



Proceedings of the
32nd Linear Accelerator Conference
(LINAC2024)
(at a glance)

Proceedings at a glance of the 32nd Linear Accelerator Conference (LINAC2024)

DATE: August 25-30, 2024

ISBN: 978-3-95450-219-6

ISSN: 2226-0366

DOI: 10.18429/JACoW-LINAC2024

Editorial Board: Kelly Jaje (ANL), Kip Bishofberger (LANL), Ryan Brody (ANL), Gustavo Bruno (ANL), Jan Chrin (PSI), Cathy Eyberger (ANL), Maggie Montes (SLAC), Denise Skiadopoulos (ANL), Ling Wang (MSU/FRIB), Kent Wootton (ANL)

Copyright © 2024 by JACoW — Creative Commons Attribution 4.0 — Publishing Policies & Ethics

BREAKING THROUGH 100 mA H⁻ ION SOURCE OUTPUT CURRENT AT SNS*

B. X. Han†, R. F. Welton, C. M. Stinson, V. J. Andzulis, G. P. Terszakowec, C. Piller, S.-H. Kim
Spallation Neutron Source, Oak Ridge National Laboratory, Oak Ridge, TN, USA

Abstract

The performance of the SNS H⁻ ion source was significantly improved over the years with a primary emphasis on operational lifetime and reliability. The recent developments in support of the SNS Proton Power Upgrade (PPU) have resulted in a remarkable boost in the ion source output current, increasing from the existing capability of ~60 mA to more than 100 mA. This paper briefly reviews the ion source reliability improvements and discusses the design and diagnostics of recent beam current enhancement.

INTRODUCTION

The Spallation Neutron Source (SNS) at Oak Ridge National Laboratory is a large-scale accelerator-based pulsed neutron facility. The accelerator system of the SNS includes a 65 keV injector, a 2.5 MeV RFQ, a high energy Linac chain (warm Linac + superconducting Linac), and a proton accumulator ring. The injector consisting of a H⁻ ion source and an electrostatic LEBT provides H⁻ beams with the required current intensity and time structure for the SNS operation. SNS has recently undertaken a major upgrade to double the proton beam power from 1.4 MW to 2.8 MW, which involves Linac beam energy upgrade from 1.0 GeV to 1.3 GeV, Linac beam current increase from ~35 mA to ~50 mA, and a reduction of chopped beam fraction. The SNS H⁻ ion source reliably supported the SNS 1.4 MW operation in the past couple of years with ~55 mA beam current operating at 6% duty-factor (1.0 ms, 60 Hz) covering 3-4 months long SNS run cycles. This established performance of the ion source could reach the requirements set forth by the new beam power goal. However, it is essential to have a sufficient beam current margin to allow operational flexibility and reliability.

THE SNS H⁻ ION SOURCE

The SNS ion source is a multicusp-confined, RF-driven, Cs-enhanced H⁻ ion source. This type of ion source was developed at Lawrence Berkeley National Laboratory (LBNL) initially for the Super-conducting Super Collider project and then for the Spallation Neutron Source project in 1990s and early 2000s. Since the ion source was operated at SNS starting in 2002, it has been further developed for long lifetime (several months), highly reliable, persistent high current (up to 60 mA) H⁻ beams for 1.0 ms pulses repeating at 60 Hz [1-9]. Figure 1 shows a cutaway view of the SNS H⁻ ion source with its key components denoted. The ion source plasma is driven by a 2 MHz RF through a porcelain-coated, water-cooled copper-tube RF antenna.

* Work supported by UT-Battelle, LLC, under contract DE-AC05-00OR22725 with the US Department of Energy (DOE)

† Email: hanb@ornl.gov

The 2 MHz RF is capable of operating at 60 Hz with 1 ms pulse length and a power level up to 80 kW for high-density plasma generation. To facilitate fast and reliable ignition and buildup of the 2 MHz high-density plasma pulses, a low-density background plasma is generated and maintained in the same chamber with a continuous, low power (~300 W) 13.56 MHz RF applied on the same antenna. A pair of rod magnets provide plasma filtering for creating a low electron temperature plasma region favorable for H⁻ formation. A solid reaction Cs dispenser system (Cs₂CrO₄ + Zr, Al) is used for ion source cesiation. A Mo cone located near the ion source outlet aperture enhances H⁻ yield through negative ion conversion on its properly cesiated surface area. The co-extracted electrons are separated from the H⁻ beam and dumped on the e-dump electrode by a transverse magnetic field generated in the ion source extraction region by an array of magnets that are embedded in the outlet electrode. The extracted H⁻ beam is coupled into an electrostatic LEBT which transports and injects the beam to the RFQ.

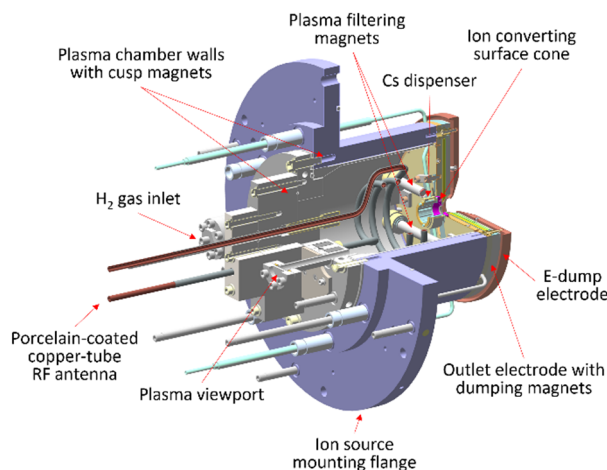


Figure 1: A cutaway view of the SNS H⁻ ion source.

The significant improvements which have contributed to the high-performance ion source operation include:

- Quality improvements of antenna coating (material composition, layer thickness, and rigorous inspection) allowing the ion source lifetime extension from the original 2-3 weeks to >4 months.
- RF systems improvements (relocation of RF amplifiers from ion source high voltage deck to ground potential, frequency shift and amplitude modulation at the start and end of the 2 MHz RF pulses, optimization of 13.56 MHz RF matching) enhancing the ion source plasma ignition and operational reliability.

STATE-OF-THE-ART PHOTOCATHODES FOR BRIGHT-BEAM AND SPIN-POLARIZED-BEAM GENERATION

Oksana Chubenko*, Northern Illinois University, DeKalb, IL, USA

Abstract

Due to their key properties, photoemission-based electron sources (photocathodes) are now widely used to generate bright and spin-polarized electron beams for advanced accelerator applications. The performance of these applications is limited by the quality of the photocathodes. Therefore, research and development of high-quality photocathodes with superior brightness and, where required, spin-polarization that can endure realistic photoinjector conditions is crucial. This paper will cover some of the latest advancements in photocathodes for generating bright and spin-polarized electron beams.

INTRODUCTION

Cutting-edge electron accelerator applications, such as X-ray Free Electron Lasers (XFELs), Ultrafast Electron Diffraction (UED) and Microscopy (UEM), as well as particle colliders including the Electron-Ion Collider (EIC), require high-quality electron beams. The quality of electron beams is characterized by their brightness. To enhance beam quality, it is essential to understand the factors that limit brightness. For high-charge-density applications, one key limitation of the 4D brightness B_{4D} is the accelerating electric field \mathcal{E} at the photocathode surface, which determines the maximum charge density that can be extracted without degrading brightness

$$B_{4D} \propto \frac{\mathcal{E}^n}{MTE}, \quad (1)$$

where n varies between 1 and 2, depending on the photoinjector design. Another critical factor is the mean transverse energy (MTE) of the photoemitted electrons. MTE is defined as the average kinetic energy of emitted electrons in the direction perpendicular to the beam propagation. Due to different effects, the MTE of electrons emitted from conventional photocathodes is limited to several 100s of meV, which is nearly an order of magnitude larger than the theoretically predicted MTE limit ($MTE_{\min} \approx k_B T \approx 25$ meV at room temperature, where k_B is the Boltzmann constant and T is the temperature). Typical factors that limit MTE include the requirements for high charge density, the disordered nature of photocathode materials, surface roughness, and work function variations.

For high-energy-physics and nuclear-physics experiments that rely on spin-polarized electron sources, it is important to have very high electron spin polarization (ESP), which is defined as the degree to which the spin is aligned with a given direction and is given by

$$ESP = \left| \frac{N_{\uparrow} - N_{\downarrow}}{N_{\uparrow} + N_{\downarrow}} \right|, \quad (2)$$

where N_{\uparrow} and N_{\downarrow} is the number of electrons with spins parallel and antiparallel to the direction of beam propagation, respectively. The ability of photocathodes to generate spin-polarized electron beams stems from the unique band structure of the photocathode materials. The maximum achievable ESP in experiments is determined by fundamental scattering mechanisms within these materials.

The overall quality of a photocathode is described by its quantum efficiency (QE), which is defined as the ratio of the number of emitted electrons N_{e^-} to the number of incident photons $N_{\hbar\omega}$

$$QE = \frac{N_{e^-}}{N_{\hbar\omega}}. \quad (3)$$

Photocathodes with higher QEs can produce electron beams with higher intensities.

Many applications require photocathodes with a prompt response time, which refers to the time it takes for a photocathode to emit electrons in response to incident light. The response time depends on the material's electron escape time, which is the time required for photoexcited electrons to reach the surface and escape into the vacuum.

It is also important to have a robust photocathode with long operational time, which means that photocathodes must operate under realistic photoinjector conditions. The photocathode reliability and stability under high electric-field loads and large laser fluences are crucial for sustained experimental operations.

Evidently, the quality of the electron beam is directly limited by the quality of the photocathode. Detailed theoretical photoemission modeling, combined with advanced photocathode characterization techniques, can be utilized to improve the performance of traditional electron sources and develop new ones with enhanced capabilities. Here, we will review some theoretical and experimental approaches towards generating high-quality electron beams for bright and spin-polarized applications.

PHOTOCATHODES FOR BRIGHT-BEAM APPLICATIONS

Traditionally, many accelerator facilities use metallic photocathodes to generate electron beams. Operating metallic photocathodes with photoexcitation energy close to the photoemission threshold results in low MTE but also yields low QE. While QE can be enhanced by increasing the photoexcitation energy, this also leads to an increase in MTE. For high-current, high-brightness applications, photocathodes can, in principle, operate near the photoemission threshold under high laser fluences. However, recent theoretical [1] and experimental [2] studies have shown that non-linear processes, such as multi-photon absorption, limit the MTE of electrons photoemitted from Cu to several hundred meV.

* chubenko@niu.edu

THIN GOLD LAYERS ON NIOBIUM FOR SRF CAVITIES*

S. Seddon-Stettler[†], M. Liepe, T. Oseroff, N. Sitaraman

Cornell Laboratory for Accelerator-based ScienceS and Education (CLASSE),
Ithaca, New York, United States

V. Do, H. Lew-Kiedrowska, S. J. Sibener, University of Chicago Department of Chemistry
and James Franck Institute, Chicago, Illinois, United States

C. Wang, National Cheng Kung University, Tainan, Taiwan

Abstract

New materials beyond the standard bulk niobium have the potential to greatly improve the performance of Superconducting Radio Frequency (SRF) cavities. Specifically, thin coatings of non-oxidizing normal conductors such as gold have the potential to improve the key RF performance metric of quality factor. We present progress on depositing thin gold layers onto 2.6 GHz SRF cavities and testing their RF performance.

INTRODUCTION

Superconducting Radio-Frequency (SRF) cavities underlie current cutting edge accelerator technology on a variety of scales. Typically, SRF cavities are manufactured from bulk niobium, several millimeters thick, and are given a variety of chemical and thermal treatments to improve their performance [1]. Though the niobium is thick, the RF field excited in the cavity interacts with the cavity most strongly at the surface, specifically within (approximately) the first 40 nm [2]. Because of this, engineering and optimization of the surface of niobium has become a strong focus of research and development for improving SRF cavity performance [1].

When exposed to atmosphere, the surface of niobium forms a complex, multi-phased oxide [3, 4]. By volume, the oxide is composed primarily of the pentoxide, Nb_2O_5 , then lower phases including NbO_2 , NbO , and other lower phases. The pentoxide can be removed by thermal treatments at reasonable temperatures, but not the lower phases [5]. The electronic properties of the oxide, and therefore its interaction with RF fields, are affected in many subtle ways by different cavity treatments. The lower phases of the oxide may have some normal conducting properties [3], which may inhibit cavity performance at energies relevant to accelerator applications. However, due to the complexity and irregularity of the oxide, it is difficult to study in isolation.

Work at Cornell University and elsewhere proposed to remove the oxide entirely, then replace it with a thin layer of a non-oxidizing normal conductor such as gold [6–8]. That work showed promise for improving cavity RF performance at very thin (sub-nm) layer thicknesses of gold.

We have previously presented preliminary work towards developing a gold passivation technique that could be applied on a full-scale SRF cavity [9, 10]. Here we discuss progress towards a fully plated 2.6 GHz SRF cavity, including progress on the electrodeposition process and development of a suitable cavity.

ELECTRODEPOSITION OF GOLD

A major challenge of applying a thin layer of gold to an SRF cavity is the choice of deposition method. Many deposition methods common to materials science applications are not able to accommodate the large size and irregular geometry of a typical 1.3 GHz SRF cavity. Furthermore, removal of all oxide layers requires a chemical treatment of hydrofluoric acid in an inert atmosphere in order to prevent the oxide from reforming. Given these requirements, we are developing an electroplating system capable of depositing thin layers of gold on niobium substrates that can be performed entirely within an inert atmosphere glovebox [10].

Our electroplating setup uses a commercially available sodium gold sulfite electroplating solution, which has a deposition rate that scales linearly with current density. Deposition thickness in electrochemical processes also scales linearly with time. In order to deposit very thin films of gold, we have developed a custom timing circuit that can reliably deliver very low quantities of current over very short intervals of time [10]. During the process, the current is monitored using an ammeter and recorded digitally, resulting in a trace of current vs. time. An example such trace is shown in Fig. 1. This together with the geometry of the substrate receiving the deposit allows for estimation of the deposited thickness of gold.

SAMPLE CHARACTERIZATION

Optimization of an electroplating process for use on an SRF cavity requires regular characterization of the films produced by the process. There are two main tools for this: X-Ray Photoelectron Spectroscopy (XPS), which scans over binding energies to identify elements and chemical phases present on a sample, and Scanning Electron Microscopy (SEM), which allows for visual characterization of deposited films. An example XPS scan of a thinly plated niobium sample, showing the presence of gold but with very low counts per second (indicating a very thin film of gold), is shown in Fig. 2.

* Work supported by U.S. National Science Foundation under Award PHY-1549132, the Center for Bright Beams, the U.S. Department of Energy under Award DE-SC0024137, and the NSF Materials Research Science and Engineering Center (MRSEC) at the University of Chicago, Grant No. NSF-DMR-2011854.

[†] sgs238@cornell.edu

MITIGATION OF LONGITUDINAL BEAM LOSSES IN THE FRIB LINAC

A. Gonzalez*, A.S. Plastun, P.N. Ostroumov

Facility for Rare Isotope Beams, Michigan State University, East Lansing, MI, USA

Abstract

The linear accelerator at the Facility for Rare Isotope Beams (FRIB) at Michigan State University uses a thin liquid lithium film for charge stripping of high-intensity heavy ion beams. Energy straggling and energy loss of the beam in the inherently non-uniform lithium film affects the energy distribution in the beam. This can lead to non-linear “tails” in the longitudinal phase-space beam distribution after bunching at the two 161 MHz room-temperature Multi-Gap Bunchers (MGBs) between the stripper and the next accelerating segment. Some particles in these “tails” are lost in the downstream accelerator cryomodules. To mitigate these losses, we have designed a room-temperature IH-type buncher cavity with a resonant frequency of 322 MHz, the second harmonic of the MGBs. The new harmonic cavities will be installed next to each MGB, linearizing the waveform of the effective bunching voltage and eliminating the formation of non-linear “tails.” The increase in the energy acceptance of the post-stripper part of the accelerator reached over 50% according to our simulations. We present the electromagnetic design of this cavity along with beam dynamics simulations that demonstrate how the losses are mitigated. The construction and installation of the cavity are being pursued as an accelerator improvement project.

INTRODUCTION

The FRIB linear accelerator is a state-of-the-art superconducting heavy ion linear accelerator. As shown in Fig. 1, the accelerator contains three linear accelerating segments and two 180 degree bending sections. For more efficient acceleration, a charge stripper is located after the first accelerating segment (LS1). Two options are available for charge stripping: a carbon foil for low intensity beams, and a thin liquid lithium film for high intensity beams [1]. Downstream of the stripper, we use two 161 MHz Multi-Gap Bunchers (MGBs) [2] to keep the beam longitudinally bunched before entering the second accelerating segment (LS2). Figure 2 shows a zoomed-in view of the layout between the stripper and the entrance to LS2.

When the lithium stripper is used, energy straggling, energy loss and non-uniformities in the film cause a large energy spread in the beam after the stripper. This means the longitudinal beam size is large when the beam arrives at the first MGB (MGB01). The large longitudinal beam size leads to non-linear “tails” in the longitudinal phase space distribution after the beam experiences the sinusoidal 161 MHz effective bunching voltage at MGB01. Particles in these “tails” are lost in the LS2 cryomodules. The lost fraction of the beam does not exceed 10^{-4} , which corresponds to

a temperature increase of up to 0.3 K in the beam pipe in the LS2 cryomodules during 10 kW beam power on target operation [3]. As beam power ramps up to our ultimate goal of 400 kW [4], the temperature increase in the cryomodules will also ramp up, which may lead to degradation of SRF cavities due to field emission. Therefore, it is necessary to mitigate these losses.

Beam dynamics studies showed that the losses can be eliminated if the MGB effective voltage is linearized. To do this, we have designed a Second Harmonic Buncher (2HB) cavity to be installed downstream of each MGB as seen in Fig. 2. This new cavity will have a resonant frequency of 322 MHz, which is twice the resonant frequency of the MGBs. The effect of this second harmonic is shown in Fig. 3. The effective bunching voltage waveform of the combined harmonics, shown in orange, has a significantly longer linear region than the waveform of the 161 MHz MGB only.

BEAM DYNAMICS

We used the particle tracking code TRACK [5] to simulate the effect of the new cavities on the beam dynamics. First, we examined the effect of building only one 2HB and installing it downstream of MGB01 versus the effect of building two 2HBs and installing them downstream of each MGB. We simulated the longitudinal acceptance from the lithium stripper to the end of LS2 for three cases: no 2HBs added, one 2HB added downstream of MGB01, and two 2HBs added: one downstream of MGB01 and the other downstream of MGB02. The results can be seen in Fig. 4. From these plots, it is apparent that while installing one 2HB leads to a significant increase in energy acceptance, the highest energy acceptance is achieved when two 2HBs are installed.

The linearizing effect of the second harmonic can be directly seen in Fig. 5. To clearly demonstrate the effects of the new cavities, we created an artificial beam distribution with an exaggerated energy spread at the stripper and simulated it with TRACK from the stripper to the entrance of LS2, taking snapshots of the longitudinal distribution at the exit of 2HB1 and 2HB2. In the top plot, when 2HB1 is on, there are much fewer particles in the non-linear “tails” on the edges of the beam distribution compared to the case when 2HB1 is off. In the bottom plot, the distribution with the largest linear region is when both second harmonic bunchers are activated. In Fig. 6, it can be seen that when both 2HBs are activated, all particles in the simulation fit inside the longitudinal acceptance of LS2, whereas some particles are lost in the other cases. This further validates the decision to build and install two 2HBs.

* gonzalea@frib.msu.edu

HIGH Q AND HIGH GRADIENT PERFORMANCE OF THE FIRST MEDIUM-TEMPERATURE BAKING 1.3 GHz CRYOMODULE

J. Zhai[†], W. Pan, F. He, R. Ge, Z. Mi, P. Sha, S. Jin, R. Han, Q. Wang, H. Lin, Z. Zhang, M. Li, M. Sang, L. Sun, T. Zhao, B. Liu, X. Yang
Institute of High Energy Physics, Chinese Academy of Sciences, Beijing, China

Abstract

World's first 1.3 GHz cryomodule containing eight 9-cell superconducting radio-frequency (RF) cavities treated by medium-temperature furnace baking (mid-T bake) was developed at the Institute of High Energy Physics (IHEP), Chinese Academy of Sciences. The 9-cell cavities in the cryomodule achieved an unprecedented high average intrinsic quality factor (Q_0) of 3.8×10^{10} at 16 MV/m and 3.6×10^{10} at 21 MV/m in the horizontal test. The cryomodule can operate stably up to a total continuous wave (CW) RF voltage greater than 193 MV, with an average cavity usable accelerating gradient of more than 23 MV/m. The results significantly exceed the specifications of Circular Electron Positron Collider (CEPC) and Dalian Advanced Light Source (DALIS) and the other high repetition rate free electron laser facilities (LCLS-II, LCLS-II-HE, SHINE, S³FEL etc.). This contribution reviews the cryomodule performance and discusses some important issues in cryomodule assembly and testing.

INTRODUCTION

High Q_0 1.3 GHz cryomodules operating in the CW mode are critical technology for several major scientific projects under construction or being planned in the world. For example, Shanghai High Repetition Rate X-ray FEL and Extreme Light Facility (SHINE) [1], Shenzhen Superconducting Soft X-Ray Free Electron Laser (S³FEL) [2], and high duty cycle upgrade of the European XFEL [3]. High Q_0 will save a large part of the construction and operational cost of the cryogenic system for these projects.

The successful commissioning and operation of Linac Coherent Light Source II (LCLS-II) at SLAC first time demonstrated high Q_0 cavity in a CW superconducting RF linac [4] with nitrogen-doping (N-doping) technology [5]. Fermilab and JLAB has achieved even ambitious performance goals in LCLS-II-HE prototype and production cavities and cryomodules by improving the nitrogen doping technology [6-8].

Medium-temperature baking (mid-T bake) is a novel high Q_0 recipe discovered in 2019 [9-11] by Fermilab. KEK simplified the implementation of the recipe by mid-T baking of the unassembled cavity in a normal vacuum furnace (so called mid-T furnace baking) [12], which is more accessible than the original in-situ mid-T bake.

KEK's systematic investigations showed that 300 C bake has the highest Q_0 [13].

Based on Fermilab and KEK's experience on single cell cavities, IHEP further simplified mid-T furnace bake procedure to only one bulk EP (without light EP) and successfully applied it first time to 1.3 GHz 9-cell cavities in October 2020 [14, 15]. Since then, fourteen mid-T 9-cell cavities have been tested with high reliability by industrial vendors. Researches from other labs [16-19] also confirmed the mid-T furnace bake a reproducible and stable recipe for high Q_0 cavities. In June 2023, a 1.3 GHz cryomodule with eight mid-T furnace baked 9-cell cavities was assembled and tested at IHEP and achieved world leading high Q_0 and high gradient.

There are some distinct advantages of mid-T bake compared to nitrogen doping [20]. Mid-T bake has been widely applied successfully to large grain cavities [21, 22], other frequencies and shapes [23, 24] and even carried out without furnace [25]. In particular, mid-T furnace bake high Q_0 recipe was recently adopted for the low-beta 650 MHz 5-cell cavities for Fermilab's PIP-II project [26]. The ongoing and future high repetition rate FEL and ERL projects (e.g. SHINE, S³FEL, DALIS, PERLE and high duty cycle upgrade of European XFEL etc.), as well as the energy frontier circular lepton colliders (CEPC, FCC-ee) are all considering to use mid-T furnace bake treatment for their large number of cavities.

Therefore, demonstration of mid-T bake cavity performance in a real cryomodule is becoming essential for the development and practical application of this novel high Q_0 technology. In this contribution, we report the performance of the world's first mid-T bake cryomodule.

CRYOMODULE ASSEMBLY AND INSTRUMENTATION

The cryomodule structure and assembly procedure are similar to LCLS-II cryomodules which is modified from Euro-XFEL design. The 12 m long cryomodule (Fig. 1) contains eight 1.3 GHz 9-cell cavities, eight power input couplers, eight tuners with piezos, one conduction-cooled superconducting magnet and one BPM. Measures to reduce microphonics were adopted according to LCLS-II experience [27]. To avoid contamination risk, the cavity string was kept in vacuum after leak check all through to the horizontal test. To reduce the multipacting processing time, the cavity string was also pumped by a turbo molecular pump whenever possible during the cold mass

[†] zhajy@ihep.ac.cn

ACCELERATOR DESIGN CHOICES FOR A COMPACT, ELECTRON-DRIVEN, PULSED NEUTRON SOURCE

L. M. Wroe, A. Latina, J. Olivares Herrador, S. Stapnes, W. Wuensch, CERN, Geneva, Switzerland
G. Kharashvili, F. Plewinski, DAES SA, Geneva, Switzerland

Abstract

Neutron scattering is an indispensable technique in material science research for providing solutions to important engineering challenges, including the ever-growing demand for more efficient batteries and fuel-cells. There are, however, limitations in the access and availability to the necessary neutron beams and this is worsening as nuclear research reactors continue to shut down. As a result, there appears to be market demand for an affordable, medium-flux, compact, accelerator-driven neutron source optimised for deployment in an industrial setting. In this paper, we present an overview of the beam specification and the high-level design choices for an electron linear accelerator that is optimised to drive such a facility.

INTRODUCTION

The use of neutron beams for neutron scattering measurements finds a broad range of applications in the field of material science [1]. In particular, neutron scattering techniques can be exploited to develop advanced battery and fuel-cell materials and manufacturing techniques [2–4], as well as to measure the material stresses and strains within material samples [5–7]. Such neutron scattering experiments and measurements are typically undertaken in large-scale facilities that utilise spallation sources (such as the Spallation Neutron Source at the Oak Ridge National Laboratory in Tennessee, US [8] and the European Spallation Source under construction in Lund, Sweden [9]) or nuclear research reactors (such as the High Flux Reactor at the Laue-Langevin Institute in Grenoble, France [10]).

However, the landscape of available neutron facilities is shifting as nuclear facilities continue to close despite the ever increasing demand for access to neutron beams [11]. Compact Accelerator-driven Neutron Sources (CANS) are a potential answer to this problem and, despite a reduced neutron flux at the sample compared to higher-end facilities, they offer a series of attractive benefits. These include, for example, the ability to develop and use advanced sample environments and instrumentation dedicated to focused topics, the provision of high ‘access agility’, the production of less radioactive waste, and the fact that nuclear licensing is not required [12].

Currently, there are no commercial-off-the-shelf CANS available to industry, universities, nor research centers. A collaboration therefore formed between DAES SA and CERN in 2023 to further develop the so-called VULCAN (Versatile ULtra-Compact Accelerator-based Neutron source) instrument that has been jointly developed between 2021 – 2024 by DAES SA, the Danish Technological Insti-

tute, and Xnovotech. VULCAN is a compact and affordable, non-destructive, CANS-based testing instrument that generates a cold neutron beam for neutron scattering measurements. It is purpose-built for implementation in an industrial setting and optimised for the in-situ analysis of battery and fuel cell electrodes, as well as for the measurement of internal stresses inside thick metallic and ceramic components.

Essential to the VULCAN design is its compactness. A conceptual visualisation of such a facility is shown in Fig. 1. The core parts are:

- **Electron linac:** A compact, pulsed electron-based linear accelerator that delivers 35 MeV electrons with an average beam power on the order of a kW to the Target-Moderator-Reflector (TMR).
- **Radiofrequency source:** A radiofrequency power source that drives the electron linac.
- **Target-Moderator-Reflector (TMR) assembly:** A compact setup optimised for the conversion of the incident electron beam into a cold neutron beam with the desired properties.
- **Neutron guide:** A neutron guide to provide time-of-flight measurements.
- **Hexapod and detector:** A hexapod on which to position the material sample and a detector with which to take measurements.

The collaboration between DAES SA and CERN has two aims. One is to benchmark the performance of a prototype TMR and the second is to develop a conceptual design of an electron linear accelerator optimised for VULCAN.

This paper focuses on the high-level design choices made for the electron linac design. We begin with a discussion of the electron beam specification and the accelerator design parameters that are to be optimised. The impact this has on the high-level accelerator design is then outlined.

ELECTRON BEAM SPECIFICATION

Table 1 provides the specification on the electron beam and accelerator design for the VULCAN facility.

The underlying reasons behind this electron beam specification are:

- **Beam energy and spread:** The neutron yield per unit of electron beam power incident on a tungsten target increases rapidly between 7 – 30 MeV. Bremsstrahlung processes produce more photons with energies that have a significantly larger cross-section for exciting the giant

PERFORMANCE OF THE FERMILAB LINAC INJECTOR

D. C. Jones*, D. Bollinger, V. Kapin, Fermi National Accelerator Laboratory, Batavia, USA

Abstract

The Fermilab Linac injection line consists of a 35 keV magnetron-type H^- ion source, two-solenoid Low Energy Beam Transport (LEBT), 201 MHz 4-rod 750 keV Radio Frequency Quadrupole (RFQ), and a Medium Energy Transport (MEBT) containing 4 quadrupoles and a bunching cavity. The injector delivers 25 mA, 48 μ s pulses to the drift-tube Linac at a repetition rate of 15Hz. The transmission efficiency of the injector has been lower than expected since commissioning. Recent beam current measurements suggest that the beam is primarily lost upstream of the RFQ exit. Numerical simulations indicate that ions passing through the non-linear field region of the solenoids could produce a beam with an increased emittance resulting in up to 50% of the LEBT beam current failing to meet the RFQ acceptance. An aperture restriction was installed upstream of the first solenoid to remove these ions. This report describes the results of measurements and simulations as well as the LEBT tuning.

INTRODUCTION

The Fermi National Accelerator Laboratory (FNAL) LINAC H^- injector was upgraded from a Cockcroft–Walton 750 keV DC accelerator to a 201 MHz 4-rod 750 keV Radio Frequency Quadrupole (RFQ) injector as part of the 2012 Proton Improvement Plan for the FNAL complex. The H^- injector line currently consists of a 35 keV magnetron-type H^- ion source, two-solenoid Low Energy Beam Transport (LEBT), 201 MHz 4-rod 750 keV Radio Frequency Quadrupole (RFQ), and a Medium Energy Transport (MEBT) containing 4 quadrupoles and a bunching cavity [1].

The transmission efficiency from the ion source to the start of the LINAC is approximately 40% which is significantly lower than expected. Previous studies looking at the transmission efficiency focused on the MEBT and other beamline qualities [2]. In addition, recent data exploring the possibility that the LEBT is the main cause of the inefficiency has been presented [3].

In this paper, we explore the use of an aperture restriction just upstream of the first solenoid to explore the possibility of better matching the LEBT beam to the RFQ acceptance. This report describes the results of measurements and simulations.

NOTICING THE PHASE SPACE SPIRALLING

Due to the compact nature of the H^- injector the ion source, LEBT, and RFQ have no emittance diagnostics. The first set of emittance diagnostics is at the entrance of the drift-tube LINAC (DTL). To investigate the emittance of the beam

* dcjones@fnal.gov

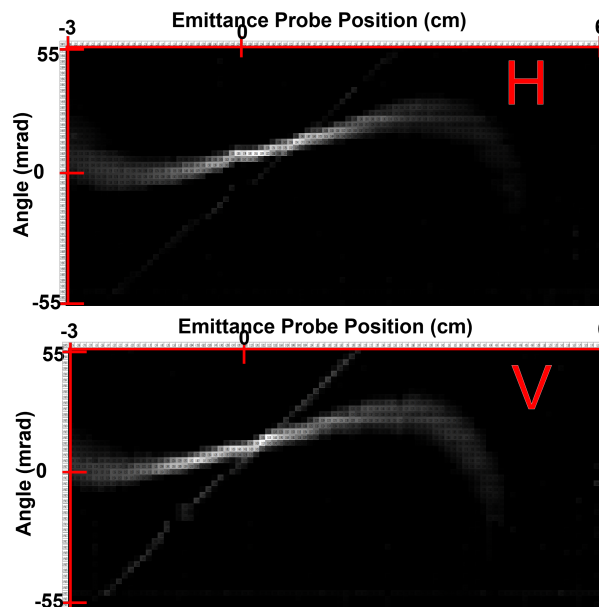


Figure 1: Heat maps from the ion source test bench emittance probes

downstream of the ion source an ion source test bench with a similar ion source and single solenoid was used. Heat Maps from the ion source test bench are shown in Fig. 1.

The shown phase space spiral is in both transverse planes. This suggests a linear "stick"-like shape of the beam in phase spaces at the ion source which is then filamented in the solenoid field.

We suspect that this filamentation is due to the beam interacting with the non-linear magnetic field region in the solenoid. Assuming a "stick"-like shape of the beam in phase space CST Particle Studio (PS) simulations were run under full neutralization conditions and the results showed growth and dilution of the beam emittance in the LEBT. This growth and dilution of the beam emittance in the LEBT results in a mismatch with the elliptic RFQ acceptance resulting in high beam loss. Further simulations indicate that an aperture restriction upstream of the first solenoid will assist in forming a beam emittance matched to the RFQ acceptance in size and shape, shown in Fig. 2.

The simulation results show that without the aperture restriction, the beam is filamented in the X-X' and Y-Y' planes resulting in many of the particles falling outside of the RFQ acceptance (red ellipse). When an aperture restriction with a diameter of 46 mm was simulated to be just upstream of the first solenoid most of the particles fell within the RFQ acceptance.

STANDING WAVE DIELECTRIC DISK ACCELERATING STRUCTURE DESIGN AND FABRICATION

S. Weatherly*¹, C. Jing², E. Wisniewski¹, D. Doran, J. Power
Argonne National Laboratory, Lemont, IL, USA

B. Freemire, Euclid Beamlabs, USA

T. Abe, Accelerator Laboratory, High Energy Accelerator Research Organization, Japan

¹also at Illinois Institute of Technology, Chicago, USA

²also at Euclid Beamlabs, Bolingbrook, USA

Abstract

A Dielectric Disk Accelerator (DDA) is a metallic accelerating structure loaded with dielectric disks to increase coupling between cells, thus high group velocity, while still maintaining a high shunt impedance. This is crucial for achieving high efficiency high gradient acceleration in the short rf pulse acceleration regime. Research of these structures has produced traveling wave structures that are powered by very short (~9 ns), very high power (400 MW) RF pulses using two beam acceleration to produce these pulses. In testing, these structures have withstood more than 320 MW of power and produced accelerating gradients of over 100 MV/m. The next step of testing these structures will use a more conventional, klystron power source. A new standing wave DDA structure is being fabricated for testing on the Nextef2 test stand at KEK. Simulation results of this structure show that at 50 MW of input power, the DDA produces a 457 MV/m gradient. It also has a large shunt impedance of 160 M Ω /m and an r/Q of 21.6 k Ω /m. Cold testing of this structure will be conducted late summer 2024 with high power testing to be done in the fall.

INTRODUCTION

The future path for accelerators are compact, high energy linear machines. In order to minimize the footprint, high gradient accelerating cavities need to be developed. Dielectric Disk Accelerators (DDA) researched here are X-band dielectric disk loaded metallic structures are a promising candidate to be used in future accelerators. These structures have high shunt impedances and high accelerating gradients [1].

To produce high accelerating gradients, high peak input RF power are required and to limit the risk of breakdown, short RF pulses are used [2]. These pulses are created using Two Beam Acceleration (TBA). A high charge drive beam is produced and sent through a Power Extractor and Transfer Structure (PETS) [3]. This decelerates the drive bunch and transfers the created RF power packet to the DDA that accelerates a witness beam. The RF pulse length produced by the PETS in this research is ~9 ns.

In this paper we will review the outcomes of previous DDA experiments and discuss plans to test a new standing wave DDA on a klystron test stand at KEK.

PREVIOUS DDA PROTOTYPES

Initially, two single cell DDA structures were designed and high power tested [4,5]. A clamped design was selected for new designs due to difficulties with brazing on previous prototypes. During high power testing, the clamped single cell DDA withstood 321 MW of input power and achieved an accelerating gradient of 102 MV/m [6]. The test ran up to the amount of available RF power. During the experiment there were no optical signs of breakdown and in review of the recorded RF pulses during data processing there were also no signs of breakdown. After testing, the single cell clamped DDA was disassembled and visually inspected. Damage was found where the faces of the copper components meet when clamped. Figure 1 shows the damage. Since the damage was located outside the RF volume it was likely caused by uneven and insufficient clamping during assembly.



Figure 1: Damage seen on the copper and ceramics from the single cell DDA high power experiment.

Multicell DDA Structure

Following the success of the single cell clamped structure, a multicell clamped structure was designed and tested. The fabricated and assembled structure is seen in Fig. 2.

Structure Simulation The original design of the multicell DDA involved seven dielectric disks that made up six cells. The design emphasized maximizing the shunt impedance of the structure while also keeping the accelerating gradient as high as possible. Simulations were done in both CST and COMSOL [7, 8]. Table 1 summarises the simulation results for the six cell structure.

* sweatherly@hawk.iit.edu

SIMULTANEOUS ACCELERATION OF PROTON AND H-MINUS BEAMS IN RFQ

S. S. Kurennoy, Los Alamos National Laboratory, Los Alamos, NM, USA

Abstract

The Los Alamos Neutron Science Center (LANSCE) accelerator complex delivers both protons (p) and negative hydrogen ions (H⁻) and provides various beam patterns simultaneously to multiple users. The LANSCE linac front end is still based on Cockcroft-Walton voltage generators that bring proton and H⁻ beams to 750 keV. An upgrade of the front end to a modern, RFQ-based version is now under consideration. The most promising upgrade option is based on acceleration of two continuous beams, p and H⁻, injected simultaneously into a single RFQ, which has never been done before. We use an existing CST model of a proton RFQ to model simultaneous acceleration of proton and H⁻ beams as a proof of principle for such an RFQ operation.

INTRODUCTION

The 800-MeV proton linac at LANSCE operates since 1972 and now delivers both proton and negative hydrogen ion (H⁻) beams of different flavors (time patterns, bunch charges) to five user facilities simultaneously [1]. The initial beam acceleration to 750 keV is still provided by ageing Cockcroft-Walton (C-W) generators. Various options for the front-end upgrade have been under consideration for a long time [2]. The most promising option is based on simultaneous acceleration of two continuous beams, p and H⁻, in a single RFQ. While it is known that a proton RFQ can also accelerate H⁻ ions, RFQ working simultaneously with two beams, p and H⁻, has not been demonstrated.

We will use an existing CST Studio [3] model of the 4-rod RFQ that was originally developed to replace the proton C-W injector at LANSCE, see in [4], while keeping the H⁻ injection unchanged. The 201.25-MHz RFQ was designed to accelerate protons to 750 keV, fabricated by Kress GmbH, and delivered to LANL in 2015. However, detailed 3D modeling [5] indicated difficulties of integrating such a new proton injector in the existing front end.

One important goal for the upgraded LANSCE front end is that it should provide all beam flavors available now. The most challenging is a special case of H⁻ beam, which consists of single bunches with increased bunch charge, about 300 pC, separated by long intervals of 1.8 μ s – the so-called MPEG beam. The MPEG bunches are delivered from the linac at 800 MeV directly to targets, mainly for time-of-flight experiments. Compared to regular H⁻ bunches (called LBEG), which are injected into the Proton Storage Ring at 800 MeV and follow at 201.25-MHz repetition rate (\sim 5-ns period), the higher charge in MPEG bunches is achieved by chopping about 25-30 ns of continuous H⁻ beam at 750 keV and applying an energy tilt for velocity bunching. MPEG bunches are not well matched to the linac, which is tuned to beam flavors with higher average power, and a significant fraction of the MPEG beam,

up to 2/3, is lost in the drift tube linac, well before it reaches its target, see in [6]. Generating a single high-charge bunch out of an RFQ is a challenge: it will likely be accompanied by undesirable satellite bunches, which will need to be removed (chopped) in the following transport line, Medium Energy Beam Transfer (MEBT).

MODELING RFQ IN CST STUDIO

CST Model of RFQ

The 201.25-MHz 4-rod RFQ was designed to accelerate proton beams from 35 keV to 750 keV. Its CST model [4] is shown in Fig. 1. Note the unusual coordinate system, which came with the RFQ CAD model: the beam moves from right to left, in the negative x -direction. The RFQ vacuum vessel, in light blue, is 175-cm long, 34-cm wide, and 30-cm high (along the stem direction, z). The rods are supported by 24 stems, with movable tuning plates mounted between stems. The EM fields of the operating mode were calculated with eigensolver in CST MicroWave Studio.

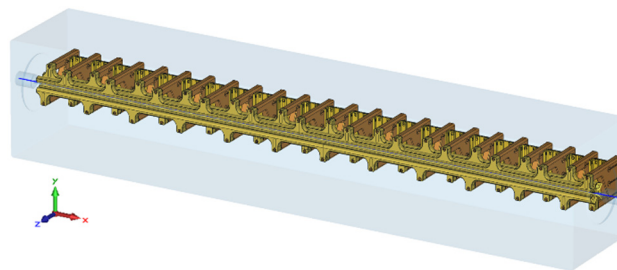


Figure 1: Vacuum volume of RFQ CST model (outer box walls not shown).

The model was used to study beam capture and acceleration with 35-keV proton macro-particle distributions generated by Parmila (L.J. Rybarczyk) and matched to the RFQ for a few different currents. The macro-particles are evenly distributed in phase within one RF period. The Parmila distributions were reformatted into CST Particle Studio (PS) input – all particles are injected in a fixed plane at different times corresponding to their RF phases. For PS simulations we typically inject into RFQ 10 RF periods with 10K macro-particle per period, i.e., 100K particles. Some results of PS particle-in-cell (PIC) simulations [4] with different currents are presented in Table 1, where the units for emittances are π mm·mrad. The initial normalized r.m.s. transverse emittance is $\epsilon_t = 0.2 \pi$ mm·mrad in both transverse planes. The output normalized r.m.s. emittances are marked as horizontal ϵ_h , vertical ϵ_v , and longitudinal ϵ_s , referencing the usual lab coordinates, because the RFQ box is rotated by 45° w.r.t. the beam axis (x here), so that the tuning plates are not vertical as in Fig. 1 but are inclined at 45° to the floor.

HIGH PULSED POWER MEASUREMENTS OF SUPERHEATING FIELDS FOR SRF MATERIALS*

N. Verboncoeur[†], A. Holic, M. Liepe, T. Oseroff, R. D. Porter[‡], J. Sears, L. Shpani
Cornell Laboratory for Accelerator based ScienceS and Education (CLASSE), Ithaca, NY, USA

Abstract

The Cornell High Pulsed Power Sample Host Cavity (CHPPSHC) is a new system designed to measure the superheating field of candidate superconducting RF (SRF) materials, giving insight into their operational limits. This system is designed to reach peak magnetic fields of up to 0.5 T in only a few microseconds, allowing us to achieve a purer magnetic field quench on the sample. We present an overview of the CHPPSHC system and proof of principle data from a niobium sample.

INTRODUCTION

Improving the accelerating gradient, E_{acc} , of superconducting radio-frequency (SRF) cavities is a desirable goal for the next generation of accelerators. The upper limit on E_{acc} for a given material is set by its superheating field, B_{SH} , and the cavity geometry. Niobium cavities are the current standard and has a B_{SH} of ~ 200 mT corresponding to a maximum E_{acc} of ~ 50 MV/m in an elliptical cavity [1]. The SRF community has been investigating other materials [2, 3] including Nb_3Sn , which is predicted to have a B_{SH} of ~ 400 mT [4, 5]. This corresponds to an upper limit on E_{acc} of ~ 100 MV/m.

To date, there has not been satisfying experimental measurements of Nb_3Sn 's superheating field. Previous attempts have been made, however these experiments have been severely limited by thermal effects. The superheating field is an extremely temperature-dependent property, so even a small amount of heating can lower the quench field. Here, we explore the Cornell High Pulsed Power Sample Host Cavity (CHPPSHC), a sample host structure specifically designed to measure the limiting magnetic fields of candidate SRF material samples [6, 7].

THE CORNELL HIGH PULSED POWER SAMPLE HOST CAVITY

The CHPPSHC must be able to reach fields exceeding the predicted B_{SH} of Nb_3Sn fast enough that heating does not have a significant effect on the measurement. The CHPPSHC utilizes a 1 MW klystron with pulse lengths on the order of $10 \mu s$. Past experiments at Cornell were done with 1.3 GHz elliptical cavities, but maximum fields were thermally limited due to pulse lengths of $50 - 100 \mu s$ [1]. The CHPPSHC's geometry is designed to charge quickly by exploiting field enhancement along the sharp edge of the sample. A simulation of the magnetic field in the cavity is shown in Fig. 1.

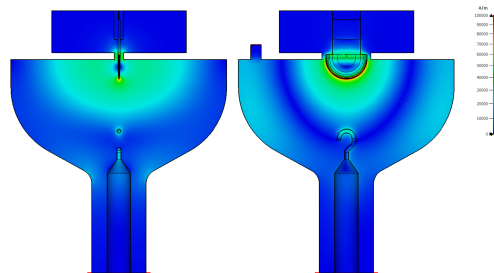


Figure 1: Simulation of peak magnetic fields along $x = 0$ (left) and $z = 0$ (right) planes of the CHPPSHC in CST Microwave Studio. The design exploits field enhancement to reach significantly higher peak fields on the sample edge. An upper bound of 1×10^5 A/m was set on the color scale for visibility purposes. The peak field on the sample is $\sim 4 \times 10^5$ A/m corresponding to ~ 500 mT.

The peak field on the sample edge is enhanced by a factor of 500 due to this effect, which allows the system to reach a maximum field of ~ 500 mT in only $\sim 10 \mu s$ [6].

The simulation also calculates the quality factors of various components of the system. While superconducting, the sample accounts for less than 0.001 % of losses. When the sample is normal conducting at 300 K, the losses on the sample reach ~ 70 % of losses. The resulting sharp drop in the system's Q_0 is large enough that it will be evident in RF power data when the sample has quenched.

PULSED RF DATA

Before investigating Nb_3Sn , baseline data for a niobium sample is necessary to ensure that quench information can be accurately extracted from our measurement results. A niobium sample was prepared using the same processes applied to a niobium cavity, receiving a bulk chemical polish, electropolishing, and a 5 hr 800 C bake. The sample was cleaned with DI water in a class 100 cleanroom before being assembled into the copper host structure.

The host cavity is tested in helium over a temperature range from 2 K to 9 K and driven by a 1 MW klystron. Before taking pulsed data, a system calibration is done in continuous wave (CW) operation to determine the loaded quality factor, Q_L , the coupling, β , and field calibration. In Fig. 2, an example pulsed operation data point is shown. B_{pk} is calculated from the RF data using the results of the CW calibration and the CST simulation.

Figure 2 shows a pulse that exhibits “overfilling” behavior where the cavity continues to fill despite the sample quenching. This makes it more difficult to accurately identify the quench field as the underlying mechanisms become more complex.

* Supported by U.S. Department of Energy Grant No DE-SC0008431

[†] nmv39@cornell.edu

[‡] Now at SLAC, Menlo Park, California, USA

LOW ENERGY MULTI-BEAM DYNAMICS IN NOVEL LANSCE FRONT END

Y. K. Batygin, Los Alamos National Laboratory, Los Alamos, New Mexico, USA

Abstract

The proposed novel 100 MeV injector for the LANSCE Accelerator Facility [1] is designed to replace the existing 750-keV Cockcroft-Walton-columns-based injector. The new Front End includes two independent low-energy transports for H^+ and H^- beams merging at the entrance of a single RFQ, with the subsequent acceleration of particles in the new Drift Tube Linac. The challenge of the design is associated with the necessity of simultaneous acceleration of protons and H^- ions with different beam currents, beam charges per bunch, beam emittances, and space charge depression, in a single RFQ and DTL, while injection beam energy is reduced from 750 keV to 100 keV. Acceleration of various beams in a single RFQ provides less flexibility for optimal adjustment of acceleration and focusing parameters concerning the existing LANSCE setup. The paper discusses multi-beam dynamics in the proposed injector.

FORMATION ON MULTI-BEAM STRUCTURE IN LEBT

A unique feature of the LANSCE accelerator facility is its simultaneous acceleration and delivery of various beams to multiple targets [2]. Protons with energy of 100-MeV are delivered to the Isotope Production Facility (IPF), while the 800-MeV H^- beam is distributed to four experimental areas: the Lujan Neutron Scattering Center equipped with the Proton Storage Ring (PSR), Weapons Neutron Research Facility (WNR), Proton Radiography (pRad), and Ultra-Cold Neutron facility (UCN). To reduce long-term operational risks and to realize future beam performance goals in support of the laboratory missions, we develop a novel Front End including a high-brightness Radio-Frequency Quadrupole (RFQ) based injector [1, 3, 4], see Fig. 1. The low-energy part of the novel injector includes two independent transports for the proton and H^-

beams with multiple flavors of the beams merging at the entrance of a single RFQ.

Details of the time structure of accelerated beams are given in Ref. [1]. The multi-beam structure is achieved in Low Energy Beam Transport through a combination of chopper and RF bunchers. Among all the beams, the H^- beam delivered to the WNR facility exits only as a combination of single bunches, separated by long time intervals, while other beams are trains of bunches with various pulse lengths.

Figure 2 illustrates only two modes of chopper operation: long pulse mode for the beam injected into the Proton Storage Ring, and short pulse mode used for the preparation of single bunches for WNR facility. The chopper is normally energized so that no beam gets through. An electrical pulse of length 25 ns and 290 ns for short and long bunch modes, respectively, travels along the chopper allowing the un-chopped part of the beam pulse to pass through, see Fig. 3. The minimum width of the chopper pulse is determined by the chopper's rise time, which is about 10 ns. The long bunch pulses feed the chopper at the rate of 2.8 MHz, which corresponds to one pulse every 358 ns, which is the revolution time for the Proton Storage Ring. Following the chopper, the leading and trailing edges of the beam are bent vertically, which affects the beam emittance.

Figure 4 illustrates the formation of a single WNR bunch using the short pulse mode of the chopper. The chopper cuts ~ 25 ns beam followed by beam energy modulation in the 16.77 MHz Low-Frequency Buncher. In the downstream drift space, the energy modulation is transformed into beam density compression resulting in a single WNR bunch with a substantially larger charge per bunch than that obtained by 201.25 MHz acceleration of other beams. The WNR bunch is then accommodated in the 201.25 MHz RF

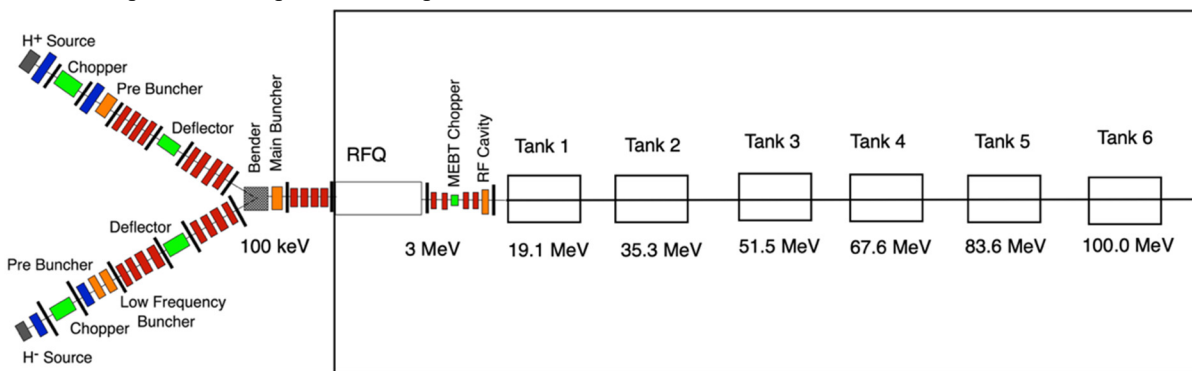


Figure 1: Layout of the proposed 100 MeV LANSCE Front End Accelerator Facility [1].

batygin@lanl.gov

BEAM OPTICS DESIGN OF A PROTOTYPE 20 KW CONDUCTION-COOLED SRF ACCELERATOR FOR MEDICAL STERILIZATION *

A. Saini[†], C. Edwards, I. Gonin, Y. Ji, T. Kroc, N. Solyak, V. Yakovlev, Fermilab, Batavia, IL, USA

Abstract

Superconducting technology has significantly advanced the capabilities of particle accelerators, facilitating higher beam-power operations for fundamental research at a comparatively lower cost. However, the conventional implementation of superconducting technology introduces complexities in the form of cryogenic plants, cryogenic distribution systems and substantial construction and operational cost. In response to these challenges, recent research efforts at Fermilab have been dedicated to the development of a cryogen-free, conduction-cooled Nb₃Sn-based superconducting technology. This paper outlines the beam optics design of a 20-kW conduction-cooled compact superconducting accelerator for medical sterilization. The paper reviews both the physics and practical constraints associated with high beam-power operation within the context of industrial applications. The focus is on providing insights into the potential of this innovative technology to overcome existing challenges and pave the way for more accessible and efficient industrial particle accelerators.

BACKGROUND

Superconducting Radio Frequency (SRF) accelerating structures provide higher accelerating fields with minimal power dissipation, making them highly energy-efficient and capable of delivering significant energy-gains. These advantages make SRF technology the preferred choice for particle acceleration in large research facilities. Despite its potential to extend the particle accelerators into emerging applications and enhance the efficiency of existing processes, SRF technology has not yet been fully adopted in the commercial sector. This is mainly due several practical challenges associated with conventional SRF accelerators, including (a) the significant initial capital investment required to establish an SRF facility, (b) comparatively a larger footprint of the overall infrastructure, (c) complexity of routine operation and maintenance associated with cumbersome systems such as cryo-plant and cryogenic distribution and (d) need for highly skilled personnel to manage and maintain the facility. To overcome these challenges, recent research and development efforts at Fermilab have been focused on developing enabling technologies to simplify and reduce the construction and operational cost of SRF particle accelerators for a variety of energy and environmental applications including but not limited to medical sterilization, treatment of potable and

wastewater, sludge, removing pollutants from stack gas-es, medical wastes and many more [1].

20 KW COMPACT SRF ACCELERATOR

A team of researchers and engineers at Fermilab has been working to develop a prototype cryogen-free, conduction cooled [2] Nb₃Sn based, 20 kW, Continuous Wave (CW), electron SRF accelerator. Note that, Nb₃Sn coated cavities significantly reduce cryogenic losses and allow for operation at higher temperature (i.e., 4. K vs 2.0 K). This, in turn, enables the replacement of complex cryogen-based cooling systems with commercially available cryocoolers, resulting in a smaller infrastructure footprint, highly reliable and simplified superconducting operation with minimal expert's involvement. Thus, this prototype SRF accelerator represents a significant milestone in establishing the feasibility of beam accelerating using conduction cooled Nb₃Sn SRF technology. A successful demonstration will set the stage for building a full-scale, high power SRF accelerator facility, aimed at providing megacurie-level capabilities as a replacement for Cobalt-60 (Co-60) irradiation facilities.

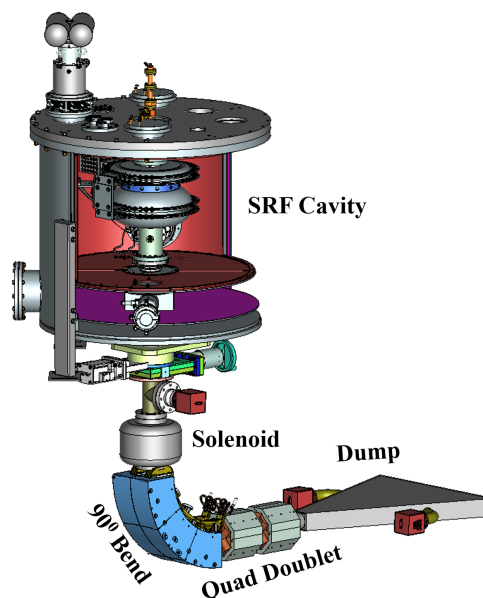


Figure 1: Render view of 20 kW prototype accelerator.

The accelerator is designed to deliver 12.5 mA electron beam current at 1.6 MeV in CW regime. Figure 1 shows rendered view of 20 kW prototype accelerator beamline. Its critical components can be organized into three major sections: (a) Integrated electron gun, (b) SRF section and (c) Beam delivery system.

* Work supported by Fermi Research Alliance, LLC under contract no. DE-AC02-07CH11359 with the DOE, USA

[†] asaini@fnal.gov

AUTOMATION OF RF TUNING FOR MEDICAL ACCELERATORS*

F. H. O'Shea[†], J. D. Cruz, A. Edelen, SLAC National Accelerator Laboratory, Menlo Park, CA, USA
J. Edelen, M. Henderson, RadiaSoft, LLC, Boulder, CO, USA

Abstract

RadiaSoft is developing machine learning methods to improve the operation and control of industrial accelerators. Because industrial systems typically suffer from a lack of instrumentation and a noisier environment, advancements in control methods are critical for optimizing their performance. In particular, our recent work has focused on the development of pulse-to-pulse feedback algorithms for use in dose optimization for FLASH radiotherapy. The PHASER (pluridirectional high-energy agile scanning electronic radiotherapy) system is of particular interest due to the need to synchronize 16 different accelerators all with their own noise characteristics. This presentation will provide an overview of the challenges associated with RF tuning for a PHASER-like system, a description of the model used to evaluate different control schema, and our initial results using conventional methods and machine learning methods.

FLASH RADIATION THERAPY

There is empirical evidence for increased tumor control probability and decreased normal tissue complication probability when ultrahigh dose rates are used to treat cancerous tumors, so-called FLASH radiation therapy [1]. An example of the FLASH effect is given in Fig. 1. Current systems used for radiation therapy typically deliver dose at the ≤ 1 Gy/min rate, while evidence for the FLASH effect typically occurs at ≥ 40 Gy/s. In either case, the expected dose is approximately 10 Gy, meaning that, for FLASH, the total treatment time is less than 250 ms, and usually much less. As such, new accelerator technology is required to deploy FLASH in the clinic [2, 3]. One such proposed system is the PHASER (pluridirectional high-energy agile scanning electronic radiotherapy) [4].

A schematic of the PHASER system is shown in Fig. 2. The PHASER uses 16 beams (as opposed to a gantry) to allow fast tracking of targets that are monitored via an integrated computed tomography (CT) scanner. The RF macropulse length will be 300 ns long. The second generation PHASER, which will treat patients directly with electrons, also plans to use pulse shaping of the photo-cathode laser to allow for intensity-modulated radiation therapy without a slow multi-leaf collimator. These new features require a new kind of fast control (well sub-second) that is able to use the CT images to help determine where to apply the planned dose [5]. Artificial intelligence is a candidate suite of solutions for everything from tracking tumor motion to controlling the dose profile.

* This work is supported by the DOE Office of Science Office of Accelerator Research Development and Production award number DE-SC0023641.

[†] foshea@slac.stanford.edu

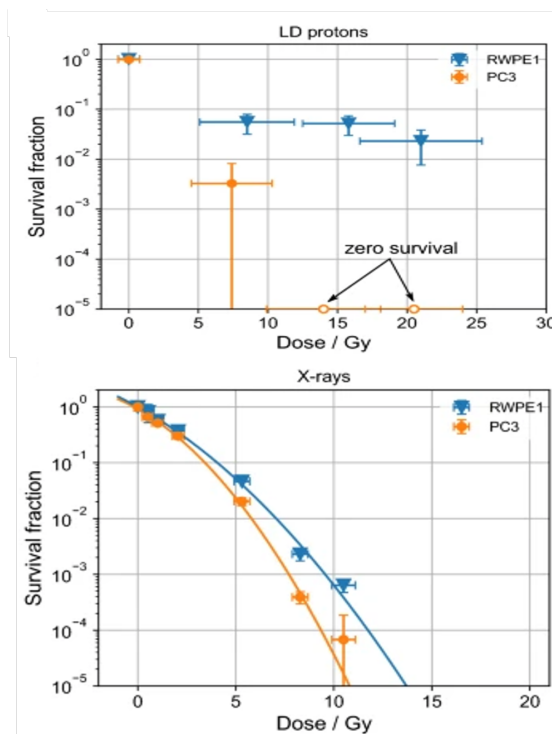


Figure 1: Survival fraction of human prostate cells after a FLASH treatment from protons (top) and a normal treatment from x-rays (bottom). Normal cells are denoted RWPE1 and cancerous cells are denoted PC3. Image adapted from [6] under the Creative Commons Attributions License [7].

Herein, we present some initial results on controlling some relevant RF system properties of the PHASER. After constructing an accessible model of power combination from multiple klystrons, we will show that the system admits solutions using both reinforcement learning and linear regression.

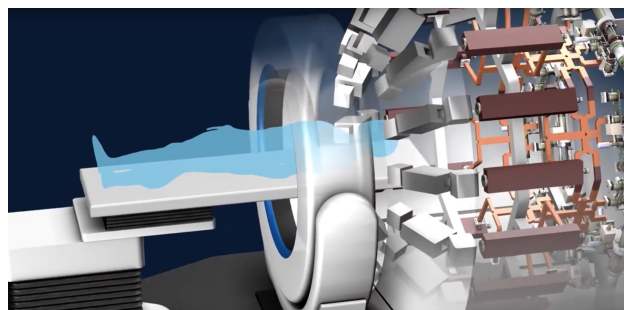


Figure 2: Conceptual design of the PHASER system showing the 16 linacs directed towards a patient phantom. The white ring that shares an isocenter with the accelerator beams is a computed tomography (CT) scanner. Image courtesy of Greg Stewart/SLAC National Accelerator Laboratory.

ALBA INJECTOR RELIABILITY IMPROVEMENT WITH AN 80 MeV LINAC BEAM

R. Muñoz Horta, D. Lanaia, F. Pérez, ALBA Synchrotron, Cerdanyola del Vallès, Spain

Abstract

The ALBA injector consists of a 110 MeV Linac, a Linac-to-Booster Transfer Line (LTB) and a full energy Booster that further accelerates the electrons up to 3 GeV. The Linac consists of two pre-bunchers (PB1 at 500 MHz and PB2 at 3 GHz) a buncher and two accelerating structures (AS1 and AS2). The whole system is powered by two pulsed 37 MW klystrons at 3 GHz. To overcome an eventual klystron failure the injector has been adapted to keep operative at lower Linac beam energy. In 2014 the injection into the Booster was optimized for a Linac beam of 67 MeV, which is the energy achieved using only one klystron. However, the procedure of switching the injector from a Linac beam of 110 MeV to a 67 MeV one is not straightforward and it requires to be periodically updated. After a recent waveguide modification the RF-power sent to the first accelerating structure is equally distributed between both accelerating structures. As a result, a Linac beam of 80 MeV is achieved using only one klystron. The injection into the Booster in this mode is expected to be efficient and stable enough to be set as the nominal Linac operation mode. Furthermore, setting the nominal Linac beam energy at 80 MeV the injector operation will be assured by the hot-spare klystron in case of klystron failure

INJECTOR VERSALITY

An overview of the whole ALBA injector [1] is shown in Fig. 1. The Linac is placed in a separate bunker whereas the Booster is placed in the same tunnel than the Storage Ring. The Booster lattice has a four-fold symmetry with a circumference of 249.6 m. On-axis injection from the Linac to the Booster is achieved by using a single septum and a single kicker.

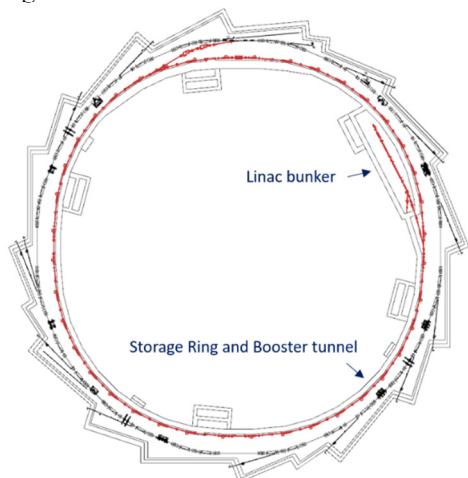


Figure 1: Schematics of the ALBA Synchrotron. All the injector elements are marked in red.

Since 2012 the nominal operation mode of the Linac is a 108.5 MeV beam consisting of 40 bunches with a total charge of 0.2 nC and 0.05 nC/bunch. In this mode klystron 1 (KA1) feeds the 3 GHz bunching cavities (PB2 and BU) and the first Accelerating Section (AS1) whereas klystron 2 (KA2) feeds exclusively AS2.

Injector operation versatility was first improved in 2014 by installing an S-band switching system in the Linac waveguide that allows using KA2 instead of KA1 in case of KA1 failure [2]. The schematics of the Linac waveguide with the implemented S-band switching system is shown in Fig. 2.

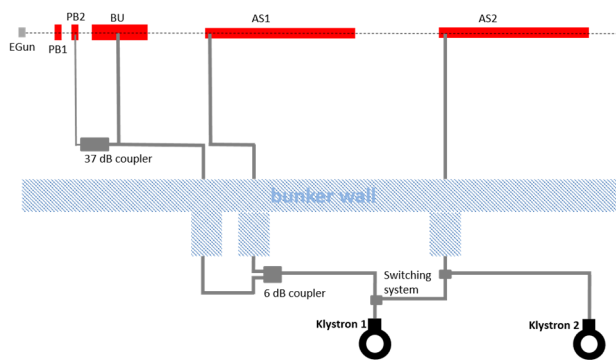


Figure 2: Schematic of the Linac RF-cavities and its waveguide system, including the S-band switching system installed in 2014.

Powering only the bunching part and AS1 with KA1 the Linac delivers a 67 MeV whereas using KA2 the beam achieved is limited to 60 MeV due to arcs in the waveguide. The power distribution of the nominal operation mode at 108.5 MeV and of the two low energy modes using only one klystron are shown in Table 1.

Table 1: RF-Power Distribution of the Current Operation Modes of the ALBA Linac

Mode	Energy [MW]	KA1 [MW]	KA2 [MW]	BU [MW]	AS1 [MW]	AS2 [MW]
Nominal	108.5	30	13	5.8	19	11.5
KA1 only	67	26		5.2	17	
KA2 only	60		22	4.5	16.2	

The whole injector (LTB, pulsed elements and Booster) was then adapted to make possible the injection (and further acceleration to 3GeV) of the low energy beam delivered by the Linac using only one klystron. Beam capture into the Booster at low beam energies was achieved despite difficulties due to non-linear effects in the Booster magnetic fields [3]. The magnetic field distortions are produced by eddy currents induced at the bending magnet vacuum chambers. These effects become more significant at lower

EXTRACTING CRITICAL BEAMLINE ELEMENT MISALIGNMENTS FROM DATA USING A BEAM SIMULATION MODEL*

A. Ravichandran[†], B. Mustapha, Argonne National Laboratory, Lemont, IL, USA

Abstract

Successful implementation of AI/ML models for online tuning of accelerators highlights the need for accurate simulation of beamline elements. Deployment of such models requires the inclusion of realistic element misalignments during the simulation process. This paper presents an original method to determine misalignments across entire beamlines and apply them to the previously developed TRACK simulation model. Validation has been performed using experiment data in this study for a newly commissioned section of ATLAS called the Argonne Material Irradiation Station (AMIS) and an existing straight lattice known as the PII-BOOSTER. A preliminary study for the AMIS line shows the average difference in beam transmission between experiment and simulation for 28 tuning cases has dropped from ~46% without steering to ~16% after applying steering and further down to ~6% after accounting for 4 quadrupole misalignments in the simulation. Given these values and the well-established accuracy of the TRACK model, major deviations in element positions could be narrowed down enabling engineers to perform the necessary alignment corrections, and possibly eliminating the need for some steering elements. Predictability of the TRACK code has been shown to significantly improve after applying realistic alignment and steering corrections.

INTRODUCTION

Simulation of beamline elements is vital in the design of new lattices and making modifications to existing structures. However, even the most advanced models fail to accurately replicate experimentally measured data due to misalignment in lattice elements. Moreover, codes such as Methodical Accelerator Design software (MAD-X) that employ transfer matrices to simulate FODO lattices currently do not have the capability to account for such miscellaneous errors. The TRACK beam dynamics code developed at Argonne National Lab employs the particle tracking approach in which equations of motion are solved using Runge-Kutta based solvers. This approach is more amenable to account for misalignments. A recent update to the TRACK code has incorporated a separate misalignment function that can be setup along with the other elements when building up the lattice for simulation. Both rotational and translational misalignments in three dimensions can be accounted for via this function. Although currently used only for quadrupole misalignments, the tool supports simulating misalignments for most other types of elements.

Misalignment in accelerator components may lead to emittance growth, beam losses and breakup of the beam.

* Work supported by the U.S. Department of Energy, Office of Science-Basic Energy Sciences, under Contract No. DE-AC02-06CH11357.

[†] aravichandran@anl.gov

Although misalignment in beam position monitors do not deflect the beam, they significantly compromise the effectiveness of any optimization that is implemented to tune the device. Ganesh Tiwari et al., [1] report on the effects of transverse spatial misalignment on the performance and stability of X-ray free electron oscillators. Given the current trend in development of smaller accelerators, Silva et al., [2] present a statistical method to determine the tolerances in misalignment of a set of lenses for such small machines. As part of this method, particle losses as a function of alignment accuracy of optical elements in a lattice is found. Marco Venturini et al., [3] present a method to model particle ray tracing through misaligned elements by sandwiching the transfer-map for aligned elements between two transformations, one applied at the entrance and one at the exit. Beam-based alignment methods account for misalignments without evaluating the values associated with each element of a lattice. The work presented in this research in contrast, offers an attractive alternative approach using the TRACK code to determine actual values of misalignment associated with quadrupoles. These values could then be used both in simulations to correct for error in predictions and during the design processes of new lattices by making suitable modifications. Two methods are proposed to this extent.

TRANSMISSION BASED MISALIGNMENT

This section provides a procedure to determine misalignment in quad elements along a single straight lattice solely employing experimentally measured values of transmission across the lattice. A straight lattice section known as the PII-BOOSTER line at the ATLAS LINAC was used to this extent (Fig. 1).

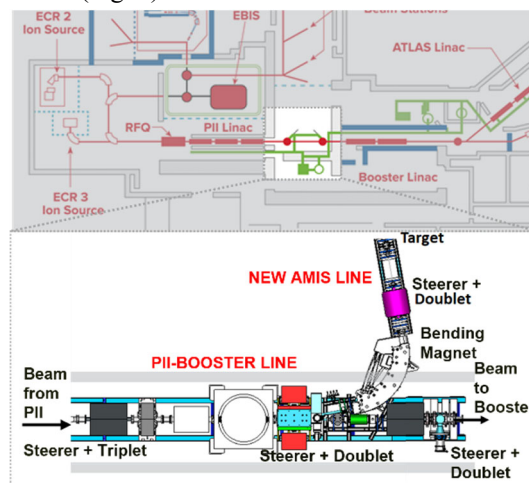


Figure 1: PII-BOOSTER lattice.

APPLICATION OF SURVEY AND ALIGNMENT TECHNIQUES FOR BEAMLINE INSTALLATION*

A. F. Grabenhofer[†], Argonne National Laboratory, Lemont, IL, U.S.A.

Abstract

The installation and alignment of new beamlines and beamline components is necessary at any accelerator facility. The equipment and methods used to perform these precision driven tasks must be accurate, reliable, and above all, easily repeatable. Using coordinate measuring machines (CMM), laser trackers, combined with Spatial Analyzer (SA), Autodesk Inventor, and other custom tools, it is possible to rapidly and accurately take an idea from model to reality, as shown through the construction of the ATLAS Multi-User beamline.

OVERVIEW

Accelerator beamline construction, with some variation in tools, follows a relatively simple process: design and installation. I will focus on the installation and alignment of the beamline devices. This process starts with design and site preparation, direct measurements, fiducialization of parts, and finally installation and alignment.

DESIGN AND SITE PREPARATION

Design preparation is simply the analysis of the final design, allowing the design to go from a CAD model into the real-world dimensions and values. Often this is done by using the dimensions already known: length, width, height, diameter, etc. With this information, I start looking at the environment where the construction will take place. Correlation of the design and environment is important, as many devices may require permanent fixtures. The 80 degree bending magnets for the ATLAS Multi-User Upgrade (AMUU) are 6600 lb magnets that require steel stands anchored into concrete. Placement of these stands is vital as once they are installed, they cannot be repositioned without great effort (new concrete, etc.).

In addition to the stands, the magnets themselves define the path for the new beamline. While they have some adjustment with the stands, they need to be as close as possible to perfect prior to the final alignment (anything more than a 1-inch offset could result in a failed installation). From the CAD model of the installation, we know where the bending magnets should be placed relative to existing beamline devices (also important for achromatic¹ beam delivery). For correlating the CAD model to the environment, we need monuments.

*Work supported by U.S. Department of Energy Office of Science, Office of Nuclear Physics, under contract number DE-AC02-06CH11357 and used resources of ANL's ATLAS Facility, which is DOE Office of Science User Facility

[†]agrabenhofer@anl.gov

¹Achromatic beam delivery means that the beam has the same phase-space profile entering and exiting a section of beamline

Monuments

Monuments are fixed reference points in the environment, usually target holders for laser tracker targets or probe tips, but can be anything *as long as they are globally fixed* (they cannot be moved without great effort). Monuments serve two purposes: to correlate the CAD model and the environment and to allow the precision measuring devices to locate themselves in the environment. In the case where no monuments exist, monuments may be chosen or placed after some reference data is taken.

DIRECT MEASUREMENTS

Direct measurements are just that: data taken directly with the measurement device. In the case for the AMUU, I use both laser tracker (Leica AT960) and portable CMM (Hexagon Absolute ARM 85 shown in Fig. 1) to perform all the measuring both the environment and installed devices.



Figure 1: Leica AT960 (left) and Hexagon Absolute ARM 85 (right).

For the AMUU, I started by taking direct measurements of the currently installed beamline which the new beamline was to be added to. This served as my initial reference data and allowed me to add *monuments* (small magnetic holders) to the existing structure to serve as my device locating points as well as reference points for any future changes. I was able to correlate the data between the existing beamline and the CAD model (which included the existing section of beamline as well as the new sections) in SA (Fig. 2).

AN OVERVIEW OF MICROPHONICS IN CEBAF AND CURRENT MODERATION TECHNIQUES*

P. Owen[†], T. Powers, Jefferson Lab, Newport News, USA

Abstract

Superconducting RF (SRF) structures are susceptible to frequency detuning from external vibrations and modal mechanical resonances in the structure. These small disturbances, known as microphonics, require additional RF power in CW accelerating structures since the frequency is constantly shifting. In the Jefferson Lab CEBAF accelerator, time and frequency data of this frequency shift have been recorded for many years, allowing a retrospective analysis of different microphonics-mitigation techniques. Some of these techniques are specific to the design of each CEBAF cryomodule, for example implementing BNNT damping material on the cavity string. Other techniques are universal such as affixing vacuum lines and reinforcing waveguide structures.

MICROPHONICS

In a resonant structure such as an SRF cavity, the resonant frequency is a function of the structure's geometry. Any vibration will deform the geometry slightly and the corresponding resonant frequency.

Superconducting cavities have a very narrow bandwidth (10s–100s of Hz). For on crest beam, the required RF power is given by the following:

$$P = \frac{(\beta + 1)L}{4\beta Q_L(r/Q)} \left\{ (E + I_0 Q_L(r/Q))^2 + \left(2Q_L \frac{\delta f}{f_0} E \right)^2 \right\}, \quad (1)$$

where $\beta \cong Q_0/Q_1$, E is the accelerating gradient in V/m, I_0 is the beam current in amperes, f_0 is the frequency of the RF drive, (r/Q) is the normalized shunt impedance of the cavity in Ω/m , L is electrical length of the cavity in meters, and δf is the difference between the frequency of the RF source and that of the cavity.

Every structure or cryomodule design will have different natural frequencies for mechanical resonance. It is up to the designer of a cryomodule to predict these frequencies and ensure they do not align with frequencies commonly found in the accelerator tunnel environment which would excite the natural resonance. The CEBAF C100 cryomodule resonances have been well studied through simulation and modal testing at various stages of assembly [1]. The cavity string is suspended in a space frame with nitronic rods. It is further constrained by the waveguides, tuners, and cryogenic beam pipe transitions to the insulating vacuum vessel.

There are four primary resonant modes which affect the cavity geometry. The lowest frequency mode, occurring at

10 Hz, occurs as the entire cavity string moves along the beam line direction. The next significant mode, 20 Hz, occurs as one half of the cavity string moves 180° out of phase with the other half. The third significant mode occurs at 40 Hz and are the resonances of individual cavity, which can be transferred to neighboring cavities as there are no bellows in between cavities. The fourth mode is a 90 Hz mode where the tuner stack tends to oscillate in a horizontal plane.

All these frequencies are approximate and vary per cavity and per cryomodule. Furthermore, these modes can interact with each other. For example, when a tuner motor operates it will induce a 90 Hz oscillation in the corresponding cavity. If this happens to be in phase with a 10 Hz string mode, the 10 Hz mode can be amplified and cause a cavity trip. For some cavities this is the typical form of a microphonics trip [2].

When peak microphonics exceed the available RF power and control system phase margin, the cavity will go into a fault state which interrupts beam operations. As microphonics in C100 cryomodules have adversely affected beamtime at CEBAF, much effort has been made to reduce the sources or impact of microphonic vibration. There are many types of cryomodule in the accelerator, however the C100 cryomodule design is particularly susceptible to vibration [1].

SOURCES AND MITIGATIONS

Mechanical resonances of the structures can be excited by both transient and continuously occurring sources and resonate within the cryomodule structure with minimal damping. Additionally, one can get driven vibrations that are excited by external sources. Some of the more universal sources are discussed below, along with current mitigation techniques used in CEBAF.

Waveguides

Waveguides carry RF power from klystrons or amplifiers in above-ground service building to a cavity in the underground accelerator tunnel (Fig. 1). These are long rigid structures, approximately 25 feet in length. Transfer function measurements were conducted on the waveguide with an instrumented hammer and accelerometer to excite the structure and measure the modal transfer function.

The tests showed significant resonances at 10, 24, 44, and 78 Hz. A series of Unistrut braces were installed to stiffen the waveguides combined with Sorbothane® pads to dampen the motion [3]. The reinforcing structures successfully damped the resonant modes of waveguides as is shown in Fig. 2. This method of dampening is relatively easy to test for and implement.

* Work supported by the U.S. Department of Energy, Office of Science, Office of Nuclear Physics under contract DE-AC05-06OR23177.

[†] powen@jlab.org

PHOTOCATHODE DRIVE LASER UPGRADE FOR THE ADVANCED PHOTON SOURCE LINAC*

J. Dooling[†], W. Berg, A. Lumpkin, P. Piot, Y. Sun, K. P. Wootton, A. Zholents
Argonne National Laboratory, Lemont, IL, USA

Abstract

We discuss the need for a new photo-cathode (PC) gun drive laser for the Advanced Photon Source Upgrade (APS-U) linac. As context, the characteristics associated with the current system are presented. The proposed new drive laser is based on a Ytterbium (Yb) gain medium and is capable of multi-kHz operation (although presently only 30 Hz is needed for injection into the particle accumulator ring in support of APS-U). The pulse charge specification is 1 nC.

INTRODUCTION

In a photoinjector system the main components are the rf gun, the photocathode, and the drive laser matched in wavelength and pulse energy to generate sufficient charge for the application. With our present Cu photocathode quantum efficiency, the UV harmonic near 260 nm is needed to obtain the micropulse-charge target in support of the Advanced Photon Source Upgrade (APS-U) operations and linac experiments. A Ytterbium-based photocathode gun drive laser is proposed for the linac to replace the existing antiquated Nd:Glass laser. The proposed laser will readily operate at 30 Hz providing 0.3 mJ of 257-nm UV radiation per pulse yielding 1 nC from our Cu cathode, s-band gun in support of user operations. In addition, the laser allows generation of lower-charge, low-emittance electron beams for high-brightness experiments in the APS Linac Extension Area. An advantage of updating the PC Gun drive-laser is that the gun beamline includes a 3-meter-long s-band accelerating structure; this provides an additional 35-40 MeV of energy at the linac output over what is presently available from either of the two thermionic-cathode guns. Higher linac output energy is essential for high-charge operation of the new storage-ring. We outline the laser physics requirements for our LCLS-I-style PC gun and summarize the expected beam performance.

CASE FOR A NEW PC GUN DRIVE LASER

Our present Nd:Glass CPA drive laser does not have sufficient energy to generate the 1-nC micropulse charge at 30 Hz specified for operations support, and it is no longer supported by the vendor. Our focus is on the Pharos laser systems built by Light Conversion. Light Conversion specializes in Ytterbium (Yb)-based femtosecond laser sources for industrial, medical, and scientific applications.

Advantages

- Modern laser system with controls and diagnostics (turn key)—less effort required to maintain the laser
- Yb-based fiber lasers are competitively priced, and offer better stability and reliability than conventional Titanium-Sapphire systems.
- SLAC National Laboratory is moving to these systems and away from Ti:Sapphire-based lasers
- Backup source for operations
- Low-emittance beams for high-brightness experiments (e.g., Advance acceleration concepts, Compton backscattering, Microbunching)
- Improved timing stabilization, reduced jitter
- Calibration of fast diagnostics (e.g., impulse response function for fast detector deconvolution)
- Yb-based system has a broader gain-bandwidth allowing for shorter pulses than the present Nd-based system. Yb mode-locked pulses can be as short as 50 fs.
- The Yb-doped medium lases between 1030 and 1070 nm with an upper excited state in the 970-980 nm range. This allows for efficient diode laser pumping. Nd also has this advantage, but the difference between the Nd upper excited state, 808 nm and the lasing level, 1053 nm, is greater leading to a larger quantum defect which appears as lost as heat in the laser medium.
- Operating with a fundamental wavelength at 1 micron is inherently safer than 700-800 nm (Ti:Sapph).

Disadvantages

- Quenching where the excited atoms emit spontaneously rather than via cavity-defined stimulated emission.

EXISTING ND:GLASS CPA SYSTEM

Oscillator and Amplifier

The existing PC gun laser is based on a chirped-pulsed amplifier (CPA) design employing an oscillator seed followed by a regenerative amplifier (regen), utilizing Nd:Glass as the gain medium [1, 2]. In 2010, the amplifier flash-lamps were replaced with high-efficiency, high-power 805-nm laser diodes, significantly reducing thermal loading on the phosphate-glass laser rods. The 1.8-m folded-cavity regen is shown schematically in Fig. 1. This system as well as the oscillator (not shown) will be replaced.

Though diode pumping greatly reduced thermal effects in the 3-mm diam. Nd:Glass laser rods, operation at a sustained 30-Hz rate has been problematic. Figure 2 shows the effect on energy per pulse and spot size as the laser rep rate is varied from 2 to 30 Hz. The APS-U linac operates in a 30-Hz burst mode and injects into the particle accumulator

* Work supported by the U.S. D.O.E., Office of Science, Office of Basic Energy Sciences, under contract number DE-AC02-06CH11357.

[†] dooling@anl.gov

RF TUNING ANALYSIS OF A 750 MHz CARBON RFQ FOR MEDICAL APPLICATIONS*

G. Moreno[†], D. Gavela, M. Lopez, P. Calvo,
A. Rodríguez, J. Etxebarria, C. Oliver, J. M. Pérez, CIEMAT, Madrid, Spain
J. Giner, ICMUV, Paterna, Spain
J. M. Carmona, M. Alvarado, X. Arrillaga, AVS, Elgoibar, Spain
U. Etxebeste, Egile Mechanics S.L., Gipuzkoa, Spain
A. Lombardi, A. Grudiev, CERN, Geneva, Switzerland

Abstract

This work is part of the development study of a linac injector for hadron therapy with carbon ion beams. The initial cavities of the future injector consist of two 750 MHz Radio Frequency Quadrupoles (RFQ), which are based on the compact CERN High-Frequency RFQ. These RFQs are designed to accelerate the ions from 15 KeV/u to 5 MeV/u. Each RFQ, with a length of more of 2 meters, comprises four individual modules and 32 tuners, 8 per module.

Certain design choices, manufacturing imperfections, and misalignments lead to local variations in the frequency and field distribution within the RFQs. The tuning procedure corrects these perturbations in the TE210 operating mode using a bead pull system and movable tuners.

The aim of this article is to determine the maximum field correction achieved through this tuning without affecting the beam dynamics. For this purpose, a set of electromagnetic deviations that introduces significant dipole components to the cavity is simulated, using CST Studio. Using the tuning algorithm, this EM deviation is corrected in a realistic way.

INTRODUCTION

CIEMAT, in the framework of the IKERTU project, leads a national collaboration that includes both industrial companies and research centers. This project aims to develop an optimized linear carbon ion injector, named LINAC6+, for use in hadron therapy. Carbon ions have proven to be more precise and effective than conventional radiotherapy in treating certain types of cancer. However, the technology of the accelerators required for this therapy needs further development to optimize their performance and efficiency [1]. For this reason, the project focuses on the technological advancement of LINAC6+, which could be integrated into the initial phase of a synchrotron or a complete linac.

The study aims at enhancing efficiency and compactness while maintaining a careful beam dynamics design. The baseline linac layout involves an EBIS ion source, 750 MHz RFQ and IH-DTL cavities, capable of providing C6+ ion beams up to 10 MeV/u with currents of 190 μ A and pulses of 5-10 μ s at repetition rates of 200-400 Hz.

Two RFQs have been designed at CERN for this purpose [2], adapted from the compact design of the proton HF-RFQ [3], with an special trapezoidal vane modulation that enhances acceleration efficiency. Table 1 lists the main specifications of the first RFQ.

Table 1: Main Specifications of the First RFQ [4]

Parameter	Value
Frequency	749.48 MHz
Length L	235 cm
Intervane Voltage V_0	50 kV
Surface Power Loss P_0	244 kW
External Quality Factor Q_{ext}	5000
Coupling Strength	1.35
Number of Tuners	32
Number of Couplers	4
Number of Vacuum Ports	12

Certain manufacturing imperfections, and misalignments, both in the areas of the apertures and in the more external regions, lead to variations in the capacitance and inductance of the cavity. These changes will result in a shift in the cutoff frequency f_{co} , and consequently, in the voltage distribution as follows [4]:

$$\frac{\delta V}{V} = \pi^2 \left(\frac{L}{\lambda}\right)^2 \frac{\delta f_{co}}{f_{co}} = -\frac{\pi^2}{2} \left(\frac{L}{\lambda}\right)^2 \left(\frac{\delta C}{C} + \frac{\delta L}{L}\right) \quad (1)$$

This variation in voltage will also be reflected in the magnetic fields of each quadrant. This can be quantified by the following three components: a quadrupole component Q and two dipole components D_S and D_T , defined as:

$$Q = \frac{B_1 - B_2 + B_3 - B_4}{4}, D_S = \frac{B_1 - B_3}{2}, D_T = \frac{B_2 - B_4}{2}$$

The appropriate sign must be assigned to account for the alternating orientation of the TE210 quadrupole mode field in the four quadrants B_i . In the absence of any errors, the dipole components D_S and D_T would be zero, and the quadrupole component Q would correspond to the correct magnetic field in each quadrant.

In the case of misalignment, the tuning process involves correcting the mixing of resonant dipole fields by adjusting

* Work supported by local Basque government through IKERTU-II project, ZE-2021/00050

[†] gabriela.moreno@ciemat.es

STUDY OF MANUFACTURING ERRORS IN 750 MHz RFQ USING ELECTROMAGNETIC SIMULATIONS*

G. Moreno Fernández-Baíllo[†], D. Gavela Pérez, P. Calvo Portela, M. León López, A. Rodríguez Páramo, J. Etxebarria, C. Oliver Amorós, J. M. Pérez Morales, CIEMAT, Madrid, Spain
 J. Giner Navarro, ICMUV, Paterna, Spain
 J. M. Carmona, M. Alvarado Martín, X. Arrillaga, AVS, Elgoibar, Spain
 U. Etxebeste Rodríguez, Egile Mechanics S.L., Gipuzkoa, Spain
 A. Lombardi, A. Grudiev, CERN, Geneva, Switzerland

Abstract

As an initial part of a future linac for hadron therapy, two 750 MHz Radio Frequency Quadrupoles (RFQs) have been preliminarily designed by CERN, based on the compact HF-RFQ model. These RFQs aim to accelerate carbon ions from 15 KeV/u to 5 MeV/u. Each RFQ is composed of four individual modules.

Manufacturing imperfections and misalignments can result in local variations in the frequency and electromagnetic field distribution within the RFQs. In this study, we focus on analyzing the electromagnetic sensitivity to possible modifications in the structure of a single RFQ module. Additionally, we evaluate how the combination of these irregularities can generate significant dipole errors, even when they remain within the specified dimensional tolerances. For this purpose, electromagnetic simulations are conducted using CST Studio.

INTRODUCTION

CIEMAT is working in the design of a carbon ion linear accelerator, the LINAC6+, for medical applications in hadron therapy. This accelerator, still under development, aims to provide a more precise and effective treatment against cancer cells, with a better energy modulation than current synchrotrons [1]. The initial part of the linac injector includes two 750 MHz RFQs, to accelerate carbon ions C^{6+} up to 5 MeV/u, based on a compact design of the proton CERN HF-RFQ [2]. The design and manufacturing of this kind of RF structures is currently in progress in the framework of Spanish innovation projects withing Spanish industry (IKERTU and CPP 03/2023 project).

This cavity, operating in the resonant TE210 mode, consists of four vanes that act as alternating voltage electrodes RF period (Fig. 1). Each pair of adjacent electrodes has an opposite polarization, with an absolute value of $V_0 \cos(\omega_0 t)$.

There are two main features of the RFQ that will enable a significant breakthrough in the field of particle accelerator cavities. On the one hand, the reduction in cavity length by minimizing the adiabatic bunching section. Negatively, this characteristic results in increased transmission loss, similar to the proton HF-RFQ [2]. On the other hand, the introduc-

tion of a trapezoidal vane modulation to improve acceleration efficiency [3], [4]. In Table 1 the specifications of the RFQ are shown:

Table 1: Summary of the RFQ specifications. The reduction in values due to the use of trapezoidal vanes compared to the standard vanes is shown in parentheses [3], [4].

Parameter	Value
Frequency	749.48 MHz
Vane Length	4.6 m (-20%)
Module Length	~ 580 mm
RF Peak Power	480 kW (-20%)
Input Beam Current	0.19 mA
Minimum Aperture	0.67 mm
Transmission	50%
Maxime Surface Field	51 MV/m

RFQ cavities can be considered as a transmission line model due to the spatial separation of the electric and magnetic fields [5]. The quadrants Q_1 , Q_2 , Q_3 , and Q_4 (see Fig. 1) can be replaced by equivalent inductance-capacitance circuits in parallel, where C_i and L_i are the capacitance and inductance per unit length of each quadrant Q_i . In the case of perfect RFQs, the capacitive and inductive impedances are constant and equal to each other. However, if the cavity experiences displacements between vanes or in the external structure, the values C_i and L_i are affected by perturbations.

Modifications in capacitance and inductance create a mix of modes within the cavity, altering the electromagnetic fields and creating dipole components. In the case of voltage, it will change $U = U_0 = (V_0, 0, 0)$ to a displacement equal to $U = U_0 + \delta U = (V_0, 0, 0) + (\delta U_Q, \delta U_S, \delta U_T)$ [6]. The values are defined in the basis $U = |U_Q, U_S, U_T|$, which is a linear combination of the inter-electrode voltages present in each quadrant (A_i) [7]:

$$U_Q = \frac{A_1 - A_2 + A_3 - A_4}{4}$$

$$U_S = \frac{A_1 - A_3}{2}$$

$$U_T = \frac{A_2 - A_4}{2}$$

assigning the appropriate sign to account for the alternating orientation of the TE210 quadrupole mode field in the four quadrants.

* Work supported by local Basque government through IKERTU-II project, ZE-2021/00050, and Spanish CDTI CPP 03/2023 project.

[†] gabriela.moreno@ciemat.es

DESIGN OF BPMs FOR A 750 MHz HADRONTHERAPY LINAC

A. Rodríguez[†], P. Calvo, J. Etxebarria, G. Moreno, C. Oliver, M. León, D. Gavela,
J. M. Perez, CIEMAT, Madrid, Spain
J. M. Carmona, A. Tato, AVS, Elgoibar, Spain

Abstract

This work presents the design of Beam Position Monitors for a 750 MHz Linac for hadrontherapy studies.

BPMs will be installed in different sections of the Linac, operating at different energies, from the RFQ exit at 5 MeV/u to the end of the line after IH cavities at 10 MeV/u. The BPMs will allow measurement of the beam position, phase and time of flight (tof) measurements. Therefore, they are fundamental for commissioning and operation of the prototype hadrontherapy Linac.

In the analysis we compare the expected signal from stripline and button BPMs using analytical and CST models, studying the BPMs dimensions and response at different energies, and BPMs sensitivity for position, phase and tof measurements.

INTRODUCTION

The LINAC6+ is a project currently under development, with the goal of performing radiobiology studies for hadrontherapy using a Carbon 6+ beam. The Beam Position Monitors (BPMs) are crucial diagnostics both for the accelerator commissioning and during operation. The BPMs will be installed at different Linac sections after the RFQ, giving information about the beam position and phase, and allowing energy measurements through time of flight.

The LINAC6C+ will be composed of an ion source and LEBT up to 15 keV/u, a 750 MHz RFQ up to 5 MeV/u [1] and IH cavities up to 10 MeV/u [2]. The Linac will operate with beam pulse currents of 190 μ A, with pulse durations of 5-10 μ s at repetition rates of 200-400 Hz [3]. In Table 1 the expected BPM operation parameters are described.

For the design of the BPMs we have first studied the expected signal using analytical formulae, and then performed electromagnetic simulations using CST. The analysis allows comparison of stripline and button BPM, characterizing the expected signal for the definition of requirements for the amplification electronics.

Table 1: Main Operational Parameters for the BPMs

Parameter	Value
RF Frequency	750 MHz
Beam Energy	5-10 MeV/u
Beam Pulse Current	190 μ A
Beam Pulse Duration	5-10 μ s
Repetition Rate	200-400 Hz

* Work supported by CPP 03/2023

[†] angel.rodriguez@ciemat.es.

IMAGE CURRENT

When the beam passes through a Linac section an image (or wall) current is induced in its surrounding conducting elements. If electrodes are installed, they pick-up the signal, and with a configuration of four electrodes the beam position can be measured.

For the estimation of the BPMs signal first the image signal at the electrode location is estimated [4]:

$$I_{image}(\omega) = -\frac{I_{bunch}(\omega)}{2\pi} \cdot s(\omega) \quad (1)$$

$$s(\omega) = \alpha \cdot \frac{I_0(gR)}{I_0(gR)} + 2 \sum_{n=1}^{\infty} \frac{1}{n} \frac{I_n(gR)}{I_n(gR)} \cdot [\sin(n(\alpha/2 - \varphi)) - \sin(n(\alpha/2 + \varphi))] \quad (2)$$

The image current depends on the bunch current in the frequency domain $I_{bunch}(\omega)$, the position of the beam ($r; \varphi$), the beam energy ($\gamma\beta$) the beampipe radius (R) and aperture (α). The aperture α for a stripline BPM is its width angle, and for a button bpm of radius r_b is $\alpha = 2\pi \cdot r_b/4R$. $I_n(x)$ are the modified Bessel function of order n and $g = \frac{\omega}{\beta\gamma c}$ the dependence on energy.

For the LINAC6+ BPMs the expected pulse current is 190 μ A with a bunched structure of $\sigma \sim 20$ ps at 750 MHz. Solving Eq. (1) and applying Fourier transform, the results in time domain are obtained. In Figure 1 we show the bunch current and its image current. For low beta beams the signal is distorted, since the field is not transversal, and the observed signal duration increases from $\sigma \sim 20$ ps on the beam to ~ 150 ps on the image signal.

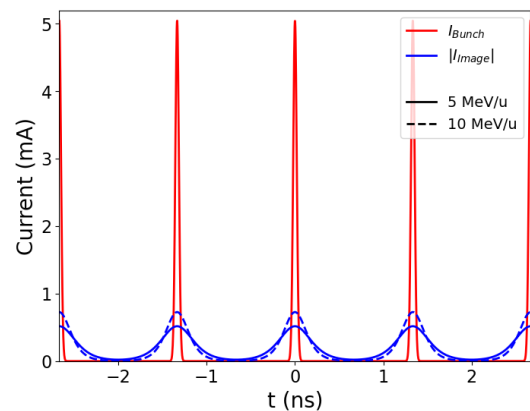


Figure 1: Bunch current and image current for a beam with pulses of 190 μ A at 750 MHz and 20 ps bunches.

OVERVIEW OF ACCELERATING STRUCTURE RESEARCH ACTIVITIES AT IHEP*

J. R. Zhang[†], C. Meng, H. Shi, N. Gan, O. Xiao, X. Li, X. He,
X. Ma, J. Liu, D. He, Z. Zhou, J. Li, Y. Li, J. Gao
IHEP, Beijing, China

Abstract

In electron linear accelerators, the improvement of the acceleration gradient of the acceleration structure has been a continuous research topic for scientists, which can reduce the construction cost of the entire accelerator by increasing the accelerating gradient. For the CEPC and HEPS projects at IHEP, S-band 3 meters long and C-band 1.8 meters long accelerating structure has been developed. The operating frequencies are 2860 MHz, 2998.8 MHz and 5720MHz respectively. CEPC linac is 30 GeV with S & C-band structures in the TDR phase. The high-power test gradient of S-band accelerating structure reach the 33MV/m. The C-band structures also designed and waiting for high power test. HEPS is 500 MeV linac injector and already conditioning for one year. The maximum gradient achieved with the beam during commissioning was approximately 26 MV/m with a beam current of 7 nC. During actual operation, it has been functioning at around 20 MV/m. The electron beam has remained stable up to the present time.

INTRODUCTION

In an electron linear accelerator, the RF field is used to accelerate the electron beam. The accelerating structure is a crucial component that converts the RF field energy generated by the power source into the beam energy. High-gradient accelerating structures can provide higher acceleration levels in a shorter distance, thereby enhancing the efficiency and performance of the accelerator. In other words, they can achieve the required acceleration energy within a shorter length. That will not only save space but also reduce construction and operating costs.

The Circular Electron Positron Collider (CEPC) is a large circular electron-positron collider project being developed by the Institute of High Energy Physics (IHEP) in China. The injector linac of the CEPC is a 30 GeV normal-conducting (NC) linear accelerator, which includes a linear section and a 1.1 GeV damping ring (DR) [1]. In the design of the linac, an S-band structure is used before the DR, and a C-band structure is used after the DR to increase the accelerating gradient and reduce costs. Additionally, we will focus on and develop more advanced accelerator technologies to improve the performance of the linac and reduce construction costs.

High Energy Photon Source (HEPS) linear accelerator operates on a 500 MeV S-band system. With the construction phase now successfully concluded, the linac can deliver a maximum stable beam current of 7 nC to the booster.

* Work supported by NKPSTRD & HEPS, a major national science and technology infrastructure in China.

[†] zhangjr@ihep.ac.cn

DESIGN OF RF SYSTEM AND DEVELOPMENT OF ACCELERATING STRUCTURES

During the Technical Design Report (TDR) phase for the CEPC, adjustments were made to the injector linac to achieve a better balance with the booster. Compared to the CT coil dipole magnet, the key advantages of the iron-core dipole magnet are low cost and low power loss. In order to control the production cost and power loss, the injection linac energy of the booster is increased from 10 GeV to 30 GeV [2,3]. Even considering the increase of linac cost, the overall price of the injection including linac and booster is still decreasing.

The 30 GeV linac provides electron and positron beams for the booster, with 1.1 GeV damping ring for the positron beam. The linac parameters shows in Table 1. Figure 1 shows the layout of the CEPC linac. The total length of the linac from start to end is about 1.6 km. Thermal cathode electron gun is used to produces 10 nC bunch charge. The energy on the positron target is 4 GeV. Conventional scheme (fixed target with FLUX) is selected for the positron source.

Table 1: CEPC Linac Parameters

Parameter	Symbol	Unit	Baseline
Energy	E_{e^-}/E_{e^+}	GeV	30
Repetition rate	f_{rep}	Hz	100
Bunch charge	-	nC	1.5 (3)
Energy spread	σ_E	-	1.5×10^{-3}
Emittance	ϵ_r	nm	6.5

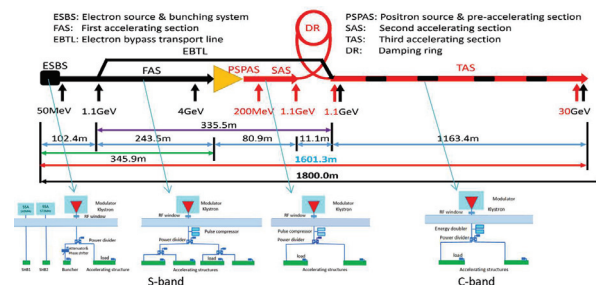


Figure 1: Layout of 30 GeV CEPC linac.

The RF system includes a bunching system and main accelerating structures. The bunching system comprises of two sub-harmonic cavities with frequencies of 158.89 MHz and 476.67 MHz, and one 2860 MHz S-band accelerating structure. For the total 30 GeV linac, there are

DESIGN AND TEST OF DOUBLE SPOKE SUPERCONDUCTING CAVITY TUNER FOR CSNS-II *

Z. Mi ^{†1}, M. Liu¹, W. Zhou¹, W. Pan¹, R. Ge¹, C. Zhang¹, F. He¹, J. Zhai¹, M. Xu¹
 Institute of High Energy Physics, CAS, Beijing, China
¹also at University of Chinese Academy of Sciences, Beijing, China

Abstract

The China Spallation Neutron Source phase II (CSNS-II) upgrade design will increase the total beam power from 100 kW to 500 kW and boost the beam energy from 80 MeV to 300 MeV in the linac by adding a superconducting linear accelerator to the existing accelerator complex. The double spoke resonator is used in the energy range of 80 MeV to 165 MeV. To compensate the frequency change due to manufacturing uncertainty, Lorentz force, beam loading, He pressure and microphonics, a new type tuner is designed for the double spoke superconducting cavity. The tuner is mounted on the side of the cavity, and each module contains two tuner systems. In this paper, the structure and working principle of the tuner are designed and analysed, also the testing result of the tuner with the double spoke Resonator and cryomodule prototypes are introduced.

INTRODUCTION

The baseline and main parameters for upgrade SRF system of CSNS-II have been public [1, 2]. IHEP is developing 324 MHz double superconducting RF cavities for CSNS-II, the structure is shown in Fig. 1. In order to increase the beam power from 80 MeV to 165 MeV, and also with the beam peak current increase from 15 mA to 50 mA, twenty double Spoke superconducting cavities with $\beta_0=0.5$ are used, as the scheme shown in Fig. 2. Each cryomodule contains two 324 MHz superconducting cavities, for a total of ten this cryomodules. The spoke cavity operates in pulse mode and is mainly affected by Lorentz force, to adjust the cavity resonance frequency to the accelerator frequency during operation is essential to the RF system stable and have a perfect transmission of the radiofrequency power to the beam, also reduce reflection power. The cavity parameters as shown in Table 1, to meet the requirements of 324 MHz double Spoke cavities, newly tuner system is designed. Two type tuners have been designed and test for the performance verification. Due to the lever tuner are widely used for SRF cavity to tuning frequency for install and maintains easily, lever tuner has been chosen as the basic structure. And adopts the structure of motor tuner (slow tuning) and piezo tuner (fast tuning). Assembled the two type tuners and cavity in the cryostat, and completed the warm temperature (300 K) test and cold test (2 K). The research objectives include verify the tuner's design and overall structure, evaluate its performance at different temperatures, and assess its effectiveness in achieving the desired tuning capabilities

* Work supported by China spallation resources phase II project & Youth innovation promotion association CAS

[†] mizh@ihep.ac.cn

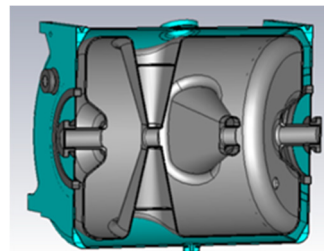


Figure 1: 324 MHz double spoke cavity 3D model.

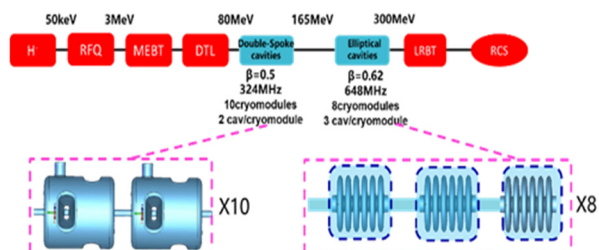


Figure 2: CSNS-II linear accelerator upgrade scheme.

Table 1: Parameters of Double Spoke Cavity

Parameters	Value	Units
Frequency	324	MHz
Aperture	50	mm
Operating temperature	2	K
B 0	0.5	--
Ep/Eacc	4.1	--
Bp/Eacc	9.2	mT/(MV/m)
G	120	Ω
R/Q	410	Ω
Operating gradient	7.3	MV/m
Operating frequency	25	Hz
Cavity stiffness	~ 10	N/um
Tuning sensitivity	100	kHz/mm
K1 (tow beam pipe free)	-12.54	Hz/(MV/m) ²
K1(one beam pipe free)	-10.47	Hz/(MV/m) ²
df/dp	-0.773	Hz/mbar
Frequency	324	MHz

ADVANCEMENTS IN Nb₃Sn GROWTH FOR SRF TECHNOLOGY

L. Shpani*, M. U. Liepe, Cornell University, Ithaca, NY

V. Do, H. Lew-Kiedrowska, S. J. Sibener, C. Wang, University of Chicago, Chicago, IL

Abstract

Nb₃Sn is the most promising alternative material for the future of superconducting radio-frequency (SRF) technology, steadily advancing towards practical applications. Having a critical temperature twice that of niobium, Nb₃Sn offers the potential for developing smaller, more powerful, and more efficient accelerators. We have designed a comprehensive study to synthesize and characterize substrate treatments at nucleation temperatures following the thermal vapor diffusion growth process to improve the uniformity of Nb₃Sn coatings, pushing its performance closer to fundamental limits.

INTRODUCTION

Having a critical temperature two times that of Nb and a potential to achieve twice the accelerating fields compared to Nb cavities, Nb₃Sn is the most promising alternative material for the future of SRF technology [1–4]. Nb₃Sn cavities can reach high quality factors (>10¹⁰) at ~ 4 K liquid helium temperatures, and thus can be operated efficiently at 4 K as opposed to niobium cavities which are typically operated at 2K [4]. Employing Nb₃Sn cavities will significantly reduce the cost and complexity of SRF technology, making SRF technology accessible at a smaller scale and to a variety of applications, such as wastewater treatment, medical isotope production, and ultrafast electron diffraction [1]. While there has been significant progress in research and development of Nb₃Sn cavities, there still remain practical challenges in the synthesis of this material that need to be addressed for the performance of this material to come closer to its theoretical limitations. The state of the art growth method for Nb₃Sn cavities is thermal vapor diffusion, where a Nb cavity is put inside a high vacuum furnace along with a tin source and a nucleating agent of tin chloride (SnCl₂) and heated at high temperatures (> 900 °C) where the A15 Nb₃Sn structure formation is thermodynamically favorable. More details of the coating process can be found in [2, 3, 5].

Synthesizing a uniform layer of the right stoichiometry on the complex cavity surface is crucial for achieving high quality factors and high accelerating gradients. A common culprit for premature cavity quenches and degraded cavity performance are tin depleted regions [3–5]. There are a few ways that we can help avoid these tin depleted regions. Growing an amorphous Nb₂O₅ layer on the Nb substrate before Nb₃Sn growth has been shown to result in less tin depleted regions compared to the native oxide [5]. Recent studies have shown that altering this anodic pentoxide can help promote more uniform nucleation of tin at early stages of growth [2].

The main hypotheses to describe the mechanism behind the role of the oxide are the increased surface area of the amorphous Nb₂O₅ film compared to the native oxide, and the thermodynamic role of oxygen in aiding the initial stages of the alloying process [6].

Anodic Growth of Niobium Oxide

Anodic niobium oxides are well studied outside the field of SRF and accelerator physics for a variety of applications in other disciplines such as solar cells and chemical sensing [7]. When niobium is made the anode of electrolytic cell, anodic oxidation is one of several reactions that can occur in competition with other reactions such as anodic dissolution or oxygen evolution [8]. The mechanism behind this anodic oxide growth is illustrated in in Fig. 1. The final properties, chemistry, and morphology of the anodic Nb₂O₅ are influenced by the operating conditions, namely the temperature, current density, terminating voltage, the pH and chemical composition of the electrolyte.

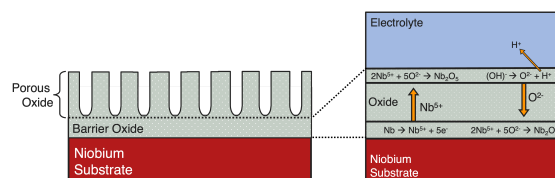


Figure 1: Simplified illustration of the anodic pentoxide growth. First, the barrier oxide layer growth (right) happens at the oxide/electrolyte interface through the outward migration of Nb⁵⁺ cations, and at the oxide/metal interface through the inwards migration of O²⁻ anions. If the oxide is soluble in the electrolyte, a porous oxide layer is formed at the oxide/electrolyte interface (left).

When the oxide is soluble in the electrolyte, we can synthesize porous oxide surfaces at the electrolyte/oxide interface. Niobium oxide is attacked by HF and by alkali electrolytes with pH ≥ 14 [8]. Studies have been done on anodic Nb₂O₅ with various growth conditions and porosity of the surface of these films have been characterized and a voltage-thickness relationship has been established [7–9].

The study done at Cornell University [5] found that anodizing Nb substrates in 10%w/w NaOH with terminating voltages of 15, 30, and 50 V all resulted in more uniform Nb₃Sn layer coverage compared to the native oxide, but there was no significant difference (to the limits of EDX measurement) between these three voltages. Another study [10] reported tin droplets to be bigger and more sparsely distributed when anodized in NH₄OH at 50 V as opposed to 30 V. This discrepancy could be explained by the use of different electrolytes and potentially different current density limits.

* ls936@cornell.edu

HIGH PULSED POWER MEASUREMENTS OF SUPERHEATING FIELDS FOR SRF MATERIALS*

N. Verboncoeur[†], A. Holic, M. Liepe, T. Oseroff, R. D. Porter[‡], J. Sears, L. Shpani
Cornell Laboratory for Accelerator based ScienceS and Education (CLASSE), Ithaca, NY, USA

Abstract

The Cornell High Pulsed Power Sample Host Cavity (CHPPSHC) is a new system designed to measure the superheating field of candidate superconducting RF (SRF) materials, giving insight into their operational limits. This system is designed to reach peak magnetic fields of up to 0.5 T in only a few microseconds, allowing us to achieve a purer magnetic field quench on the sample. We present an overview of the CHPPSHC system and proof of principle data from a niobium sample.

INTRODUCTION

Improving the accelerating gradient, E_{acc} , of superconducting radio-frequency (SRF) cavities is a desirable goal for the next generation of accelerators. The upper limit on E_{acc} for a given material is set by its superheating field, B_{SH} , and the cavity geometry. Niobium cavities are the current standard and has a B_{SH} of ~ 200 mT corresponding to a maximum E_{acc} of ~ 50 MV/m in an elliptical cavity [1]. The SRF community has been investigating other materials [2, 3] including Nb_3Sn , which is predicted to have a B_{SH} of ~ 400 mT [4, 5]. This corresponds to an upper limit on E_{acc} of ~ 100 MV/m.

To date, there has not been satisfying experimental measurements of Nb_3Sn 's superheating field. Previous attempts have been made, however these experiments have been severely limited by thermal effects. The superheating field is an extremely temperature-dependent property, so even a small amount of heating can lower the quench field. Here, we explore the Cornell High Pulsed Power Sample Host Cavity (CHPPSHC), a sample host structure specifically designed to measure the limiting magnetic fields of candidate SRF material samples [6, 7].

THE CORNELL HIGH PULSED POWER SAMPLE HOST CAVITY

The CHPPSHC must be able to reach fields exceeding the predicted B_{SH} of Nb_3Sn fast enough that heating does not have a significant effect on the measurement. The CHPPSHC utilizes a 1 MW klystron with pulse lengths on the order of $10 \mu s$. Past experiments at Cornell were done with 1.3 GHz elliptical cavities, but maximum fields were thermally limited due to pulse lengths of $50 - 100 \mu s$ [1]. The CHPPSHC's geometry is designed to charge quickly by exploiting field enhancement along the sharp edge of the sample. A simulation of the magnetic field in the cavity is shown in Fig. 1.

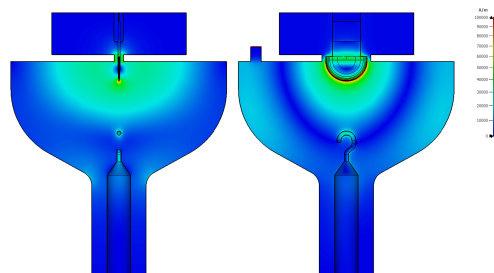


Figure 1: Simulation of peak magnetic fields along $x = 0$ (left) and $z = 0$ (right) planes of the CHPPSHC in CST Microwave Studio. The design exploits field enhancement to reach significantly higher peak fields on the sample edge. An upper bound of 1×10^5 A/m was set on the color scale for visibility purposes. The peak field on the sample is $\sim 4 \times 10^5$ A/m corresponding to ~ 500 mT.

The peak field on the sample edge is enhanced by a factor of 500 due to this effect, which allows the system to reach a maximum field of ~ 500 mT in only $\sim 10 \mu s$ [6].

The simulation also calculates the quality factors of various components of the system. While superconducting, the sample accounts for less than 0.001 % of losses. When the sample is normal conducting at 300 K, the losses on the sample reach ~ 70 % of losses. The resulting sharp drop in the system's Q_0 is large enough that it will be evident in RF power data when the sample has quenched.

PULSED RF DATA

Before investigating Nb_3Sn , baseline data for a niobium sample is necessary to ensure that quench information can be accurately extracted from our measurement results. A niobium sample was prepared using the same processes applied to a niobium cavity, receiving a bulk chemical polish, electropolishing, and a 5 hr 800 C bake. The sample was cleaned with DI water in a class 100 cleanroom before being assembled into the copper host structure.

The host cavity is tested in helium over a temperature range from 2 K to 9 K and driven by a 1 MW klystron. Before taking pulsed data, a system calibration is done in continuous wave (CW) operation to determine the loaded quality factor, Q_L , the coupling, β , and field calibration. In Fig. 2, an example pulsed operation data point is shown. B_{pk} is calculated from the RF data using the results of the CW calibration and the CST simulation.

Figure 2 shows a pulse that exhibits “overfilling” behavior where the cavity continues to fill despite the sample quenching. This makes it more difficult to accurately identify the quench field as the underlying mechanisms become more complex.

* Supported by U.S. Department of Energy Grant No DE-SC0008431

[†] nmv39@cornell.edu

[‡] Now at SLAC, Menlo Park, California, USA

DESIGN OF A QUADRIPARTITE WAKEFIELD STRUCTURE FOR FREE ELECTRON LASER APPLICATIONS

Y. Ji¹, C. Lei¹, J. Shao^{1*}, Y. Yu¹, J. Sun², Zongbin Li¹, L. He¹, H. Wang¹,
J. Wei¹, W. Wei¹, W. Wang¹, J. Yang², W. Zhang², X. Yang²

¹Institute of Advanced Science Facilities, Shenzhen, China

²Dalian Institute of Chemical Physics, Dalian, China

Abstract

Wakefield structures are broadly employed in free electron laser (FEL) facilities for beam manipulation. Compared with cylindrical geometries, planar structures are typically preferred due to their increased flexibility, allowing for tunable wakefield strength through gap adjustment. However, these planar configurations can induce time-dependent quadrupole wakefields, which require careful compensation in various applications. To address this issue, we propose a novel structure design incorporating four identical corrugated elements which are independently controllable. By adjusting the gaps between orthogonal pairs, the quadrupole wakefield can be either fully compensated to avoid emittance growth or significantly amplified to enhance beam mismatch for slice lasing control. This manuscript presents both the physical and mechanical design of the proposed structure, as well as the planned proof-of-principle experiment.

INTRODUCTION

Wakefields are induced when a charged bunch traverses a corrugated or dielectric pipe. Structure-based wakefield acceleration represents a promising approach to achieve gradients significantly higher than those attained by conventional techniques [1–3]. Furthermore, wakefield have been demonstrated to be effective tools for beam manipulation in FELs, where the short-range wakefield from the bunch head can alter the longitudinal or transverse momentum of the tail [4–18]. Initially, wakefield structures were employed in FELs as dechirpers to mitigate the linear energy chirp introduced for magnetic bunch compression [4, 5, 7]. Since then, these structures have been adapted for a broader range of applications, such as passive linearization [6, 13], slice lasing control [8, 10–12, 14, 15], and passive deflection [9, 17, 18].

The Shenzhen Superconducting Soft X-Ray Free-Electron Laser (S³FEL) is a newly proposed, high repetition-rate FEL facility featuring multiple undulator lines that lase in the 1–30 nm range [19]. Wakefield structures are under development to serve as dechirpers and as key components for advanced FEL modes. Their performance is crucial to achieving high lasing quality in S³FEL.

Most FEL facilities apply planar structures with two corrugated plates, where the longitudinal wakefield strength can be adjusted by varying the gap. However, quadrupole wakefield is introduced in addition to the longitudinal wakefield due to the asymmetric geometry. The time-dependent

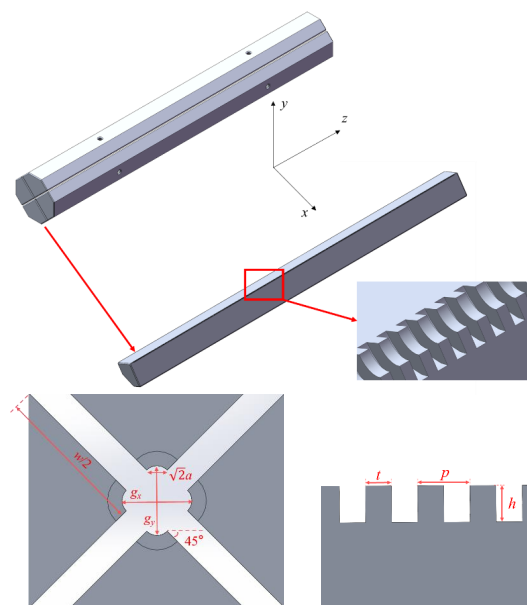


Figure 1: Schematic layout of the quadripartite wakefield structure.

quadrupole wakefield can cause beam mismatch and emittance growth, which usually require compensation by placing two pairs of plates orthogonally and maintaining nearly symmetric average β functions throughout the structures [7]. Conversely, purposely enhancing beam mismatch via the quadrupole wakefield can be exploited for slice lasing control, by individually matching the slices into different undulators [10, 11]. Consequently, it would be desirable to introduce a structure that provides flexible and independent control of both longitudinal and quadrupole wakefield.

Therefore, we propose a novel wakefield structure consisting of four identical elements. By adjusting the gaps between orthogonal pairs, the quadrupole wakefield can be either fully compensated or significantly amplified, while the impact to the longitudinal wakefield is moderate. Such design allows for flexible manipulation of bunch slice properties for various applications.

PHYSICAL DESIGN

The quadripartite wakefield structure comprises four identical corrugated plates, each independently controlled by a pair of high-precision motors, as illustrated in Fig. 1. The corrugation of each plate can be designed either as a quarter-circle curve or flat, without affecting the fundamental work-

* shaojiahang@mail.iasf.ac.cn

SINGLE BUNCH AND MULTI BUNCH OPERATION WITH SINGLE KLYSTRON USING A PROGRAMMABLE SLED SYSTEM

A. Tropp, P. Gu, C. Christou†
Diamond Light Source, Oxfordshire, UK

Abstract

The Linac for Diamond Light Source has been running with two 3 GHz klystrons, powering two 5.2m-long accelerating structures to deliver 100 MeV electron beam since the start of operation. By introducing a SLED RF pulse compressor system to generate a pulse capable to power both structures from one klystron, redundancy and reliability will be improved. With a 5 μ s total pulse, it is possible to charge the SLED cavities for 4 μ s and generate a high peak pulse for the last 1 μ s able to power both structures. An arbitrary waveform generator function was implemented in digital low-level RF to generate a flat top pulse, which can be utilized for both single bunch and multi bunch operation. Details of the waveguide network, low-level RF design and high-power operation will be described. Results from full energy operation will also be shown.

LINAC MODIFICATIONS

Diamonds original Linac configuration can be seen in Fig. 1 on the left. To use both klystrons to power the RF pulse compressor, a new configuration of the waveguide had to be designed. The first design with SLED did not use compressed RF pulse for the bunching structures as can be seen in the middle configuration layout in Fig. 1. This was later changed, and the final design layout was made, shown on the right side of Fig. 1.

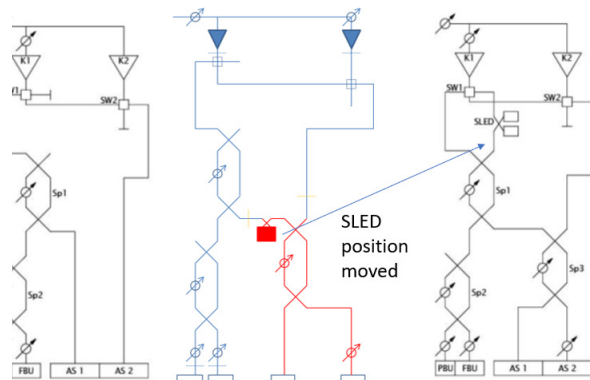


Figure 1: Linac configurations from start to finish of project. Initial without SLED (left), Intermediate (middle), final design (right).

This design allows either of the klystrons to power the pulse compressor by using two RF switches SW1 and SW2. After the pulse compressor the power will first be split to the bunching structures FBU and PBU. After this the remaining power goes through a splitter SP3 which

splits the power between the two accelerating structures AS1 and AS2. By changing the switches both klystrons can also be used as in the old configuration.

A High-power RF window capable of withstanding a peak power of 70 MW was also installed directly after the SLED, see Fig. 2. This window is based on the PAL design [1], and the design change from 2856 MHz to 2998 MHz lowered the power limit slightly.

The final installation was done in March 2024 and allowed carrying out high power tests.

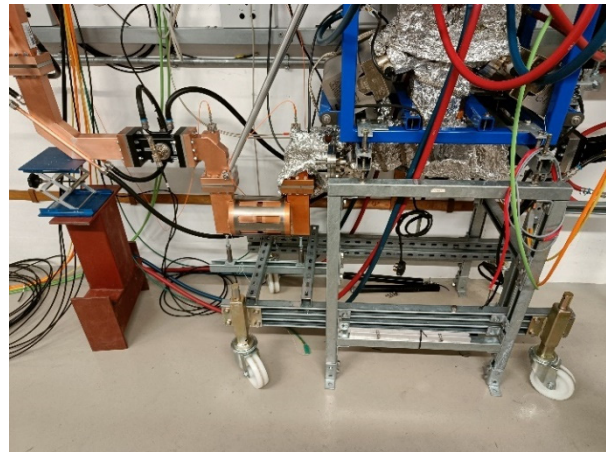


Figure 2: SLED and window assembly inside Linac.

DIGITAL LOW-LEVEL RF

The DLLRF is based on the Micro Telecommunications Computing Architecture (MicroTCA) standard. It was chosen for its reliability, modularity and scalability. The DLLRF consists of a 2U MTCA.4 chassis, a MCH, an AMC computer board, a Struck SIS8300-KU card and a Struck DWC8VM1 RTM with supporting clock/local oscillator (LO)/reference generation RF circuits, see Fig. 3.

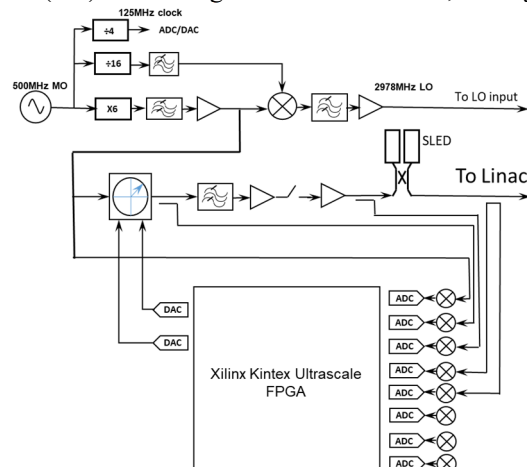


Figure 3: Schematic for the digital low-level RF.

† Present address DESY, Hamburg, Germany

C-BAND RF SYSTEM FOR THE SAPS TEST BENCH

Hui Zhang¹, Zhencheng Mu², Hexin Wang², Zhixin Xie², Linyan Rong², Bo Wang²,
Maliang Wan², Shimin Jiang²

¹Spallation Neutron Source Science Center, Dongguan, China

²Institute of High Energy Physics, Beijing, China

Abstract

This work describes a C-band RF system for the SAPS (Southern Advanced Photon Source of China) test bench linear accelerator. SAPS' RF testing system comprises of a photocathode electron gun and a 2-metre-long equal gradient acceleration device. The klystron power source delivers energy to the photocathode electron gun and the travelling wave acceleration structure, respectively. Test the photocathode electron gun first, followed by the travelling wave acceleration structure. We investigated a short-pulse C-band spherical pulse compressor. The photocathode electron gun's preliminary high-power testing is now complete.

INTRODUCTION

To improve the beam quality of photocathode microwave electron guns, increase the gradient inside the electron gun to lower heat and space charge emissivity. The photocathode electron gun cavity is designed to achieve an acceleration gradient of 150 MV/m. A 2-meter-long travelling wave acceleration structure is put at the back end of the photocathode electron gun to increase the energy and stabilise the emissivity of the electron beam emitted by the gun.

The RF system's function is to deliver enough power to the electron gun cavity to achieve a gradient of 150 MV/m, as well as RF power to the travelling wave acceleration structure to ensure that its gradient satisfies the design criteria. Figure 1 shows the layout design for the electron gun and accelerator tube.

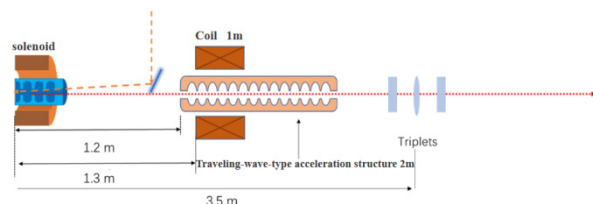


Figure 1: Layout of electron gun and accelerator tube.

RF SYSTEM

The components of the C-band RF system include a circulator, directional couplers, rectangular waveguides, a spherical pulse compressor, and more. Figure 2 display the C-band RF power source system's composition diagram. The klystron, circulator, and pulse compressor which are positioned in the system as seen in Fig. 3 are the most important parts of the RF power system.

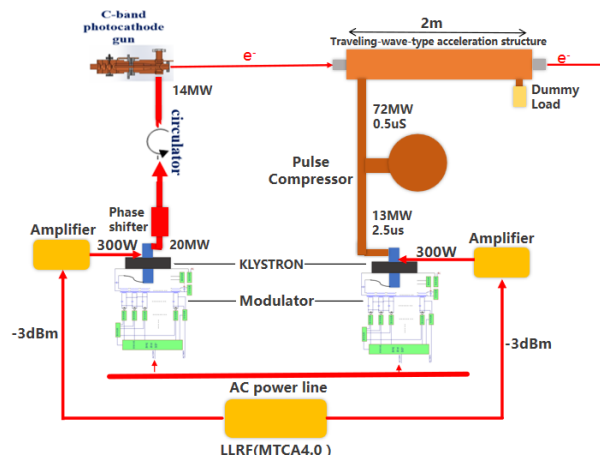


Figure 2: Composition of C-band RF power source.

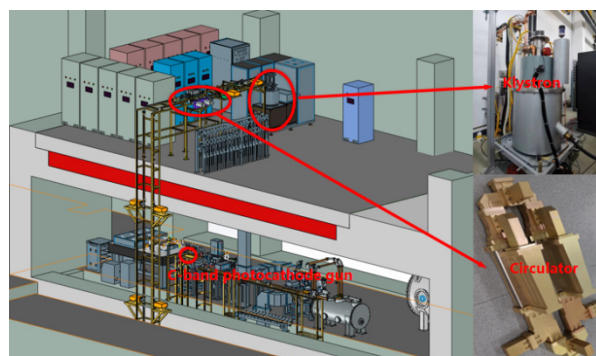


Figure 3: RF system schematic diagram.

Klystron

The traveling wave acceleration structure and the photocathode electron gun in the SAPS experimental device will each require one klystron with a 20 MW output power. High throughput electron optical system, highly dependable microwave output system, and high-efficiency beam wave interaction system are all features of C-band klystron. The klystron mainly comprises an electron optics system, a beam-wave interaction section, and a collector [1]. The designed klystron, with a working frequency of 5712 MHz, peak power of 50 MW, repetition rate of 50 Hz, and pulse width of 2.5 μ s, satisfies the performance criteria of high gradient acceleration devices. Operational stability was taken into account when testing the klystron, and an RF pulse width of 1.2 μ s was employed.

When the klystron was tested with an RF pulse width of 1.2 μ s and a repetition rate of 5 Hz, the output power reached 45 MW. Figure 4 shows the power display.

AN ALTERNATIVE DESIGN SCHEME FOR CSNS-II MEBT DYNAMICS

Qiyu Kong^{*1}, Huachang Liu^{1,2}, Jun Peng^{1,2}

Spallation Neutron Source Science Center, Dongguan, China

¹also at Institute of High Energy Physics, Chinese Academy of Sciences (CAS), Beijing, China

²also at University of Chinese Academy of Sciences, Beijing, China

Abstract

The China Spallation Neutron Source (CSNS) has been operating at a stable beam power of 160 kW since March 2024, marking a significant 60% increase from its original design capacity. The ongoing CSNS upgrading project, known as CSNS-II. As part of this upgrade, a versatile Medium Energy Beam Transport (MEBT) system has been meticulously studied and redesigned to meet the stringent requirements for beam control in the presence of strong space charge effects. The MEBT system boasts several key functions and features, including beam chopping for optimizing beam structure, scrapers for confining and removing beam halo particles. Detailed studies on beam performance, in conjunction with the main linac, have been carried out and are presented in this article.

INTRODUCTION

The China Spallation Neutron Source (CSNS) leverages a high-energy proton accelerator to generate neutrons for a diverse array of scientific investigations [1]. The high-energy proton accelerator complex initiates with the 81 MeV H^- linear accelerator, consists of a 50 keV H^- ion source, a low energy beam transport line (LEBT), a 3 MeV Radio Frequency Quadrupole (RFQ), a medium energy beam transport line (MEBT), an 81 MeV Alvarez-type Drift Tube Linac (DTL) [2]. Then, H^- ion is stripping injected into rapid cycling synchrotron (RCS), where they are accelerated to 1.6 GeV.

The ongoing upgrade of the CSNS, known as CSNS-II, aims to enhance the linac peak current to 50 mA while the energy increase to 300 MeV, facilitated by a superconducting accelerator featuring Double-Spoke Resonators (DSR) [3] and Elliptical Resonators (EllipR). The layout of the linac in CSNS-II is illustrated in Fig. 1. Upon the successful completion of this upgrade, CSNS-II is poised to become the pioneering user open facility to deploy a superconducting linac as an RCS injector.

Table 1: The Main Parameters of the CSNS Linac in Phase-I and Phase-II

Parameter	Phase-I	Phase-II
Output energy (MeV)	81	300
Peak current (mA)	15	50
Repetition rate (Hz)	25	50
RF frequency (MHz)	324	324&648
Duty factor (%)	0.625	1.25

* kongqy@ihep.ac.cn

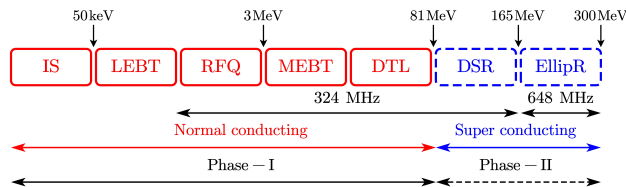


Figure 1: The layout of linac in CSNS-II.

The MEBT currently in operation at CSNS underwent joint commissioning with the DTL in 2018, at an energy level of approximately 3 MeV, which for high-intensity beam is a section dominated by space charge effect, making emittance growth seemingly inevitable. However, the functions it possesses are relatively simple and may not suffice to address the challenges posed by increased intensity, including emittance growth. In response to these evolving requirements, a series of research initiatives have been undertaken to develop a multi-functional MEBT dynamics scheme tailored to meet the demands of the CSNS-II project. This innovative approach aims to enhance the capabilities of the MEBT system to effectively manage emittance growth and other associated challenges arising from the intensified beam currents, thereby ensuring the continued success and optimal performance of the CSNS-II facility.

DESIGN PHILOSOPHY AND CONSIDERATIONS

In high-intensity accelerator facilities, the damage caused by beam losses due to various factors should be kept as low as possible along the linac, typically adhering to an acceptable threshold of 1 W/m for majority high-power particle accelerators [4]. Among all kinds of different possible beam loss sources in CSNS-II, the beam loss existing in MEBT or can be solved in MEBT mainly has the following three mechanisms:

- The linac in CSNS is equipped with a beam chopper at the LEBT with approximately a 20 ns rising edge [5]. It is important to note that the rising edge comprises several micro-pulses that are not entirely chopped.
- With CSNS-II operating at a beam current approximately five times higher than the existing facility, it is crucial to optimize beam halo at the entrance of the DTL.

CHOPPER SYSTEM

A pre-chopper in LEBT together with a chopper in MEBT is an effective solution to mitigate beam loss as in the SNS [6].

SIMULATION AND EXPERIMENT STUDY OF PROTON GENERATED BY RESIDUAL GAS STRIPPING IN CSNS

Qiyu Kong^{*1}, Huachang Liu^{1,2}, Jun Peng^{1,2}

Spallation Neutron Source Science Center, Dongguan, China

¹also at Institute of High Energy Physics, Chinese Academy of Sciences, Beijing, China

²also at University of Chinese Academy of Sciences, Beijing, China

Abstract

The CSNS consists of an H^- linac as injector, the interaction of the residual gas with H^- particles will strip the electrons to produce associated protons within the LEBT, which follow the H^- into the subsequent accelerating structure. In order to avoid the adverse effects of proton loss on the device, the feasibility of employing a bump for associated proton separation at the MEBT was investigated firstly using multiparticle tracking simulations. Beam experiment was carried out in the existing CSNS MEBT device, in which the transverse profile signals of the associated protons were observed. Intensity of the associated proton with and without the bump separation are compared downstream the DTL, which proves bump separation is an effective method for the removal of associated protons. The simulation and experimental results can provide scheme references for solving the associated proton problem faced in CSNS-II.

INTRODUCTION

The China Spallation Neutron Source (CSNS) leverages a high-energy proton accelerator to generate neutrons for a diverse array of scientific investigations [1]. The proton accelerator complex presently consists of an 81 MeV H^- linear accelerator and a 1.6 GeV Rapid Cycling Synchrotron (RCS), as shown in Fig. 1. The linac consists of a 50 keV H^- ion source, a low energy beam transport line (LEBT), a 3 MeV Radio Frequency Quadrupole (RFQ), a medium energy beam transport line (MEBT), an 81 MeV Alvarez-type Drift Tube Linac (DTL) [2]. The H^- linac is an injector of RCS, and the charge-exchange injection is adopted to mitigate the space-charge effects. Protons are finally extracted to the target where generates neutron.

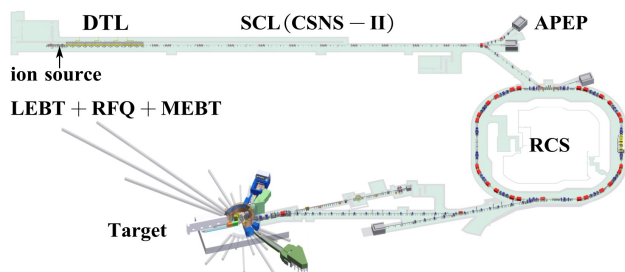
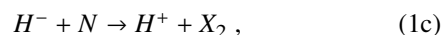
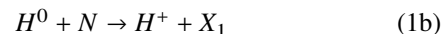
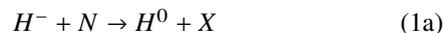


Figure 1: The layout of proton accelerator in CSNS.

Generation of Associated Proton

H_2 gas flows from the ion source into vacuum pumps in LEBT, H_2 gas is ionized to positive ion such as H_2^+ after colliding with H^- particles to neutralize space charge force. A small fraction of H^+ and H^0 are generated by electron stripping of H^- particles with residual gas [3]. The stripping process is described by Eqs. (1a)-(1c) [4]:



where N is the remnant gas molecule, and X, X_1, X_2 are the other products.

Transportation of Associated Proton

Processes and protons have been observed in other facilities, such as SNS and LAMPF, protons will be absorbed by electrodes of quadrupoles in LEBT immediately. However, CSNS adopts solenoids focusing for LEBT to mitigate the emittance growth with the help of space-charge neutralization effect. In that case, a substantial fraction of the H^+ will reach the RFQ and gradually bunched around the RF phase shifted by 180 degrees with respect to the phase of the H^- bunch. Even worst, H^+ particles can be eventually accelerated to the same energy with H^- of 3 MeV as they have almost the same charge-to-mass ratio with opposite charge. According to the particle tracking simulation, H^+ can transport through the MEBT and captured by DTL. Finally, H^+ will be accelerated to 80 MeV, because there is no RF frequency jump within MEBT and DTL. 80 MeV H^+ is deflected to Associated Proton beam Experiment Platform (APEP) which is opposite to that of H^- [5].

Considerations for Associated Proton Removal

The ongoing upgrade of the CSNS, known as CSNS-II, aims to enhance the linac peak current to 50 mA while the energy increase to 300 MeV, facilitated by a superconducting accelerator featuring Double-Spoke Resonators (DSR) [6] and Elliptical Resonators (EllipR). Most importantly, the Elliptical Resonators operate at RF frequency of 648 MHz, which is twice of the DTL and RFQ. In that case, associated H^+ will be lost in resonators of 648 MHz. In order to avoid contamination of the superconducting resonators, the removal of associated protons generated by residual gas stripping should be considered in advance. Series of research and experiments have been conducted.

* kongqy@ihep.ac.cn

RECENT RESULTS OF THE HIGH GRADIENT S-BAND ACCELERATING MODULE FOR FERMI ENERGY UPGRADE

M. Trovò*, N. Shafqat, F. Gelmetti, M. Milloch, A. Milocco
Elettra Sincrotrone Trieste S.C.p.A., Trieste, Italy

R. Fortunati, R. Zennaro, Paul Scherrer Institute (PSI), Villigen, Switzerland

Abstract

FERMI is the seeded free electron laser (FEL) user facility at Elettra laboratory in Trieste, operating in the VUV - soft X-ray spectral range. In order to extend the FEL radiation to shorter wavelengths, an energy increase from 1.5 GeV to 2.0 GeV is required in the linear accelerator (linac). This result is achievable by replacing the present old sections with the newly designed accelerating sections that can work at high gradient with lower transverse wakefields. A new high-gradient (HG) module was built and installed at the FERMI linac. We report here the recent experience on the conditioning and the results on the e-beam energy gain in operation.

INTRODUCTION

The FERMI FEL, located at the Elettra Sincrotrone research center in Trieste, Italy is the 4th generation light source operating in Extreme-Ultraviolet (EUV) to the soft X-rays range. FERMI is presently driven by a 1.5 GeV, S-band normal conducting linear accelerator (linac), outlined in Fig. 1.

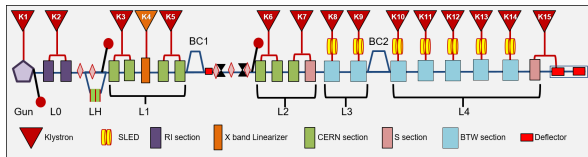


Figure 1: FERMI FEL linac layout (*cartoon not to scale*).

The upgrade plan of the FERMI aims to extend the FEL wavelength range to cover the nitrogen and oxygen K-edge by increasing the electron beam energy up to 2.0 GeV and the peak current greater than 1 kA [1]. The upgrade plans the replacement of the old accelerating sections, starting from the seven, 6.4 m long, Backward Travelling Wave (BTW) structures in the high energy part of the linac (L3 and L4) which are limited presently to a maximum gradient of 24 MV/m. These BTW structures would be replaced with the newly designed HG modules (one HG module consists of two HG structures with length of 3.0 m each) that are designed to operate reliably up to an accelerating gradient of 30 MV/m as shown in Fig. 2 [2].

This energy upgrade will enable the FERMI to generate the photon beam up to one keV energy. In the first step, two such new HG structures are installed in place of S0a and

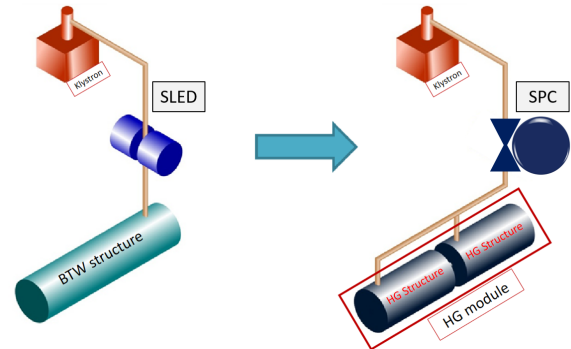


Figure 2: Sketch of the FERMI upgrade plan unit.

one deflector at K15 increasing the beam energy to 1.7 GeV. In the next phase, 14 new HG structures would replace the present BTW sections reaching the final goal of 2.0 GeV. The first 3.0 m HG structure was conditioned and high-power tested at the cavity test facility of Elettra from May 2022 to August 2022. After receiving the 2nd HG structure first HG module was installed at FERMI linac during the summer shutdown in September 2022 for commissioning with the beam. Since that time the K15 operation is characterized by a rotation between conditioning mode and acceleration for user operations.

BRIEF UPGRADE PLAN OVERVIEW

The HG structures are constant gradient type accelerating structures operating in $2\pi/3$ phase advance mode [3, 4]. These HG structures are designed to operate reliably at an accelerating gradient of 30 MV/m with a very low breakdown rate (BDR) with low wakefields. The HG structures are fed using a customized version of dual-fed EC-type couplers as they have lower surface fields as compared to their MC counterparts [5]. All the geometrical parameters of an accelerating cell are summarised in Table 1.

A short prototype was built at Paul Scherrer Institute (PSI) in Switzerland with the aim to verify the feasibility and reliability of the upgrade. The short prototype was fabricated using a technique developed at PSI which produces a tuning-free structure by adhering to very tight tolerances [6]. A high-power S-band test facility with the BOC type pulse compressor and National Instrument (NI) diagnostic hardware was commissioned at Elettra for conditioning and high-power testing of the short prototype [7]. The complete history of conditioning and high-power operation along with the exhaustive post-processing of the conditioning data is covered in [8].

* mauro.trovo@elettra.eu

TRANSVERSE BEAM DYNAMICS SIMULATIONS BENCHMARKED WITH ESS BILBAO INJECTOR MEASUREMENTS FOR ISOLDE ISRS PROJECT*

D. Fernández Cañoto[†], K. Altenmüller, I. Bustinduy, S. Masa, R. Miracoli, J. L. Muñoz, S. Varnasseri, ESS Bilbao Consortium, Zamudio, Spain

Abstract

A multi-harmonic buncher cavity, MHB, is being designed by ESS Bilbao for the HIE-ISOLDE ISRS project at CERN, to bunch beam pulses with 5 keV/u input energy. The MHB will be tested with the ESS Bilbao light-ion injector. Transverse beam dynamics simulations were carried out to analyse preliminary measurements from hydrogen beams produced at 5 and 10 keV. Results have demonstrated that ESS Bilbao injector can produce H^+ and H_2^+ beams with 5 keV/u, for an optimum characterization of the MHB cavity.

INTRODUCTION

A multiharmonic buncher cavity, MHB, will be installed before the HIE-ISOLDE RFQ to bunch beam pulses with a 5 keV/u input energy or $\beta = 0.00328$ at 10% of RF frequency [1]. The MHB will consist of two copper electrodes with 20 mm bore diameter installed inside a cross shaped vessel [2]. The cavity designed by ESS Bilbao will be tested with ESS Bilbao injector. This injector was designed for an extraction voltage of 45 kV and consists of a 2.7 GHz Electron Cyclotron Resonance (ECR) ion source, and a Low Energy Beam Transport line, LEBT [3].

Beams required for MHB characterization can be produced with ESS Bilbao injector using H^+ accelerated at 5 keV or H_2^+ at 10 keV, but due to the fact that both extraction voltages are far from ideal injector configurations, preliminary analysis of measurements were necessary. Cations of H^+ , H_2^+ , and H_3^+ in different ratios are formed from H_2 molecules depending on ionization energy, which characteristics would lay on ECR parameters like gas pressure, magnetic field configuration, or microwave power [4]. Additionally, identification and control of any beam species are important for proton therapy, spallation sources, or particle physics applications [5].

LEBT LAYOUT

Beam dynamics simulations are performed throughout LEBT, which layout with main longitudinal positions, Z_{pos} , and bore diameters, Φ , is shown in Fig. 1. The LEBT consists of a 45 kV extraction column, two solenoid magnets, $SOL1$ and $SOL2$, and four vessels for allocation of beam diagnostics. Beam currents are measured with the following current transformers: ACCT1 positioned before $SOL1$ and ACCT2 after $SOL2$; ACCT3 and ACCT4 after a 20 mm diameter collimator, COL_{20} , being separated by a $\Phi = 63$ mm diameter drift pipe 210 mm long. The MHB system will

be installed in between ACCT3 and ACCT4. The MHB electrodes will have the same diameter as COL_{20} , and the cross shaped vessel similar Φ and length as the drift pipe.

MEASUREMENTS

Measurements were carried out for hydrogen beams extracted at 5 and 10 keV. Figure 2 shows measured 2D maps of beam current, I_m , versus $SOL1$ and $SOL2$ excitation currents, I_{SOL1} and I_{SOL2} at ACCT2, ACCT3, and ACCT4. I_m at ACCT3 and ACCT4 presented similar values and patterns with contributions from different species, due to mass-to-charge ratio and collimation effects.

SIMULATIONS

The General Particle Tracer (GPT) code [6] has designed the extraction electrode optical system design of ESS Bilbao injector [7], and was used to simulate single H^+ , H_2^+ , and H_3^+ beams at 5 and 10 keV. Electromagnetic fields for extraction electrodes and LEBT solenoids were calculated with COMSOL Multiphysics [8]. Simulations were performed for the same magnetic fields considered for measurements. Measured beam currents at ACCT1 were nearly constant, and their mean values were used as inputs. For 5 keV beams: $I_{i-5keV} = 1.1$ mA; and for 10 keV: $I_{i-10keV} = 3.2$ mA.

Figure 3 illustrates simulated 2D maps of beam currents, I_s , at ACCT2, ACCT3, and ACCT4 Z_{pos} versus solenoids current for 5 keV beams. The optimum beam current transmission regions at ACCT2 Z_{pos} show vertical belt shapes, but after COL_{20} at ACCT3, and ACCT4 we notice optimum transmission regions are at weaker fields with hyperbolic triangular shape, and at stronger fields with a hyperbolic curved shape, only noticed for H^+ and H_2^+ species, since for H_3^+ would be out of range.

It was found that XZ -trajectories for beams extracted at any field configuration within a hyperbolic triangular region, for example a 5 keV H^+ beam from Fig. 3(c) being $I_{SOL1} = 45$ A and $I_{SOL2} = 32.5$ A presented normal focusing having one focal point, but within a hyperbolic curved region like at $I_{SOL1} = 55$ A and $I_{SOL2} = 70$ A, the beam was over focused showing two focal points. Figures 4(a) and 4(b) illustrates both cases.

Optimum extraction regions for H^+ , H_2^+ , and H_3^+ beam simulated at 10 keV were similar to the 5 keV maps from Fig. 3, but slightly displaced to stronger field values, due to Lorentz centripetal forces.

* Project funded by Spain Government under grant agreement Experiment ISRS-ISOLDE (BOE-A-2023-16885).

[†] dfernandez@essbilbao.org

UPDATE ON ESS-BILBAO RFQ LINAC

J. L. Muñoz*, I. Bustinduy, N. Garmendia, J. Martín, D. Fernández-Cañoto, P. González, A. Conde, A. Zugazaga, A. Kaftoosian, ESS-Bilbao Consortium, Zamudio, Spain

Abstract

The ESS-Bilbao RFQ fabrication is completed. The RFQ will operate at 352.2 MHz and will accelerate a 45 mA proton beam from 45 keV up to 3.0 MeV. The RFQ is build up of 4 copper segments, for a total length of 3.2 m. Each segment is composed of 4 subparts, 2 major and 2 minor vanes, that are assembled together by using bolts, vacuum and RF gaskets, with no brazing used in the procedure. This approach enables possible corrections in the assembly. The machining of all the segments has now finished. The RFQ structure has been assembled and the several tests have been carried out on it. In this paper we present aspects of the mechanical fabrication of the RFQ, the results of the vacuum tests of the whole structure, with all the tuners and couplers inserted. The low power RF measurements, frequency spectrum, quality factor and tuning operations by bead pull technique. Fabrication and testing of the components (tuners, couplers, pickups) are also presented. The operation of the RFQ is initially planned for low duty cycle, simplifying water cooling engineering and couplers design. The tests at low duty cycle will enable to define the required facilities for the use of the RFQ at its nominal power for future steps.

INTRODUCTION

The machining of the ESS-Bilbao Radio Frequency Quadrupole (RFQ) [1, 2] has been completed. This RFQ will be part of the proton injector for the ARGITU compact accelerator-based neutron source [3]. Designed to accelerate protons from 45 keV to 3.0 MeV, the RFQ operates as a pulsed linear accelerator (linac) at 352.2 MHz with a duty cycle of up to 5%.

To achieve the necessary acceleration and transmission characteristics, the RFQ must be precisely machined and assembled. The ESS-Bilbao RFQ is composed of four segments, each consisting of four vanes. Unlike traditional designs, these segments are not brazed together; instead, polymeric vacuum gaskets and RF contact elements are used in the assembly (as described in [1, 2]) to guarantee vacuum and electrical and thermal contact. Main characteristics of the RFQ are summarized in Table 1.

The machining, assembly and characterization of individual segments have finished, and results are presented here. The assembly of the whole structure is in process.

It is relevant to point out that power couplers have already been built and have been tested in low and high RF power. One coupler was attached to the RFQ already in operation at ISIS-FETS facility and tested with nominal peak power, for low duty cycle, as already reported in Ref. [4].

Table 1: ESS-Bilbao RFQ Main Characteristics

Parameter	Value
Type	4 vane
Particle	Protons
RF frequency	352.2 MHz
Intervane voltage	85 kV (uniform)
Energy	45 keV → 3.0 MeV
Design current	60 mA
Input emittance (rms norm)	$0.25 \pi \cdot \text{mm} \cdot \text{mrad}$
Duty cycle	Up to 10%
Kilpatrick factor	1.85
Number of cells	273
R_0	3.44 mm
ρ/R_0	0.85
Input/Output matcher	16.674 mm / 14 mm
Total length	3.12 m (3.66 λ)
Number of segments	4 (about 800 mm each)
Method of assembly	Polymeric vacuum gaskets
Plunger tuner ports	16 per segment

RFQ FABRICATION

Segments Machining

Each segment is itself an assembly of four components, two major vanes and two minor vanes (Fig. 1). Major vanes include the ports for tuners, couplers and pick-ups, as well as the vacuum ports. All components incorporate vane cooling channels that run along the segment. Each component is machined starting from a block of raw material (copper grade ASTM B248 C10100, ISO Cu-OFE), and subsequently machined in several steps until the final geometry is achieved. During the fabrication process several metrology controls are realized in order to verify that there are no deviations from the plan.

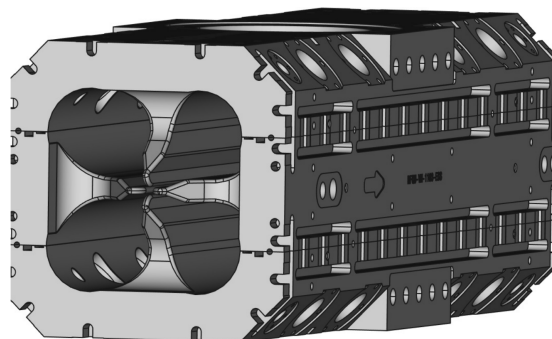


Figure 1: Model view of a segment, showing the minor and major vanes, the vacuum and RF seals grooves, as well as some details of the exterior.

* jlmunoz@essbilbao.org

A CRYOGENIC DIELECTRIC PULSE COMPRESSOR

S. V. Kuzikov[†], Euclid Techlabs LLC, Bolingbrook, IL

Abstract

Efforts aimed at developing klystron parameters have made significant progress in recent years [1]. However, the ultimate parameter list of connected pulse compressors (PCs) has been given insufficient attention. We propose to develop a new high efficiency, high power gain pulse compressor based on the use of a dielectric storage resonator (100% dielectric filling factor) that is operated at a cryogenic temperature (77 K). It is well known that, at cryogenic temperatures, a copper cavity can gain a much higher Q factor. However, at cryogenic temperatures, the RF loss tangent of some dielectric materials also decreases substantially ($\tan\delta \sim 10^{-9}$ for Sapphire at 10 K). This inspires our effort to develop dielectric resonators for PCs with an intrinsic quality factor, Q_0 , that is several orders of magnitude higher than the Q_0 for all metallic resonators at room temperature, and at least twice as high as for cryogenic copper cavities. In addition, the dielectric storage cavity can make the PC system more compact and lower their cost. We anticipate improving the parameters of the well-known SLED-II PCs. We consider both a passive PC (switched with a fast change of the klystron's phase) as well as an active PC (which requires a fast RF switch).

CRYOGENIC HIGH-Q RESONATORS

Two of the best-known pulse compression systems used for room temperature RF accelerators are the SLED and SLED-II PCs (Fig. 1). Both of these use hollow copper storage resonators (SLED) or delay lines (SLED-II) that accumulate RF energy from an incident RF pulse [2, 3]. The resonators work in low-loss TE_{01} or higher order axisymmetric modes. Unlike the SLED PC that has a decaying output pulse, the SLED-II was designed to provide a flat-top output RF pulse that is the best shape for feeding accelerating structures. The compressed pulse arises when the phase of the incident RF pulse is sharply changed by 180° . These PCs are often called passive PCs because the properties of the resonators or delay lines are never changed. A pair of resonators or delay lines are fed by a -3-dB hybrid coupler that protects the RF source from the undesirable reflection that occurs during the transient process of RF power accumulation. The SLED PC can provide up to $9\times$ power gain, P_g (ratio of the output pulse power to the incident pulse power). For maximum power gain, the efficiency (η), defined as the ratio of the energy in the output pulse to the incident energy, is very low. Typically, SLED works with power gain ~ 4 , in which case the compression ratio, C_r (ratio of incident pulse length to the length of the compressed pulse) equals 6. The efficiency in this case can be as high as 67% [2].

[†] s.kuzikov@euclidtechlabs.com

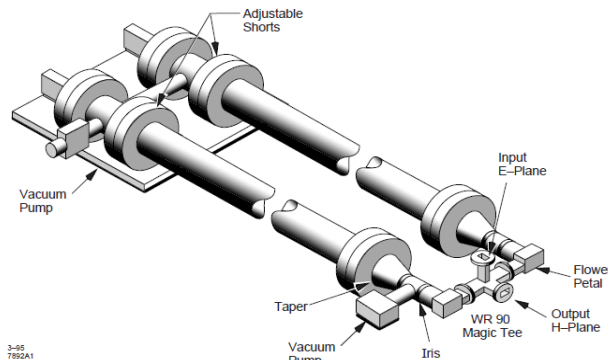


Figure 1: SLED-II layout. Tested with 12.065-cm diameter waveguide, 22.5-m in length (150-ns round-trip RF transit time) [2].

The obtainable parameters for the compression, power gain, and efficiency depend on the internal losses of the PC. Obviously, the lower the losses, the higher these parameters will be. To reduce the losses in the storage resonators, one can cool them down. Another idea is to substitute low-loss dielectric waveguides for the copper waveguides that are typically employed. Additional loss reduction can be obtained using dielectric materials at cryogenic temperature, taking advantage of the fact that, below some threshold temperature, the losses in all types of dielectrics go down as the temperature is decreased. Table 1 summarizes the properties of two of the most appealing dielectric materials, Magnesia and Sapphire, in X-band at different temperatures. The data for Magnesia are taken from Refs. [4, 5]. Sapphire, a particular type of Corundum crystal (another one is Ruby), was well characterized in Refs. [6, 7].

Table 1: Properties of Materials at Cryogenic Temperatures in X-Band

Material	300 K	77 K	45 K
Magnesia	$\epsilon=9.64$ $\tan\delta=7\cdot 10^{-7}$	$\epsilon=9.64$ $\tan\delta=1\cdot 10^{-7}$	-
Sapphire	$\epsilon=11.6$ $\tan\delta=1\cdot 10^{-5}$	$\epsilon=11.36$ $\tan\delta=1\cdot 10^{-8}$ - $1\cdot 10^{-7}$	$\epsilon=11.34$ $\tan\delta=5\cdot 10^{-9}$ - $1\cdot 10^{-7}$
Quartz	$\epsilon=4.4$ - 4.6 $\tan\delta=1\cdot 10^{-4}$	$\epsilon=4.4$ - 4.6 $\tan\delta=2\cdot 10^{-6}$ - $1\cdot 10^{-5}$	$\epsilon=4.4$ - 4.6 $\tan\delta=2\cdot 10^{-6}$ - $1\cdot 10^{-5}$

Let us consider a rod packed in a quartz envelope (see Fig. 2). Good guiding properties come from the effect of total internal reflection (TIR). A wave propagating in a dielectric rod (made of Magnesia or Sapphire) with a high refractive index does not leak into a medium, like vacuum or quartz, which has a low refractive index. Remarkably, this configuration does not contain any dielectric-vacuum interfaces at a field level that can cause multipactor discharge.

ACCELERATING STRUCTURES FOR THE FCC-ee PRE-INJECTOR COMPLEX: RF DESIGN, OPTIMIZATION, AND PERFORMANCE ANALYSIS

A. Kurtulus, A. Grudiev, A. Latina, CERN, Geneva, Switzerland
S. Bettoni, P. Craievich, J.-Y. Raguin, Paul Scherrer Institut, Villigen, Switzerland

Abstract

The Future Circular Collider electron-positron (FCC-ee) pre-injector complex demands high-performance RF accelerating structures to achieve reliable and efficient acceleration of beams up to 20 GeV. In this study, we describe an analytical approach to RF design for the traveling-wave (TW) structures including a pulse compression system to meet the rigorous specifications of the FCC-ee pre-injector complex. The fundamental mode at 2.8 GHz and Higher Order Mode (HOM) characteristics were determined through the utilization of lookup tables and analytical formulas, enabling efficient exploration of extensive parameter ranges. Optimization of the structure geometry and in particular the iris parameters was performed to address key challenges including maximizing effective shunt impedance, minimizing surface fields, and effectively damping long-range wakes through HOM detuning. Moreover, we investigated the impact of beam-loading effects on the bunch-to-bunch energy spread. Comprehensive thermal and mechanical analyses were carried out to evaluate the impact on the accelerating structure performance during operation at a repetition frequency of 100 Hz.

INTRODUCTION

The proposed new baseline for the FCC-ee injector complex [1] includes an updated high-energy linear accelerator (HE linac). This design enhancement increases the number of bunches per RF pulse from two to four while reducing the repetition rate to 100 Hz. Each bunch will have a charge of 5 nC, an rms length of 1 mm, and a bunch spacing of 25 ns.

The following section provides an update on the RF design, optimization, and performance analysis, including the methodology and specific structural features of the HE linac.

RF DESIGN METHODOLOGY

A parametric study was conducted to optimize accelerator structure design. Lookup tables were generated to rapidly assess the impact of aperture radius a and iris thickness d on the first twenty HOMs of a convex cell at the synchronous frequencies. The primary design goal was to enhance shunt impedance relative to previous S-band structures [2]. The target structure was defined by an RF frequency of 2.8 GHz, RF phase advance ψ of 120° per cell, and a length L_s of 3 meters. An average aperture of 0.12λ [3] (equivalent to 12.85 mm) was selected as a suitable compromise between beam dynamics and RF considerations. The long-range transverse wake is damped through the detuning of dipole modes, eliminating the necessity for additional damping

elements. This is accomplished by tapering the aperture and iris thickness while maintaining an average aperture of 0.12λ . The design constraint requires that the transverse wakefield potential W_t remains at or below 0.1 V/pC/mm/m within the time range of 25 to 100 ns.

A SLED-type [4] RF pulse compressor was analytically designed and implemented to further optimize the performance. This device increases the peak amplitude of the RF pulses and shortens their duration by storing energy in a cavity and then releasing it in a compressed form. The resultant boost in peak RF power significantly impacts the electric field strength within the accelerator cavities, which is essential for achieving the target acceleration gradients. Consequently, the effective shunt impedance $R_{\text{eff}} = \langle G(t = T_k) \rangle^2 L_s / P_k$ (where $\langle G(t = T_k) \rangle$ is the average gradient at beam injection, L_s is the length of the structure, and P_k is the klystron power), which measures the efficiency of RF power transfer to the beam, was carefully evaluated.

OPTIMIZATION OF THE RF STRUCTURE

A parametric sweep was conducted to optimize the HE linac RF structure design based on shunt impedance calculations. Using a lookup table, iris thicknesses ranging from 2.04 mm to 6.2 mm were tested to maximize shunt impedance.

To assess tapering effects, the delta Δ parameter was introduced as an offset relative to the constant aperture structure, adjusting the first and last cell apertures while maintaining a linear variation between them. Positive delta values resulted in down-tapering (larger first cell aperture, smaller last cell), and negative values led to up-tapering. Delta was varied from -4 mm to 4 mm in 0.2 mm steps, and the highest shunt impedance was identified. Finally, a wakefield analysis was conducted using frequency-domain parameters of 20 lowest HOMs, with designs selected based on analytically calculated wakefields that remain below 0.1 V/pC/mm/m , refining the linac's aperture and iris thickness for optimal performance.

Figure 1 presents the results of a parametric sweep of maximum effective shunt impedance as a function of the delta parameter. The red traces depict the effective shunt impedance values under conditions where transverse wakefields are not constrained, providing a baseline for comparison. In contrast, the blue traces illustrate the effective shunt impedance when the transverse wakefield is limited to a threshold of 0.1 V/pC/mm/m . We observed that a delta of 2 mm achieves the highest effective shunt impedance while meeting wakefield constraints and exhibiting a low surface electric field

VARIABLE POLARIZATION SELF-LOCKED STREAKING OF ELECTRONS IN TIME WITH A PAIR OF CORRUGATED STRUCTURES

A. Malyzhenkov*, A. Aksoy, R. Corsini, W. Farabolini, A. Gilardi, A. Latina, P. Korysko¹
CERN, Geneva, Switzerland

¹also at University of Oxford, Oxford, United Kingdom

Abstract

Corrugated structures have recently been utilized for the time-resolved diagnostics of electron bunches and free-electron-laser (FEL) pulses across several FEL facilities: SwissFEL at PSI and European XFEL at DESY. This approach is simple and cost-effective, based on the self-streaking of electrons with a transverse wakefield enhanced in such structures. In this work, we optimize the design of a corrugated streaker for the wide range of beam parameters of the CERN Linear Electron Accelerator for Research (CLEAR). We report on the fabrication of corrugated plates with various corrugation parameters and their initial installation for in-air measurements at CLEAR. Variable polarization streaking can be achieved either by mechanically rotating the plates or by utilizing two pairs of corrugated streakers. Additionally, we emphasize that when streaking in the vertical (or horizontal) direction with one structure, the undesired quadrupole wakefield can be compensated by the second orthogonally oriented streaker. This allows for a significant improvement in the resolution of the method.

INTRODUCTION

CLEAR is a user facility providing an electron beam with a wide range of parameters for user experiments, summarized in Table 1 [1–4]. The layout of the CLEAR beamline is shown in Fig. 1 featuring several Test Areas for the experiments. Characterization and control of the bunch length, temporal profile distribution, and longitudinal phase space of the electron bunch are of great importance for several user experiments. Currently, such diagnostics are realized by utilizing an S-band transverse deflector driven by a dedicated klystron. The transverse deflector has a footprint of around 20 cm, excluding the waveguides, and provides a temporal resolution of ~ 100 fs for 200 MeV electron beams when measuring the streaked beam at the MTV390 screen [5].

All test areas are located downstream of the transverse deflector and the first measurement screen. Therefore, non-invasive shot-to-shot online diagnostics of the bunch length are currently not available at CLEAR, although experiments could benefit from such capabilities. Moreover, temporal diagnostics may be of significant interest for monitoring beam properties in the second beamline planned to be implemented at CLEAR, using the bending magnet BHB0400 to direct the beam in the opposite direction from the Vesper Test Area. In this work, we explore a cost-effective and elegant approach of employing a corrugated passive streaker for

Table 1: CLEAR Beam Parameters

Parameter	Value
Bunch charge	0.005 – 1.6 nC
Bunch length RMS	0.1 – 10 ps
Beam Energy	30 – 220 MeV
Beam Energy Spread	< 0.2% rms (< 1 MeV FWHM)
Bunch frequency	1.5 or 3.0 GHz
Norm. emittance	1 – 20 μm
Bunches per pulse	1 – 150
Max. pulse charge	~ 90 nC
Repetition rate	0.8333 – 10 Hz

temporal diagnostics, which was successfully implemented at SwissFEL [6] and EXFEL [7].

SIMULATION RESULTS

Each corrugated streaker installed at SwissFEL is approximately 1 m long, consisting of two pairs of corrugated streakers attached to micron-precision moving motors, with the entire setup integrated into a vacuum chamber [6, 8]. The approximate cost of a single unit is around 110 kCHF, which is roughly an order of magnitude less than that of an active C-band or X-band deflecting cavity with a power supply [6]. However, even this amount is still a significant investment for a single diagnostic system in a small medical accelerator or an electron linac at an irradiation facility such as CLEAR.

In comparison to the 6 GeV beam energy at SwissFEL, the maximum beam energy at CLEAR is limited to 200 MeV. For this energy, and considering that the shortest bunch length at CLEAR is approximately 100 fs, we optimized the design of the corrugated plates to minimize production cost and footprint. Another characteristic worth comparing is the active S-band deflector installed at CLEAR, which is approximately 20 cm long, excluding the waveguides and power supply system. We performed a series of numerical simulations assuming a corrugated plate length of only 10 cm and validated that the streaking effect, even for the shortest bunches at CLEAR, is well-pronounced and would enable reconstruction of the temporal profile of the electron bunch with a resolution similar to that of the active S-band deflector.

Figure 2 shows the results of numerical simulations at a measurement screen placed 0.5 m downstream from the corrugated streaker. In these simulations, we use the analytical model from [9] for plates with 500 μm corrugation,

* alexander.malyzhenkov@cern.ch

STUDIES OF SINGLE AND MULTI-BUNCH INSTABILITIES IN LINACS USING RF-TRACK

A. Latina, CERN, Geneva, Switzerland

Abstract

In high-intensity linacs, bunch-to-bunch effects due to the excitation of short and long-range wakefields can lead to beam instabilities and beam breakup. Wakefields can be due to resistive or geometric effects excited in the RF structures or in the beam pipe. From version 2.3.0 onwards, the particle tracking code RF-Track has been modified to implement a multi-bunch beam model that simplifies and optimises the calculation of single and multi-bunch effects. The effect of wakefields on the beam is assessed by computing the action amplification due to incoming jitter. The jitter amplification due to multi-bunch effects is evaluated using a 1 GeV electron linac example.

INTRODUCTION

Linacs for high-energy physics colliders, medical applications, compact X-ray sources, such as Inverse Compton Scattering sources, and compact accelerator-based neutron production require high-intensity beams. When high-intensity beams are injected into linacs, intensity-dependent effects such as beam loading and short- and long-range wakefields in the accelerating structures must be considered. The effect of beam loading is primarily to reduce the effective accelerating gradient available in the RF structures as high-charge bunches travel through them. The effect of wakefields degrades the beam quality by causing transverse deflections, energy loss, emittance growth, energy spread increase and ultimately, beam breakup. In this paper, we focus on evaluating the effect of wakefields on beam jitter, both in single and multi-bunch operation, using the CERN tracking code RF-Track [1]. This code can also simulate the effects of beam loading, as presented in Ref. [2].

RF-Track v2.3.0

Initially developed for the design and optimisation of a medical proton and light ion linac [3], RF-Track has evolved over the years to extend its simulation reach and range of applications, becoming the primary design tool for many projects and studies: e.g., the “Deep Electron FLASH Therapy” (DEFT) facility [4], the positron sources of SuperKEKB [5], the CLIC and FCC-ee injector linacs [6, 7], Inverse Compton scattering sources [8], and the cooling channel of a future muon collider [9].

Up to version 2.3.0, RF-Track could only simulate single bunches. It was still possible to simulate bunch-to-bunch long-range effects using the standard trick of creating a single “super bunch” with all individual bunches suitably separated in time. This workaround, while working in some cases, introduced several inconveniences: it complicated the post-processing of the output data to separate the individual

bunches; it undermined the simulation of single-bunch effects such as short-range wakefields or space-charge, whose algorithms are designed to operate in the short-range regime.

In version 2.3.0, the tracking core of RF-Track has been rewritten to handle multi-bunch beams rather than single bunches, introducing the new object Beam. In RF-Track, a “Beam” is a set of single bunches that the user can specify individually at arbitrary distances from each other. The main innovation and benefit of the new object is that it allows a specialised implementation of long-range collective effects for multi-bunch beams. For example, specific single-bunch effects such as space charge are applied to each bunch individually, while bunch-to-bunch effects such as long-range wakefields can be computed considering the large spacing between bunches using a dedicated long-range algorithm. In addition, accessing information about each bunch and analysing the results after tracking is now much easier. The new “Beam” model also increases flexibility, for example, by allowing the user to simulate bunch trains where some bunches are single particles while others are multi-particles, thus speeding up simulations where one needs to focus on a specific bunch. Moreover, the bunches can be arbitrarily and irregularly spaced, have different charges and even be of different species.

It should be noted that these changes have been implemented to maintain backward compatibility with older simulation scripts, so when the user is working with single bunches, RF-Track behaves in the same way as in previous versions.

Example of Beam Definition

The following lines provide an example declaration of a train consisting of 30 equally spaced bunches:

```
% Define a bunch
bunch = Bunch6d(mass, charge, q, phase_space);
% Define the train structure
num_of_bunches = 30; % train length
bunch_spacing = 1/3 * ns; % bunch spacing
% Define a beam
B0 = Beam(bunch, bunch_spacing, num_of_bunches);
```

If “LINAC” is an arbitrary beamline, then `B1 = LINAC.track(B0)`; is the outgoing train, where `B1{1}` is the first bunch, `B1{2}` is the second, etc.

JITTER AMPLIFICATION

Single-bunch Short-range Wakefields

A detailed explanation of the Wakefield models implemented in RF-Track was presented in Ref. [10]. The effect of short-range wakefields on a bunch, in addition to introducing correlated energy spread and slice emittance growth, is also

BEAM LOADING COMPENSATION IN CHARGE-VARYING SCENARIOS WITH RF-TRACK

J. Olivares Herrador^{*1,2}, A. Latina¹, N. Fuster-Martinez², B. Gimeno², D. Esperante^{2,3}

¹CERN, Geneva, Switzerland

²Instituto de Física Corpuscular (IFIC); CSIC-University of Valencia, Paterna, Spain

³Department of Electronic Engineering—ETSE, University of Valencia, Burjassot, Spain

Abstract

High intensity linacs based on compact accelerating RF structures suffer from beam loading effects, which result into a bunch-to-bunch energy loss as a consequence of the beam-induced excitation of the fundamental accelerating mode. To track charged particles under this effect, the code RF-Track implemented a beam loading module in version 2.2.2. For ultrarelativistic scenarios in travelling-wave structures, the simulation tool was limited to trains of bunches with equal charge per bunch. In this work, we present the latest update of the beam loading module in version 2.3.0, extending its capabilities to account for this effect in trains with different charges per bunch and allowing the performance of beam loading compensation studies in these scenarios.

INTRODUCTION

The Beam Loading (BL) effect is the gradient reduction that occurs in accelerating radiofrequency (RF) structures, when the particles traveling through it excite the fundamental mode, which exhibits a decelerating longitudinal electric field. Energy conservation requires that bunches lose energy in order to excite the mentioned mode [1]. In addition, given that standard operation discourages the damping of the fundamental mode, each bunch-induced excitation will last in the cavity for a long time. For this reason, consecutive bunches can also lose energy when they are affected by the beam induced field left by earlier ones.

A self-consistent module to simulate BL effects upon particle tracking was implemented in RF-Track's version 2.2.2 [2]. It is based on the power-diffusive model derived in Ref [3], which, for travelling-wave (TW) structures, gives the following gradient reduction equation:

$$-\frac{\partial G}{\partial t} = v_g \frac{\partial G}{\partial z} + \left(\frac{\partial v_g}{\partial z} - \frac{v_g}{r} \frac{\partial r}{\partial z} + \frac{\omega}{Q} \right) G + \frac{\omega r}{2} \mathcal{F} \tilde{I}, \quad (1)$$

where G is the gradient, ω the angular frequency, v_g the group velocity of the cavity, Q its unloaded quality factor, r/Q the normalized shunt impedance per unit length, \mathcal{F} the time-transit factor and \tilde{I} is defined as:

$$\tilde{I} = \beta_z \frac{q_{\text{bunch}}}{T} F, \quad (2)$$

with F being the form-factor of the bunch, q_{bunch} its total charge, β_z its average longitudinal velocity (normalized by the speed of light c) and T the RF period.

* javier.olivares.herrador@cern.ch

Version 2.2.2 calculated beam loading effects based on the resolution of Eq. (1) prior to tracking, as bunches with equal charge and velocity c were assumed. This limits the simulation of scenarios where particles are lost along the accelerator, or where trains with different charge per bunch are injected. For this reason, a more flexible algorithm has been implemented in version 2.3.0, whose major upgrades are presented in this conference proceedings at [4].

FLEXIBLE BEAM LOADING MODEL

The longitudinal electric field (E_z) of the fundamental mode of a lossless TW structure can be written, by means of the Floquet theorem, as the superposition of several spatial harmonics ($l \in \mathbb{Z}$) as:

$$E_z(z, t) = \text{Re} \left[\sum_{l=-\infty}^{\infty} E_l \exp(-j(k_l z + \omega t)) \right], \quad (3)$$

where j is the imaginary unit, $E_l \in \mathbb{R}$ is the amplitude of each harmonic and k_l its wave number, which satisfies the following property:

$$k_l - k_{l-1} = \frac{2\pi}{L}. \quad (4)$$

where L stands for length of each periodic cell.

Usually, TW structures are designed in a way that the phase velocity of one harmonic, l^* , is c and $k_{l^*} = \omega/c$. In this case, for an ultrarelativistic particle, the gradient reads as:

$$\begin{aligned} G(z) &= \frac{1}{L} \int_0^L dz E_z(z, \frac{z}{c}) = \\ &= \frac{1}{L} \sum_{l=-\infty}^{+\infty} E_l \int_0^L \cos\left(\frac{2\pi(l-l^*)z}{L}\right) dz \\ &= \sum_{l=-\infty}^{+\infty} E_l \left[\frac{\sin(2\pi(l-l^*))}{2\pi(l-l^*)} \right] = E_{l^*}. \end{aligned} \quad (5)$$

Equation (5) provides a physical meaning to the accelerating gradient: It is the amplitude of the spatial harmonic whose phase velocity synchronizes with the beam velocity.

Therefore, solving Eq. (1) for a single particle (G_{single}), one can compute the longitudinal electric field excited by this particle as $E_z(z, t) = \text{Re} [G_{\text{single}}(z, t) \exp(-j\omega(z/c - t))]$. With this, the longitudinal wakefield (w_l) caused by this particle upon a test particle located at a distance s can be defined as [5]:

$$w_l(s) = \frac{c}{q_{\text{single}}} \int_{-\infty}^{\infty} dt E_z(ct - s, t). \quad (6)$$

DIRECT INJECTION EXTRACTION SYSTEM INTO A HIGH FREQUENCY RADIOFREQUENCY QUADRUPOLE FOR MEDICAL APPLICATIONS

A. Mamaras^{†1}, M. Koopmans, J. B. Lallement, A. M. Lombardi, F. di Lorenzo, E. Pasino, D. Sampsonidis¹, CERN Geneva, Switzerland
¹also at AUTH, Thessaloniki, Greece

Abstract

As part of CERN's medical application research, a compact electrode system (< 30 cm) has been designed to facilitate low-current, multiparticle beam extraction and matching to a high-frequency RFQ. This study explores the innovative extraction system design and evaluates its simulation performance. Superfish (SF) and CST Studio Suite were employed to export the 2D and 3D electric field maps of the extraction system for beam dynamics simulations. Beam dynamics simulations using the Travel code have confirmed the system's ability to deliver a high-quality, low-current particle beam fully matched to a 750 MHz RFQ, capable of accelerating particles with a q/m ratio of $\frac{1}{2}$ to 1. This paper provides an overview of the key design considerations, geometry layout, and beam dynamics results.

INTRODUCTION

Hadron therapy is a well-established and effective treatment method for severe cancer cases [1]. In hospital environments, the typical accelerator complex used for hadron therapy comprises a linac pre-injector and a synchrotron that delivers the beam to treatment rooms. Standard linac pre-injectors include an ion source with its extraction system, a Low Energy Beam Transport Line (LEBT), and a Radiofrequency Quadrupole (RFQ), which accelerate and transport the beam to the next accelerating structure.

The need for sustainability and high daily performance has driven research towards designing a more compact and efficient accelerator facility. This approach aims to reduce the required space and power consumption while ensuring a high-performance, reliable, and user-friendly machine. At CERN in the framework of NIMMS a new compact extraction system has been developed to provide a multiparticle beam directly to the RFQ, eliminating the need for a LEBT and efficiently meeting low-current injection requirements.

DESIGN METHODOLOGY

The extraction system is envisioned to integrate into an experimental setup comprising a commercial RF ion source from National Electrostatics Corp. (NEC) [2] and a two-cavity RFQ operating at 750 MHz. This RFQ is capable of accelerating ions with a charge-to-mass ratio (q/m) of $\frac{1}{2}$ to 1, e. g. $^{12}\text{C}^{6+}$, $^4\text{He}^{2+}$ or H^+ , for hadron therapy [3]. Therefore, the new extraction system must be specifically designed not only to accelerate the beam to the desired energy of the RFQ but also to focus and match the beam with the Twiss parameters required by the first RFQ cavity's [†]aristeidis.mamaras@cern.ch

matching plane (MP), as detailed in Table 1. The RFQ MP is a critical reference plane at the entrance of the first RFQ cavity, where the beam parameters must be precisely matched to ensure optimal beam transmission (total acceptance) and acceleration.

Table 1: Transverse Acceptance Parameters of the First RFQ Cavity

Twiss Parameters	X plane	Y plane
Alpha	0.26	0.32
Beta / mm/mrad	0.01	0.01
Total Acc. Norm / mm · mrad	~0.80	~0.79

The extraction system consists of a fixed-shaped source electrode mounted on the plasma chamber, a puller electrode, and two additional electrodes to ensure versatility and adaptability to a wide range of particle types and energies while adjusting the matching to the input plane of the first RFQ cavity. The nominal energy provided by the extraction system is 15 keV/u, set by the input energy accepted by the first RFQ cavity with the extracted current ranging up to several μA . Given that the source initially provides a probe extraction energy of 1 keV, the remaining potential difference for extraction is 14 kV. The electrodes are metallic hollow discs with apertures sized to be at least 1.5 times the total transverse beam size in both planes, preventing electrode damage from potential beam loss.

These losses may result from possible misalignments in the extraction system or the divergence of the extracted beam. To address this, the electrodes have been designed with a thickness of 5 mm, capable of withstanding current losses up to tens of μA . To determine the optimal design configuration that meets the characteristics of the RFQ MP listed in Tables 1 and 2, a minimization algorithm incorporating the model of aperture lenses was developed [4].

Table 2: Key Characteristics and Optimized Parameters of the Extraction System

System Characteristics	
Electrodes Thickness / mm	5
Particle beam energy / keV/u	15
Probe voltage / kV	1
Total potential difference / kV	14
Total system length, d_{tot} / cm	< 30
Drift length, d_{drift} / cm	10
Optimised params	$V_{1,2}, d_{1,2,3}, r_{1,2,3}$

The algorithm defined the optimal combination of potential $V_{1,2}$ and distances $d_{1,2}$ of the two additional electrodes, as seen in Fig. 1, following a mismatch function that

ANALYSIS OF THE PANOFSKY-WENZEL THEOREM IN PILLBOX CAVITIES WITH A BEAM PIPE

L. M. Wroe, A. Latina, S. Stapnes, W. Wuensch, CERN, Geneva, Switzerland
R. J. Apsimon¹, M. Southerby¹, Lancaster University, Lancaster, United Kingdom
¹also at Cockcroft Institute, Warrington, United Kingdom

Abstract

In this paper, we derive the multipolar form of the change in transverse and longitudinal momenta of an ultra-relativistic charged particle that traverses a harmonic TM_{mn0} mode in a pillbox cavity with a beam pipe. The relevant equations are first formalised before presenting results from the numerical integration of RF cavity field maps. In particular, we show that the radial dependence of the change in transverse and longitudinal momenta through a TM_{mn0} mode has polynomial, and not Bessel, dependence.

INTRODUCTION

In 1956, Panofsky and Wenzel derived their eponymous theorem stating that the change in transverse momentum Δp_{\perp} of a rigid particle of charge e and ultra-relativistic velocity $\vec{v} = c\hat{z}$ which traverses an RF cavity supporting a mode l of resonant angular frequency ω_l and longitudinal electric field E_z is [1, 2]

$$\Delta p_{\perp}(r, \theta) = -i \frac{e}{\omega_l} \int_{-L/2}^{L/2} \nabla_{\perp} E_z(\vec{r}, t) dz. \quad (1)$$

Here L is a longitudinal length that is sufficiently longer than the RF cavity such that electromagnetic fields decay to a negligible value, $E_z(r, \theta, |z| > L) \sim 0$, and the integral limits in Eq. 1 can be replaced with $L \rightarrow \infty$.

In the case of the ultra-relativistic particle having coordinate $z = 0$ at $t = 0$ such that $t = z/c$ and the harmonic RF cavity mode having phase ψ at $t = 0$ such that $E_z(\vec{r}, t) = E_z(\vec{r})e^{i(\omega_l t + \psi)}$, Panofsky-Wenzel's Eq. 1 becomes

$$\Delta p_{\perp}(r, \theta) = -i \frac{e}{\omega_l} \int_{-\infty}^{\infty} e^{i(\omega_l z/c + \psi)} \nabla_{\perp} E_z(\vec{r}) dz. \quad (2)$$

Thus the change in transverse momentum is simple to calculate if the longitudinal electric field is known completely.

A completely general representation of the spatial component of the longitudinal electric field for a standing-wave mode l in an RF cavity is derived in Ref. [3] as

$$\begin{aligned} E_z(\vec{r}) &= \int_{-\infty}^{\infty} dk \frac{e^{ikz}}{\sqrt{2\pi}} \sum_{m=0}^{\infty} \tilde{g}_m(k) R_m(\kappa_l r) \cos(m\theta - \phi_m) \\ &= \sum_{m=0}^{\infty} E_{z,m}(r, z) \cos(m\theta - \phi_m). \end{aligned} \quad (3)$$

In this formalism, $\tilde{g}_m(k)$ has the same units as the electric field and represents the strength of the multipole of order m and ϕ_m is the orientation of the multipole of order m ($\phi_m = 0$

is normal and $\phi_m = \pi/2$ skew). Furthermore,

$$R_m(\kappa_l r) = \begin{cases} J_m(\kappa_l r), & k < k_l; \\ I_m(\kappa_l r), & \text{otherwise,} \end{cases} \quad (4)$$

where $\kappa_l^2 = |k^2 - k_l^2|$ and $k_l = \omega_l/c$ is the wavenumber of the mode.

In this representation, $\tilde{g}_m(k)$ has no dependence on radius. Therefore, if the longitudinal field E_z is completely known on the surface of a cylinder of radius a , $g_m(k)$ can be explicitly calculated as

$$\tilde{g}_m(k) = \frac{1}{R_m(\kappa_l a)} \int_{-\infty}^{\infty} \frac{dz}{\sqrt{2\pi}} e^{-ikz} E_{z,m}(a, z). \quad (5)$$

By solving Eq. 5, the longitudinal electric field is then also calculable at any point in the cavity using Eq. 3 and, from this, so too is the change in transverse momentum by Panofsky-Wenzel's Eq. 2 which becomes

$$\begin{aligned} \Delta p_{\perp} &= -i \frac{e}{\omega_l} \int_{-\infty}^{\infty} \nabla_{\perp} \left(\int_{-\infty}^{\infty} \frac{dk}{\sqrt{2\pi}} e^{ikz} e^{i(k_l z + \psi)} \right. \\ &\quad \left. \sum_{m=0}^{\infty} \tilde{g}_m(k) R_m(\kappa_l r) \cos(m\theta - \phi_m) \right) dz. \end{aligned} \quad (6)$$

From here, we present analytical and numerical results from field map integrations using MATHEMATICA [4] to derive the form of the change in transverse momentum through TM_{mn0} modes in RF cavities.

PILLBOX CAVITIES WITH BEAM PIPES

Figure 1 shows a pillbox cavity with a beam pipe and the relevant parameters used for this analysis: G is the cell length, R the cavity radius, a the beam pipe radius, and L the field map length.

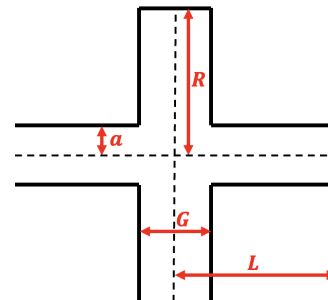


Figure 1: Cross-section of a pillbox cavity with beam pipe.

DESIGN OF A HELIUM ION LINEAR ACCELERATOR FOR INJECTION IN A PARTICLE THERAPY SYNCHROTRON AND PARALLEL PRODUCTION OF RADIOISOTOPES*

L. Nikitovic^{1, 2, †}, T. Torims² and M. Vretenar¹

¹European Organization for Nuclear Research (CERN), Geneva, Switzerland

²Riga Technical University (RTU), Riga, Latvia

Abstract

Interest in helium ions for cancer therapy is growing, motivated by their superior conformality as compared to protons or carbon. Clinical trials are starting, using beams produced by large carbon synchrotrons. To exploit the potential of this new ion, a compact synchrotron is being designed to accelerate helium and protons at treatment energies, for about half the size of a carbon machine. The helium linac is designed to operate at a higher duty cycle than the one required for synchrotron injection. Beam pulses can be sent to target-producing radioisotopes, in particular alpha emitters to be used for targeted alpha therapy of cancer.

The 352 MHz linac is made of 3 sections. To increase the efficiency with respect to a standard Drift Tube Linac (DTL), the first section from 1 to 5 MeV/u is made of a Quasi-Alvarez DTL, a structure combining high efficiency and smooth beam optics. Only this section is powered when injecting helium ions into the synchrotron. The second and third sections of the DTL type have energies of 7.1 MeV/u, the threshold for the production of ²¹¹At, the most widely used alpha emitter, and 10 MeV/u, for the production of other radioisotopes.

INTRODUCTION

Helium ions can be effectively used for production of several radioisotope species of medical interest, in particular those used for Targeted Alpha Therapy (TAT). This technique involves linking alpha-emitting radioisotopes to a carrier that is injected and absorbed by cancerous cells, thus delivering an intense and localized radiation dose. Investigations of the usage of TAT on tumors such as prostate cancer, neuroendocrine tumors, or brain cancers are progressing, with several ongoing clinical trials [1].

In parallel, there is a renewed interest in directly using helium ions for cancer treatment, related to their better conformality compared to protons or carbon ions [2]. Treatment of deep-seated tumors at beam energy of 250 MeV/u can be realized after acceleration in a compact synchrotron of the He²⁺ beam provided by a linac injector [3, 4].

To satisfy both requirements above, the design of a linear accelerator that can inject helium ions into a therapy synchrotron and produce in parallel a wide range of therapeutic radioisotopes is presented in this paper. Modifying the synchrotron injector linac with the addition of two

accelerating tanks and dimensioning cooling system and power supplies for operation at higher duty cycle can provide with minor investment an effective system for radioisotope production. Operation at 50 Hz repetition frequency with pulse length of 2 ms (10 % duty cycle) can provide enough radioisotope doses as required by a medium-size hospital [5]. One linac pulse out of 50 will go to the synchrotron that operates at 1Hz repetition frequency.

The layout of the complete facility for helium ion therapy and production of radioisotopes is presented in Fig. 1 [4]. After the linac, a magnet allows choosing the beam destination between the radioisotope production target and the synchrotron.

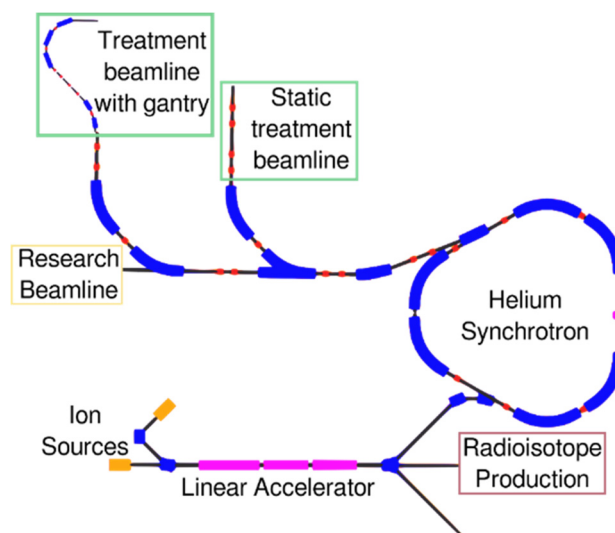


Figure 1: Layout of compact cancer therapy facility [4].

LINAC DESIGN

The linac as synchrotron injector must deliver 5 mA of He²⁺ ions at the energy of 5 MeV/u, as required for multi-turn injection [4]. For production of ²¹¹At, the most promising alpha emitter for TAT [6], the linac has to provide an additional acceleration up to 7.1 MeV/u. An additional section to 10 MeV/u allows production of other radioisotopes like ⁴⁷Sc, ⁶⁷Cu and ¹²³I [7-9].

The proposed linac is made of three cavities, all at 352 MHz frequency. The first structure is a Quasi-Alvarez Drift Tube Linac (QA-DTL) [10]. This structure has been selected since it presents a higher shunt impedance compared to a conventional DTL, and for light ions has comparable shunt impedance to IH-DTL structures with cleaner beam optics [11]. The QA-DTL is followed by two

* This study was partially supported by the European Union H2020 research and innovation programme under GA 101008548 (HITRIplus).

† lazar.nikitovic@cern.ch

THE FOUR BEAM DESTINATIONS FOR THE COMMISSIONING OF THE ESS NORMAL CONDUCTING LINAC

Elena Donegani^{*,1}, Vincent Bertrand², Ibon Bustinduy³, Viatcheslav Grishin¹, Tara Hodgetts⁴, Carlos Neto¹, Anders Olsson¹, Laurence Page¹, Marcos Ruelas⁴, Tom Shea¹

¹European Spallation Source (ESS) Lund, Sweden

²Pantechnik, Bayeux, France

³ESS Bilbao, Zamudio, Spain

⁴RadiaBeam Technologies, Santa Monica, CA, USA

Abstract

The commissioning of the Normal Conducting Linac (NCL) of the European Spallation Source (ESS) in Lund (Sweden), started in September 2018 and was completed in July 2023. The four NCL commissioning phases required the design, procurement, test, installation and operation of four distinct beam destinations in order to safely dump the proton beam and measure the current of protons with energy of 75 keV in the LEBT, 3.6 MeV in the MEBT, 21 MeV in the DTL1, and up to 74 MeV in the DTL4.

Each beam destination was operated under UHV, and designed to be as compact as possible while withstanding the Fast Tuning mode (62.5 mA, 5 μ s, 14 Hz), and the Slow Tuning mode (62.5 mA, 50 μ s, 1 Hz). The EPICS-based control system was fundamental for five main reasons: (1) the control of the motion in and out of the beam line, (2) the high voltage control in the [0, -1000 V] range, (3) the monitoring of the water cooling systems, (4) the proton current measurements and (5) the timing synchronization with the overall ESS NCL. Key milestones and measurements results are described to demonstrate the proton transport at the nominal current of 62.5 mA during each of the four commissioning phases.

THE ESS NCL COMMISSIONING: HISTORICAL BRIEFING FROM THE POINT OF VIEW OF THE BEAM DESTINATIONS

The European Spallation Source (ESS [1]) is located in Lund (Sweden) and it will be a 5 MW pulsed neutron source once 2 GeV protons will be accelerated onto the ESS tungsten target. Once fully commissioned, the ESS proton accelerator will produce 2.86 ms long protons pulses at a repetition rate of 14 Hz. The nominal proton current of the ESS accelerator is 62.5 mA. The commissioning of the ESS Normal Conducting Linac (NCL) was completed in four stages between 9/2018 and 7/2023 (see Fig. 1). Correspondingly, four beam destinations (namely LEBT, MEBT, DTL1 and DTL4 FC i.e., Faraday cups) were workhorses to safely dissipate the beam power and measure the proton current as well as the pulse length (see Table 1). The beam destinations were more compact and less expansive with respect to the usually

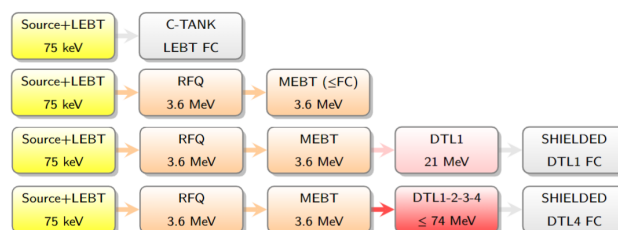


Figure 1: The four phases of the commissioning with the location of the beam destinations.

bulky beam dumps. Radiation transport calculations were performed to design the beam destinations, to quantify the beam-induced activation, to enable the SCL installation in parallel to the NCL commissioning, and for dismantling purposes within a few weeks of cool-down. Thermo-mechanical simulations were fundamental to define the operational limits in planned, unplanned and potential failure scenarios. The control system was based on EPICS [2] and enabled the successful operation of all the beam destinations that required water cooling, motion in/out of the beam line, HV to suppress secondary electrons, timing synchronization and the data acquisition. The proton current was measured between 0.1 mA to 62.5 mA with an accuracy of better than 1% and a time resolution better than 1 μ s. In this paper, highlights and key references are given for each unique beam destination.

SOURCE TUNING WITH THE LEBT FC

The beam destination in the Low Energy Beam Transport (LEBT) section of the ESS linac was designed at ESS and manufactured by Pantechnik [3]. It contributed to the test of the ESS source at the INFN LNS in Italy, and then to the LEBT commissioning at the ESS. It can withstand 2.86 ms long pulses of 75 keV protons at the nominal current and 14 Hz (see Fig. 2, with pulses acquired during the first test of the LEBT chopper at 12 kV). For instance, the optimal source settings were found with the LEBT beam destination by scanning five key parameters [4]: the three coils confining the magnetic field inside the plasma chamber within the ESS source, the input RF power to the magnetron and the hydrogen flux. Moreover, the LEBT beam destination quantified the impact of the source repeller on the space charge compensation in the extraction region [5].

* elena.donegani@ess.eu

INTEGRATED APPROACH FOR ESS PERSONNEL SAFETY SYSTEMS

J. Lastow[†], A. Farshidfar, A. Abujame, A. Nordt, A. Andersson, A. Petrushenko, C. Webber, D. Plotnikov, D. Daryadel, J. Gustafsson, J. Grönvall, L. Nunes, M. Zmuda, M. Carroll, M. Eriksson, M. Mansouri, N. Naicker, P. Holgersson, R. Foroozan, V. Harahap, Y. Takzare
European Spallation Source ERIC, Lund, Sweden

Abstract

The European Spallation Source (ESS) is a state-of-the-art research facility currently under construction in Lund, Sweden. Upon project delivery, ESS will host the most powerful linear proton accelerator and a spallation target capable of producing the brightest neutron source in the world. In order to enable safe commissioning and operation of these potent systems, each system has a dedicated personnel safety system (PSS). Together they make up the ESS PSS, an integrated system of several PSS across the facility. These systems communicate with each other through a centralised interlink system, and together determine if the facility is ready for proton beam generation in the Accelerator and consequently neutron production at the Target Station. This paper provides a summary of the inner workings, along with a discussion on the approach and proposed strategies for overcoming the identified challenges.

INTRODUCTION

The European Spallation Source (ESS) facility consists of three main parts: the accelerator, target station, and a suite of neutron instruments.

The ion source, which is the first part of the accelerator, generates protons through evaporating electrons from hydrogen gas. The protons are then lead through normal conducting and superconducting accelerating structures to reach 96 % of the speed of light. The proton beam is then directed through a dogleg with bending magnets to the target station, which is referred to as Beam on Target (BoT). During normal operation, this is the primary beam destination. However, in certain circumstances, the beam may be directed to beam stops distributed in the accelerator tunnel. At the target station, the high-energy protons collide with a rotating tungsten target wheel, which releases neutrons through spallation. The neutron beams are then moderated, tuned and guided through a shielding structure (referred to as the Bunker) to experimental stations referred to as neutron instruments. There, researchers can use the particles as a probe for studying the inner structure, as well as the dynamic behaviours, of a selected sample for a broad range of scientific fields and endeavours. The initial instrument suite consists of 15 neutron instruments and one test beamline [1].

There are a number of hazards related to these systems, mainly radiation-related hazards such as prompt ionizing radiation from the proton beam and neutron beams, and gamma radiation from the target and moderators. ESS employs systems and administrative procedures to ensure the

safety of personnel in the presence of radiation. In this regard, the key systems are the personnel safety systems (PSS). They are primarily safety interlock systems, which ensure that sources of prompt radiation are switched off to protect personnel in beam enclosures (e.g. accelerator tunnel, experimental stations, etc.) from exposure to prompt radiation, prevent entry to beam enclosures while sources are energized, and switch them off when designated predefined access functions are violated. Each part of the machine has a dedicated PSS: Accelerator PSS (ACC PSS), Target Station PSS (TS PSS), Bunker PSS, and several Instrument PSS. The full scope of PSS also includes e.g. accelerator test stands.

BACKGROUND

The PSS are designed consistently across the ESS facility in order to reduce design, installation, commissioning and maintenance cost and effort, and more importantly to improve system reliability. Each PSS is built using fail-safe Programmable Logic Controllers (PLC) and distributed Input/Output (I/O) modules with redundant sensors and actuators. Safety Instrumented Functions (SIF) are derived from the risk assessment and hazard analyses process, following the functional safety standard IEC 61511 [2]. The boundaries of the area in which PSS is responsible for mitigating designated hazards, i.e. *PSS controlled areas*, are also defined in the process. The SIFs are defined to e.g. switch off the hazardous equipment if an intrusion into the area is detected by the position monitoring switches on the access doors, or if an emergency switch-off button (ESOB) is pressed. For example, regarding an instrument PSS that entails closing a beam shutter (or *instrument shutter*) to block neutron particle flow to the experimental station. There are also SIFs related to radiation monitors that interface the PSS, e.g. a radiation monitor by the instrument shutter verifies the shielding integrity of the shutter when it is closed. If these radiation monitors alarm, the hazardous equipment is also switched off.

INTEGRATED SYSTEM

The personnel safety systems at ESS operate independently to support the safe operation of various parts of the machine and neutron instruments. However, they need to also work in concert to mitigate designated hazards. Most hazard controls methods are implemented locally, but in certain circumstances, a PSS requires to escalate an issue to ESS PSS and switch off the proton beam to target. The systems need to communicate with each other, and together determine if the facility is ready for proton beam genera-

[†] jessica.lastow@ess.eu

BEAM LOSS MECHANISMS IN THE PIP-II LINAC AND BEAM TRANSFER LINE AT FERMILAB*

Abhishek Pathak[†], Olivier Napoly, Fermi National Accelerator Laboratory, Batavia, IL, USA

Abstract

Beam loss in high-intensity H- linacs, such as the PIP-II linac at Fermilab, is a critical challenge that requires comprehensive study and understanding to ensure efficient and safe operation. This study explores the various beam loss mechanisms encountered in the PIP-II linac and its beam transfer line, drawing parallels from other high-intensity H- linacs. Key loss mechanisms include residual gas stripping, where H- ions interact with residual gas molecules leading to electron detachment; field stripping, caused by the interaction of H- ions with magnetic fields; and intra-beam stripping, resulting from interactions within the beam itself. Beam halo formation, particularly due to Twiss function mismatch, is another significant source of beam loss, which can be exacerbated by Landau damping mechanisms. Adhering to the 1 W/m loss criterion is essential to maintain hands-on maintenance capability and ensure the longevity of the accelerator components. By understanding these mechanisms and implementing targeted mitigation strategies, the PIP-II linac can achieve its design goals while maintaining safe and efficient operations.

INTRODUCTION

The Proton Improvement Plan-II (PIP-II) [1] at Fermilab features an 800-MeV superconducting linear accelerator (Linac) and a comprehensive beam transfer line [2] to enhance H- delivery to the Booster (see Fig. 1). The superconducting Linac, composed of continuous wave (CW)-capable structures and cryomodules, operates with an average H- beam current of 2 mA and accelerating the beam from 2.1 MeV to 0.8 GeV.

At such high beam intensities, beam transmission is of great concern, as the beam loss mechanisms in an H- linac like PIP-II are more numerous than in a proton linac. Some of the primary sources of the beam loss in a H- ion linac involves Intra-beam stripping, magnetic stripping, gas stripping, black body radiation, RF transient from the ion source, dark current from ion source, H+ capture and acceleration, and beam halo formation followed by beam mismatch along different sections of the linac or along the Beam Transfer Line. This article primarily investigates three of these mechanisms: intra-beam stripping, magnetic stripping, and beam halo formation due to beam mismatch.

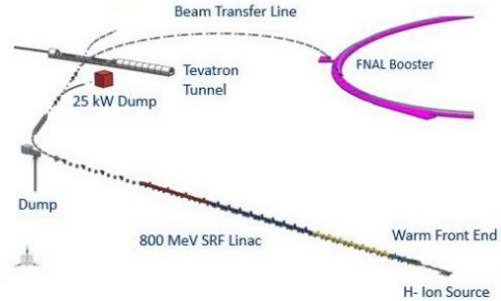


Figure 1: Schematic layout of the PIP-II Linac and associated beam transfer line: The diagram illustrates the 800 MeV SRF Linac, warm front end, H- ion source, beam transfer line, and the connection to the FNAL Booster.

INTRABEAM STRIPPING

Intrabeam stripping is a key beam loss mechanism in high-intensity H- ion accelerators, occurring when electrons are stripped from H- ions due to Coulomb interactions within the beam. This process can result in the production of neutral hydrogen atoms (H⁰) or protons (H⁺), leading to potential beam losses.

The probability of intrabeam stripping per unit length, P_{strip} , is given by:

$$P_{\text{strip}} = N \cdot \frac{\sigma_{\text{strip}}}{8\pi^2 \sigma_x \sigma_y \sigma_z \gamma^2} \cdot F(v_{\text{rel}}) \quad (1)$$

where N is the number of particles per bunch, σ_{strip} is the stripping cross-section, σ_x , σ_y , and σ_z are the RMS beam sizes, γ is the Lorentz factor, and $F(v_{\text{rel}})$ is a form factor that depends on the relative velocity between particles.

The stripping cross-section σ_{strip} is expressed as:

$$\sigma_{\text{strip}} = \frac{C}{v_{\text{rel}}^2} \quad (2)$$

where C is a constant dependent on the beam parameters, and v_{rel} is the relative velocity between particles. The form factor $F(v_{\text{rel}})$, which accounts for the distribution of velocities within the beam, is:

$$F(v_{\text{rel}}) = \left(\frac{2 - \sqrt{3}}{\sqrt{3}(\sqrt{3} - 1)} \right) \left(\frac{v_x + v_y + v_z}{\sqrt{v_x^2 + v_y^2 + v_z^2}} - 1 \right) + 1 \quad (3)$$

Analysis of the PIP-II superconducting linac and Beam Transfer Line shows that the fractional particle loss rate, total particle loss, fractional power loss, and cumulative power loss are within acceptable limits. As illustrated in Fig. 2, the fractional particle loss rate ($\frac{1}{N} \frac{dN}{ds}$) and integrated particle

* This manuscript has been authored by Fermi Research Alliance, LLC under Contract No. DE-AC02-07CH11359 with the US Department of Energy, Office of Science, Office of High Energy Physics.

[†] abhishek@fnal.gov

COLD TEST RESULTS OF PRE-PRODUCTION PIP-II SSR2 CAVITIES WITH HIGH-POWER COUPLERS IN THE FERMILAB SPOKE TEST CRYOSTAT*

A. Sukhanov[†], C. Contreras-Martinez, C. Grimm, B. Hanna, B. Hansen, S. Kazakov, T. Khabiboulline, M. Parise, D. Passarelli, Y. Pischalnikov, D. Porwisiak, V. Roger, J. Subedi, A. Syed, P. Varghese, S. Wijethunga, V. Yakovlev, Fermilab, Batavia, IL, USA

Abstract

As part of the PIP-II project at Fermilab, a pre-production cryomodule featuring 325 MHz Single Spoke Resonator type 2 (SSR2) superconducting RF cavities is under construction. These SSR2 cavities are fabricated by industry partners and undergo initial cold testing at our collaborating institution, IJCLab in France, utilizing low-power coupler. Subsequently, the cavities are subjected to final qualification at Fermilab, complete with tuner and high-power coupler assemblies. This paper provides an overview of the ongoing efforts dedicated to high-power testing of jacketed SSR2 cavities in the Spoke Test Cryostat (STC) at Fermilab. Performance parameters obtained from these tests are presented, offering valuable insights into the cavities' operational characteristics and readiness for integration into the PIP-II cryomodule.

INTRODUCTION

The Proton Improvement Plan-II project (PIP-II) is built at Fermilab to deliver intense neutrino beam to LBNF-DUNE experiment [1]. PIP-II utilizes continuous-wave (CW) Superconducting RF (SRF) linac to accelerate H^+ ions up to 800 MeV. For efficient performance PIP-II linac is composed of five different types of cavities. Thirty five Single Spoke Resonator Type-2 (SSR2) cavities operating at 325 MHz and assembled in seven cryo-modules accelerate beam from 35 to 185 MeV [2].

Seven pre-production jacketed SSR2 cavities were fabricated by the Fermilab industry partners. Six of these cavities from one of the vendors were initially cold tested at IJCLab in France with low-power coupler (LPC). Results of this testing were discussed elsewhere [3]. SSR2 cavities from IJCLab and one from the second vendor were delivered to Fermilab for assembly with tuner and high-power coupler (HPC) and final testing and qualification at the Fermilab Spoke Test Cryostat (STC) before installation into the pre-production SSR2 cryo-module.

The Fermilab STC facility (see Fig. 1) is capable of cold testing of four out of five types of PIP-II SRF cavities: both 325 MHz SSR type 1 [4] and type 2, and 650 MHz 5-cell elliptical Low and High beta (LB650, HB650) cavities [5]. RF tests at STC could be performed in LPC and HPC configurations. Initially, SSR2 cavities received at Fermilab from IJCLab, were tested with LPC to verify and

cross-check testing procedures between different test setups in our institutions. Five such tests were performed on two cavities [3]. One SSR2 pre-production cavity was delivered to Fermilab recently from another vendor. Initial performance evaluation of this cavity was performed at STC in LPC setup.

After initial verification, cavities were assembled with high-power coupler and tuner. In this paper we report on ongoing efforts of HPC testing of SSR2 cavities at STC.



Figure 1: Spoke Test Cryostat facility at Fermilab.

STC TEST SEQUENCE

Cavity Preparation and Installation

Jacketed SSR2 cavities were shipped to Fermilab assembled with LPC and under vacuum in RF/beamline volume. When no verification with LPC at STC were required, or after the STC LPC testing, cavities underwent installation of high-power coupler [6]. Cavities assembled with HPC were delivered to STC for installation of tuner and instrumentation. Typical instrumentation setup included temperature sensors at the cavity Helium vessel (top, bottom, middle), tuner arm and motor windings, coupler ceramic window flange and 5 K and 80 K intercepts; magnetic sensors at the vessel and beam pipe; heater at the coupler ceramic window flange. Subsequently, cavities were inserted into the STC cryostat, Fig. 2, where air (warm) side of the coupler was assembled and connected to the RF distribution system and thermal connection of the coupler 80 K intercept to the STC high-temperature thermal shield (HTTS) was done. Note, that because STC did not have low-temperature thermal shield, coupler 5 K intercept was not connected. After making cryogenic and beamline vacuum

* This manuscript has been authored by Fermi Research Alliance, LLC under Contract No. DE-AC02-07CH11359 with the U.S. Department of Energy, Office of Science, Office of High Energy Physics.

[†] ais@fnal.gov

HIGH ORDER MODES SPECTRA MEASUREMENTS IN 1.3 GHz CAVITIES FOR LCLS-II*

A. Lunin†, T. Khabiboulline, A. Sukhanov, V. Yakovlev, Fermilab, Batavia, USA

Abstract

Fermilab recently completed production and testing of 1.3 GHz cryomodules for the LCLS-II project. Each cryomodule consists of eight TESLA-shaped superconducting elliptical cavities equipped with two High Order Mode (HOM) coupler ports. Measurement of the HOM spectrum is part of the incoming quality control of cavities at room temperature and the final qualification cold test of cryomodules at the Cryomodule Test Facility (CMTF). In this paper we describe the procedure for measuring the HOM spectrum along with further data processing. Finally, we present accumulated statistics of individual HOM frequencies and quality factors related to various cavity vendors and discuss the possible contribution of HOMs to heat loads and beam dynamics.

INTRODUCTION

Advances in superconducting technologies result in realization of many projects of particle accelerators operating both in continuous mode and in modes with high duty factors of the beam current (XFEL, LCLS-II, ILC). Superconducting (SRF) cavities are a good resonant system with a spectrum of modes having very high-quality factors. A beam of charged particles can potentially cause resonant excitation of a particular High Order Mode (HOM) and lead to both large beam power losses and dilution of the beam emittance. Due to the nature of SRF cavities, they have a random eigen spectrum, and coherent HOM excitation becomes an inherently probabilistic problem that is very difficult to evaluate [1]. Note that knowing the exact HOM stochastics, we can estimate the regenerative beam breakup instability, which is critical for machines with high beam current. Thus, direct measurement of the HOM parameters under operating conditions allows us to obtain a reliable model of the interaction of the beam with the

cavity HOM spectrum. In addition, monitoring HOM spectra allows any deviations to be identified earlier and notifies the supplier of non-conforming cavity fabrication. As part of the LCLS-II collaboration, Fermilab was responsible for the production and testing of twenty 1.3 GHz cryomodules [2]. For technological purposes, two independent companies (vendor A and vendor B) with approximately equal contributions were selected to manufacture SRF cavities. When a cavity is received from a vendor, it follows standard cryomodule assembly procedures, including a series of incoming quality checks (QC). Figure 1 shows the workflow for final assembly of the LCLS-II cryomodule in the high-bay ICB building and subsequent high power RF testing at the dedicated Cryomodule Test Facility (CMTF) at Fermilab. Measurements of the HOM spectra of the cavities were taken during tests in the CMTF after the cooling the cryomodule to 2K and tuning all fundamental power couplers (FPC) to a nominal external coupling of 4E7. After post-processing the raw data, the sorted HOM parameters are recorded in the online traveller database for each delivered cryomodule.

RF MEASUREMENTS OF HOM SPECTRA

The layout of the 9-cell 1.3 GHz cavity for the LCLS-II project is illustrated in Fig. 2. The cavity has an FPC port and three auxiliary ports, including two downstream and upstream HOM couplers. To measure the HOM spectrum, we recorded signal transmission from HOM1 ports to HOM2 ports. Since the cryomodule is being tested inside a concrete cave used as radiation shielding, there are approximately 20 meters of $\frac{3}{8}$ -inch diameter Heliax coaxial cables connecting the auxiliary ports to the low-power electronics rack located outside the cave. These HOM cables were temporarily used to connect to the vector network analyser (VNA) ports to measure the S21 transmitted signal. Typical

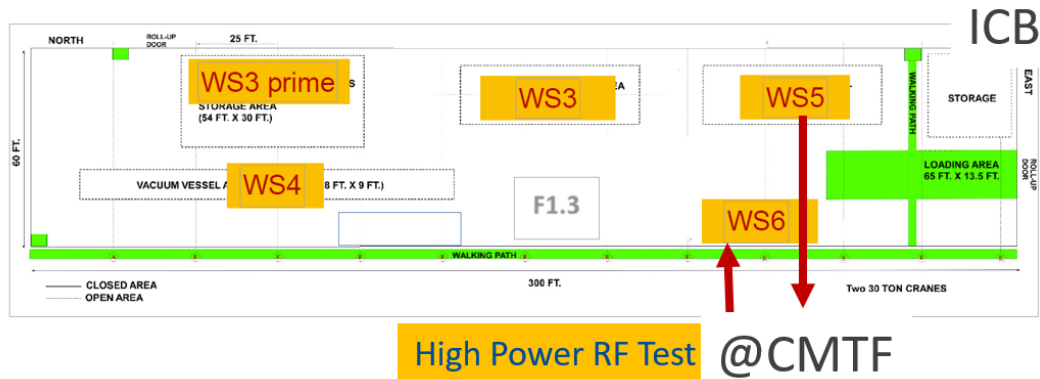


Figure 1: LCLS-II cryomodule assembly workflow at a series of workstations (WS) in the high-bay ICB building and final RF testing in the CMTF facility at Fermilab.

* Work supported by Fermi Research Alliance, LLC under Contract No. DE-AC02-07CH11359 with the U.S. Department of Energy

† lunin@fnal.gov

SUCCESSFUL CLEANROOM INSTALLATION OF PIP-II SSR2 COUPLER USING ROBOTIC ARM *

C. Narug[†], D. Passarelli, G. Wu, M. Parise, T. Aiazzi,
D. Bice, J. Helsper, Fermilab, Batavia, IL, USA
C. Denton, Northern Illinois University, Dekalb, IL, USA
A. Ciaramella, University of Pisa, Pisa, Italy

Abstract

To minimize the risk of contamination during the assembly of SRF cavities, remote installation techniques are needed. Recent developments at Fermilab have initiated the process of employing robotics for cavity assembly. Various alignment strategies were prototyped and evaluated. A remotely controlled robotic arm was successfully used to align and install couplers on prototype PIP-II SSR2 cavities in a cleanroom environment. This process highlights the potential for extending these techniques to the installation of other cavities and associated components in the future.

MOTIVATION

To reduce the risk of contamination on the superconducting surfaces of SRF cavities, specialized assembly tooling sets are typically employed to attach components in a cleanroom environment. Each new assembly application often necessitates the development of a unique set of tooling and corresponding procedures. Despite efforts to standardize tooling across projects [1], contamination risks persist, primarily due to manual operation and adjustments by technicians. To address this issue, Fermilab has initiated work on utilizing robotic arms for the assembly of Superconducting Radio Frequency (SRF) cavities, aiming to significantly minimize contamination. The first intended application for this assembly process is the assembly of couplers onto the Proton Improvement Plan-II (PIP-II) Single Spoke Resonators Type 2 (SSR2) cavities.

ASSEMBLY CELL

When selecting a suitable robotic arm, key considerations included safety features, cleanroom compatibility, payload capacity, and ease of use. After evaluating the options available on the market, a 6-axis robotic arm was chosen. This cobot, with a payload capacity of 16 kg, is certified for use in cleanrooms up to ISO 14644-1 Class 5. The robotic arm also come equipped with various safety features, remote control capabilities and force-sensitive tool flanges that allow the arm to stop automatically in the event of a collision. Additionally, the arm can be programmed via an attached tablet, which reduces the development time for specific applications [2].

In preparation for testing assembly methods on the actual SRF cavity, an initial assembly was conducted at a dedicated

test station outside of the cleanroom. This test station was constructed using the same components as the final setup, including cavity supports and rail systems, to closely replicate the cleanroom environment. Multiple test assemblies were performed using 3D-printed components, which allowed for the rapid iteration and evaluation of designs for attaching the coupler to the robotic arm and supporting the cavity on the structure. The flexibility of 3D printing enabled quick modifications, providing valuable insights before producing cleanroom-compatible components. The layout of the test station is shown in Fig. 1.

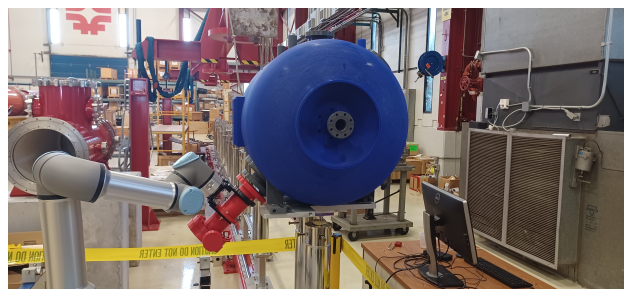


Figure 1: Test station setup for initial robotic assembly trials.

Using these prototype components, four potential assembly processes were developed. These methods were used to create a series of pre-programmed waypoints for the robotic arm, which would later be applied in the cleanroom. Before relocating the setup to the cleanroom, a successful assembly was carried out using a plastic cavity and coupler, as well as with a prototype coupler and a prototype cavity that required reprocessing. The effectiveness and specifics of each of these methods will be discussed in detail later in this paper.

INSTALLATION PROCESS

Using the procedure developed at the test station, the installation of the coupler onto the cavities was performed in a cleanroom at Fermilab. To prepare for assembly, all components were thoroughly cleaned before being brought into the cleanroom. The coupler was then mounted onto the robotic arm using a set of L-bracket tooling, with alignment pins installed on the flange of the coupler.

To prepare the cavity for the installation, four bolts were removed from the flange, which was then blown with pure nitrogen to eliminate any particles. The robotic arm was used to position the coupler and align it with the cavity. This aligned position was saved as a waypoint. Afterward, the

* Work supported by Fermi Research Alliance, CONF-24-0248-TD

[†] cnarug@fnal.gov

STANDARDIZATION OF ANCILLARY INSTALLATION TOOLING FOR SRF CAVITIES AT FERMILAB *

C. Narug[†], M. Parise, D. Passarelli, L. Ristori, H. Park,
V. Rogers, J. Helsper, Fermilab, Batavia, IL, USA
C. Denton, I. Salehinia, Northern Illinois University, Dekalb, IL, USA

Abstract

For assemblies of cavities in cleanrooms, single-use tooling systems are made for the alignment and installation of ancillary components such as couplers and bellows. To minimize the number of tooling sets created, a design has been created to standardize alignment features to allow for assembly of different components with one set of tooling. A prototype set of tooling has been developed to with the required degrees of freedom for multiple assemblies while minimizing deformation during the assembly process. Prototype designs have been created for PIP-II SSR2 and 650 Cavities and for AUP Crab Cavities. Using 3D printing, this tooling can be quickly adjusted to allow for different ancillary components. The development process and status of the design will be discussed.

INTRODUCTION

In the pursuit of higher gradient Superconducting Radio Frequency (SRF) cavities, there is a need to further reduce contamination inside superconducting cavities. One of the primary sources of contamination occur during the installation of ancillary components during production. To reduce sources of contamination, alignment tooling is used to support components while increasing the distance of people to the open cavities. To serve as backups for the robotic assembly procedures being developed [1], a set of universal component installation tooling has been developed. The primary purpose of the redesign of the tooling was for the Proton Improvement Plan-II (PIP-II) Single Spoke Resonators Type 2 (SSR2) Cavities. For this project the tooling was initially designed for the only the coupler installation processes. Additional requirements by the PIP-II project required expanding the use of the tooling for installing 650 MHz cavity coupler assemblies. Additional design feedback has been received from projects, such as for the High Luminosity LHC Accelerator Upgrade Project's (AUP) Crab Cavities. Feedback and design details have been refined to allow the tooling to be used for all of the projects and future projects to allow for the tooling to be used with minimal functional changes.

Previous Tooling

The initial set of tooling was developed exclusively for use for the installation of SSR2 couplers. This tooling can be seen in Fig. 1. The tooling had multiple drawbacks that made it difficult to use in a production environment. The

specific issues faced with the tooling were that there were too many points of adjustment, the structure was unstable, and the internal mechanisms limited the orientation of the components.

Expanding on some of the limitations, the adjustment mechanism in the tooling had redundant points of contact for aligning components. For example, to the horizontal position was held and aligned using two threaded rods. This mechanism required tightening and loosening threaded rods to gradually shift the coupler horizontally and vertically. The multiple adjustable mechanisms led to a design that was inherently unstable and which had difficulty supporting components. The mechanisms also limited the

Due to the combination of adjustment features used, the orientation of the adjustment assembly was limited. The mechanism that was most limited by these features was the mechanism that pushed the assembly along the track. The mechanism was a threaded rod with a foot that pushed the main alignment tooling along the track. While the mechanism did allow for smooth sliding as the foot was not fixed to the main alignment tooling, it also made the mechanism unable to support different orientations and required the device to be mounted at 45 degrees. These limitations in the initial tooling design were the initial motivation for redesigning the overall tool design.

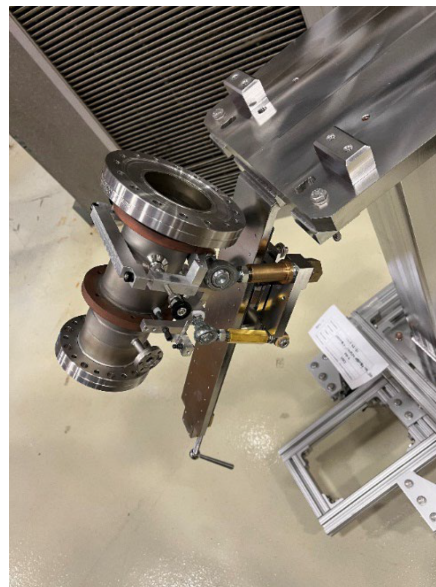


Figure 1: Initial SSR2 coupler alignment tooling.

* Work supported by Fermi Research Alliance, CONF-24-0249-TD

[†] cnarug@fnal.gov

TESTING OF THE SSR2 SRF CAVITY TUNER FOR PIP-II at 2 K*

C. Contreras-Martinez[†], A. Sukhanov, P. Varghese, M. Parise, Y. Pischalnikov,
J. Holzbauer, D. Passarelli, V. Roger, Fermilab, Batavia, IL, USA

Abstract

The PIP-II linac will include thirty-five 325 MHz Single Spoke Resonators Type 2 (SSR2) cavities. Each cavity will be equipped with a tuner for resonance control. The tuner consists of mechanical frame with a motor for coarse frequency tuning and a piezoelectric actuator for fine frequency tuning. The tuner was tested for the first time at Fermilab on an SSR2 cavity. This dressed cavity-tuner system was tested at the single spoke testing cryostat (STC) in Fermilab at 2 K. The tuner performance was evaluated and is presented. Lastly, cavity-tuner mechanical modes were measured via the piezos.

INTRODUCTION

The SSR2 cavities are one of five classes of superconducting RF (SRF) cavities that will form part of the proton improvement plan (PIP)-II linac under construction at Fermilab. The cavities use an SRF tuner to keep them on resonance to accelerate the beam to the specified energy efficiently. The cavity will use a double lever tuner which is similar in design to the SSR1 tuner [1]. It can compensate for slow-coarse frequency detuning as well as fast-fine frequency detuning.

The tuner can only compress the cavity; therefore, the frequency of the warm cavity is set to have a positive frequency offset of ≤ 130 kHz (see Table 1) when cooled to 2 K. The slow-coarse frequency component of the tuner, composed of a stepper motor, is used to compensate for this deviation. Microphonics and helium pressure fluctuation require the use of a fast-fine frequency tuning component. The fast-fine tuner component consists of two piezoelectric actuator capsules. Accelerated lifetime and irradiation tests at Fermilab demonstrate that the stepper motor and piezo will survive prolonged operation far exceeding the typical linac lifetime of 25 years [2,3].

The frequency tuner performance was measured when the SSR2 cavity was cooled to 2 K. Additionally, the mechanical modes of the cavity-tuner system were measured via the piezos. The cavity was placed in the Spoke Resonator Test Cryostat (STC) facility at the Meson Detector Building (MDB) at Fermilab, pictured in Fig. 1. The results are compared to the project specifications [4] and to the results from the Irène Joliot-Curie laboratory (IJCLab) test in France [5].

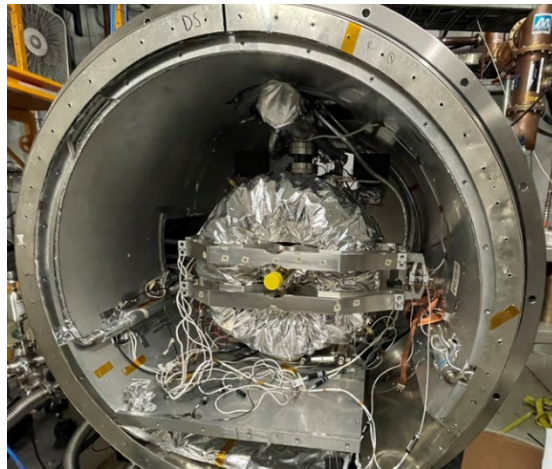


Figure 1: 325 MHz SSR2 cavity with tuner and other ancillaries installed at the MDB facility.

SLOW-COARSE TUNING COMPONENT

Pivoting Motor Lever Dislocation

After installing the tuner on the cavity the tuner probe gap was set to 1 mm. This gap is between the two probes on the tuner arms and cavity. The purpose of the gap is to avoid any excessive compression of the cavity by the tuner during cool down and measure the frequency change of the cavity solely due to cool down effects. The initial frequency (shown as 0 position in Fig. 2) is the frequency due to cool down effects (tuner was disengaged). An estimate of 60 k steps is needed to close the 1 mm gap between the probes and cavity (though due to cooldown effects it was expected to be less). During initial motor checks prior to closing the cryostat the shaft turning direction was checked. Applying negative steps to stepper motor will move the tuner probes to compress the cavity.

Once the cavity was cooled to 2 K the motor was actuated with minus 60 k steps and tuner probes must have moved by ~ 1 mm (see Fig. 2 named 1st movement). However, the cavity frequency did not change. After not seeing a response from minus 60 k steps doubt settled that the perhaps the wrong motor direction was applied. Positive steps were then used and after plus 60 k steps from 0 steps (see Fig. 2 second movement) no response was observed. The original direction (negative steps) was tried again.

After operating the stepper motor for minus 120 k steps from the 0th position the probes compressed the cavity (see Fig 2). The number of steps from the 0th position until first contact translates to 2 mm on the gap (See Fig. 2). After

*This manuscript has been authored by Fermi Research Alliance, LLC under Contract No. DE-AC02-07CH11359 and DE-AC02-76SF00515 with the U.S. Department of Energy, Office of Science, Office of High Energy Physics.

[†] ccontrer@fnal.gov

EMITTANCE MEASUREMENTS WITH WIRE SCANNERS IN THE FERMILAB SIDE-COUPLED LINAC *

E. Chen, R. Sharankova, A. Shemyakin, J. Stanton
Fermi National Accelerator Laboratory, Batavia, USA

Abstract

The Fermilab Side-Coupled Linac accelerates H⁺ beam from 116 MeV to 400 MeV through seven 805 MHz modules. Twelve wire scanners are present in the Side Coupled Linac and four are present in the transfer line between the Linac and the Booster synchrotron ring. These wire scanners act as important diagnostic instruments to directly collect information on the beam's transverse distribution. The manipulation of the conditions of wire scanner data collection enables further characterization of the beamline, such as calculating emittance and the Twiss parameters of the beam at select regions, which we present here.

INTRODUCTION

The Fermilab Side-Coupled Linac accelerates 116.5 MeV H⁺ beam to 400 MeV via 805 MHz side-coupled cavities [1]. The cavities are organized into seven main modules (Modules 1-7) with four sections in each module, as well as a transition section (Module 0) composed of 805 MHz buncher (B) and Vernier (V) cavities, Fig. 1.

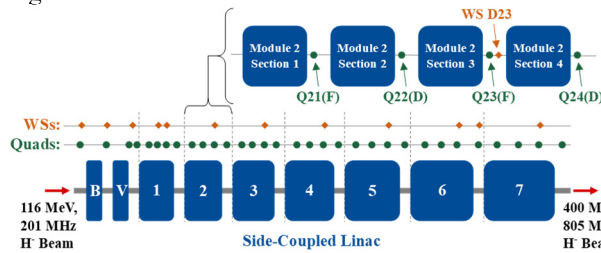


Figure 1: Schematic of the Fermilab Side-Coupled Linac and representative layout inside Module 2. Naming convention for diagnostic instruments follows the structure of Q_{mn} (quads, green dots) or D_{mn} (WSs, orange diamonds), where m = module number and n = section number.

Diagnostic, steering, and focusing elements are present in between sections and modules, including an alternating FODO lattice of quadrupoles [1] and 12 wire scanners (WSs) throughout the Side-Coupled Linac [2]. The WSs yield transverse profiles in the X and Y directions (Fig. 2), as well as in a 45° direction not discussed here.

The abundance of these diagnostic devices in the Side-Coupled Linac facilitates the use of WSs to measure the transverse emittance and the Twiss parameters of the H⁺ beam. Such measurements have not been performed in more than a decade [2]; however, we seek to experimentally characterize the present state of the Fermilab Linac. Here we present the results of the recent study analyzing transverse beam properties in the Side-Coupled Linac.

* This manuscript has been authored by Fermi Research Alliance, LLC under Contract No. DE-AC02-07CH11359 with the U.S. Department of Energy, Office of Science, Office of High Energy Physics.

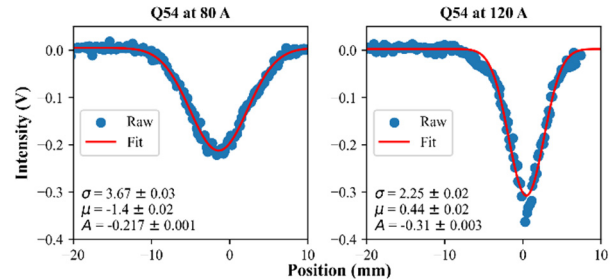


Figure 2: Example of vertical (Y) wire scans from quadrupole scan Q54-D63 with Q54 at 80 A and 120 A.

MEASUREMENTS OF EMITTANCE AND TWISS PARAMETERS

The transverse emittance and Twiss parameters were measured via two methods: a quadrupole scan and a beam width measurement at several locations in a drift space.

To reduce the duration of the wire scans, the scan procedure was modified to run at a constant speed. Previously, the wire frame was moved in steps, requiring significant time to equilibrate at each position and an overall scan time of 10-15 minutes. This long scan time is incompatible with a quadrupole scan, in which a large number of wire scans is required. Instead, the modified procedure collects position and intensity data on each beam pulse while moving the wires at a constant speed across the beam pipe, reducing scan time tenfold to 1.25 minutes and demonstrating comparable data quality [3]. The step in space between the points is defined by the wire frame speed and pulse frequency. To address the low signal-to-noise ratio, the beam profile width is characterized by the standard deviation of the fitted Gaussian function σ_{RMS} . The use of beam width from the Gaussian fit additionally allows inclusion of scans with incomplete beam profiles due to insufficient scan range. The RMS errors associated with the Gaussian fit are assigned to all points shown in Figs. 3 and 4. A Python program was written to schedule the wire scans and vary the quadrupole current for the quadrupole scan, enabling faster collection.

Data for both methods were collected in July 2024 with 18.7 mA beam at the output of the Linac and 5 Hz pulse frequency. For the quadrupole scan, wire scans taken when moving the frame both “in” and “out” of the beam pipe with a 5 μs pulse length. For the propagation in free space experiment, data were taken in both the “in” and “out” directions and averaged.

Quadrupole Scan

In the thin-lens approximation, the quadrupole scan is defined by the characteristic equation in Eq. (1).

DATA ACQUISITION AND CHARACTERIZATION SOFTWARE FOR RADIO-FREQUENCY (RF) SYSTEMS

S. K. Suthar*, B. Popovic

Accelerator Systems Division, Argonne National Laboratory, Lemont, IL, USA

Abstract

In accelerator physics, radio-frequency (rf) systems play a pivotal role in particle beam acceleration and diagnostics. This work presents a graphical interface designed with Python for interaction with rf instruments, enabling efficient data acquisition, processing, and visualization. Leveraging advanced software tools, the system enables efficient management and analysis of rf data. This capability is crucial for optimizing experimentation and streamlining data flow. The modular architecture is implemented on various systems and is demonstrated with the current 200kW Solid State Amplifier (SSA) test setup at the Advanced Photon Source.

INTRODUCTION

Measurement and characterization of rf systems involve a variety of instrumentation, but retain the fundamental process of experimentation: measurement, acquisition, processing, and modelling. The Advanced Photon Source (APS) has a variety of rf systems and structures in operation. To streamline interfacing with these systems, instrumentation can be automated and centralized. Creating these capabilities allows for powerful organization and handling of rf data, which is important for advanced characterization.

METHODOLOGY

Python is employed as the primary development tool for this project. Libraries such as vxi-11, pyvisa, and rs-instrument are used for instrument communication. For data processing matplotlib, numpy, and an in-house rf-based toolbox are used. This choice of software provides compatibility and modularity for the proposed use case. Furthermore, streamlining, centralizing, and automating data acquisition for rf instruments allows for an organized scheme to characterize rf systems. Additionally, industry standard touchstone files are supported for import and exportation of scattering parameters.

DEVELOPMENT

Figure 1 shows some modules of the full GUI. The developed software tool contains modules to interface with many instruments including: Vector Network Analyzers (VNAs), pulsed and CW power meters, and signal generators. By using standardized instrumentation protocols, implementing support for additional instruments can be done easily. Additionally, the system incorporates various functions to process and visualize data.

* sohumksuthar@gmail.com | ssuthar@anl.gov

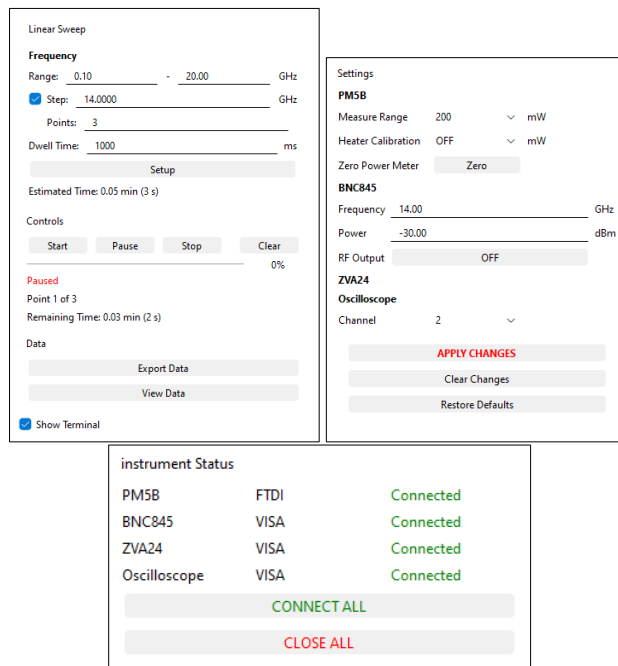


Figure 1: Instrument and experiment modules Left: Experiment module for running sweeps, Right: Settings module for instrument parameter control, Bottom: Instrument connection interface.

As seen in Fig. 2, the plotter module facilitates the analysis of scattering parameter data. A multitude of parameters can be derived from datasets and visualized in various different plot types. Also, various traces and measurements can be overlapped to allow for comparative analyses.

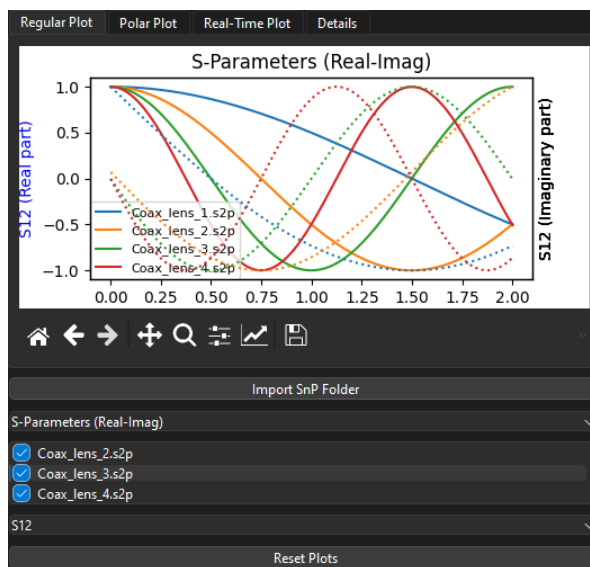


Figure 2: Reader-friendly plotter module.

GRIDDED RF GUN DESIGN FOR SRF LINAC APPLICATIONS

I. Gonin[†], C. Edwards, S. Kazakov, T. Khabiboulline, T. Nicol, A. Saini, N. Solyak,
J.C.T. Thangaraj, V. Yakovlev, FNAL, Batavia, IL, USA
M. Curtis, K. Gunther, HeatWave Labs, Inc., Watsonville, CA, USA

Abstract

The thermionic gridded gun is described which generates short electron bunches for further acceleration in a Nb3Sn conduction cooled SRF linac. The gun is built into the first cavity of the 250 keV injector [1] for the 20 kW, 10 MeV, 1.3 GHz CW conduction cooled one-cavity linac. The beam current is 2 mA. The RF gun design is presented as well as the results of perveance measurements, which are in a good agreement with the design parameters. The design of the RF resonator of the gun is presented also. The beam generated by the gun is matched to the injector to provide lack of current interception in the SRF cavity.

GENERAL

The concept of compact linear electron accelerators for industrial application suggested in [2] is based on use of Nb3Sn conduction cooled SRF cavities. This concept allows both high energy ≈ 10 MeV and high power of MW level. One of the most serious limitations of the beam power is the beam current interception in the SRF cavity cooled by few cryo-coolers which provide power removal of ~ 2 - 2.5 W each at 4.5 K. Therefore, power loss in the SRF cavity caused by intercepted electrons should not exceed ~ 1 W, or $\sim 1.e-6$. It means that a source of electrons should provide short bunches without tails, which may be defocused by RF field and reach the cavity surface. In addition, the beam should have considerably low transverse emittance preventing strong beam diameter increase in the cavity. To generate these short bunches, we suggested to use gridded RF gun [3]. RF field is applied to the gun cathode – grid gap together with the bias deceleration DC voltage. This scheme provides electron injection in very narrow phase domain, few degrees, and therefore, generation of very short bunches. On the other hand, this scheme provides lack of long bunch tails. Initially the gun has been designed for 650 MHz, 1.8 MeV linac prototype which is under construction at IARC [3]. It will be installed directly into the SRF cavity. For 1.3 GHz prototype [2] a special room-temperature injector has been designed [1] which provides the 250-300 keV beam for the SRF accelerator. This concept potentially allows higher beam power than the scheme with immersed gun, because high power and consequently high beam current (up to 100 mA at very short, $<10^9$ pulses) requires considerably big cathode diameter, and therefore, large black body radiation and cavity contamination caused by the cathode material evaporation. The design of a thermionic electron source which can either be directly connected to a superconducting cavity or be part of a normal conducted injector cavity is described.

[†] gonin@fnal.gov.

The direct connection option is applied in a prototype $1\frac{1}{2}$ cell 650 MHz SRF cavity capable of delivering a 12.5 mA average beam current with a beam power of 20 kW. As an external option we present the development of a CW normal conducting 1.3 GHz RF injector which consists of a gridded RF gun integrated with the first cell of a copper booster cavity. The electron source concept is presented including the cathode-grid assembly and the gun resonator design.

THE RF GUN DESIGN

The RF gun consists of the cathode-grid assembly and the gun RF resonator. Fig. 1 show a 3D cross-section of the cathode-grid assembly [3]. The assembly contains the cathode-grid part, the transition support part, the socket part with the ceramic window which subdivide the vacuum cathode part and air RF resonator, and the socket.

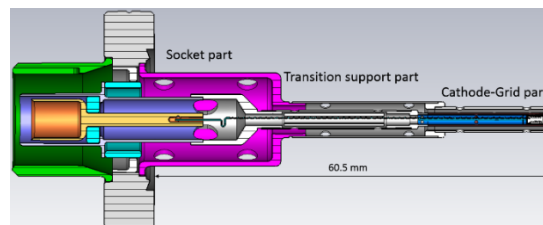


Figure 1: Cross-section of the cathode-grid assembly.

The beam optics is determined by the shape of the grid extension electrode with Pierce angle. It has an impregnated cathode of 612M type with a 1.8 eV work function to provide electron current density greater than 10 A/cm² at emitter temperature of 1050°C. The cathode $\varnothing = 1.5$ mm to provide low heat load (< 1 W). The grid is placed at the distance of 150 microns from the cathode. The cathode has planar shape. The grid is attached to the Pierce angle electrode. The grid transparency is higher than 80%. Planar geometry of the cathode and grid is less sensitive to dimensional errors and misalignments. A heater filament should be designed to avoid the heater magnetic field on the cathode. The heater power level < 2 W. The gun cathode-grid unit engineering design is made by HeatWave Labs (HWL).

Figure 2 shows the cathode-grid area with details of the heater. An outer conductor and the grid are grounded. The cathode and heater are at a DC bias voltage. To minimize the heater power, the cathode is mounted using a support sleeve made of 25 μ m (0.001”) thick molybdenum/rhenium alloy with an additional hole pattern to reduce the thermal path to emulate a 12.5 μ m thick sleeve. To reduce thermal radiation, a special thermal shield of a 25 μ m thick Mo/Re has been added to the design.

STRATEGIES FOR MITIGATING RESIDUAL MAGNETIC FIELD EFFECT ON PRE-PRODUCTION PIP-II SSR2 CRYOMODULE PERFORMANCE*

J. Bernardini[†], D. Passarelli, M. Parise, V. Roger, Y. Xie, G. Romanov, F. Lewis, A. Hogberg
FNAL, Batavia, USA

Abstract

This paper outlines the strategy aimed at mitigating the adverse effects of residual magnetic fields on the performance of pre-production SSR2 superconducting cavities within the context of the PIP-II project at Fermilab. Residual magnetic fields can significantly impact cavity performance, leading to reduced quality factor. To address this challenge, our strategy integrates various approaches including magnetic shielding, careful selection of materials, quality controls aimed at measuring magnetic permeability, magnetic hygiene to reduce residual magnetic field at the installation phase. Additionally, experimental studies are being planned to analyze the behavior of the cavities under different magnetic field conditions, and the effectiveness of advanced demagnetization procedures.

INTRODUCTION

The Proton Improvement Plan II (PIP-II) project [1] at Fermilab is an upgrade to the existing accelerator complex, designed to power the world's most intense high-energy neutrino beam for the LBNF-DUNE experiment. The PIP-II Linear Accelerator (Linac) features five different types of Superconducting Radio Frequency (SRF) accelerating cavities, each housed in distinct cryomodules (CMs) [2–4], and equipped with high-power RF couplers and frequency tuners:

- 162.5 MHz Half Wave Resonators (HWR).
- 325 MHz Single Spoke Resonators type 1 and type 2 (SSR1 and SSR2) [5, 6].
- 650 MHz 5 cells low beta and high beta (LB650 and HB650) [7, 8].

The CMs containing the HWR, SSR1, and SSR2 cavities also include superconducting focusing lenses and beam position monitors (BPMs). The focusing lenses are superconducting magnets that combine a solenoid with bucking coils and four independently powered corrector coils. The HWR focusing lenses are convection cooled in a bath of 2 K liquid Helium, while the SSR focusing lenses are conduction cooled through copper straps thermally connecting the solenoid and corrector coils to the 2-phase Helium return pipe.

All PIP-II cryomodules feature a global magnetic shield designed to attenuate the magnetic field at the cavities' surfaces. The acceptable magnetic field is 50 mG for HWR, 15

mG for SSR1 and SSR2, and 5 mG for LB650 and HB650 cavities. The more stringent requirement for LB650 and HB650 CMs is met by adding a local cold magnetic shield surrounding the cavities. Moreover, for the SSR1 and SSR2 CMs, all components inside the cold mass must have a relative magnetic permeability $\mu_r < 1.02$ and a maximum residual magnetic field of less than 5 mG at zero distance from the surface when the focusing lenses are off. When powered, the focusing lenses must have a fringe field of less than 10 G on the surface of a cylinder, centered on the focusing lens, with a diameter of 0.7 m and a length of 0.84 m.

Such requirements aim at minimizing the degradation in the Q_0 of the cavities from horizontal testing in the Spoke Test Cryostat (STC) to CM configuration. Indeed, a Q_0 degradation was observed for prototype SSR1 cavities when comparing the results from STC to cryomodule testing [9, 10].

PASSIVE MITIGATION STRATEGY

Passive mitigation techniques begin during the design phase by prioritizing the use of non-ferromagnetic materials such as Titanium Gr. 5 and Gr. 2, Aluminum and Copper alloys. For example, in the cavity's helium jacket, the material was changed from SS 316L (used in the prototype SSR1 CM) to Titanium Gr. 2 (used in pre-production SSR2 and production SSR1 and SSR2 CMs) [11].

When austenitic stainless steel is used, it is crucial that its relative magnetic permeability is less than 1.02. However, SS 316L (UNS S31603, EN 1.4404) does not always meet this requirement [12]. Despite this, SS 316L remains the material of choice for pre-production SSR2 BPMs, edge-welded bellows, frequency tuners, and most hardware and mechanical supports used in the CM.

Relative Magnetic Permeability of Components in SS 316L

To ensure the relative magnetic permeability of components in SS 316L stays below 1.02, solution annealing is employed. When annealing is applicable, the process involves: initial machining of the stock material, heating to 1420 K (the duration must ensure that the core of the material reaches this temperature), water quenching, and final machining.

In case of TIG welded joints between parts in SS 316L, ER310 and ER316LMn bare wires are used as filler material [13]. Several tests were performed by TIG welding tubes in SS 316L, having initial $\mu_r < 1.01$, with different filler materials, results are summarized in Table 1.

* Work supported by Fermi Research Alliance, LLC under Contract No. DEAC02-07CH11359 with the United States Department of Energy, Office of Science, Office of High Energy Physics.

[†] jbernard@fnal.gov

INTEGRATION OF COMPUTER VISION SYSTEM TO TRACK THE ALIGNMENT OF SRF CAVITIES INTO THE TEST CRYOSTAT FOR PIP-II AT FERMILAB*

J. Bernardini[†], D. Dillman, S. Zorzetti, F. Lewis, M. Parise, V. Roger, D. Passarelli,
Fermi National Accelerator Laboratory, Batavia, IL, USA

A. Gonzalez, Université Paris-Saclay, IRFU-CEA, Gif-sur-Yvette, France

N. Kumar, ISIS Neutron and Muon Source, Rutherford Appleton Laboratory, Harwell, Didcot, UK

Abstract

PIP-II cryomodules use a computer vision system (H-BCAMs system) to monitor the alignment of SRF cavities and focusing lenses during assembly, testing, and operation. This contribution details the integration of the H-BCAMs into the Spoke Test Cryostat (STC) at Fermilab, which is utilized for cold testing SRF cavities prior to their integration into the string assembly. Thermal and structural finite element analyses were employed to estimate the cavities' deformations, to be validated during cold testing in the STC using H-BCAMs. Notably, this marks the first instance of H-BCAMs integration into a cryostat and operation within a cryogenic environment.

INTRODUCTION

The geometric axes of Superconducting Radio Frequency (SRF) cavities and magnets installed in the Proton Improvement Plan II (PIP-II) [1] cryomodules (CMs) are aligned during the string assembly phase. This alignment must be maintained throughout the cryomodule assembly, transport, and operational phases. The alignment requirements for cavities and magnets in Single Spoke Resonators Type 1 (SSR1) and Type 2 (SSR2) CMs are detailed in Table 1.

Table 1: PIP-II Alignment Requirements

Cavities	Value
Transverse cavity alignment error, mm RMS	<1
Angular cavity alignment error, mrad RMS	≤10
Solenoids	Value
Transverse cavity alignment error, mm RMS	<0.5
Angular solenoid alignment error, mrad RMS	≤1

H-BCAMs[®] [2] are optical instruments first used in high energy physics during the HIE ISOLDE experiment at CERN [3] and later adapted for PIP-II. The H-BCAMs system has been successfully employed to monitor the alignment of SRF cavities in prototype SSR1 and HB650 CMs [4–6].

The alignment established during the assembly phase must account for the movements that cavities and magnets experi-

* Work supported by Fermi Research Alliance, LLC under Contract No. DEAC02-07CH11359 with the United States Department of Energy, Office of Science, Office of High Energy Physics.

[†] jbernard@fnal.gov

ence as the CM is cooled from ambient temperature to 2 K. Both vertical and transversal displacements of the axes of cavities and magnets are estimated using coupled thermal and structural Finite Element Analyses (FEA) performed in ANSYS [7] and are also measured directly during cavity testing in the STC. Each PIP-II cavity, equipped with a frequency tuner and high-power RF coupler, must be cold-tested and qualified in the STC before being integrated into the CM string.

The installation of H-BCAMs in the STC enables the measurement of target movements, which are strategically mounted on the helium vessel of SRF cavities, during cooldown. These displacements help determine the vertical and transversal movement of the cavity's axis, which can then be applied as an offset during the string assembly phase. In Fermilab-style CMs [8–10], string components are individually mounted on support posts and interconnected by edge-welded bellows [11]. The flexibility provided by these bellows allows for independent movement of each cavity and magnet using a dedicated alignment system [12, 13].

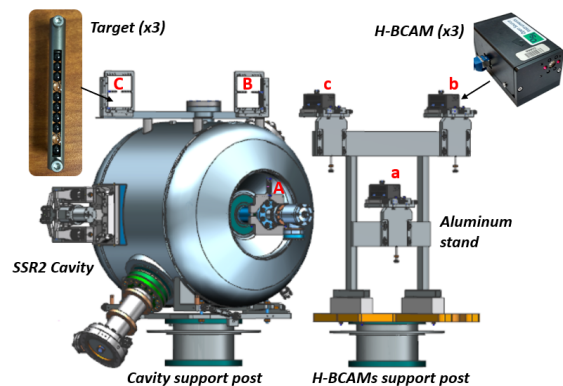


Figure 1: Measurement set-up used in the STC. Three H-BCAMs (a, b, and c) face the three targets (A, B, and C) mounted on the SSR2 cavity.

MEASUREMENT SYSTEM

The STC is equipped with a pair of G-10 support posts, which are intercepted by a liquid nitrogen-cooled thermal shield. These support posts provide thermal insulation, keeping components at 2 K separate from those at ambient temperature. As shown in Fig. 1, one post supports the SSR2 cavity, while the other supports an aluminum stand that holds

SUCCESSFUL INTERNATIONAL VALIDATION TEST SHIPMENT OF THE PIP-II HB650 CRYOMODULE TRANSPORTATION SYSTEM*

J.P. Holzbauer[†], J. Helsper, J. Ozelis, A. Wixson
Fermi National Accelerator Laboratory, Batavia, IL, USA
M. Kane, STFC-UKRI, Warrington, UK

Abstract

The PIP-II Project will receive fully assembled cryomodules from CEA and STFC-UKRI as in-kind contributions. Damage to these cryomodules during transport is understood to be a significant risk to the project, so an extensive testing and validation program has been executed to mitigate this risk. The centerpiece of this effort was the successful shipment, from FNAL to STFC-UKRI and back, of a prototype HB650 cryomodule with cold testing before and after shipment to verify no functionality changes from shipment. Building on an escalating test transport program, the prototype cryomodule was shipped to the UK and back using realistic logistics, handling, instrumentation, and planning. The process of executing this shipment, lessons learned, and plan moving forward will be presented here.

INTRODUCTION

The PIP-II SRF linac is composed of five cryomodule types at 3 sub-harmonics of 1.3 GHz (162.5, 325, and 650 MHz) [1]. The 650 MHz section of the linac is composed of two cryomodule types, Low-Beta (LB) and High-Beta (HB). The PIP-II Project has significant international contributions in almost every part of the machine, and the 650 section is no exception. The LB modules are being designed and produced by CEA in France while the HB modules are produced by STFC-UKRI in the UK as in-kind contributions to the project. The PIP-II project has adopted the strategy of convergent design, aligning the techniques and technologies between different modules as much as possible. This allows convergent mitigation of the transportation risks for the LB and HB modules from the partner labs in Europe to FNAL. Transportation experts at all three labs have worked closely to ensure that a consistent and systematic approach is used for assessing and mitigating the risks of these critical cryomodule transports.

TRANSPORT SYSTEM VALIDATION STRATEGY

The systematic approach to transportation and transport validation has been adopted by PIP-II driven by past experience with cryomodule shipping for LCLS-II [2]. This includes the choice to forego sea and rail, relying on air transport for the transatlantic segments. The following major stages are chosen to systematically validate the integrated

transport system design (cryomodule plus shipping frame) while minimizing risk to critical equipment.

1. Detailed specification, design, and review of the HB650 transport frame in collaboration between FNAL and STFC-UKRI [3, 4]
2. Fabrication, integration of HB650 transport frame with cryomodule analog (Dummy Load), realistic testing with Dummy Load to validate isolation and handling performance, first locally via road and then from to STFC-UKRI, validating air transport and handling [5, 6]
3. Local road testing with a cold-tested and validated prototype HB650 (pHB650) to reverify isolation performance as well as any module-internal resonances
4. Realistic transport of the pHB650 module from FNAL to STFC-UKRI and back, concluding with second cold-test to assess impacts of transatlantic shipment on cavity performance [7]
5. Design optimization of HB650 and LB650 transport frames by the respective partner labs [8].

All stages of this validation effort have been completed successfully including the cold re-validation of the cryomodule performance. This paper will describe the final shipment of the pCM to the UK and back, including major lessons learned.

TRANSPORT SYSTEM DESIGN

The HB650 transport system, designed by STFC-UKRI, is a tessellated steel frame meant to enclose the cryomodule during transport, isolating the CM during transport with wire-rope isolators sized for the weight and shocks/vibrations expected during transport. The model of the transport system (frame, isolators, and CM) can be seen in Fig. 1. The frame is covered in plywood panels during transport to prevent access and protect from weather. Access ports were added to allow instrumentation inspection during transport, viewing windows in case of customs inspections, and labeling for ease of assembly.

During the fabrication, dummy load testing, and final validation with CM, this design was fundamentally found to be sound with minor changes proposed. These lessons learned mostly consisted of:

- Revisit and improve all connections, especially on outer panels, which will see wear and tear of multiple shipments. The more robust these materials and attachment points can be, the better

* Work supported by Fermi Research Alliance, LLC under Contract No. DE-AC02-07CH11359 with the United States Department of Energy.

[†] jeremiah@fnal.gov

PERFORMANCE OF PIP-II HIGH-BETA 650 CRYOMODULE AFTER TRANSATLANTIC SHIPPING*

J. Ozelis[†], M. Barba, J. Bernardini, C. Contreras-Martinez, D. Crawford, J. Dong, V. Grzelak, P. Hanlet, J. B. Holzbauer, Y. Jia, S. Kazakov, T. Khabiboulline, J. Makara, N. Patel, V. Patel, L. Pei, D. Peterson, Y. Pischnalnikov, D. Porwisiak, S. Ranpariya, J. Steimel, N. Solyak, J. Subedi, A. Sukhanov, P. Varghese, T. Wallace, M. White, S. Wijethunga, Y. Xie, S. Yoon
Fermilab, Batavia, USA

Abstract

After shipment to the Daresbury Lab and return to Fermilab, the prototype HB650 cryomodule underwent another phase of 2K RF testing to ascertain any performance issues that may have arisen from the transport of the cryomodule. While measurements taken at room temperature after the conclusion of shipment indicated that there were no negative impacts on cavity alignment, beamline vacuum, or cavity frequency, testing at 2K was required to validate other aspects such as tuner operation, cavity coupling, cryogenic system integrity, and cavity performance. Results of this latest round of limited 2K testing will be presented.

INTRODUCTION

The PIP-II Superconducting Linac features 23 cryomodules of 5 different types. The highest energy section of the Linac is comprised of 9 Low-Beta (LB) 650 MHz cryomodules with 4 cavities, and 4 High-Beta (HB) cryomodules with 6 cavities. Except for a prototype HB cryomodule, the remaining 650 MHz cryomodules (including the refurbishment of the HB650 prototype cryomodule) are to be assembled by international partners (CEA and INFN for LB, UKRI's Daresbury Lab for HB) as in-kind contributions to the PIP-II project. As a result, 13 of the cryomodules to be used in the PIP-II Linac will require that they undergo transatlantic shipment to the US.

Reducing the risk that this transatlantic shipment results in performance degradation or damage to these cryomodules is paramount. To that end two approaches have been taken to understand the environmental conditions posed by such transport and to mitigate risks:

- Shipment of a fully instrumented “dummy load” to perform preliminary verification of shipment methods and transport fixtures
- Shipment of the prototype HB650 cryomodule (HB650 pCM) to Daresbury Lab after completion of 2K testing at Fermilab's PIP2IT facility, and re-test upon return

Shipment of the dummy load was performed during summer 2022. As reported elsewhere [1], the results indicated that the fixturing and processes (adopted from similar

experience shipping LCLS-II cryomodules from FNAL to SLAC) worked extremely well, and minor changes were pursued to incorporate lessons learned.

The shipment of the actual pCM took place late in 2023, after the first round of RF testing of the cryomodule at 2K to characterize initial performance was completed in the PIP2IT facility at Fermilab. The shipment configuration, preparation, and process for shipment of the completed HB650 pCM is described in detail in [2].

TRANSPORT-CRITICAL CRYOMODULE PERFORMANCE PARAMETERS

A number of critical performance parameters or system/component functionalities were the primary focus of the post-transport study. These include :

- Insulating vacuum integrity
- Beamline vacuum integrity
- Cryogenic circuit integrity
- Cavity alignment preservation
- Tuner operation
- Cryogenic valve actuator operations
- Instrumentation
- High-power coupler Qext
- Cavity performance (gradient, field emission, and quality factor)
- Thermal performance consistency

Each of these areas were subject to test/measurement, and results to be compared with performance observed before shipment.

TEST APPROACH AND PLAN

Upon return from the UK, the HB650 pCM was partially re-assembled, as the top port and its internal components (e.g., heat exchanger, thermal and magnetic shields) and power coupler air-side components were removed for transport. This re-assembly activity also provided an opportunity to make several modifications to the cryomodule cryogenic systems and mechanical structure, based on results and analysis from earlier thermal studies. A check valve was installed in the 2K relief line, additional MLI was added, and temperature sensors and heaters were installed on the cryogenic valve thermal intercepts, to better characterize heat transfer and examine the possibility of thermo-acoustic oscillations [3].

* This manuscript has been authored by Fermi Research Alliance, LLC under Contract No. DE-AC02-07CH11359 with the U.S. Department of Energy, Office of Science, Office of High Energy Physics.

[†] ozelis@fnal.gov

HIGH PRESSURE RINSE SIMULATIONS FOR PIP-II SRF CAVITIES*

M. Parise[†], T. Aiazzi, D. Passarelli

Fermi National Accelerator Laboratory (Fermilab), Batavia, IL, USA

Abstract

The implementation of High Pressure Rinse (HPR) not only ensures thorough cleaning of the inner high purity niobium surface of Superconducting Radio Frequency (SRF) cavities, but also unlocks their full potential for achieving peak performance. By effectively removing contaminants and impurities, HPR sets the stage for enhanced superconducting properties, improved energy efficiency, and superior operational stability. A simulation tool has been developed, facilitating the accurate prediction of both the quality and effectiveness of the rinsing process before its execution in the cleanroom. This tool, the focus of this paper, stands as a pivotal advancement in optimizing Superconducting Radio Frequency (SRF) cavity preparation. Furthermore, our paper will also present correlations with cavity cold testing results, demonstrating the practical applicability and reliability of the simulation predictions in real-world scenarios.

INTRODUCTION

The performance of Superconducting Radio Frequency (SRF) cavities showcases the state-of-the-art of what we can achieve with today's technology. As we push the boundaries of particle acceleration, the fabrication and processing of these cavities emerge as critical factors that determine their performance. This is particularly true for non-elliptical cavities, whose intricate geometries present additional challenges. Unlike the Tesla-shaped cavities, for which standard processes have been refined and optimized over time, non-elliptical cavities demand a reevaluation of existing methodologies. Their complex shapes not only necessitate advanced manufacturing techniques but also call for innovative processing solutions to ensure optimal performance. Field Emission (FE) issues have been a persistent bottleneck during the cold testing phase of jacketed Single Spoke Resonators Type 2 (SSR2) ([1], [2], [3], [4]) for PIP-II (PIP-II [5]), where the presence of particulate contaminants has severely impaired the cavity's functionality. This paper investigates the cleaning of SSR2 cavities. The motivation behind this study stems from the difficulties in achieving an effective high-pressure rinse. Due to the cavities' convoluted geometry, standard water jet cleaning procedures fail to reach, or effectively clean, all surfaces. This inadequacy is attributed to the limitations in water jet coverage and the dynamics of fluid interaction with the cavity walls. The efficiency of the rinse is contingent upon several factors: the angle between the water jet and the cavity surface, the duration for which specific areas are subjected to the high-pressure water, and the distance from the nozzle to the surface at the point of

impact. It is hypothesized that the angle of incidence plays a pivotal role in the cleaning process, where certain angles may enhance the rinse effectiveness, while others may lead to suboptimal results. Similarly, the time of exposure and the distance of the water jet from the surface are critical parameters that determine the force exerted by the water jet, and consequently, its cleaning efficacy. In the context of this work a new tool to simulate the HPR cavity surface coverage, efficiency, time of exposure and nozzle to surface distance has been developed (see also [6], [7]). Additionally, The code has been meticulously crafted to significantly reduce computational time. This efficiency enables the execution of optimization processes that would otherwise be impractical due to their iterative nature. By minimizing the time required for each run, the code facilitates a level of optimization that was previously unattainable. By fine-tuning the angles at which the high-pressure water strikes the cavity surfaces, we can significantly enhance the rinse, ensuring that all areas are effectively reached and contaminants are removed. This leads to a direct improvement in the performance of the cavities by mitigating field emission issues, which is a critical step forward in the maintenance and operation of advanced particle accelerators.

DEVELOPMENT OF THE SIMULATION TOOL

Process Description and Input Parameters

The HPR process is performed in a controlled cleanroom environment to ensure the performance of SRF cavities. Central to this process is a wand equipped with a series of nozzles, typically ranging from 2 to 8, through which high-pressure water is directed onto the cavity surfaces. These nozzles, often sourced from commercial vendors, are designed to spray water at specific angles referred to as the water jet angle. To accommodate the varying geometries of SRF cavities, the nozzles can be oriented at different angles. This parameter, which could be termed as the nozzle orientation angle, is crucial for optimizing the cleaning coverage. These angles are the azimuthal and polar angles. Also nozzles may be spaced at a certain distance along the wand axis. Although this distance is small compared with the dimension of the cavity it is included in the model. The wand itself is engaged in a relative motion with the cavity, which may involve rotation and translation at certain speeds to ensure comprehensive cleaning. Although the cavity itself may rotate and translate, it is the relative motion between the two that is of importance. Low beta cavities, such as the SSR2 cavities with their four ports, present unique challenges due to their complex geometry. In our simulations, the wand is positioned vertically or slightly tilted with respect to the

* Work supported by Fermi Research Alliance, LLC under Contract No. DE-AC02-07CH11359 with the United States Department of Energy

[†] mparise@fnal.gov

PLANNED FUTURE UPGRADES OF LINEAR IFMIF PROTOTYPE ACCELERATOR (LIPAc)

F. Cismondi, D. Duglue, H. Dzitko, A. Jokinen, F. Scantamburlo, F4E, Garching, Germany
T. Akagi, Y. Carin, D. Gex, K. Masuda, I. Moya, M. Sugimoto, IFMIF/EVEDA Project Team,
Rokkasho, Japan

K. Hasegawa, K. Hirosawa, K. Kondo, K. Kumagai, QST, Rokkasho, Japan

P. González, ATG, Barcelona, Spain

IFMIF/EVEDA Integrated Team with CEA, CIEMAT, INFN, Italy

Abstract

The Implementing Agencies of the Broader Approach (BA) agreement, namely Fusion for Energy (F4E) and National Institutes for Quantum Science and Technology (QST), are developing the Accelerator Facility validation activities that aim at demonstrating the acceleration of 125 mA D⁺ beam up to 9 MeV in continuous wave (CW) [1,2]. This is the main goal of the Linear IFMIF Prototype Accelerator (LIPAc) under installation, commissioning and operation in Rokkasho, Japan.

LIPAc has been operated until June 2024 in its Phase B⁺ configuration, which consists of all the beamline except the SRF Linac (high duty cycle operation results up to 5 MeV are reported by T. Akagi in this conference).

In parallel, the upgrades for several systems are being designed and procured taking into account the lessons learned so far during commissioning and operation and will be the main object of this paper. These systems are: a new injector encompassing a new design of beam production and extraction system together with LEBT; a new RF system based on SSPA technology for the RF-RFQ, whose full-scale prototype is being manufactured and validated in 2024; a new set of RF-RFQ power couplers with improved design to overcome the limitations suffered by the couplers currently installed in LIPAc.

INTRODUCTION

The LIPAc [1, 2] in its Phase B⁺ configuration consists of a 100 keV injector, a 5 MeV Radio-Frequency Quadrupole (RFQ) accelerator, a Medium and High Energy Beam Transport lines (MEBT and HEBT respectively) and a Beam Dump (BD). Its final configuration will include a Superconducting Radio-Frequency (SRF) Linac and will target to commission a beam in CW of 125 mA at 9 MeV. A temporary MEBT Extension Line (MEL) replaced the SRF linac during Phase B⁺.

The beam generated at the ion source has an emittance below 0.3π .mm.mrad at the entrance of RFQ. The LIPAc commissioning is currently on-going at Rokkasho Institute for Fusion Energy [3]. In 2019 the beam commissioning campaigns achieved RFQ acceleration at nominal current 125 mA, 5 MeV at low duty cycle (DC) of ~ 0.1 % (1ms pulse) [4, 5]. Since the installation of the HEBT and the DP in 2020 and 2021, a deuteron beam of around 20 mA at

0.01 % duty cycle was transported up to the High-Power Beam Dump in December 2021 [6, 7].

ENHANCED INJECTOR

The LIPAc Injector CW commissioning campaigns have been conducted with $\phi 9$, $\phi 10$, $\phi 11$, and $\phi 12$ mm plasma electrodes (PE) apertures. By using the $\phi 11$ mm PE, a total current of 150 mA was extracted in CW (11 hours continuous operation) with D⁺ fraction of 91% (D⁺ = 137 mA), and a low emittance (0.24π mm mrad). Also, by using a $\phi 12$ mm PE, CW operation and a total current of 160 mA were achieved, but the emittance increased to 0.3π mm mrad and the beam current stability deteriorated. The $\phi 11.5$ mm is considered the optimum electrode diameter for stable extraction of the target CW current [8, 9], and was used during the Phase B⁺.

General Layout and Design Features

The upgrade of the Injector (see Fig. 1) should encompass studies of the current CW campaigns and the beam operation results to identify the best design options for the injector subparts. It is likely that the most important efforts and changes will target to upgrade the accelerator column and the Emittance Meter Unit (EMU). The efforts will nevertheless not be limited to optimize those components, but rather to design a full upgraded injector.

For the EMU, the development of an optimized design target to improve its overall performance. It is very important for LIPAc to study the possibility to perform emittance measurements up to at least 10%DC. The optimized design can be based on the improvement of the cooling system, the better choice of the materials to maximize the heat dissipation and minimize deformations, an upgrade of its LCS, and the improvement of the manufacturing. The upgrade of the accelerator column will target to improve the overall performance in particular the stability at high duty cycle and continuous wave operation modes. Elements to take into account for the design upgrade are the optimization of the distance between the electrodes, the profiles of the electrodes, the improvement of the behaviour against the voltage breakdown, the optimization of the magnetic field into the plasma chamber, the magnetic shielding between the plasma chamber and the electrodes, and the capability to check the electrodes mechanical alignment.

During the LIPAc injector campaigns a quicker than expected degradation of the Boron Nitride (BN) disk was

STUDIES OF TRANSVERSE EMITTANCE GROWTH IN CSNS LINAC DTL*

J. Peng^{1,2,†}, Y.L. Han^{1,2}, Z.P. Li^{1,2}, Y. Li^{1,2}, Y. Yuan^{1,2}, X.Y. Feng^{1,2}, M.Y. Huang^{1,2}, S. Wang^{1,2},
S.N. Fu^{1,2}, H. Liu^{1,2}

¹Institute of High Energy Physics, Chinese Academy of Sciences, Beijing, China

²Spallation Neutron Source Science Center, Dongguan, China

Abstract

The transverse emittance at the exit of the China Spallation Neutron Source (CSNS) DTL is measured regularly every year. However, recently, the measured transverse emittance growth became larger than the historical data. It is also bigger than the simulated emittance. The process of measurement, data analysis and matching methods used are almost the same. Several factors contributed to the transverse emittance growth are analysed and presented in this paper. Compared to other factors, longitudinal mismatch contributes the most growth.

INTRODUCTION

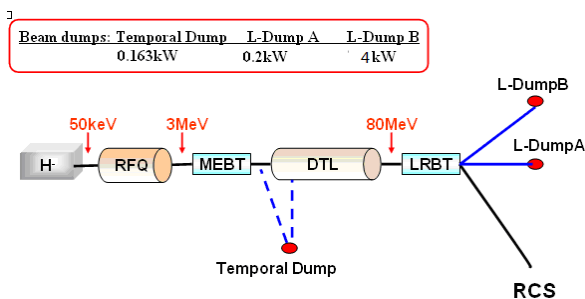


Figure 1: CSNS linac layout.

The CSNS is designed to accelerate proton beam pulse to 1.6GeV at a 25Hz repetition rate while striking a solid metal target to produce spallation neutrons. The accelerator aims to provide 100kW of proton beam power with more than 90% reliability. In 2024, the beam power is increased to 160kW with more than 93% reliability. The accelerator complex consists of an 80MeV H⁻ linac as the injector and a 1.6GeV rapid cycling proton synchrotron (RCS), as shown in Fig. 1 [1]. The linac consists of a 50keV H⁻ ion source, a 3MeV RFQ, an 80MeV DTL, and several beam transport lines. Table 1 shows the main parameters of the CSNS linac.

The transverse beam emittance at the exit of the DTL is measured regularly. However, this year, the transverse beam emittance increase about 25% compared to the recorded value. In 2021, the horizontal and vertical rms emittance is 0.346 and 0.337 π mm mrad at the beam current of 15mA. For this year, the horizontal and vertical rms emittance is 0.434 and 0.399 π mm mrad at the same current. Although the transverse rms emittance grew about

25%, the activation levels throughout the linac didn't increase. It kept less than 7mrem/hour at 30cm. And the beam profile obtained from the wire scanner measurement at the exit of the DTL also didn't show any significant beam halo, indicating that the beam didn't mismatch seriously.

Table 1: Main Parameters of the CSNS Linac

	Ion Source	RFQ	DTL
Input Energy (MeV)		0.05	3.0
Output Energy (MeV)	0.05	3.0	80
Pulse Current (mA)	20	10	10
RF frequency (MHz)		324	324
Chop rate (%)		50	50
Duty factor (%)	1.3	1.05	1.05
Repetition rate (Hz)	25	25	25

Several factors contributing to transverse emittance growth are analysed, including mismatch and incomplete transverse lattice. We also performed beam experiments to solve these issues.

EMITTANCE GROWTH STUDIES

Mismatch

Discrepancies between the physical model and actual machine parameters are common, and these differences can typically be minimized using beam-based calibration methods [2]. The CSNS MEBT consists of ten quadrupoles and two bunchers, which are utilized for longitudinal and transverse matching. The equivalent slicing model method is employed to construct magnet models [3], incorporating the fringing field effect. The amplitude and phase of two bunchers are determined using the phase scan signature method [4]. A pair of FCTs after each buncher is used to measure the beam phase difference during cavity amplitude and phase scanning. By matching the measured beam phase difference to the simulated beam phase differences, the cavity phase and amplitude can be determined. However, as the pair of FCTs is close to the buncher and the voltage of the buncher is small compared to an accelerating cavity, results in insufficient precision of the amplitude calibration. Discrepancies between the amplitude from the matching calculation and the actual RF setting can lead to transverse emittance growth.

* Work supported by National Natural Science Foundation of China (11505201)

† pengjun@ihep.ac.cn

PROGRESS IN THE DEVELOPMENT OF THE CRYOMODULES FOR CSNS-II SUPERCONDUCTING LINAC

M. Xu†, R. Ge, M. Li, Z. Chang, K. Zhu, J. Zhou, Y. Han, W. Zhou, Z. Mi, F. He, Z. He

Institute of High Energy Physics, Chinese Academy of Sciences, Beijing, China

Abstract

The China Spallation Neutron Source phase II (CSNS-II) upgrade design will increase the total beam power from 100 kW to 500 kW and boost the beam energy from 80 MeV to 300 MeV in the linac by adding a superconducting linear accelerator to the existing accelerator complex. Its proton linac will include 18 superconducting cavity cryomodules. It is composed of one string of Spoke cavity cryomodule and another string of elliptical cavity cryomodule. The nominal operating temperature for the cavities is 2 K, with 50~60 K thermal shielding. This paper introduces the thermo-mechanical design and expected operation of the CSNS-II spoke cavity cryomodule and elliptical cavity cryomodule, it also include the horizontal test results about the prototype of Spoke cavity cryomodule with two cavities.

INTRODUCTION

The China Spallation Neutron Source (CSNS) is the first pulsed neutron source facility in developing countries. CSNS locates at Dalang Town of Dongguan City, the heart of the Guangdong-Hong Kong- Macao Greater Bay Area. The China Spallation Neutron Source phase II (CSNS-II) upgrade design will increase the total beam power from 100 kW to 500 kW and boost the beam energy from 80 MeV to 300 MeV in the linac by adding a superconducting linear accelerator to the existing accelerator complex. Based on superconducting radiofrequency technologies, the superconducting linear accelerator will operate for the first time a 90 meter long section of niobium cavities.

It is composed of 10 Spoke cavity cryomodules and 8 elliptical cavity cryomodules. Paired in 18 cryomodules, each cavity will generate an accelerating pulsed field of 9MV/m. The cryogenic system is the specialised technical systems and can be further divided into two subsystems: the linac cryoplant and the test stand and instruments cryoplant. The linac cryoplant will provide all the cooling to the 18 cryomodules containing the superconducting RF cavities. The PID design of the linac cryoplant is finished. The test stand and instruments cryoplant have been finished commissioning and under normal operation for more than 3 years.

A prototype of double Spoke cavity cryomodule housing two superconducting Spoke cavities and their RF power couplers is now being fabricated and assembled. It provides the cryogenic environment for their normal operation in a 2K saturated superfluid helium bath: a 60 K thermal shield, a cold magnetic shield enclosed cavities, and integrates all the interfaces necessary to be operational

within the linac machine. This prototype has finished the cryogenic horizontal test at Platform of Advanced Photon Source Technology R&D (PAPS) site and then it is prepared to transport to CSNS site.

LINAC CRYOPLANT

The linac cryoplant provides cooling at three nominal temperature levels : 45 K to 60 K for the thermal shields of the cryomodules, valve boxes, 60 K thermal intercepts of the power coupler and beam pipe and distribution system; 5 K for the power coupler thermal intercepts and 2 K for the SRF cavities. The linac consists of 18 cryomodules operating at 324 MHz for the Spoke cavities and 648 MHz for the elliptical cavities. The CSNS-II cryomodules are individual cryogenic units and are cooled in parallel by the cryogenic distribution system. Figure 1 is a flow schematic for the helium distribution system of superconducting linac. Figure 2 shows the layout of the superconducting linac.

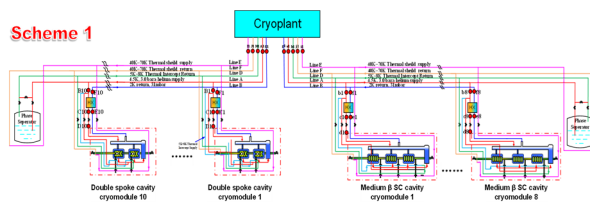


Figure 1: Flow schematic for the helium distribution system of CSNS-II superconducting linac.

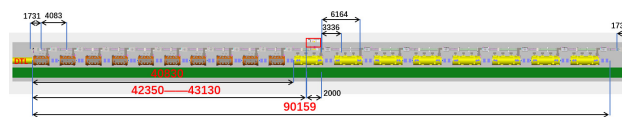


Figure 2: The layout of the superconducting linac.

MECHANICAL DESIGN

The superconducting linac of CSNS-II includes two types of cryomodules, one is Spoke cavity cryomodule and another is elliptical cavity cryomodule. A cut view of the Spoke cavity cryomodule is shown on Fig. 3. The two double Spoke cavities are installed along the axis of the vacuum vessel. Cold tuning systems are vertical mounted at the side of helium bath of cavity, which face toward the end head assembly of the vacuum house to facilitate the maintenance operations. Cold magnetic shields cover the helium bath of cavity. The RF power couplers are horizontal installed and its thermal anchors are connected to the corresponding cold source by copper braided tapes. The bi-phase pipe is positioned horizontally on the top of the cavities. The cold mass is surrounded by the thermal shield.

NEUTRALIZER-BASED LONGITUDINAL BUNCH PROFILE MEASUREMENT DESIGN*

C.E. Taylor[†], H. Andrews, E.C. Huang, J.W. Lewellen, C. Rohde, R.T. Thornton
Los Alamos National Laboratory, Los Alamos, New Mexico, USA

Abstract

The Longitudinal Profile Monitor (LPM) system aims to measure and control particle beam tails in high-power particle accelerators. Using a picosecond laser, portions of H⁻ ion beams are neutralized into H⁰ atoms for detection. Despite challenges in laser synchronization and hardware installation, progress was made in laser system development, beamline hardware installation, and magnet system integration. This project advances diagnostic technology and workforce development, positioning LANL at the forefront of H⁻ beam diagnostics. Continued programmatic efforts will focus on overcoming remaining challenges and completing the development of this diagnostic tool.

INTRODUCTION

The neutralizer-based LPM project has been a pivotal endeavor in advancing the field of particle accelerator diagnostics. This project, initiated to tackle the challenges associated with measuring and controlling the tails or halos of high-power particle beams, has involved intricate planning, extensive collaboration, and the integration of cutting-edge technology [1, 2]. As we reach a critical juncture in the project's timeline, it is essential to reflect on the journey so far, the technical progress made, the challenges encountered, and the outcomes achieved. Here, we provide a comprehensive overview of the project's development, highlighting key milestones and setting the stage for future advancements.

Particle accelerators like those at the Los Alamos Neutron Science Center (LANSCE) and the Spallation Neutron Source (SNS) are essential tools in both scientific research and national security missions. These accelerators generate high-energy beams of particles that are used in a variety of applications, from fundamental physics research to the maintenance of the national nuclear stockpile. However, one of the persistent challenges in operating these accelerators is the presence of beam tails or halos—portions of the beam that contain only a small fraction of the total beam current but can have significant consequences if not properly managed. Even small beam losses can lead to radiation generation, component activation, and physical damage to the accelerator itself. Thus, developing a reliable method to measure and control these tails is of paramount importance.

* This work benefitted from the use of the LANSCE accelerator facility. Work was performed under the auspices of the US Department of Energy by Triad National Security under contract 89233218CNA000001.
[†] cetaylor@lanl.gov

BACKGROUND AND OBJECTIVES

The primary objective of this project was to develop a non-perturbative diagnostic tool capable of accurately measuring the longitudinal profile of H⁻ ion beams within accelerators. Traditional diagnostic methods often require intercepting the beam, which can be disruptive to the accelerator's operation [3]. Our approach was different. We proposed using a picosecond (ps) laser to selectively neutralize portions of the beam, converting H⁻ ions into neutral H⁰ atoms (Fig. 1). This process allows for the measurement of the beam's profile without significantly disrupting the beam's operation, making it a transformative advancement over existing diagnostics.

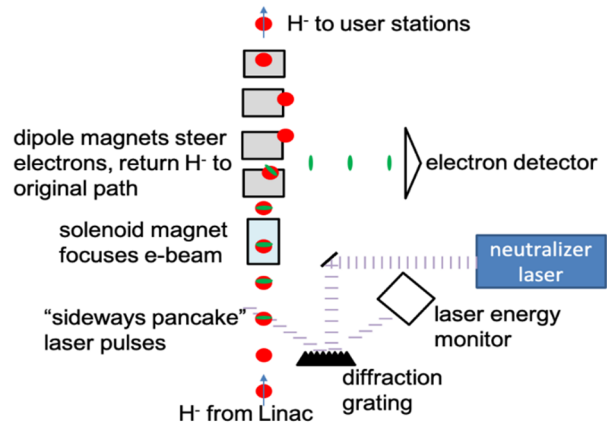


Figure 1: Schematic of the diagnostic.

The project was designed with several specific technical goals in mind:

- 1. Measurement of self-neutralization rates:** Understanding how H⁻ ions naturally convert to neutral atoms within the accelerator. Initially, this was considered critical for calibrating the diagnostic tool. However, it was later determined that collecting the stripped electrons would provide the necessary data without requiring the measurement of self-neutralization rates.
- 2. Measurement of the longitudinal bunch profile:** Achieving a resolution of approximately 1 ps was essential for capturing the fine details of the beam structure. This high resolution would allow us to measure the bunch length and tail amplitude with unprecedented precision.
- 3. Detection of shadow bunch amplitudes and profiles:** Beam tails extending to at least 4 σ from the bunch center were of particular interest. By accurately measuring these tails, we could minimize radiation production and optimize the beam transport process.

GENERALIZATION ABILITY OF CONVOLUTIONAL NEURAL NETWORKS TRAINED FOR COHERENT SYNCHROTRON RADIATION COMPUTATIONS *

C. Leon[†], P.M. Anisimov, N. Yampolsky, A. Scheinker

Applied Electrodynamics Group, Los Alamos National Laboratory, Los Alamos, NM, USA

Abstract

Coherent synchrotron radiation (CSR) has a significant impact on electron storage rings and bunch compressors, inducing energy spread and emittance growth in a bunch. Calculating the effects of CSR is computationally expensive, severely limiting the use of simulations. Here, we explore utilizing neural networks (NNs) to model the 3D wakefields of electrons in circular orbit in the steady state condition. NN models were trained on both Gaussian and more general bunch distributions, which evaluate much faster than physics-based simulations. Here, we explore how well the models generalize, by testing their ability to: 1) extrapolate to Gaussians with smaller/larger widths 2) predict on distributions never encountered before (out of distribution generalization) using smoothed uniform cubes. We see the models are able to generalize, which makes them potentially useful in the design and optimization of accelerator apparatuses by enabling rapid searches through parameter space.

INTRODUCTION

Coherent Synchrotron Radiation (CSR) can significantly alter the distribution of electrons moving in circular orbit, such as in an electron storage ring or a bunch compressor. For emitted wavelengths, λ , much larger than the bunch size, then at λ -resolution the bunch looks point-like, and the N_e electrons look like they're all undergoing nearly identical motion. Consequentially, the radiation emitted by these electrons are approximately in phase and adds up coherently, resulting in an intensity of $\mathcal{O}(N_e^2)$. This can significantly distort the bunch phase space distribution. In the ultra-relativistic limit, this primarily causes the tail and center of the bunch to lose energy while the head gains, leading to an increase in emittance.

The electromagnetic (EM) field produced by a charged point particle in motion is given by the well-known Liénard-Wiechart (LW) fields [1–3]:

$$\mathbf{E} = \frac{q}{4\pi\epsilon_0} \left(\frac{\mathbf{n} - \boldsymbol{\beta}}{\gamma^2(1 - \mathbf{n} \cdot \boldsymbol{\beta})^3 \rho^2} + \frac{\mathbf{n} \times (\mathbf{n} - \boldsymbol{\beta}) \times \dot{\boldsymbol{\beta}}}{c(1 - \mathbf{n} \cdot \boldsymbol{\beta})^3 \rho} \right) \Big|_{ret.}, \quad (1)$$

$$\mathbf{B} = \frac{1}{c} \mathbf{n} \times \mathbf{E}, \quad (2)$$

where the *ret.* signifies that the expression must be evaluated at the retarded time to ensure causality.

* Work was supported by the Los Alamos National Laboratory Laboratory Directed Research and Development (LDRD) DR project 20220074DR.
[†] cleon@lanl.gov

The total force an electron experiences due to the radiation emitted by other electrons in the past is called the wakefield, $W(\mathbf{r}, t)$. To find it, one must integrate the Lorentz force, $F(\mathbf{r}, t)$, generated by the LW fields in Eqs. (1) and (2) along the past light cone:

$$W(\mathbf{r}) = \int_{\Delta} d^3r' \lambda(\mathbf{r}', t') F(\mathbf{r}', t') \Big|_{ret.}, \quad (3)$$

where Δ signifies the past light cone, time in the integrand is the retarded time and $\lambda(\mathbf{r}', t')$ is the number density. The computational storage needed to do the evaluations at the retarded times and the computational expense of $\mathcal{O}(N_e^2)$ interactions, with typical bunch sizes of $N_e \sim 10^{10}$, for each time step makes designing practical software for CSR calculations a formidable task. To deal with the complexities, many approximations are commonly used, such as the 1D approximation [4]. Even in the specific case of circular motion in the 1D approximation, though, the incorporation of CSR effects in a simulation can increase the running time of the simulation by an order of magnitude [5]. This makes many conventional simulations far too slow for some applications, such as a thorough exploration of parameter space to optimize accelerator component design. With the production of smaller bunch sizes in accelerator facilities, the need for a fast and accurate account of 3D CSR has become important.

Machine learning (ML) can speed up simulations to provide real-time virtual diagnostics which can be used for real-time adaptive beam control. For example, in [6] the first approach to adaptive ML was demonstrated combining a deep learning with adaptive feedback [7] for automatic control of the longitudinal phase space of the LCLS FEL electron beam. They can also be used to speed up accelerator simulations [8, 9]. Convolutional neural network (CNN) computations utilize matrix multiplications and several parallelized operations and with modern GPU's, which are optimized for such tasks, can be performed rapidly. Hence, a CNN trained on CSR simulations data can lead to very fast computations.

Previous work has investigated the use of ML surrogate models to speed up CSR calculations. Mayes and Edelen used a dense neural network in the 1D case to speed up CSR calculations [10]. CNN's in particular have been utilized in the 2D transient case [11].

Here, we take previous CNN models trained to predict the fully 3D wakefields generated by electrons at steady-state [12] and see their generalization ability. Specifically, we investigate at how well it performs at extrapolating to

COLLIMATIONS SYSTEMS STUDIES AT LANSCE

C.-M. Alvinerie[†], E.-C. Huang, S. Sosa Guitron, C. Taylor, J. Upadhyay
Los Alamos National Laboratory, Los Alamos, New Mexico, USA

Abstract

At the Los Alamos National Neutron Science Center (LANSCE), the LANSCE Modernization Project (LAMP) includes beamline studies that could help the operation. For the PSR, reducing or at least controlling the beam losses could maximize the beam current delivered to the users and extend the run cycle via shortening the maintenance period. One of the approaches would be to install collimations that are not present at LANSCE. Preliminary results are discussed in this proceeding to evaluate various possibilities of collimation systems along the high energy beam transport and/or in the ring.

INTRODUCTION

The Los Alamos Neutron Science Center, illustrated in Fig. 1, is a unique facility with several applications for engineering and science studies. In this facility, the Drift Tube Linac and the Side Coupled-Cavity Linac accelerates a H-beam up to 800 MeV to deliver it to multiple user stations requiring different beam structures.

In this configuration, the Proton Storage Ring (PSR) compresses a long macro pulse of protons (625 μ s) at a nominal 800 MeV energy into a short pulse of 290 ns. This empowers the Manuel Lujan Neutron Scattering Center for experiments using spallation neutrons. Facility users would prefer a higher beam current for a better signal-to-noise ratio. However, this current is limited by the beam losses, among other reasons.

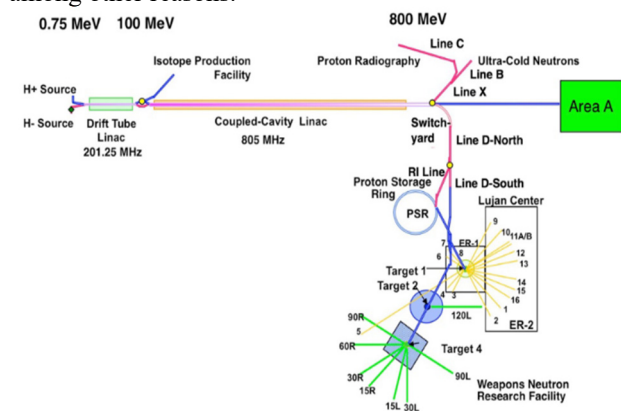


Figure 1: Overview of the LANSCE facility [1].

Radiations produced by beam losses require long cool-down time and prevent hands-on maintenance after the beam production period. Reducing beam losses will produce less radiation in the PSR and potentially shorten the maintenance time required. Furthermore, the beam inside the ring can be imperfect due to instabilities like the electron-proton instability [2]. This instability describes the

[†] calvinerie@lanl.gov

interaction between an electron cloud potentially produced from lost particles and the subsequent proton bunches. Therefore, it could be reduced by at least controlling the beam losses.

Prospective studies are explored to reduce or at least controlling the beam losses in the PSR. One of the solutions would be to install collimation systems, not currently present at LANSCE. For several years, beam collimation systems are a scientific subject in different high-energy facilities (accelerators and/or rings) as at SNS [3], Fermilab [4], J-PARC [5], LHC [6] and PIP-II [7]. This proceeding presents a study for potential locations of collimation systems at LANSCE to control beam losses. First, we introduce collimation systems that could be applied at LANSCE. Then, we will discuss on the collimation choice for the LANSCE facility. Finally, we will briefly propose a beam collimation experiment.

BEAM COLLIMATION

The collimation systems are chosen depending on several factors, such as beam characteristics (species, energy), type of collimation to be operated (off-momentum, etc.) or location of collimators in the accelerator and/or ring.

At LANSCE, beam losses appear notably from downstream the linac to the PSR. This facility works in a similar way as the SNS facility. So, based on collimator systems locations at SNS, two different collimation possibilities are discussed: around the stripping foil in PSR and/or downstream the linac (Switchyard and Line D-North areas).

The first solution could be a collimation system around the stripping foil in the PSR. The idea is to install a collimator after the stripping foil and capture the partially stripped particles and send them to the beam stop. To avoid a full collimator due to space constraints, detail studies are undergoing to identify optimal collimation scheme. This will not be included in this proceeding.

The second solution, around the Switchyard and Line D-North areas, is then presented more in details. Downstream the linac, the beam is composed of H- particles. Among all the different collimation systems, collimation with stripping foils is particularly efficient for H- beam [8-10]. It represents a simple mechanism to remove the beam halo, an important source of beam losses in the ring. By using stripping foils, the H- halo particles are converted in H+ ones, creating a different trajectory from the main bunches. There are two ways to deal with the H+ beam: absorbing them locally by a collimator (absorbers) or transport them to a beam dump. In this case, the H+ beam (stripped particles) is separated from the H- beam (unstripped particles) thanks to a magnetic field and transported to a well shielded beam dump. Having only one beam dump for the stripped particles instead of having a full collimator system inside the line has a better efficiency and the advantage to

DTL STUDIES FOR THE LANSCE FUTURE FRONT-END UPGRADE AT LANL*

D. V. Gorelov[†], D. A. Dimitrov, L. D. Duffy, E. Henestroza, S. S. Kurennoy, S. I. Sosa
Los Alamos National Laboratory, Los Alamos, NM, USA

Abstract

LANSCE accelerator complex was successfully supporting nuclear science research at LANL for more than 50 years. However, the need of the upgrade of the linear accelerator becomes immanent due to development of the modern accelerator technology, and due to inevitable aging of the existing equipment. The first stage of the planned upgrade of the linear accelerator at LANSCE includes the replacement of the outdated proton and H- Cockroft-Walton (CW) sources with the modern RFQ accelerator, and development of the new DTL. The proposed DTL is designed to accelerate protons and H- ions simultaneously, just as the existing accelerator, from 3 MeV – the output energy of the RFQ, to 100 MeV, that will allow us to keep existing Coupled Cavities Linac (CCL) intact. Presently existing megawatt-class RF power amplifiers will be used in the proposed new DTL. The details of the proposed design of the DTL will be given in the present paper. The details will include the main linear accelerator parameters, like synchrotron and betatron oscillations frequencies, as well as the developed techniques for the design studies.

INTRODUCTION

LANSCE accelerator modernization project (LAMP) is the first stage of the upgrade of the linear accelerator facility at Los Alamos National Laboratory (LANL). This project proposes replacement of the existing CW ion sources for protons and H- with new Low Energy Beam Transport (LEBT) at 100 keV, a new RFQ accelerator, and new Medium Energy Beam Transport (MEBT) at 3 MeV. A new DTL will be designed to accelerate beams up to 100 MeV.

SCOPING STUDIES PRINCIPLES

The main limitations of the DTL design are the existing RF power amplifiers at frequency 201.25 MHz and maximum power ~ 2 MW each. We have 6 of those tubes, called Diacrodies, and hence we are planning to have 6 accelerating DTL tanks with rf power requirements below 2 MW each.

The other hard limitation is the existing tunnel, that the new DTL will be placed in. The total length of the tunnel and the available RF power dictate the range of the accelerating gradient values, that can be used in the new DTL.

We are planning to use Permanent Magnet Quadrupoles (PMQ) magnets for transverse focusing in the drift tubes, since the available technologies give us the desired results

* This work benefited from the use of the LANSCE accelerator facility. Work was performed under the auspices of the US Department of Energy by Triad National Security under contract 89233218CNA000001.

[†] gorelov@lanl.gov

without the drawbacks of the electrostatic magnets scheme, that is used in the existing DTL at LANSCE.

We start the design process with choosing of the suitable synchrotron and betatron oscillation frequencies along the DTL by finding adequate transverse focusing period length and PMQs strength, that can be achieved in practice. The focusing lattice F0D0 was found to satisfy our requirements for the beam dynamics, where “O” represent empty drift tubes, and “F” and “D” – focusing and defocusing quadrupole in horizontal transverse plane respectively. The result of our choice is presented in Figs. 1 and 2. The nomenclature of the variables correspond to Refs. [1,2].

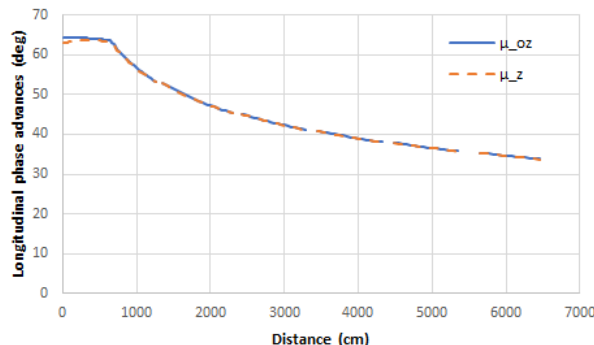


Figure 1: Synchrotron oscillations phase advance per focusing period for negligible beam current and for the design beam current of 35 mA.

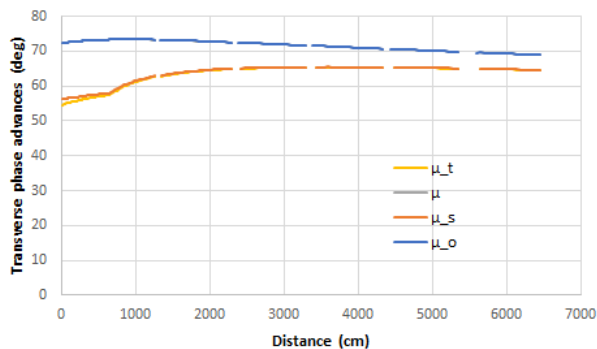


Figure 2: Betatron oscillations phase advance per focusing period for negligible beam current and for the design beam current of 35 mA.

The presented combination of the phase advances avoids the dangerous parametric resonance anywhere along the DTL, as well as stay below 90° , which is the limit of stable region for beam with high current [3]. Sufficient adiabatic continuity of the oscillation frequencies was preserved and

ONLINE MULTI-PARTICLE MODEL FOR LANSCE PHYSICS TUNE-UP WITH HPSim*

E.-C. Huang[†], P. M. Anisimov, A. J. Braido, M. J. Kay, L. J. Rybarczyk[‡], J. K. K. Quemuel
Los Alamos National Laboratory, Los Alamos, NM, USA

[‡]also at COMPA Industries Inc., Los Alamos, NM, USA

Abstract

The accelerator at the Los Alamos Neutron Science Center (LANSCE) delivers beam to five user facilities, including the Isotope Production Facility (IPF), the proton Radiography (pRad), Ultra-Cold Neutron (UCN), Lujan Center and the Weapon Neutron Research (WNR). The high-power operation of the LANSCE accelerator is often limited by the level of beam losses, especially for IPF and the Lujan Center which require higher average current. Longitudinal halos and tails, one of the major source beam losses, could be easily generated via longitudinal mismatch under present bunching scheme and the large uncertainties of cavity power measurements. We present a GUI with an online multi-particle model based on HPSim. This could potentially help the beam physicists intuitively determine the quality of the longitudinal capture after each phase scan, and therefore, reduce the beam losses due to longitudinal mismatch.

INTRODUCTION

The acceleration and bunching scheme of the LANSCE linac contains the following steps (Fig. 1): Both H^+ and H^- DC beams are accelerated by their respective Cockcroft-Walton (CW) generator to 750 keV. An H^- beam chopper creates the desired timing structure for different user facilities, and the WNR beam goes through an additional low-frequency buncher [1]. Afterwards, both species are bunched by their respective Pre-Buncher (PB) before entering a common Main Buncher (MB). The bunchers transform the DC beam into the basic 201.25-MHz micro-bunch structures before the beam enters the Drift Tube Linac (DTL). During operation, around 20-30% of the beam falls outside of the DTL longitudinal acceptance and is lost in the DTL. Furthermore, since the beam fills almost the whole phase range of the initial DTL acceleration bucket, halos and tails could easily form from a longitudinal mismatch in the subsequent accelerating modules in both DTL and the 805-MHz Side-Coupled Cavity Linac (CCL).

To clean up the tails and halos generated by the longitudinal mismatch, it normally takes operators 1-2 weeks to fully ramp up the current and lower the beam losses to acceptable range every year after the initial physics tune-up. Empirically, the first three of the four DTL modules were adjusted the most to reduce tails/halos formed in the early stage. LANSCE relies on the physics

tune-up at the beginning of each run cycle, as we still yet cannot reliably return to past stable operation points. However, the physics tune-up procedures do not currently address the halos/tails. For the DTL, an absorber/collector pair [2] is used to measure the beam current above a given energy threshold under a phase scan. The present procedure only considers three measured parameters: the Full Width Half Maximum (FWHM), which represents the phase width of the acceleration bucket, the relative phase in the bucket, and peak-to-valley ratio (PVR) for the first module to constrain the effects of the bunchers. For the CCL, we use Beam Position and Phase Monitors (BPPMs) for signature matching of a phase scan. This ensures the beam, on average, is correctly accelerated [3]. However, this method does not easily demonstrate the picture of the longitudinal capture. While many other facilities rely on power measurements for each cavity to return to known amplitude setpoints, LANSCE has also attempted such effort [4]. However, LANSCE has yet to reliably reproduce cavity amplitude setpoints based on power measurements due to aging cavities and the problematic performance of klystrons [5]. Therefore, beam-based signature matching is the only reliable method for us to determine the amplitude setpoints of each CCL module.

Therefore, an online multi-particle model for the physics tune-up is critical for LANSCE to reduce the initial optimization time by operators for every run cycle. In this proceeding, we present an online software tool based on the GPU-based HPSim [6-8] that quickly converts the phase scan results into intuitive pictures of the longitudinal capture.

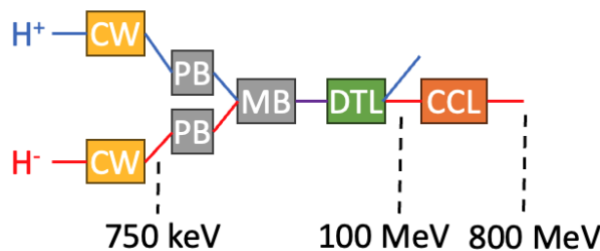


Figure 1: A schematic of LANSCE acceleration and bunching scheme. Both H^+ and H^- beam go through their respective Cockcroft-Walton (CW) generator and Pre-Buncher (PB), and merge into the same Main Buncher (MB). The beam delivered to WNR also goes through a Low Frequency Buncher (LFB) before the PB. The Drift Tube Linac (DTL) accelerates both H^+ and H^- to 100 MeV while the Side-Coupled Cavity Linac (CCL) accelerates H^- to 800 MeV.

* This work was supported by Los Alamos National Laboratory's Laboratory Directed Research and Development (LDRD) Program under project 20230409MFR.

[†] en-chuan@lanl.gov

DESIGN OF A MULTI-PURPOSE LEBT FOR THE LANSCE FRONT END UPGRADE*

E. Henestroza†, S. Sosa Guitron, S. Kurennoy, D.A. Dimitrov, J. Upadhyay
Los Alamos National Laboratory, Los Alamos, NM, USA

Abstract

The Los Alamos Neutron Science Center (LANSCE) facility at LANL is considering an upgrade of its front end, from the source to the end of a 100 MeV Drift Tube Linac (DTL). One of the main features of LANSCE is that it delivers several types of bunching systems to five users (Isotope Production Facility, Lujan Neutron Scattering Center, Ultra Cold Neutron Center, Proton Radiography Facility “pRad” and the Weapons Neutron Research Facility “WNR”). The first three users accept bunch trains modulated at 201.25 MHz produced from quasi-DC beams. The WNR facility requires the delivery of sub-nanosecond bunches every 1.8 μ s. At present the bunching system for the WNR beam is prepared in a 750 keV Low Energy Beam Transport (LEBT) lattice. The proposed upgrade will need to manipulate short bunches for WNR at an energy of 100 keV to be injected into a 3 MeV RFQ. The quasi-DC beams can be charge-compensated by the ionization of background gas, which cannot be done for the short bunches of WNR. A similar situation happens with the pRad beams. At such low beam energy, the uncompensated space charge of the bunch will require a special LEBT design that will work simultaneously for all types of beams to be delivered by the LANSCE upgrade. We will describe a new LEBT layout for the LANSCE Front End Upgrade that will be able to deliver the required beam bunches to all facilities.

INTRODUCTION

The Los Alamos Neutron Science Center (LANSCE) accelerator delivers high intensity proton beams for fundamental science and national security applications since 1972. LANSCE is capable of simultaneous H^+ and H^- beam operations to multiple experiments requiring different time structures. This is achieved upstream in the facility with a combination of two 750 kV Cockcroft-Walton (CW) generators, a chopper and radiofrequency cavity pre bunchers, and a Drift Tube Linac to accelerate the beam to 100 MeV. The proposed LANSCE Modernization Project (LAMP) is evaluating critical machine upgrades necessary for continuous beam operations in decades to come. A significant component of LAMP is replacing the two CW with a dual-species 3-MeV Radiofrequency Quadrupole (RFQ). This change requires a full re-design of the LANSCE front-end accelerator to deliver the existing and expanded capabilities of the facility.

A design of a concept for a Front End Upgrade of the LANSCE Linac has been set up to perform a start-to-end

* This work benefitted from the use of the LANSCE accelerator facility. Work was performed under the auspices of the US Department of Energy by Triad National Security under contract 89233218CNA000001.

† henestroza@lanl.gov

modeling of the system at the current development stage. The components of the design are shown in Fig. 1. The sequence of the components is correct; however, the sketch is not to scale.

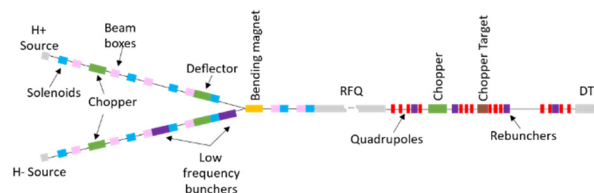


Figure 1. Concept for a LANSCE Front End Upgrade.

The LANSCE Upgrade front-end concept discussed here evolved from a design described in a previous report [1]; the H^- and H^+ ion sources, the RFQ and the MEBT have not changed. Here we will discuss the design of a multi-purpose LEBT that will work simultaneously for all types of beams to be delivered by the LANSCE upgrade.

CHARGE COMPENSATION IN THE LEBT

The LANSCE Front End Upgrade is required to deliver 625 μ s beam macro pulses with specific time structures to the present users. A chopper located in the H- LEBT provides such bunching systems.

The use of a 100 keV beam to inject into the 3 MeV RFQ that replaces the Cockcroft-Walton generators turns the LANSCE 750 keV LEBT into a 100 keV LEBT, thereby increasing the space charge force substantially: $(750/100)^{1.5} \sim 20$. Therefore, there is a large difference in the beam dynamics in the 100 keV LEBT among beam pulses that can or cannot be charge compensated.

To study the beam dynamics in the LEBT, we can group the five types of beam structures in two groups.

The macropulses delivered to Lujan Neutron Scattering Center, Ultra Cold Neutron Center and Isotope Production Facility can be treated as long (625 μ s) quasi-DC beams where we expect to have in the 100 keV LEBT a large charge-compensation by ionization of the background gas [2]. This type of macropulses will be referred as **LBEG**-type beams. The H^+ beam delivered to the Isotope Production Facility is a DC beam, but the other two H^- beams are basically 625 μ s pulses where 70 ns slices are removed every 360 ns.

The Weapons Neutron Research Facility requires the delivery of sub-nanosecond bunches every 1.8 μ s at the target. At present the bunching system for the WNR beam is prepared in a 750 keV LEBT where the macropulse is chopped every 1.8 μ s to provide a 30 ns beam bunch to a 16.67 MHz Low Frequency Buncher that compresses the pulse to ~ 5 ns to match the frequency (201.25 MHz) of the 750 keV-100 MeV DTL. Due to the sparsity of this time

NEW CONCEPTS FOR A HIGH POWER 805 MHz RF AMPLIFIER FOR LANSCE USING GALLIUM NITRIDE SEMICONDUCTORS*

J. T. M. Lyles[†], J. D. Alvarez Prieto, S. A. Baily, M. S. Barrueta, J. T. Bradley III, E. N. Brown, M. C. Brown, J. L. Castellano, B. N. Comiskey, T. W. Hall, S. I. Kwon, M. S. Prokop, S. Rocha, M. B. Rodriguez, P. J. Van Rooy, S. J. Russell, J. A. Valladares, A. S. Waghmare
Los Alamos National Laboratory, Los Alamos, NM, USA

Abstract

Los Alamos Neutron Science Center (LANSCE) uses a coupled-cavity linac (CCL) to accelerate H- beam from 100 to 800 MeV. This was the first CCL put into operation anywhere in 1972 and is powered by forty-four 1.25 MW 805 MHz klystrons developed in the same era. A new initiative is underway to develop a replacement RF power amplifier that fits in place of one klystron with HV modulator tank and is functionally equivalent or better in RF performance. Conventional LDMOS transistors based on silicon have reduced power above 500 MHz and are also limited in peak power by the maximum drain voltage (50-65 volts). Changing wireless infrastructure is causing leading manufacturers to introduce and discontinue products within a decade. Long term operation of LANSCE requires continuity of product availability. We have chosen leading-edge high voltage Gallium Nitride (GaN) on Silicon Carbide transistors to be able to reduce the number of active devices and the complexity of power combing. GaN has inherent higher temperature and voltage capability. We are testing devices for 3.6 kW of saturated power at 100 volts, and improvements are underway. Combining technology is also under study as part of the overall system.

INTRODUCTION

LANSCE has operated as a 800 MeV proton and H- linac since 1972. Presently protons of 100 MeV from the drift tube linac are used for isotope production while a subsequent CCL accelerates H- beam from 100 to 800 MeV. This normal conducting structure is powered by forty-four 1.25 MW 805 MHz klystrons, which all together provide approximately 44 MW of peak RF power and 5.3 MW of average power. These mod-anode klystrons are still available using the same design as the original tubes. The LANSCE linac is expected to continue operation until 2050, and there are growing concerns about relying solely on this vacuum electron tube technology for 25 more years. Mean time between failure for current klystrons is shorter than it was for the original production tubes [1]. They rely on 86 kV beam voltage from conventional mains power

* Work supported by the U.S. Department of Energy through the Los Alamos National Laboratory, operated by Triad National Security, LLC, for the National Nuclear Security Administration of U.S. Department of Energy (Contract No. 89233218CNA000001). Research presented in this article was supported by the Laboratory Directed Research and Development program of Los Alamos National Laboratory under project number 20240723DI.

[†] jtml@lanl.gov

supplies and capacitor banks, which present their own set of technical difficulties that are beyond the scope of this paper.

A new initiative is underway to develop a replacement RF power amplifier that can fit in the space of one klystron with a HV modulator tank. This will use a multitude of Solid-State Amplifiers (SSA) combined to produce the equivalent or better performance than the klystron. Peak power capability has been a hallmark for vacuum tubes, where the thermal mass is large and the peak to average power ratio is unity (CW) to as high as ten. For a SSA, the best approach is operating in continuous mode, and this has enabled SSAs to replace klystrons or inductive output tubes at dozens of synchrotrons and storage rings worldwide [2]. Pulsed operation, such as for the LANSCE CCL, requires considering the intrinsic peak capability of the individual junctions or channels inside transistors. Transistors require matching circuits adjacent to the input and output terminals, using discrete capacitors, inductors and microstrip lines. The functional block of transistor (single or push-pull device) plus matching is a pallet. This is the basic building block of all SSA.

TRANSISTOR CONSIDERATIONS

Silicon transistors using laterally-diffused metal-oxide semiconductor (LDMOS) construction are often rated at a maximum operating DC (drain to source) voltage of 50-75 volts. LDMOS is a mature technology from multiple manufacturers and has powered wireless communication for decades. They can be made from large wafers in conventional silicon foundries so the price per watt is attractive. These devices can generate up to 2 kW of saturated peak power below 500 MHz but at 805 MHz the gain and peak power drops. The drain to source capacitance of these devices, related to their construction, limits further improvement in their frequency-power product. As upcoming wireless technology such as 6G requires considerably more bandwidth into GHz bands, LDMOS is less viable, and new transistor technologies have come into use.

Gallium Nitride (GaN) on Silicon Carbide (SiC) is a high electron mobility transistor that is becoming available from multiple sources [3]. The wide bandgap of the semiconductor allows for higher breakdown voltage rating while operating at increased channel temperature. GaN RF transistors operating above 100 volts DC are now available [4, 5] at UHF and L band. Matching of the drain terminal to fifty Ohm transmission line is easier as the transistor load impedance is proportional to the RF drain voltage. When comparing transistors it is important to understand the class

LATENT EVOLUTION MODEL FOR TIME-INVERSION OF SPATIOTEMPORAL BEAM DYNAMICS*

M. Rautela^{†,1}, A. Williams¹, A. Scheinker¹

¹Applied Electrodynamics (AOT-AE), Los Alamos National Laboratory, Los Alamos, NM, USA

Abstract

The problem of estimating upstream six-dimensional phase space given downstream measurements of charged particles is an inverse problem of growing importance. In this work, we propose a latent evolution model (LEM) to invert the forward spatiotemporal beam dynamics. In this two-step self-supervised deep learning framework, we first use a conditional variational autoencoder (CVAE) to transform 6D phase space projections of a charged particle beam into a lower-dimensional latent distribution. We then autoregressively learn the inverse temporal dynamics in the latent space using a long-short-term memory (LSTM) network. The coupled VAE-LSTM framework can predict 6D phase space projections in upstream accelerating sections given single or multiple downstream phase space projections as inputs.

INTRODUCTION

Particle accelerators are complex, time-varying, high-dimensional systems governed by hundreds to thousands of radio-frequency (RF) cavity and magnet parameters. The dynamics of charged particle beams in accelerators emerges as spatiotemporal phenomena, characterized by the temporal evolution of a six-dimensional phase space (x, y, z, p_x, p_y, p_z) . The solution of such dynamical systems can be computationally demanding due to the intricate interplay between temporal evolution and detailed spatial features. Machine learning and deep learning methods have shown significant promise for challenging different spatiotemporal dynamical problems. Recently, latent evolution models (LEM) have gained traction for solving various dynamical systems [1–5]. The key idea is to decompose the learning problem into spatial and temporal learning, which are later coupled to make predictions.

Recent applications of Latent Evolution Models (LEM) for addressing beam dynamics in particle accelerators have shown significant progress. In Refs. [6–8], an adaptive virtual 6D phase space diagnostic was developed, where an autoencoder compresses high-dimensional 6D phase space projections into a low-dimensional latent space. Adaptive feedback within this latent space is then used to track the properties of an unknown, time-varying beam as accelerator parameters evolve. In Refs. [9, 10], a conditional variational autoencoder combined with an autoregressive LSTM is employed to generate and predict beam dynamics throughout the accelerator based on initial module measurements.

* Work supported by the LANL LDRD Program Directed Research (DR) project 20220074DR

[†] mrautela@lanl.gov

The solution of inverse problem to estimate upstream phase space is essential for characterizing the beam in earlier sections of the accelerator, which in turn helps to understand beam dynamics, minimize beam losses, and optimize accelerator performance. However, limited studies are conducted on predicting the upstream phase space of charged particles based on downstream measurements. In Ref. [8], an adaptive ML approach has been proposed to map output beam measurements to input beam distributions. In Ref. [11], neural networks are integrated with differentiable particle tracking to learn mappings from measurements to initial phase space distributions.

In this paper, we propose a latent evolution model (LEM) that predicts the upstream 6D phase space from downstream measurements. The model uses a conditional VAE to learn the low-dimensional latent distribution of 15 unique phase space projections, followed by an autoregressive LSTM to reverse the forward temporal dynamics in the latent space. This coupled network enables the prediction of upstream phase space projections based on single or multiple downstream measurements.

METHODS

Charged Particle Beam Dynamics

The behavior of charged particles in accelerators is influenced by numerous parameters, such as radio frequency cavity fields and magnetic field strengths. These parameters are manually adjusted to minimize beam loss, but this process is time-consuming, often leading to suboptimal performance. Additionally, limited non-destructive beam measurements and short run times complicate data collection. It is crucial to understand beam dynamics for optimal accelerator performance. More details about the optimization and tuning challenges of the LANSCE accelerator are given in Ref. [12].

The dynamics of a beam's phase space density function are governed by the relativistic Vlasov equation

$$\frac{\partial \rho}{\partial t} = -\mathbf{v} \cdot \nabla_{\mathbf{x}} \rho + \frac{\partial \mathbf{p}}{\partial t} \cdot \nabla_{\mathbf{p}} \rho, \quad (1)$$

$$\frac{\partial \mathbf{p}}{\partial t} = q (\mathbf{E}(x, y, z, t) + \mathbf{v} \times \mathbf{B}(x, y, z, t)), \quad (2)$$

with \mathbf{v} and \mathbf{p} representing velocity and relativistic momentum:

$$\mathbf{v} = \left(\frac{dx}{dt}, \frac{dy}{dt}, \frac{dz}{dt} \right), \quad \mathbf{p} = (p_x, p_y, p_z) = \gamma m \mathbf{v},$$

$$\gamma = \frac{1}{\sqrt{1 - v^2/c^2}}, \quad v = |\mathbf{v}|, \quad (3)$$

where c is the speed of light [13]. The electromagnetic fields, \mathbf{E} and \mathbf{B} each have external and beam-based sources.

HIGH-VOLTAGE FEED DESIGN FOR ELECTROSTATIC POTENTIAL DEPRESSION IN AN RF ACCELERATOR*

M. Sanchez Barrueta†, H. Xu, Los Alamos National Laboratory, Los Alamos, USA

Abstract

Space-borne accelerator technologies suffer from significant electron beam loss during beam acceleration and excessive energy spread of the output beam. Los Alamos National Laboratory is proposing a deployable and compact solution using electrostatic potential depression (EPD) to achieve higher bunching, lower beam loss, and smaller energy spread, with an electron bunch repetition rate of 5.7 GHz. This buncher system involves two EPD sections, each electrically insulated from the RF cavities and with a separate high voltage power supply, whose leads will have to reach through vacuum and the insulator to bias the specific section of the buncher. This presents considerable challenges due to the triple junction problem and the presence of parasitic radiofrequency leaking through the electrostatic high voltage gaps.

INTRODUCTION

In compact radiofrequency (RF) accelerator applications, the electron beam source is usually a direct-current (DC) electron gun. If the DC electron beam is sent directly into the RF accelerator, only a very small portion of the beam will fall within the desired longitudinal acceptance of the RF accelerator. In order to maximize the DC electron beam capture in the RF accelerator, in large-scale, facility accelerators, meter-long buncher sections are used in the beamline. Those buncher structures consume external RF power at a megawatt (MW) level. For compact accelerators, the high-power buncher scheme is inefficient, and thus unadoptable.

Recently, at Los Alamos National Laboratory (LANL), a novel type of electron beam buncher is under development [1]. The buncher is intended for application on a space-borne electron RF accelerator, and it is intended for the purpose of increasing the usable portion of the DC beam generated, meanwhile keeping the energy spread of the electron bunch at a low level. Such an electron beam buncher will significantly benefit space missions where an RF accelerator is entailed, such as the Beam-Plasma Interactions Experiment (Beam PIE) [2].

The electron beam buncher was designed based on a compact, high-efficiency klystron architecture [3], the unique feature of which is the utilization of electrostatic potential depression (EPD) inserts. In the klystron architecture, an EPD insert, or section, refers to a short section of the metallic beam pipe that is applied with a negative high voltage (HV). The HV-biased beam pipe is insulated from other parts of the klystron, which are grounded. The

EPD sections cause the electron beam bunching formation to take place over a very short distance, allowing the entire klystron circuit to be compact. In this proceeding, we report the basic architecture of the electron beam buncher and introduce the design considerations of the HV feed as well as the insulators. We also discuss the parasitic mode excitation by the pre-bunched electron beam transiting across the HV gaps of the EPD sections. Our electromagnetic and particle-in-cell (PIC) simulations were performed using the CST Simulation Suite [4].

BUNCHER CONCEPTUAL DESIGN

The buncher architecture takes after a two-cavity klystron circuit, assisted by the EPD sections for achieving compactness, as presented in Fig. 1. An electron gun generates pulsed DC electron beam, and the solenoid focuses the electron beam into the buncher circuit. Inside the buncher, the beam focusing is provided by permanent magnets, which were designed to be tunable [1], as inspired by an ongoing project at SLAC [5]. The input cavity provides the initial energy modulation by the longitudinal RF electric field, at a frequency of 5.7 GHz. When the modulated, or pre-bunched, electron beam enters the first EPD section (EPD-1), its average kinetic energy is significantly reduced. However, the energy difference among the electrons is preserved. As a result, the wave-break in the longitudinal phase space occurs over a very short distance. When the electron beam leaves EPD-1, its original kinetic energy is recovered. The idler cavity in the downstream then further adjusts the longitudinal phase space of the electron beam to allow subsequent enhancement of the bunching formation. The function of EPD-2 is identical to EPD-1, maximizing the bunching level over a short distance. The bunched electron beam then enters the 5.7-GHz RF accelerator in the downstream.

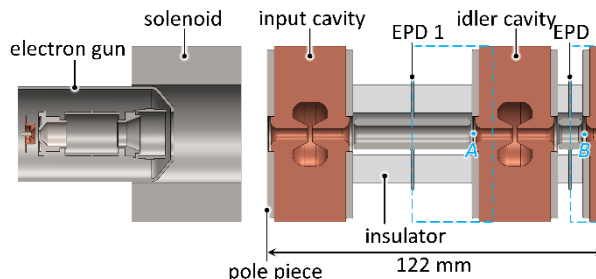


Figure 1: Electron buncher two-cavity conceptual design illustration. Permanent magnets between each two pole pieces are suppressed. Point A and B are placed at the center of the re-acceleration gaps of the EPD-1 and EPD-2 sections, respectively. The blue-colored rectangles are intended for parasitic mode discussion in a later section.

* Work supported by the Laboratory Directed Research and Development program of Los Alamos National Laboratory under project number 20240136ER.

† msb@lanl.gov

LINAC MODULE PHASE SCAN IN HPSim*

M. J. Kay[†], P. M. Anisimov, A. J. Braido, E.-C. Huang, J. K. K. Quemuel, L. J. Rybarczyk
Los Alamos National Laboratory, Los Alamos, NM, USA

Abstract

The side-coupled cavity linac (CCL) at the Los Alamos Neutron Science Center (LANSCE) is tuned by matching a single-particle model to the RF phase signature of the modules. In the future, the High-Performance Simulator (HPSim), a GPU-powered, 6-D particle tracking code, will be used to reveal additional information that will assist with tuning. In this proceeding, the status of the HPSim-based Phase Scan Signature Matching (PSSM) routine is presented, along with the outlook for its future implementation.

INTRODUCTION

The LANSCE accelerator at Los Alamos National Laboratory (LANL) supplies beam to five user facilities and simultaneously accelerates H^+ and H^- [1]. The CCL is made up of 44 accelerating modules, which accelerate the H^- beam from 100 MeV to 800 MeV (Fig. 1). The 805-MHz RF field that powers each module is supplied by a different klystron, causing the amplitude and phase of the RF inside one module to be independent of all others. As a result, each module must be tuned individually before the start of the run-cycle. PSSM is used to tune the CCL modules, in which the phase of the H^- beam after a module is measured while the RF phase is scanned over a full cycle [2]. A fitting algorithm then attempts to match the output of a single-particle model to the measured phase scan signature to extract parameters necessary to tune the module.

The High-Performance Simulator (HPSim) code will complement the single-particle model used in PSSM by revealing additional information about the tune. HPSim is a 6-D particle tracking code that is powered by GPUs [3]. The code was developed at LANL and contains a detailed model of the LANSCE linac. The signature feature of HPSim is its speed, which allows it to be used as an online simulation tool to assist with beam recovery during startup [4, 5]. HPSim can give information about the bunching and RF capture quality that the single-particle model cannot. In this proceeding, it is shown that HPSim reproduces an archived phase scan signature measurement as accurately as the single-particle model, while also retaining the full 6-D beam distribution.

CCL MODULE TUNE-UP

Tuning a CCL module amounts to ensuring the RF field amplitude and output beam energy are at the design values and that the beam exits the module properly bunched. The two “knobs” available for tuning are the RF amplitude setpoint (ASP) and phase setpoint (PSP). Although neither is

* This work was supported by Los Alamos National Laboratory’s Laboratory Directed Research and Development (LDRD) program under project number 20230409MFR.

[†] mkay@lanl.gov

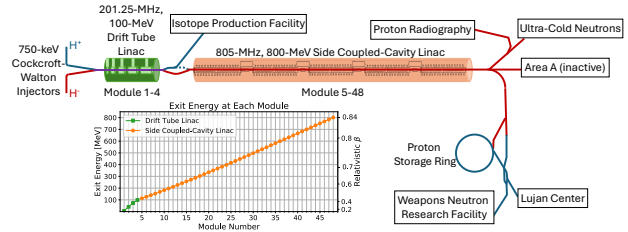


Figure 1: The LANSCE accelerator and user facilities.

calibrated to match the actual value, there is a one-to-one relationship. Tuning a CCL module is an iterative processes that uses PSSM to determine the correct ASP and PSP.

Phase Scan Measurement

PSSM requires the beam phase to be measured at a point after the module. A beam position and phase monitor (BPPM) measures the phase of the beam relative to a 201.25-MHz reference signal (Fig. 2). First, the RF is turned off, and the BPPM measures the phase of the beam after it drifts through the module. Then, the RF is turned on, and the BPPM measures the phase of the accelerated beam while the PSP for the RF is scanned between $\pm 180^\circ$. The difference between the phases measured with the RF on and off is plotted over the range of PSPs to produce the phase scan signature curve.

Phase Scan Signature Matching

A fitting algorithm then attempts to reproduce the phase scan signature with a single-particle model. An example of a fit for CCL module 5 is shown in Fig. 3. The fit is used to extract three parameters: the fractional amplitude of the RF field, the input beam energy offset, and the input beam phase offset. The best-fit values of those parameters are used to calculate the output energy of the beam at each

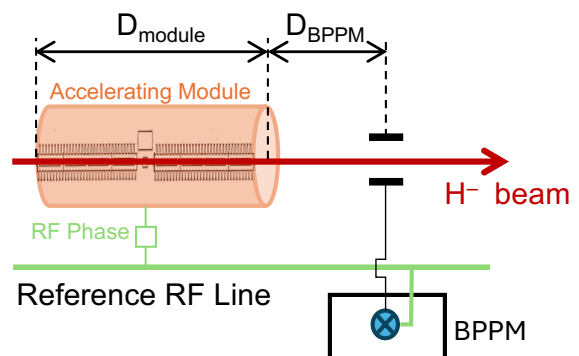


Figure 2: Phase scan measurement setup.

LANSCE ACCELERATOR INSTRUMENTATION AND CONTROL TECHNOLOGY CHOICES*

M. Pieck†, C. D Hatch, H. A. Watkins, E. E. Westbrook
Los Alamos National Laboratory, Los Alamos, NM, USA

Abstract

From being the first computer-controlled accelerator, through its 52-year long operational history, today the LANSCE Instrumentation and Control (I&C) system shows little resemblance to its early days. However, its maintainability depends on the ability to restore, or repair failed systems. Complicating this task is the undeniable fact that technology has significantly evolved over the last decades and that older components and systems, while still performing their function, have become obsolete and un-maintainable. When a technology migration path isn't viable to ensure I&C system maintainability, the only alternative is to upgrade to a new technology. Consideration needs to be given so that the new technology platform seamlessly integrates with the existing I&C infrastructure while allowing for technological progress. We discuss from the LANSCE's I&C engineering perspective the universal challenges older facilities are facing. We also provide a I&C system architecture overview.

LANSCE USER FACILITY

The Los Alamos Neutron Science Center (LANSCE) has been in operations for over 52 years. The multifunctional facility has grown over the years and now has five distinct state-of-the-art experimental facilities which provide the scientific community with intense sources of protons and neutrons, with the capability of performing experiments supporting civilian and national security research [1]. Without a properly functional LANSCE accelerator none of these experimental facilities could fulfill their mission. Hence, it is critical to plan for and appropriately fund the upkeep of the necessary LANSCE accelerator systems.

INTRODUCTION

Technological advancements have revolutionized control systems, making them smarter, more efficient and transformative. Control systems have surpassed previous limits offering intelligent features. This progress has ushered in an era of automation and machine learning, shaping a world of new possibilities.

An Accelerator Instrumentation and Controls (I&C) system reality check, is that many of the accelerator facilities around the world are lasting longer, extending their end-of-life. At the 2024 Accelerator Reliability Workshop,

an informal survey revealed that numerous facilities are more than 40, and 50 years old with a few of them even older than 60 years.

During the lifetime of a facility, some of the I&C systems have been very likely modernized. Moreover, as an accelerator increases in size and complexity so do its I&C systems. As a result, I&C systems have often accumulated a wide variety of hardware form factors and software methodologies that challenge maintainability and longevity. I&C engineers are faced with the daunting task of maintaining and modernizing their systems, often under the tight budgetary and schedule constraints of an operating accelerator facility with an enduring mission.

ACCELERATOR I&C SYSTEM LIFESPAN

External observers may perceive an accelerator I&C system as operating "just fine", while others, usually those who are "arms deep" into things, can have a totally different opinion. System complexity, component diversity and interdependencies, deferred maintenance, and technology obsolescence all have significant and compounding effects on overall I&C system maintainability and lifespan.

Accelerator I&C lifespan information is not widely published, and the information that is published does not provide a complete picture. This is probably, at least in part, because large accelerator I&C systems don't get upgraded in their entirety all at once.

Driven by budgetary and operating schedule constraints, I&C engineers often focus on partial upgrades to keep up with technology maturation of individual systems. Consequently, accelerator I&C systems continuously undergo some form of modernization effort. Hence it is difficult to report on their exact lifespan. Nevertheless, it is important to understand the lifespan expectancy of systems since it directly impacts future work scope, related labor, material needs, and consequently required funding.

Given that accelerator I&C systems rely for the most part on industry standards, one can often find life expectancy information for single vendor-based systems. It becomes more challenging when systems are composed of multiple components from different vendors. This may be complicated by software and hardware interdependencies.

Lifespan information about general category is available: Switches: 5–7 years. Routers: 3–4 years. Firewalls: 5–8 years, instrumentation 10–15 years, PLCs/Industrial automation controller 10–20 years, desktop computer 5–7 years, FPGAs 3–5, windows operating system ~10 years, Linux operating system 10 years. I&C engineers need to understand, document, and track the specific lifespan for their equipment to address the risk to support operations in a pre-emptive manner.

* This work was supported by the U.S. Department of Energy through the Los Alamos National Laboratory. Los Alamos National Laboratory is operated by Triad National Security, LLC, for the National Nuclear Security Administration of U.S. Department of Energy (Contract No. 89233218CNA000001).

† pieck@lanl.gov, LA-UR-24-28976

UPDATE ON THE STATUS OF THE LOS ALAMOS NEUTRON SCIENCE CENTER ACCELERATOR MODERNIZATION*

S. J. Russell[†], J. Bradley, E. Brown, B. Carlsten, G. Dale, M. Gulley, J. Lyles, J. Tapia
Los Alamos National Laboratory, Los Alamos, NM, USA

Abstract

The Los Alamos Neutron Science Center (LANSCE) accelerator is a MW-class H-/H+ 800 MeV linear accelerator that serves five distinct user facilities that support Los Alamos National Laboratory (LANL) national security missions, commercial applications, and the Department of Energy Isotope Program (DOE IP). Now into its sixth decade of continuous operation, major accelerator systems are showing their age with decreased reliability and diminished vendor support due to equipment obsolescence. With plans to continue LANSCE operations for several more decades, LANL is exploring different avenues to modernize large portions of the accelerator. We will present the current status of those plans and an overview of supporting R&D.

THE LOS ALAMOS NEUTRON SCIENCE CENTER

In 1972 the Los Alamos Meson Physics Facility (LAMPF) began operations for a 20-year basic nuclear physics program. The most powerful proton beam in the world, until the early 2000s, LAMPF pioneered technologies such as the side coupled cavity linear accelerator and dual species acceleration. When its original mission ended, LAMPF was re-branded as the Los Alamos Neutron Science Center (LANSCE) and repurposed as a user facility for nuclear weapon stockpile stewardship, basic science, industry, and isotope production [1]. Highlighting the versatility of the machine, LANSCE currently supports five distinct user end stations (Fig. 1):

- Isotope Production Facility (IPF) – IPF produces medical and other isotopes for the DOE IP, short-lived isotopes for defense programs, counter and non-proliferation, and criticality safety studies
- Proton Radiography (pRad) [2] – pRad employs 800 MeV protons to do dynamic imaging of shock and detonation events.
- Ultra-Cold Neutron Facility (UCN) [3] – Unique probe for basic nuclear physics science.
- Lujan Neutron Scattering Center (Lujan Center) [4, 5] – Provides spallation neutrons for neutron scattering and imaging and provides neutrons for materials science.
- Weapons Neutron Research Facility (WNR) [5] – Enables nuclear physics for defense programs, counter-

proliferation, and criticality safety. Serves as a user facility for electronics testing for industry and global security agencies.

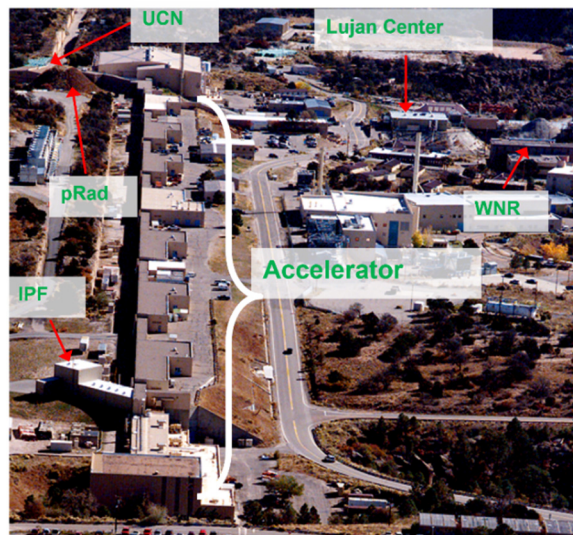


Figure 1: LANSCE [1].

LANSCE PRESENT STATUS AND FUTURE PLANS

LANSCE Present Status

In 2008 LANL embarked on an eight-year program to upgrade targeted LANSCE systems to both restored historical operating capability and to sustain future operation [6]. This involved an upgrade of the 201.25 MHz radiofrequency (RF) system that drives the LANSCE drift tube linear (DTL) accelerator, which accelerates the beam to 100 MeV, and procurement of 45 new 805 MHz klystrons from Communications and Power Industries to serve as spares for the 805 MHz High Power RF (HPRF) system, which powers the LANSCE coupled cavity linear (CCL) accelerator and boosts the beam energy from 100 MeV to 800 MeV. These new tubes are nominally identical to the original 1960s era design and were delivered by the end of 2014. The 201.25 MHz system upgrade was completed in 2016 [7].

Although this modest sustainment effort did in fact achieve its purpose, ensuring operation of LANSCE until 2020, it was not a long-term solution. LANL and the National Nuclear Security Agency (NNSA) have since realized that operation of LANSCE is needed until at least 2050. However, at 52 years of age modernization of the facility is now essential as reliability is now a major concern (Fig. 2). In 2019, for example, a crack developed in one of the four DTL tanks due to decades of thermal cycling. Fortunately, the location of the damage was accessible and was

* Work was performed for U.S. Department of Energy by Triad National Security, LLC, contract 89233218CNA000001 and through the Laboratory Directed Research and Development program of Los Alamos National Laboratory, under project number 20240723DI

[†] srussell@lanl.gov

AUTOMATION OF SAMPLE ALIGNMENT FOR NEUTRON SCATTERING EXPERIMENTS

B. Pritchard, M. Henderson, J. P. Edelen, RadiaSoft LLC, Boulder, CO, USA

Abstract

Sample alignment in neutron scattering experiments is critical to ensuring high quality data for the users. This process typically involves a skilled operator or beamline scientist. Machine learning has been demonstrated as an effective tool for a wide range of automation tasks. RadiaSoft in particular has been developing machine learning tools for a range of accelerator applications including beamline automation. In this poster we will present recent developments for selecting and aligning multiple samples at the HB-2A powder diffractometer at the High Flux Isotope Reactor (HFIR).

INTRODUCTION

Neutron beam diffraction experiments are a critical tool for determining the atomic structure and physical characteristics of materials. The HB-2A diffractometer at Oakridge National Laboratory (ORNL) provides data primarily for the purpose of determining the magnetic structure of powder samples [1]. HB-2A has an open instrument layout and multiple rotational and translational degrees of freedom that allow for rapid cycling between up to three samples placed on the sample stage at a time (see Fig. 1), where a concentrated neutron beam of constant wavelength supplied by the High-Flux Isotope Reactor (HFIR) interacts with the samples. Neutron detectors partially encircling HB-2A are used to capture the resulting neutron diffraction data, and a diagnostic neutron camera at the end of the beamline provides a 2D view of the sample orientation and location within the beam.

Currently, HB-2A relies on a skilled operator to manually identify approximate sample centroids in the diagnostic camera images and align the samples with the neutron beam. Operators use a graphical user interface (GUI) to initiate motor controls, a procedure which must be repeated continuously over an experiment to achieve the manual adjustments needed to keep the sample correctly placed within the beam. Although this process is relatively straightforward and sufficient for achieving the scientific goals of an experiment, it requires the expenditure of labor hours by highly skilled beamline scientists whose time could be better spent on higher-level operations and experiment planning. The alignment process at HB-2A and other beamlines is therefore a prime target for automation.

SAMPLE SEGMENTATION PROBLEM

In previous work, images from the diagnostic neutron camera at HB-2A have been used to orient the sample within the beam using both the standard manual procedures as well as an automated alignment procedure recently developed by

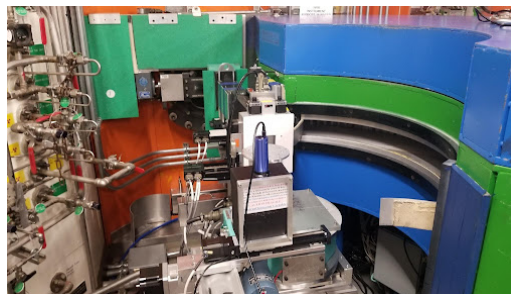


Figure 1: HB-2A sample stage.

RadiaSoft. The automated procedure makes use of a UNet, a type of convolutional neural network (CNN) used in machine vision [2], to produce binary masks of sample images which are then used to identify sample centers and align them within the neutron beam. However, the automated alignment processes currently deployed at HB-2A rely on the condition that the masks produced by a UNet contain only a single contiguous sample. The use of a multi-sample environment to enhance experimental efficiency at the beamline therefore poses a challenge for automated alignment, as secondary and tertiary samples cannot easily be excluded from diagnostic camera images under most circumstances.

In order to address the automation challenge posed by the multi-sample environment at HB-2A, we have begun to augment the alignment procedure to include an additional instance segmentation task. In this task, masks that contain binary information indicating whether or not each pixel contains a sample are processed to add an additional label that indicates which (if any) sample is present in the pixel. We utilized a basic form of connected component analysis (CCA) to achieve this processing by computing average 1D image and sample mask profiles, segmenting pixels belonging to distinct clusters, and assigning group labels based on the segmentation. This process is described in more detail below, and is now being integrated into the alignment software deployed at HB-2A.

METHODS

Static Imagery

Static images from the diagnostic neutron camera as well as masks available from previous work were used in development and testing. All software developed for this purpose was written in Python and tested using a command line interface and the *rscontrols* framework developed by RadiaSoft [3]. To ensure the best outcome possible and provide a greater level of robustness to the segmentation efforts, two separate segmentation approaches were tested. The first approach attempted to produce sample segmentation using just the raw neutron camera image data (Fig. 2, left) which is

LOW-LEVEL RF SYSTEM DEVELOPMENT FOR A C-BAND LINAC

J. P. Edelen*, J. Einstein-Curtis, RadiaSoft LLC, Boulder, CO, USA
 A. Diego, M. Kravchenko, R. Berry, RadiaBeam, Santa Monica, CA, USA
 J. Krasna, COSYLAB, Ljubljana, Slovenia

Abstract

RadiaSoft and RadiaBeam are partnering on the development of a low level RF control system to support a 100 MeV C-Band LINAC. Our system utilizes a Keysight data acquisition system and arbitrary waveform generator to drive the LINAC. The controllers are fully integrated with EPICS and are actively being commissioned. In this presentation we will provide an overview of the design architecture, discuss details of the epics integration, and show initial results controlling a photoinjector.

INTRODUCTION

The Low-Level Radio Frequency (LLRF) control system is primarily responsible for delivering RF to amplifiers, receiving and processing signals for the various RF diagnostics, and control of the RF cavities to include phase, amplitude, and frequency. When building a LLRF system there are a number of design considerations that lead to the choice of frequency parameters, digital vs analog, and how to modulate the RF signals. One of the most common architectures utilizes an intermediate frequency that is used for digitization and an analog system to perform up and down conversion [1]. However, base-band modulation has also been used, for example the Swiss FEL utilized such an architecture [2]. Additionally, modern electronics are making systems that perform direct digital down-conversion more popular [3]. For C-Band there are limited commercial options for direct digital sampling that are also cost effective for a modest scale system. This is largely due to the development time required and operating in unusual modes such as the first Nyquist band. Moreover, the technical challenges associated with base-band modulation and noise mitigation makes a digital system operating at an intermediate frequency more attractive. As such we chose to build a COTS system based on digitization at a reasonable intermediate frequency with cost effective solutions. Figure 1 shows a functional block diagram of our COTS LLRF system. Here we highlight the notable interconnections and signals. For this system, we have a common local oscillator that is distributed to all of the analog electronics. The digital system generates a clean reference signal that is re-distributed to the LLRF system as a phase reference and also distributed to the timing system and the laser system for phase locking. The parameters for the LLRF system are given in Table 1.

This paper provides an overview of the digital and analog components of the LLRF system as well as measurement of losses through the downconverter and amplitude stability measurements. We also describe the EPICS integration at

* jedelen@radiasoft.net

Table 1: Parameters for the LLRF System

Parameter	Value
RF	5712 MHz
IF	100 MHz
LO	5812 MHz
Laser	476 MHz
Sample Rate	500 MS/s
ADC	14 bit
DAC	16 bit

a high level and provide a brief overview of the high level applications used to control the accelerator.

DIGITAL SYSTEM DESIGN

The digital system is comprised of an M3102A PXIe Digitizer from Keysight and an M3201A PXIe Arbitrary Waveform Generator also from Keysight. Our AWG resolution is 16 bit at a 500 MS/s sample rate. The digitizer resolution is 14 bit at a 500 MS/s sample rate.

The choice of intermediate frequency is largely determined by the available digital components and the constraints on RF filtering, This typically is in the 10 – 100 MHz range. Our initial choice of the intermediate frequency is 100 MHz. This is to allow for good isolation between IF signals, RF signals, and baseband signals. When converting from RF to IF, the RF signal at 5712 MHz is mixed with the LO at 5810 MHz. This will generate a 100 MHz signal and a 11524 MHz signal. The 11.5 GHz signal will be filtered out using analog components leaving the 100 MHz signal. The IF signals will be digitized at a rate of 500 MS/s which is readily available with modern digitizers. The choice of a digital system that is 2.5x Nyquist will provide higher signal quality while maintaining a reasonable cost. The digitizers have a bandwidth of up to 200 MHz and we will show results of our system with an IF of up to 175 MHz. To extract the RF waveforms the 100 MHz signal is mixed digitally with another 100 MHz signal giving a baseband waveform and a 200 MHz signal. In order to resolve the cavity dynamics, we need a minimum of 20 MHz bandwidth at baseband. Having 200 MHz of space between the baseband signal and the secondary signal generated by the IF downmixing relaxes the constraints on the filter design and reduces the need for high order filters that cause ringing and other unwanted effects.

The arbitrary waveform generator has built in I/Q modulation for phase coherent signal generation. It can generate sinusoidal signals with envelope and phase modulation all synchronized to an internal reference clock. The DACs are 16 bit which provides a high level of precision for the RF

COMMISSIONING AND PERFORMANCE OF A C-BAND LLRF SYSTEM AT RADIABEAM

J. P. Edelen*, J. Einstein Curtis, RadiaSoft LLC, Boulder, USA
 A. Diego, M. Kravchenko, R. Berry M., RadiaBeam, Santa Monica, USA
 J. Krasna, COSYLAB, Ljubljana, Slovenia

Abstract

RadiaBeam and RadiaSoft have been developing a LLRF system for a 100 MeV C-band LINAC. The system is based on a Keysight PXIE arbitrary waveform generator and ADCs. We are in the process of commissioning our system and validating its performance. In this presentation, we will provide details on amplitude and phase calibration, improvements to signal conditioning, comparisons between measurements and simulations, and performance of our pulse to pulse feedback scheme.

INTRODUCTION

RadiaSoft is leading the development of a LLRF system in support of a C-band test accelerator being constructed at RadiaBeam. This machine contains staged acceleration which requires phase synchronization between cavities and therefore a complete LLRF system. The system is comprised of a digital arbitrary waveform generator that produces a modulated 100 MHz signal, an analog upconverter that mixes the 100 MHz signal up to 5712 MHz, an analog downconverter that mixes measured signals down to 100 MHz, and a digitizer that records the 100 MHz signals for processing by our LLRF software. Our system also comprises timing and reference signal generation. The parameters for the LLRF system are provided in Table 1.

Table 1: Parameters for the LLRF System

Parameter	Value
RF	5712 MHz
IF	100 MHz
LO	5812 MHz
Laser	476 MHz
Sample Rate	500 MS/s
ADC	14 bit
DAC	16 bit

This paper is focused on improvements to the signal processing performed in software, calibration of our measurements, and initial performance of our pulse-to-pulse feedback algorithms.

SIGNAL CONDITIONING

Our system performs signal processing in software after recording raw 100 MHz pulses. After the ADC records the signal, it is passed through our EPICS IOC to a Python

* jedelen@radiasoft.net

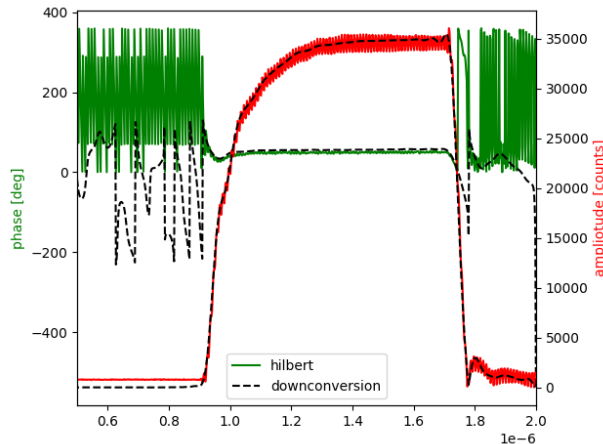


Figure 1: Amplitude (red) and phase envelope (blue) for the *hilbert* method of envelope detection and the improved envelope reconstruction using a traditional downconversion implemented in Python (black dashed).

modules. Specifically, we utilize the `scipy.signal` function *hilbert* [1], to reconstruct the amplitude and phase of the 100 MHz signals. The function uses Fourier transforms to build a complex representation of the input time domain signal. While an efficient envelope detection method, we have noticed the resulting waveforms have residual noise, Fig. 1. A frequency analysis of these waveforms, Fig. 2, shows the spectra of the *hilbert* reconstruction of the amplitude signal with a 100 MHz component and a 200 MHz component. To correct for this we implemented a traditional downconversion in the Python signal processing module. Here we mix the incoming 100 MHz signal with a 100 MHz reference followed by a low pass filter to remove the higher harmonics. The resulting signals and frequency spectra are shown in the dashed lines in both Figs. 1 and 2 respectively. Here we can see that the improved method for extracting the signal envelopes no longer have the 100 MHz and 200 MHz leakage and the envelopes signals are significantly smoother.

SIGNAL CALIBRATIONS

During commissioning we calibrated the signals measured in the ADCs to be in units of megawatts. The ADC has a range of plus-minus four volts. The losses in the system were measured using a network analyzer and are provided in Table 2. Here we are considering two channels measuring forward power for the two LINAC sections. The directional couplers are identical to three significant figures along with the attenuators. The cables had some slight variation and

AN RF SIMULATOR FOR CONTROL SYSTEM DEVELOPMENT

M. Henderson, D. Abell, D. Bruhwiler, J. P. Edelen, J. Einstein-Curtis
 RadiaSoft LLC, Boulder, CO, USA

A. Diego, R. Agustsson, RadiaBeam, Santa Monica, CA, USA

Abstract

Simulation tools are critical to the prototype and validation of control algorithms prior-to and during commissioning of LLRF systems. Moreover, for industrial systems, diagnostics that are available on test systems and in laboratory accelerators are not always available in the field. RadiaSoft has been developing an RF simulator suite that allows for rapid prototyping of control algorithms in a fully integrated epics environment. As part of this process, we have performed extensive testing and bench-marking using a novel C-band test cavity with a range of diagnostics. This poster provides an overview of the simulator, the physical models which make it up, and results for an example system with two cavities and other typical hardware elements.

INTRODUCTION

Most particle accelerator facilities feature some number of RF cavities and associated low-level (LLRF) control systems, whether as primary mechanisms for acceleration or for use in other subsystems (e.g., injection modules). However, utilizing these devices for secondary purposes such as controls development can be costly in both time and resources, and can impede normal experimental operations.

To that end, RadiaSoft has designed, tested, and deployed a robust RF simulator for developing LLRF control algorithms, input-output control (IOC) software, and user interfaces (UI). The simulator is integrated with the EPICS framework for experimental controls, and can be run through a number of modalities, including basic command line interfaces, Python scripts or Jupyter notebooks, and direct EPICS connections. It describes RF signal propagation using a standard scattering matrix approach and cavity dynamics using an effective circuit model derived in previous work for application to superconducting cavities.

Using our simulator, we have successfully tested several practical LLRF feedback control methods (including PID loops and filters), modeled systems of interest for research applications, and even studied the use of machine learning as a means for noise reduction in industrial RF systems. The simulator itself has been key to the success of these and other ongoing efforts, and will be described in greater detail below.

RF SYSTEM MODELING

Cavity Model

Development of our RF simulator began with a simple effective RLC circuit model which accounts for a number of system characteristics, including: coupling and quality factors, frequency, drive amplitude and phase, pulse duration, and cavity detuning. The associated model dynamics are

based on equations previously derived in [1] and [2], and an additive white Gaussian noise (AWGN) model for simulated measurements. Simulation is carried out by solving a differential equation for the voltage transmitted by a cavity, which is a function of both the current transmitted voltage and effective applied current supplied to the cavity:

$$\frac{d\mathbf{V}_t}{dt} = \begin{bmatrix} -\omega_{1/2} & -\Delta\omega \\ \Delta\omega & -\omega_{1/2} \end{bmatrix} \mathbf{V}_t + \frac{\omega_{1/2} R_L}{m} \mathbf{I}_f \quad (1)$$

where

$$\mathbf{V}_t = \begin{bmatrix} \text{Re}(V_t) \\ \text{Im}(V_t) \end{bmatrix}, \quad \mathbf{I}_f = \begin{bmatrix} \text{Re}(I_f) \\ \text{Im}(I_f) \end{bmatrix} \quad (2)$$

are the transmitted voltage and forward current, respectively. The half-bandwidth $\omega_{1/2}$, coupling factor m , and loaded cavity resistance R_L are all parameters of the cavity itself, and their relationship with the effective circuit model parameters can be found in [1] and [2]. The voltage reflected by the cavity can be similarly computed [2] given a system reference impedance Z_0 using the equation:

$$\mathbf{V}_r = \begin{bmatrix} \text{Re}(V_r) \\ \text{Im}(V_r) \end{bmatrix} = \frac{1}{m} \mathbf{V}_t - \frac{Z_0}{2} \mathbf{I}_f \quad (3)$$

RF Signal Chain

With an RF cavity model implemented, we then extended the generator-to-cavity system used in [1] and [2] to include a number of additional hardware elements commonly employed in RF systems. In order to properly simulate the much more complicated propagation dynamics that can result from the addition of such elements, we chose to describe incoming (**a**) and outgoing (**b**) RF waves at the ports of each element as power waves using a standard scattering matrix approach [3] such that:

$$\mathbf{b} = S \mathbf{a} \quad (4)$$

where the dimension of **a**, **b**, and S are determined by the number of ports on an element, and the elements of S (the scattering matrix, are determined by the internal function of the element. For example, the scattering matrix for an ideal two-port RF transmission line (e.g., a coaxial cable or an RF waveguide) of length l is simply:

$$S_{Line} = \begin{bmatrix} 0 & e^{-(\alpha+i\beta)l} \\ e^{-(\alpha+i\beta)l} & 0 \end{bmatrix} \quad (5)$$

where α and β are the typical attenuation and propagation constants of the waveguide. The scattering matrix for some elements, such as the four-port “magic tee” signal splitter, can be derived geometrically:

LLRF AND PULSE-TO-PULSE CORRECTION FOR A COMPACT LINAC*

J. Einstein-Curtis[†], J. Edelen, M. Kilpatrick, RadiaSoft LLC, Boulder, CO, USA

R. Augustsson, R. Berry, A. Diego, S. Thielk

RadiaBeam Technologies, LLC, Santa Monica, CA, USA

B. Hong, Z. Li, C. Liu, J. Merrick, E. Nanni, L. Ruckman,

S. Tantawi, F. Zuo, SLAC National Accelerator Laboratory, Menlo Park, CA, USA

Abstract

The advent of c-band and x-band technology has made it possible to reduce the footprint of linear accelerators. Additionally, for industrial systems a more compact linac is an enabling technology for burgeoning applications in security and defense. A key aspect to operating these machines in an industrial environment is stabilization of the amplitude and phase signals for the cavities. In this poster we present the design and recent results for a LLRF and pulse-to-pulse correction scheme utilizing an RFSoc based FPGA system.

INTRODUCTION

Radio-frequency (RF) particle accelerators rely on consistent and stable RF sources to operate in an optimal regime. In particular, developers of industrial accelerators are looking into ways to have higher RF power levels for more energetic beams, while also decreasing the system cost envelope. Accomplishing both of these goals while maintaining a high-quality beam over the entire flat-top of an accelerating pulse is a significant challenge, requiring both a synchronization of the timing and power systems involved in addition to active correction to account for system-wide variations due to equipment or environmental concerns.

It is essential to reduce the need for complex processing algorithms when designing to minimize system cost when manufacturing at scale. We have developed a pulse-by-pulse correction scheme that acts on system nonlinearities on an inter-pulse time frame. This algorithm is designed to generate a stable and flat forward power signal, using this signal as an analogue for cavity voltage. Although our reported method has limitations due to the lack of intra-pulse correction, it allows for a simple correction scheme without requiring high-performance, low-latency hardware close to the accelerating structure, increasing system complexity and cost. The correction algorithm has been developed to work in any EPICS [1] environment where the RF waveform is available as an EPICS process variable.

We implemented this scheme using prototype hardware consisting of an AMD Xilinx ZCU216 RF-SoC evaluation kit, a custom trigger board, and supporting RF hardware [2–4]. The software platform is built on a SLAC-

developed software platform known as *rogue* [5]. This leads to complications with system design for an industrial accelerator due to the need to minimize components, but also allows for clear functional compartmentalization and opportunities for SWaP+C minimization.

SIMULATION

We developed a system RF simulator to minimize the need for actual hardware testing time. The simulator was used to test a variety of control algorithms, including PID and Kalman filter methods. The simulator was originally designed without signal delays or certain types of nonlinearities, which allowed for better processing speed, and was connected to EPICS PVs to integrate with the controller algorithm. The system has several unusual design features, including every two cavities a feed and load, requiring the ability to decouple individual cavity effects from a minimal number of readback signals.

Results from the inter-pulse PID method can be seen in Fig. 1. Both the PID and Kalman filter controllers performed successfully, with the Kalman filter results shown in Fig. 2. These responses clearly show the ability for the algorithm, with proper tuning, to generate a flat waveform from an originally uneven waveform.

LOW-POWER TESTING

Initial testing with RF was performed using the RF-SoC LLRF system along with a conditioning pre-amplifier, pre-klystron RF amplifier, and the cavity structure. We used this testing to refine the calibration algorithms and startup routine, determining a procedure for setting proper delays and the corresponding window in the readback signal for controller operation. This testing turned out to have additional benefits as the high power system was unavailable due to equipment failure or bunker availability several times throughout the project. Figures 3 and 4 show the algorithm actively stabilizing the forward power signal and the calculated drive waveform. The initial 5 counts of the generated signal are not a part of the integral portion of the PID accumulator to avoid attempting to correct for any effects resulting from RF or klystron turn-on. The end of the generated waveform also shows the resultant effect due to amplifier turn-off. Note the misalignment in time between the measured forward amplitude and generated drive waveform.

* This material is based upon work supported by the Defense Advanced Research Projects Agency under Contract Numbers 140D0423C0006 and 140D0423C0007. The views, opinions, and/or findings expressed are those of the author(s) and should not be interpreted as representing the official views or policies of the Department of Defense or the U.S. Government.

[†] joshec@radiasoft.net

ESS INSTALLATION PROGRESSES

H. Przybilski*, on behalf of the European Spallation Source ERIC

Abstract

The installation of the superconducting part of the ESS Linac is progressing towards the first operation at 870 MeV on the beam dump in January'25. A pilot installation of 1 spoke and 1 elliptical cryomodule was conducted in the superconducting (SCL) part of the ESS tunnel in spring 2023, to practice the installation sequence as well as to complete the cryogenic distribution system (CDS) commissioning. Currently a total of 13 spoke and 14 elliptical cryomodules (9MB + 5HB) are being installed to allow 2 MW capabilities for the first phase of the project. Overall, 30 elliptical cryomodules will be delivered to extend the power reach to 5MW. At the time of the conference the linac will be in the technical commissioning phase.

INTRODUCTION

The European Spallation Source (ESS) in Lund, Sweden [1], is currently entering into the commissioning phase after years of construction. The linear accelerator (linac) will drive the most powerful neutron spallation source. The linac is composed of both a normal and a superconducting section, which will deliver an average ultimate beam power of 5 MW at 2 GeV. The first and current phase intends to deliver a maximum power of 2 MW, followed by 3 MW in 2027. Figure 1 describes the layout of the linac as well as the energy for the initial phase of operation.

The Normal Conducting Linac (NCL) section was completed in September 2023 with the installation of the fifth Drift Tube Linac (DTL) tank. The DTL is delivered by the Italian in-kind partner INFN. A section in this paper will introduce some key parameters of the DTL as well as results of the conditioning up to DTL-4.

Regarding the Superconducting Linac (SCL) French in-kind institutes contributed with three types of cryomodules (CM): spoke cryomodules from IJC Lab, Orsay, medium-beta elliptical (MB) and high-beta elliptical (HB) cryomodules from CEA Saclay. All cryomodules must undergo Site Acceptance Test (SAT) prior to their installation in the ESS tunnel. The spoke CM were tested at FREIA laboratory in Uppsala, Sweden. The elliptical CM on the other hand are tested in the Test Stand 2 (TS2) at ESS.

At the time of the conference, all 13 spoke, 9 MB and 5 HB (out of 21) cryomodules are installed in the linac. The installation of the last systems and technical commissioning phases are now overlapping in order to start the cooldown of the entire linac by October'24.

This paper will highlight some achievements in the NCL and relate some key installation and commissioning processes in the SCL.

* henry.prybilski@ess.eu

DTL CONDITIONING HIGHLIGHTS

The ≈ 38.8 m ESS DTL is designed to accelerate the proton beam from 3.62 MeV up to 89.8 MeV. The five cavities are now fully installed and tested in the linac tunnel. Moreover, in 2023 DTL-1 to DTL-4 were RF conditioned to full power and beam commissioned with maximum peak current at short pulses. From the SCL installation perspective, the NCL conditioning could happen thanks to a 2 m thick concrete wall separating the two areas.

The DTL-1 experience allowed significant enhancement of the field quality and the conditioning time of the next cavities. Results and improvements regarding low power field tuning [2] and RF conditioning strategy are presented at this conference.

The automated conditioning of the DTLs starts at $10 \mu\text{s}$ -10 kW-1 Hz, stepping up to full power in the cavities at 3.2 ms ≈ 1.2 MW-14 Hz. The 4 DTLs reached the nominal field and duty cycle ($P_{ave} \approx 60\text{kW}$) in March'23, including long stability run with more the 95% RF ON over 12 hours. The RF parameters measured at low power were then confirmed at high power. The RF pick-ups of the DTLs present a calibration error of $\pm 5\%$, as expected from the measurement error propagation of the attenuation. More details can be found in Refs. [3, 4].

During the last beam commissioning campaign in 2023, the milestone of transporting and accelerate a $50 \mu\text{s}$ beam pulse at nominal current to the end of DTL-4 was achieved. Phase scan, longitudinal acceptance measurements, beam loading based measurements were used to find the correct RF amplitude and phase set point of the four DTLs. The results of those methods are in good agreement, with some optimisation to be done in the next commissioning phases [4, 5].

In September'23, after completing the beam commissioning at 74 MeV and the removal of the concrete wall, the last DTL tank (DTL-5) was installed in the tunnel (Fig. 1). After the conclusion of the high power tests, the RF windows and power couplers were assembled in May'24 [4]. The DTL-5 is now connected to the rest of the subsystems and ready for the integrated tests scheduled before high power conditioning in November'24.

SCL INSTALLATION

This section will present the spoke and elliptical CM preparation and installation in the ESS tunnel as well as the first integrated tests performed on the water cooling systems.

CM Installation

The recent activities regarding the CM pilot installation of 1 spoke CM and 1 MB, and the CM preparation were presented at both SRF'23 [6] and IPAC'24 [7, 8]. The purpose of the pilot installation in Q2-2023 was to demonstrate the

FIRST TWO YEARS OF FRIB OPERATION*

P. N. Ostroumov[†] and J. Wei, on behalf of FRIB team
Facility for Rare Isotopes Beams, Michigan State University, East Lansing, MI, USA

Abstract

The Facility for Rare Isotope Beams (FRIB), a major nuclear physics facility for research with fast, stopped, and reaccelerated rare isotope beams, was successfully commissioned and has been in operation for the past two years. Various ion beam species have been accelerated up to 300 MeV/u and delivered to the target. FRIB routinely provided 10 kW primary beams on target over the past year, a factor of 10 above used at the beginning of user operation. Recently, a record-high 10.4 kW of uranium beam, the most challenging for accelerator systems, was delivered to the target, and three new isotopes were discovered during a short 24-hour run. We developed a 21.9-kW Se-82 beam a month ago (in July 2024) and provided it for the first observation of neutron-rich rare isotopes. Every incremental step in energy and power of primary beams allows us to gain valuable experience in the facility's safe operation and provides directions for further improvements. Several accelerator improvement projects are being pursued for further power ramp-up, improving the accelerator availability, delivering more time for science, and preparing for the ultimate 400 kW beam on target.

INTRODUCTION

FRIB will provide access to 80% of all isotopes predicted to exist in nature. FRIB construction started in 2013 and was completed in 2022, on cost and ahead of schedule. The FRIB facility is based on a heavy-ion CW superconducting driver linac, capable of accelerating uranium ions to 200 MeV/u and higher energies for lighter ions with 400 kW power on target [1]. A detailed description of the layout of the linac and beam commissioning results has been presented in previous publications [1-4]. The linac consists of

- A Front End (FE) composed of two Electron Cyclotron Ion Sources (ECR), Low Energy Beam Transport (LEBT), Radiofrequency Quadrupole (RFQ) and Medium Energy Beam Transport (MEBT);
- Linac Segment 1 (LS1) containing 104 Superconducting (SC) Quarter Wave Resonators (QWR) and 39 SC solenoids;
- Folding Segment 1 (FS1) containing a liquid lithium charge stripper, an achromatic 180-degree bending system, Charge Selection Slits (CSS) with the beam absorber for unwanted charge states;
- Linac Segment 2 (LS2) containing 168 Half Wave Resonators (HWR) and 24 SC solenoids;

* This material is based upon work supported by the U.S. Department of Energy, Office of Science, Office of Nuclear Physics and used resources of the FRIB Operations, which is a DOE Office of Science User Facility under Award Number DE-SC0023633.

[†]ostroumov@frib.msu.edu

- Folding Segment 2 (FS2) containing an achromatic 180-degree bend;
- Linac Segment 3 (LS3) with 52 HWRs, 6 SC solenoids, and 80-meter beam transport;
- The Beam Delivery System (BDS) containing a 75-degree achromatic bend and a final focusing system to create a 1-mm beam spot on the target.

In this paper, we report the results of ongoing developments to support experiments with various ion beam species and the beam power ramp-up up to 21.9 kW. We also discuss Accelerator Improvement Projects (AIP) and R&D initiatives to reach the ultimate beam power of 400 kW. To date, the primary ion beams of ¹⁸O, ²⁰Ne, ²⁸Si, ³⁶Ar, ⁴⁰Ar, ⁴⁸Ca, ⁶⁴Zn, ⁷⁰Zn, ⁸²Se, ⁸⁶Kr, ¹²⁴Xe, ¹⁹⁸Pt, and ²³⁸U, at various beam energies from 130 MeV/u up to 300 MeV/u have been delivered to the target and used to produce more than 270 unstable isotopes for 44 nuclear physics experiments.

OPERATIONAL EXPERIENCE

FRIB production runs for the science experiments commenced in May 2022. FRIB provided 4300 and 4200 hours of beamtime in FY23 and FY24, respectively, with 94% availability to support nuclear physics experiments [5]. About 25% of the beamtime goes to restoring, tuning, and studies of primary beams. In addition, 2000 hours every year are provided for Single Event Experiments (SEE) at beam energies of various ion species from 10 to 40 MeV/u. A total of 44 nuclear physics experiments have been conducted since the commencement of user operation. Once the development of primary and secondary beams is complete, the delivery of isotopes to the experiments has been highly stable. Some adjustments of the ECR were required, especially for metal beams, to maintain constant beam power on target. The SRF cavities are operated at slightly lower fields than the design to facilitate stable operation and provide a margin for quick recovery in the case of possible failure of some cavities. However, there has been no cavity failure during the production runs in the past two years. The Machine Protection System (MPS) operated as expected [5, 6]. The lithium charge stripper contribution to the facility downtime was dominant last year. Maintenance on the Lithium Charge Stripper requires a significant amount of thermal cool-down time before accessing the containment enclosure.

DEVELOPMENT OF ION BEAMS

Development of Linac Tune

The development of the linac tune for a new ion beam starts with the pre-calculated setting of all beam optics devices and RF cavities for the entire linac. The RF cavities' phases and amplitudes for any given ion species and its en-

SPIRAL2 OPERATIONS AND FUTURE PLANS

A. K. Orduz*, M. Di Giacomo, J-M. Lagniel, A. Leduc, G. Normand
Grand Accélérateur National d'Ions Lourds (GANIL), Caen, France

F. Bouly, A. Plaçais

Univ. Grenoble Alpes, CNRS, Grenoble IN2P3, LPSC-INP Grenoble, France

Abstract

GANIL (Grand Accélérateur National d'Ions Lourds) started the operation of the SPIRAL2 superconducting linac in 2022. Experiments in the Neutron For Science (NFS) room, specific beam dynamics studies and different technical improvements are carried out during its operation in the second half of each year, after the run of the cyclotrons in the first half of the year. Up to now, accelerated particles are mainly D^+ and $^4He^{2+}$ with energies between 7 and 20 MeV/A. First linac tunings with $^{18}O^{6+}$ and $^{40}Ar^{14+}$ ion beams at energies between 7 and 14.5 MeV/A were also carried out to prepare the Super Separator Spectrometer (S^3) experimental area commissioning. The paper presents a summary of the beam time distribution during the second year of operation, preliminary results of specific studies on cavity failure recovery and on pressure variation in the warm linac sections induced by beam losses.

INTRODUCTION

The successful acceleration of the H^+ , D^+ and $^4He^{2+}$ beams to their nominal energies was performed during the linac commissioning between 2019 and 2021 [1]. These beams were also sent to the NFS room for initial tests and experiments [2]. Since 2022, SPIRAL2 delivers beams for physics experiments (mainly at NFS) and to carry out different studies on beam dynamics, diagnostics and others accelerator systems. The beam dynamics studies performed were mainly related to heavy-ion tunings for the Super Separator Spectrometer (S^3) commissioning and to linac tunings in case of cavity failure [3].

This article focuses on machine study results during the second year of SPIRAL2 operation. The first part presents the 2023 operation timetable and the results of the first heavy-ion acceleration to 14.5 MeV/A. The second section describes the results of the acceleration of a $^4He^{2+}$ beam in the linac in the case of cavity #6 failure. Finally, preliminary results on the pressure variation in the linac warm sections with heavy-ion beams are presented.

SPIRAL2 OPERATION

The SPIRAL2 beam operation in 2023 was approximately 3 months from August 28 to November 19 (Fig. 1). Six physics experiments and two main preparatory studies for S^3 were successfully conducted. The time for physics experiments represented 34.6% of which 83% was with D^+ beams between 9 and 47 μA mean intensity on target, mainly with

a selection of 1 bunch /100 using the Single Bunch Selector (SBS). For 13.5% of the total time used for machine studies, 6% was used for beam dynamics studies with $^4He^{2+}$, $^{18}O^{6+}$ and $^{40}Ar^{14+}$ beams. Tests were performed on heavy-ion acceleration at nominal energy and on linac operation in case of cavity failure, among others.

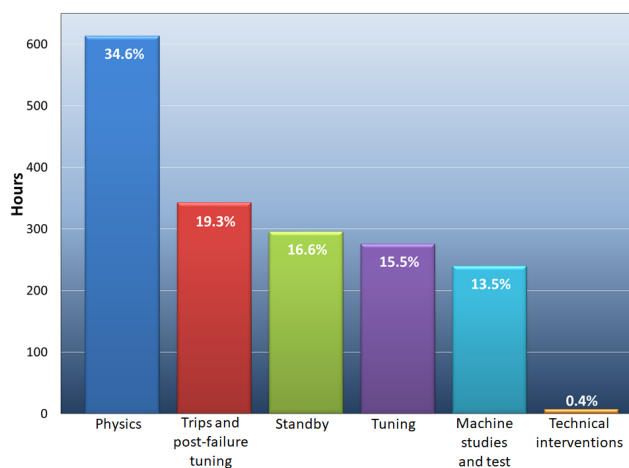


Figure 1: SPIRAL2 beam time sharing in 2023.

Heavy-ion beams $^{18}O^{6+}$ and $^{40}Ar^{14+}$ were tuned and accelerated in 2022 up to 7 MeV/A, the energy requested by S^3 [4]. In 2023 a 50 μA $^{18}O^{6+}$ beam was tuned up to the project nominal energy of 14.5 MeV/A (Fig. 2).

A power ramp-up to 2 kW with a $^{18}O^{6+}$ beam at 14.5 MeV/A was performed to qualify the tuning (Fig. 3). The strategy was to accelerate the beam with a peak current of 50 μA through the linac and to increase the pulse length up to 100% duty cycle.

LINAC TUNING WITH A MISSING CAVITY

Since 2022, dedicated studies have been conducted on linac operation in case of missing cavity. The procedure started optimizing the linac parameters using TraceWin for a specific missing cavity, then tuning the machine and finally minimizing the beam losses. This last step is performed slowly increasing the beam power and monitoring the diagnostics in the linac and HEBT [1]. In the case of a very first low β cavity failure the debunching between two cavities is so high that beam losses cannot be avoided. As the energy increases the debunching decreases, so if one of the mid or last low β cavities fails, it is more or less easier to recover a beam dynamics without losses. To do so, one must retune one or two upstream cavity and all downstream cavities to recover the required longitudinal acceptance, the price to

* angie.orduz@ganil.fr

DEVELOPMENT OF WET NITROGEN DOPING TO IMPROVE THE PERFORMANCE OF HALF-WAVE RESONATORS*

Yuting Wu[†], Andrei Ganshyn, Chris Compton, Ethan Metzgar, Kenji Saito, Kyle Elliott, Laura Popielarski, Sang-hoon Kim, Spencer Combs, Taro Konomi, Ting Xu, Walter Hartung, Wei Chang, and Yoolim Cheon

Facility for Rare Isotope Beams - Michigan State University, East Lansing, USA

Abstract

A new surface treatment method is being developed, wet nitrogen doping, in which nitric acid is added during electropolishing (EP). In the first trial on a FRIB $\beta = 0.53$ half-wave resonator (HWR), a high quality factor ($Q_0 = 8 \times 10^{10}$) was observed at 2 K at low field (accelerating gradient ≤ 0.5 MV/m) without an anti- Q slope. It is known that the Q_0 can be increased by shortening the mean free path via surface contamination by oxygen. Low-temperature baking (LTB) can allow oxygen to diffuse into the surface to a depth similar to the RF penetration depth. However, nitrogen cannot diffuse via LTB. Therefore, the mechanism for increasing Q_0 with N-doping has not been clearly understood. First results and analyses for HWR wet N-doping will be presented.

INTRODUCTION

An effort is underway at FRIB to increase the quality factor (Q_0) and accelerating gradient (E_{acc}) of superconducting radio-frequency (SRF) $\beta = 0.53$ half-wave resonators (HWRs, 322 MHz), along with the production of a spare HWR cryomodule for the FRIB linac. This effort is oriented toward better accelerator maintainability and mitigation of possible cavity performance degradation in long-term operation. Four objectives were identified: (1) Achieve higher E_{acc} using electropolishing (EP) and low-temperature baking (LTB) in lieu of buffered chemical polishing (BCP); (2) Increase Q_0 to $\geq 2 \times 10^{10}$ at $E_{acc} = 12$ MV/m by reducing the residual magnetostatic field; (3) Develop an EP procedure with wet nitrogen doping; and (4) Develop a BCP procedure without high field Q -slope (HFQS). Objectives 1 and 2 were successfully completed in 2023; the results of Objective 1 were reported at the last SRF Conference [1]. This paper reports on the first results of Objective 3.

MOTIVATION

A $Q_0 \geq 3 \times 10^{10}$ at 12 MV/m was reached in a FRIB $\beta = 0.53$ HWR with EP, LTB, and remnant field reduction (Objective 2). However, efforts are ongoing to further improve Q_0 . It is well-established that furnace nitrogen doping can generate an anti- Q slope for SRF cavities and thereby increase Q_0 at high field [2]. An alternative nitrogen doping procedure is being studied for FRIB cavities, with the hope

of achieving similar results with simplified preparation steps. This new recipe is called wet-nitrogen doping or EP (HNO_3); nitric acid is added to the traditional EP acid (a 10:1 mixture of 98% sulfuric acid and 49% hydrofluoric acid). The goal is to deliver nitrogen to the SRF surface during EP rather than adding N-doping as an additional furnace treatment step.

Wet doping was first developed by K. Saito and T. Higuchi to mitigate hydrogen Q -disease for mechanically-polished and EP'ed cavities [3]. K. Saito recently revisited and found that the EP (HNO_3) recipe can increase Q_0 , as seen in Fig. 1. EP (HNO_3) was used to remove 50 μm , followed by LTB. A high Q_0 was seen up to $E_{acc} \approx 20$ MV/m with subsequent HFQS, similar to results from furnace nitrogen doping [2].

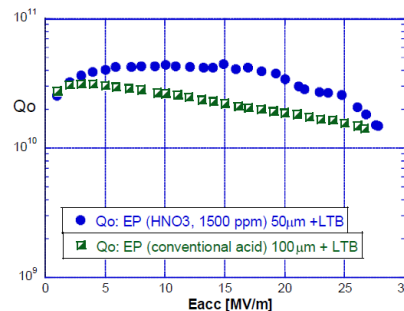


Figure 1: Measured quality factor as a function of gradient for EP'ed and wet-doped ILC-type cavities (1.3 GHz) at KEK.

CAVITY PREPARATION AND COLD TEST CONDITIONS

For the initial tests, 120 μm was removed from the SRF surface with wet doping EP. Three cold tests were performed after wet doping: Test 1 was right after 120 μm removal and high pressure water rinsing; Test 2 was after LTB at 120° C for 48 hours; Test 3 was after an overnight 100 K “soak.” LTB is effective to increase Q_0 for FRIB EP'ed HWRs [1], which provided the impetus for Test 2. Since the SRF surface should be mostly doped with nitrogen rather than oxygen, and N does not diffuse at 120°C [4], we expect minimal benefit from LTB. The 100 K soak tests whether hydrogen is present on the SRF surface to produce Q -disease.

Additional tests were done after furnace hydrogen degassing and removal of an additional 25 μm with EP (HNO_3). Degassing is considered to reset the wet nitrogen doping, because nitrogen is also removed from the SRF surface, and

* Work supported by the U.S. Department of Energy, Office of Science, DE-S RC114424

[†] wuyu@frib.msu.edu

ANTHEM PROJECT, CONSTRUCTION OF A RFQ DRIVEN BNCT NEUTRON SOURCE

A. Pisent, F. Grespan, C. Baltador, L. Bellan, M. Comunian, V. Conte, J. Esposito, L. Ferrari, E. Fagotti, M. Montis, Y.K. Ong, A. Palmieri, A. Selva, INFN/LNL, Legnaro, Italy
 P. Mereu, C. Mingioni, M. Nenni, E. Nicoletti, INFN sezione di Torino, Torino, Italy
 A. Passarelli, M.R. Masullo, INFN sezione di Napoli, Napoli, Italy
 V. Vercesi, S. Bortolussi¹, INFN sezione di Pavia, Pavia, Italy
¹also Università degli studi di Pavia, Pavia, Italy

Abstract

The project Anthem, funded within the Next Generation EU initiatives, foresees the realization of an innovative accelerator based BNCT (Boron Neutron Capture Therapy) facility in Caserta, Italy.

The INFN (LNL, Pavia, Napoli, Torino) is in charge of the design and construction of the epithermal neutron source, that will assure a flux of $10^9 \text{ s}^{-1} \text{ cm}^{-2}$ with characteristics suited for deep tumors treatment. The driver is a cw RFQ, able to produce proton beam of 30 mA at 5 MeV, impinging on a beryllium target. Specific challenges are related to the medical application of the device. In the paper an overview of the project will be given.

INTRODUCTION

New neutron sources based on compact high intensity linacs have recognized advantages respect to reactors and spallation sources for medical (and many other) applications.

One of the pilots of the project ANTHEM (Advanced Technology for Human centered Medicine) is aiming to the realization of an intense source of epithermal neutrons for Boron Neutron Capture Therapy (BNCT) for deep-seated tumour treatment. Such neutron source is based on a high intensity linear accelerator under realization at INFN (Istituto Nazionale di Fisica Nucleare), Legnaro National Laboratory, Pavia, Napoli and Torino units.

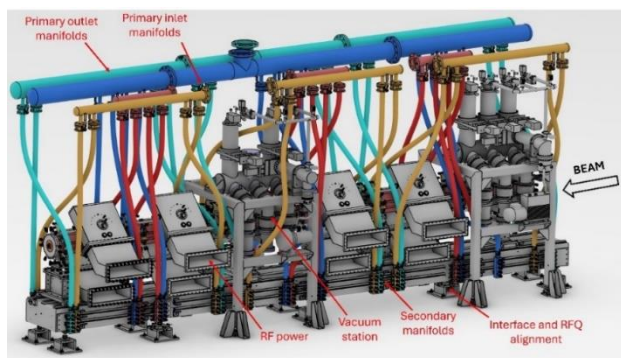


Figure 1: The RFQ integration on the new support.

The accelerator is a Radio Frequency Quadrupole able to accelerate 30 mA of protons up to 5 MeV. The RFQ (Figs.1 and 2), together with the ion source TRIPS was developed in the last years in the framework of TRASCO project at INFN LNL and LNS respectively.

The proton accelerator is coupled to a high-power beryllium target. For BNCT application this neutron source promises unique performances in terms of neutron flux and spectra (very low gamma and fast neutrons components) as needed for a successful therapy.

Table 1: ANTHEM BNCT Main Parameters

Ion source	MDIS	Proton energy 80 keV
Accelerator	RFQ	352.2 MHz, 7.13 m long
Final energy	5 MeV	
Beam current	30 mA	accelerated
Duty cycle	CW	50% duty cycle possible
p-n Converter	Beryllium	150 kW, 1 kW/cm^2
Neutron source intensity	$\sim 10^{14} \text{ s}^{-1}$	entire solid angle, Ave. neutron energy 1.2MeV
At BNCT port	$\sim 10^9 \text{ s}^{-1} \text{ cm}^{-2}$	epithermal
RF power	1.0 MW	
Power consumption	$\sim 3.5 \text{ MVA}$	

The proposal of a neutrons source based on TRASCO RFQ for BNCT has a quite long history as SPES-BNCT [1] and MUNES projects [2]; for these R&D programs the construction of the facility was not funded, but many technological issues were solved.

Therefore, when in 2022 the group of physicists from INFN, and the group of medical doctors and biologists from Vanvitelli University met with the strong motivation to build a BNCT facility, many elements were clear and a successful proposal could be prepared in short time. Table 1 summarizes the main parameters of ANTHEM BNCT. In this paper we shall concentrate in accelerator and target aspects.



Figure 2: The 3 RFQ segments at INFN-LNL.

BEAM COMMISSIONING OF THE FIRST HELIAC CRYOMODULE

J. List^{* 1,2}, W. Barth^{1,2,3}, C. Burandt^{1,2}, F. Dziuba¹, V. Gettmann^{1,2}, T. Kürzeder^{1,2}, R. Kalleicher^{1,2,3}, S. Lauber^{1,2}, M. Miski-Oglu^{1,2}, H. Podlech⁴, U. Scheeler¹, H. Vormann¹, S. Yarymyshev^{1,2}

¹ GSI Helmholtzzentrum für Schwerionenforschung GmbH, Darmstadt, Germany

² HIM Helmholtz Institute Mainz, Mainz, Germany

³ KPH Johannes Gutenberg-University Mainz, Mainz, Germany

⁴ IAP Institut für Angewandte Physik, Frankfurt am Main, Germany

Abstract

The superconducting heavy ion HELmholtz LInear ACcelerator (HELIAC) is designed to meet the needs of the Super Heavy Element (SHE) research and material science user programs at GSI in Darmstadt. The beam energy can be varied smoothly between 3.5 and 7.3 MeV/u, with an average current of up to 1 mA and a duty cycle of 100 %. Recently the first cryomodule CM1 was fully commissioned and tested. CM1 comprises three Crossbar H-mode (CH)-type accelerating cavities, a CH-rebuncher, and two superconducting solenoid lenses. Following the commissioning of the cryogenic supply- and RF-systems, a successful beam test was conducted at the end of 2023. A Helium ion beam was successfully accelerated to the design energy of 2.7 MeV/u. The beam energy could be varied continuously between 1.3 MeV/u and 3.1 MeV/u without any significant particle losses inside the cryomodule. In June 2024 a Argon ion beam was accelerated to the design energy of 2.7 MeV/u. This contribution covers the construction and commissioning of the first HELIAC cryomodule and the results of the beam test campaign.

(HELIAC) [1–4] is foreseen to be constructed on the GSI campus. It will provide for continuous wave (CW) heavy ion beams of smoothly variable energies between 3.5 and 7.3 MeV/u with a mass to charge ration A/Z between 1 and 6. HELIAC comprises a normal conducting injector and the SC main accelerator [2]. The injector consists of an Electron Cyclotron Resonance Ion Source (ECR), a radio frequency quadrupole (RFQ), and two alternating phase focusing (APF) interdigital H-mode (IH) cavities [5, 6] for acceleration up to 1.4 MeV/u. The SC part comprises four separate cryomodules, each consisting of three SC crossbar H-mode (CH) cavities [7–9] for beam acceleration, a SC rebuncher and two SC solenoid lenses with integrated steering coils, as well as two cold beam position monitors (BPMs).

Highlighted in Fig. 1 the first of the series HELIAC cryomodule CM1, (called Advanced Demonstrator) was assembled in the clean room of Helmholtz Institute Mainz (HIM), transported to GSI and tested with a $^4\text{He}^{2+}$ and $^{40}\text{Ar}^{8+}$ beam provided by the GSI High Charge State Injector (HLI) [10].

CRYOMODULE ASSEMBLY AND INSTALLATION

INTRODUCTION

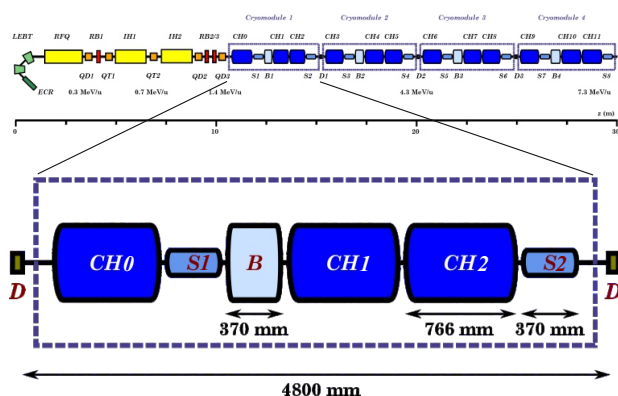


Figure 1: Sketch of the HELIAC (top) and the first cryomodule (CM1), referred to as the Advanced Demonstrator (bottom).

To sustain and enhance the research programs in superheavy ions, material sciences, and biophysics at GSI Helmholtz Centre for Heavy Ion Research (GSI), the superconducting (SC) heavy ion Helmholtz Linear Accelerator



Figure 2: Fully assembled cold string on rail system.

After the previous test of the first of series cavity CH0 in 2018 with beam [11], the cavity was transported back to HIM to be assembled together with the remaining components of the coldstring of CM1 in the HIM clean room [12].

The assembly procedure of the cold-string components in the clean room consists of an initial cleaning of all components in an ultrasonic bath, followed by a conductivity rinse. The cavities are subjected to a high pressure rinse (HPR) treatment at the manufacturer. Solenoids and bellows are cleaned with HPR in the clean room. After drying, the components are mounted on a trolley that runs on a rail system (Fig. 2). The cold part of the power couplers [13] are first as-

* j.list@gsi.de

BEAM EMITTANCE AND TWISS PARAMETERS FROM PEPPER-POT IMAGES USING PHYSICALLY INFORMED NEURAL NETS*

I. J. Knight[†], Georgia Institute of Technology, Atlanta, GA, USA
B. Mustapha, Argonne National Laboratory, Lemont, IL, USA

Abstract

In the field of accelerator physics, the quality of a particle beam is a multifaceted concept, encompassing characteristics like energy, current, profile, and pulse duration. Among these, the emittance and Twiss parameters—defining the size, shape, and orientation of the beam in phase space—serve as important indicators of beam quality. Prior studies have shown that carefully calibrated statistical methods can extract emittance and Twiss parameters from pepper-pot emittance meter images. Our research aimed to retrieve these parameters with machine learning (ML) from a transverse image of the beam after its propagation through a pepper-pot grid and subsequent contact with a scintillating plate. We applied a Convolutional Neural Network (CNN) to extract the x and y emittances and Twiss parameters (α and β), producing a six-dimensional output by simply looking at the image without calibration information. The extraction of divergence-dependent parameters, such as α and emittance, from a single image presented a challenge, resulting in a large Symmetric Mean Absolute Percentage Error (SMAPE) of 30%. To mitigate this issue, our novel method that incorporated image data from two points along the particles' propagation path yielded promising results. β prediction achieved a low SMAPE of 10.5%, while α and emittance predictions were realized with a 16.5% SMAPE and 13.3% SMAPE, respectively. Our findings suggest the potential for improvement in ML beam quality assessment through multi-point image data analysis.

BACKGROUND

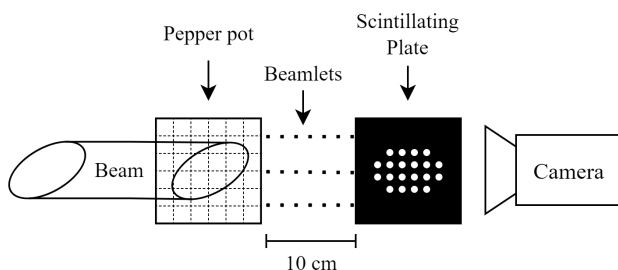


Figure 1: Pepper-pot emittance meter arrangement.

At the Argonne Tandem Linear Accelerator System (ATLAS), images of the beam are captured using a pepper-pot (PP) emittance probe. A pepper-pot is a plate with holes in

* This work was supported by the U.S. Department of Energy, under Contract No. DE-AC02-06CH11357. This research used the ATLAS facility, which is a DOE Office of Nuclear Physics User Facility.

[†] ianknight@gatech.edu

it placed transverse to the beam splitting it into beamlets. In a PP emittance probe system, beamlets travel a short distance then hit a scintillating plate which fluoresces in those locations, see Fig. 1. An image of the plate is then captured by a camera, see Fig. 2.

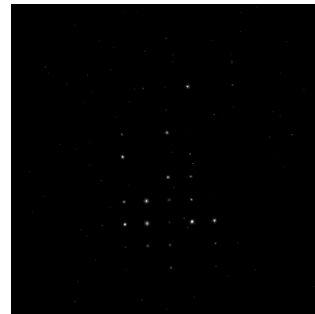


Figure 2: Real-world pepper pot image.

The beam envelope, the x and y extent of the beam, exist in physical space; phase space is a theoretical space defined by the momentum and physical positions of particles in the beam. Particles have position and momentum in three dimensions, for this reason there are 3 separate phase space ellipses in the absence of coupling. The longitudinal coordinate, z, is the direction the beam travels, and the (x, y) plane or transverse plane contains the image that PP metering captures.

$$\gamma x^2 + 2\alpha x x' + \beta x'^2 = \epsilon \quad (1)$$

where x' and y' represent momentum.

$$\frac{1 + \alpha}{\beta} = \gamma \quad (2)$$

The distribution of momenta and position of particles when projected onto a phase plane generate an ellipse, referred to as the phase space ellipse. Twiss parameters (α , β , γ) and emittances (ϵ) define the size, shape, and orientation of the phase space ellipses as in Eq. (1). Beta is proportional to the extent of the beam, horizontal or vertical, in physical space. Emittance is the area of the phase space ellipse, and in physical space, it relates to the spread of the beam. Alpha is the correlation of position and momentum. Visually, it describes the tilt of the beam in phase space.

Problem Definition

Our PP images, defined in physical space, do not fully capture information about particles' momenta as they show a snapshot in time while momentum describes a process that changes over time. To extract the Twiss parameters from

CRYOMODULE OPERATION EXPERIENCE FOR THE FRIB CONTINUOUS-WAVE SUPERCONDUCTING LINAC*

W. Chang[†], Y.-L. Cheon, Y. Choi, X. Du, W. Hartung, S. Kim, T. Konomi, S. Kunjir, H. Nguyen, K. Saito, Y. Wu, T. Xu, D. Zhang, S. Zhao

Facility for Rare Isotope Beams, Michigan State University, East Lansing, MI, USA

Abstract

The superconducting (SC) driver linac for the Facility for Rare Isotope Beams (FRIB) includes 46 cryomodules for acceleration of heavy ions to 200 MeV/u. FRIB cryomodules have been supporting sustainable and reliable delivery of high-power heavy ion beams, including 10 kW uranium beams, to the target for production of rare isotopes for user experiments in nuclear physics. The linac operates in continuous-wave mode for maximum utilization of beam from the ion source. A total of 104 quarter-wave resonators (QWRs; $\beta=0.041$ and 0.085 ; 80.5 MHz) equipped with stepper-motor frequency tuners and frictional mechanical dampers are operated at 4 K. A total of 220 half-wave resonators (HWRs; $\beta=0.29$ and 0.53 ; 322 MHz) equipped with pneumatic frequency tuners are operated at 2 K. We will present resonance control and phase stability performance as well as experience with tuner systems in linac operation. FRIB cavities are designed to be operated at a peak surface electric field of approximately 30 MV/m. We will present cavity field emission performance over the years of linac operation and discuss field emission reduction measures such as pulsed RF conditioning (presently in use) and plasma processing (in development). Automation is a key aspect of efficient delivery of beams to users. We will present our experience with automation of SC devices such as start-up, shut-down, and fast recovery from an RF trip as well as performance tracking of linac SC devices.

INTRODUCTION

The Facility for Rare Isotope Beams (FRIB) is a 400 kW superconducting linac which accelerates stable ions up to uranium to energies of ≥ 200 MeV/u [1]. The linac has a folded layout with 3 accelerating segments and 2 folding segments, as shown in Fig. 1. The linac has a total 324 superconducting radio frequency (SRF) cavities and 69 superconducting (SC) solenoids. The quarter-wave resonators (QWRs) in Linac segment 1 (LS1) operate at 4.5 K; the half-wave resonators (HWRs) in Linac Segment 2 and 3 operate at 2 K; all SC solenoids operate at 4.5 K [2].

Beam is delivered to the target at full energy or to the FRIB Single Event Effects (FSEE) experimental station downstream of Segment 1. On 22 December 2023, the FRIB linac reached a record high beam power of 10.4 kW

Uranium with energy up to 177 MeV/u. The facility is currently delivered 10 kW primary beam power for users. An increase in beam power to 20 kW is planned in 2024 [3].

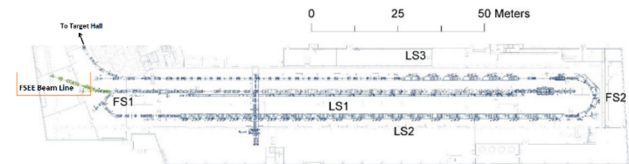


Figure 1: Layout of the FRIB driver linac.

CRYOMODULE PERFORMANCE AND IMPROVEMENTS

Cavity Field Level and Field Emission

Figure 2 shows the achievable average accelerating gradient (E_{acc}) for each cryomodule. Though some cavities are operated at lower field, neighbouring cavities can operate at higher E_{acc} , such that the average gradients are above the design goals.

Figure 3 shows the measured field emission (FE) X-rays from the cavities. Compared with 3 years ago (FRIB cryomodule commissioning), a few cavities have stronger FE X-rays. Conservative administrative limits are used to keep the X-rays below ~ 10 mR/hr for most cavities to reduce the risk of further performance degradation. As a result, a few of the cavities are operated below their design field, as mentioned above.

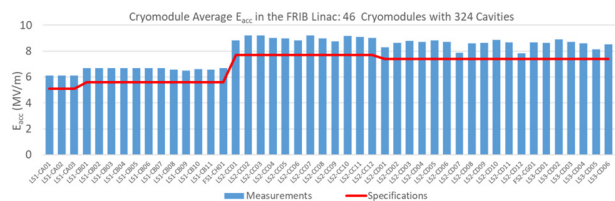


Figure 2: Average gradients in the FRIB cryomodules.

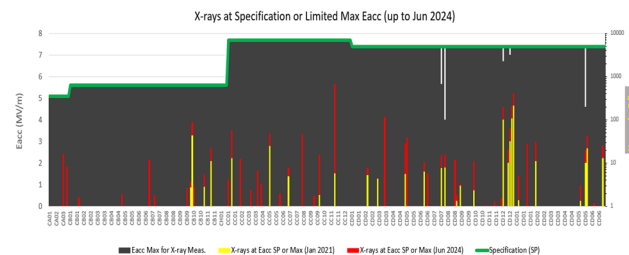


Figure 3: Field emission X-rays in the FRIB Linac.

High power pulsed RF conditioning and in-situ plasma processing can reduce field emission. Several cavities improved after pulse conditioning [4]. Plasma processing has

*This work is supported by the U.S. Department of Energy, Office of Science, Office of Nuclear Physics and used resources of the Facility for Rare Isotope Beams (FRIB) Operations, which is a DOE Office of Science User Facility under Award Number DE-SC0023633.

[†]chang@frib.msu.edu

EVALUATION OF WAKEFIELD MITIGATION FOR UPGRADING THE ATF FINAL FOCUS BEAMLINE

Y. Abe*, K. Kubo¹, N. Terunuma¹, T. Okugi¹, KEK, Tsukuba, Japan
¹also at The Graduate University for Advanced Studies, SOKENDAI

Abstract

The KEK-ATF is an R&D facility for the final focus system to develop the nanometer beam technology required for the International Linear Collider. The vertical beam size growth as a function of the bunch intensity was observed at the virtual interaction point (IP), which is mainly caused by wakefield. ATF is the best research environment for the study of wakefield effects on the nanometer small beam. The evaluation results of wakefield effects show that cavity BPM and vacuum flange have strong effects on the small beam. We are planning to upgrade the ATF-FF beamline to reduce wakefield effects on the small beam. First, an internal shield was inserted into the vacuum flange, one of the strong wakefield sources, to evaluate the mitigation of the wakefield effect. As a result, it was demonstrated that the wakefield effect of the ICF70 flange can be mitigated by the RF shield to the same level as that of a straight pipe.

INTRODUCTION

The KEK-ATF (Accelerator Test Facility) is an R&D facility for the final focus system to develop the nanometer small beam (small beam) technology required for the International Linear Collider (ILC) [1]. ATF consists of LINAC, Damping Ring (DR), Extraction (EXT) beamline and Final Focus (FF) beamline [2, 3]. Figure 1 shows the layout of the beamline after the DR. A low emittance beam is generated at DR [4,5] and focused with the EXT and FF beamline to focus the electron beam to 37 nm at the virtual interaction point (IP) [6]. Table 1 shows the nominal beam parameters for the nanometer small beam study. In 2016, it was confirmed that the vertical beam size at IP reached 41 nm [7].

Wakefield is an electromagnetic field generated by charged particles passing through a structure in a beamline that has geometrical shape changes. The excited wakefield acts as a kick to the backward of the bunch, distorting its distribution. It induces the bunch position change and the beam size growth. It is important to study the wakefield effects on the beam to develop advanced accelerators that require small beam technology. ATF is the best research environment for the detailed evaluation of wakefield effects on the small beam because the nanometer small beam with low emittance is generated, and the bunch center position and beam size can be measured using high-precision monitors [8–10].

The vertical beam size growth as a function of the bunch intensity at the IP has been observed at ATF, which is mainly caused by wakefield. We are planning to upgrade the FF beamline to mitigate wakefield effects on the small beam by reducing the wakefield source from the beamline. The

impacts of the ICF70 flange, which is one of the strong wakefield sources, as a single component of the wakefield source were experimentally evaluated. In addition, The wakefield mitigation by inserting an internal RF shield into ICF70 flanges was confirmed. This paper reports the evaluation results and the current status of the work to upgrade the beamlines to reduce the effects of the wakefield.

Table 1: Nominal Beam Parameters for the Small Beam Study

Parameter		Unit	Value
Beam energy	E	GeV	1.3
Max. bunch population	Q	$10^9 e^-/\text{bunch}$	20
Bunch length	σ_z	mm	7
Energy spread	σ_E	%	0.08
Vertical emittance	ε_y	pm.rad	12
Beta function at the IP	β_y	mm	0.1

IMPACTS OF EACH WAKEFIELD SOURCE ON THE SMALL BEAM

Table 2 lists wakefield sources (the vacuum components, beam monitors, collimators, etc.) in EXT and FF beamlines and the amount of installations. The excited wakefield on each wakefield source was calculated by GdfidL, which is an electromagnetic field simulation code [11]. In addition, a new wakefield model was constructed to evaluate the wakefield effects on the small beam [12]. The impact of each wakefield source on the small beam caused by the orbit fluctuation is expressed as $W_{y,j}(y = 1\text{mm}, z) \sum_i \beta_{y,j,i}$ [13]. Figure 2 shows the evaluation result of wakefield effects on the small beam of each type of wakefield source. It illustrated that cavity BPM and ICF70 flange have strong effects on the small beam.

EVALUATION OF THE WAKEFIELD MITIGATION AS A SINGLE COMPONENT

The cross-section of the ICF70 flange is shown in Fig. 3. We planned to insert a cylindrical RF shield made of stainless steel, as shown in Fig. 3, into the ICF70 flange to hide the gap. In this section, we described the evaluation results of the wakefield effects caused by the ICF70 flange on the small beam and mitigation by the RF shield. The effects were evaluated by the orbit response method as a single component of Wakefield source [14–16].

The effect of the wakefield kick caused by a single wakefield source on the beam can be quantified by the orbit response downstream from the wakefield source. This method

* abeyuki@post.kek.jp

ON FORCED RF GENERATION OF CW MAGNETRONS FOR SUPERCONDUCTING ACCELERATORS*

G. Kazakevich[#], R.P. Johnson, Muons, Inc., Newport News, VA, USA
 T. Khabiboilline, G. Romanow, V. Yakovlev, Fermilab, Batavia, IL, USA
 Ya. Derbenev, JLab, Newport News, VA, USA

Abstract

CW magnetrons, developed for industrial RF heaters, were suggested to power superconducting RF (SRF) cavities of accelerators due to magnetrons higher efficiency and lower cost comparing to traditionally used klystrons, IOTs or solid-state amplifiers. CW magnetrons are regenerative RF generators with a huge regenerative gain. This causes regenerative instability with a quite large noise. Traditionally CW magnetrons operate at the anode voltage above the threshold of self-excitation. Stabilized by a small injection-locking signal they were proposed to drive SRF cavities. Then the magnetrons generate the injection locked oscillations and generate noise. This may preclude use of CW magnetrons in some SRF accelerators. We developed described below a mode for forced RF generation of CW magnetrons when the injected forcing signal provides start up and the regenerative noise is suppressed. The mode is most suitable for powering high Q-factor SRF cavities.

INTRODUCTION

High-power CW magnetrons, designed and optimized for industrial RF heaters, but driven by an injection-locking signal, were suggested in number of works to power SRF cavities in accelerators due to higher efficiency and significantly lower cost of generated RF power per Watt than traditionally used RF amplifiers (klystrons, IOTs, solid-state amplifiers). The RF amplifiers driven by a master oscillator serve as coherent low noise RF sources. The CW magnetrons are regenerative RF generators with a huge regenerative gain of the resonant system to start up reliably with a self-excitation by noise even if the tube is powered by a DC power supply. Very large regenerative gain causes a regenerative instability with a large level regenerative noise. Traditionally the magnetrons operate in the self-excitation mode, i.e. with the anode voltage above the self-excitation threshold, at a small injection-locking signal, $P_{Lock} \approx -20$ dB_C or less of the magnetron power P_{Mag} . In this case the regenerative noise of a CW magnetron violates a necessary correlation of the tube start up with its injection-locking; the magnetron may be launched by the noise or Power Supply (PS) ripples via side bands, but not by the injection-locking signal. Such probability is considered in the presented work. A novel method of forced RF generation of CW magnetrons eliminating start up by noise and PS ripples is briefly described below. The method was

tested in experiments with CW magnetrons of microwave ovens.

OPERATION OF A CW MAGNETRON INJECTION-LOCKED BY A SMALL SIGNAL

We consider operation of a CW magnetron as it is traditionally assumed, in the self-excitation mode, at an injection-locking signal with low power P_{Lock} .

The effective bandwidth of injection-locking Δf , at the locking signal is expressed by the following equation [1]:

$$\Delta f = \frac{f_0}{2Q_L} \sqrt{\frac{P_{Lock}}{P_{Mag}}} \quad (1)$$

Here: f_0 is the instantaneous magnetron frequency, Q_L is the magnetron loaded Q-factor, P_{Mag} is the magnetron output power. For the 2.45 GHz, free running microwave oven magnetron type 2M137-IL the effective bandwidth $\Delta f_{FR} \approx 4.5$ MHz [2]. Out of the effective bandwidth the magnetron cannot be injection-locked at the given P_{Lock} .

Then the probabilities of the injection-locking process w_{Lock} and a free running operation w_{FR} ($P_{Lock} = 0$) for this 2.45 GHz, CW tube one can estimate as:

$$w_{Lock} \sim \frac{\Delta f}{\Delta f_{FR}}, \text{ and } w_{FR} \sim \frac{\Delta f_{FR} - \Delta f}{\Delta f_{FR}} \quad (2)$$

The probabilities estimates vs. P_{Lock} are shown in Table 1.

Table 1: The Values of w_{Lock} and w_{FR} vs. P_{Lock} .

P_{Lock}	Δf ,	w_{Lock}	w_{FR}
-10 dB	3.87 MHz	~0.86	~0.14
-20 dB	1.22 MHz	~0.27	~0.73
-30 dB	0.39 MHz	~0.09	~0.91

Thus, probability of the injection-locked generation of such RF source may be less than probability of the free running generation caused by noise. The noise oscillations are much less in magnitude than the injection-locked ones. Since the average time of motion of charges in the interaction space towards the anode is $\sim f_0^{-1} \ll Q_L / \pi f_0$ (the latter is a filling time of the magnetron resonant system), this results in a notable quasi-continuous noise spectrum. It is a disadvantage for operation of the self-exciting magnetrons with low locking signal for high Q-factor SRF cavities. The distorted spectra of the RF sources with an intense quasi-continuous noise may preclude required suppression of parasitic modulations (microphonics, etc.) and may increase the beam emittance in SRF accelerators.

Impact of power of the injection-locking signal on the spectral density of noise power for the 2.45 GHz microwave oven free running magnetron plotted in Fig. 1 [3]

* Supported by scientific collaboration of Muons, Inc and Fermi National Accelerator Laboratory, Fermi Research Alliance, LLC under CRADA-FRA-2023-0029.

[#]e-mail: gkazakevitch@yahoo.com; grigorv@muonsinc.com

PRELIMINARY MEASUREMENT OF 4D BEAM PHASE SPACE DISTRIBUTION USING A SLIT EMITTANCE METER SYSTEM

S. Lee*, S.H. Moon, D.-H. Kim, H.-S. Kim, H.-J. Kwon
Korea Multipurpose Accelerator Complex,
Korea Atomic Energy Research Institute, Gyeongju, Korea

Abstract

Transverse emittances are generally measured in horizontal and vertical phase space separately as 2D projections of 4D phase space without any correlations between them. It is true only if their degrees of freedom are independent. Recent studies show that there exists correlation across conjugate pairs. This correlation can affect beam dynamics and cause beam loss. In our study, we sought to measure 4D beam phase space distribution with possible correlations. For this purpose, we used a direct method of measuring the 4D phase space distribution using slits. A set of 4 slits is used to slice the beam into a specific volume of the 4D phase space, and the charge inside each volume is measured. KOMAC has a test bench called BTS (Beam Test Stand) which consists of a microwave ion source, LEBT, a 200 MHz RFQ and two beamlines. At one of the beamlines, we have just installed slit emittance meter system to measure 4D beam phase space distribution. This paper presents our slit emittance meter system and shows preliminary experimental results thereof.

INTRODUCTION

Beam diagnostics research for measuring high power beam distribution becomes more important and is studied in several laboratories [1–4]. Especially in high power accelerators, nonlinear space charge forces cause beam loss which can lead to radio-activation of the accelerator components. It is important to understand the beam phase space distribution fully to reduce uncontrolled losses for the safe hands-on maintenance. In this paper, we present works of measuring 4D beam phase space distribution specified below:

- Slit emittance meter and its installation in BTS.
- Measurements of 4 D beam phase space distribution with all possible correlations across conjugate pairs $x - x'$, $y - y'$, $x - y'$, $y - x'$, $x - y$ and $x' - y'$.
- Reconstruction of x , y , $x - x'$, $y - y'$, $x - y'$ and $y - x'$ beam distributions from the 4 D phase space distribution $f(x, x', y, y')$ measurement.
- Comparison between measured and reconstructed beam distributions.
- Calculation of 4D emittance.

SLIT EMITTANCE METER

Slit emittance meter uses two pairs of slits installed at a distance $L = 0.5$ m. Fig. 1 (a) shows the cross-sectional view of the chamber with a pair of vertical and horizontal slits.

These slits are driven by a set of linear motion manipulator and a stepper motor. The beam is directed to first slit pair (slit 1 and 2 for x_1 and y_1 positions) and chopped into flat beamlets. This beamlet is spread with initial angular spreads in x and y , and then passes through the second slit pair (slit 3 and 4 for x_2 and y_2 positions). After passing through all the slits, the final beamlet is measured as the beam current at the collector. By repeating these measurements at various combinations of slit positions, the entire phase space $f(x, x', y, y')$ can be directly measured as $x = x_1$, $y = y_1$, $x' = (x_2 - x_1)/L$ and $y' = (y_2 - y_1)/L$. The slit emittance meter is installed in the straight beamline of the BTS. BTS consists of a microwave ion source, a LEBT (low energy beam transport) system, a RFQ (Radio Frequency Quadrupole) accelerator, quadrupole magnets and beam diagnostics tools such as current transformer, faraday cups and wire scanners as shown in Fig. 1 (b). The slit emittance meter is installed as seen in Fig. 1 (c).

4D PHASE SPACE MEASUREMENT

The slit emittance meter installed in the BTS (Fig. 1 (c)) is set to measure multi-dimensional phase space distributions with certain combinations of slits. When measuring $x' - y'$, all 4 slits are used, which took more than 50 hours-long measurement time. And the $x' - y'$ data can be used to reconstruct its sub-dimensional distributions, that is, the $x - x'$, $y - y'$, $x - y'$ and $y - x'$ distributions. In this section, we show experimental results and compare directly measured distributions with distributions reconstructed from $x' - y'$ data.

Measurements of Beam Phase Space Distribution

$x - x'$, $y - y'$ and $x - y$ beam phase space distributions are measured using the $x_1 - x_2$, $y_1 - y_2$ and $x_1 - y_1$ slit pairs with the moving step of 0.5 mm respectively. For $x - y'$ and $y - x'$ beam phase space measurements, we used three slits, *i.e.* $x_1 - y_1 - y_2$ and $x_1 - y_1 - x_2$ pairs. For $x' - y'$ beam phase space measurements, all four slits are used. These measurement results are shown in Fig. 2 with phase space ellipses (yellow dotted lines) of their emittances and twiss parameters obtained from the beam phase distribution. The emittance and twiss parameters are summarized in Table 1.

Reconstruction of Beam Phase Space Distribution

$x' - y'$ measurement data is a function of beam intensity with respect to x_1 , y_1 , x_2 and y_2 which can be written as,

$$I(x_1, y_1, x_2, y_2) = I(x, y, x', y') \quad (1)$$

* shl@kaeri.re.kr

STATUS OF THE L-BAND GUN DEVELOPMENT AT PITZ

A. Oppelt[†], N. Aftab, Z. Amirkhanyan, P. Boonpornprasert, D. Dmytriiev, J. D. Good, A. Grebinyk, M. Gross, A. Hoffmann, L. Jachmann, D. Kalantaryan, W. Köhler, M. Krasilnikov, X. Li, Z. Lotfi, F. Müller, S. Philipp, C.R. Richard, F. Riemer, F. Stephan, G. Vashchenko, S. Zeeshan

DESY, Zeuthen, Germany

D. Bazyl, M. Bousonville, F. Brinker, A. Ermakov, A. Jeromin, D. Lipka, C. Martens, L. Schaper, S. Vilcins-Czvitkovits, DESY, Hamburg, Germany
X.-Y. Zhang, Tsinghua University, Beijing, China

Abstract

Gun5, the new generation of high-gradient normal conducting 1.3 GHz RF guns for linac-driven free-electron lasers like FLASH and European XFEL is under development at the Photo Injector Test facility at DESY in Zeuthen (PITZ). Its improved cell geometry and cooling concept allow for RF pulse durations of up to 1 ms at 10 Hz repetition rate, at gradients of ~60 MV/m at the cathode. Gun5 is also equipped with an RF probe for measurements of the RF field inside the gun.

The first gun of this type, Gun5.1, is in operation at PITZ since April 2022. Gun5.2 will be commissioned at the FALCO conditioning facility at DESY in Hamburg, starting in June 2024. This gun is equipped with a balanced (symmetric) RF waveguide feed to the coaxial power coupler to prevent a coupler kick and thus improve the beam quality delivered by the electron source.

Further guns are currently in the manufacturing process. In parallel, studies towards a more reliable cathode spring design are ongoing, in order to overcome observed issues during the high duty cycle operation of Gun5.1. This article will give an overview on all those developments.

INTRODUCTION

For 25 years, the development of electron sources for linac-driven Free Electron Lasers (FELs) like FLASH and European XFEL takes place at the Photo Injector Test Facility at DESY in Zeuthen. Over the years, the facility developed into a place for accelerator R&D, but the original purpose of optimizing electron guns is still one pillar of the PITZ research program.

The PITZ gun is an L-band (1.3 GHz) normal conducting 1 ½ cell standing wave copper cavity operated in π -mode. In total, 10 different electron sources (guns) have passed through the PITZ facility over the years. During this time, 5 optimized gun setups have been delivered to FLASH, and 3 to European XFEL.

With time, the operations specifications for the electron gun have changed towards more demanding parameters, in terms of gradient and pulse length, as well as in terms of stability and reliability. The currently envisaged operation parameters are an RF pulse length of up to 1 ms at a repetition rate of 10 Hz, and an operation gradient of 60 MV/m, corresponding to an RF power input of up to 6.5 MW into the gun cavity. At these parameters, the RF gun has to fulfill the user requirements in terms of stability and reliability.

Gun5 is the latest generation of electron guns for high duty cycle operation with improved stability and reliability [1]. Compared to the previous Gun4 type, it has an optimized cell geometry with elliptical irises for higher RF efficiency and reduced surface field strength which shall allow for more stable and reliable operation. It furthermore has an optimized water cooling which allows cooling of up to ~65 kW average power. Thus, it permits higher duty cycle operation. Improved rigidity of the cavity will reduce the deformation over the up to 1 ms long RF pulse (pulse heating). Another new feature is the existence of in-cavity RF probe(s) which allow a direct control of the RF field in the cavity and thus facilitate LLRF regulation. It furthermore allows the use of a new, symmetric RF distribution system by means of a symmetric power coupler which has the additional advantage of reducing the power load on the needed RF windows by 50% by the use of two input arms. Several cavities of Gun5 type are being produced and will replace the currently used Gun4 type cavities at FLASH and European XFEL.

GUN5.1

Gun5.1 is the prototype gun and is in operation at PITZ since April 2022. It still uses the old RF distribution system from the Gun4 type described in [2]. As reported in [2], the operation of Gun5.1 at PITZ was limited by short interruptions within the first part of an RF pulse, so-called minibreakdowns, occurring at higher average power settings. In 2023, the gun conditioning focused on the study of this phenomenon which was found to be related to a cathode spring problem that finally manifested in August 2023. The cathode spring was therefore exchanged but the operation stability did not improve significantly. Since the gun will be exchanged in the near future, it was decided to finish the planned physics program despite the instabilities, and to use Gun5.1 afterwards as testbed for a new cathode spring development, which is described below.

GUN5.2

The design of Gun5.2 (and all subsequent guns) is slightly different from the prototype, Gun5.1. It has a reinforced cathode backplane, two pickups, and minimally corrected inner dimensions in order to better match the resonance frequency after production. The tuning parameters are reported in Table 1 and compared to the values from Gun5.1. The effect of correcting the inner cavity dimensions on the frequency after production is clearly visible.

SMITH-PURCELL RADIATION STUDIES TOWARDS A COMPACT HIGH-RESOLUTION LONGITUDINAL DIAGNOSTIC

B. Stacey*[†], W. Kuropka, T. Vinatier
Deutsches Elektronen-Synchrotron DESY, Hamburg, Germany
W. Hillert
Universität Hamburg, Hamburg, Germany

Abstract

A new longitudinal diagnostic has been proposed, the SPACEChip (Smith-Purcell ACcElerator Chip-based) diagnostic, which can infer information about the temporal profile of a particle bunch from the Smith-Purcell radiation spectrum generated when the bunch passes close to a dielectric grating. This is done using the bunch form factor after retrieving the phase information. A simulated dielectric grating has been excited by Floquet modes to investigate the angular distribution of the Smith-Purcell radiation. Progress on the SPACEChip experimental campaign at the ARES linac at DESY will be reported, along with the expected photon yield from the structure with the ARES operational parameters.

INTRODUCTION

When a charged particle bunch passes close to a periodic change in refractive index, i.e. a grating of dielectric material, it is induced to radiate via the Smith-Purcell radiation (SPR) mechanism [1] as demonstrated in Fig. 1. The emis-

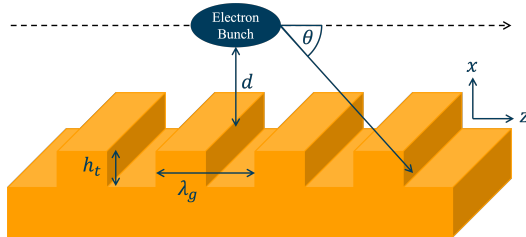


Figure 1: 3D model of SPR emission.

sion mechanism of SPR can be interpreted as the diffraction of the electron field [2]. SPR is spectrally dispersed and in-vacuum emission is governed by,

$$\frac{1}{\beta} - \cos(\theta) = \frac{m\lambda}{\lambda_g}, \quad (1)$$

where $\beta = v/c$, v is the velocity of the particle, c is the speed of light in a vacuum, θ is the angle of emission, m is the diffraction order, λ is the wavelength of the radiation, and λ_g is the period of the grating. For $m \neq 0$, Eq. (1) describes SPR of order m ; for $m = 0$, it describes Cherenkov radiation.

* also at Universität Hamburg, Hamburg, Germany

[†] blae.stacey@desy.de

The power radiated per angle is described by the angular distribution relation [2],

$$\frac{dP_m}{d\Omega} = \frac{eIm^2L}{2\lambda_g^2\epsilon_0} \frac{\sin^2\theta}{\left(\frac{1}{\beta} - \cos\theta\right)^3} |R_m|^2 e^{-\frac{d}{h_{int}}}, \quad (2)$$

where e is the elementary charge, I is the beam current, L is the length of the grating, ϵ_0 is the permeability of free space, and d is the impact parameter. $|R_m|^2$ is the radiation coefficient, which is discussed in detail for metallic rectangular and volume strip gratings in [3, 4]. h_{int} is the interaction length of the electron field virtual photons with the electron bunch,

$$h_{int} = \frac{\lambda\beta\gamma}{4\pi}, \quad (3)$$

where $\gamma = (1 - \beta^2)^{-1/2}$ is the Lorentz factor. Equation (2) assumes that the radiation is emitted in the x - z plane, as depicted in Fig. 1.

The use of SPR as a longitudinal bunch length diagnostic is not a new concept, however previous work has mostly involved using metal gratings [5–8]. Here, dielectric gratings are proposed, which can be produced with very high precision at low cost, due to advanced manufacturing techniques in the computer industry.

The reconstruction of the longitudinal bunch current profile is done through the use of the form factor. The radiated power consists of incoherent radiation, S_{inc} which is proportional to the horizontal charge profile of the bunch, and coherent radiation, S_{coh} , when the bunch length is shorter than λ_g , which is proportional to the entire three-dimensional current profile of the bunch. The total radiated power for a bunch of N_e electrons is,

$$\left(\frac{dP_m}{d\Omega}\right)_{N_e} = \left(\frac{dP_m}{d\Omega}\right)_1 (N_e S_{inc} + N_e^2 S_{coh}(\omega)), \quad (4)$$

where the form factor for the coherent radiation, S_{coh} , is given by,

$$S_{coh} = \left| \int_0^\infty X e^{-\frac{x}{\lambda_e}} dx \right|^2 \left| \int_{-\infty}^\infty Y e^{-ik_y y} dy \right|^2 \times \left| \int_{-\infty}^\infty T e^{-i\omega t} dt \right|^2, \quad (5)$$

where the charge distribution inside the bunch is assumed to be $q(x, y, t) = X(x)Y(y)T(t)$, λ_e is the evanescent wavelength and represents the coupling efficiency between the beam and the grating, k_y is the y component of the wave vector, and ω is the frequency of the radiation.

LIMITATIONS OF THE EuXFEL 3RD HARMONIC CRYOMODULE IN HIGH DUTY CYCLE OPERATION

B. Richter*, A. Bellandi, J. Branlard, A. Heck, M. Herrmann, K. Kasprzak
Deutsches Elektronen-Synchrotron DESY, Hamburg, Germany

Abstract

Future High Duty Cycle (HDC) operation scenarios of the European X-ray Free Electron Laser (EuXFEL) promise increased bunch repetition rate and photon delivery, at the cost of changing system requirements and moving away from the current mode of Short Pulse (SP) operation. To assess whether the third harmonic cryomodule design is also suitable for Long Pulse (LP) and Continuous Wave (CW) operation, key parameters of the spare module are examined at the Accelerator Module Test Facility (AMTF). For Radio-Frequency (RF) related energy efficiency, the cavity resonance tuning precision and the loaded quality factor tuning range are investigated. As performance indicators, limitations on attainable cavity gradient and RF stability are quantified. The results show that the module in its current design is insufficient for LP at high duty cycles and CW at the required operating points. The installed 3-stub tuners only yield maximum loaded quality factors between 5.3×10^6 and 1.9×10^7 , and the mechanical cavity tuner prohibits tuning precision within the intended cavity half bandwidth. Also, some higher order mode couplers do not allow CW operation at required gradients. Nevertheless, closed-loop RF stability measured in single cavity control is comparable to that of the third harmonic system of EuXFEL.

INTRODUCTION

The European X-ray Free Electron Laser (EuXFEL) is a hard X-ray light source for matter and technology research providing the highest brilliance in the world. It is driven by a linear accelerator providing a bunched electron beam with energies up to 17.3 GeV. Therefore, 800 superconducting cavities are operated in Short Pulse (SP) operation mode with a Radio-Frequency (RF) flat top length of $650 \mu\text{s}$ at 10 Hz pulse repetition rate. Electron bunches are accelerated during these flat tops at a repetition rate of up to 4.5 MHz.

To optimize bunch train utilization, a High Duty Cycle (HDC) upgrade of the linac allows to increase both the bunch spacing and the number of bunches per second at the same time. Different scenarios include substantially longer flat tops of tens to hundreds of ms and reduced RF repetition rates, called Long Pulse (LP), or even Continuous Wave (CW) operation. However, such an upgrade demands careful evaluation of required modifications to the machine.

Numerous R&D activities have been carried out since 2007, mostly related to the cryomodules and periphery of TESLA-type 1.3 GHz accelerating cavities. However, implications to the 3.9 GHz third harmonic system of the EuXFEL

were not investigated until 2017 [1], when the spare third harmonic cryomodule X3M2 was assembled.

The main focus of this work is determining the limitations of the third harmonics cryomodule in its current state for HDC operation. The resulting need for modifications depends on the specifications of the target operating point, which have not yet been decided.

CRYOMODULE X3M2

The third harmonic system at EuXFEL has been in operation since December 2015. It is used to linearize the longitudinal beam phase space curvature induced by the first accelerating module in the injector section, enabling to maintain beam quality in subsequent bunch compressors and the main linac. In the current EuXFEL setup, the 8 cavities of the cryomodule X3M1 are operated in vector sum, driven by a single klystron.

In 2018, the third harmonic spare module X3M2 passed the acceptance test for SP operation and has been installed in the Accelerator Module Test Facility (AMTF) since then. All cavities achieved electric field strengths of 20 MV/m without field breakdown.

To assess whether the module is suitable for LP and CW operation, the test bench was equipped with a 1 kW Solid State Amplifier (SSA), ready for operation since March 2023. The system is set up in single cavity control configuration. However, the available infrastructure is limited to provide 300 W drive power to the Fundamental Power Couplers (FPC).

LIMITATIONS AND STABILITY

Efficient HDC operation requires changes to several interdependent parameters of the system:

Without beam, the obtainable gradient E_{cav} depends on the provided driving power P_{drive} , the loaded quality factor Q_L , and the detuning Δf from cavity RF resonance,

$$E_{\text{cav}} = \frac{2}{l_{\text{cav}}} \cdot \frac{\left(\frac{r}{Q}\right) Q_L P_{\text{drive}}}{\sqrt{1 + \left(\Delta f \cdot \frac{2Q_L}{f_{\text{gen}}}\right)^2}},$$

where l_{cav} is the cavity length, (r/Q) the normalized cavity shunt impedance, and f_{gen} the generator frequency. The approach of reducing power demand through high loaded quality factors thus requires precise resonance control, as the impact of uncompensated disturbances on field stability increases. Besides, the maximum allowable gradient is bounded by the heat transport limit of the cryogenic system,

* bozo.richter@desy.de

REACHING DESIGN ELECTRON ENERGY AT FLASH AFTER LINAC UPGRADE

V. Ayvazyan^{*}, J. Branlard, C. Christou, K. Honkavaara, V. Katalev, D. Kostin, J. Roensch-Schulenburg, L. Schaper, C. Schmidt, S. Schreiber, M. Wienczek, B. Yildirim
Deutsches Elektronen-Synchrotron DESY, Hamburg, Germany

Abstract

The FLASH 2020+ project at DESY includes, among other modernizations, an increase of the electron beam energy. Two accelerator modules were replaced and the RF distribution of other modules was optimized. The limiting factors such as cavity breakdown and field emission were identified and measured through dedicated studies. At a later stage, based on these measurements, adjustments to the high-power distribution were proposed and the optimal operating point was demonstrated to achieve the design electron energy of 1.35 GeV with the nominal RF pulse length at FEL lasing conditions. After proper optimization and tuning of the low-level RF parameters, the linac successfully operated at maximum energy and delivered FEL radiation in the wavelength range below 3.2 nm. The measurement results as well as the achieved cavity gradients with energy gains are presented.

INTRODUCTION

The FLASH [1] linac is based on TESLA superconducting RF technology and is built with accelerating modules (ACC) with eight superconducting RF cavities each. Currently seven ACC's are installed in the linac. In 2022, during the first stage of the FLASH2020+ upgrade project [2], two accelerator modules were replaced and other modules had their RF distribution scheme optimized to increase the beam energy [3, 4]. The modules are powered either by a 5 MW or 10 MW (multi-beam) klystron. The cavities are operating in a pulsed mode. The low-level RF system is used to maintain beam stability. An RF regulation system provides field control for the RF gun and for superconducting modules with the vector-sum group of cavities [5]. RF power is distributed from a high-power klystron to the cavities via a forked set of waveguides. With the vector-sum concept, one klystron powers a set of up to 16 cavities. The synchronism of the incident waves to the cavities is ensured by waveguide tuners in front of each cavity which allows phase adjustment for individual cavities. A frequency tuning mechanism (stepper motor and piezo) is used to operate the cavities on resonance. Each accelerating cavity has one input coupler for RF power and a pickup antenna to measure the cavity field. The probes measure the field directly inside the cavities. The measured fields are digitized and further processed to calculate the vector-sum. After comparison with the set-point, a feedback correction is applied to the klystron drive. Standard operation includes algorithms such as multiple input multiple output-based feedback controller, adaptive feedforward and beam loading compensation.

^{*} valeri.ayvazyan@desy.de

NEW ACCELERATING MODULES IN OPERATION

During the FLASH linac upgrade the two oldest and weakest accelerator modules (ACC2 and ACC3) were replaced by new ones with an adapted waveguide RF power distribution and a new 10 MW klystron to feed 16 cavities. The new modules were installed with a specially tailored waveguide RF power distribution to achieve highest total energy for the new cavity gradient distribution. After installation, both modules were successfully tested with beam at FLASH. The RF station could be operated providing an energy gain up to 465 MeV, with routine operation between 400 and 460 MeV since October 2022. Prior to this replacement, ACC2/3 was operated at a maximum 330 MeV energy gain. Therefore, the two refurbished modules significantly contributed to increasing the maximum FLASH electron beam energy.

Achieved Gradients at ACC2/3

For high energy runs the confirmed operational gradients for ACC2 vary from 26.2 MV/m to 30.8 MV/m. The gradients variation at ACC3 are in a range of 23.3 MV/m to 31.7 MV/m (Fig. 1).

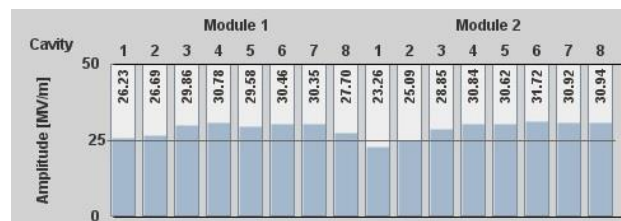


Figure 1: ACC2/3 gradients (peak) at energy 460 MeV. Modules are operated off-crest to allow beam compression.

RF DISTRIBUTION OPTIMIZATION FOR OTHER MODULES

The original RF distribution scheme for ACC4/5 was linear. The klystron output RF power was equally distributed among the cavities. Before the shutdown upgrade, the gradient hard limits (i.e. quench) were measured for each cavity. Figure 2 shows ACC4/5 gradient distribution before shutdown. Based on these measurements, an RF waveguide distribution was tailored and assembled. After start-up of the machine it turned out that the new dominating limiting factor was field emission (gamma radiation) of some cavities in ACC4. The investigations were carried out under nominal RF pulse operation and the maximum operational gradient limit as well as the limiting mechanism of individual cavities were determined. Either

INFLUENCE OF ENVIRONMENTAL PARAMETERS ON CALIBRATION DRIFT IN SUPERCONDUCTING RF CAVITIES

Y. Sun*, A. Bellandi, J. Branlard, B. Richter, A. Eicher¹, C. Schmidt, H. Schlarb
Deutsches Elektronen-Synchrotron DESY, Hamburg, Germany
¹also at Hamburg University of Technology, TUHH, Germany

Abstract

Precisely calibrating superconducting Radio-Frequency (RF) linear accelerators is crucial for accurately assessing cavity bandwidth and detuning, which provides valuable insights into cavity performance, facilitates optimal accelerator operation, and enables effective fault detection and diagnosis. In practice, however, calibration of RF signals can present several challenges, with calibration drift being a significant issue, especially in settings prone to humidity and temperature fluctuations. In this paper, we delve into the effect of environmental factors on the calibration drift of superconducting RF cavities. Specifically, we examine long-term calibration drifts and explore how environmental variables such as humidity, temperature, and environmental noise affect this phenomenon. The results show that environmental factors, particularly relative humidity, significantly influence calibration drifts. By analyzing these correlations, appropriate compensation algorithms can be designed to mitigate and eliminate these effects, thus optimizing calibration accuracy and stability.

BACKGROUND

The European X-ray Free-Electron Laser (European XFEL) is one of the most advanced facilities utilizing Superconducting Radio Frequency (SRF) technology, providing researchers with unprecedented capabilities in probing the structure and dynamics of matter at the atomic scale. The European XFEL relies heavily on the stability and accuracy of the SRF cavities to ensure the high quality of the X-ray pulses. Precisely calibrating RF cavities is crucial for accurately assessing cavity bandwidth and detuning, which provides valuable insights into cavity performance, facilitating optimal accelerator operation.

A key challenge in the operation of SRF cavities is the phenomenon of calibration drift, which, if not managed properly, can lead to significant performance degradation. Various environmental parameters, such as temperature and humidity fluctuations, and mechanical vibrations, can influence this drift, necessitating robust calibration and compensation mechanisms.

The Low-Level RF (LLRF) control system plays a crucial role in maintaining the stability of the RF fields within the SRF cavities. The LLRF system continuously monitors and controls the RF signals to generate precise and stable RF fields required for X-ray free-electron laser pulses, including the compensation for any deviations caused by environmen-

tal factors. However, calibration drift remains a persistent issue despite the advanced control algorithms employed as they rely on the calibration.

The Drift Compensation Module (DCM) [1] has been developed as part of the LLRF system to address this challenge. It is specifically designed to mitigate the effects of calibration drift by dynamically adjusting the calibration parameters in real-time. However, it is important to note that DCM only calibrates the probe signal, not the drift of forward and reflected signals.

Accurate measurements of the RF forward V_F^m and the reflected signals V_R^m are critical for calculating cavity bandwidth and detuning. Ideally, the sum of V_F^m and V_R^m should equal the RF probe signal V_P^m . However, in practice, the finite directivity of waveguide directional couplers and the drift caused by environmental parameters impact the accuracy of the RF forward and reflected signals, thus degrading the performance of the accelerator.

This paper investigates the long-term calibration drift in superconducting RF cavities and examines the influence of environmental factors on this phenomenon. By analyzing the correlation between these variables, we found that the calibration error or drift could be predicted based on environmental factors. Additionally, calibration coefficients can be accurately forecasted, offering a promising calibration method for SRF cavities operating in Continuous Wave (CW) mode.

RF SIGNAL CALIBRATION AND CALIBRATION DRIFT

Long-term Calibration Drift

The original virtual probe is defined by the sum of the measured forward $V_F^m \in \mathbb{C}$ and reflected $V_R^m \in \mathbb{C}$ RF signals, expressed in In-phase and Quadrature (I&Q) form as

$$V_P^v = V_F^m + V_R^m \quad (1)$$

Ideally, the virtual probe V_P^v should be equal to the measured RF probe signal $V_P^m \in \mathbb{C}$. However, as mentioned above, in practice, the finite directivity of waveguide directional couplers and drift due to environmental parameters can affect the measurement of the RF forward and reflected signals, leading to calibration errors. Formally, calibration error is defined as the difference between the measured probe signal V_P^m and the virtual probe V_P^v , denoted as:

$$E_C = V_P^m - V_P^v = V_P^m - (V_F^m + V_R^m) \quad (2)$$

* yue.sun@desy.de

MACHINE LEARNING-BASED NON-DESTRUCTIVE MEASUREMENT OF BUNCH LENGTH AT FRIB*

J. Wan[†], A. Plastun, P. N. Ostroumov

Facility for Rare Isotope Beam, Michigan State University, East Lansing, MI, USA

Abstract

A machine learning-based virtual diagnostic approach for bunch length measurement is proposed. Utilizing multiple measurements of bunch length at the Facility for Rare Isotope Beams (FRIB) accelerator, a neural network model is trained to learn the correlations between the spectra of the beam position monitors' (BPMs) signals and the bunch length. This model enables rapid prediction of bunch length at BPM locations without compromising beam quality.

INTRODUCTION

The Facility for Rare Isotope Beams (FRIB) [1], operated by Michigan State University, is a national user facility for advanced nuclear physics research. Since the commencement of user operation in May 2022 the primary beam power has been steadily increased from 1 kW to 20 kW [2]. To ensure the high-power beam delivery with no beam losses, accurate measurement of the ion beam properties is crucial. For example, the bunch length measurements are very important for matching stripped multiple charge-state beams and for optimizing the accelerator performance. Traditional instruments for measuring the bunch length of ion beams are destructive see, for example, Bunch Shape Monitor (BSM) [3] that can interrupt the beam and also are not suitable for continuous monitoring.

To address this challenge, a virtual diagnostic approach is proposed. This involves training a machine learning [4] model to learn the correlations between signals from non-destructive Beam Position Monitors (BPMs) and the longitudinal bunch length. While BPMs typically measure the beam's transverse position and phase, by analyzing the spectra of BPM signals, we can infer information about the longitudinal properties. As a result, the model is expected to predict bunch lengths at BPM locations in a non-destructive manner.

DATA PREPARATION

Figure 1 shows the FRIB accelerator layout. Ion beams are accelerated in the inner linac segment 1 (LS1), followed by the folding segment 1 (FS1). A BSM is installed downstream of the LS1, next to the charge strippers.

Five BPMs around the BSM are selected, which are defined as 2212, 2223, 2248, 2278, and 2313, according to their locations. The BSM is installed between BPM 2248

and BPM 2278. Four superconducting bunching cavities are installed upstream of those BPMs. The 80.5 MHz, 161 MHz, 241.5 MHz, and 322 MHz signal harmonics for those BPMs are collected as input data of the machine learning model.

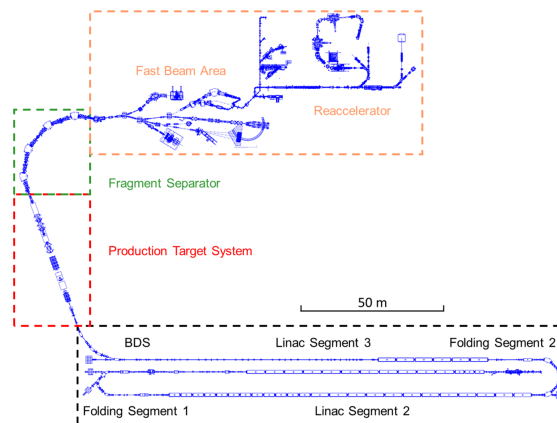


Figure 1: Layout of the FRIB accelerator.

The goal of this project is to derive the bunch lengths at the BPM locations from their signal spectra. Since direct measurement at these locations is not feasible, we employ simulation tools to estimate the bunch lengths by tracking the ion beam from the superconducting bunching cavities through FS1.

To determine the initial beam parameters in the simulation, we conducted a series of bunch length measurements at the BSM location by varying the field strength of the cavities from 0 to 5.5 MV/m as shown in Fig. 2. With the aid of TRACK [5], a particle-in-cell (PIC) macroparticle tracking code, the initial beam parameters are fitted by a Particle Swarm Optimization (PSO) [6] optimizer based on the measured data. A resolution term σ_{res} representing the uncertainties introduced by the BSM resolution is also included in the fitting. The measured bunch length is determined by $\sigma_{\text{measured}} = \sqrt{\sigma_{\text{real}}^2 + \sigma_{\text{res}}^2}$, where σ_{real} is the real bunch length.

Considering that the resolution of the BSM is comparable with the RMS bunch length of the focused beam, resolution-related terms may compromise the precision of the measurements. To reduce the impact of this term, we opt to focus on the geometric bunch length that covers 80% of the particles, which is larger than the RMS bunch length by a factor of 2-3, depending on the beam phase space distribution.

It is important to note that for a Gaussian beam, the error introduced by the BSM resolution tends to increase on the 80% geometric length, making this approach ineffective in

* Work supported by the U.S. Department of Energy, Office of Science, Office of Nuclear Physics, under Award Number DE-SC0024707 and used resources of the FRIB Operations, which is a DOE Office of Science User Facility under Award Number DE-SC0023633.

[†] wan@frib.msu.edu

MACHINE LEARNING ENABLED MODEL PREDICTIVE CONTROL FOR THE RESONANCE FREQUENCY OF THE FRIB RFQ*

J. Wan[†], S. Zhao, Y. Hao, W. Chang, H. Ao

Facility for Rare Isotope Beams, Michigan State University, East Lansing, MI, USA

Abstract

Frequency detuning of the radio-frequency quadrupole (RFQ) at the Facility for Rare Isotope Beams (FRIB) is managed by a cooling water control system. Efficiently controlling the RFQ frequency remains challenging due to the system's time-delayed behavior. To address this, we propose using a machine learning-based model predictive control (MPC) approach. In this work, a long short-term memory (LSTM) network is trained to project the variables into a higher-dimensional space, and a Koopman network is trained to predict the behavior of RFQ frequency detuning given control actions. With the machine learning-based MPC controller, the control time is expected to be reduced by a factor of 2.

INTRODUCTION

The Facility for Rare Isotope Beams (FRIB) [1] is a user facility for nuclear physics research built at Michigan State University. The radio frequency quadrupole (RFQ) at FRIB is designed to accelerate single and two-charge state ion beams from 12 KeV/u to 0.5 MeV/u. To control the temperature-sensitive resonance frequency of the RFQ, a cooling water system is designed to automatically control the temperature of the RFQ with a proportional–integral–derivative (PID) controller in case of the frequency detuning [2]. Due to the thermal process and the water transport delay, the control process usually needs ten to twenty minutes to eliminate the frequency detuning.

In this work, we propose to use a model predictive control (MPC) method based on a machine learning model to shorten the control time. The machine learning model is a deep Koopman network consisting of a long short-term memory (LSTM) neural network [3]. With the deep Koopman model, we can obtain accurate predictions of the frequency behavior of the RFQ, so as to apply it to MPC for better control performance.

DEEP KOOPMAN NETWORK MODEL

The deep Koopman network, based on Koopman operator theory [4], has emerged as an innovative method of predicting the behavior of dynamical systems [5]. A deep Koopman network aims to linearize the variable x_t of a dynamical system to a higher-dimensional representation ϕ_t using a neural network called encoder. The time-dependent behaviour of ϕ_t can be described by a linear operator \mathcal{K} .

* Work supported by the U.S. Department of Energy Office of Science under Cooperative Agreement DE-SC0023633, the State of Michigan, and Michigan State University.

[†] wan@frib.msu.edu

By converting the variable from ϕ space to x space with another neural network called decoder, the behaviours of the dynamical system can be predicted.

$$\phi_t = \phi(x_t) \quad (1)$$

$$\phi_{t+1} = \mathcal{K} \phi_t. \quad (2)$$

In this work, an LSTM network is selected to learn the time-delayed information, including the temperature, pressure and flow of the cooling water related to the RFQ system (see Fig. 1). The linearized observable is then advanced with a linear operator \mathcal{K} . To predict the behavior of the RFQ frequency, a decoder is typically required to reconstruct the RFQ frequency from the high-dimensional observable. However, in this work, we utilize a modified observable function that combines the time series of frequency F with the original observable ϕ . This structure eliminates the need for an additional decoder, simplifying the prediction process.

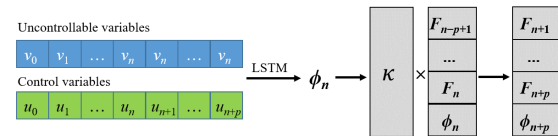


Figure 1: Layout of the deep Koopman model. $\{v_0, v_1, \dots, v_n\}$ and $\{u_0, u_1, \dots, u_n\}$ represent the time-delayed data, where u is the control variable. ϕ_n is a linearized observable function. \mathcal{K} represent the Koopman operator and F_n is frequency detuning at time n .

MODEL TRAINING AND EVALUATION

With operational data from FRIB, a deep Koopman network is trained. The data is divided into two sets for training and testing purpose. As illustrated in Fig. 2, the model demonstrates strong predictive capabilities on the test data for both high detuning and low detuning scenarios. These findings suggest that the model has successfully captured the complex relationship between multiple input variables and the RFQ frequency behavior.

It is important to note that certain variables, such as the forward power of the RFQ cavity, can strongly impact the RFQ resonance frequency in a non-delayed manner. These variables are generally stable and only occasionally experience rapid changes due to cavity trip or other accidents during regular operations, which can cause substantial frequency detuning. It is observed that including these extreme cases in the training is not always advantageous. Using that extreme data in the training can lead to poorer performance

TOMOGRAPHY DEVELOPMENT AT ATLAS*

A. D. Tran[†], Y. Hao, Michigan State University, East Lansing, MI, USA
B. Mustapha, Argonne National Laboratory, Argonne, IL, USA

Abstract

Beam tomography is a method for reconstructing the higher-dimensional beam from its lower-dimensional projections. This provides an understanding of the beam's transverse phase space, enabling better modeling and predicting downstream beam loss. We will show methods of extrapolating confidence intervals of our reconstructed beam and explore a new beam tomography algorithms using Markov Chain Monte Carlo (MCMC).

INTRODUCTION

Beam tomography allows for the reconstruction of the beam transverse phase space, which is very useful in optimizing accelerator performance, predicting and reducing beam loss, and understanding beam behavior. It can aggregate existing beam measurement devices, which capture projectional measurements of the beam, to reconstruct a higher-dimensional beam phase space, such as the 4D transverse space (two positional and two momentum).

Current techniques for direct higher-dimension tomography in accelerators use algebraic reconstruction technique (ART) [1], machine learning (ML) [2], or maximum entropy technique (MENT) [3]. ART and MENT are limited by computer memory, while ML requires a differentiable simulation. However, it is efficient and not limited by memory. All of these methods need an accurate beamline model to back-propagate projectional information about the beam, and not having this produces errors in the reconstruction.

This paper uses quad scans, simultaneous algebraic reconstruction technique (SART), and MCMC to arrive at different conclusions about the initial beam phase space. We will show a method to extrapolate a confidence interval using SART, and showcase the limitations of MCMC as a potential algorithm for fast approximation of the phase space.

METHODOLOGY

We will consider a linear system for our study and limit our study to 4D. Beam tomography aims at retrieving the beam distribution in phase space at location A, e.g., $f(\mathbf{X}) = f(x, x', y, y')$ using the lower dimension measurement at location B, $P(x, y)$ or its projections. Let $M(\mathbf{X}, \mathbf{Q}): \mathbb{R}^4 \rightarrow \mathbb{R}^4$ be the transfer map between A and B with \mathbf{Q} as the vector of the accelerator tuning parameters such as the strength of quadrupole. The beam will be assumed to be centered to ignore the effect of offsets.

* This work was supported by a sub-award from Argonne National Laboratory and by the U.S. Department of Energy, under Contract No. DE-AC02-06CH11357.

[†] tranant2@msu.edu

Data Collection and Processing

The data was collected over three days in November 2023, and two primary data collection phases focused on beam emittance and beam tomography measurements. For the first phase, a quadrupole scan was performed by varying individual quadrupoles while keeping the others constant. Data was collected by adjusting quadrupoles 6 and 7, as seen in Fig. 1 to measure the beam emittance.

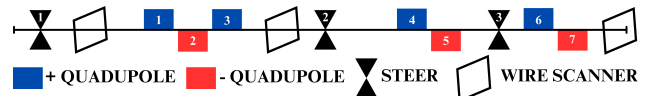


Figure 1: A section of the ATLAS Beam Line.

Since the method of specifying desired beam settings was unavailable, the beam settings were varied randomly. The last four quadrupoles and two steerers were adjusted within set bounds to manipulate the phase space sufficiently. The aim was to maintain low beam loss since tomography accuracy requires high accuracy and minimal beam loss. This dataset was collected overnight to create set A. An autoencoder-decoder analysis was employed on Set A to generate alternative beam settings with high transmission. While Set B successfully increased transmission, it did so at the cost of reducing the angular range, which is needed for accurate beam tomography reconstruction. An angular range of 180 degrees is required for precise rebuilding, and the reduced range in Set B, around $33^\circ - 57^\circ$, limit this accuracy.

Various methods were used to filter and preprocess the data for analysis. These involve filtering beam settings with over 100% transmission and those below 90% transmission. Transmission over 100% is not possible and represent an error with the faraday cups while 90% was chosen to remove settings with high beam loss. Projections were also fitted to a gaussian curve with a vertical offset. The offset was subtracted to establish a zero baseline, and an R-square score was calculated to evaluate the fit. Data with an R-squared score below 0.8 was discarded. The beam may also be offset from the center, so a horizontal shift was applied to zero the mean of the distributions. Due to different signal gains, the integrated projections differ for each beam profile, so these were normalized to ensure consistency across projections. Finally, to account for beam loss, the normalized projections were scaled according to the transmission ratio, ensuring that changes in beam transmission were accurately reflected.

Quad Scan

Quad scans [4] were performed to extract the beam emittances and sizes. Assuming this is an uncoupled system, let Σ_0 be the beam matrix at the reconstructed location where

SIMULATIONS OF FIELD EMITTERS AND MULTIPACTING IN PIP-II SINGLE SPOKE RESONATOR TYPE-2*

J. Brown[†], T. Xu, Facility for Rare Isotope Beams, East Lansing, USA

D. Passarelli, G. Romanov, A. Sukhanov, Fermi National Accelerator Laboratory, Batavia, USA

Abstract

It has been found in benchmark tests that some Single Spoke Resonator Type-2 (SSR2) cavities have early field emission onset as well as strong multipacting barriers. A longstanding hypothesis is that field-emitted electrons in the high electric field accelerating gap can migrate and ignite multipacting bands in the low electric field regions of the cavity periphery. In this study, we use simulation techniques to examine multipacting behavior in SSR2 cavities from electrons seeded in common field emitter locations. Additionally, we investigated seed locations for areas in SSR2 cavities which may have poor coverage during high pressure water rinsing and compared the multipacting behavior.

INTRODUCTION

Single spoke resonators have been used in numerous projects to provide acceleration of hadrons and heavy ions in the low to medium velocity regimes in accelerators [1]. The Proton Improvement Plan-II (PIP-II) at Fermi National Accelerator Lab will be powered by a continuous-wave superconducting linac designed to accelerate H^- ions up to 800 MeV [2]. PIP-II will utilize 35 SSR2 cavities to accelerate the ions from 35 MeV to 185 MeV [3]. The operational fields from CST eigenmode solver and cavity geometry can be seen in Fig. 1.

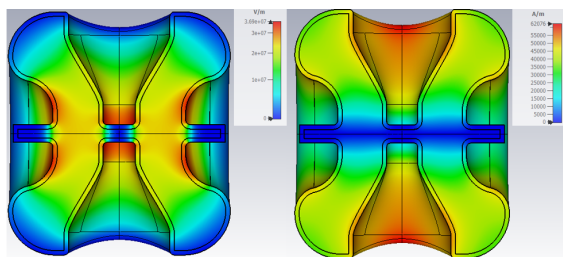


Figure 1: Electric and H-fields respectively for the $f_0 = 325$ MHz operational mode and accelerating electric field amplitude of $E_{acc} = 11.5$ MV/m for SSR2.

SSR2 production and benchmark testing for PIP-II has been ongoing. Early preliminary testing of SSR2 cavities has shown strong field emission below 5 MV/m accompanied with stronger multipacting barriers [4, 5]. This work aims to

* Funding agency: This manuscript has been authored by Fermi Research Alliance, LLC under Contract No. DE-AC02-07CH11359 with the U.S. Department of Energy, Office of Science, Office of High Energy Physics. This material is based upon work supported by the U.S. Department of Energy, Office of Science, Office of Nuclear Physics under Award Number DE-SC0018362.

[†] brownjac@frib.msu.edu

answer whether field emission can provide an explanation for the increased multipacting strength and ignition.

SIMULATIONS

For this study, we utilized the particle-in-cell (PIC) and eigenmode solvers from CST Studio Suite. The eigenmode solver is used to simulate the eigenmode electromagnetic fields in SSR2 with the stored energy normalized to 1 J, which are then exported to the PIC solver. An amplitude parameter can be used in simulations to scale the eigenmode fields and can be swept to examine particle behavior at different accelerating electric fields (E_{acc}). Much of the model and simulation setup for this study is based on previous studies for different prototypes of SSR2 and other cavities [6, 7]. The cavity walls have a secondary emission yield model for Niobium that has been baked out at 300 °C from the CST material library.

The PIC solver allows us to set the seed location and charged particle characteristics. It is theorized that common field emitter locations lie in the high electric field regions. For SSR2 this is on the beam cup and iris areas along the inner conductor. Previous work has explored multipacting in SSR2, from which we will be able to compare results from different seeds. Electron seeds previously used and our field emitter seeds can be seen on the cavity in Fig. 2.

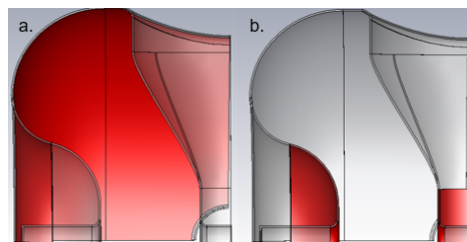


Figure 2: a) Seed locations (in red) for previous simulation work, which we will call global seeds. b) Field emitter location seeds.

Our simulations run for 35 RF periods, which corresponds to ~ 107 ns for SSR2's operational frequency of $f_0 = 325$ MHz. The number of emitter locations has a lower bound due to the mesh, but to keep computation costs low, 64 emitter locations was chosen. The charge emission distribution in the PIC solver is natively set to Gaussian in time. To keep the particles as close to discrete charges as possible, a large temporal standard deviation is used to obtain a flat distribution. A table containing the other distribution settings can be seen in Table 1. Additionally, space charge effect is accounted for in our simulations.

FEASIBILITY STUDY FOR DUAL HIGHER-ORDER-MODES FOR PLASMA PROCESSING OF FRIB SUPERCONDUCTING COAXIAL RESONATORS *

P. Tutt[†], W. Chang, K. Elliot, W. Hartung, S-H Kim, T. Xu

Facility for Rare Isotope Beams, Michigan State University, East Lansing, MI, USA

P. Berrutti, Brookhaven National Laboratory, Upton, NY, USA

Abstract

In-situ plasma processing is a promising technique to reduce field emission in superconducting radio-frequency cavities and thus maintain maximum accelerator performance for long-term operation. Continuous-wave accelerators such as FRIB are more challenging than pulsed accelerators due to relatively weak coupling ($Q_{\text{ext}} = 2E6$ to $1E7$ for FRIB) via the fundamental power coupler (FPC). This results in an unfavorable mismatch at room temperature and makes fundamental-mode plasma processing difficult. Hence we have investigated the use of higher-order modes (HOMs) with less FPC mismatch. Several HOMs are promising for lower-mismatch plasma generation. However, HOMs often present a less favorable plasma distribution. To improve the plasma distribution, we are studying techniques to drive the plasma with two HOMs simultaneously. Plasma development results will be presented for FRIB $\beta = 0.085$ quarter wave resonators including ignition threshold measurements and plasma distribution assessments.

INTRODUCTION

Development of plasma processing, an in-situ method to recover performance degradation of superconducting radio frequency (SRF) cavities, is underway at the Facility for Rare Isotope Beams (FRIB). FRIB supports nuclear physics experiments by providing heavy ion beams with energies up to 200 MeV per nucleon using SRF quarter-wave resonators (QWRs) and half-wave resonators (HWRs) [1]. User operations at FRIB began in May 2022; potential future performance degradation of cryomodules is a concern [2]. Hence, in-situ methods for plasma processing of FRIB cavities are being developed. Several groups have investigated the effectiveness of plasma processing on SRF cavities [3–7]. Reductions in field emission after plasma processing have been seen in several trials on FRIB cavities [8].

Recent plasma processing trials on the FRIB $\beta = 0.085$ QWR have used HOMs for sustaining plasma due to their improved mismatch [8]. HOMs have the disadvantage of multi-lobed electric field distributions, with the plasma tending to ignite in only 1 of the lobes, resulting in a plasma distribution that lacks the symmetry of the E-field, and hence

producing uneven coverage of the surface for plasma cleaning. One proposed solution is to use dual-driven higher-order modes (HOMs). Dual-mode excitation of plasma has been demonstrated at ORNL and FNAL in multi-cell elliptical cavities [4, 6]. In this paper, the feasibility of dual-driven modes in FRIB's $\beta = 0.085$ QWR to promote better plasma uniformity and sustain higher plasma densities will be explored.

RF SYSTEM AND MODIFIED QWR

To drive 2 resonant modes in the cavity simultaneously, the RF system was modified from the typical setup used at FRIB [8]. The modified RF system is similar to the system used for dual-tone excitation of LCLS-II cavities at FNAL [6]. The QWR's tuning plate and bottom flange were modified to add 2 viewports for a better view of the cavity interior, as shown in Fig. 1. The extra viewports are aligned with the accelerating gaps; a third viewport is installed on one of the beam ports.

HOMS FOR DUAL-TONE

To determine what HOMs may be suitable for dual-tone, CST Microwave Studio (MWS) [9] was used to simulate the electromagnetic field distribution for HOMs up to twenty times the accelerating mode frequency (80.5 MHz). Plasma measurements were then done for modes with favorable field distributions and coupling strengths.



Figure 1: FRIB $\beta = 0.085$ QWR with modified tuning plate (left) and bottom flange (right).

MWS Simulation

The QWR was simulated with the FPC in its nominal position at room temperature. HOMs were sorted according to their coupling strength, field distribution, and maximum field on the coupler tip (CT). Results for interesting HOMs are shown in Table 1. Coupling strength and maximum field

* This material is based upon work supported by the U.S. Department of Energy, Office of Science, Office of Nuclear Physics and High Energy Physics and used resources of the FRIB Operations, which is a DOE Office of Science User Facility under Award Number DE-SC0023633 and DE-SC0018362.

[†] tutt@frib.msu.edu

ANOMALOUS FREQUENCY SHIFTS NEAR T_c OF FUNDAMENTAL AND HIGHER-ORDER MODES IN MEDIUM-VELOCITY 644 MHz SUPERCONDUCTING ELLIPTICAL CAVITIES*

S. M. Moskaitis, Y.-L. Cheon, S. Kim, P. N. Ostroumov

Facility for Rare Isotope Beams, Michigan State University, East Lansing, MI, USA

Abstract

Recent studies indicate the magnitude of an anomalous decrease in the resonant frequency, so-called frequency dip, near critical temperature of superconducting niobium cavities, T_c , correlates to the cavity quality factor, Q_0 , and impurities introduced into the superconducting niobium surfaces, such as nitrogen or oxygen. We measured frequency dips in both 644 MHz fundamental mode (FM) and 1.45 GHz higher-order mode (HOM) of single-cell elliptical cavities for FRIB energy upgrade (FRIB400) R&D. These measurements were performed in cavities with the following surface treatments: (1) electropolished (EP) only, (2) nitrogen-doped (N-doping), and (3) medium-temperature (mid-T) baked and then hydrofluoric (HF) acid rinsed. We will present measured frequency dips and compare them to cavity Q_0 performance in the FM. Frequency-dependent behavior of frequency dips with various surface treatments will also be discussed as our experimental setup has a unique feature compared to previous studies, which allows for measurement of frequency dips in different modes within the same cavity, in other word, on the same surfaces.

INTRODUCTION

Recent study of bulk superconducting radiofrequency (SRF) niobium cavities has shown a relation between resonant frequency, frequency dip magnitude (denoted $|f_{\text{dip}}|$), and anti-Q slope [1].

These relations previously found between resonant frequency, $|f_{\text{dip}}|$, and anti-Q slope are of particular interest in the FRIB400 project. This project aims for $Q_0 = 2 \cdot 10^{10}$ at the accelerating gradient E_{acc} of 17.5 MV/m, operated at 2 K. The study of $|f_{\text{dip}}|$ and its cavity-to-cavity behavior could give directions towards producing a 644 MHz 5-cell elliptical cavity for the FRIB400 with lower BCS resistance at the operating E_{acc} , possibly through the realization of anti-Q slope in these 644 MHz cavities, which has not been observed yet in mid-GHz frequency range cavities.

EXPERIMENTAL SETUP

We used three elliptical single-cell niobium SRF cavities in our study. These single-cell cavities have resonant fre-

quencies 644 MHz for their FM and 1.45 GHz for the selected HOM, TM020. These cavities all went through an initial bulk EP, after which the treatment was specific to each cavity. One cavity was nitrogen-doped at 800°C for 2 minutes at 25 mTorr and no annealing under vacuum at 800°C, so-called 2N0 doping, followed by post-doping 5 μm EP. Another cavity was baked at 330°C in the vacuum furnace for 3 hours, followed by a hydrofluoric acid (HF) rinse. The third cavity was simply left with its standard EP as a baseline comparison. These cavities will be referred to as N-doping, mid-T Baking, and baseline EP, respectively.

The dual-mode frequency and temperature measurements of these cavities were performed using the following steps. Lakeshore Cernox-1050 Resistance temperature detectors (RTDs) were placed on the cavity for temperature measurements. The dunk dewar, in which one of the cavities was installed, was initially cooled down and liquid helium was accumulated at 4.5 K. We then pumped down the dewar to 30 – 50 Torr, and started to warm up the cavity at a constant pressure. This is to eliminate the df/dp effect such that the measured frequency is solely a function of temperature. A heater located at the bottom of the dunk dewar was used to control the warm-up speed; we found that once the liquid level was below the cavity assembly, the boil-off of liquid helium enhanced by the heater actually slowed down the cavity warm-up speed. With this technique, we could achieve the warm-up rate slower than 0.05 K/min at around T_c , which was useful to take precise measurement of f_{dip} .

We used two Vector Network Analysers to measure both FM and HOM simultaneously. The FM was amplified up to 3 – 5 W by a 644 MHz amplifier and driven to the cavity through a standard high-power RF transmission line. On the other hand, the HOM was driven via the reflected port of the bi-directional coupler in the RF transmission line. The pickup RF signal was split by a 3-dB splitter and each of them went to the FM/HOM VNA. We could detect almost the same RF power level between FM and HOM because coupling strength of both input and pickup couplers is much higher in the HOM compared to the FM: S21 is approximately 60 dB higher.

For each frequency dataset, the electron mean free path of the cavity surface, l , was found by fitting the experimental data. To do this fitting, the experimental frequency data was converted to penetration depth, $\lambda(T)$, as represented by [2]:

$$\lambda(T) - \lambda(T_0) = \frac{G}{\mu \cdot \pi f^2} (f(T) - f(T_0)), \quad (1)$$

*This material is based upon work supported by the U.S. Department of Energy, Office of Science, Office of Nuclear Physics and High Energy Physics and used resources of the FRIB Operations, which is a DOE Office of Science User Facility under Award Number DE-SC0023633 and DE-SC0018362.

RF PULSE CONDITIONING TO REDUCE FIELD EMISSION IN FRIB SRF CRYOMODULES*

Y.-L. Cheon[†], S. Kim, W. Chang, W. Hartung, T. Xu

Facility for Rare Isotope Beams, Michigan State University, East Lansing, MI, USA

Abstract

The superconducting radio-frequency (SRF) linear accelerator (linac) for the Facility for Rare Isotope Beams (FRIB) has been operating for user experiments since May 2022, using 104 quarter-wave resonators (80.5 MHz) and 220 half-wave resonators (322 MHz) operating with peak surface electric fields (E_{peak}) ranging from 27 MV/m to 33 MV/m. Field emission (FE) can limit the maximum accelerating gradients in SRF cavities and may worsen over time during long-term operation. RF pulse conditioning has been a useful technique to reduce FE in FRIB cryomodules for commissioning and user operations. In this paper, we will present RF pulse conditioning results and analysis for about 50 cavities, performed in cryomodule bunker tests and the linac tunnel. During conditioning, we observe "electrical breakdown", a rapid ($<1 \mu\text{s}$) collapse of the field, which usually leads to a significant reduction in FE X-rays. On the other hand, when a thermal breakdown ($\sim\text{ms}$ decay time, also known as quench) occurs, opportunities for further conditioning at higher field are limited and FE X-rays may not be significantly improved.

INTRODUCTION

Field-emitted electrons from the niobium surface of superconducting radio frequency (SRF) cavities are accelerated by the RF field and strike the cavity walls, generating Bremsstrahlung X-rays. The emitters that generate the dominant field emission (FE) are likely located near the region of the peak surface electric field (E_{peak}), depending on the surface cleanliness. The FE electrons and associated X-rays can negatively impact the cavity performance by limiting the maximum achievable accelerating gradient (E_{acc}) or increasing the cryogenic heat load [1–3].

Field emission in FRIB cavities has been tracked and monitored during cavity Dewar tests, cryomodule bunker test, and linac beam commissioning [4]. In the Dewar certification tests, FE was significantly reduced in a number of cavities by repeating preparation steps ("FE reworks") such as ultrasonic cleaning, high pressure rinsing, acid etching, and mechanical polishing [5, 6]. These FE reworks could be done relatively easily at the cavity certification stage, in contrast to the cryomodule test stage. On the other hand, RF pulse conditioning was found to be useful to mitigate FE in FRIB cryomodules. Pulse conditioning in the cryomodule is

facilitated by the over-coupled fundamental power coupler (FPC), which is in contrast the matched couplers used for Dewar tests. A statistical analysis of RF pulse conditioning effects on the FE performance of FRIB cryomodules will be discussed in this paper.

PULSE CONDITIONING

In bunker cryomodule tests and in-tunnel cryomodule tests, we first measured FE X-rays as a function of E_{acc} in continuous wave (CW) mode, and then attempted pulse conditioning if significant X-rays were produced below the operating gradients. Pulse lengths of 30 to 50 ms were used (the RF fill time being a few tens of ms), with repetition rate of 1 Hz.

Electrical/Thermal Breakdown

Figure 1 shows the results of pulse conditioning in bunker tests (Fig. 1(a)) and in the linac tunnel (Fig. 1(b)). During conditioning, we observed two types of rapid drops in the transmitted RF power:

- A rapid collapse in the field, faster than $1 \mu\text{s}$, which we classify "electrical breakdown" (EB) [7].
- A decay taking of order 1 ms, due to "thermal breakdown" (TB). This is faster than the normal decay dominated by the external quality factor of the FPC.

The FE onset field is significantly improved after EB, in contrast to TB. This is consistent with EB theory [7, 8]: the emitter is heated by the field emission current, leading to a local increase in pressure of vacuum and exciting a local discharge in which the emitter is explosively "burned out."

In TB, the emission current heats up the superconducting niobium cavity surfaces, causing a quench (transition from superconducting to normal conducting) before a local discharge can occur. This may explain why FE is not greatly improved after TB. In TB cases, if we attempt a shorter pulse (closer to the fill time) with higher peak power, we do not see a significant benefit. Generally, if pulse conditioning is limited by TB, it is difficult to induce EB after all.

The in-tunnel FE conditioning results (Fig. 1(b)) are divided into three cases: (1) during beam commissioning (2018-2021); (2) after user operation (2022-present); and (3) outliers in the statistical analysis such as non-conforming cavities in bunker tests or one case of FPC cold cathode gauge failure [9]. The FE observed in the bunker tests is likely due mainly to particulate contamination during cryomodule assembly since, in most cases, the cavities did not show significant field emission at the design field in the

* Work supported by the U.S. Department of Energy, Office of Science, Office of Nuclear Physics and used resources of the FRIB Operations, which is a DOE Office of Science User Facility under Award Number DE-SC0023633.

[†] cheon@frib.msu.edu

DEVELOPMENT OF BI-ALKALI ANTIMONIDE PHOTOCATHODES FOR A 1.3 GHZ SUPERCONDUCTING RF PHOTO-INJECTOR*

Z. Yin[†], W. Hartung, T. Konomi, S. Kim, T. Xu,

Facility for Rare Isotope Beams, East Lansing, MI, USA

J. W. Lewellen, Los Alamos National Laboratory, Los Alamos, NM, USA

J. Smedley, SLAC National Accelerator Laboratory, Menlo Park, CA, USA

Abstract

Superconducting Radio Frequency (SRF) photo-injectors offer the possibility of producing low-emittance electron beams in continuous wave operation. Among the various photo-emissive materials, bi-alkali antimonide is favored for its high quantum efficiency (QE) at visible light wavelengths. A development effort at FRIB is oriented toward the integration of advanced photo-cathodes into an SRF photo-injector. This paper describes improvements to the cathode preparation chamber, first cathode depositions, and characterization trials. A K_2CsSb film was produced with a notably extended dark lifetime, albeit with a modest QE of approximately 2%. Extensive spectral response analyses of the layer were conducted, along with thorough assessments of measurement procedures and hardware. This presentation offers insights into the factors contributing to the low measured QE and describes plans for improving the cathode preparation chamber and the experimental procedures.

INTRODUCTION

Electron beams with low emittance are vital for a wide range of accelerator-based applications, including free-electron lasers, Thomson scattering sources, and ultrafast electron diffraction. Superconducting Radio Frequency (SRF) photo-injectors are particularly promising for generating low-emittance electron beams in continuous wave (CW) operation [1].

In 2022, an SRF photo-injector system [2], including a photo-cathode coating chamber, a 1.3 GHz 1.5-cell jacketed cavity, and a precise frequency tuner, was transferred from the High Energy Accelerator Research Organization (KEK) to the Facility for Rare Isotope Beams (FRIB). The R&D focus at FRIB now includes the integration of innovative photo-cathodes within the SRF photo-injector framework. Bi-alkali antimonide photo-cathodes, particularly K_2CsSb , are attractive due to their high quantum efficiency (QE) in visible light [3]. These materials have demonstrated QE of several percent with green light in various photo-injector laboratories [4-7], and notable long-term stability was observed in SRF photo-injector experiments at Brookhaven National Laboratory (BNL) in 2021 [7]. This paper discusses the development and experimental outcomes of photo-cathode materials, specifically detailing the use of the photo-cathode chamber at FRIB for deposition on niobium and P-type silicon substrates.

* Work supported by MSU and the Department of Energy Contract DE-AC02-76SF00515

[†] yin@frib.msu.edu

PHOTOCATHODE CHAMBER

The photocathode chamber serves two primary functions: (1) depositing the K_2CsSb photocathode and (2) transferring the coated cathode to the SRF gun cavity without contamination. In addition, it also allows measurement of cathode QE versus wavelength. Prior to coating, the cathode undergoes a heat cleaning at over 400°C to eliminate residual gas and is then allowed to cool to room temperature. A 10 nm layer of antimony (Sb) is deposited on the substrate heated to 130°C. The substrate temperature is then increased to 140°C for deposition of potassium (K) until the QE saturates at ~530 nm. Finally, the substrate is cooled to 120°C for cesium (Cs) deposition until the QE once again saturates. Essential equipment includes 3 evaporation sources, a thickness gauge, heaters, temperature sensors, and a setup for real-time QE measurement.

An integrated load-lock system facilitates the safe transfer of the cathode to the SRF gun cavity under vacuum. The photo-emissive film is susceptible to poisoning by residual gas, necessitating an ultra-high vacuum (UHV) environment ($< 1e-8$ Pa). This requires a full UHV system, including a scroll pump, a 340 l/s turbo-molecular pump (TMP), a 300 l/s ion pump, and a 900 l/s(H_2O) non-evaporable getter (NEG) pump. The layout is shown in Fig. 1.

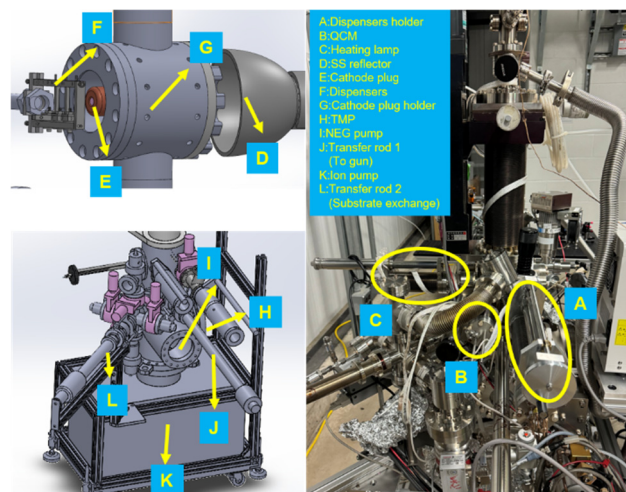


Figure 1: Photocathode chamber drawings (left) and photograph of the as-built system (right).

A NOVEL TEST CAVITY SETUP FOR SURFACE CONDUCTIVITY MEASUREMENTS OF ADDITIVE MANUFACTURING SAMPLES

M. Mayerhofer¹, G. Dollinger¹, R. Helm¹, J. Sonpar², H. Hähnel²
¹Bundeswehr University Munich, 85579 Neubiberg, Germany
²Goethe University Frankfurt, 60438 Frankfurt am Main, Germany

Abstract

Additive Manufacturing (AM) has the potential to increase the performance of radio frequency (rf) cavity resonators while cutting manufacturing costs. To leverage this potential, AM processes and potentially post-processing techniques must be tailored to cavity requirements. Additionally, conventional manufacturing's quality assurance methods must adapt to the AM case requiring numerous studies on additively manufactured test bodies. We introduce a compact rf cavity design, enabling cost-effective and precise studies of the surface conductivity of test bodies. The test body is mounted on a dielectric holder inside a cylindrical rf cavity made of aluminum. The geometry of the test body corresponds to a rod which allows simple and cost-effective production, post-processing and evaluation. The test body's surface conductivity is extracted from a measurement of the quality factor (Q_0) of the cavity. Depending on the geometry of the test body, Q_0 values of over 10,000 can be achieved for copper test bodies. Thereby, the test body is responsible for up to two-thirds of the total cavity loss. Studies will be presented demonstrating the precision of surface conductivity determination via Q-measurement and the impact of uncertainties in test body position and geometry

INTRODUCTION

Conventional manufacturing of RF cavity resonators is expensive and design constraints limit performance [1,2]. Studies show that additive manufacturing (AM), especially Laser Powder Bed Fusion (L-PBF), have the potential to produce higher-performing cavities at lower costs [3–11]. For example, optimized cooling channels can improve cooling efficiency. However, after printing, AM cavities show higher surface roughness than conventionally manufactured ones, decreasing surface conductivity (σ_S). Current post-processing techniques aim to reduce this roughness to achieve desired quality factors (Q_0) [8, 11]. Nevertheless, predicting the surface roughness- σ_S relationship remains challenging, necessitating direct Q_0 measurements on whole AM cavities or cavities with AM manufactured complex internal geometries [3, 4, 8].

These geometries are time-consuming and expensive to produce. Moreover, these complex geometries make it difficult to compare different post-processing methods and to characterize the part's surface. We propose a test cavity setup for rapid, precise σ_S evaluation on simple test bodies. The symmetrical geometry of the test bodies allows uniform post-processing and straightforward roughness analysis. Hence, this setup enables an efficient comparison of post-processing

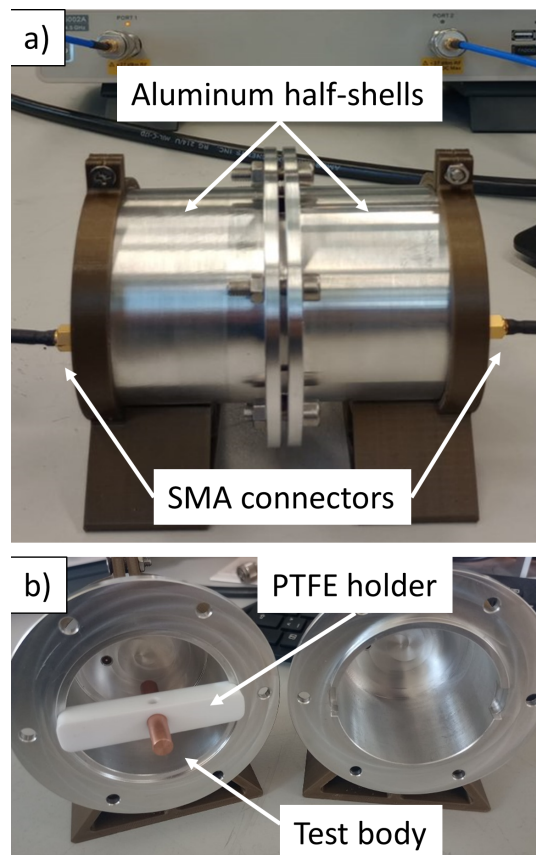


Figure 1: Test cavity a) mounted and connected to the VNA and b) in individual parts

methods and an optimization of the RF cavity manufacturing process without the need for complex and costly geometries. A cost-effective and uniform generation of an empirical data set can be achieved for the development of a Roughness- Q_0 methodology.

MATERIALS AND METHODS

The test cavity setup is shown in Fig. 1a. Two bolted aluminum half-shells form the actual cavity. Each half-shell is equipped with an SMA connector for coupling of the rf signal. The disassembled test cavity is shown in Fig. 1b. The test body, mounted on a holder made of PTFE, is located in the center of the test cavity. In this study, three test bodies are examined: one made of oxygen-free copper annealed for 3 hours at 530 °C, one made of oxygen-free copper that was not annealed, and one additively manufactured from

SURFACE FINISHING OF ADDITIVE MANUFACTURING PARTS FOR PARTICLE ACCELERATORS *

H. Hähnel^{1†}, B. Dedić, Institute of Applied Physics, Goethe University, Frankfurt a. M., Germany
¹also at Helmholtz Forschungsakademie Hessen für FAIR (HFHF), Frankfurt a. M., Germany

T. Torims, A. Ratkus, Riga Technical University, Riga, Latvia

M. Vedani, T. Romano, Politecnico di Milano, Italy

M. Vretenar, CERN, Geneva, Switzerland

M. Pozzi, Rösler Italian S.R.L, Concorezzo, Italy

E. Chyhyrynets, R. Caforio, C. Pira, INFN Laboratori Nazionali di Legnaro, Legnaro (PD), Italy

N. Kunkel, Technische Hochschule Mittelhessen (THM), Friedberg, Germany

Abstract

Significant progress towards the suitability of Additive Manufacturing (AM) metal parts for the production of linear accelerator components has been made in recent years. One significant factor for the suitability of AM parts to produce linac rf structures is the surface quality of the parts. Due to the inherently higher surface roughness of AM metal parts, post-processing is necessary to reach surfaces suitable for rf operation. We present most recent results of surface post-processing trials with AM parts from stainless steel.

INTRODUCTION

Additive manufacturing (AM) of stainless steel and pure copper parts for the manufacturing of critical parts for linear particle accelerators is an interesting prospect for cost reduction of these typically very complex structures [1–9]. First implementations of stainless steel parts use an oversize print that is CNC machined and then copper plated with the rest of the linac cavity [10–12]. The main benefit there is the inclusion of complex cooling channels within the parts. These implementations therefore still need very costly and time consuming machining of the surface to achieve the dimensional accuracy and surface roughness needed. However, to fully harness the potential cost savings of metal AM, this step should be eliminated. To reach this goal, we need to identify surface finishing (polishing) processes, that can produce parts with low surface roughness ($R_a < 1 \mu\text{m}$) while maintaining the dimensional accuracy of the part or at least show predictable mass removal of the part geometry.

In this paper, we summarize the current state of a study to try to answer these questions for steel AM parts. To this end, a small, cheap to print test geometry was developed to evaluate as many geometrical scenarios as possible to differentiate the different processes tested (see Fig. 1).

* Work supported by: BMBF 05P21RFRB2.

This project has received funding from the European Union's Horizon 2020 Research and Innovation programme under grant agreement No 101004730 and is supported by the Latvian Council of Science under grant agreement VPP-IZM-CERN-2022/1-0001.

Development of PEP technology financed from: PNRR MUR project PE0000023-NQSTL.

[†] haehnel@iap.uni-frankfurt.de

TEST GEOMETRIES

The aforementioned test geometry is shown in Fig. 2, where the purpose of the different features is noted. In addition to different simple geometric features to stress test surface finishing techniques, a short stem with a modified drift tube structure from an IH-DTL is positioned on top of the part for evaluation of a more realistic scenario as found in linac structures [3]. The test part measures 61 mm×20 mm×55 mm and is therefore more cost-effective than printing full large linac geometries just for testing.

At this time, a total of 12 of these test samples have been printed at the company Rosswag (samples 1–5) as well as by colleagues at THM Friedberg with a focus on high part accuracy (samples 6–12), as shown in Fig. 1. While samples 9–12 were not sandblasted (SB) after printing (see Fig. 3), all other parts were sandblasted after printing to remove residual powder from the parts surface.

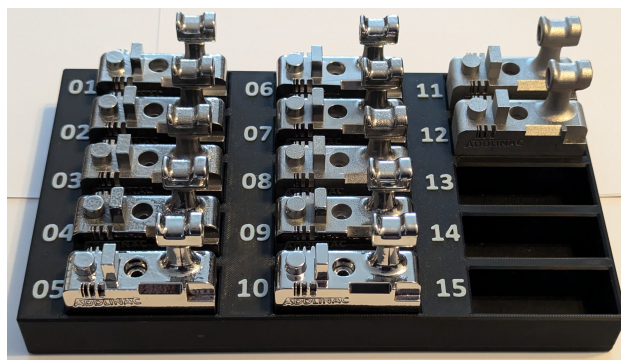


Figure 1: Test geometries in sorting rack. Samples 11 and 12 are still unprocessed.

SURFACE FINISHING PROCESSES

Test samples were sent to different companies and researchers for surface finishing with different techniques. The processes used for this study so far are summarized in Table 1. The processes include two trials with vibratory mass finishing (PERS, Rösler), which is known to be able to produce very smooth parts at higher processing times. One potential

CURRENT STATUS OF BEAM COMMISSIONING AT THE FRANKFURT NEUTRON SOURCE

H. Hähnel^{1,2*}, A. Ateş¹, L. Bauer¹, B. Dedić¹, K. Kümpel¹,
C. Wagner¹, H. Podlech^{1,2}, U. Ratzinger^{1,2}, C. Zhang^{1,2,3}

¹Institute of Applied Physics, Goethe University, Frankfurt, Germany

²Helmholtz Forschungsakademie Hessen für FAIR (HFHF), Frankfurt, Germany

³GSI Helmholtz Centre for Heavy Ion Research, Darmstadt, Germany

Abstract

The Frankfurt Neutron Source FRANZ will be a compact accelerator driven neutron source utilizing the ${}^7\text{Li}(p, n){}^7\text{Be}$ reaction with a 2 MeV proton beam. Following successful beam commissioning of the 700 keV proton RFQ, further beam experiments including emittance measurements are currently ongoing. Preparations for conditioning and commissioning of the IH-DTL are running in parallel to the current beam measurement campaign. We report on the current status of commissioning towards a 2 MeV proton beam.

INTRODUCTION

The Frankfurt Neutron Source (FRANZ) is a compact accelerator driven facility originally initiated in the early 2000s [1–6]. It is designed to provide a 2 MeV proton beam for neutron production via the ${}^7\text{Li}(p, n){}^7\text{Be}$ reaction [7]. The produced neutrons with a thermal spectrum around 30 keV can be used for a number of experiments in the fields of applied physics and experimental astrophysics [8].



Figure 1: Photograph of the current FRANZ LEBT beamline (Aug. 2022).

Significant progress on the driver linac was made recently. The commissioning of the new CHORDIS ion source [9, 10] in late 2020 was a first milestone. Since the CHORDIS ion source only provides a 35 keV proton beam, an electrostatic post-accelerator was developed and commissioned at IAP to reach the desired beam energy of 60 keV [11]. After stable operation was confirmed, the Low Energy Beam Transport line (LEBT), see Fig. 1, was commissioned and the beam was transported up to the point of injection into the RFQ-Accelerator. The 60 keV beam is now in routine operation at the FRANZ. This presents an important milestone for the initial beam commissioning of the FRANZ facility. Meanwhile, emittance measurements to further improve an efficient injection into the RFQ have been performed.

* haehnel@iap.uni-frankfurt.de

RFQ RETROFIT

A change of the RFQ injection energy to 60 keV, necessitated a redesign of the RFQ electrodes. The new beam dynamics design is based on the so-called SEGLER method and the resulting electrode geometries were developed in 2022 [12, 13]. Production of the new electrodes was ordered in summer 2022. The RFQ retrofit and low level rf tuning was finished in summer of 2023. Following that, rf conditioning and finally beam commissioning were performed.

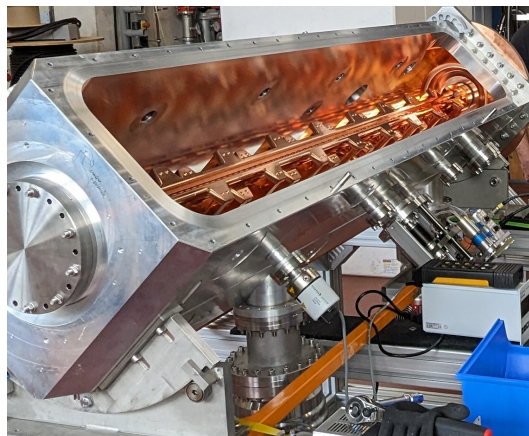


Figure 2: FRANZ RFQ after installation of the new electrodes and successful delivery to IAP Frankfurt with the lid open for final RF tuning.

RF TUNING

After the installation of the new RFQ electrodes at the company Neue Technologien GmbH (NTG) in Gelnhausen (see Fig. 2), the final RF tuning was performed on site in collaboration with IAP. A total of 18 tuning plates had to be installed and adjusted to tune the final frequency of 175 MHz of the RFQ while maintaining a flat voltage distribution over the whole length of the RFQ. For the measurements, the frequency shift introduced by a small dielectric plastic cylinder placed on top of the electrodes is recorded at a position above each tuning plate to deduce the flatness. This process took about two days with numerous iterations, until the results were satisfactory. The final field flatness was within $\pm 3\%$ which is a typical acceptable value for a four rod RFQ (see Fig. 3 (left)).

DEVELOPMENT OF A COMPACT RF COUPLER UTILIZING ADDITIVE MANUFACTURING

J. D. Kaiser^{*†1,2}, A. Ateş¹, H. Hähnel^{1,2}

¹Institute of Applied Physics, Goethe University, Frankfurt a. M., Germany

²Helmholtz Forschungsakademie Hessen for FAIR (HFHF), Frankfurt a. M., Germany

Abstract

Additive manufacturing (AM) has established itself as a powerful tool for rapid prototyping and the production of complex geometries. For use in a 433 MHz IH-DTL cavity, a CF 40 coupler is being developed that is manufactured from pure copper using a 3D printing process and has a water cooling concept that cannot be realized using conventional methods. The coupler consists of a ceramic window which is cooled on both sides, an outer conductor with spiral cooling channels and a cooled inner conductor. Thanks to its modular design, the individual components can be easily replaced. The ideal transmission is frequency-dependent and was adjusted by fine-tuning the inner conductor structure in CST-Simulations. A prototype made of aluminium was built for verification purposes.

COUPLER DESIGN

For high power testing of a 3D-printed IH cavity [1–3], the coupler currently in use is to be replaced by a 3D-printed coupler with full water cooling to withstand higher thermal loads. A Teflon vacuum window is currently in use and will be replaced by a ceramic one in the form of a simple disk (Degussit AL23 by Kyocera). As a result, the design has been completely revised and adapted to the HF properties of the ceramic (see Fig. 1).

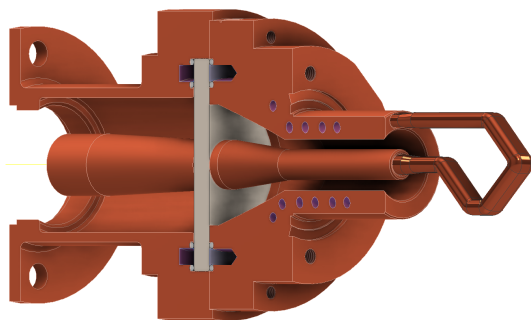


Figure 1: Half section view of the advanced compact CF 40 coupler.

The ceramic is sealed with O-rings, enabling cost-effective manufacturing and quick replacement of the window if damaged. To offset the additional capacitance caused by the separation of the inner and outer conductor sections due to the ceramic, the outer radius of the inner conductor

* kaiser@iap.uni-frankfurt.de

† Work supported by BMBF 05P21RFRB2

is tapered to reduce the radial capacitance between the inner and outer conductors. The coupler is composed of a total of six individual parts. The components in the vacuum are produced using additive manufacturing, while those on the atmosphere side are made conventionally, as they lack cooling channels within the solid material. The individual parts (see Fig. 2) were delivered at the beginning of August and are currently undergoing surface treatment and finishing in the workshop.



Figure 2: Raw parts before post-processing.

RF-Transmission Optimisation

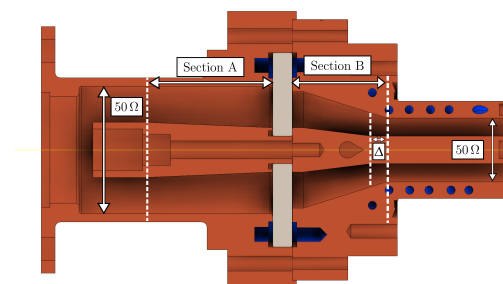


Figure 3: Schematic representation of the internal geometry of the coupler with cone lengths A, B and offset Δ , which are significant for the frequency setting.

The transmission line is composed of five sections (see Fig. 3). The input and output sections follow the standard 50 Ω coaxial geometries, while the middle section, which includes the ceramic window, is shaped according to the

A NEW RFQ FOR THE CARBON THERAPY INJECTOR AT HIT HEIDELBERG

U. Ratzinger[†], S. Altürk, H. Hoeltermann, Bevatech GmbH, Mörfelden-Walldorf, Germany
R. Cee, T. Haberer, A. Peters, Heidelberg Ionenstrahltherapie Centrum, Heidelberg, Germany
H. Hähnel, H. Podlech, C. Zhang, Goethe-Univ. Frankfurt, Frankfurt am Main, Germany
M. Schuett, GSI Helmholtzzentrum für Schwerionenforschung GmbH, Darmstadt, Germany

Abstract

The tumor therapy facility HIT at Heidelberg is in operation with light ion beams up to carbon since 2006. The 7 A MeV, 216.8 MHz synchrotron injector linac with a total length of 5 m was designed for the ion C^{4+} from an ECR ion source. The RFQ accelerates the beam from 8 A keV up to 400 A keV and is at present a bottleneck in beam transmission. After a careful analysis of the beam quality along the Low Energy Beam Transport system LEBT and the RFQ it was decided by HIT to order a new RFQ from Bevatech with higher beam acceptance and with tight mechanical tolerances. Other features are optimized entrance and exit gaps by including longitudinal field components, which are characteristic for 4-Rod-RFQs. A complete dipole compensation along the mini-vane electrodes is another improvement. This RFQ is scheduled to replace the old one in 2026.

INTRODUCTION

The carbon therapy injector linac [1] was originally developed for the Heidelberg HIT facility and was reproduced for CNAO in Pavia, MIT in Marburg, SPHIC in Shanghai and with a modified RFQ and intertank section ITS for MedAustron, Wiener Neustadt. These 21 MV injectors run reliably since many years. Recently, higher pulsed beam injector currents are requested in new efforts to make the therapy treatment faster and/or more efficient.

To reach a compact and efficient linac design 25 years ago, the layout was optimized for an 8 A keV beam from the LEBT with a normalized rms emittance of 0.125 mm mrad. However, less than half the beam current delivered by the all-permanent magnetic ECR-source Superannogun [2] fits into that phase space at the RFQ injection point. At the HIT facility the beam losses are located at the RFQ and ITS, which consists of a quadrupole doublet and xy- steerer only. The injector linac at present delivers 45 to 50 $\mu A C^{4+}$.

With the RFQ redesign a significantly higher transmission along the RFQ and an improved matching into the ITS are intended – resulting in a factor two of beam current improvement at the injector exit. Full transmission of the beam as delivered by the LEBT will not be possible due to measured norm. 90% rms beam emittances of around 0.3 mm mrad.

[†] U.Ratzinger@iap.uni-frankfurt.de

RFQ BEAM DYNAMICS

The beam emittances at the end of the LEBT were measured and analysed carefully for all types of ion beams applied at HIT. It was then concluded, that the new RFQ will be based on normalized rms emittances of 0.25 mm mrad. Higher RFQ acceptances would not pay off in the overall performance of the injector linac due to the limitations along the ITS and the IH-DTL, which will not be rebuilt.

For local technical reasons the total RFQ tank length was limited to a maximum of 1492 mm. A view on the new RFQ is shown by Fig. 1.

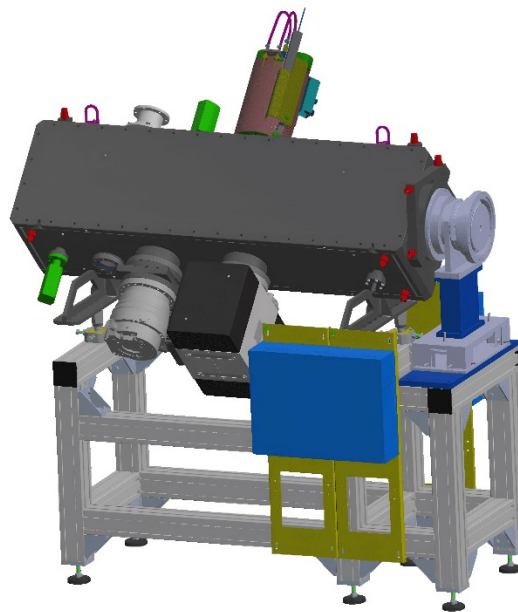


Figure 1: View on the new RFQ design and the existing ITS (quadrupole doublet and steerer) at the right side.

The beam dynamics simulations were performed with RFQGen [3] and used a compact layout along the bunch formation [4, 5]. The simulation of the end gaps including the longitudinal field components [6] were managed by tracking the particles with TraceWin [7] through the electric fields as calculated by CST-Studio-Suite [8]. As the longitudinal end-gap voltages are in the order of magnitude of the vane-voltage one has to minimize the transit-time-factor of the entrance gap close to zero to avoid strong influence on the bunch-forming process along the RFQ. That means, that the effective gap length has to be an integer multiple n of $\beta_i \lambda = 5.73$ mm. The choice was $n = 2$. The radial matcher consists of 4 cells. The length between the

PHASE SETTING ISSUES FOR THE SPIRAL2 LINAC

M. Di Giacomo [†], J-F. Leyge, Ch. Jamet, A. Orduz, P. Salou, GANIL, Caen, France

Abstract

The SPIRAL2 superconducting LINAC accelerates beams of different species, in a large energy range. During operation, the beam requested by the physics can change quite often and it is mandatory that beams that have already been tuned can be obtained again by simple application of the machine parameters already used. This reduces the accelerator retuning time and increases the machine availability for the physics experiences.

Voltages and more particularly phases of all the cavities are among the crucial parameters for a quick retuning. Proper beam tuning is monitored via the BPM (Beam Position Monitor) system.

This paper focuses on the RF and beam phase issues, reminds the way the reference frequency distribution, the LLRF and the BPM work and are used in the tuning procedures, and summarizes the upgrade foreseen to improve the phase setting and monitoring reliability.

INTRODUCTION

The accelerator is presently operated with only one experimental hall: NFS (Neutron For Science), which mainly requires protons and deuterons beams. Nevertheless, a second one: S³ (Separated Superconducting Spectrometer), dedicated to heavy ion physics is under commissioning, and a second injector (NEWGAIN project) is being constructed to extend the ion variety as shown in the last column of Table 1.

During operation, the beams may vary depending on the user requirements. Particle changes occur 4 to 6 times per

run under current conditions, and will increase in the coming years. For a quick retuning, it is mandatory to ensure that previously tuned beams are reproducible through the simple application of the machine parameters already used, among which voltages and more particularly phases of all the cavities. Cavity phase setting stability depends on the reliability of the reference frequency distribution and of the LLRF.

Table 1: Spiral2 Beams

Particles	H+	D+	IONS	
A/Q	1	2	3	7
Max Current [mA]	5	5	1	0.34
Max Energy [MeV/A]	33	20	14	7
Max Beam Power [kW]	165	200	44	17

REF. FREQUENCY DISTRIBUTION

The SPIRAL2 accelerator works at a single frequency of 88.0525 MHz and the master oscillator (MO) is a commercial synthesiser, with stability around 10⁻⁶.

This MO signal is amplified to drive a transmission line (TL) containing several directional couplers and ended on a matching load as shown in Fig. 1. The amplifier is a 1 kW unit, expected to be used at ~710 W (58,5 dBm) for operation margins, whose output power is stabilized within better than 1%. The TL is a 7/8" one (rated for ~7 kW), running aside à water-cooled rubber pipe whose temperature is stabilized at 26±2 °C, and is almost 40 meters long. A thermal case envelopes the TL and the pipe, from the first to

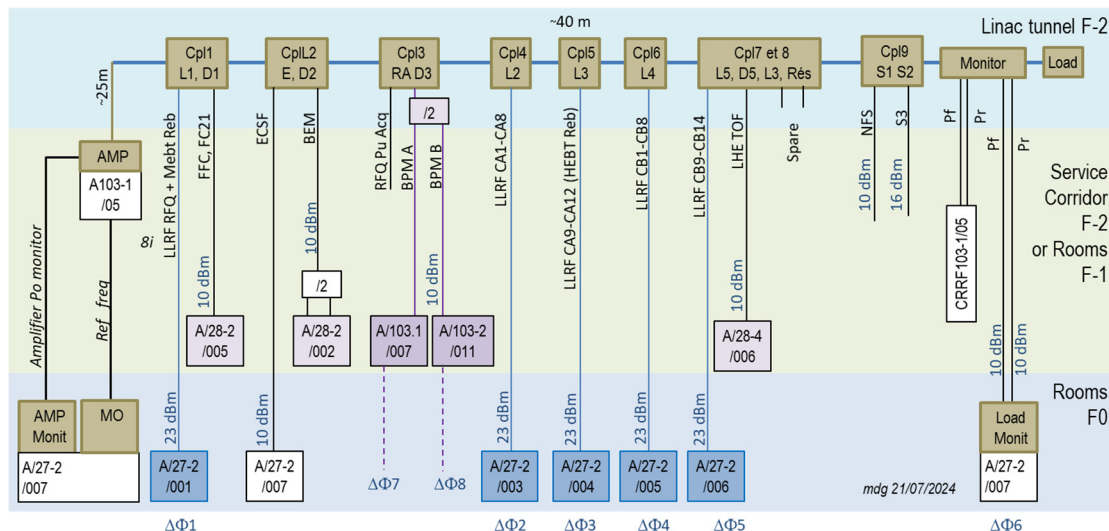


Figure 1: Schematics of the reference frequency distribution for LLRF and diagnostics.

PROGRESS AND STATUS OF THE FAIR PROTON LINAC

C. Kleffner, A. Schnase, A. Seibel, C. Muehle, C. Will, G. Schreiber, K. Knie, M. Rodionova, M. Vossberg, M. Schuett, P. Forck, R. Hettinger, S. Udrea, S. Puetz, T. Sieber, V. Srinivasan
 GSI Helmholtzzentrum für Schwerionenforschung GmbH, Darmstadt, Germany
 H. Hähnel, U. Ratzinger, Goethe Universität Frankfurt, Frankfurt, Germany

Abstract

The progress and status of the high intensity short pulse 325 MHz proton linac driver for the FAIR facility in Darmstadt is described. The proton linac is designed to deliver a beam current of 70 mA at an energy of 68 MeV. The design of the normal conducting CCH cavities was carried out in collaboration with our partners at the IAP Frankfurt and industrial partners. First bead pull measurements have been successfully performed on the CCH prototype. This prototype cavity is intended for later final production and copper plating. The construction of the ladder RFQ has been completed together with first rf measurements at levels up to 400 W. The RFQ has been delivered to FAIR and high power rf tests are expected to be performed on site during the next year. The proton driver, along with the antiproton chain of the FAIR project, has been postponed due to a re-prioritisation of the FAIR project and is now in a frozen state. All delivered components need to be brought to a state that is consistent with the project objectives. This will allow a smooth re-launch in the future. The status of this process is described in this paper.

OVERVIEW

The main characteristics and structure of the proton linac [1, 2] are shown in Fig. 1 and Table 1. It consists of a 2.45 GHz ECR source generating 100 mA of 95 keV protons followed by a low-energy beam transport line (LEBT), a 4-Rod ladder RFQ and six normal conducting crossbar cavities of CCH and CH type arranged in two sections. The design provides for the proton beam to go directly to the proton beam dump or with two 45° dipoles to the injection beam line in front of the SIS18 synchrotron.

Table 1: Proton Linac Main Parameters

Particle	Proton (H ⁺)
Ion source	95 keV
MEBT energy	3 MeV
CCH section	33 MeV
Final energy	68 MeV
Pulse current	70 mA
RF-frequency	325.224 MHz
Rep. rate	2,7 Hz

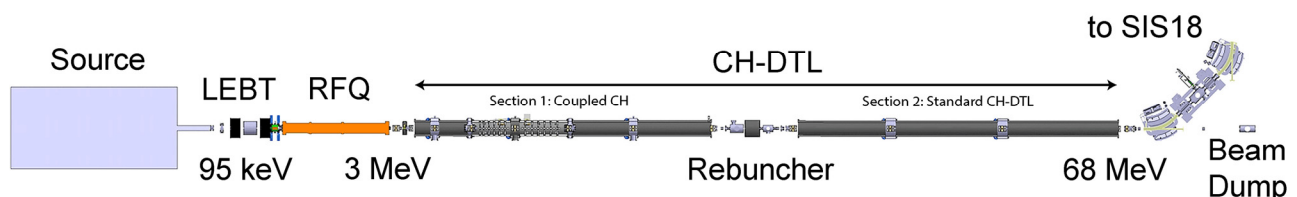


Figure 1: Layout of the FAIR Proton Linac.

CH-DTL

It is planned to complete the first of the series of CCH coupled cavities, the CCH1, and put it into operation with RF [3]. The CCH1 cavity was manufactured by PINK and delivered to GSI last year in a version with clamped drift tube connectors. Low level RF bead pull measurements were performed on site to verify the basic RF characteristics of the cavity. Final electroplating tests on a dummy will be carried out next year as a prerequisite for final production of the CCH1. At GSI the CCH1 cavity was set up on the RF testbench (Fig. 2) to be able to perform bead pull measurements. The cavity was supplied with a complete set of movable tuners for all 17 possible tuner locations. In total, measurements were carried out with more than 120 different tuner positions (Fig. 3).

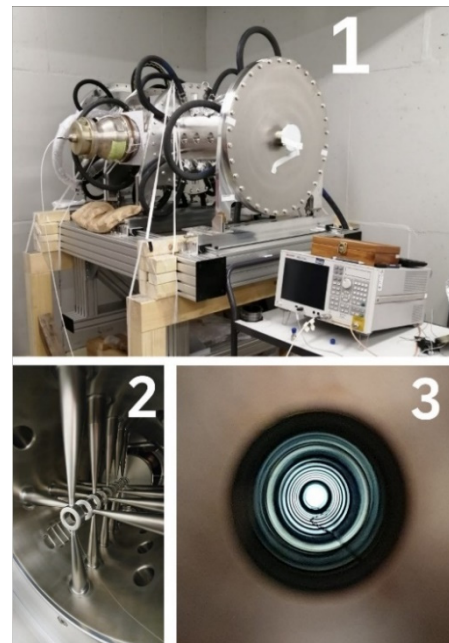


Figure 2: CCH1 cavity in preparation for bead pull measurements (1). Photo of the first CCH1 section (2). Photo tele shot along all drift tubes of the cavity (3).

HIGH CURRENT MACHINE CAMPAIGN WITH VARIOUS ION SPECIES AT GSI UNILAC

H. Vormann^{1,*}, W. Barth^{1,2,3}, F. Dziuba^{1,2}, S. Lauber^{1,2}, J. List^{1,2},
M. Miski-Oglu^{1,2}, U. Scheeler¹, M. Vossberg¹, S. Yarymyshev¹
¹ GSI Helmholtz Centre for Heavy Ion Research, Darmstadt, Germany
² HIM Helmholtz Institute Mainz, Mainz, Germany
³ KPH Johannes Gutenberg University Mainz, Mainz, Germany

Abstract

After dedicated machine upgrade measures at the GSI UNILAC (UNiversal Linear ACcelerator), a high current beam campaign has been performed recently. The presented results were successfully accomplished, including newly installed electrodes for the superlens (short RFQ-type matching section). Beam experiments have been conducted with high intensity proton beam (1.2 mA), carbon (1 mA $^{12}\text{C}^{6+}$) and nitrogen beam (6.5 mA $^{14}\text{N}^{7+}$) dedicated for pion production. A record argon beam intensity of 28 mA ($^{40}\text{Ar}^{11+}$) has been obtained at gas stripper section. A sufficiently high stripping efficiency of 35% applying a pulsed N_2 gas stripper target could be realized. By achieving high-current performance for medium-heavy ions, a further step has been taken towards fulfilling the FAIR requirements for space charge dominated operation. In this contribution the results of machine experiments are summarized, in particular the performance enhancement at the High Current Injector (HSI).

INTRODUCTION

The UNILAC is utilized for all ions of different masses from protons to uranium. It consists of different ion source terminals, the High Current Injector HSI with the adjacent stripping section, the poststripper, a chain of ten single gap resonators and the transfer channel to SIS18 (Fig. 1, [1–6]).

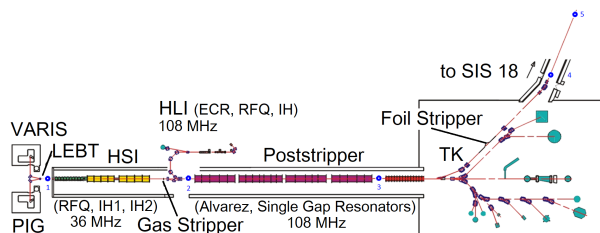


Figure 1: Overview of the GSI UNILAC (UNiversal Linear ACcelerator).

In the HSI ion beams are accelerated from 2.2 keV/u to 1.4 MeV/u with an RFQ and two IH-DTL-tanks. The poststripper contains five Alvarez type DTL-tanks and a chain of ten single gap resonator cavities. The nominal output beam energy is 11.4 MeV/u. Lower energies can be chosen by individually turning off Alvarez cavities, fine tuning is accomplished with the single gap resonator chain.

* h.vormann@gsi.de

ION BEAM INVESTIGATIONS

In November and December 2023 measurement campaigns have been conducted with high intensity light and medium ion beams (protons, carbon, nitrogen, argon).

HSI-superlens-operation suffered from performance restrictions until 2022. Therefore, since 2023 high intensity heavy ion beam operation is again possible and has even been significantly improved.

HSI RFQ and Superlens Optimization

The HSI-RFQ RF performance was significantly degraded in 2017/2018, due to damages of the electrodes' copper surface from a long period of being held under atmosphere conditions, during repair measures in the one year shutdown 2017. After the replacement of its electrodes in 2019, the RFQ is again able to accelerate all ion species, up to mass to charge ratio of 62 [5].

The HSI superlens also showed degradation effects. As a consequence the superlens rods have been exchanged in 2023, requiring additional RF-retuning, applying a modified RF plunger design. Collimation of the horizontal beam size were introduced to avoid beam loss inside the superlens cavity. The superlens upgrade resulted in a full performance recovery.

Proton and Carbon Beam Investigations

Proton beam generated by stripping the CH_3 beam (MUCIS) from HSI was accelerated to the maximum intensity at UNILAC and SIS18 and maximum energy of 4.7 GeV/u. From 1 mA $^{15}\text{CH}_3^{1+}$ at 1.4 MeV/u, a proton beam intensity of up to 1.2 mA at the end of the transfer channel could be reached (70% of UNILAC design limit). Intensity optimization suffered from an exceptional unstable beam position, due to insufficient stability of the power supply of a dipole magnet. Higher proton beam intensity is possible, if operation of the DTL tanks at a nominal synchronous phase of -30° would be applied. Nevertheless, an intensity of up to $1 \cdot 10^{11}$ particles on SIS flattop could be achieved.

Proton beam operation was conducted with dedicated Alvarez RF phase settings, as already used in regular operation since 2021: The synchronous phase is shifted from -30° (regular for heavy ions) to -57° , so a reasonable (not too low) RF power can be applied, leading to poststripper oper-

UPDATE ON THE INTENSE HEAVY ION DTL PROJECT ALVAREZ 2.0 AT GSI

L. Groening*, T. Dettinger, M. Heilmann, M. S. Kaiser, S. Mickat
GSI Helmholtzzentrum für Schwerionenforschung, Darmstadt, Germany

Abstract

The Alvarez-type post-stripper DTL at GSI accelerates intense ion beams with $A/q \leq 8.5$ from 1.4 to 11.4 MeV/u. After more than 45 years of operation, it suffers from aging and its design does not meet the requirements of the upcoming FAIR project. Prototyping of a new 108 MHz Alvarez-type DTL has been completed and series components for the 55 m long DTL are under production and have been delivered partially. This report summarizes the actual status of Alvarez 2.0 at GSI and sketches the future path to completion.

INTRODUCTION

Like the current DTL, the new section will accelerate ions up to the injection energy of the subsequent synchrotron SIS18. All species up to the mass-to-charge ratio of $A/q=8.5$ are accelerated, corresponding to FAIR's reference ion of $^{238}\text{U}^{28+}$ [1]. Five cavities with lengths of about 11 m each are operated at 108.4 MHz with peak powers of up to 1.35 MW including beam loading. Figure 1 plots the new DTL together with some RF-design details of the first cavity. The normal conducting DTL covers a beam repetition rate of up to 10 Hz with flat top RF-pulse length of up to 1.0 ms corresponding to the beam pulse length. Within

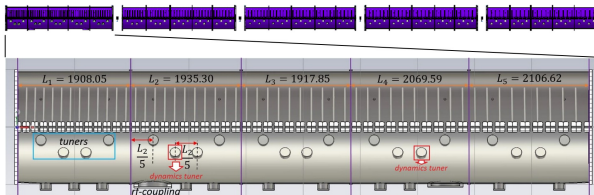


Figure 1: New post-stripper DTL Alvarez 2.0 under construction at GSI.

the cavities, transverse FDDF focusing is provided with a zero current phase advance of 65° . The large intensities cause transverse tune depressions of up to 40% along the first cavity [2]. Longitudinal focusing is from RF-phases of -30° along the first three cavities and -25° along the last two ones. Cavities are separated by four identical inter-tank sections [2] which serve for 3D beam envelope matching by three quadrupoles and one re-buncher. The inter-tank sections provide also for a beam current and phase probe, a sector valve, and a transverse beam profile measurement set-up.

Although the machine is mainly designed as an injector for the synchrotron SIS18, several low-energy experiments

shall be served as well. The DTL design allows for switching off the RF-power of the last cavities while the transversely focusing quadrupoles inside the drift tubes remain switched on. Accordingly, the DTL output energies correspond to the individual cavity exit energies of 3.212, 5.173, 7.142, 9.237, and 11.318 MeV/u. The quadrupoles are pulsed, such that focusing can be adapted individually to each ion species and design energy; the latter can be changed between the individual DTL pulses, i.e., within less than 100 ms. The DTL design is described in detail within the dedicated Technical Design Report [3] and the main design parameters are listed in Table 1.

Table 1: Main Design Parameters of GSI's New Post-Stripper DTL Alvarez 2.0 [3]

Parameter	Value
Ion A/q	≤ 8.5 ($^{238}\text{U}^{28+}$)
Input beam energy	1.358 MeV/u
Output beam energy	3.212 – 11.318 MeV/u
Electrical beam current	1.76 emA · A/q
Transv. tune depression	$\leq 40\%$
Beam pulse duration	0.2 – 1.0 ms
Beam repetition rate	≤ 10 Hz
Number of cavities	5
RF-frequency	108.408 MHz
Max. RF-power per cavity	1.35 MW
RF-sources per cavity	1
Transv. focusing scheme	FDDF
Total length	55 m

PRODUCTION OF CAVITIES

Each of the five cavities comprises five cavity sections from stainless steel. The mantle has a strength of 12 mm. Its roundness with a tolerance of the average radius of $-0/+0.3$ mm has been achieved by rolling without milling as well as the tolerance in length of ± 0.1 mm. The mantle is equipped with external cooling channels. Of special concern is the high quality of the inner surfaces for subsequent bright Cu-plating. The surface must be free of voids and its roughness R_a must not exceed $0.3 \mu\text{m}$. Production has been started in summer 2022 at one single manufacturer (see Fig. 2), after successful testing of a fully RF-operated FoS cavity section [4]. Effective duration of production is about seven weeks per section, including also the 5×2 cavity end plates. The sections of the first cavity have been delivered in spring 2024 and those of the second cavity in

* la.groening@gsi.de

CONSIDERATIONS AND FINDINGS ON BEAM VORTICITY DYNAMICS

L. Groening*, GSI Helmholtzzentrum für Schwerionenforschung, Darmstadt, Germany

Abstract

Rotation of beams is usually quantified through angular momentum rather than through vorticity. However, the difference of the two transverse eigen-emittances is linked more strongly to vorticity than to angular momentum. It has been found that the dynamics of vorticity has remarkable similarity to the dynamics of the beam envelope along channels of solenoids and quadrupole triplets. Transport matrices of vorticity, corresponding phase advances, and Twiss parameters look very similar and are partially even identical to their counterparts concerning envelopes. Corresponding to emittance, the quantity of vortissane, being a constant of motion, is defined. Unlike emittance, for vorticity-dominated beams, it may take imaginary values causing imaginary Twiss parameters and negative or zero phase advances along a finite beam line section.

ANGULAR MOMENTUM AND VORTICITY

The rms angular momentum of a particle beam is defined through the beam's second moments as

$$L := \langle xy' \rangle - \langle x'y \rangle. \quad (1)$$

Usually, the angular momentum is regarded as the quantification of rotation being justified by its outstanding role in physics. Nevertheless, other quantities may serve for this purpose as well, among them for instance the beam vorticity

$$\mathcal{V} = A \int_A [\vec{\nabla} \times \vec{r}'] \cdot d\vec{A}, \quad (2)$$

obtained from the rotation of the derivative of the particle beam position and the beam rms area

$$A^2 := \langle x^2 \rangle \langle y^2 \rangle - \langle xy \rangle^2. \quad (3)$$

The above expression for vorticity may be re-phrased [1] as

$$\mathcal{V} = \langle y^2 \rangle \langle xy' \rangle - \langle x^2 \rangle \langle yx' \rangle + \langle xy \rangle (\langle xx' \rangle - \langle yy' \rangle). \quad (4)$$

Figure 1 illustrates the difference between angular momentum and vorticity using an ellipse performing two types of rotation.

Determining the angular momentum and \mathcal{V}/A reveals for the rigid rotation [1]

$$L_{rig} = \frac{\omega}{4} a^2 (1 + r^2), \quad (5)$$

$$(\mathcal{V}/A)_{rig} = \frac{\omega}{2} a^2 r, \quad (6)$$

while for the intrinsic rotation one obtains

$$L_{int} = \frac{\omega}{2} a^2 r, \quad (7)$$

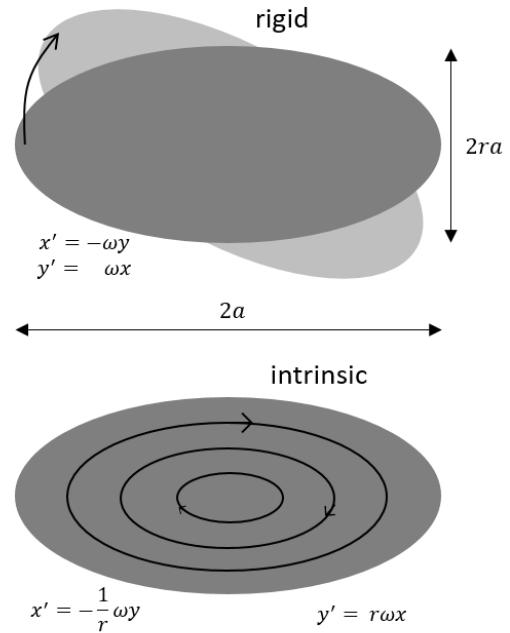


Figure 1: Ellipse with aspect ratio r performing a rigid rotation (upper) and an intrinsic rotation (lower).

$$(\mathcal{V}/A)_{int} = \frac{\omega}{4} a^2 (1 + r^2). \quad (8)$$

The expressions for L and \mathcal{V}/A flip when flipping from rigid to intrinsic rotation. Additionally, for extreme aspect ratios of $r \ll 1$ or $r \gg 1$, the rigid rotation has just angular momentum and vanishing \mathcal{V}/A (relatively), while the intrinsic rotation has just \mathcal{V}/A but vanishing angular momentum (relatively). Another special case is the circle ($r = 1$) and just for objects with cylindrical symmetry, angular momentum is equal to vorticity

$$L = \mathcal{V}/A. \quad (9)$$

Vorticity enters into beam dynamics through its tight relation to the two transverse eigen-emittances ε_1 and ε_2 [2] of a beam. The latter are equal to the two projected rms emittances, if and only if all correlations between the two transverse planes have been removed to zero. Removing them preserves the eigen-emittances and changes the projected emittances.

Transverse beam eigen-emittances are calculated through beam rms moments as

$$\varepsilon_{1/2} = \frac{1}{2} \sqrt{-tr[(CJ)^2] \pm \sqrt{tr^2[(CJ)^2] - 16 \det(C)}}, \quad (10)$$

with

* la.groening@gsi.de

HIGH PERFORMANCE MEGAWATT URANIUM BEAMS AT GSI UNILAC

W. Barth^{1,2,3,†}, F. Dziuba^{1,2}, S. Lauber^{1,2}, J. List^{1,2}, M. Miski-Oglu^{1,2}, U. Scheeler¹, H. Vormann¹,
M. Vossberg¹, S. Yaramyshev^{1,2}

¹ GSI Helmholtzzentrum für Schwerionenforschung, Darmstadt, Germany

² Helmholtz Institute Mainz, Germany

³ Johannes Gutenberg-Universität Mainz, Mainz, Germany

Abstract

The 50 years operating GSI-UNILAC (Universal Linear Accelerator) as well as the heavy ion synchrotron SIS18 will serve as a high current short pulse heavy ion injector for the FAIR (Facility for Antiproton and Ion Research) synchrotron SIS100. This contribution presents the results of the full performance high current uranium beam machine experiment campaign at UNILAC, conducted in the last three years. In order to determine the behaviour of uranium beams, the transverse beam emittance at five selected measurement positions along the complete UNILAC have been measured for the first time in several machine investigation runs. A significant improvement in beam brilliance was achieved after several upgrade measures at the High Current Injector (HSI) by using the pulsed hydrogen stripper at 1.4 MeV/u. It could be shown that extremely low horizontal emittances, i.e. very high brilliances, are achieved along the complete UNILAC up to the SIS18 injection. Besides high intense uranium beams with charge state 28+ also 1.5 Megawatt-multi charge beams, comprising 27+, 28+, 29+ uranium ions, commonly recharged primarily to charge state 73+ using a carbon foil, were investigated and a record uranium beam current of 3.6 emA has been achieved.

INTRODUCTION

Besides the High Charge State Injector (HLI) accelerating highly charged ions from an ECR ion source of CAPRICE-type, the High Current Injector (HSI), fed by two ion source terminals and a low energy beam transport system (LEBT), serve as injector linac for the GSI-UNILAC (Fig. 1). The HSI comprises a 36 MHz IH-RFQ (2.2 keV/u up to 120 keV/u) and an IH-DTL with two separate tanks, accelerating the beam up to the final HSI-energy of 1.4 MeV/u. After stripping and charge state separation the Alvarez DTL provides for beam acceleration up to 11.4 MeV/u. In the transfer line (TK) to the synchrotron SIS18 a foil stripper and another charge state separator system can be used. In order to provide the highest heavy ion beam currents (15 emA, U²⁸⁺), as required for FAIR, the HSI must deliver up to $2.8 \cdot 10^{12}$ U⁴⁺ ions per pulse [1-2]. With the AC beam transformers installed behind each accelerator cavity and along all transport sections, the beam transmission in all sections can be permanently monitored and measured with high precision. The positions of the emittance meters, used for the measurements presented in this paper, are shown in Fig.1.

† email address: w.barth@gsi.de

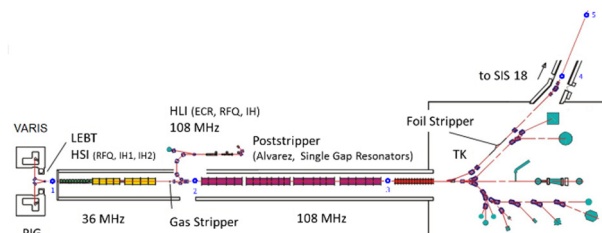


Figure 1: GSI-UNiversal Linear ACcelerator; emittance meters at LEBT (1), gas stripper section (2), poststripper (3), transfer line (4 and 5) are shown in blue marks.

UNILAC-UPGRADE MEASURES

For the recent uranium beam campaigns at UNILAC, a novel multi-hole extraction system for extracting a high brilliant ion beam from the VARIS ion source [3-4] was used. Moreover, the HSI RFQ has been equipped with new mini-vane electrodes so that it could be again operated at nominal RF-voltage for uranium operation by applying a dedicated conditioning and development program. The HSI-superlens also recently underwent an extensive upgrade programme. The electrodes were also replaced, so that uranium levels could be applied again without any problems. To prevent beam losses in the tank, the electrodes were protected by a suitable aperture diaphragm.

During preparation stage of the superlens upgrade, the beam emittances before and behind HSI-RFQ for high current argon-beam have been measured again after more than 12 years; the measured beam emittances are about 50% lower compared to the long past campaign. By measuring the RF-voltage influence on the beam emittance, it was possible to show that the RFQ-working point corresponds to minimum transversal emittance growth (see Fig. 2). Backtracking of measured beam emittance to RFQ-exit and subsequent forward tracking resulted in optimized superlens matching. A minimum beam spot at superlens entrance was confirmed by a profile measurement. Due to field strength limitations of the intermediate quadrupole duplet in front of the superlens, the optimum uranium beam matching (avoiding further beam losses) could be accomplished only by a new quadrupole duplet with increased field gradients.

The upgrade measures facilitated an extensive machine optimizing program and thus the success of this measurement campaign. The already used pulsed hydrogen stripping target [5] has been further optimized to enable for increased gas densities [6], as well as to determine the maximum achievable average charge state. It was found,

MODELING BEAM DYNAMICS IN THE HELIAC ADVANCED DEMONSTRATOR

S. Lauber^{*1,2}, W. Barth^{1,2,3}, C. Burandt^{1,2}, F. Dziuba^{1,2,3}, R. Kalleicher^{2,3},
T. Kürzeder^{1,2}, J. List^{1,2,3}, M. Miski-Oglu^{1,2}, U. Scheeler¹, H. Vormann¹, S. Yaramyshev^{1,2}

¹ GSI Helmholtzzentrum für Schwerionenforschung GmbH, Darmstadt, Germany

² HIM Helmholtz Institute Mainz, Mainz, Germany

³ KPH Johannes Gutenberg-University Mainz, Mainz, Germany

Abstract

A crucial milestone towards the final expansion stage of the HELIAC (HElmholtz LInear ACcelerator at GSI Darmstadt) is the commissioning of the first fully equipped cryo module, the so-called Advanced Demonstrator. The cryo module comprises three superconducting crossbar H-mode accelerating cavities, a rebuncher and two superconducting solenoids. For modelling the beam dynamics of the Advanced Demonstrator test setup, the actual 3D electromagnetic field distributions of the cavities and solenoids are used. The digital model was linked to beam-based measurements of the longitudinal and transverse beam density distribution to realistically calculate the beam propagation along the 20 m long setup. The beam dynamics findings gained during the cryo module commissioning are presented.

INTRODUCTION

The first cryo module (CM1) of the Helmholtz Linear Accelerator (HELIAC) [1, 2] was subject to the first full integration test in the end of 2023. The cryo module is equipped with four superconducting crossbar H-mode (CH) cavities [3–5] and two superconducting magnets for beam acceleration and focusing. An Ar^{8+} and He^{2+} ion beam (delivered by the GSI HLI) was utilized to investigate the beam acceleration capabilities of the cryo module unit. Finally, the cryo module provided beam energies up to 3.1 MeV/u with He^{2+} , exceeding the foreseen 2.7 MeV/u design energy.

The cryo module has a minimal selection of beam diagnostics. Only cold beam position monitors are generally available, but have not been operated in the forementioned beamtime. For a better understanding of the employed beam dynamics concept of the superconducting CH cavities (namely EQUidistant mUltigap Structure (EQUUS) [2, 6, 7]) in practice, further knowledge about the beam transport within the cryo module is desired. Through the use of a digital twin of the accelerator and a beam representation based on measurements, it is possible to visualize the beam dynamics as it passes the accelerator. This allows a more precise understanding of the accelerator performance in terms of transmission and beam quality.

METHOD

The beamline has been modelled using the in-house developed beam dynamics solver Aperture3D [8] based on

* s.lauber@gsi.de

Python. The software can be utilized with the highest flexibility to fit in the dynamic readout of the control system. The application is able to display specific plots, it is intended to be extended continuously.

Aperture3D

Aperture3D is a multi-particle code designed to describe beam dynamics in linear accelerators. It calculates the propagation of charged particles through 3D electromagnetic fields. The propagation is calculated in two steps. In the first step, the space charge forces acting on each particle (and other external forces if required) are calculated. All these external forces are intended to have a relatively long evaluation time. After calculation of the external forces, the particles are integrated through the electromagnetic fields by using the Runge–Kutta 4 method, considering the 3D electromagnetic fields $E(x, y, z, t)$ and $B(x, y, z, t)$ and the (for the second step temporarily static) external forces, until the beam propagated several RF-periods. After this distance, the beam shape has changed sufficiently in order to justify updating and recalculating all external forces, avoiding manifold updates per RF period. The Python package *Numba* is employed to balance the benefits of Python and the high performance capabilities of compiled languages. Thus, the high computational workload can be managed by utilizing CPU-parallel execution.

Beamline Model

A beamline model for the existing beamline has been built using Aperture3D, incorporating the HLI partially and the HELIAC cryo module CM1 (see Fig. 1). The beamline description and modelling starts at the exit of the HLI IH cavity at a beam energy of 1.4 MeV/u due to the availability of sufficient beam diagnostics. This allows both, the longitudinal and the transverse characterization of the beam. At positions in the injector with lower energies, the longitudinal reconstruction of the beam density is not feasible due to the lack of required instrumentation. Also, the prediction of the beam dynamics inside the RFQ and IH are very demanding and should be established extremely careful. As the main scope of this investigation is the beam dynamics inside the cryo module, the calculations inside and before the IH are not required.

For the modelling of the beamline, the position of all beamline magnets, quadrupoles, solenoids, steerers and normal and superconducting cavities must be considered. Fur-

PHOTOCATHODE STUDY IN SRF GUN-II AT HZDR

R. Xiang[†], A. Arnold, S. Gatzmaga, G. Hallilingaiah, A. Hoffmann, P. Murcek, R. Niemczyk, A. Ryzhov, J. Teichert, Helmholtz-Zentrum Dresden-Rossendorf, Dresden, Germany

Abstract

HZDR's SRF Gun-II is an excellent demonstration of SRF technology application in the field of electron sources operating in continuous wave mode. As well known, quality of the photocathode is crucial for operational stability and reliability of an SRF gun. In this contribution, various studies on Cs₂Te cathodes, including cleaning, preparation, transport/insertion, RF and beam operation will be summarised. We will look back at the achievements and open issues, and discuss possible improvements and further development.

INTRODUCTION

Development of high-quality electron photo-sources is a key research field in particle accelerator technologies, which is crucial for both fundamental and applied research. It is widely acknowledged that quality of photocathodes plays an essential role in enhancing the stability and reliability of photo-injectors [1]. A "perfect" photocathode should provide a high quantum efficiency (QE) at a standard laser wavelength, long lifetime, fast response and low thermal emittance.

For the development of SRF guns at HZDR, metal cathodes (copper, magnesium) and a type of semiconductor photocathodes, Cs₂Te, have been selected. During last years, with Cs₂Te photocathodes the SRF Gun-II has been able to provide stable beams for accelerator users [2].

HZDR SRF GUN-II AND CATHODES

HZDR SRF gun-II was built for the super-radiant THz source at ELBE SRF accelerator. Currently, the SRF gun-II is providing more than 1000 hours beam time yearly for ELBE.

The SRF gun-II includes a 3½ cell 1.3 GHz cavity with chock cell and a SC solenoid in a cryostat, and a load-lock system for cathode exchange. It is operated with Cs₂Te cathodes driven by a 260 nm laser. The bunch charge is up to 250 pC at the repetition rate of 50 kHz or up to 80 pC at 13 MHz. The kinetic energy is limited to 3.5 MeV by field emission in the SRF cavity.

A highlight of HZDR SRF gun-II is that the cavity gradient has not significantly degraded despite multiple cathode exchanges. Even after overheated Cs₂Te evaporated in the gun in 2017, it was possible to recover the cavity. This well demonstrates possibility of routine operation of an SRF gun.

By now, 31 cathodes have been in use in SRF gun-II, including 2 bulk-Cu plugs, 3 Cs₂Te on Mo plugs, 12 bulk Mg cathodes, and 14 Cs₂Te on Cu plugs (see Fig. 1). Copper was employed as the commissioning cathode. The

work function of Cu (4.6 eV) is relatively high, and its quantum efficiency (QE) of 1×10^{-5} at 260 nm is insufficient for routine beam production. In the context of medium bunch charge mode, a magnesium cathode is a promising candidate. Magnesium is a metal with a low work function of 3.6 eV, while its QE can reach 0.5% after ps UV laser cleaning [3]. Despite its lower QE compared to Cs₂Te, Mg offers the benefits of a longer operational lifetime, reliable compatibility, and minimal risk of contaminating the niobium cavity.

Since May 2020, Cs₂Te photocathode (with a band gap of 3.3 eV and an electron affinity of 0.2 eV) has demonstrated favorable QE and a prolonged operational lifetime in the ELBE SRF gun-II [4]. Due to the overheating observed in the cathodes within the SRF gun cavity, the decision was taken to use high conductive copper (OFHC) instead of Mo plugs, despite the inherent challenges associated with utilising copper as a substrate for Cs₂Te. Cs₂Te on Cu plugs have been prepared at HZDR and have demonstrated successful operation within SRF gun-II during the THz user beam time as well as possibility of high average current (up to 1 mA) operation.

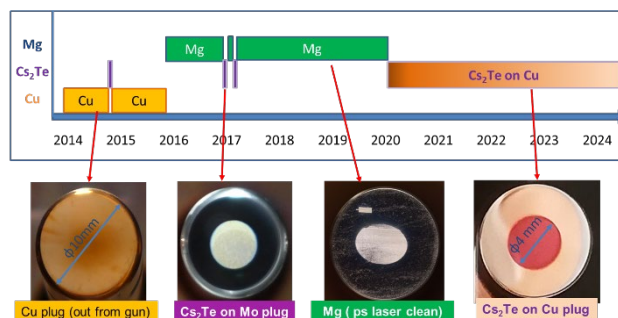


Figure 1: Cathodes used in SRF Gun-II.

CS₂TE PREPARATION PROCESS

The Cs₂Te photocathodes were prepared in the HZDR cathode laboratory and transported to the SRF gun via a vacuum transfer system. In the course of our experiments, the Cs₂Te cathodes on the mechanically polished plugs and those on the diamond-turning finished plugs exhibited nearly identical photoemission quality and also the same dark current in the gun. The plugs were meticulously cleaned in a cleanroom. To maintain the surface free of any contamination, chemical cleaning, dry ice cleaning, and 350°C baking in a vacuum were employed.

During the preparation process, the plug was kept at 120°C by means of a halogen lamp. First, tellurium was

[†] xiang@hzdr.de
TUPB034

DEVELOPMENT OF AN INTEGRATED MONITOR SYSTEM FOR REAL-TIME RELATIVE PHASE MEASUREMENT BETWEEN THE CAVITY-RF AND BEAM

E. Cicek*, Z. Fang, Y. Fukui, K. Futatsukawa, T. Miyao, S. Mizobata, KEK, Ibaraki, Japan
J. Kamiya, K. Moriya, S. Shinozaki, JAEA, Tokai, Naka, Ibaraki, Japan
Y. Sato, NAT Corporation, Tokai, Naka, Ibaraki, Japan

Abstract

In a linear accelerator, phase drift in upstream cavities can adversely affect downstream cavity synchronization, leading to momentum drift and beam loss. J-PARC LINAC employs different phase reference signals for beam monitoring and RF systems, hindering direct comparison. Recent observations revealed susceptibility of reference signals to environmental effects in the Klystron Gallery. Hence, a thorough observation of the relative phase between cavity-RF and beam is imperative. Addressing this, we took advantage of the newly developed MicroTCA.4-based monitor digitizers to meticulously analyze RF signals from cavity pick-up and beam signals from existing fast current transformers dedicated to measuring beam phase. Initial results show enhanced long-term stability in the relative phase with a shared RF reference. A beam study was also conducted wherein deliberate alterations were made to the cavity-RF phase settings via the LLRF system to detect their impact on the phase drift of downstream cavities. The system recorded downstream beam oscillations prompted by phase drift in upstream cavities. Our work elucidates a real-time monitoring strategy for relative phase detection.

INTRODUCTION

The linear accelerator (LINAC) in Japan Proton Accelerator Research Complex (J-PARC) comprises a negative hydrogen (H^-) ion source (IS), a radio-frequency quadrupole (RFQ) linac, a drift-tube linac (DTL), a separated-type drift-tube linac (SDTL), and an annular ring coupled structure (ACS). This configuration also includes a 50-keV low-energy beam transport line (LEBT), a 3-MeV medium-energy beam transport line (MEBT1) with two crucial buncher cavities (Buncher1 and Buncher2), and an RF chopper. The assembly extends through a 191-MeV medium-energy beam transport line (MEBT2) and culminates in the linac-to-3-GeV synchrotron beam transport line (L3BT), as illustrated in Fig. 1 [1,2]. The LINAC is equipped with various beam monitoring devices, including fast current transformers (FCTs) dedicated to beam phase and energy measurements [3,4].

In linear accelerators, phase drift in upstream cavities can disrupt synchronization in downstream cavities, resulting in momentum drift and potential beam loss. The LINAC uses different phase reference signals for beam monitoring and RF systems, complicating direct comparisons. Specifically, the RF distribution system operates at frequencies of

312 MHz and 960 MHz [5], while beam monitor functions at 324 MHz. Recent observations have also highlighted the susceptibility of reference signals to environmental influences in the Klystron Gallery. Consequently, a direct measurement of the relative phase between the cavity-RF and beam is crucial.

To address this challenge, we utilized a micro telecommunications computing architecture (MicroTCA.4)-based beam-monitor digitizer [6], a device within the monitoring infrastructure developed for beam diagnostics purposes. The board of the digitizer includes eight analog-to-digital converters (ADCs) operating at a maximum of 370 MSPS with 16-bit resolution and 800-MHz bandwidth, as well as two digital-to-analog converters [7]. The DC-coupled ADCs measure signals from FCTs and slow current transformers, while 324-MHz RF signals from the beam position monitors are acquired using AC-coupled ADCs. Our objective was to precisely analyze RF signals from cavity pick-ups and beam signals from existing FCTs. Our investigation started with long-term measurements to monitoring long-term stability. Furthermore, we conducted a beam study to evaluate the impact of intentional modifications to the cavity-RF phase settings at the RFQ, Buncher2, and SDTL01 locations, as indicated by the dashed blocks in Fig. 1. This study aimed to assess the influence of these adjustments on the phase drift in downstream cavities and investigate phase relationship between cavity-RF and beam, thereby providing insights into improving the LINAC.

LONG-TERM MEASUREMENTS

Phase detectors are utilized for beam phase measurements in the LINAC [8]. In this study, a setup was established using phase detectors, buffer amplifiers, and newly developed monitor digitizers to capture signals from multiple FCT monitors and measure the long-term relative phase (see Fig. 2). The 324-MHz RF signal from a cavity is routed to the digitizer through a phase detector, while 324-MHz signals from the FCTs are routed through phase detectors and connected to the digitizer via buffer amplifiers. A consistent 324-MHz monitor RF reference (REF#1~REF#4, REFCLK) is distributed to phase detectors and the digitizer and used to compute cavity-RF and beam phases from each ADC channel.

The newly developed monitor digitizers, intentionally placed at various locations in the Klystron Gallery, facilitated a week-long measurement of the relative phase be-

* ecicek@post.kek.jp

RF REFERENCE PHASE CONTROL SYSTEM IN THE SuperKEKB INJECTOR LINAC

T. Miura^{†1}, H. Katagiri, T. Kobayashi¹, T. Matsumoto¹, KEK, Tsukuba, Japan
¹also at The Graduate University for Advanced Studies (SOKENDAI), Hayama, Japan

Abstract

The radio-frequency (RF) reference phase in the SuperKEKB injector linac has been specially controlled for stable beam injection into the main rings (HER/LER). The phase control system contains three parts: MOFB, MOPS, and SECT35PS. MOFB is the phase feedback system for drift compensation between the linac master oscillator (LMO) of 571.2 MHz and ring MO (RMO) of 508.9 MHz which has a frequency ratio of 49/55 to the LMO. The MOPS is an MO phase shifter for injection phase control. The LMO phase must smoothly shift to the injection phase for the HER or LER rings at a repetition rate of 50 Hz. However, the laser system of a photocathode RF gun for the HER beam does not accept such rapid phase changes. Therefore, MOPS was developed to satisfy the requirements of the laser system and injection phase control. SECT35PS is the phase shifter of the 2856 MHz RF reference downstream of the positron damping ring (DR) located in the middle of the linac. The DR is operated at the same frequency as the main rings, 508.9 MHz. The linac RF reference phase at the downstream of the DR is changed from pulse to pulse by the bucket selection system to increase the synchronization probability for the bucket selection of LER ring. In this paper, we describe an RF reference phase control system in the SuperKEKB injector linac.

INTRODUCTION

The KEK injector linac [1] is a facility that delivers low emittance and high bunch-charge electron/positron beams to the SuperKEKB HER/LER rings. Figure 1 illustrates the

layout of the radio-frequency (RF) reference control and distribution system [2]. The linac master oscillator (LMO) (Keysight E8663D) is 571.2 MHz, and the main ring master oscillator (RMO) is 508.9 MHz. The frequency ratio between LMO and RMO is 55:49, and the common frequency is 10.385 MHz. Both the LMO and RMO are generated by inputting 10 MHz, which is 510 MHz of the main master oscillator (MMO) divided by 51, as the signal generator synchronization signal. For the SuperKEKB, a photocathode RF gun with a laser system was introduced to produce the low-emittance electron beams for HER, and a positron damping ring (DR) was constructed in the middle of the linac for the low-emittance positron beams for the LER. To accommodate these upgrades and ensure stable beam injection into the rings, three new phase control systems are introduced for the RF reference in the injector.

The first is an MO phase feedback module (MOFB), introduced for drift compensation between the LMO and RMO. If the phase drifts, the beam injection phase changes and the injection efficiency worsens. The MOFB is required for stable injection and is placed immediately after the LMO.

The second is an MO phase shifter (MOPS) for injection phase control. The LMO phase must shift smoothly to the injection phase for the HER or LER rings every 20 ms which corresponds to a linac repetition rate of 50 Hz. However, the laser system of the photocathode RF gun does not accept such rapid phase changes. Therefore, MOPS has been developed to satisfy the requirements of the laser system and injection phase switching. The MOPS has two

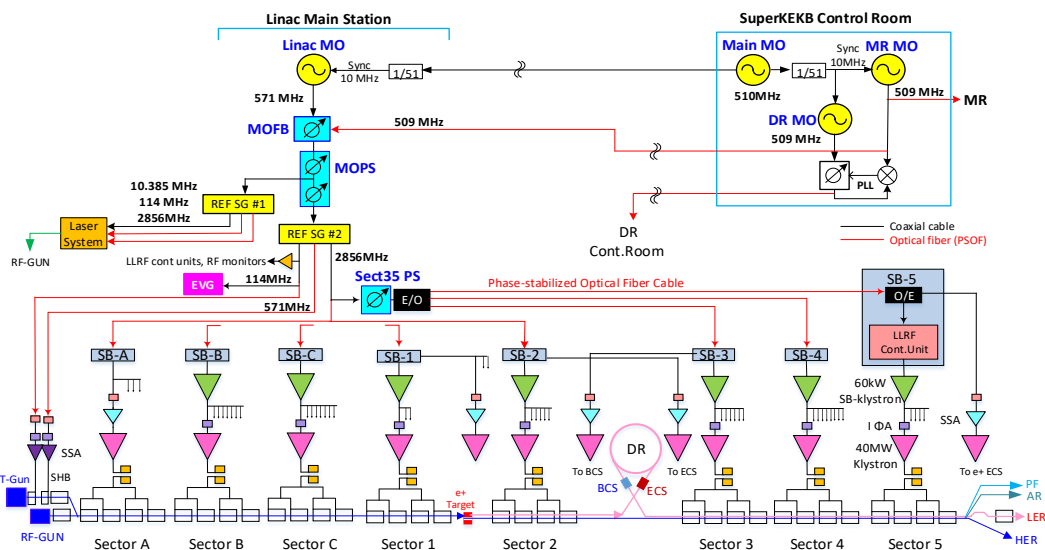


Figure 1: Layout of the RF reference control and distribution system at SuperKEKB injector linac.

[†] takako.miura@kek.jp

DEVELOPMENT OF NEW PULSE DRIVER FOR HIGH POWER PULSED MAGNET

T. Natsui[†], KEK, Ibaraki, Japan

Abstract

The KEK injector linac injects electron and positron beams into four rings: the high-energy ring (HER), low-energy ring (LER), PF ring, and PF-AR. The HER and LER are SuperKEKB main rings. The PF ring and PF-AR are light source rings. These rings require several beams with different charges and energies. The LER beam is a positron. Simultaneous four-ring top-up injections were achieved in 50 pps. We have already installed pulsed magnets downstream of the linac for pulse-to-pulse difference beam injection. Pulsed quadrupole magnets require a pulsed current of 300 A. For these pulse magnets, we use an energy-recovery-type pulse driver. We can change the optics using these pulsed quadrupole magnets and drivers.

However, the quadrupole magnet has a small aperture. It cannot be installed in the upstream section because of its large beam size; in particular, the positron primary electron beam has the largest beam size. Thus, we installed a new larger-aperture quadrupole magnet and high-power pulse driver. The magnet current was 600 A, and the required power was approximately four times higher than that of the old driver. In the summer of 2023, large-aperture quadrupole pulsed magnets were installed upstream of the linac. The power of the new pulse driver was 600 A at 400 V, which is an energy-recovery type. We achieved high efficiency with a simple pulse-width control. We intend to introduce this high-power and high-efficiency pulse driver.

INTRODUCTION

KEK has four storage rings for the electron/positron collider rings and two light source rings. The collider rings are the high-energy ring (HER) and the low-energy ring (LER), which are the SuperKEKB main rings [1]. The PF ring and PF-AR are light source rings. Table 1 lists the injection beam specifications for each ring. As the requirements of the beams were different, we changed the linac

acceleration conditions. We achieved simultaneous top-up injection of the four rings using two types of electron guns and several pulse magnets [2]. Figure 1 shows a schematic of the KEK electron/positron injector linac. We used a photocathode RF gun to generate the HER low-emittance electron beam. The required emittances were 40 and 20 mmrad in the horizontal and vertical directions, respectively. The other gun is a thermionic DC gun for the positron primary electron beam, which had a high charge of 10 nC per bunch. The DC gun is also used for the light source rings (PF and PF-AR). A positron beam is generated by hitting a tungsten target in a flux concentrator (FC) with primary electrons [3]. A damping ring was used to reduce the emittance of the positron beam. The damping ring was installed between Sectors 2 and 3, as shown in Fig. 1. In Sectors 3-5, all the quadrupole magnets (Q magnets) are pulsed magnets. Downstream of the damping ring, the transverse beam sizes were small in all modes; therefore, a pulsed Q magnet with a 20 mm aperture could be used. This small-aperture-type magnet is called the PM_32_4 type. The Q magnets in Sectors 3-5 were replaced by pulsed Q magnets in 2017 [4]. The inductance of the Q magnet was 1.0 mH, and the maximum pulse current was 330 A. The pulse driver raises a current within 3 msec at a voltage of 220 V. However, these pulsed Q magnets and pulse drivers cannot be used upstream of the injector because of the large positron primary beam size. In the bending sector (J-arc), we could not independently match the beams because the Q magnets were DC magnets.

Table 1: Specifications of Each Beam

Ring	Beam	Energy	Charge
HER	Electron	7.0 GeV	4.0 nC
LER	Positron	4.0 GeV	4.0 nC
PF ring	Electron	2.5 GeV	0.3 nC
PF-AR	Electron	6.5 or 5 GeV	0.3 nC

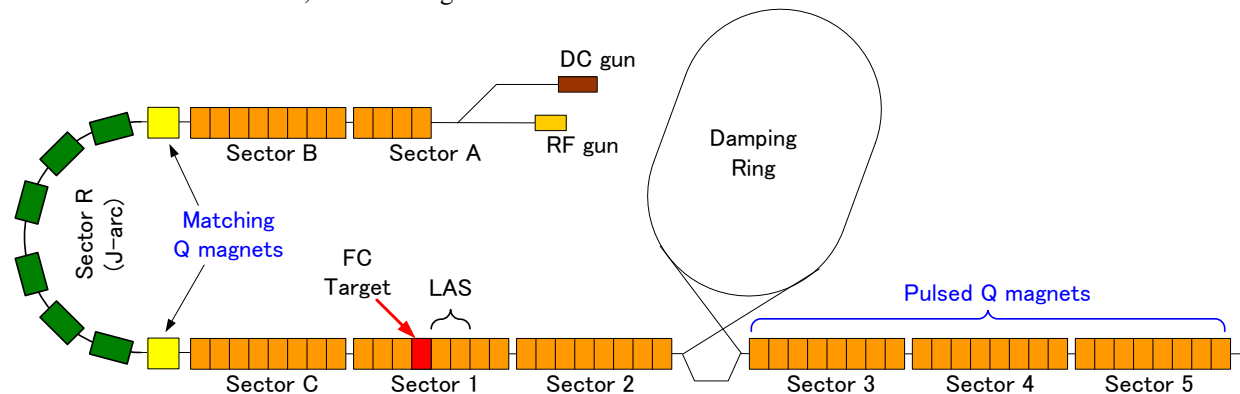


Figure 1: KEK injector linac consisting of eight acceleration sectors and a 180° bending sector. Sectors 3 to 5 have a pulsed Q magnet. The new large-aperture quadrupole magnets were installed in the summer of 2023 for matching.

[†] takuya.natsui@kek.jp

CIRCULAR MODES FOR LINACS*

Onur Gilanliogullari[†], Pavel Snopok, Illinois Institute of Technology, Chicago, IL, USA
Brahim Mustapha, Argonne National Laboratory, Lemont, IL, USA

Abstract

Circular mode beams are beams with non-zero angular momentum and strong inter-plane coupling. This coupling can be achieved in linear accelerators (linacs) through magnetization of electrons or ions at the source. Depending on the magnetization strength, the intrinsic eigenmode emittance ratio can be large, which produces intrinsic flatness. This flatness can either be converted to real space flatness or can be maintained as round coupled beam through the system. In this paper, we discuss rotation invariant designs that allow circular modes to be transported through the lattice while accelerating the beam and maintaining its circularity. We demonstrate that with rotation invariant designs the circularity of the mode can be preserved as round beam while maintaining intrinsic flatness to be converted to flat beam for high brightness or injected into a ring.

INTRODUCTION

Space charge effects at low energies are the limiting factor for achieving high-intensity high-quality beams. This limit originates from two sources. Firstly, the current limit due to extraction at the source. Secondly, the space charge limit due to self Coulomb repulsion force and charge density within the beam. Space charge forces are equivalent in the transverse plane when the beam is round. When the beam is flat, the quality parameters such as beam brightness and luminosity are enhanced due to small geometric beam size in one dimension. At the same time, flat beams can not maintain high currents due to space charge effect, which tends to equilibrate the beam sizes. Circular modes are round beams with intrinsic flatness and non-zero angular momentum as discussed in Refs. [1, 2].

Since space charge forces depend on the beam distribution in space, circular modes behave in a similar fashion to uncorrelated round beams while maintaining their intrinsic flatness.

Magnetized beams can also be classified as circular modes, where the beam experiences only one part of the solenoid's fringe field, which translates the canonical angular momentum to mechanical angular momentum. Extension of Bush's theorem discusses the angular momentum conversion from the magnetic field strength as discussed in Ref. [3].

In this paper, we will provide the background and define circular modes through coupling vectors. We will discuss formation of circular modes at the source and present rotational-invariant linac lattice designs.

* This work was supported by the U.S. Department of Energy, under Contract No. DE-AC02-06CH11357.

[†] ogilanli@hawk.iit.edu

CIRCULAR MODE OPTICS

Due to coupling, phase space vector parameterization is expressed through coupled optics as shown in Ref. [4]. Phase space vector, $\vec{z} = [x, x', y, y']^T$, can be written as

$$\vec{z} = \frac{1}{2}\sqrt{\epsilon_1}\vec{v}_1 e^{i\psi_1} + \frac{1}{2}\sqrt{\epsilon_2}\vec{v}_2 e^{i\psi_2} + c.c., \quad (1)$$

where $\epsilon_{1,2}$ are the eigenmode emittances, $\psi_{1,2}$ the betatron phases, *c.c.* stands for complex conjugate, and $\vec{v}_{1,2}$ are the eigenvectors given by

$$\vec{v}_1 = \begin{pmatrix} \frac{\sqrt{\beta_{1x}}}{i(1-u)+\alpha_{1x}} \\ \frac{\sqrt{\beta_{1x}} e^{i\psi_1}}{\sqrt{\beta_{1y}} e^{i\psi_1}} \\ -\frac{i u + \alpha_{1y}}{\sqrt{\beta_{1y}}} \end{pmatrix}, \quad \vec{v}_2 = \begin{pmatrix} \frac{\sqrt{\beta_{2x}} e^{i\psi_2}}{-i u + \alpha_{2x}} \\ \frac{\sqrt{\beta_{2x}}}{\sqrt{\beta_{2y}}} \\ -\frac{(1-u)i + \alpha_{2y}}{\sqrt{\beta_{2y}}} \end{pmatrix}. \quad (2)$$

Here $\beta_{1x}, \beta_{1y}, \beta_{2x}, \beta_{2y}$ are the coupled betatron functions, $\alpha_{1x}, \alpha_{1y}, \alpha_{2x}, \alpha_{2y}$ the alpha functions, u the strength of coupling and $\psi_{1,2}$ the phases of coupling. As mentioned earlier, circular mode beams are intrinsically flat, $\epsilon_2 \ll \epsilon_1$ with flatness ratio defined as $\mathcal{R} = \epsilon_1/\epsilon_2$. Due to intrinsic flatness, mode 2 contribution to phase space is small and the hase space vector can be written as

$$\begin{aligned} x &= \sqrt{\epsilon_1\beta_{1x}} \cos \psi_1, & y &= \sqrt{\epsilon_1\beta_{1y}} \cos(\psi_1 - \nu_1), \\ x' &= \sqrt{\frac{\epsilon_1}{\beta_{1x}}} (-\alpha_{1x} \cos \psi_1 - (1-u) \sin \psi_1) \\ y' &= \sqrt{\frac{\epsilon_1}{\beta_{1y}}} (-\alpha_{1y} \cos(\psi_1 - \nu_1) - u \sin(\psi_1 - \nu_1)). \end{aligned} \quad (3)$$

The phase of coupling determines the shapes of beam projections onto the different phase space planes. The projection onto real space is given by

$$\begin{aligned} \frac{x^2}{2\sigma_x^2} - \frac{2\tilde{\alpha}}{\sigma_x\sigma_y}xy + \frac{y^2}{2\sigma_y^2} &= 1 - \tilde{\alpha}^2, \\ \tilde{\alpha} &= \frac{\epsilon_1\sqrt{\beta_{1x}\beta_{1y}}\cos\nu_1 + \epsilon_2\sqrt{\beta_{2x}\beta_{2y}}\cos\nu_2}{\sqrt{\epsilon_1\beta_{1x} + \epsilon_2\beta_{2x}}\sqrt{\epsilon_1\beta_{1y} + \epsilon_2\beta_{2y}}}, \end{aligned} \quad (4)$$

where the beam distribution can be tilted in the (x, y) space. Disregarding mode 2 contribution will simplify the projection equation to

$$\frac{x^2}{2\sigma_x^2} - \frac{2xy}{\sigma_x\sigma_y} \cos \nu_1 + \frac{y^2}{2\sigma_y^2} = \sin^2 \nu_1. \quad (5)$$

In order to satisfy round beam condition, the phase of coupling needs to be $\pi/2$ and the optics functions, $\beta_{1x} = \beta_{1y} = \beta_0$. Furthermore, based on circular mode properties, the strength of coupling is determined to be $u = 1/2$. This leads to interesting relations, such as

DESIGN UPDATE OF THE POWER COUPLERS FOR THE SINGLE-SPOKE RESONATORS IN INSTITUTE FOR RARE ISOTOPE SCIENCE

J. Yoon*, Y.-W. Jo, Y. Jung, Y.-K. Kim

Institute for Rare Isotope Science, Daejeon, Republic of Korea

D. Cha, D.-K. Lee, Vitzro Nextech Co., Ltd., Ansan, Republic of Korea

Abstract

A heavy-ion accelerator facility was constructed for the Rare Isotope Science Project (RISP) at the Institute for Rare Isotope Science (IRIS) in Daejeon, Korea. A cryomodule with quarter-wave resonators (QWRs) and half-wave resonators (HWRs) was installed in the SCL (Superconducting Linac) 3 tunnel, and the initial beam commissioning using argon beams has been completed. Additionally, a cryomodule with single-spoke resonators (SSRs), power couplers, and tuners is currently under development for the SCL2 project. The geometry of the fundamental power couplers (FPCs) for the SSRs is a coaxial capacitive type based on a conventional 3-1/8 inch Electronic Industries Alliance (EIA) 50 Ω coaxial transmission line with a single ceramic window. A multi-physics analysis, incorporating electromagnetic, thermal, and mechanical aspects, was conducted to evaluate the design of the power coupler for the SSRs. This paper presents the results of the multi-physics analysis and the current design status of the power coupler for the SSRs.

INTRODUCTION

SCL2 consists of two cavity types, SSR1 and SSR2, with a resonant frequency of 325 MHz. The difference between SSR1 and SSR2 is the ratio of the particle's velocity to the speed of light, denoted as $\beta = v/c$, with values of 0.3 and 0.51, respectively. Additionally, the accelerating voltage differs, being 2.35 MV for SSR1 and 4.2 MV for SSR2. While the fundamental power coupler (FPC) for each cavity type must have different design characteristics, the FPC design for SSR1 and SSR2 can be the same due to their resonant frequency of 325 MHz; the main differences of the FPC are the required power and optimum external quality factor. In this study, we present the updated design of the FPC for 325 MHz SSRs at IRIS. The main parameters are listed in Table 1.

Table 1: Main Parameters of the FPC

Parameter	Value
Operating frequency	325 MHz
Reflection coefficient (FPC only at 325 MHz)	< -20 dB
Operating power (Nominal)	3 kW
Operating power (SSPA)	7 kW
Optimum external quality factor	5.2×10^6
Impedance of the vacuum section	90 Ω
Impedance of the air section	50 Ω

* foryjy12@ibs.re.kr

DESIGN UPDATE

To minimize the emission of electrons, the impedance had to be increased, which consequently reduced the diameter of the antenna (vacuum section) compared to a conventional 3-1/8-inch Electronic Industries Alliance (EIA) 50- Ω coaxial transmission line (TL). Figure 1 shows the difference between the previous design and the updated design.

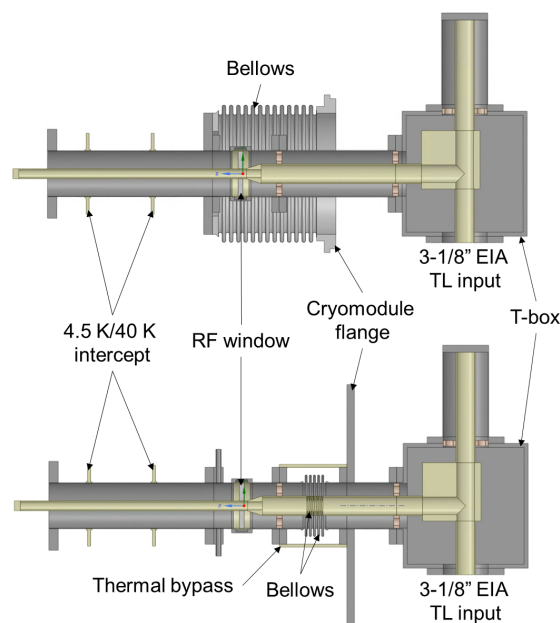


Figure 1: (top) Previous design and (bottom) updated design.

Since the dimensions of the inner conductor are the same in both cases, the results of the electromagnetic field analysis are also identical. The outer conductors are plated with 10 μm of copper, approximately three times the skin depth ($\delta_{Cu,325\text{MHz}} = 3.62 \mu\text{m}$). The T-box allows the supply of RF power to the power coupler via a coaxial transmission line and includes an inner conductor cooling line. The updated design features bellows on the outer and inner conductors within the cryomodule to protect the RF window from mechanical overload [1, 2].

This design allows for the addition of three pick-up ports to monitor arc discharge, electronic emission, and vacuum level variations, which helps prevent RF window breakage. To avoid dew point conditions on the RF window, two Kapton film heaters (maximum 25 W) are attached to the outer conductor on the RF window section to maintain room temperature.

PRELIMINARY DESIGN OF TRANSVERSE DEFLECTING STRUCTURE SYSTEMS FOR SHENZHEN SUPERCONDUCTING SOFT-X-RAY FREE ELECTRON LASER

Z. Li[†], J. Shao, Q. Huang, L. Wei, Institute of Advanced Science Facilities, Shenzhen, China
J. Yang, W. Zhang, Dalian Institute of Chemical Physics, CAS, Dalian, China

Abstract

Transverse Deflecting Structures (TDS) are commonly used in Free Electron Laser (FEL) facilities for the measurement of longitudinal information of electron beam, including bunch length, temporal distribution, slice emittance, etc. Shenzhen Superconducting Soft-X-ray Free Electron Laser (S³FEL) is a high-repetition-rate FEL recently proposed for scientific research and applications. In S³FEL, TDSs that work at S-band (2997.222 MHz) and X-band (11988.889 MHz) will be utilized for the diagnosis and analysis of longitudinal phase space of electron bunches along the beamline. In this manuscript, we present the preliminary design of both S-band and X-band TDS systems of S³FEL, including system layout, deflecting structures, pulse compressors, RF distribution networks, etc. Additionally, we introduce a new parallel-coupled TDS cavity with variable polarization for multi-dimensional phase space diagnostics.

IASF & S³FEL

Institute of Advanced Science Facilities, Shenzhen (IASF), founded in 2020, is a multi-disciplinary research institute responsible for Shenzhen's large-scale science facilities' whole life cycle planning, construction, operation, and maintenance. The Institute is located in Guangming District, which aims to be the science center of Shenzhen.

At this stage, two projects are being proposed: Shenzhen Innovation Light-source Facility (SILF), and Shenzhen Superconducting Soft X-ray Free Electron Laser (S³FEL) as shown in Fig. 1. Both are planning to be constructed in Guangming District, Shenzhen [1].



Figure 1: Architectural rendering of S³FEL.

S³FEL was approved in May, 2023, aiming to generate MHz-repetition-rate soft X-ray FEL using superconducting acceleration technology [2] at rates up to 1MHz (Fig. 2 and Table 1).

[†] lizongbin@mail.iasf.ac.cn

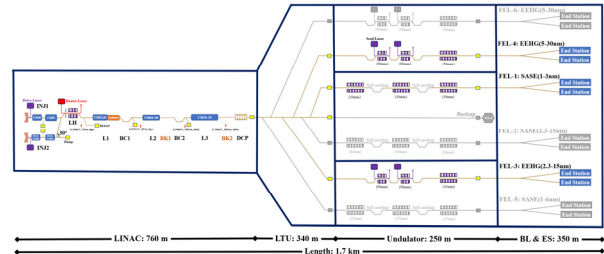


Figure 2: Layout of S³FEL.

Table 1: Main Parameters of S³FEL

Parameter	Unit	Value
Beam Energy	GeV	2.0~2.5
Charge	pC	100
Rep. Rate	MHz	1
FEL Wavelength	nm	1~30

TDS SYSTEMS OF S³FEL

Transverse Deflecting Structures (TDS) are designed for longitudinal and transverse phase-space diagnostics in S³FEL. The RF frequencies of TDS systems are decided according to bunch energy and bunch length. When bunch energy ≤ 300 MeV, S-band TDSs will be applied with an RF frequency of 2997.222 MHz. When bunch energy > 300 MeV, X-band TDSs will be used with a frequency of 11988.889 MHz. Totally 5 S-band TDS units and 5 X-band ones are considered as listed in Table 2.

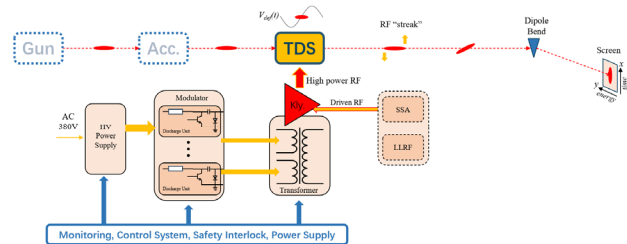


Figure 3: TDS system.

TDSs are powered by klystron as shown in Fig. 3. Each TDS unit contains TDS, waveguide network, klystron, modulator, HV power supply, etc.

X-band TDS

As mentioned above, the deflecting voltage of X-band TDSs should be no less than 24 MeV (@1 GeV bunch energy) and 48 MeV (@2.5 GeV bunch energy). A conventional LOLA-type TDS [3] scheme is being considered for now.

Limited by klystron technology and the budget, we take

DEVELOPMENT OF THE SUPERCONDUCTING HWR CAVITIES FOR NICA PROJECT

Z. H. Liang^{1,2†}, M. Xu^{1‡}, J. Y. Wang¹, C. L. Li¹, Q. T. Huang³, T. Tan¹, L. B. Liu¹, P. A. Xiang³,
S. X. Zhang¹, H. Guo¹, P. R. Xiong¹, Y. He¹

¹Institute of Modern Physics, Chinese Academy of Sciences, Lanzhou, China

²University of Chinese Academy of Sciences, Beijing, China

³Advanced Energy Science and Technology Guangdong Laboratory, Huizhou, China

Abstract

Nuclotron-based Ion Collider fAcility (NICA) is an accelerator complex under construction in JINR, in which superconducting linac-injector can accelerate protons up to 20 MeV and light ions to 7.5 MeV/u. To achieve this design target, a 325 MHz, $\beta = 0.21$ niobium half-wave resonator (HWR) called HWR1 was developed jointly by IMP and JINR. This paper optimizes the electromagnetic design of NICA cavity, designs the mechanical structure (including helium jacket) and gives the results of multi-physical studies. Simulation results show that $E_{pk}/E_{acc} = 5.88$, $B_{pk}/E_{acc} = 9.96$ mT/(MV/m). In addition, the niobium cavity has been fabricated and vertically tested, the magnetic shield and helium jacket are in the process of electron beam welding, and the cryomodule will be assembled in the next 1~2 months.

INTRODUCTION

The NICA project in Russia is a major scientific initiative focused on exploring the properties of dense nuclear matter. Located at the Joint Institute for Nuclear Research (JINR) in Dubna, NICA aims to recreate conditions similar to those of the early universe by colliding heavy ions at high energies. The facility consists of a complex of accelerators, including a superconducting synchrotron and two collider rings, designed to accelerate ions and polarized protons. The primary goal of NICA is to study the phase transitions between hadronic matter and quark-gluon plasma, providing insights into the fundamental forces governing particle interactions. Through its unique capabilities, NICA will play a critical role in advancing our understanding of strong interactions and the structure of matter under extreme conditions [1-4].

The existing linear injector LU20 has been in operation for 50 years and is now considered outdated. As a result, the superconducting linear accelerator LILac has been developed as a new injector [5-6]. The Institute of Modern Physics, Chinese Academy of Sciences (IMP, CAS), optimized the electromagnetic design of the HWR1 cavities within this superconducting linac, manufactured a prototype, and tested it.

CAVITY DESIGN

Electromagnetic Design

The design of the HWR1 seeks to achieve a balanced compromise between optimal RF performance, adequate mechanical properties, and ease of fabrication and surface preparation. The initial focus is on optimizing the RF properties of the HWR cavity, with the goal of minimizing heat load and maximizing the accelerating gradient. This is achieved by targeting a higher R/Q_0 (where R is the shunt impedance and Q_0 is the unloaded quality factor), a higher geometry factor (G), and lower peak surface fields (B_{pk}/E_{acc} and E_{pk}/E_{acc}) to avoid field emission.

To achieve these objectives, the HWR1 is designed with a taper-shaped inner conductor and a ring-shaped drift tube, which minimizes the peak surface fields. At the same time, the outer conductor is kept cylindrical to ensure ease of fabrication. Two rinsing ports are opened on each side to facilitate post-processing of the superconducting cavity. The thicker port on the outer conductor is the coupling port of the fundamental power coupler (FPC), and the thinner port on the opposite side is the signal extraction port.

The final optimized RF parameters of the cavity are presented in Table 1. And the cavity electromagnetic field distribution are presented in Fig. 1.

Table 1: RF Parameters of HWR1

Parameters	Value	Unit
Frequency	325	MHz
β_{opt}	0.21	
Beam Aperture	30.00	mm
G	59	ohm
R/Q	299.82	ohm
$L_{eff} (\beta\lambda)$	193.84	mm
E_{p}/E_{acc}	5.88	
B_{p}/E_{acc}	9.96	mT/(MV/m)
Cavity Diameter	194	mm
Cavity Height	471	mm

* Work supported by Chinese Academy of Sciences "The Development of High Stability Cryomodule [E129812YR0]", National Key R&D "Next generation heavy ion accelerator key components cooperation development [E01O591KJ0]".

† Email: liangzehua@impcas.ac.cn

‡ Corresponding author, Email: xumx@impcas.ac.cn

SUPERCONDUCTING $\beta=0.40$ HALF-WAVE CAVITY DESIGN FOR CiADS*

Z. H. Liang^{1,2†}, M. Xu^{1‡}, S. X. Zhang¹, L. B. Liu¹, J. Y. Wang¹, Y. M. Chu^{1,2,3}, H. Guo¹, T. C. Jiang¹, S. C. Huang¹, C. L. Li¹, P. A. Xiang³, Q. T. Huang³, P. R. Xiong¹, S. H. Liu¹, T. Tan¹, Z. J. Wang^{1,3}, F. F. Wang¹, Y. He¹

¹Institute of Modern Physics, Chinese Academy of Sciences, Lanzhou, China

²University of Chinese Academy of Sciences, Beijing, China

³Advanced Energy Science and Technology Guangdong Laboratory, Huizhou, China

Abstract

A 325 MHz, optimal $\beta = 0.40$ niobium half-wave resonator (HWR) called HWR040 for the superconducting driver linac of the China initiative Accelerator-Driven subcritical System (CiADS) has been designed and analyzed at the Institute of Modern Physics, Chinese Academy of Sciences (IMP, CAS). The linac requires 60 HWR040s to accelerate protons from 45 MeV to 175 MeV. This paper mainly presents a design scheme of HWR040 and a new method of aluminum-niobium composite with liquid helium partially immersed cavity. Meanwhile, electromagnetic field optimization, mechanical structure design and heat transfer simulation are carried out, to predict the behavior of the cavity under practical operating process.

INTRODUCTION

The CiADS is a major scientific infrastructure currently under construction in China. This system comprises three main components: a high-current, high-power superconducting proton linac working in continuous wave (CW) mode, a spallation target, and a subcritical reactor.

The proton beam generated by a proton source is transmitted through a low energy beam transport line, an RFQ, and a medium energy beam transport line before entering the superconducting acceleration section. This section consists of 9 HWR010s, 24 HWR019s, 60 HWR040s, 30 Ellip062s, and 28 Ellip082s cavities, capable of accelerating a 5 mA proton beam to 630 MeV. The HWR040s section cover an energy range of 45-175 MeV [1]. Given the high cost of cryogenic systems, for CiADS to achieve commercial viability, the low-beta superconducting sections will need to operate at 4.2 K. However, at this temperature, the superconducting cavities are inevitably affected by the vaporization of liquid helium and vibrations from the cryogenic system.

The bandwidth of the superconducting cavity generally in the range of a few hundred hertz. Any deformations caused by various disturbances can lead to frequency shifts, or cavity detuning. If the detuning is significant and over the bandwidth of the cavity, it can cause a notable decrease in RF power delivery efficiency and may also

increase beam energy spread, leading to operational instability of the superconducting cavities.

When low-beta cavities operating in CW mode, frequency detuning due to Lorentz forces does not vary over time, making pressure fluctuations in the helium the primary factor affecting the stability of the cavity operation. While tuners can partially compensate for frequency shifts caused by helium pressure fluctuations, frequent tuner motor movements can introduce issues such as electromechanical resonance. Therefore, it is essential to enhance the mechanical stability of the HWR, through reducing their helium pressure sensitivity coefficient to ensure that pressure fluctuations do not affect the stable operation of the cavities under the current cryogenic system conditions [2].

This paper proposes a method to solve these issues by optimizing the electromagnetic design and utilizing an aluminum casting technique to modify the surface morphology of the superconducting cavity in contact with liquid helium. Based on this new concept, the Al/Nb composite HWR040 has been designed.

ELECTROMAGNETIC DESIGN

Layout of RF Design

Due to their complex structure, low and medium beta superconducting cavities are prone to field emission even after BCP surface treatment, particularly when the surface peak electric field (Epk) exceeds 30 MV/m. At the same time, to meet the requirements specified by the accelerator physics design, the operating Epk for the 325 MHz HWR040 cavity has been set at 28 MV/m. This cavity was designed and optimized using CST Studio Suite [3].

The electromagnetic design focused on minimizing the Epk/Eacc and Bpeak/Eacc while maximizing (R/Q)*G as much as possible. To achieve this, the inner conductor of the HWR040 was designed with a Tapper-type featuring a larger opening. The main coupling port is located on the sidewall of the cavity, and four cleaning ports are positioned on the upper and lower end caps respectively, allowing high-pressure rinsing (HPR) water pipes to extend deep into the cavity without significantly affecting the electromagnetic field distribution. This ensures that the inner surface of the cavity can be thoroughly cleaned during the HPR process. The cavity vacuum model and electromagnetic field distribution are presented in Fig. 1.

And Fig. 2 shows the transit time factor (TTF) curve of this cavity. Table 1 lists the main RF parameters of this cavity.

* Work supported by Chinese Academy of Sciences "The Development of High Stability Cryomodule [E129812YR0]", and the Large Research Infrastructures "China initiative Accelerator Driven System [2017-000052-75-01-000590]".

† Email: liangzehua@impcas.ac.cn

‡ Corresponding author, Email: xumx@impcas.ac.cn

MAXIMUM ENTROPY PHASE SPACE TOMOGRAPHY UNDER NONLINEAR BEAM TRANSPORT

L. W. Liu^{*1,2,3}, Z. J. Wang^{1,2,3}, J. C. Wong^{1,2,3}, Y. Du^{1,2,3}, T. Zhang^{1,2,3}, H. Y. Zhou^{1,2,3}, B. H. Ma^{1,2,3},
C. G. Su^{1,2,3}, M. Yi³, L. Y. Gong^{1,2}, T. Y. Li^{1,2,3}, T. L. Wang^{1,2,3}, Y. M. Chu^{1,2,3}

¹Institute of Modern Physics, Chinese Academy of Sciences, Lanzhou, China

²University of Chinese Academy of Sciences, Beijing, China

³Advanced Energy Science and Technology Guangdong Laboratory, Huizhou, China

Abstract

Obtaining the complete distribution of a beam in high-dimensional phase space is crucial for predicting and controlling beam evolution. Previous studies on tomographic phase space reconstruction often required linear beam optics in the relevant transport section. In this paper, we show that the method of maximum entropy tomography can be generalized to incorporate nonlinear transformations, thereby widening its scope to the case of nonlinear beam transport. The improved method is verified using simulation results and potential applications are discussed.

INTRUDUCTION

Tomography is a general term for the reconstruction of a high-dimensional distribution using multiple low-dimensional profiles. The maximum entropy tomography is to select the high-dimensional distribution with the maximum information entropy as the reconstruction solution under the premise of satisfying the profiles. One characteristic of this method compared with other tomography methods is that it can clearly identify the most suitable solution according to the principle of maximum entropy. A detailed discussion of maximum entropy theory can be found in Ref. [1]. The previous use of the entropy-maximum tomography method to reconstruct the four-dimensional phase space distribution using two-dimensional profiles is the Ref. [2]. In this paper, we extend the application of entropy maximum tomography to nonlinear situation, so that our reconstruction is no longer limited by the mapping relationship between the directions where the profiles are located, and can accept the profiles without an upper limit of number. The position of the measured profile is called the measurement point, and the position of the reconstructed result is called the reconstructed point. In the following part of this paper, we discuss the entropy-maximum tomography when the mapping between the distribution of reconstructed points and the distribution of measured points is nonlinear. In the part of simulation verification, we take the beam from the reconstructed point to the measurement point through a sextupole with adjustable intensity as an example, and use 12 two-dimensional profiles of the measurement point to reconstruct the four-dimensional distribution of the reconstructed

point position. This work will certainly help to control the motion state of the beam in the accelerator [3].

NONLINEAR MAXIMUM ENTROPY TOMOGRAPHY

For a four-dimensional distribution $\rho(x, x', y, y')$ to be solved, its information entropy $H[\rho]$ is in the form Eq. (1). Here we use the same form of four-dimensional information entropy as in Ref. [2].

$$H[\rho] = - \iiint \rho(x, x', y, y') \ln \rho(x, x', y, y') dx dx' dy dy' \quad (1)$$

The j -th of the n profiles measured is denoted as $g(u_j, u'_j)$, which is a projection of the four-dimensional distribution $\rho(u_j, u'_j, v_j, v'_j)$ on a two-dimensional plane (u_j, u'_j) and should satisfy the constraint condition Eq. (2).

$$G_j = g(u_j, u'_j) - \iint \rho(f_j(x, x', y, y')) dv_j dv'_j \quad (2)$$

The f_j in Eq. (2) represents the mapping from four-dimensional space (x, x', y, y') to four-dimensional space (u_j, u'_j, v_j, v'_j) . This is a generalized mapping, which can take any form that can be determined. (u_j, u'_j, v_j, v'_j) is an orthogonal four-dimensional space composed of the two axes of the plane in which we measure the j -th projection and the other two axes that are orthogonal to them.

Create a new function $K[\rho]$ with n Lagrange multipliers λ , where n is the number of constraints.

$$K[\rho] = H[\rho] + \sum_{j=1}^n \iint \lambda(u_j, u'_j) G_j[\rho] du_j du'_j \quad (3)$$

The ρ that maximizes $H[\rho]$ is denoted by ρ^* , and when ρ is ρ^* , the partial derivative of $H[\rho]$ with respect to ρ needs to be 0.

$$\frac{\partial K[\rho]}{\partial \rho} = - \iiint \left(\ln \rho^* + 1 + \sum_{j=1}^n \lambda(u_j, u'_j) \right) dx dx' dy dy' \quad (4)$$

From Eq. (4), we can write the form of the solution for ρ^* . We can know that it is a four-dimensional function composed of n two-dimensional functions multiplied together, and the plane in which these two-dimensional functions reside each corresponds to a different plane in which the projection resides. We can rewrite it as Eq. (5). Where C is some constant that we don't care about when we only take the

* liuliwen@impcas.ac.cn

A COMPARISON OF RMS MOMENTS AND STATISTICAL DIVERGENCES AS WAYS TO QUANTIFY THE DIFFERENCE BETWEEN BEAM PHASE SPACE DISTRIBUTIONS

Y. Du^{*,1,2,3}, Z. J. Wang^{1,2,3}, J. C. Wong^{1,2,3}, L. W. Liu^{1,2,3}, C. G. Su^{1,2,3}, M. Yi³, L. Y. Gong^{1,2}, T. Zhang^{1,2,3}, H. Y. Zhou^{1,2,3}, B. H. Ma^{1,2,3}, Y. M. Chu^{1,2,3}, T. Y. Li^{1,2,3}, T. L. Wang^{1,2,3}

¹Institute of Modern Physics, Chinese Academy of Sciences, Lanzhou, China

²University of Chinese Academy of Sciences, Beijing, China

³Advanced Energy Science and Technology Guangdong Laboratory, Huizhou, China

Abstract

Accurately assessing the difference between two beam distributions in high-dimensional phase space is crucial for interpreting experimental or simulation results. In this paper, we compare the common method of RMS moments and mismatch factors, and the method of statistical divergences that give the total contribution of differences at all points. We first show that, in the case of commonly used initial distributions, there is a one-to-one correspondence between mismatch factors and statistical divergences. This enables us to show how the values of several popular divergences vary with the mismatch factors, independent of the orientation of the phase space ellipsoid. We utilize these results to propose evaluation standards for these popular divergences, which will help interpret their values in the context of beam phase space distributions.

INTRODUCTION

In the research fields of beam transport line design, beam diagnostics, phase space tomography and so on, accurately assessing the difference between two beam distributions in high-dimensional phase space is crucial for interpreting experimental or simulation results [1–3]. A common approach to quantify these differences is through the use of RMS moments and mismatch factor, which gauges the overlap of RMS boundaries [4]. Another more detailed approach is to use statistical divergences, which give the total contribution of differences at all points, commonly including: Kullback-Leibler divergence, Jensen-Shannon divergence, Total Variation distance, Hellinger distance, collectively referred to as f-divergence [5–9]. This paper compares these two different methods, aiming to find the connection between them.

BASIC TERMS

RMS Moments and Mismatch Factor

Considering a beam distribution centered at the origin of the (x, x') phase space, if we conduct RMS statistics on it, we can obtain the following covariance matrix:

$$\Sigma = \begin{pmatrix} \langle xx \rangle & \langle xx' \rangle \\ \langle x'x \rangle & \langle x'x' \rangle \end{pmatrix}. \quad (1)$$

* duyuu@impcas.ac.cn

This is a symmetric matrix constituted by four second-order moments. Each Σ corresponds to a quadratic form RMS phase ellipse equation

$$\mathbf{x}^T \Sigma^{-1} \mathbf{x} = 1, \quad (2)$$

where $\mathbf{x} = (x, x')^T$ is the 2D phase space coordinates of the beam.

The mismatch factor measures the difference between two ellipses in phase space that have the same center and area but do not completely overlap. They both have the form of Eq. (2) and share the same RMS emittance. If one ellipse can exactly enclose the other after being scaled by a certain proportion, then the mismatch factor is defined as the value of this scaling factor minus 1. The commonly used calculation formula is as follows [10]:

$$M = \left[1 + \frac{\Delta + \sqrt{\Delta(\Delta + 4)}}{2} \right]^{1/2} - 1, \quad (3)$$

where

$$\Delta = \Delta\alpha^2 - \Delta\beta\Delta\gamma, \quad (4)$$

with $\Delta\alpha$, $\Delta\beta$ and $\Delta\gamma$ being the differences in Twiss parameters between the two phase ellipses.

f-Divergence

The f-divergence is a class of methods used to measure the difference between two probability distributions, defined as follows (1D):

$$D_f[p(x)||q(x)] = \int q(x) f\left[\frac{p(x)}{q(x)}\right] dx; \quad (5)$$

where $p(x)$ and $q(x)$ are the probability density functions of two distributions. $f(\cdot)$ is a convex function and satisfies $f(1) = 0$. Different $f(\cdot)$ correspond to different statistical divergences. This paper selects four popular divergences to study the beam distribution, with corresponding forms and calculation formulas are shown in Table 1.

THE RELATIONSHIP BETWEEN MISMATCH FACTOR AND F-DIVERGENCE

Theorem 1 *In 2D phase space, there is a one-to-one correspondence between the f-divergence and the mismatch factor for two beam distributions with elliptical symmetry.*

DEVELOPMENT OF AN X-BAND LLRF PROTOTYPE FOR THE EUPRAXIA@SPARC_LAB LINAC*

P. D. Meruga^{†1}, B. Baričević, M. Cargnelutti, Instrumentation Technologies, Solkan, Slovenia
 L. Piersanti, M. Bellaveglia, B. Serenellini, INFN - Laboratori Nazionali di Frascati, Frascati, Italy
 A. Mostacci, Sapienza University of Rome, Rome, Italy
¹also at Sapienza University of Rome, Rome, Italy

Abstract

EuPRAXIA stands for “European Plasma Research Accelerator with eXcellence In Applications”. It's a next generation free-electron laser (FEL) aimed at developing a compact, cost-effective particle accelerator based on novel wake-field accelerator technology. Traditionally, high-energy physics requires higher acceleration voltages, so developing the X-band acceleration technology, enables the possibility to achieve high gradients with very compact structures. The EuPRAXIA LINAC injector comprises one S-Band and two X-Band sections, achieving a max beam energy of 1 GeV. Low-Level Radio Frequency (LLRF) systems are crucial for RF station synchronization and machine stability at femtosecond precision. Currently, there are no commercially available X-band LLRF solutions, especially for pulse processing and control in the 100 ns range. This project aims to develop an X-band LLRF prototype, in collaboration with INFN, tailored to meet EuPRAXIA@SPARC_LAB LINAC's demands. Once confirmed on a real testbench, the prototype will be used as a starting point for the industrialization into a commercial instrument. This paper presents the architecture and preliminary results of the prototype.

INTRODUCTION

In recent years, the field of particle accelerators has witnessed significant advancements, driven by the need for compact, cost-effective, and high-performance systems. Among these innovations, the EuPRAXIA (European Plasma Research Accelerator with eXcellence In Applications) project stands out as a pivotal initiative aiming to develop the world's first compact accelerator based on plasma technology [1]. Within this framework, the SPARC_LAB LINAC (Sorgente Pulsata e Amplificata di Radiazione Coerente_Laboratori Nazionali di Frascati Linear Accelerator) plays a crucial role.

The EuPRAXIA SPARC_LAB LINAC, housed at the INFN-LNF (Istituto Nazionale di Fisica Nucleare - Laboratori Nazionali di Frascati) in Italy, is designed to serve as a testbed for advanced acceleration techniques and beam manipulation. Figure 1 shows the machine layout of the SPARC_LAB LINAC combining the conventional radio-frequency (RF) linear acceleration that includes 1 S-band RF gun, 4 S-band and 16 X-band RF structures with state-

of-the-art plasma acceleration, aiming to achieve unprecedented beam quality and energy efficiency.

The integration of these technologies is expected to address some of the fundamental limitations of traditional accelerators, such as size, cost, and energy consumption.

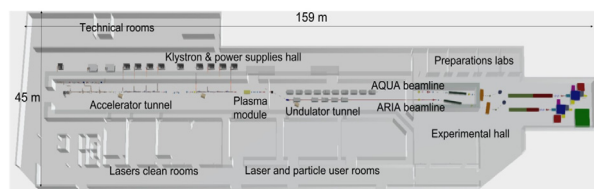


Figure 1: EuPRAXIA@SPARC_LAB machine layout [2].

A key component of this innovative system is the development of the X-Band Low-Level Radio Frequency (LLRF) system. The X-Band LLRF system is crucial for precise control of the accelerating fields, ensuring stability and high performance of the electron beam. Operating at higher frequencies than traditional S-Band systems, the X-Band technology offers significant advantages in terms of reduced accelerator size and enhanced accelerating voltage gradients in the order of 60 MV/m. This development is instrumental in achieving the compact and efficient design goals set by the EuPRAXIA project.

This paper provides a comprehensive overview of the EuPRAXIA X-band LLRF prototype requirements, detailing the architecture of the prototype, the realization of the prototype which includes the development and assembly. The results from initial experimental runs, highlighting the prototype's front-end performance in terms of amplitude and phase stability are presented.

Requirements

The below Table 1 describes the EuPRAXIA X-band LLRF prototype requirements that provides the input and the starting point towards the development of the prototype. The main requirements are the prototype operates in pulsed mode at a carrier frequency of 11.994 GHz, with a master oscillator input level of 0 dBm. It utilizes pulse length of 100 ns and a greater than equal to 250 MHz sampling rate for precise control and signal processing. The front-end should handle the input levels up to +20 dBm and require a bandwidth greater than 20 MHz to process the 100 ns pulses. The back-end should provide output level at +10 dBm with a rise time of 10-12 ns, maintaining signal integrity. The system should have a low added amplitude noise (0.01-0.05% RMS) and phase noise (0.01-0.015 degrees RMS) over 400 pulses, ensuring high signal fidelity. With two RF input channels and one RF output channel, an

* This project has received funding from the European Commission Horizon Europe Research and Innovation Programme under Grant Agreement no. 101073480 and the UKRI guarantee funds.

[†] phanideep.meruga@i-tech.si

TUNING OF ESS DTLs

C. Baltador[†], A. Palmieri, F. Grespan, A. Pisent
INFN – LNL Legnaro, Italy

Abstract

The normal conducting part of ESS LINAC in Lund (Sweden) uses 5 DTL cavities, provided by INFN LNL as in-kind partner, to accelerate 60 mA proton beam from 3.62 MeV to 90 MeV. DTL1 have been tuned, installed in the accelerator tunnel and RF conditioned in 2021-2022, DTL2, 3 and 4 in 2022-2023, while DTL5 has been tuned and installed in summer 2023, but not yet conditioned. All the DTLs were equipped with tuning elements like tuners and post couplers (PCs), but the challenges experienced during the tuning of DTL1 has resulted in a change of tuning strategy, which effectively reduced the timeframe to tune the other cavities from months to days. The aim of this paper is to give an overview of the achieved results of tuning procedure performed on the DTLs.

INTRODUCTION

European Spallation Source (ESS) [1] is a proton linac driven neutron source, under construction in Lund, Sweden. The last section of the normal-conducting part of the linac feature a drift-tube linac (DTL), composed by five tanks, provided by INFN LNL [2]. DTL tanks are composed by 4 stainless steel modules. Drift tubes (DTs) are distributed along the tank, hold in place by vertical stems.

All DTL components suffer of mechanical tolerances and despite the use of sophisticated alignment instrumentation, like laser trackers, relative alignment cannot be perfect. These mechanical imperfections, which can also be enhanced by thermal effects, cause random local change in the capacitance of the DTL cells, moving the accelerating field away from the reference one, defined to be the same through all the gaps. To ensure optimal performance and accurate acceleration of the beam to match the desired beam dynamics, these perturbations must be compensated with a proper tuning of the cavity.

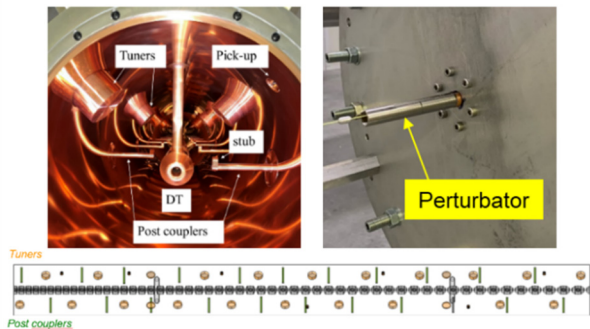


Figure 1: Internal view of one DTL tank (left). A metallic cylinder inserted in the last cell of the DTL to perturb the cavity (right). Tuners and PCs distribution along the DTL Tank (down).

[†] carlo.baltador@lnl.infn.it

To tune the cavity, DTL tanks feature accordable elements (see left hand side of Fig. 1):

- **Tuners:** make the cavity resonate at the correct frequency
- **Post couplers (PCs):** stabilize the field with respect to sources of local frequency detuning [3].
- **Stubs:** placed at PC tips make the accelerating field uniform along the tank length.

In the case of ESS DTL, the number of tuners and PCs are summarized Table 1. Note that the number of PCs of Tanks 1 and 2 don't match the number of DTs: the number of PCs was chosen following a criterion of a sufficient number of post couplers per metre [4].

Table 1: Main Tank Parameters

Tank	DTs	Tuners	PCs	E_0 [MV/m]
1	60	26	24	3.00
2	33	26	17	3.16
3	28	26	28	3.07
4	26	26	25	3.04
5	22	26	22	3.13

FIELD MEASUREMENT

The measurement of the accelerating field in the cavity is carried out with usual bead pulling technique: by inserting a small diamagnetic bead, a volume change ΔV (perturbation) of the cavity is induced, which shifts the resonant frequency ω_0 . The bead can be driven through all the gaps of the DTL with a dielectric (nylon) wire, whose path is guided by a series of pulleys and moved by an electric motor. For ESS DTLs, a fishing line and an aluminium bead were used.

By using a Vectorial Network Analyzer (VNA) to drive low RF power into the cavity, frequency is locked and a phase shift $\Delta\phi$ rather than a frequency shift are recorded. The two are related by the relation:

$$\Delta\phi = -\tan^{-1} \left[Q_L \left(\frac{\omega_0}{\omega_0^*} - \frac{\omega_0^*}{\omega_0} \right) \right], \quad (1)$$

where ω_0^* is the frequency with the bead and Q_L is the 'loaded' Q of the cavity. Bead perturbation is cancelled inside the DTs, giving a profile with peaks at the gaps and valleys in the DTs. It is then possible to derive the E_z field from the phase shift thanks to the Slater perturbation theorem [5].

By integrating the obtained E_z field over the gap length L , the accelerating field E_0 is obtained for each gap:

$$E_{0i} = \frac{1}{L_i} \int_0^{L_i} E_z(z) dz. \quad (2)$$

To reduce the noise coming from the measurements, it is possible to integrate over the length l of the bead, using the peakfield method [6], which uses the theoretical field

INFN LASA IN-KIND CONTRIBUTION TO ESS ERIC PROJECT

D. Sertore*, M. Bertucci, A. Bosotti, E. Del Core, F. Fiorina, L. Monaco, R. Paparella, P. Spruzzola
 INFN Milano - LASA, Segrate, Italy
 C. Pagani¹, Università degli Studi di Milano, Segrate, Italy
¹also at INFN Milano - LASA, Segrate, Italy

Abstract

INFN Milano - LASA recently concluded its in-kind contribution to European Spallation Source Eric, providing the 36 Superconducting Medium Beta cavities that will allow boosting the proton beam energy from 216 MeV to 571 MeV. The performances of the last four cavities, treated with Electro-Polishing as main processing step, are presented and compared with the results obtained on the remaining cavities treated with Buffered Chemical Polishing. The overall performance of the delivered cavities and lessons learned during the cavities production stages are also discussed.

INTRODUCTION

INFN Milano - LASA has taken on the responsibility of the Italian In-Kind contribution to the European Spallation Source (ESS) ERIC, specifically in the development of the Superconducting (SC) Medium Beta Cavities. We have developed the electromagnetic design for these cavities, optimizing it with consideration of mechanical requirements, industrial feasibility, and adherence to the ESS interface requests. The importance of this last point should not be underestimated, as it has been instrumental in ensuring a seamless assembly of the cavities in their cryomodule at CEA Saclay. The key parameters of the INFN Medium Beta cavities are summarized in Table 1.

Table 1: ESS Medium Beta Cavities Main Parameters

Parameter	Value
R_{iris}	50 mm
Geometrical β	0.67
π -mode Frequency	704.42 MHz
Acc. length	0.855 m
Cell-to-cell coupling k	1.55 %
π - $5\pi/6$ mode sep.	0.70 MHz
Geometrical factor G	198.8 Ω
Optimum beta, β_{opt}	0.705
Max R/Q at β_{opt}	374 Ω
E_{acc} at β_{opt}	16.7 MV/m
E_{peak}/E_{acc}	2.55
E_{peak}	42.6 MV/m
B_{peak}/E_{acc}	4.95 $\frac{mT}{MV/m}$
Q_0 at nominal gradient	$>5 \times 10^9$
Q_{ext}	7.8×10^5

In the SC linac, the Medium Beta ($\beta=0.67$) cavities will intercept the 62.5 mA proton beam from the Spoke section

* daniele.sertore@mi.infn.it

(256 MeV) and accelerate it to 571 MeV, preparing it for injection into the High Beta cryomodules. These modules will then boost the beam to its final energy of 2 GeV.

The 5 MW average power proton beam will operate in pulse mode at 14 Hz, with each pulse lasting 2.86 ms. The long beam pulse operation was a significant factor in the project decision to use superconducting cavities, as it allows us to achieve the project parameters while maintaining cost-effectiveness. Furthermore, there is a pressing need to operate the cavities at a high accelerating gradient to attain the required energy within the projected accelerator footprint. Upon reaching the target station, the proton beam will generate a neutron beam through the spallation process [1]. Once operational, the European Spallation Source ERIC is set to become the world's most intense neutron source [2].

This paper provides an update on the status of cavity production, with a particular focus on the recovery actions undertaken to qualify cavities that were initially performing below expectations, incorporating lessons learned during the recovery process.

CAVITY PRODUCTION AND TESTING

The ESS Medium Beta cavities production is based on the “build to print” schema inherited from our previous work for European XFEL SRF cavities [3, 4]. To ensure high quality, strict guidelines for cavity production and a comprehensive Quality Control and Quality Assurance plan are enforced during the entire cavity production process [5].

Based on the ESS requirements, we have chosen to treat the cavities using a Buffered Chemical Polishing (BCP) process, both in bulk and as a final treatment. The final treatment, known as the “Final BCP”, is part of the cavity preparation necessary to assemble the cavity before the Vertical Test at cryogenic temperatures, required for cavity qualification. To accommodate the high cavity delivery rate required by the project, most of the qualification tests were conducted at DESY, utilizing the AMTF infrastructure [6].

However, for specific cavities, we utilized the LASA infrastructure, which is not able to sustain the series test rate but is equipped with advanced diagnostic tools capable of identifying quench and field emission sources that could potentially limit the cavity performance [7].

A total of thirty-two cavities met ESS specifications, while the last four, with lower performance, were accepted by the project and installed in the first cryomodule, where beam matching from the Spoke section to the elliptical section requires less demanding acceleration fields. All the cavities were subsequently integrated into cryomodules at CEA

RF AND MULTIPACTING ANALYSIS OF THE HIGH-POWER COUPLERS OF IFMIF/EVEDA RFQ AND ESS DTL

F. Grespan, C. Baltador, L. Bellan, M. Campostrini, M. Comunian, E. Fagotti, L. Ferrari, A. Palmieri, A. Pisent, C. Roncolato, INFN- LNL, Legnaro, Italy
 D. Nicosia, L. Page, R. Zeng, ESS, Lund, Sweden
 L. Y. Gong, IMP, Chinese Academy of Sciences, Lanzhou, China
 F. Cismondi, F. Scantaburlo, IFMIF/EVEDA Project Team, Rokkasho, Japan
 A. De Franco, QST, Rokkasho, Japan
 H. Kobayashi, KEK, Tsukuba, Japan

Abstract

The performances and failure cases of the power couplers of the IFMIF/EVEDA RFQ and ESS DTLs have been analysed with dedicated high-power test campaigns and Multi-Pacting (MP) simulation methods. The paper presents test and simulation methodology, results, and inputs for the next activities.

INTRODUCTION

IFMIF/EVEDA RFQ power couplers

Eight tetrode RF amplifiers at 175 MHz - numbered 1A...4A, 1B ... 4B - feed the IFMIF/EVEDA RFQ [1] for 1.6 MW total power capability. The net power need is $P_{TOT}[1.3MW] = P_{cav}[650kW] + P_{beam}[650kW]$. Beam performances in pulsed mode have been demonstrated in 2019 [2]. In RF conditioning beam loading is absent, so each coupler operates with $P_{REV} \approx 13\%$. The couplers (Fig. 1) are coaxial magnetically coupled loops, without bias. A coaxial planar alumina window separates vacuum from air, vacuum sealing being provided by Viton O-rings. The impedance matching between window and line is given by reducing the inner conductor radius. RF windows are coated with 1.5 -3 nm TiN layer. The alumina is not directly water cooled. The couplers have been designed and tested on a test cavity at full power (200 kW-CW) at INFN-LNL in 2015 [3].

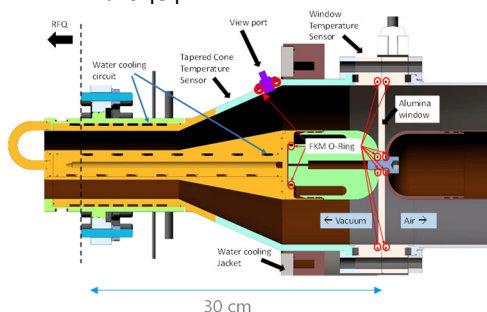


Figure 1: Sketch of the IFMIF coupler. The diagnostics and the positions of Viton O-ring are shown.

During RFQ RF conditioning operations toward CW [4] (2019-2023), 5 of the 8 couplers showed anomalous temperature increases of the external conductors. Two improvements of cooling capability have been implemented: in 2019 water jackets were applied on the external conductor. In 2023 the inner conductor cooling was improved, after

finding O-rings melted, once reached 60% average power. In the same inspection the alumina was found coloured, as well as the copper inner conductor (Fig. 2). Nonetheless, in November 2023, after reaching 25% average power, a vacuum leak occurred again.

An experimental and theoretical analysis of the electron activity in the couplers was carried out to clarify the power heat source capable to heat the O-ring at melting temperature (180°C).

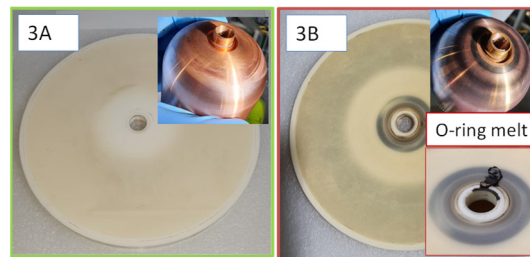


Figure 2: Status of "cold" (left) and "hot" (right) coupler.

ESS DTL's Power Couplers

One 2.9 MW klystron at 4% duty cycle feeds each of the 5 DTLs (352 MHz). The net power need is $P_{TOT}[2.2MW] = P_{cav}[1.1MW] + P_{beam}[1.1MW]$, coupled to the cavity by 2 iris couplers placed on the bottom of the DTLs. The air-vacuum separation between cavity and wave guide is provided by a pillbox-type alumina RF window, water cooled and coated with 2 nm TiN layer. Windows are connected to the coupler box with a WR2300 HH flange (Fig. 3). The windows have 2 view ports (air and vacuum sides). The sealing between the RF window and coupler box is an EPDM gasket, without RF joint protections. The RF windows were tested to full power in 2020.

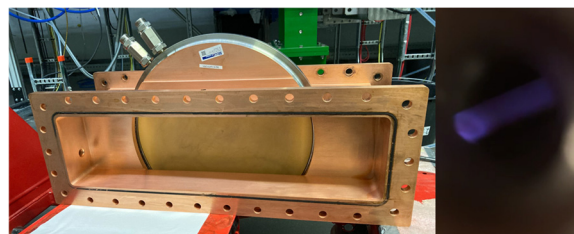


Figure 3: One of the ESS DTL RF windows. Brown coloration melted O-ring and light is shown.

In 2023 DTL1-2-3-4 started high power RF operation at ESS Lund, reaching full performances [5]. But, after 6 weeks of operations, light started on both vacuum and air

ESS DTL: FINAL INSTALLATION AND FIRST COMMISSIONING RESULTS UP TO 74 MeV

F. Grespan^{†,1}, C. Baltador, L. Bellan, M. Comunian, M. Montis, A. Palmieri, A. Pisent
INFN-LNL, Legnaro, Italy

T. Bencivenga, P. Mereu, C. Mingioni, M. Nenni, E. Nicoletti, INFN-Torino, Torino, Italy
B. Jones, Y. Levinsen, R. Miyamoto, N. Milas, L. Page, C. Plostinar, R. Zeng, ESS, Lund, Sweden
¹also at ESS, Lund Sweden

Abstract

The Drift Tube Linac (DTL) for the European Spallation Source (ESS ERIC) will accelerate proton beam up to 62.5mA peak current from 3.62 to 90 MeV. The 5 cavities are now fully installed and tested in the linac tunnel. Moreover, in 2023 DTL1 to DTL4 have been RF conditioned to full power and beam commissioned with max peak current at short pulses. Relevant results of these activities are presented in this paper.

INTRODUCTION

Status of Installation.

A total of 5 cavities of the Drift Tube Linac (DTL5) for the European Spallation Source (ESS ERIC) were installed in September 2023 (Fig. 1), following completion of beam commissioning at 74 MeV [1]. Tests were undertaken for vacuum leaks, alignment, and the RF parameters were validated. The assembly of RF windows and power couplers was completed in May 2024, after the high-power tests reported in Ref. [2]. The DTL5 is now connected to the cooling skid and ready for a series of integrated tests scheduled before high power conditioning in November 2024.

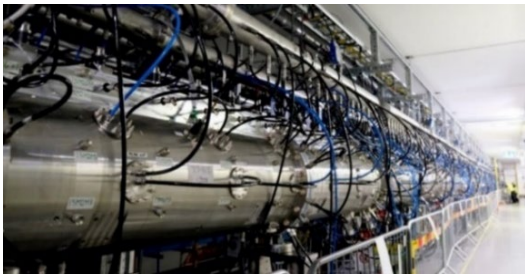


Figure 1: The 5 DTLs now installed in the ESS tunnel.

DTL5 comprises 23 cells, i.e., 22 drift tubes (DTs). The installation of DTs on the modules and module-to-module assembly follows the sequence described in Ref. [3]. Each assembly step is monitored with a laser tracker and leak tested. The total DT transverse errors specifications are ± 0.1 mm, and take into account the machining errors of DTs and girders, and the positioning errors of DTs in the modules, the PMQs inside DTs and module-module alignment. Transverse PMQ alignment is within specifications (± 0.1 mm) with the only exception of the high energy end plate. Longitudinally, the maximum gap-gap error is $< \pm 0.3$ mm, with the corresponding phase errors within the tolerance (< 0.5 deg). The process of tuning and stabilization

with Post Couplers (PCs) equipped with stubs is extensively described in Ref. [4]. The adjustable aluminium tuners and PCs are replaced with machined copper parts and cavity parameters are recorded (Table 1, Fig. 2).

Table 1: DTL5 RF Parameters (VNA Measurements)

	Parameters	Design	Measured
DTL5	Freq. [MHz]	352.21	352.266 (in vacuum, no RF power, 18°C)
	Coupl. factor [β]	1.84	1.95
	Q0 (SFish/1.25)	43415	43307
	E0 flatness [%]	± 2	± 1.15
	Tilt.Sens.	N.A.	± 4.5 %/MHz

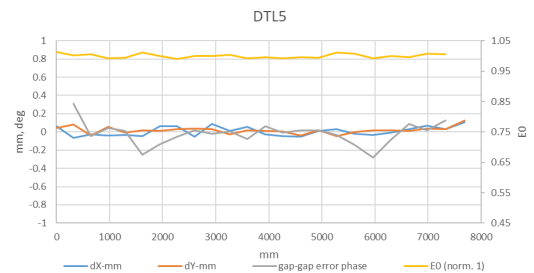


Figure 2: E0, gap-gap phase error and DT transverse alignment of DTL5.

“As Built” Simulations

The data in Fig. 2, together with the data of DTL1-2-3-4 [5], are the inputs for the beam dynamics “as built” model. The simulation run with nominal current, 62.5 mA and nominal input beam rms emittances, 0.28/0.28/0.39 mm mrad. Steerers are activated to counteract PMQ misalignments, the max used steerer strength is 1 mT*m, with max possible strength 1.4 mT*m. The run is without losses with output emittances comparable with nominal case (Fig. 3).

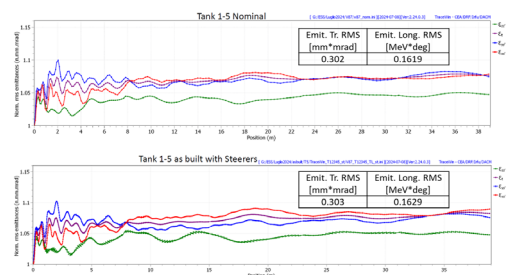


Figure 3: Nominal and “as built” DTL’s emittances.

DESIGN AND OPTIMIZATION OF A C-BAND RF PULSE COMPRESSOR FOR A VHEE LINAC FOR FLASH RADIOTHERAPY

G. Torrisi*, G. S. Mauro and G. Sorbello², INFN-LNS, Catania, Italy

A. Curcio, L. Faillace and B. Spataro

INFN Laboratori Nazionali di Frascati, Italy

L. Giuliano⁵, M. Migliorati⁵, A. Mostacci⁵ and L. Palumbo⁵

SBAI, Sapienza University of Rome, Italy

²also at University of Catania, Catania, Italy ⁵also at INFN-Sezione di Roma, Italy

Abstract

In this paper, the design of a compact C-band SLED RF Pulse Compressor for a Very High Electron Energy (VHEE) FLASH machine is presented. A spherical cavity RF pulse compressor - selected because of its compactness and relative ease of fabrication - is adopted to compress the $5 \mu\text{s}$ RF pulse, down to $1 \mu\text{s}$ obtaining a peak power gain greater than 5. Both the RF and thermo-mechanical design have been carried out, including a sensitivity study to evaluate the mechanical tolerances, possible tuning methods, and the cooling system. The main parameters of the full RF design (spherical storage cavity + mode converter/polarizer) and the final mechanical design of the structure are presented.

INTRODUCTION AND MOTIVATION

This paper presents the complete design of a C-band (5.712 GHz) spherical pulse compressor for a Very High Electron Energy (VHEE) FLASH machine. VHEE [1] irradiations could represent a valid technique to apply the FLASH effect [2] in clinical use to treat deep tumors. The design strategy and electromagnetic characteristics of the C-band linac for VHEE FLASH radiotherapy is presented in [3]. The translation of FLASH therapy - a novel cancer treatment technique, aims to control the tumor-grown sparing the healthy tissue from radiation damage increasing the therapeutic index - into clinical practice, especially for treating deep-seated tumors, necessitates achieving Very High Electron Energy (VHEE) levels within the 50-150 MeV range [4, 5]. The output beam energy can be increased by enhancing the RF peak power at the expense of RF pulse width by using a pulse compressor. This system called "SLAC Energy Doubler (SLED)", firstly proposed and applied in [6], has been widely used elsewhere according different schemes such as the Binary Pulse Compression (BPC) [7], SLED-II [8], Barrel Open Cavity (BOC) pulse compressor [9] and single spherical cavity pulse compressor [10]. The latter is also the one selected for this work: it is composed of a "special" 3 dB coupler (also acting as a circular polarizer) and a single spherical energy storage cavity (compared with the traditional SLED where two cylindrical cavities are adopted).

At La Sapienza University of Rome, in collaboration with the Italian Institute for Nuclear Research (INFN), the de-

* giuseppe.torrisi@lns.infn.it

velopment of a high gradient C-Band FLASH linac demonstrator is ongoing to test and validate all the C-Band key components necessary for a VHEE Linac (see Fig. 1).

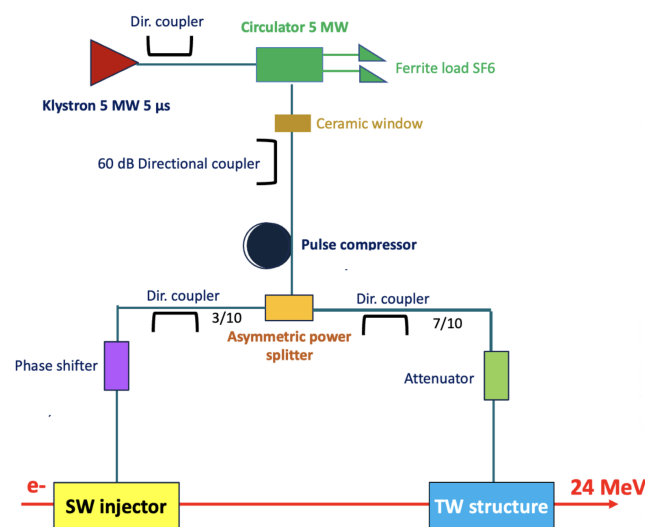


Figure 1: VHEE FLASH linac general layout [3].

DESIGN OF THE SPHERICAL PULSE COMPRESSOR

A spherical cavity RF pulse compressor – selected because of its compactness and relative ease of fabrication – is adopted to compress the RF pulse obtaining a peak power gain greater than 5. The spherical cavity pulse compressor, visible in Fig. 2 (b), is composed of a 3 dB coupler (also acting as a circular polarizer, converting the input TE_{10} mode into two, 90-deg shifted, circular TE_{11} output modes) and a single spherical energy storage cavity. These two subsystems have been firstly designed separately and then assembled together to obtain the complete device. For the spherical cavity, two degenerated TE_{114} (see Fig 2(b)) have been chosen as operating modes because of their high unloaded quality factor, $Q_0 = 134 \times 10^3$.

RF Design and Tuning

The simulated S-Parameters of the pulse compressor by CST Frequency Domain Solver are shown in Fig. 3. The minimum value of $|S_{21}|$ is about -2 dB at the frequency $f_0 = 5.712$ GHz. The corresponding coupling coefficient β is calculated to be about 8.

R&D ON SRF AT INFN LASA

L. Monaco[†], M. Bertucci, M. Bonezzi, A. Bosotti, E. Del Core, F. Fiorina, R. Paparella, D. Sertore,
P. Spruzzola, INFN Milano LASA, Segrate, Italy
C. Pagani¹, Università degli Studi di Milano, Segrate, Italy
¹also at INFN Milano - LASA, Segrate, Italy.

Abstract

Sustainability and cost reduction are key factors for the development of future large particle accelerators. This motivated INFN LASA to initiate an INFN-funded R&D program dedicated to improving the performance of SRF Nb cavities in terms of quality factor (High-Q) and accelerating gradient (High-G).

The R&D program will start by exploiting state-of-the-art surface treatments on 1.3 GHz single-cell prototypes, in view of a possible industrialization process for large-scale productions.

Integrating part of this program is the upgrade of our vertical test facility to enable qualification of such high-performance cavities. Ongoing activities include the construction of a new dedicated cryostat, which minimizes Liquid Helium consumption, reduces the impact of trapped magnetic flux and provides a wide range of diagnostics for quench, field emission, and magnetic flux expulsion studies.

INTRODUCTION

The SRF group of INFN Milano - LASA has a long experience in the field of niobium (Nb) superconducting (SC) cavities and related accessories, with research and development activities also dedicated to the industrialization of this technology aimed at in-kind contribution to international projects such as E-XFEL, ESS and, recently, PIP-II [1-4].

Maintaining and reinforcing this excellence and expertise is important in view of future high-performance accelerators (such as lepton colliders and light machines) that aim for even better performance for SRF cavities to meet greater sustainability, cost reduction and short footprint (as for example stated by the ESPP - European Strategy for Particle Physics) [5]. Therefore, R&D programs dedicated to the study and improvement of cavity surface and thermal treatments to achieve High-Q and High-G performance prove to be crucial activities.

The demonstration of how this approach is shared by many worldwide parties is supported by similar 3-4 years programs financed not only nationally as by INFN (with main focus on future projects as ILC, Muon Collider, FCC, etc.), but also by international collaboration as ITN (ILC Technology Network) that aim to reach High-G with good Q_0 at the ILC goal [6]. In this context, FCC is aiming for 20 MV/m with 3E10 while ILC expects 31.5 MV/m with 1E10 in operation. In particular ITN, that is still under formal finalization between all the partners, is a worldwide technology network that aims to study some critical aspects

highlighted in IDT (ILC Development Teams) during the preparatory phase of ILC. For ITN, INFN contributes to SRF themes (cavities, cryomodules and ancillaries) working with our colleagues from EU labs involved and coordinated by CERN. Among the various tasks, we will take care of the development and optimization cavities treatments, of their industrialization, and we will work on the harmonization of the EU/US pressure vessel code (PED and ASME) with the Japanese HPGS (High Pressure Vessel Code), that will allow installing up to two European cavities in the demonstrator cryomodule that it will assemble at KEK. This activity is important in view of the future international projects where it will be essential to have world-wide contributions compliant with local regulations.

Furthermore, a four-year EAJADE EU Marie Curie program plays a crucial role in these activities since, sponsoring staff exchange between young EU researchers and well-known labs and universities in US and Japan, will enrich and improve the knowledge exchange in the SRF fields.

OUR R&D STRATEGY

The strategy we propose consists of an R&D phase based on single cells at 1.3 GHz (reference frequency for these activities) for the development of treatments that allow the High-Q to be extended towards the high gradient. Once these treatments will be consolidated, an essential step will be their transfer to multicell cavities in view of a possible large-scale production. This activity is synergic with the SRF group's current program towards future colliders (ILC, Muon Collider, FCC, etc.).

Moreover, the R&D activities here described, in particular the High-Q part, will be synergic and it will profit of the on-going developments and studies in our group for the optimization of the 650 MHz (1st sub harmonic of 1.3 GHz) PIP-II cavity treatments, that asks to reach a very high Q_0 but at modest accelerating gradient.

Within our reference time frame (3-4 years), the plan for developing the activities we propose, based on 1.3 GHz technology, can be summarized in:

- High-Q/High-G recipe development on 2 single-cell cavities. This activity will start from baseline process (E-XFEL like) and then it will include further treatments such as two-step baking, mid-T baking, etc. Moreover, we will test the cavities not only at LASA but also in other laboratories (i.e. CEA) for performance cross-check.
- Transfer of selected treatments to multicell, with 2 9-cells, addressing the industrialization and QA/QC process implementation in preparation for a future large-scale production.

[†] laura.monaco@mi.infn.it

DESIGN AND TEST OF C-BAND LINAC PROTOTYPES FOR ELECTRON FLASH RADIOTHERAPY

L. Giuliano*, E. Anelli, E. Chiadroni², M. Coppola, A. De Gregorio¹, L. Ficcadenti¹, S. Farina¹,
D. Francescone¹, G. Franciosini¹, M. Magi¹, M. Migliorati¹, A. Mostacci¹, L. Palumbo¹, V. Patera¹,
F. Perondi, R. Remetti, A. Sarti¹, Sapienza University of Rome, Italy
D. Alesini, F. Cardelli, M. Carillo, A. Curcio, R. Di Raddo, L. Faillace, G. Franzini, A. Gallo,
L. Piersanti, B. Spataro, A. Vannozzi, INFN - LNF, Frascati, Italy
G. Cuttone, G. S. Mauro, G. Sorbello, G. Torrisi, INFN - LNS, Catania, Italy
M. Di Francesco, G. Felici, SIT - Sordina IORT Technology Spa, Aprilia, Italy

¹ also INFN-Roma, Italy

² also INFN-LNF, Italy

Abstract

FLASH Therapy [1], a novel cancer treatment technique, aims to control the tumor-grown sparing the healthy tissue from radiation damage, increasing the therapeutic index. Translating FLASH therapy into clinical practice, especially for treating deep-seated tumors, necessitates achieving Very High Electron Energy (VHEE) levels within the 50-150 MeV range [2]. In the framework of the SAFEST project [3–7], Sapienza University, in collaboration with INFN, is actively developing a compact C-band linac demonstrator at the energy of 24 MeV (loaded) with a 100 mA peak current. This paper provides insights into the design strategy and electromagnetic characteristics, focusing on prototype testing and tuning conducted at the Sapienza Accelerator Laboratory. The progress of this innovative linac represents a step toward realizing an advanced FLASH VHEE source in cancer treatment.

INTRODUCTION

FLASH radiotherapy (RT) has attracted significant attention within the cancer research community due to its potential to effectively treat tumors while minimizing damage to surrounding healthy tissues. Preclinical studies have shown that delivering electron radiation in extremely short bursts (less than 100 ms) at ultra-high instantaneous dose rates (exceeding 10^6 Gy/s) can significantly reduce toxicity in healthy tissues while maintaining therapeutic efficacy against cancer.

The first experiment involving FLASH-RT was conducted by V. Favaudon and his team at Institut Curie in 2014 [1]. Since then, various in-vivo and in-vitro radiobiological studies have reported substantial sparing of normal tissues, nevertheless, more research is necessary to fully comprehend the advantages and limitations of FLASH-RT and to identify the best clinical applications. Currently, only a limited number of dedicated electron linacs are employed for experimental research, with ongoing studies and technological advancements aimed at developing more compact and cost-effective linacs for high-energy electrons. The ultimate goal is to

adapt these linacs for the treatment of deep-seated tumors using Very High Energy Electron FLASH radiotherapy.

At La Sapienza University of Rome, in collaboration with the Italian Institute for Nuclear Research (INFN), we are developing a high gradient C-Band (5.712 GHz) FLASH linac demonstrator [8] with the aim of testing all key components necessary for a VHEE Linac (Fig. 1). The first stage of the demonstrator consists of a compact Standing Wave (SW) bi-periodic structure operating in $\pi/2$ mode followed by a high-gradient traveling wave (TW) structure, with a phase advance of $\frac{2}{3}\pi$, intended to accelerate the electron beam up to 24 MeV (loaded with 100 mA pulse current), the maximum energy being limited by radio-protection constraints in the University laboratory.

In this paper, we present the status of the design and construction of the prototype which has to deliver ultra-high dose rate (UHDR) pulses typical of the FLASH regime [9], as reported in Table 1.

Table 1: Most Used Parameters for FLASH Irradiation

Symbol	Description	Value
PRF	Pulse repetition frequency	> 100 Hz
t_p	Electron pulse width	0.1-4.0 μ s
t_i	Total irradiation time	< 100 ms
\bar{D}	Time-averaged dose rate	> 100 Gy/s
\dot{D}_p	Dose-rate in a single pulse	> 10^6 Gy/s
D_p	Dose in a single pulse	> 1 Gy

The facility will offer an adaptable platform for conducting radiobiology experiments using both in-vitro and in-vivo samples, and it will support the development and testing of innovative devices for precise measurements and monitoring of electron beam parameters in FLASH conditions.

FACILITY PARAMETERS AND LAYOUT

The proposed basic system (Fig. 1) is composed of a standing wave injector and a traveling wave accelerating structure. A continuous electron beam of about 220 mA is generated by a DC gun with a pulse length of 1 μ s. The accelerating structures are powered by a 5 MW klystron with an RF pulse length of 5 μ s. The klystron output feeds a pulse

* lucia.giuliano@uniroma1.it

FAST CHOPPER LINE FOR DONES

M. D'Andrea[†], L. Bellan, L. Ferrari, F. Grespan, A. Palmieri, A. Pisent, INFN-LNL, Legnaro, Italy
M. Di Giacomo, GANIL, Caen, France

Abstract

The International Fusion Materials Irradiation Facility – DEMO-Oriented Neutron Early Source (IFMIF-DONES) will provide a deuteron beam of unprecedented intensity for irradiation and characterization of materials to be used in fusion reactors. In recent years, the possibility to use a small fraction of this beam for other applications in parasitic mode was discussed. This has the potential to not only enlarge the user community without perturbing the main operation, but also allow characterization measurements for beam quality management purposes. Considering various requirements and constraints, the most promising option for the extraction towards such a parasitic line involves the use of a meander-line travelling-pulse beam deflector at the start of the High Energy Beam Transfer (HEBT) line. This paper describes preliminary studies aiming at a first definition of the structure, materials and geometrical parameters of the meander-line deflector.

INTRODUCTION

The definition of which materials shall be used for the construction of nuclear fusion reactors is a crucial part of the European roadmap towards fusion electricity. To be validated and qualified, these materials must be exposed to neutron irradiation comparable to what is expected in a fusion reactor. The construction of IFMIF-DONES (referred to as DONES in the following for simplicity), the staged version of a facility capable of producing neutrons with the required energy spectrum and fluence, was launched in March 2023 in Escúzar, Spain, as part of the European Fusion Roadmap. The neutron flux (10^{18} neutron/m²/s) will be produced by a deuteron beam accelerated to 40 MeV hitting a liquid lithium target. The main parameters of the DONES accelerator systems are reported in Table 1. More details on the facility can be found in [1–4].

Table 1: Main DONES Accelerator Nominal Parameters

Particle	D ⁺ (p)
Peak current [mA]	125
Beam energy [MeV]	40 ± 5 FWHM
β_{beam}	0.204
Beam power [MW]	5
RF frequency [MHz]	175

In the past years, the possibility to extract a small fraction of the beam and devote it to different applications (e.g. physics experiments or beam characterization), without perturbing the main operation, was discussed. Preliminary explorations of this concept determined that it is particularly interesting if 1 bunch over 1000 of the fully accelerated 40 MeV beam can be extracted keeping the 125 mA

peak current intact. The bunch separation must therefore take place after the full acceleration is completed, i.e. in the HEBT. The most promising solution to achieve this setup involves the use of a meander-line travelling-pulse beam deflector to separate the selected bunch, coupled with electrostatic and magnetic septa to complete the extraction.

PRELIMINARY STUDIES

In a meander line beam deflector, a travelling electric field pulse is applied between two electrodes around the beam. If the rise/fall time and length of the impulse are properly set, the electric field will act only on a selected bunch, without perturbing the path of the others. However, the propagation speed of the signal along the beam trajectory must be reduced to be synchronized to the selected bunch. For this purpose, the electrodes can be meander-shaped, as already done in various facilities [5–7].

Preliminary investigations were carried out to identify a suitable location in the HEBT (shown in Fig. 1) for the installation of the meander line [8]. This is mainly driven by the minimum achievable rise/fall time, as this puts a hard limit to the bunch-by-bunch separation if the rest of the beam must remain untouched. Since there is no longitudinal focusing, and therefore the beam increases its phase spread as it travels along the line, the separation must take place at the beginning of the HEBT. Considering a minimum achievable rise/fall time of 2-3 ns [9, 10], the suitable region is restricted to the first 3.5 m of the line. Simulations performed with TraceWin [11] for a typical DONES bunch show that all particles are contained within 1.77 ns [8]. Therefore, an electric field pulse with a 2 ns plateau was considered for the preliminary design.

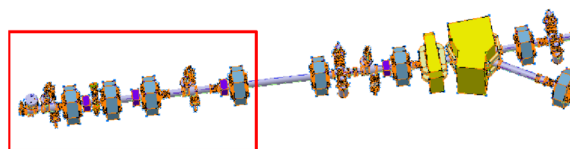


Figure 1: Sketch of the DONES HEBT [12]. The region considered for the installation of the meander-line deflector is highlighted in red.

MEANDER LINE DESIGN

Several different solutions for the meander-line deflector design were conceived [8]. The one considered in the following includes a total of three separate meander sections installed in succession, followed by dedicated septa to complete the separation of the bunch. The main parameters of this setup are reported in Table 2.

The design of a meander line is driven by the synchronization between the electric field pulse along the line and the bunch to be deflected. This depends also on the dielectric material chosen to separate the line conductor from the

[†] marco.dandrea@lnl.infn.it

STATUS OF THE INFN LASA IN-KIND CONTRIBUTION TO PIP-II PROJECT

R. Paparella[†], M. Bertucci, M. Bonezzi, A. Bosotti, E. Del Core, F. Fiorina, L. Monaco, D. Sertore, P. Spruzzola, INFN Milano LASA, Segrate, Italy
 C. Pagani¹, Università degli Studi di Milano, Segrate, Italy
¹also at INFN Milano - LASA, Segrate, Italy
 H. Park, G. Wu, J. Ozelis, Fermilab National Accelerator Laboratory, IL USA

Abstract

The status of INFN LASA in-kind contribution to the PIP-II project at Fermilab is reported in this paper. The effort for the series production of the 38 INFN LASA designed, 5-cell cavities with beta 0.61 for the LB650 section of the linac commenced and the status of ongoing activities and major procurements is here conveyed. At the same time, preliminary tests on INFN LB650 cavity prototypes are progressing in order to optimize the complete preparation and qualification cycle. All cavities will be produced, and surface treated in industry to reach the unprecedented performances required, qualified through vertical cold test at state-of-the art infrastructures and delivered as installation ready at the string assembly site.

INTRODUCTION

The Fermilab Proton Improvement Plan II (PIP-II) Linac is designed to deliver a 1.2 MW H- beam upgradable to multi-MW to enable LBNF and DUNE neutrino physics projects [1]. The 800 MeV beam will be injected into the upgraded Booster Ring via a linac-to-booster transfer line and it will then proceed to the Main Injector Ring.

The PIP-II linac features a flexible time structure for its 0.55 ms, 2 mA beam pulse in order to satisfy different experimental needs, with radiofrequency (RF) components capable of supporting continuous-wave (CW) operations.

A key section of the linac is the 650 MHz superconducting part with geometric beta factor of 0.61 (LB650) that encloses 36 five-cell elliptical cavities in 9 cryomodules, accelerating beam from 177 MeV to 516 MeV.

Target cavity accelerating gradient is set at 16.9 MV/m with a quality factor higher than $2.4 \cdot 10^{10}$, an unprecedented working point for this type of resonators [2].

The complete series of 38 SC cavities (36 plus 2 spares) will be handed over to the project once qualified through cold vertical test and they will be in a ready-for-string-assembly configuration: jacketed, fully dressed and under vacuum.

THE PIP-II LB650 CAVITY

INFN LASA provided the electromagnetic and mechanical design for the LB650 resonator, fully compatible to the performances and technical interfaces posed by the project as well with beam pipes and flanges, power coupler, helium tank, tuner.

Key design parameters and target performances of the INFN designed LB650 resonator are shown in Table 1, the

cavity in its final configuration upon delivery to string assembly site is instead shown in Fig. 1.

Table 1: Design Parameters of LB650 Cavity

Parameter	Value
$\beta_{\text{geometric}}$	0.61
Frequency	650 MHz
Number of cells	5
Iris diameter	88 mm
Cell-to-cell coupling, k_{cc}	0.95 %
Frequency separation $\pi-4\pi/5$	0.57 MHz
Eq. diameter - IC	389.8 mm
Eq. diameter - EC	392.1 mm
Wall angle – Inner-End cells	2°
Effective length ($10 \cdot L_{\text{hc}}$)	704 mm
Optimum beta β_{opt}	0.65
$E_{\text{peak}}/E_{\text{acc}} @ \beta_{\text{opt}}$	2.40
$B_{\text{peak}}/E_{\text{acc}} @ \beta_{\text{opt}}$	4.48 mT/(MV/m)
R/Q @ β_{opt}	340 Ω
G @ β_{opt}	193 Ω
Stiffening ring radius	90 mm
Wall thickness – discs	4.5 mm
Longitudinal stiffness	1.8 kN/mm
Long. frequency sensitivity	250 kHz/mm
LFD coefficient	
- k_{ext} at 40 kN/mm -	$-1.4 \text{ Hz}/(\text{MV}/\text{m})^2$
Pressure sensitivity	
- k_{ext} at 40 kN/mm -	-11 Hz/mbar

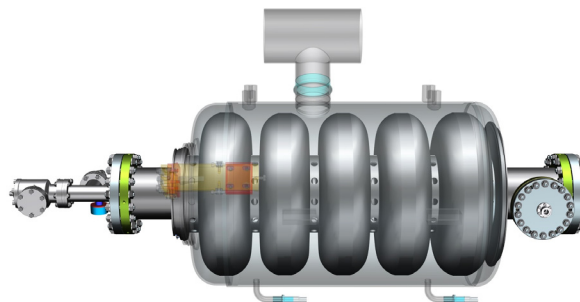


Figure 1: LB650 cavity.

Following the valuable know-how available in the PIP-II community and the preliminary R&D done and being done (described later in this paper and in more details in [3]), the target surface processing cycle for LB650 has been defined as:

ADVANCED ALGORITHMS FOR LINEAR ACCELERATOR DESIGN AND OPERATION

Y. K. Ong*¹, L. Bellan, A. Pisent, M. Comunian, E. Fagotti, D. Bortolato, M. Montis, M. Giacchini, O. Carletto, INFN-LNL, Legnaro, Italy
¹also at La Sapienza University of Rome, Italy

Abstract

In this paper, we investigate the usage of advanced algorithms, specifically Bayesian optimization, adapted for optimizing the design and operation of different linear accelerators (LINACs). The aim is to enhance the design efficiency and operational reliability and adaptability of linear accelerators. Through simulations and case studies, we demonstrate the effectiveness and practical implications of these algorithms for optimizing LINAC performances across diverse applications.

INTRODUCTION

The field of accelerator physics has advanced significantly, driven by the demand for higher performance in particle accelerators used in research, medical, and industrial applications. Conventional methods for designing and operating these complex systems, such as Nelder-Mead Simplex [1] and robust conjugate direction search [2], often rely on extensive simulations and expert knowledge due to the large and varied accelerator components and parameters needed to be tuned. Therefore, developing more efficient ways to solve complex optimization problems through advanced machine learning (ML) based algorithms are being explored.

Among the advanced algorithms, Bayesian Optimization (BO) has been gaining popularity within the accelerator community for both offline and online tuning due to its flexibility, low initialization effort, fast convergence, and robustness to noisy environments [3–5]. BO builds a probabilistic surrogate model, typically a Gaussian process [6], of the objective function. This model predicts the function's behavior and quantifies uncertainty. The optimization process iteratively selects new evaluation points based on this model, balancing exploration of the search space with exploitation of known high-performing regions. An acquisition function guides the selection of points by considering both predicted performance and uncertainty. This efficient approach finds optimal parameters with a limited number of evaluations.

In this paper, we explore the application of Bayesian Optimization in the design of the ANTHEM MEBT line and the operation of the TAP accelerator complex at INFN-LNL. We discuss the challenges in accelerator optimization, review current techniques, and present case studies demonstrating the effectiveness of Bayesian optimization.

* ysaong@lnl.infn.it

THE ANTHEM MEBT LINE

The AdvanCed Technologies for Human-centrEd Medicine (ANTHEM) project aims to develop technologies for the healthcare of chronic patients. One of its main proposals is the construction of an Accelerator-based Boron Neutron Capture Therapy (A-BNCT) facility in Caserta, Campania, Italy. This facility will utilize a high-intensity proton source with the TRASCO RFQ as the proton accelerator, operating at a frequency of 352 MHz and an output beam energy of 5 MeV at a 30 mA beam current [7]. The medium energy beam transport (MEBT) line, located after the RFQ, is responsible for transporting and manipulating the spatial distribution of the beam to the target for optimal neutron production. As presented in Fig. 1, the MEBT line design includes various magnetic elements, such as quadrupoles, a dipole, and a pair of octupoles, which utilize the tail folding technique to achieve a uniform beam distribution at the target [8]. Good beam uniformity at the target with an area of $120 \times 120 \text{ mm}^2$ is necessary to maintain the beam power deposition at around 1 kW/cm^2 for optimal neutron production and target operation.

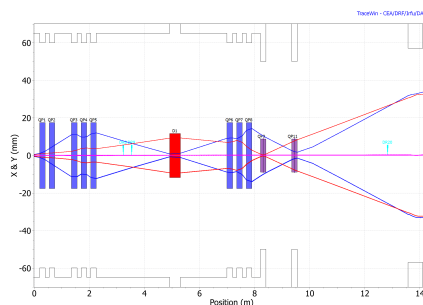


Figure 1: ANTHEM MEBT line beam envelopes with quadrupoles, dipole and octupoles being the blue, red, and purple elements respectively. Blue line: x. Red line: y.

Bayesian Optimization for Shaping the Beam Uniformity at the Target

The manipulation of the beam distribution is performed through the activation and optimization of the octupole strengths and the addition of a collimator. However, before proceeding with this step, the MEBT line was first optimized to transport the beam without losses to the target using TraceWin, a tracking program that utilizes a PIC technique to calculate the beam dynamics and exploit the space charge-induced behavior of the beam [9]. Additionally, the

BEAM TRANSIENT STUDIES FOR THE JAEA-ADS LEBT

B. Yee-Rendon*, Y. Kondo, J. Tamura, F. Maekawa, S. Meigo
Japan Atomic Energy Agency (JAEA), Tokai, Japan

Abstract

The Japan Atomic Energy Agency (JAEA) is designing a 30-MW CW proton linear accelerator (linac) for nuclear waste transmutation. Space-charge is the primary challenge in achieving low losses and high beam quality for high-power accelerators, especially at low energy levels where space-charge forces are greater. To counteract the space-charge effects, the low-energy beam transport (LEBT) uses a magnetostatic design to enable the neutralization of the beam charge, the so-called space charge compensation. The neutralization is an accumulation process that reaches a charge balance between the main beam and the opposite ionized particles. However, this equilibrium is destroyed by the chopper system used during beam ramping. During those transient regimes, the beam optics conditions are not optimal for the beam, producing considerable degradation that can end in serious damage to the accelerator. Thus, analysis of beam behavior at these periods is essential to develop a robust design and an efficient operation of the JAEA-ADS linac. This study presents the beam dynamics of neutralization build-up and chopper operation for the JAEA-ADS LEBT.

INTRODUCTION

The Japan Atomic Energy Agency (JAEA) is designing an accelerator-driven subcritical system (ADS) for nuclear waste transmutation [1]. To this end, JAEA will use a 30-MW continuous-wave superconducting proton linear accelerator [2]. As with any high-intensity accelerator, space charge is the main challenge to avoid beam losses. Therefore, the low-energy beam transport (LEBT) uses a space charge compensation (SCC) design [3] to transport the beam from the ion source to the RFQ to avoid large emittance growth caused by space-charge effects. SCC occurs when the main beam ionizes the residual gas, producing secondary particles. These secondary particles with an opposite charge regarding the main beam are trapped in the beam potential and accumulate until reaching a steady equilibrium state. This leads to a screening of the space charge forces.

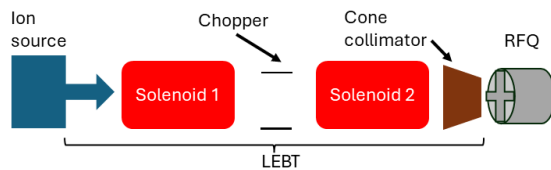


Figure 1: Schematic view of the JAEA-ADS LEBT design.

Figure 1 and Table 1 show the LEBT design and its main parameters, respectively. In this design, the chopper is

placed between the solenoids, bringing solenoid 2 closer to RFQ to achieve a more convergent beam.

Table 1: Main Parameters for the JAEA-ADS LEBT

Parameter	
Particle	Proton
Beam current (mA)	25
Beam energy (keV)	35
Solenoid length (mm)	300
Solenoid 1 position (mm)	500
Solenoid 2 position (mm)	1680
Chopper length (mm)	125
Chopper position (mm)	1347.5
Length (mm)	1960

Previous LEBT model [4] considered a piecewise constant space-charge compensation. However, experiments and studies show a more complex profile [3, 5]. Thus, this work improves the accuracy of SCC by developing a time-dependent LEBT model utilizing Warp [6] to include the ionization process. Furthermore, beam transient analysis will be utilized to determine the beam structure for nominal operation by taking into account the conditions needed to reach a steady state and the beam power ramp strategies by investigating the chopper effects.

BEAM TRANSIENT STUDIES

Transient beam studies were conducted using Warp, a 3D particle-in-cell program developed at Lawrence Berkeley National Laboratory to model high-intensity beams [7–9]. Warp is a self-consistent code, which means it can accurately simulate space charge effects in the beams.

In SCC studies, the SCC level (η) is a standard figure of merit used to evaluate the reduction in the effect of the current space charge. η is quantified as [10]:

$$\eta = 1 - \frac{\# \text{ negative particles}}{\# \text{ positive particles}}, \quad (1)$$

where # of charged particles that are contained to a certain root-means square (rms) beam size.

Another important variable is the SCC transient time (τ_{SCC}), which provides information about the time required for a particle of the beam to produce a neutralizing particle in the residual gas. τ_{SCC} is defined as [3, 5]:

$$\tau_{\text{SCC}} = \frac{kT}{\sigma_{\text{gas}} P v_b}, \quad (2)$$

where σ_{gas} is the cross-section of the beam particle to the residual gas, k is the Boltzmann constant, T is the tempera-

* byee@post.j-parc.jp

THE LINACS SIMULATION FRAMEWORK

B. Yee-Rendon*, Japan Atomic Energy Agency (JAEA), Tokai, Japan

R. A. Jameson, Goethe Universität, Frankfurt, Germany

M. Okamura, Brookhaven National Laboratory, Upton, NY, USA

C. Li, Deutsches Elektronen-Synchrotron DESY, Hamburg, Germany

P. Jiang, Institute of Modern Physics, Chinese Academy of Sciences, Lanzhou, China

J. M. Maus, NTG Neue Technologien GmbH und Co KG, Gelnhausen, Germany

Abstract

LINACS is a simulation framework for designing, simulating, and analyzing optics and beam dynamics of charged particles in particle accelerators. LINACS is an open-source software that enables the user complete control over all design and simulation parameters of RFQs. This includes beam-driven design, fully 3D simulation using precise quadrupolar symmetry, and rigorous Poisson solution for external and space charge fields. The code can handle simultaneous particle beams with analytical input distributions and allows input beam scans. The software offers a relatively short running time and provides extensive analysis techniques. This work provides a historical overview of the code, presents results from RFQ models, and discusses future developments.

INTRODUCTION

Systematic design code for linear accelerators altogether is rare, and comprehensive frameworks that include space charge physics as a primary focus and utilize an *inside out* design, i.e., a design that specifies the desired beam behavior as influenced by space charge and specifies the external field that produces that behavior, are currently only represented by LINACS [1]. As a result, the emphasis is heavily placed on design aided and followed by simulation, both of which require equal care and a framework approach. The example of RFQ design is used to illustrate this point, as it is considered the most challenging linac to design due to the beam's evolution from DC injection to the formation of accelerated bunches.

R. A. Jameson and several students at the Institut für Angewandte Physik (IAP) aimed to enhance the physics fidelity of general linacs, specifically focusing on RFQ design, simulation, and optimization [2].

The motivations included:

- Full and direct control over all parameters.
- Close the agreement between actual RFQ performance and simulations.
- Improving the physics modeling.
- Open source programs.
- Develop guidelines for model optimization.

The ultimate objective was to develop a new, open-source code called LINACS for particle accelerator design and simulation. This code would integrate the most advanced

physics that current computer technology can accommodate. It would also provide options for the designer to prioritize between accuracy and execution speed, with a clear understanding of the potential consequences. Additionally, the code would offer a versatile library of analysis capabilities.

LINACS FRAMEWORK

The LINACS framework is composed of three main codes: LINACSRfqDES, LINACSRfqSIM, and LINACSpf. The first two are specialized for RFQ design, and the last one was developed for the Alternating-Phase-Focused (APF) linacs [3]. In this report, we will focus on the RFQ codes: LINACSRfqDES and LINACSRfqSIM.

The LINACSRfqDES framework controls all RFQ parameters, including the space charge physics. This ensures that the beam is controlled in the design by requiring the root-mean-square (rms) beam envelope to be matched transversely and longitudinally at each cell. Therefore, the rms beam envelope is known at each cell. LINACSRfqDES is unique in using a good approximation of the external field (8-term multipole), applied in the design at the rms beam sizes, so that the design and LINACSRfqSIM are fully connected.

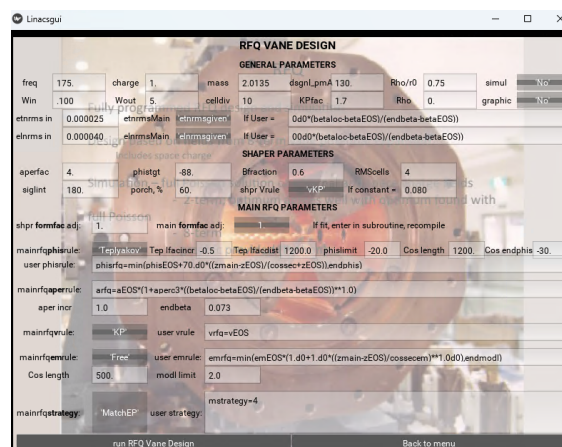


Figure 1: Graphical user interface for the RFQ design.

Figure 1 shows the graphical user interface for the RFQ design. Using this interface, the user can define the general parameters of the RFQ, shaper, and main RFQ parameters. The user has the option to choose from various predefined rules, or they can create and implement their own rules to control the parameters. The *simul* button on the top-right

* byee@post.j-parc.jp

PROGRESS OF THE SPOKE CAVITY PROTOTYPING FOR THE JAEA-ADS LINAC

J. Tamura*, Y. Kondo, B. Yee-Rendon, S. Meigo, F. Maekawa, JAEA/J-PARC, Ibaraki, Japan
E. Kako, K. Umemori, H. Sakai, T. Dohmae, KEK/iCASA, Ibaraki, Japan

Abstract

The Japan Atomic Energy Agency (JAEA) has been proposing an accelerator-driven nuclear transmutation system (ADS) as a future nuclear system. Toward the practical design of the CW proton linac for the JAEA-ADS, we are currently prototyping a low- β (≈ 0.2) single-spoke cavity. The cavity fabrication began in 2020. Most of the cavity parts were shaped in fiscal year 2020 by press-forming and machining. In 2021, we started welding the shaped cavity parts together. Each cavity part was welded together by preliminarily examining the optimum welding conditions using mock-up test pieces. So far, we have fabricated the body section and the two lid sections, and have confirmed that there were no significant problems with the cavity fabrication according to the frequency measurement of the temporarily-assembled prototype cavity.

INTRODUCTION

JAEA has been proposing an ADS as a future nuclear system to efficiently reduce high-level radioactive waste generated in nuclear power plants. In the ADS, long-lived nuclides are transmuted to short-lived or stable ones. One of the challenging R&D subjects to realize the ADS is the reliability of the accelerator [1, 2]. In the JAEA-ADS, a high-power (30 MW) proton beam with a final energy of 1.5 GeV is required with high reliability. Because the accelerator needs to be operated in CW mode, a super-conducting (SC) linac would be a suitable solution. The latest design of the JAEA-ADS linac is reported in Refs. [3, 4]. As shown in Fig. 1, the proposed linac consists of a normal-conducting radio-frequency quadrupole (RFQ), half-wave resonator (HWR), low- β and high- β single-spoke resonators (SSR1 and SSR2, respectively), and low- β and high- β elliptical cavities (ELL1 and ELL2, respectively).



Figure 1: Proposed acceleration structure of the JAEA-ADS linac.

As a first step toward the practical design of the JAEA-ADS linac, we have decided to prototype the low- β single-spoke cavity and conduct a high-field performance test of the prototype spoke cavity at liquid helium temperature. The spoke cavity prototyping will provide us with various

insights on the development of SC cavities with TEM $\lambda/2$ -mode resonance. In addition, the high-field cavity testing will provide valuable information such as how much field gradient can be achieved with reasonable stability. Therefore, both prototyping and performance testing are essential to ensure the feasibility of the JAEA-ADS linac. In this paper, the progress of the spoke cavity prototyping for the JAEA-ADS linac is presented.

CAVITY DESIGN

The prototype spoke cavity with an operating frequency of 324 MHz was designed by electromagnetic simulation [5], and its dimensional parameters were optimized for higher cavity performance [6–8]. The cross-sectional views of the designed cavity are shown in Fig. 2. The cavity's design parameters are listed in Table 1. The multipactor analysis of the designed cavity without the coupler ports was presented in Ref. [7].

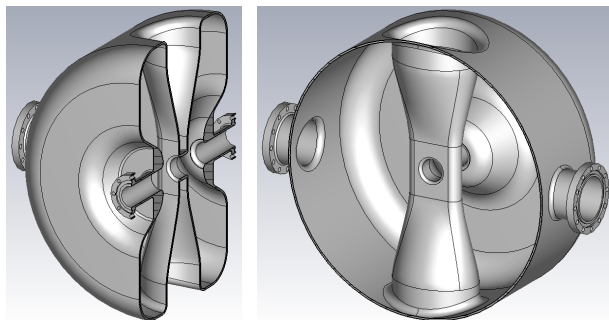


Figure 2: Cross-sectional views of the designed cavity.

Table 1: Design Parameters of the Prototype Spoke Cavity

Parameter	Value
f_0	324 MHz
β_g	0.188
β_{opt}	0.24
Beam aperture	40 mm
Cavity diameter	~ 500 mm
Cavity length	300 mm
$L_{eff} = \beta_{opt} \lambda$	222 mm
$G = Q_0 R_s$	90 Ω
$T(\beta_{opt}) = V_{acc}/V_0$	0.81
$r/Q = V_{acc}^2/\omega W$	240 Ω
E_{peak}/E_{acc}	4.1
B_{peak}/E_{acc}	7.1 mT/(MV/m)

* jtamura@post.j-parc.jp

NEW 3-MeV RFQ DESIGN AND FABRICATION FOR KOMAC

H.-S Kim*, S.-H. Moon, D.-H. Kim, S. Lee, H.-J Kwon, Korea Multipurpose Accelerator Complex, Korea Atomic Energy Research Institute, Gyeongju, Korea

Abstract

Since the second half of 2013, the Korea Multi-purpose Accelerator Complex (KOMAC) has been supporting user beam services with a 100 MeV proton linac. Given that the proton accelerator has been in operation for over 10 years and its cumulative operating time has surpassed 33,000 hours, we believe it is an opportune moment to establish a long-term plan to address the aging of the accelerator. To replace the current RFQ, which is experiencing performance degradation (particularly in reduced beam transmission), we have designed a new RFQ with several modifications. We eliminated the resonant coupling structure located in the middle of the old RFQ to simplify the design and facilitate tuning. Additionally, we increased the RFQ length from 3,266 mm to 3,537 mm to improve beam transmission efficiency in high-current mode. An error study on the new structure has shown that the design is robust against various error sources. The details of the RFQ design, along with the fabrication status, will be presented.

INTRODUCTION

The RFQ at the Korea Multi-purpose Accelerator Complex (KOMAC) was designed to accelerate a proton beam from 50 keV to 3 MeV.



Figure 1: Existing RFQ at KOMAC.

Figure 1 shows the existing RFQ at KOMAC. This RFQ was successfully commissioned and has been in operation for approximately 20 years since its initial commissioning in 2004 [1-2]. However, the performance of the RFQ has gradually degraded over time.

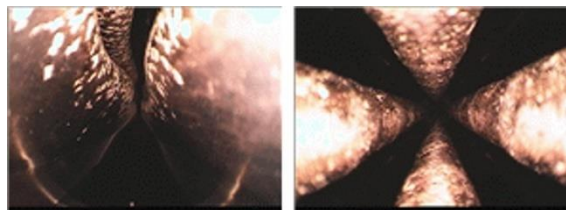


Figure 2: Observed vane electrode damage.

We suspect that the degradation in performance is due to damage to the RFQ vanes, which was confirmed through direct observation using an endoscope. We observed numerous arcing spots and surface degradation (Fig. 2).

Consequently, we have decided to design a new RFQ to replace the existing one.

DESIGN OF NEW RFQ

The new RFQ incorporates several improvements and modifications but remains quite similar to the existing RFQ. Therefore, the new RFQ parameters, as shown in Table 1, are also similar to those of the existing RFQ.

Table 1: Parameters for New RFQ

Parameter	Value
Input beam energy	50 keV
Output beam energy	3 MeV
Operating frequency	350 MHz
Transverse emittance	0.2π mm.mrad
Longitudinal emittance	0.107 deg.MeV
RFQ type	4 - vane
Vane voltage	85 kV
ρ/r_0	0.87
Length	353 cm

While many parameters remain the same, a major change in the new RFQ is the adjustment in the energy range of the gentle buncher. In the old RFQ, the energy range of the gentle buncher varied from 86.5 keV to 550 keV, whereas in the new RFQ, it ranges from 86.5 keV to 580 keV. Although this difference is only 30 keV, we found that extending the energy range improves beam transmission rates.

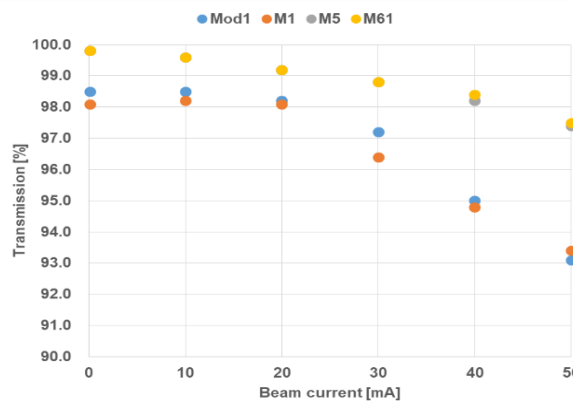


Figure 3: Beam transmission rate with various cases.

The Fig. 3 illustrates the beam transmission rate across different scenarios. Mod 1 represents the existing RFQ, while M1 is similar to Mod 1 but without the focusing

EVALUATING BEAM NEUTRALIZATION AND TRANSPORT DYNAMICS IN LASER-DRIVEN ION ACCELERATORS

H. Matsumoto^{†, 1}, H. Sakaki¹, Y. Watanabe, Kyushu Univ., Fukuoka, Japan
T. Endo, M. Hata, K. Kondo, K. Nagashima, QST, Kyoto, Japan
¹also at QST, Kyoto, Japan

Abstract

Laser-driven ion acceleration [1, 2] produces a high ion density at the source point, with a source diameter of less than one millimeter, and a bunch length of less than a few picoseconds. Typically, such a low-energy, high-density beam with short inter-ion distances causes explosive space-charge forces in the longitudinal and transverse directions, leading to significant emittance growth. However, the transverse emittance observed in the beam a few centimeters downstream of the source point is an order of over magnitude better than that of a typical RF accelerator beam [3,4]. This is because the accelerated ion beam is transported in a state like "plasma: the charge neutralized" by moving electrons, but it has not been studied in detail using particle transport simulations. To understand the beam transport dynamics, we diagnose the space charge neutralized beam by developing a novel PIC code that continuously and seamlessly simulates the laser-driven ion acceleration from the source to the beam measurement point.

LASER-DRIVEN ION ACCELERATION

Ion Acceleration Mechanism

Laser-driven ion acceleration is a method of producing MeV energy ions by irradiating a thin film target (thickness $< \mu\text{m}$) with a high intensity laser ($> 10^{18} \text{ W/cm}^2$). The ion acceleration process, Target Normal Sheath Acceleration (TNSA) [5], is shown in Fig. 1.

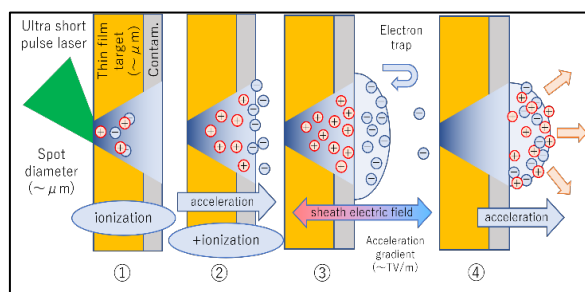


Figure 1: The mechanism of laser-driven ion acceleration.

The TNSA process is,

1. Focused high intensity laser interacts on a thin film target, and the target ionized by the electric field of the laser.
2. Produced ions and electrons are subjected to a ponderomotive force in the target normal direction. The electrons receive energy and detach from the target.

3. The detached electrons are trapped in the ion's electric field. As a result, a very strong electric field ($\sim \text{TV/m}$) is generated between ions and electrons.

4. Ions are accelerated to MeV class by generated electric field.

Thus, the TNSA process with a short-pulse laser is a micro-scale ion acceleration process, where the source diameter is less than one millimeter, and the beam direction is less than a few picoseconds at the source point.

Space Charge Neutralization

At the source, low energy and high instantaneous current ion beams are not efficiently transported downstream due to the explosive force created by space charge effects between ions. In the TNSA process, however, both electrons and ions are accelerated in the same direction, resulting in the creation of a plasma beam with charge neutralization, where both ions and electrons share the same velocity vector. The space charge force of the ion beam from the TNSA process is cancelled out by the effect of charge neutralization, a low transverse emittance is observed in the actual ion beam. Considering applications with the TNSA process ion beam, it is necessary to design an optimal beam transport system to maintain the low emittance. It can be inferred that emittance growth is caused when transient co-moving electrons are removed from the beam, such as when passing through a magnetic field in the first optics.

To design the optimal transport of this low emittance beam, a space charge simulation code is required that continuously and seamlessly calculates both the TNSA process (micro-domain: $\sim \mu\text{m}$, $\sim \text{ps}$) and the beam transport part (macro-domain: $\sim \text{m}$, $\sim \mu\text{s}$).

PARTICLE-IN-CELL SIMULATION

To understand the particle physics of TNSA beam transport, it is necessary to continuously simulate the ion and electron distribution from micro-domain to the macro-domain. In general, during macro-domain beam transport simulations, the beam is treated as a macroscopic group, and its space-charge effects are simply modelled as a linear effect to reduce computational resources. However, the model cannot simulate in detail the nonlinear emittance growth in TNSA beam transport, where the micro-domain space-charge effects between ions and electrons are constantly changing. To solve this problem, it is necessary to continuously and seamlessly simulate the ion distribution in the micro-domain and the macro-domain, a Start-to-End simulation, we are trying to develop a novel simulation using the particle-in-cell method.

[†] email address: Matsumoto.haruya.876@s.kyushu-u.ac.jp

ANALYSIS OF REDUNDANCY DESIGN AND RELIABILITY ESTIMATION OF 60 kW CW RF HPA FOR ALS-U PROJECT AT LBNL

S. Basak[†], B. Flugstad, D. Nett, K. Baptiste, LBNL, Berkeley, CA, USA
R. Kobana, K. Hirano, T. Sueishi, S. Hihara, R&K Company Ltd, Fuji City, Japan

Abstract

The two units of 60 kW CW AR RF High Power Amplifier (HPA) are critical major equipment in new RF system for ALS-U project at LBNL and so it has been designed and built with a modular redundant topology having large array of 96 RF final PA modules (each delivering ~ 700 W RF output) that are combined in parallel, and large 30 DC PS modules (each ~ 5 kW DC power) operating in parallel for achieving very high reliability (MTBF $\sim 135,000$ hours) and availability ($\sim 99.997\%$) of RF HPA which is essential design to modules failures is such that in the event up to 10% failures of RF PA modules and/or up to 15% failures of DC PS modules the HPA still can generate minimum 48 kW CW RF output that is needed for full beam power and so RF power headroom of 12 kW is built in. The operating power levels and temperatures of all components in HPA are well below to their maximum ratings for high reliability. The MBTF values of subsystems in HPA has been estimated based on components with high failures rates. The reliability probabilities having exponential distribution parameterized on failure rate were determined and the binomial distribution used for modules having redundancy. This paper presents such redundancy design analysis of HPA to such modules failures to achieve such minimum output power. Also, the Availability ($\sim 99.997\%$) and the Reliability (MTBF $\sim 135,000$ hours) Estimation analysis of the overall HPA with such redundancy to modules failures is presented.

INTRODUCTION

The ALS-U project at LBNL is aimed to create a world class facility to provide users with bright, high-coherent-flux soft x-rays that are unmatched in the world now. The ALS-U project will provide an increase in brightness and coherent flux of soft x-rays (at 1 keV) of at least two orders of magnitude beyond today's ALS capabilities. It will also provide infrared and hard x-ray capabilities comparable to the present-day ALS. There will be an upgraded Storage Ring (SR) optimized for low emittance, high soft x-ray brightness and coherent flux and a new Accumulator Ring (AR) for full-energy swap-out injection and recovery of beam bunch trains. The new AR RF system is comprised of two independent AR RF accelerating cavity subsystems, each having a low-level RF controller, an RF HPA, high power circulator, high power RF switch, rigid coaxial transmission lines, and ancillary support equipment. Each AR RF HPA will provide the requisite controlled, stable high-power RF to each normal conducting RF cavities so

as to generate the required 500 kV cavity voltage to deliver energy to the circulating electron beam in AR.

The solid-state based RF HPA is a complex piece of equipment that is the preferred topology in most Laboratories for new projects and for replacing earlier obsolete tube-based RF amplifiers because of known benefits like graceful degradation, no high voltages, high efficiency, modularity, high MTBF, and low phase noise.

The design and construction features of various subsystems in the AR RF HPA viz., AC, DC, PA modules, combiner, LCW cooling, controls, etc. has been described in Ref. [1]. The HPA has been designed and manufactured thorough a joint effort of engineers from LBNL and engineers at vendor R&K Company Ltd., Japan and a picture of the HPA taken during the factory acceptances test is shown in Fig. 1.



Figure 1: Photo of the AR RF HPA taken during FAT.

HPA MAIN SPECIFICATIONS

The HPA main specifications are tabulated in Table 1.

Table 1: HPA Main Specifications

Specification	Value
Center Frequency	500.394 MHz
1dB BW	≥ 5 MHz
1dB Output Power	≥ 60 kW CW
Input Power	≤ 0 dBm
Wall plug Efficiency	$\geq 55\%$
Group Delay	≤ 200 ns
Spurious	≤ -80 dBc
Stability (long term)	$\leq \pm 0.5$ dB ; $\leq 10^\circ$

[†]ssbasak@lbl.gov

IMPACTX SPACE CHARGE MODELING OF HIGH INTENSITY LINACS WITH MESH REFINEMENT*

C. Mitchell[†], A. Huebl, M. Garten, R. Sandberg, R. Lehe, A. Formenti, J. Qiang, and J-L. Vay
Lawrence Berkeley National Laboratory, Berkeley, CA, USA

Abstract

The code ImpactX represents the next generation of the particle-in-cell code IMPACT-Z, featuring s -based symplectic tracking with 3D space charge, parallelism with GPU acceleration, adaptive mesh-refinement, modernized language features, and automated testing. While the code contains features that support the modeling of both linear and circular accelerators, we describe recent code development relevant to the modeling of high-intensity linacs (such as beam transport for the Fermilab PIP-II upgrade), with a focus on space charge benchmarking and the impact of novel code capabilities such as mesh refinement.

BACKGROUND

High-intensity proton and ion linacs are critical to meet the needs of future colliders, spallation neutron sources, and neutrino sources. Accurate beam modeling requires high spatial resolution and particle statistics, with the ability to enable integrated start-to-end modeling with reasonable computing times, to enable large ensembles of simulation runs for optimization and for training of machine learning (ML) models, and to prepare for future Exascale computing systems, existing software must be modernized to take advantage of state-of-the-art computer hardware, including GPUs. The Beam pLasma & Accelerator Simulation Toolkit (BLAST) is an open ecosystem of codes, that can be combined with each other and with machine learning frameworks to enable integrated start-to-end simulation of accelerator beamlines for accelerator design [1]. Examples of BLAST tools include the PIC codes WarpX and ImpactX.

IMPACTX FEATURES

ImpactX [2,3] is a GPU-capable C++ successor to the Fortran code IMPACT-Z [4,5], built on the AMReX software framework [6], for modeling relativistic charged particle beams in linacs or rings. Similar to IMPACT-Z, tracking is performed with respect to the path length variable s , and space charge is included using a second order operator splitting [4]. All tracking methods are symplectic by design, and maps are used where possible for efficient particle pushing. By default, the 3D space-charge fields are computed with an iterative Multi-Level Multi-Grid (MLMG) Poisson solver [6], providing support for adaptive mesh refinement. The code provides support for commonly-used elements (drifts, quads, solenoids, dipoles, multipoles, and cavities),

as well as some specialized elements (plasma lens models, IOTA nonlinear elliptic magnet). Exact nonlinear maps are implemented for several elements (sector bends, drifts, uniform electrostatic gaps, and thin multipoles). The code is fully open to the community, and it is integrated into the BLAST software stack for interoperability with other BLAST codes.

Capabilities Added in SciDAC

ImpactX originated in an LBNL-supported LDRD as a code supporting magnetic lattice elements and high resolution space charge. As part of an ongoing HEP SciDAC-5 project [7,8], the code has undergone active development to facilitate the modeling of high intensity linacs, as part of a collaborative effort with FNAL to develop a “virtual test stand” of the PIP-II accelerator complex (Fig. 1) [9]. Capabilities added include:

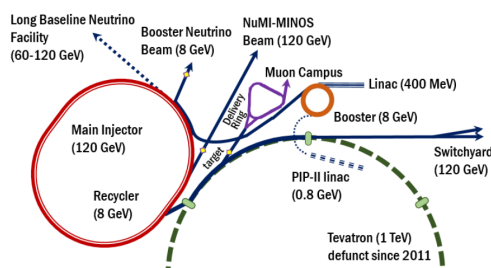


Figure 1: The Fermilab accelerator complex in preparation for the PIP-II upgrade. H^- ions are accelerated to 800 MeV in the superconducting PIP-II linac and injected into the Booster synchrotron. From there they are delivered to further accelerators and experiments.

- user control of mesh refinement (for MLMG solver)
- a 3D IGF Poisson solver with open boundaries [10]
- RF cavity models - using on-axis electric field data
- openPMD standardized format for particle output [11]
- elliptical and rectangular transverse apertures
- lost particle phase space diagnostics
- support for rotation and misalignment errors
- soft-edge magnet fringe field models (quads, solenoids)

Additional relevant tools include Python scripts for postprocessing (e.g., Twiss optics, beam visualization) and optimization (e.g., matching).

* Work supported by U.S. Department of Energy, Office of Science, Office of High Energy Physics

[†] ChadMitchell@lbl.gov

ON THE LIFE EXPECTANCE OF HIGH-POWER CW MAGNETRONS FOR SRF ACCELERATORS*

G. Kazakevich†, R.P. Johnson, Muons, Inc., Newport News, VA, USA
 T. Khabiboulline, V. Yakovlev, Fermilab, Batavia, IL, USA
 Yu. Eidelman, Eidelman Scientific Consulting, Naperville, IL, USA

Abstract

Modern CW or pulsed Superconducting RF (SRF) accelerators require efficient RF sources controllable in phase and power with a reduced cost. Therefore, utilization of the high-power CW magnetrons as RF sources in SRF accelerator projects was proposed in a number of works, e.g., [1, 2]. But typically, the CW magnetrons are designed as RF sources for industrial heating, and the lifetime of the tubes is not the first priority as it is required for high-energy accelerators. The high-power industrial CW magnetrons use the cathodes made of pure tungsten. The emission properties of the tungsten cathodes are not deteriorated much by electron and ion bombardments, but the latter causes sputtering of the cathode in the magnetron crossed fields. The sputtered cathode material covers the magnetron interior. That leads to sparks and discharges limiting magnetrons lifetime. We considered an analysis of magnetron failure modes vs. output power [3]. We developed a model of ionization of the residual gas in the magnetrons interaction space and simulated the spattering of the cathode in 100 kW CW magnetrons to estimate the life expectancy. Basing on results we proposed ways to increase the CW magnetrons longevity for SRF accelerators.

INTRODUCTION

Our consideration is based on analysis of initially developed by Burley Industries Inc. CW, 915 MHz, high-power, 10 vanes magnetrons with strapped resonant system vs. failures at power levels of 30, 50 and 75 kW [3] and analysis of impact of ionization of the residual gas in vicinity of the cathode. As it was shown in ref. [3] for 30 kW CW magnetrons with anode voltage of 12.6 kV and anode current of 2.8 A and the cathode filament power of 1.14 kW the average time in the field for new 30 kW tubes was 119 months, i.e., $\sim 20 \cdot 10^3$ hours. For 50 kW tubes at the anode voltage of 15 kV, anode current of 4 A at the filament cathode power of 0.95 kW and increased magnetic field it was $\sim 5 \cdot 10^3$ hours. The majority of failures of these tubes were caused by internal arcing. For 75 kW tubes at the anode voltage of 17.5 kV at the anode current of 5.1 A at the cathode filament power of 1.54 kW and additionally increased magnetic field the life time was less. In Ref. [3] was

noted that the internal arcing was considerably greater in tubes output power of 60 kW and more. Thus, an increase of the CW magnetrons anode voltage and current reduces the tubes life time because of internal arcing. We consider here the reasons of this.

IONIZATION OF THE RESIDUAL GAS IN A CW HIGH-POWER MAGNETRON

We consider impact of motion of electrons at operation of high-power CW magnetrons on the tubes life time with a simple model of ionization of the residual gas in a magnetron interaction space. Typical current density of tungsten cathodes is about 0.3 A/cm^2 [4]. This requires the cathode temperature of about 2500 K. An operation of the cathode at such high temperature and the cathode additional overheat caused by electron back-stream worsen the vacuum in the cathode vicinity approximately by an order of magnitude. If in a cold magnetron the vacuum pressure is typically $\leq 10^{-6}$ torr, during the tube operation the average vacuum pressure in the interaction space is increased to $\sim 5 \cdot 10^{-6}$ torr or more.

In the interaction space of operating magnetron, Larmor electrons move along trochoids during few cyclotron periods alternately approaching the cathode and anode. For 100 kW industrial, e.g., type CWM-100 kW magnetron, operating at the magnetic field of 0.238 T the anode voltage is $\approx 22 \text{ kV}$ [4]. At these parameters, the electron energy on the cyclotron orbits (closer to the cathode) is varied from approximately 0 to 10 keV for each trochoid period. The radius of the cyclotron orbit is $\approx 0.21 \text{ cm}$.

The ionization cross section of residual gases for energies of $\sim 100 \text{ eV}$ and higher is decreased approximately inversely proportional to the energy of electrons [5, 6]. Then in the estimates one can assume that in ionization of the residual gas contribute generally the Larmor electrons moving along the parts of orbits closer to cathode. It can be assumed that over several cyclotron periods the path length of the ionizing electron is of the order of the length of the Larmor orbit. Compared to high-power klystrons the smaller energy of the ionizing electrons in magnetrons results in much higher probability of ionization of residual gas by a single electron. Moreover, the modern klystrons operate at much lower pressure of the residual gas due to built-in ion pumps significantly decreasing the residual gas pressure. The ionization results in an appearance of positive ions accelerated towards the cathode. Their energy is determined by the average static electric field. In the industrial CWM-100L magnetron the ion energy is

* Supported by scientific collaboration of Muona, Inc. and Fermi National Accelerator Laboratory, Fermi Research Alliance, LLC under CRADA-FRA-2017-0026.

† e-mail: gkazakevitch@yahoo.com; grigory@muonsinc.com

DEVELOPMENT OF PHASE LOCKED OSCILLATOR FEL FOR HIGH REPETITION MID-INFRARED FREQUENCY COMBS

Y. Sumitomo, T. Kubota, K. Harada, L. Soga, T. Sakai, Y. Hayakawa
College of Science and Technology, Nihon University, Tokyo and Chiba, Japan

Abstract

The mid-Infrared region (2–5 μm) is currently a frontier of laser science with short durations, where many molecular absorbing spectrums exist. The oscillator free electron lasers have advantages against solid-state laser systems, that include the fundamental generations of high-intensity mid-IR pulses with femto-seconds scale short durations, continuous variations of the central wavelength, and the high-repetitions of pulses due to RF accelerations of electron bunches. Especially, the coexistence of high-intensities and high-repetitions at GHz scales is important for the development of mid-IR frequency combs that may open up a new direction of molecule non-linear reactions. In this paper, we report on the importance of phase-locking between FEL pulses that grow up independently due to shot noises for the mid-IR frequency combs, and the states of development of a test stand for the phase-locking system.

INTRODUCTION

We have an oscillator free electron laser (FEL) at Nihon University that equips the potential generating mid-infrared laser with a ultra-short duration less than 100 fs. The characteristics of our accelerator includes accelerations up to 100 MeV at 2.856 GHz, by RF macro pulse widths less than 20 μs , that enable FEL lasers to persist more than 10 μs in terms of macro pulse train widths. This persistent FEL laser is quite helpful to make the micro pulse length shorter but keeping the pulse energy higher since the FEL pulses needs enough durations to grow, especially at the perfect synchronization of FEL cavity against the repetition of electron pulses. In Fig. 1, we illustrate a simulation result under the perfect synchronization condition [1] using the set of

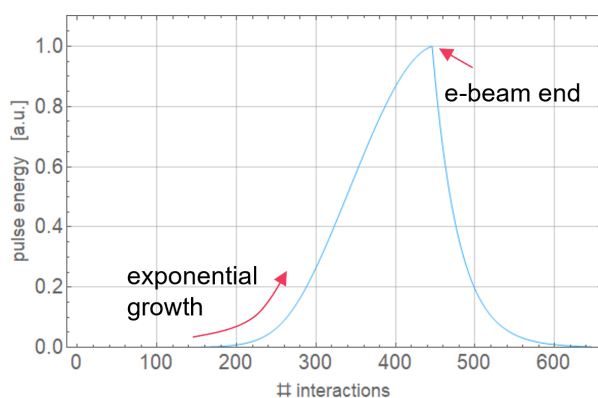


Figure 1: A simulation example of pulse growth respecting the oscillator FEL under the perfect synchronization condition [1].

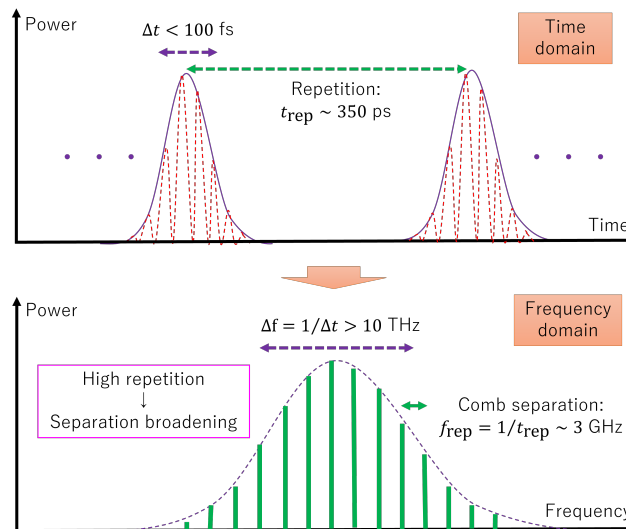


Figure 2: A schematic showing the relation between high-repetition pulses and comb separations in frequency domain.

parameter assuming our experimental operation. Also for reference, our recent experimental records show the micro pulse energy of over 1 μJ persistent among about 10 μs at the 2.856 GHz operations.

The mid-IR region is currently a frontier of laser science accompanying the recent technology generating ultra short femto-seconds scale pulses. There are many efforts devoted to generate so-called frequency combs at the mid-IR, where many topics of molecular science are related (see for instance a review article [2]). For the generations of frequency combs, the shorter pulse widths are important to have a frequency broadening so as to make enough bins in the comb. Also, the high-repetition of pulses is related to a power concentration of each bin in frequency space since the separation of bins is broadened while the total power is not changed.

We illustrate a schematic describing these relations for a better understanding in Fig. 2. In the development of solid-state lasers, the high-repetition mid-IR pulses are likely to generate by non-linear downward conversions from near-IR lasers where the efficiency of conversions is quite low. The short resonators are used for generating the high-repetition pulses over GHz ranges, but the pulse energy decreases due to the split.

Hence, we consider that the acceleration based generations of mid-IR frequency combs have advantages, for high-power pulse energy by the fundamental oscillator FEL lasers, and for the high-repetitions of pulses due to RF accelerations at GHz regions. We can also realize the ultra-short pulses of femto-seconds scale durations and make them shorter by

FIRST-PRINCIPLE BEAM-DYNAMICS SIMULATIONS OF ALPHA MAGNETS FOR BUNCH COMPRESSION OF BRIGHT BEAMS *

A. Al Marzouk[†], Northern Illinois University, DeKalb, IL, USA
P. Piot, Argonne National Laboratory, Lemont, IL, USA

Abstract

Producing bright electron beams is crucial for coherent light sources, where increasing the peak current is typically accomplished through bunch compression in magnetic chicanes. Alpha magnets, with their unique phase-space manipulation capabilities, have emerged as an attractive choice for compressing sub-10 MeV electron beams generated by radio frequency photoinjectors. This paper presents detailed numerical modeling of the beam dynamics of high-charge, bright bunches undergoing compression within an alpha magnet. The model incorporates space-charge effects and coherent synchrotron radiation, providing a comprehensive understanding of the complex interactions and behaviors of the electron beams during the compression process.

INTRODUCTION

Coherent light sources require bright electron beams with high peak currents. To increase the bunch peak current, longitudinal bunch compression in magnetic chicanes is commonly employed. This process necessitates an energy chirp in the electron bunch—a correlation between the particles' longitudinal positions and their energies—which is typically introduced by RF accelerating structures. Consequently, using chicanes for compression often requires a relatively large system and is more suitable for high energies (> 10 MeV). For compressing sub-10-MeV beams, a shorter and more compact system is desirable. In this context, alpha magnets combined with RF guns present an attractive and effective compression scheme for compact injector systems. Similarly, this class of magnet has been extensively used in conjunction with thermionic RF guns to generate bunch trains for injection into storage ring complexes. [1].

An alpha magnet can be assimilated to a half-quadrupole magnet. In the ideal alpha magnet considered in this paper, a particle injected at an angle of 40.71° to the normal of the magnet entrance exits at the same angle, regardless of its energy. The particle's trajectory within the magnet forms a path resembling the letter alpha (α). Alpha magnets were originally used as achromatic magnetic mirrors for ion beams [2]. Detailed particle dynamics in the alpha

magnet and its characteristics are described in [3]. Due to their unique phase-space manipulation capabilities, alpha magnets have garnered significant interest as bunch compression schemes for low-energy electron beams, particularly in applications like coherent light generation; see, e.g., [4–10]. The particle's path length inside the alpha magnet varies depending on its energy such that high energy electrons follow a longer path than that of the lower energy electrons. Therefore, an energy chirped beam will be compressed after passing through the alpha magnet similarly to the magnetic chicane, but with a positive chirp in this case (i.e. high-energy head and low-energy tail). The chirp can be provided by the RF photoinjector, and hence the compression can be performed at a low energy right after the gun without the need for an RF accelerating structure.

At low energies, space charge forces are particularly strong, especially for higher bunch charges. Additionally, the bending of electron trajectories through the alpha magnet causes the emission of synchrotron radiation, which becomes coherent for short bunch lengths. Therefore, detailed numerical modeling of the beam dynamics for high-charge, bright bunches undergoing compression in an alpha magnet—including space charge effects and coherent synchrotron radiation (CSR)—is essential. Studies on beam dynamics and space charge simulations are available in Refs. [11–15].

In this paper, we present beam dynamics simulations of alpha magnet bunch compression using the first-principles, large-scale CSR model, the `LW3D` code, which naturally incorporates both space charge and CSR effects. The aim is to investigate the impact of CSR on beam brightness.

SIMULATION METHOD

The basic approach to CSR involves computing the 3D electromagnetic radiation fields directly from the Liénard-Wiechert potentials. The `LW3D` code, developed by Ryne [16], is the only first-principles implementation for 3D CSR computation. It is a large-scale parallel program that calculates CSR fields on a 3D grid at each time step. These fields are then applied to the particles by interpolating them at each particle's position over time, a method referred to as the self-consistent mode of `LW3D`.

An important feature of the `LW3D` algorithm is its ability to consider arbitrary external electric and magnetic fields while most other available CSR codes are limited to dipole magnets. This feature is essential for the alpha-magnet simulation as we can easily include its fields in the code or import the field map from a file.

While CSR effects can be mitigated through shielding [17], the current implementation of the `LW3D` code does

* This work was supported by the U.S. National Science Foundation under award PHY-1549132 to Cornell University. This material is partially based upon work supported by Laboratory Directed Research and Development (LDRD) funding from Argonne National Laboratory, provided by the Director, Office of Science, of the U.S. Department of Energy under Contract No. DE-AC02-06CH11357. This research used resources of the National Energy Research Scientific Computing Center; a DOE Office of Science User Facility supported by the Office of Science of the U.S. Department of Energy under Contract No. DE-AC02-05CH11231 using NERSC award BES-ERCAP0020725.

[†] aalmarzouk1@niu.edu

ENGINEERING DESIGN OF 402 MHz NORMAL CONDUCTING COAXIAL WINDOW*

S. U. Thielk, R. Agustsson, S. Kutsaev[†], A. Pronikov, RadiaBeam LLC, Santa Monica, CA, USA

Abstract

RadiaBeam is fabricating a novel RF vacuum window for use with the Spallation Neutron Source (SNS) at Oak Ridge National Laboratory (ORNL). The window features a coaxial ceramic window between two waveguides, brazed as a single assembly. Unlike traditional pillbox window designs, this approach allows the outer diameter of the ceramic to decrease and the added benefit of water cooling the inner diameter of the ceramic. This paper covers the engineering design including details of key features, the impact of the unique RF design on manufacturability, and mechanical simulations. A status update on the fabrication is also provided with emphasis on the ceramic TiN coating and brazing process.

INTRODUCTION

The radio-frequency (RF) window is a critical aspect of most accelerator systems since it is responsible for separating the vacuum volume of the accelerating cavity from the RF power transmission line. For rectangular waveguide, this is commonly achieved by brazing a disk of dielectric material, typically alumina, into a cylinder that is then placed into the transmission line. Dimensions of the cylinder are optimized to minimize RF reflections often resulting in a diameter for the alumina window that is larger than the waveguide. For compatibility with the Spallation Neutron Source (SNS), which operates at 300-500 kW average power and 402.5 MHz, the window transitions from WR2100 waveguide (533.4 mm x 266.7 mm) on the input side to half height WR2100 waveguide (533.4 mm x 133.4 mm) on the output, or vacuum side of the assembly. The vacuum side interfaces with the iris coupler for the SNS drift tube LINAC [1]. A traditional pillbox style window for this assembly would require a ceramic diameter of approximately 330-360 mm, creating a host of challenges ranging from ceramic sourcing to excessive thermal gradients. A review of the RF design can be found in [2].

In response to this, RadiaBeam has developed a novel design that employs a coaxial window, instead of cylindrical. This approach provides several benefits. First, the diameter of the coaxial line is defined by the RF power not frequency since it operates in Transverse Electro-Magnetic (TEM) mode. The window size can be reduced to approximately 250 mm which significantly reduces the fabrication complexity and improves structural stability. Second, water cooling can be applied to both inner diameter (ID) and outer diameter (OD), instead of just the OD of the cylindrical window. Therefore, the field distribution in the

coaxial line is more uniform, which reduces dielectric losses and thermal gradients.

MECHANICAL DESIGN

The engineering design is the culminating result of the RF, thermal, and manufacturability requirements. With large internal volumes and changing cross-sectional geometries, breaking the top-level model into sub-assemblies and parts required careful consideration for machining, brazing, handling, and cost. The result is a final assembly that consists of five main sub-assemblies, as demonstrated in Fig. 1. Each sub-assembly requires multiple braze steps prior to the final braze using Gold Copper braze alloys.

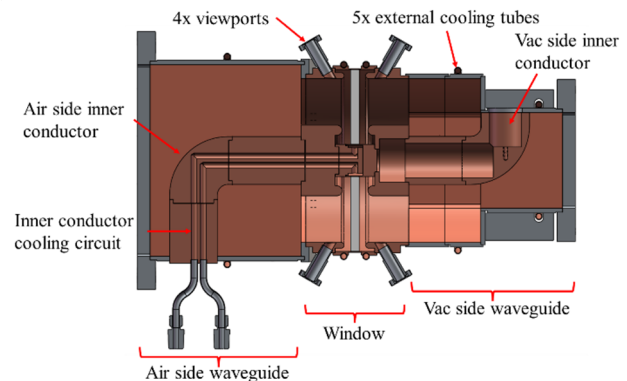


Figure 1: Cross-section view highlighting major sub-assemblies and components.

The window sub-assembly features the critical ceramic window braze. Additional details regarding the Titanium Nitride (TiN) coated Kyocera AO479U window can be found in prior publications [3, 4]. The parts brazed to the inner diameter of the ceramic form a cooling channel that places all braze joints on the air side of the assembly to eliminate risk of water to vacuum leaks. The sleeve that forms the hermetic seal with the metallized ceramic inner diameter is 1.27 mm thick. This allows the sleeve to deform during the high temperature braze to absorb the residual stress caused by the differential coefficients of thermal expansion (CTE) between copper and alumina. Additionally, the thin wall provides excellent heat transfer characteristics.

The outer diameter of the ceramic is brazed to another thin wall sleeve. During brazing, tooling constricts the thin wall to control the growth of the copper sleeve and the gap between the sleeve and the outer diameter of the ceramic at brazing temperatures. Without constrictive tooling, the differential expansion between the copper and alumina would result in a ~1.52 mm gap, far beyond the .025-.076 mm gap required for liquid braze alloy to be pulled into the joint via capillary action. Similar approaches have been demonstrated throughout literature [5-7]. Components

* This work was supported by the U.S. Department of Energy, Office of Basic Energy Science, under SBIR grant DE- SC0021552

[†] kutsaev@radiabeam.com

DESIGN OF A 25 kW FUNDAMENTAL POWER COUPLER FOR CONDUCTION COOLED Nb3Sn INDUSTRIAL LINAC*

S. U. Thielk†, R. Agustsson, S. Kutsaev, A. Pronikov, A. Martinez
RadiaBeam LLC, Santa Monica, CA, USA

J. Vennekate, G. Ciovati, R. Rimmer

Thomas Jefferson National Accelerator Facility, Newport News, VA, USA

Abstract

RadiaBeam has designed a 915 MHz, 25 kW CW Fundamental Power Coupler (FPC) to power a Nb₃Sn coated superconducting radio-frequency (SRF) cavity. Unlike traditional FPCs for SRF cavities, the device relies only on conductive cooling by cryocoolers. The baseline design was adapted from the liquid helium cooled 805 MHz SNS FPC with the notable addition of an intermediate 50 K thermal intercept and associated RF shield. Engineering design details to address the thermomechanical, manufacturability, and structural challenges will be presented. Particular emphasis will be placed on static and dynamic heat load management along with finite element analysis to validate mechanical stability. Additionally, initial manufacturing studies of the coaxial window brazing will be discussed.

INTRODUCTION

The design complexity of an FPC is rooted in the strict vacuum, thermal and mechanical requirements while ensuring the manufacturing complexity and risk is minimized. Further, these efforts must be performed iteratively with RF design to ensure efficient power coupling into a cavity. Although this paper is not focused on RF design, it is pertinent to note that the FPC is designed to operate at 915 MHz with a $S_{11} = -50.17$ dB, $S_{21} = -.006$ dB and a Q-factor between 2.96e6 to 3.3e6 with the intended Nb₃Sn coated SRF cavity. Similar to the SNS approach [1], a doorknob transition and coaxial style window were used.

A key requirement of the FPC is to transition from cryogenic temperatures near the cavity to the room temperature cryostat while minimizing the heat load to the cooling systems. In addition to the static heat transfer, heat generated from RF losses and radiation must be accounted for. SRF cavities fabricated from pure niobium operate around 2 K, typically achieved with complex and costly liquid helium systems. Nb₃Sn coated SRF cavities can operate with low losses at ~4 K, permitting the use of cryocoolers and conduction based heat removal. Without the option to route liquid helium near the FPC to cavity connection, a 50 K intercept linked to the first stage of the cryocooler can be employed. In this effort, the required heat loads were

defined as <2 W and <50 W to the SRF cavity and to the 50 K intercept, respectively. All of these factors make FPC design a multi-disciplinary effort as documented elsewhere in more comprehensive design overviews [2, 3].

MECHANICAL DESIGN

The FPC fabrication can be divided into three primary sub-assemblies as shown in Fig. 1: the doorknob, window, and outer conductor. The doorknob is responsible for transferring power from a WR975 rectangular waveguide into a coaxial port for the FPC. It consists of a welded aluminum box containing the copper doorknob and inner and outer conductor extensions. The window sub-assembly serves as the atmosphere to vacuum barrier, includes the critical fixed length antenna, and provides diagnostic ports. The positioning of the antenna tip is critical to the power coupling. Therefore, there are clear advantages to include methods to adjust the position. However, a fixed length antenna was elected as the most effective approach after comparing system requirements to manufacturing complexity. The outer conductor assembly connects the flange bolted to the cavity to the window and cryostat wall. The temperature gradient across the outer conductor sub-assembly components is accomplished by a thin-walled thermal choke and an RF shield.

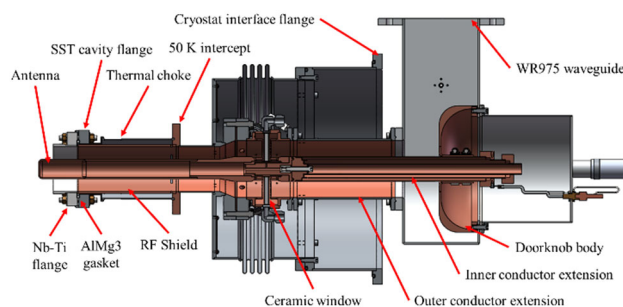


Figure 1: Cross-section of complete FPC assembly highlighting key features.

The RF shield concept was inspired by multiple publications [4- 6]. Serving as the outer conductor starting at the 50 K intercept, there is a small gap between the end of the shield and the 4.2 K cavity flange, as shown in Fig. 2. Eliminating this conduction path funnels heat from RF losses close to the cavity to the higher capacity 50 K cryocooler circuit. A small lip was added to the tip of the shield, maintaining the effectiveness while alleviating concerns about manufacturability and potential interference.

* The work was supported by U.S. Department of Energy, Office of Science, Office of Nuclear Physics via a grant from the Accelerate Innovations in Emerging Technologies program and by DOE-ARDAP via a grant from the Accelerator Stewardship program. The contribution from JLab is based upon work supported by the U.S. Department of Energy, Office of Science, Office of Nuclear Physics under contract DE-AC05-06OR23177

† sthielk@radiabeam.com

STATUS OF THE iBNCT ACCELERATOR

M. Sato[†], Z. Fang, Y. Fukui, K. Futatsukawa, K. Ikegami, H. Kobayashi, C. Kubota, T. Kurihara,
 T. Miura, F. Naito, K. Nanmo, T. Obina, T. Shibata, T. Sugimura, A. Takagi
 High Energy Accelerator Research Organization (KEK), Ibaraki, Japan
 H. Kumada, Y. Matsumoto, S. Tanaka, University of Tsukuba, Ibaraki, Japan
 T. Ohba, N. Nagura, NAT, Ibaraki, Japan
 T. Toyoshima, ATOX, Ibaraki, Japan
 H. Oguri, Japan Atomic Energy Agency, Ibaraki, Japan

Abstract

Accelerator-based boron neutron capture therapy (BNCT) has been studied worldwide. The iBNCT (Ibaraki BNCT) project began in collaboration with KEK, the University of Tsukuba, Ibaraki Prefecture, and related private companies in Japan in 2010. The iBNCT project aims to realize linac-based BNCT by irradiating a beryllium target with protons accelerated to 8 MeV. The accelerator configuration comprises an ECR ion source, a 3-MeV radio-frequency quadrupole linac, and an 8-MeV Alvarez-type drift tube linac, which is based on the Japan Proton Accelerator Research Complex linac techniques. The iBNCT project has achieved stable operation with an average proton beam current of 2 mA with a repetition of 75 Hz and a beam width of 0.92 ms. After the completion of the non-clinical studies in the fiscal year 2022, we finished preparing to start a clinical study in the year 2023 for both the medical and accelerator sides. The iBNCT project began as a Phase-I Investigator-initiated clinical trial in January 2024. In this paper, the current status of the iBNCT accelerator and its prospects are discussed.

INTRODUCTION

Accelerator-based boron neutron capture therapy (BNCT) has been extensively studied in recent years as a novel cancer therapy. It has a long history of clinical research on nuclear reactors; however, medical treatments in nuclear reactors cannot be a general treatment owing to constraints on its operation and management. Therefore, an accelerator-based BNCT has gained popularity. The iBNCT project was launched in 2010 in collaboration with the University of Tsukuba, High Energy Accelerator Research Organization (KEK), related private companies, and Ibaraki Prefecture in Japan [1]. The iBNCT project aims to realize accelerator-based BNCT with the accelerator configuration of 3-MeV radio-frequency quadrupole (RFQ) linac and 8-MeV Alvarez-type drift tube linac (DTL), whose feasibility has already been proven in the Japan Proton Accelerator Research Complex (J-PARC). Figure 1 shows a schematic of the iBNCT accelerator. The apparatus was installed at the Ibaraki Neutron Medical Research Center in Tokai, Ibaraki Prefecture, Japan. A bird's-eye view of the iBNCT accelerator can also be found in

Ref. [2]. Assuming that all the accelerator configurations are installed in a hospital, the size of the entire system should be as small as possible. As shown in Fig. 1, the proton beam passes from left to right. The primary proton beam was generated using an ECR ion source (ECR-IS) and accelerated to 50 keV under an electro-static field of 50 kV. The ECR-IS is driven by a 2.45-GHz magnetron with a maximum RF power of 3 kW. After the low-energy beam-transport line (LEBT), a 3-MeV RFQ is placed. The RFQ design was based on the J-PARC RFQ-II [3]. A 324 MHz klystron provides RF for both the RFQ and DTL simultaneously [4]. The typical rated power is 340 kW for the RFQ and 320 kW for the DTL. The medium-energy beam-transport line (MEBT) between the RFQ and the DTL contains three permanent quadrupole magnets and a beam-position monitor. After the MEBT, the DTL is placed. The design of the DTL is also based on the J-PARC DTL; however, it differs from the J-PARC DTL in its length and quadrupole magnets in the drift tubes. In the iBNCT accelerator, the output energy is optimized to be 8 MeV; thus, the length of the DTL is only 3.1 m. Another point is the application of permanent magnets for the quadrupole in each drift tube to save on electricity costs. A beam transport line (BT) of approximately 15 m in length was located after the DTL. In the straight line immediately before the neutron-generation beryllium target, a beam expander, which comprises two quadrupole and two octupole magnets, is installed alternative to expand the beam lateral size and reduce the beam intensity per unit area on the target. The beryllium target has a three-layer structure comprising 0.5-mm thick beryllium, 0.5-mm thick palladium, and 10-mm thick copper. A detailed description is provided in Ref. [5, 6]. The neutron moderator and collimator were located after the beryllium target. This apparatus not only decreases neutron energy generated by $^9\text{Be}(p, n)$ reaction from a few MeV to the epi-thermal neutron region below 10 keV but also suppresses unwanted γ -rays and high-energy neutrons for BNCT. Guidelines have been established by the IAEA for the desired neutron flux for BNCT, which requires an intensity of more than 1×10^9 n/cm²/s [7]. Therefore, high proton beam intensity is required. Thus, the iBNCT accelerator must be designed with a higher proton beam intensity than that of the J-PARC accelerator, which forms the basis for the design.

[†] masaharu.sato@kek.jp

ADVANCES IN FS SYNCHRONIZATION

M. K. Czwalinna*, J. Branlard, B. Lautenschlager, F. Ludwig, S. Schulz, H. Schlarb
Deutsches Elektronen-Synchrotron DESY, Hamburg, Germany

Abstract

Linear accelerators for FELs have very high requirements for the accuracy of synchronization. The long and short term stability is influenced by various sources of interference. In this paper it will be shown which methods of stabilization exist and how synchronization accuracy up to the single-digit femtosecond-level can be achieved.

INTRODUCTION

High precision applications at Free-Electron Lasers (FEL) pose demanding requirements on the involved reference distribution and control systems of the Linear electron accelerators (Linac). Stability requirements for the Linac are derived from the needs of user experiments, concerning photon energy stability, and the desired temporal resolution when observing dynamics on the femtosecond scale. Advanced FEL schemes as the hard x-ray self seeding, are highly sensitive to deviations from the ideal electron bunch properties in both, the transverse and longitudinal phase space. All large-scale FEL facilities require some sort of synchronization system to reach sufficient time and phase stability. Experiments in pump-probe configuration with two or more radiation sources (x-ray photons, optical laser, THz) are limited in achievable measurement resolution by pulse widths and relative timing stability in between the pump and probe pulses.

All phase-critical subsystems at a Linac are susceptible for environmental changes, including variation of the ambient temperature, changes in relative humidity and air pressure (in case of laser systems), as well as micro-phonics and other types of vibrations and ground motions. In addition to the performance demands, at user facilities also the robustness and reliability of the critical subsystems is a vital property to guarantee a long mean time between failures and high availability. Costs for installation, operation and maintenance are additional criteria. When selecting a type of synchronization system, it makes sense to consider all of the mentioned aspects. Therefore, at most facilities a hybrid solution has been realized, providing a combination of an RF-based distribution for shorter distances, and a long-haul laser-based synchronization system to fulfill the needs of the most timing critical client systems at an FEL.

SYNCHRONIZATION TECHNIQUES

Each of the possible synchronization techniques comes with its own challenges, advantages and drawbacks. For example, RF-based distribution systems have relatively low costs for small facilities and can provide many reference tap

points for the RF cavity control. However, their critical parameters concern phase drift in cables, phase uncertainties of frequency dividers and ability to recover phase offsets after power cycling of the system [1]. To improve the stability of a passive RF distribution system one has to carefully choose cabling type with temperature coefficients of $<20 \text{ fs m}^{-1} \text{ K}^{-1}$ and an optimal ambient operation temperature to minimize drifts induced by temperature variation [2]. In addition, it might be needed to actively reduce overall temperature fluctuation in the whole accelerator tunnel during operation. Passive RF-distribution systems can achieve a long-term stability of about 50 fs/day/100m [3]. However, compared to telecom optical cables, RF cables suffer with typically 3 dB/100m from power loss. For long-haul distribution systems, this requires a lower distribution frequency with local frequency and phase reconstruction, to reduce distortions along the accelerator. A purely RF-based synchronization with an interferometric phase reference line and active stabilization is under development and has demonstrated already a phase error as good as $\pm 200 \text{ fs}$ over several days for short links of $<200 \text{ m}$ [4, 5].

Another approach are pure continuous wave (CW) optical links for distributing a microwave reference frequency over optical fiber, either as amplitude modulated (AM) or frequency modulated (FM) signal. As alternative to RF oscillators also CW optical lasers or atomic clocks can serve as ultra-low noise phase reference system. CW optical systems come with the advantage of usually lower costs while still reaching timing jitter performance as good as 10 fs level. For mitigating long-term timing drifts to below $<1 \text{ ps}$ over days, a more complex implementation has to be considered, e.g. by using multiple fibers for the same link (one uni-directional and a bi-directional link) for re-calibration purpose [6, 7]. An RF-over-fiber reference distribution system has been developed for LCSL as described in [8]. It achieved an integrated residual jitter of 17.5 fs (10 Hz to 10 MHz) for a transmitted 476 MHz reference frequency. The limitation of CW reference sources in general are given by the fact that they deliver only a single frequency, reducing the variety and also the performance when phase-locking client systems to the reference source.

At SwissFEL, a CW-optical system for connecting most systems (remote microwave oscillators) has been chosen, showing less than 40 fs drift peak-to-peak over 24 h and less than 10 fs rms (10 Hz to 10 MHz) integrated jitter [9, 10]. A few pulsed optical links were added for the use of electro-optical bunch arrival time monitors, and for applying a direct laser-to-laser synchronization for the user experiments.

Such pulsed optical synchronization systems are required to fulfill highest demands on timing stability, in terms of jitter and drift, but also typically require highest investment

* marie.kristin.czwalinna@desy.de

ADAPTIVE MACHINE LEARNING WITH HARD PHYSICS CONSTRAINTS AND GENERATIVE DIFFUSION FOR 6D PHASE SPACE DIAGNOSTICS*

A. Scheinker[†], Los Alamos National Laboratory, Los Alamos, NM, USA

Abstract

Machine learning (ML) tools have been growing in popularity for accelerator applications, but still struggle with time-varying systems, for which they require lengthy brute-force re-training. LANL has developed machine learning (ML)-based tools, that utilize adaptive model independent feedback control theory together with hard physics constraints, to make the tools much more robust to distribution shift. These adaptive ML tools can extrapolate much further beyond the span of the training data and are thus much more robust for time-varying systems. This talk will give a broad overview of the challenges of various time-varying accelerator systems at various accelerator facilities (known as systems with distribution shift in the ML community) and will present adaptive ML tools for 6D phase space diagnostics of intense charged particle beams. The talk will also give a general overview of adaptive latent space tuning, which is the novel method we have developed for adaptive ML, and how we are strictly enforcing hard physics constraints in our ML tools, which traditional ML tools lack. We demonstrate our general methods for various accelerators: the 5-meter-long ultra-fast electron diffraction (UED) HiRES compact accelerator at LBNL, the kilometer long plasma wakefield accelerator FACET-II at SLAC, and the LANL ion accelerator LANSCE.

INTRODUCTION

Particle accelerators are large complex systems composed of thousands of coupled components including resonant radio frequency (RF) structures for beam acceleration and magnets for beam shaping and steering. The performance of all of these components drifts with time due to external disturbances such as environmental temperature variation, vibrations and power line fluctuations, due to ageing, and due to misalignment and shift of components during maintenance. Furthermore, the beams themselves have time-varying initial conditions due to time variation of the complex beam source properties. Changing initial conditions can strongly effect the detailed 6D phase space distributions of beams, especially for intense beams whose evolution is governed by complex collective effects such as space charge forces and coherent synchrotron radiation.

Alongside the complexity and time variation of these systems and their beams, there is a lack of detailed non-invasive beam diagnostics beyond simple 1D measurements such as beam position monitors, beam current monitors, or beam

loss monitors. The result is that accelerator beams are difficult to tune up after an outage (typically requiring weeks of effort by large teams) and are difficult to re-tune between different experiments even when the machines are running. Besides the large amount of time that is consequently wasted in re-tuning of the machines, they are also typically running at sub-optimal states with operators chasing drifts to decrease beam loss by tuning tens-hundreds of parameters by hand based on experience.

Motivated by the above, there has been a strong effort to create new tools for beam diagnostics and controls. For the EuXFEL, a convolutional neural network-based approach has been developed for generating high-resolution longitudinal phase-space (LPS) (z, E) images of the electron beam [1]. Convolutional neural networks have also been combined with destructive beam measurements to develop extremely fast virtual diagnostics for 4D tomographic phase space reconstructions [2]. Neural network-based methods have also been developed for predicting the transverse emittance of space charge dominated beams [3]. Convolutional neural networks and clustering algorithms have also been developed for predicting the longitudinal phase space of FEL beams and also to cluster these images to highlight patterns within the data [4]. Recently, very interesting methods have also been studied for phase space reconstructions based on normalizing flows [5]. One benefit of all ML-based tools is that they are by default fully differentiable models, enabling easy studies of complex input-output dependencies.

The time variation of the systems makes it clear that off-the-shelf machine learning methods cannot simply be used as they will require continuous repeated re-training based on expensive invasive beam measurements if they are applied to such systems which quickly vary with time. To overcome this difficulty, a new class of adaptive machine

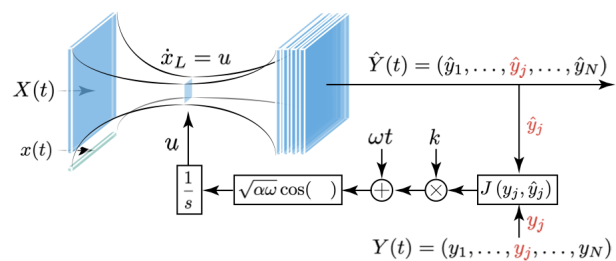


Figure 1: Adaptive latent space tuning setup in which a generative autoencoder generates all 15 projections of a beam's 6D phase space and then only those projections that can be measured non-invasively are compared to their predictions in order to track the time-varying beam with unknown and time-varying initial conditions, by adaptively tuning the low-dimensional latent embedding.

* This work was funded by the US Department of Energy (DOE), Office of Science, Office of High Energy Physics under contract number 89233218CNA000001 and the Los Alamos National Laboratory LDRD Program Directed Research (DR) project 20220074DR

[†] ascheink@lanl.gov

CRABBING CAVITY SYSTEM DEVELOPMENT FOR INTERNATIONAL LINEAR COLLIDER *

S. U. De Silva[†], Old Dominion University, Norfolk, VA, USA

Abstract

The International Liner Collider requires a crabbing system to increase the luminosity of the colliding electron bunches. The ILC has a large crossing angle that requires compensation in order to meet the luminosity requirements. There are several frequency options proposed for the crabbing cavity design. Two crab cavity designs were selected to be prototyped in the pre-lab phase, following the Down Selection Review on Crab Cavity Design held in April 2023. The two rf designs selected are the 1.3 GHz rf-dipole cavity and the 2.6 GHz QMiR cavity. This paper describes the electromagnetic and mechanical design details of the two compact crabbing cavity designs.

INTRODUCTION

The International Liner Collider (ILC) is designed to collide electrons and positrons at the speed of light with center of masses (CoM) varying from 250 GeV to 1 TeV. The baseline design CoM is 250 GeV where the 1 TeV beam energy is the proposed upgrade of the ILC. The two beams are accelerated in two separate linacs spanning over 20 km as shown in Fig. 1 [1, 2].

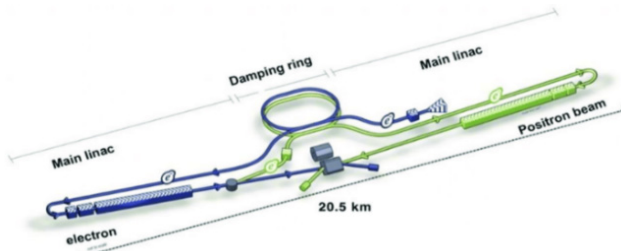


Figure 1: Layout of the Electron-Ion Collider.

The expected integrated luminosity goal of the ILC is $\sim 10^{34} \text{ cm}^{-2}\text{sec}^{-1}$. The ILC requires crabbing cavities to compensate for the luminosity degradation due to the large crossing angle of 14 mrad. Operation without crab cavities may lead to a luminosity reduction up to 80% as shown in Fig. 2. The crabbing cavities will deliver a transverse kick at the head and tail of the colliding bunches that will rotate the bunches allowing them to overlap them at the interaction point (Fig. 3) [3]. This maximizes the luminosity by increasing the number of interactions between the particles in each colliding bunch. Crabbing systems will be installed in both electron and positron beams and does not require crabbing systems to cancel the crabbing effect.

* This research used resources of the National Energy Research Scientific Computing Center (NERSC); a U.S. Department of Energy Office of Science User Facility operated under Contract No. DE-AC02-05CH11231.

This work was produced by Fermi Research Alliance, LLC under Contract No. DE-AC02-07CH11359 with the U.S. Department of Energy.

[†] sdesilva@jlab.org

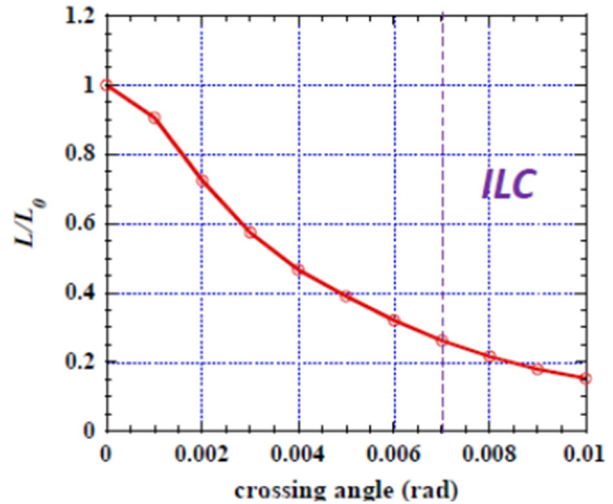


Figure 2: Luminosity degradation as a function of crossing angle for ILC.

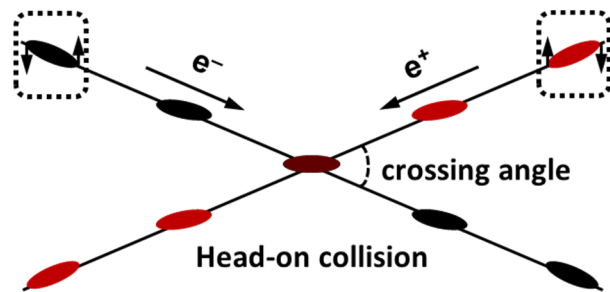


Figure 3: Crab crossing with crabbing systems for electron and positron beams.

ILC Crab Cavity Requirements

The crabbing system specifications include dimensional constraints and rf requirements as listed below [4].

Dimensional Constraints:

- Total beam line space – 3.8 m
- Separation between two beam lines < 197 mm (Fig. 4)
- Minimum crab cavity beam aperture – 25 mm

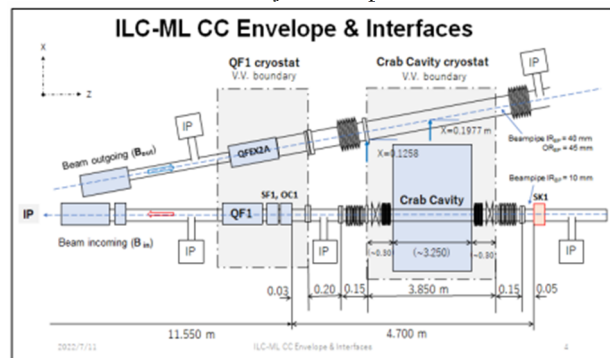


Figure 4: Beamline layout of the crabbing system.

THE DEEP ELECTRON FLASH THERAPY FACILITY

C. Rossi*, M.E. Angoletta, O. Brunner, J. Bauche, R. Corsini, J.M. Cravero, S. Doebert, B. Frisch, E. Granados, A. Grudiev, R. Key, V. Korchevnyuk, A. Latina, A. Malyzhenkov, I. Syratchev, P. Wang, W. Wuensch, CERN, Geneva, Switzerland

C. Bailat, F. Bochud, T.T. Böhlen, J. Bourhis, J. Damet, L. Desorgher, T. Garvey, J.F. Germond, W.R. Geyer, V. Gregorio, V. Grilj, F. Herrera, R. Moeckli, N. Walter
CHUV, Lausanne, Switzerland

S. Curtoni, T. Dufour, P. Liger, THERYQ, Rousset, France

Abstract

The “FLASH” effect is currently a topic of considerable interest in radio-oncology. We present the design of a novel VHEE linac, to be built and installed at CHUV (Lausanne), capable of producing electron beams which deliver radiation at dose rates and time scales consistent with the FLASH effect. The design is based on X-band radio-frequency technology, developed at CERN for the CLIC study. The e-beam properties correspond to a CHUV specification and would allow large, deep seated, tumours to be treated. Construction of DEFT (DEEP Electron FLASH Therapy) will be assured by the company THERYQ in the context of a CHUV-CERN-THERYQ collaboration.

INTRODUCTION

Radiation therapy (RT) constitutes one of the main pillars in cancer treatment, together with surgery and chemo/immuno therapy [1–3]. The conflicting requirement of sparing the healthy tissues that surround the tumor while maximizing the effectiveness in tumor control has pushed RT technologies towards fractionated dose administration together with highly conformal dose delivery systems. Besides MV photon beams, which are the workhorse of modern external beam RT, other therapeutically used particle species include protons, light ions, and electrons <25 MeV. While such modern high-precision RT treatments can provide acceptable clinical outcomes with limited side effects for many patients [1, 3] there is still a clinical care gap and a resulting clinical need for numerous cancer patients.

For such cases, hope is being generated by the observation that doses delivered at ultra-high dose rates (UHDR, average dose rate ≥ 50 Gy/s) can produce a sparing effect on healthy tissues while maintaining the effectiveness on tumoral cells compared to irradiations delivered at conventional dose rates (average dose rate ~ 0.05 Gy/s) [4, 5]. This increase of the therapeutic index by the ultra-fast dose delivery, commonly referred to as “FLASH effect”, was initially observed in the 70’s, first proposed in 2014 and has since then been independently confirmed in numerous studies using different radiation modalities and preclinical models [4–7].

The adoption of the high-gradient RF technology developed at CERN for the realization of the high-energy linear collider CLIC appeared to be the logical choice for designing

a compact FLASH-RT device capable of producing penetrating very high-energy electron (VHEE, 100 - 250 MeV) beams at UHDR to treat deep-seated tumors. In addition, supporting experiments are being carried out at the CERN facility CLEAR in relation to the creation and detection of UHDR and to the characterization of the FLASH effect.

MEDICAL BACKGROUND

The potential implications of FLASH-RT in clinical practice are profound. Conventional radiotherapy, while effective, often necessitates a delicate balance between delivering sufficient doses to eradicate tumors and minimizing exposure to surrounding healthy tissues. This balance becomes particularly challenging when treating tumors located close to critical structures and/or large and non-curable cancers such as glioblastomas for which there is a huge unmet clinical need. FLASH-RT, on the other hand, with its potential to elicit a biological selectivity between tumors and healthy tissues, may offer a breakthrough in overcoming these limitations. The reduced toxicity induced by the FLASH effect on the healthy tissue could allow for higher therapeutic doses, potentially improving either local control and overall survival rates or reducing treatment side effects for challenging cancers.

Status of Preclinical and Clinical FLASH Research at CHUV

Extensive preclinical evidence supports the potential of FLASH-RT to enhance the therapeutic ratio of RT by delivering treatments at UHDR [5–7]. In 2018, CHUV successfully conducted the first human treatment using UHDR electrons, marking a significant milestone in the clinical application of FLASH-RT [8, 9]. The patient, treated for cutaneous lymphoma, showed excellent tumor control with minimal side effects, demonstrating the feasibility and potential benefits of FLASH-RT in clinical settings. Building on this success, CHUV has initiated two human clinical trials: a dose escalation trial (IMPulse, NCT04986696) for metastasized melanoma and a Phase II trial (LANCE, NCT05724875) aimed at evaluating the treatment of localized cutaneous squamous cell carcinoma (SCC) and basal cell carcinoma (BCC) with FLASH-RT in comparison with standard of care RT. Both trials show promising preliminary outcomes.

* carlo.rossi@cern.ch

RESULTS FROM CXLS COMMISSIONING

W. S. Graves*, G. Babic, C. V. Bell, S. Botha, T. Brown, B. Cook, T. Dela Rosa, A. Dupre, K. Eckrosh, E. Everett, J. Falconer, P. Fromme, A. Gardeck, M. Holl, M. Hussain, S. Jachim, R. Jaswal, P. Jiang, R. Kaindl, R. Kirian, R. Larsen, H.-S. Lee, B. Liebich, H. Loos, X. Ma, L. Malin, A. Martinez, S. Rednour, A. Ros, E. Ros, A. Sandhu, A. Semaan, D. Smith, J. Stanton, S. Teitelbaum, S. Tilton, J. Tinlin, S. Tripathi, J. Vela, Arizona State University, Tempe, AZ, USA
V. Dolgashev, S. Tantawi, SLAC National Accelerator Laboratory, Menlo Park, CA, USA
P. D. Brown, MIT Bates Research and Engineering Center, Middleton, MA, USA

Abstract

The Compact X-ray Light Source (CXLS) is a compact source of femtosecond pulses of x-rays that is now commissioning in the hard x-ray energy range 6-20 keV. It collides the electron beam from recently developed X-band distributed-coupling, room-temperature, standing-wave linacs and photoinjectors operating at 1 kHz repetition rates and 9300 MHz RF frequency with a Yb:YAG 1030 nm laser beam operating at high peak and average power at 1 kHz repetition rate with pulse energy up to 200 mJ. We present the performance of the CXLS accelerator, laser, and timing systems, and initial x-ray results.

INTRODUCTION

Future light sources aim to improve performance, cost, and accessibility over today's instruments. CXLS uses inverse Compton scattering (ICS) to produce partially coherent synchrotron-like x-ray pulses at few hundred fs duration in the hard x-ray range. ICS-based instruments differ from the major XFEL and synchrotron facilities as well as current laboratory scale sources, thus require development of new experimental techniques, sample delivery, detector properties, controls and data analysis methods that are matched to their novel properties. These properties include lower flux than the major facilities as well as improvements in stability and precision of beam properties, and the ability to tailor integrated accelerator, laser, and x-ray beamline operations to optimize particular experiments.

CXLS INSTRUMENT AND LABS

The CXLS is constructed and now commissioning, having produced first x-rays in February 2023. The design parameters are shown in Table 1 and the layout of the source is shown in Fig. 1. It is installed in new laboratories at ASU's Biodesign Institute that were carefully constructed [1] to provide tight environmental controls and safety systems [2] for the high power equipment. Construction details include specially selected rebar in the floors and walls for low static magnetic fields, a Faraday room that encloses the high power RF transmitters, water-cooled equipment racks for low-level RF and magnet power supplies, 2 m thick floors measured at VC-E or better vibration standards under the sensitive beam equipment, and tight controls on air and water temperatures.

* wsg@asu.edu

Table 1: CXLS design performance at 0.1% and 5% bandwidth. Brilliance units are ph/(s 0.1% mm² mr²).

Parameter	0.1% BW	5% BW
Photon energy (keV)	2 - 20	2 - 20
Photons/pulse	5×10^6	1×10^8
Pulse rate (Hz)	1000	1000
Avg flux (ph/s)	5×10^9	1×10^{11}
Avg brilliance	2×10^{12}	5×10^{12}
Peak brilliance	3×10^{19}	9×10^{18}
Round RMS src size (μm)	3.0	3.0
Round RMS src angle (mrad)	4.0	4.0
RMS pulse length (fs)	< 300	< 300
RMS timing jitter (fs)	< 50	< 50

The majority of heat is transferred to water rather than air. Operation of the equipment has proved to be very stable as measured by RF phase jitter and position and timing of the beams. The reproducibility of the beams is excellent, with short start-up times each day.

The project has been constructed and run by a staff of about 20 scientists and engineers with a cohort of undergraduate students typically numbering 20, and another 5 graduate students. Students have been involved in all stages of design and construction, and routinely operate the CXLS. Our standard operations run for 10–14 hours per day rather than 24/7 due to the limited staff size.

Accelerator and RF Systems

The accelerator consists of a 4.5 cell photoinjector [3] and three 35-cm linac sections of 20 cells each, all powered by 2 RF transmitters as shown in Fig. 2. All of the accelerator structures are high efficiency standing-wave room-temperature copper structures with a repetition rate of 1 kHz and fill time of 170 ns. Peak cathode field in the photoinjector is 120 MV/m for 3 MW input power. The cathode cell is less than a half-cell so that the laser arrival timing is close to the peak applied electric field. Exit energy is 4.0 MeV.

The linacs are innovative distributed-coupling structures [4] with a high shunt impedance 165 MOhm/m making them very efficient, gradient up to 30 MV/m and peak surface E-field of 120 MV/m. The structures produce energy gain of 10 MeV each for 2 MW input power and a final max-

AUTOMATIC RETUNING OF SUPERCONDUCTING LINACS USING LightWin

A. Plaçais*, F. Bouly, E. Froidefond

Univ. Grenoble Alpes, CNRS, Grenoble INP, LPSC-IN2P3, Grenoble, France

J.-M. Lagniel, G. Normand, A. K. Orduz

GANIL, CEA/DRF-CNRS/IN2P3, Caen, France

B. Yee-Rendon, JAEA/J-PARC, Tokai, Japan

L. De Keukeleere, J. Van De Walle, SCK CEN, Mol, Belgium

Abstract

Reliability is an important feature for high-power particle accelerators. A significant proportion of beam trips come from the failure of superconducting accelerating cavities or their associated systems. Failure compensation is a technique that can limit the impact of these failures and therefore increase beam availability. Finding ideal compensation settings is, however, a difficult challenge that involves beam dynamics and multi-objective optimization, and which raises very different issues according to the linac under study. In this study, we present the LightWin tool to automatically find compensation settings in linacs. We study different compensation strategies on the MINERVA superconducting linac and present our first results on the SPIRAL2 superconducting linac.

CAVITY FAILURE COMPENSATION FOR HIGH AVAILABILITY

In order to advance the frontiers of particle physics and develop new applications, hadron accelerators are being driven towards increasing mean beam power. This tendency gives rise to numerous issues concerning accelerator design. These systems are expensive, making it important to maximize beam availability. To increase the RF-to-beam efficiency, reach higher accelerating fields, and optimize operation costs, the accelerating systems generally utilize superconducting (SC) technologies. However, these systems involve more subsystems which increase the failure risk.

Failure of cavities or their associated systems is a significant source of beam trips. Therefore, a promising solution to increase beam availability lies in cavity failure compensation. When a cavity failure is detected, the cavity is quickly detuned, and neighboring or all RF cavities are retuned. This can help maintain the beam and, in some cases, restore nominal beam conditions.

This method has already been applied successfully [1–3]. However, finding compensation settings for a given failure scenario can be complex and time-consuming. Additionally, this method is relatively new, and best practices for compensation are not well established. Furthermore, the failure compensation strategy may differ from one machine to another. This strategy depends on the linac design characteristics (*e.g.*, longitudinal acceptance) and its purpose

(type of beam and reduced velocity). Margins – foreseen by design, especially on the accelerating gradient – will also ease the application of the failure compensation scheme.

This is generally the case for Accelerator-Driven Systems (ADS). They are nuclear fission reactors driven by a stable proton beam. The beam impacts a spallation target, producing neutrons and interacting with the sub-critical nuclear core. Every prolonged interruption of the beam creates thermal constraints on the reactor structure. These interruptions also necessitate lengthy restart procedures, further reducing plant availability [4]. Thus, ADS feature a fault-tolerance design based on redundancy. The cavities are operated de-rated to their maximum capabilities, and the longitudinal acceptance of the linac is maximized by design. The requirements may differ from one project to another, but generally one should be able to recover the beam after a failure in a few seconds [5].

Considering the importance of reliability studies, the dedicated ReFiL (Reliability and fast Failure compensation methods in RF superconducting Linacs) project was launched at CNRS – IN2P3. Its objectives are to develop new RF failure mitigation techniques and assess the causes of longitudinal acceptance reduction – in particular, non-linear effects and parametric resonances in high gradient linacs [6]. The initiative currently involves the LPSC Grenoble, IJCLab Orsay and GANIL Caen French laboratories.

In the first section, we introduce the LightWin code and provide general implementation details. LightWin is a beam dynamics code developed for finding compensation settings in SC linacs. The goal is to provide a tool that can adapt to any linac to study different compensation strategies. The following sections present examples of studies and working perspectives for different linacs. The second section is dedicated to a systematic study on MINERVA. In the third section, we present the specific challenges of the SPIRAL2 SC linac, as well as the initial settings we found for a cavity failure in the low- β section.

LightWin

LightWin is an open-source code we developed for finding compensation settings [7–9]. It is mainly written in Python. It was designed with the ultimate goal of being usable on any linac, with any cavity failure compensation strategy. Its

* placais@lpsc.in2p3.fr

MATCHED TRANSPORT OF INTENSE AND COASTING BEAMS THROUGH QUADRUPOLE CHANNELS

C. Xiao*, L. Groening

GSI Helmholtzzentrum für Schwerionenforschung GmbH, Darmstadt, Germany

Abstract

Imposing angular momentum to a particle beam increases its stability against perturbations from space charge. In order to fully explore this potential, proper matching of intense coupled beams along regular lattices is mandatory. Herein, a novel procedure assuring matched transport is described and benchmarked through simulations. The concept of matched transport along periodic lattices has been extended from uncoupled beams to those with considerable coupling between the two transverse degrees of freedom. For coupled beams, matching means the extension of cell-to-cell periodicity from just transverse envelopes to the coupled beam moments and to quantities being derived from these.

INTRODUCTION

Preservation of beam quality is of major concern for acceleration and transport especially of intense hadron beams. This aim is reached at best through provision of smooth and periodic beam envelopes, being so-called matched to the periodicity of the external focusing lattice. For the time being, the quality of matching has been evaluated through the periodicity of spatial beam envelopes. This is fully sufficient as long as there is no coupling between the phase space planes (for brevity “planes”), neither in beam properties nor in lattice properties.

The TRACE-2D code [1] is well suited to provide for a matching beam line between a given initial beam matrix and a desired exit beam matrix even for a full 4D scenario. However, it is an intrinsic property of the periodic-solution problem that the initial beam matrix at the entrance of the periodic channel is unknown. Accordingly, this code cannot be applied to the present scenario in a straightforward way. This paper aims to demonstrate that a 4D-periodic cell-by-cell solution exists and demonstrates its derivation [2].

Coupled beams inhabit ten independent second-order rms moments. They are summarized within the symmetric beam moments matrix

$$C := \begin{bmatrix} \langle xx \rangle & \langle xx' \rangle & \langle xy \rangle & \langle xy' \rangle \\ \langle x'x \rangle & \langle x'x' \rangle & \langle x'y \rangle & \langle x'y' \rangle \\ \langle yx \rangle & \langle yx' \rangle & \langle yy \rangle & \langle yy' \rangle \\ \langle y'x \rangle & \langle y'x' \rangle & \langle y'y \rangle & \langle y'y' \rangle \end{bmatrix}, \quad (1)$$

and four of its elements quantify beam coupling. Beams are x - y coupled if at least one of these elements is different from zero.

The beam line being used to determine the periodic solution of an intense coupled beam along a periodic channel is sketched systematically in Fig. 1.

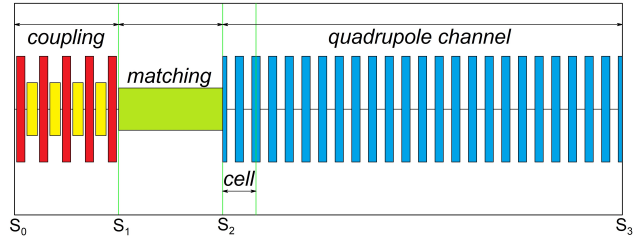


Figure 1: The beam line comprises three parts: (I) coupling production section; (II) matching section; (III) regular quadrupole doublet section (twelve cells). Space charge effects are not considered along the first two sections (see text).

At the beginning of the beam line, an uncoupled beam is assumed with beam sigma-matrix $C(s_0)$. The beam matrix at the beginning of the matching section is

$$C(s_1) = \wp \cdot C(s_0) \cdot \wp^T, \quad (2)$$

and \wp indicates the transfer matrix of the coupling section.

In order to obtain a periodic solution for this coupled beam, the details of the matching section are not required as seen in the following. However, it is modeled by a transport matrix including 16 elements (in units of m and rad)

$$\mathfrak{R}(m_1, m_2, \dots, m_{16}) = \begin{bmatrix} m_1 & m_2 & m_3 & m_4 \\ m_5 & m_6 & m_7 & m_8 \\ m_9 & m_{10} & m_{11} & m_{12} \\ m_{13} & m_{14} & m_{15} & m_{16} \end{bmatrix}. \quad (3)$$

Although initially being unknown, the 16 elements must ensure that \mathfrak{R} is symplectic. For brevity, the set of m_1, m_2, \dots, m_{16} shall be denoted by \mathfrak{N} .

MODELLING OF PERIODIC CHANNEL

For zero current, the effective focusing forces are given solely by the external lattice. The actual beam shape has no influence on them and therefore the periodic solution even for coupled beams may be found analytically. For intense beams instead, defocusing space charge forces depend on the beam shape and orientation in real space. Actually, they depend also on the spatial distribution. However, since modelling of space charge forces using rms-equivalent KV-distributions proved to work very well for matching purposes, this approach is followed here as well.

The periodic solution (zero current) meets the condition

$$C(s_2) = \mathfrak{S} \cdot C(s_2) \cdot \mathfrak{S}^T, \quad (4)$$

and the transport matrix from the exit of the coupling section s_1 to the exit of the first cell is

$$\mathfrak{U}(\mathfrak{N}) = \mathfrak{S} \cdot \mathfrak{R}(\mathfrak{N}), \quad (5)$$

* c.xiao@gsi.de

MACHINE-LEARNING-ASSISTED BEAM TUNING AT FRIB*

K. Hwang[†], Tomofumi Maruta, Tong Zhang, Qiang Zhao, Alexander Plastun, Kei Fukushima, Peter Ostroumov, Facility for Rare Isotope Beams, East Lansing, USA

Abstract

Facility for Rare Isotope Beams (FRIB) requires diverse primary ion species beams to produce rare isotopes. The beam tuning time can be reduced by employing Machine Learning (ML) techniques. In this paper, we aim to explore practical perspectives on shortening beam tuning time. Specifically, we discuss customization of Bayesian Optimization for maximum beam time utilization, and virtual diagnostics that are currently under development.

INTRODUCTION

Each experiment at FRIB requires a different ion species for the primary beam. This makes the efficient beam tuning particularly important to provide more beam time for science. We have developed high-level applications for beam tuning based on simulation of beam dynamics, classical optimization, and Machine Learning (ML) methods. Among the ML methods, Bayesian Optimization (BO) is routinely used and customized to FRIB beam tuning tasks in practical aspects including tight beam tuning time. Virtual diagnostics using data based models are under development and expected to significantly improve and expedite beam tuning procedures. Surrogate modeling of beam dynamics simulation is also being pursued and expected to further improve BO performance and other applications.

BAYESIAN OPTIMIZATION (BO)

Surrogate Model-Assisted Optimization

In this section, we explain how surrogate model-assisted optimization works. Consider the problem of finding the optimal set of controls x^* that maximize an objective $f(x)$ such that

$$x^* = \operatorname{argmax} (f(x)) \quad (1)$$

If we have a model $m(x) \approx f(x)$ that can approximate the true objective, we can find a candidate solution $x_{\text{candidate}} = \operatorname{argmax} (m(x))$ that maximizes the model as illustrated in Fig. 1. Next, consider a data-driven probabilistic model $\mathcal{P}(y|x, \mathcal{D})$ trained on online dataset $\mathcal{D} = \{(x, y = f(x))\}$, such that the model prediction of mean value approximates the objective, $\mathbb{E}_{\mathcal{P}}(y) \approx f(x)$. We can query next candidate solution $x_{\text{candidate}}$ that not only maximizes the modeled objective but also explores uncertain regions far from the existing observation points. This approach, known as Bayesian Optimization (BO), is a type of surrogate model-assisted optimization, as illustrated in Fig. 2.

* Work supported by the U.S. Department of Energy, Office of Science, Office of Nuclear Physics, under Award Number DE-SC0024707 and used resources of the FRIB Operations, which is a DOE Office of Science User Facility under Award Number DE-SC0023633

[†] hwang@frib.msu.edu

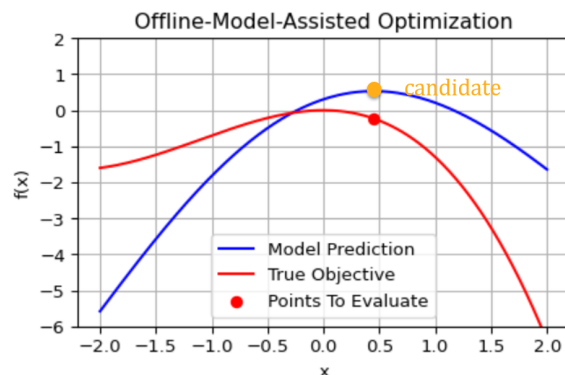


Figure 1: Illustration of surrogate model assisted optimization.

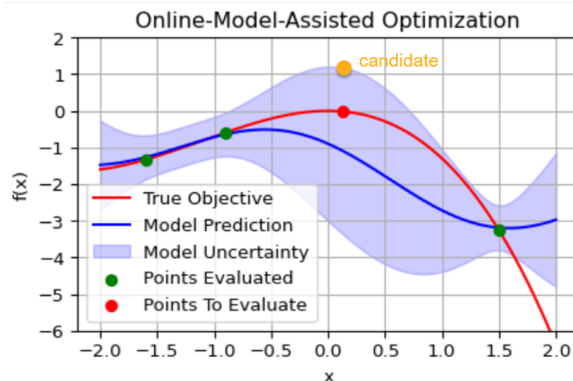


Figure 2: Illustration of Bayesian Optimization. The shaded area represents model uncertainty, which is larger in regions far from the observation points marked by green dots.

Why Bayesian Optimization?

We consider objectives that take from a few seconds to several seconds to evaluate. This includes factors such as the power supply ramping time when transitioning from an old control setting to a new one, which generally ranges from a few seconds up to 30 seconds, as well as the time required for averaging noisy measurement data. Due to the ramping time, investing a few extra seconds in averaging can result in more accurate and less noisy data, which in turn benefits the training of a more precise surrogate model. Additionally, we impose a time budget for each task, ranging from 2 to 20 minutes, depending on the problem size. This constraint typically limits the number of training data points to fewer than a few hundred.

Given this scenario, Bayesian Optimization (BO) is well-suited for the following reasons. First, BO is sample-efficient, meaning it can achieve good performance with fewer data points by strategically querying the most informative data. Moreover, the computation time for both training and query-

AN OVERVIEW OF PLASMA PROCESSING OF SRF CAVITIES AT JLAB*

T. Powers[†], T. Ganey, N. Raut, I. H. Senevirathne
Thomas Jefferson National Accelerator Facility Newport News, VA

Abstract

Plasma processing is a common technique where the free oxygen produced in a low-pressure RF plasma breaks down and removes hydrocarbons from surfaces. This increases the work function and reduces the secondary emission coefficient of the treated surfaces. Jefferson Lab has an ongoing R&D program in plasma processing. The experimental program investigated processing using argon/oxygen and helium/oxygen gas mixtures. The initial focus of the effort was processing C100 cavities by injecting RF power into the HOM coupler ports. We also developed the methods for establishing a plasma C75 cavities where the RF power is injected via the fundamental power-coupler. As part of the process development we processed, three C100 cryomodules in our off-line cryomodule test facility. In May 2023 we processed four C100 cryomodules in-situ in the CEBAF accelerator with the cryomodules returning to an operational status in Sept. 2023. The cumulative improvement in field emission free operation, as measured on a cavity by cavity basis, was 59 MeV or 24%. We recently started processing 7 cryomodules in the CEBAF accelerator in August 2024. Methods systems and results from processing cryomodules and individual cavities in the vertical test will be presented. Current status and future plans will also be presented.

METHODS

Plasma processing is being explored by a number of facilities that work with superconducting cavities [1-4]. Between 2015 and 2018 it was used to process 32 cavities in the SNS accelerator at ORNL where they achieved an average improvement in operational gradients of 2.5 MV/m [5]. Unlike helium processing which relies on ion bombardment of the field emitters, plasma processing uses atomic oxygen produced in an RF plasma to break down the hydrocarbons on the surface of the cavity. Removing this layer of dielectric material increases the work function and decrease the secondary emission coefficient [6]. Processing of SRF cavities is done at room temperature using a mixture of noble gas such as argon, neon or helium and oxygen. The discharge is operated at pressures between 50 and 300 mTorr. The current gas mixture used at Jefferson lab is 94% helium and 6% oxygen at 300 mTorr.

Gas Supply and Vacuum Systems

Process gas was supplied by a mobile cart that had a cylinder of helium or argon and a cylinder of 20% oxygen

* Funding provided by SC Nuclear Physics Program through DOE SC Lab funding announcement DE-FOA-0002670

[†] powers@jlab.org

with the remainder of the gas being helium or argon depending on the gas that was being used. The gas supply system used in the vertical test area also has a cylinder of 95% argon and 5% methane which is used to “contaminate” a cavity with hydrocarbons so that we could experiment with different processing techniques. Using a series of valves and flow controllers we were able vary the percentage of oxygen in the process gas as well as to regulate the flow and pressure in the cavities. Two mass flow controllers are used; one to regulate the pressure and one to regulate the percentage oxygen. The outlet pressure of the flow controllers is appropriately 5 Torr. The pumping system contains two turbo pumps and an RGA. In addition to monitoring the oxygen percentages the RGA is used to monitor the hydrocarbon fragments of H₂, CO, CO₂, and H₂O.

Selecting RF Frequencies for Processing

For both C75 and C100 cryomodules the RF-coupling via fundamental power coupler (FPC) is fixed and set up for cryogenic operations of a beam loaded cavity. Thus, when the cavity is at room temperature very little power is coupled to the fundamental mode and pass band modes of the cavities through the FPC. For the warm C100 cavities the ILC style HOM couplers have relatively strong coupling to the TE111 higher order modes, 1870 MHz to 2050 MHz where the power coupled into the cavity is between 20% and 95% of the power that is applied to the HOM coupler.

For the C75 cavities there is moderately good coupling through the fundamental power coupler to the first three TE111 modes. C75 cavities continued to use the glassy ceramic higher order mode loads which use waveguides to couple the HOM power out of the beam line. The cut-off frequency for these waveguides is 1966 MHz. Above this frequency RF power is coupled to the HOM loads and tends to cause a breakdown in the region of the HOM loads. Thus, we are limited to operating at frequencies below that value. The higher order modes below that frequency are coupled out through the fundamental power coupler which makes use of a half-height WR530* waveguide and are damped by a waveguide higher order mode filter. Said filter is replaced by a straight section of waveguide when we perform in situ processing.

Figure 1 shows relative electric fields as determined by a set of bead-pull and S11 measurements for the three modes that are used for processing a C75 cavity. The 1850 MHz mode has a tilt in the field pattern where the strongest field is in the cell furthest away from the fundamental power coupler (cell 5). Fortunately, that mode also had strong enough coupling that we could repeatedly ignite plasma in cell 5. We did find that it was difficult to go from no plasma to plasma on in any of the cells other

WIDE DYNAMIC RANGE DIAGNOSTICS SYSTEM FOR PRIMARY AND SECONDARY BEAMS AT FRIB*

S. Lidia†, S. Cogan, M. Cortesi, S. di Carlo, T. Larter, A. Lokey, D. McNanney, P. Nariyoshi, I. Nesterenko, S. Rodriguez, K. Saini, M. Smith, S. Zhao
Facility for Rare Isotope Beams, Michigan State University, East Lansing, MI, USA

Abstract

The FRIB diagnostics system covers an extensive range of primary and secondary beam intensities of 14 orders of magnitude and requires continuous improvements. The linac diagnostic system has provided straightforward linac commissioning and supports the development of many primary heavy ion beam species for producing rare isotopes. The diagnostics system for the secondary beam has a unique feature of detecting and measuring low-intensity rare isotope beams. This talk will report on the performance of the FRIB diagnostics system and ongoing improvements.

FRIB FACILITY

The Facility for Rare Isotope Beams (FRIB) is a high power heavy ion accelerator facility presently in operation at Michigan State University [1]. The FRIB is a power frontier accelerator facility aiming to provide two to three orders of magnitude higher beam power than existing heavy ion accelerator facilities. The FRIB linac is designed to accelerate all stable ions to energies above 200 MeV/u with beam power of up to 400 kW with Continuous Wave (CW) operation (see Fig. 1), and carrying intensities up to $\sim 10^{13}$ particles per second (pps) or currents ~ 100 eμA.

The scientific program generates demands on the functionality and operability of the facility. The ion sources and linear accelerator, and beam transport sections for the primary beam must handle intense, low energy, ion beams with velocities from 0.03c – 0.60c, and with mass-to-charge (A/Q) range 3 – 7. The linac acceptance is designed to permit lossless transport of multi-charge-state beams ($\delta Q/Q \sim 1/16$) [2].

While the FRIB linac operates in Continuous Wave (CW) mode, the electrostatic chopper allows pulsed beam operation for commissioning and tuning. As a high power accelerator, it is important to mitigate excess beam loss during tuning, and the chopper and beam attenuators play key roles to this end by permitting low peak or average power beam generation.

The high power interception devices which include the production target and beam dump, charge strippers and charge selection devices must operate in regimes of large temperature variations and thermal stresses. These are actively monitored for machine protection.

Secondary particles and rare isotopes are produced by the interaction of the primary beam with the target. This large phase space of fragments is filtered and reduced by the fragment separator beamline and instrumentation to isolate the rare isotope of interest, which typically appear at very low production rates.

DIAGNOSTIC AND INSTRUMENTATION REQUIREMENTS

To support the nuclear physics program, experimental runs are performed over periods of up to two weeks. New runs require changes to primary beam species, energy, and intensity. To facilitate these changes, the beam diagnostics and associated instrumentation must maintain sensitivity, accuracy, and speed over the entire range of beam parameters. The range of beam intensities covers many orders of magnitude between production (10^{13} pps) and beam tuning (10^6 - 10^7 pps). Oftentimes, beam tuning is performed with lower duty factor (lower average power) beams, so that signal acquisition modes must allow for short pulse durations and lower repetition frequencies.

Secondary beam production, fragment separation, and particle identification of rare isotope species impose another set of operational demands on diagnostics and instrumentation to facilitate single particle measurements at rates from 10^7 pps to 10^2 pps or lower.

Beam losses are a major concern for operation of an intensity-frontier, heavy ion accelerator. Chronic losses must be limited to permit maintenance with negligible impact to the facility's availability while fast losses must be quickly detected and stopped to prevent severe damage. High impact loss events are typically generated by failures in the RF systems or intercepting charge stripper devices. Slower losses may develop from drifts in the ion source output, slow changes to charge stripper thickness, magnet power supplies, etc.

Lastly, a new radiation effects beamline has been built and is currently operating on the FRIB linac [3]. This beamline require measurement and delivery of beam fluxes at low levels, with a minimum $\sim 10^2$ ions/cm²/s. This has necessitated the development of dosimetry instrumentation.

* Work supported by the U.S. Department of Energy Office of Science under Cooperative Agreement DE-SC0023633, the State of Michigan, and Michigan State University.

† smlidia@frib.msu.edu

COMMISSIONING OF LCLS-II*

A. Brachmann[†], SLAC National Accelerator Laboratory, Menlo Park, CA, USA
on behalf of the LCLS-II Collaboration

Abstract

This paper summarizes the current Status of the LCLS-II after initial commissioning completed in September of 2023 after achieving the formal ‘Threshold Key Performance Parameters.’ A summary of initial commissioning was presented at the IPAC-23 conference [1]. The facility has been delivering x-ray beams to the experimental areas for instrument commissioning and first experiments, while ramp-up and tuning of the accelerator and FEL continued in parallel. Challenges encountered during this time were malfunctioning of the Long Beam Loss Monitors (a key safety system component), and the onset of field emission in several cryomodules, limiting the achievable gradient.

Facility Status

The LCLS-II facility is an x-ray facility, delivering beams based on FEL’s driven by normal (NC) and superconducting (SC) accelerators. While the NC based FEL is delivering x-ray beams to users for more than a decade, the SC accelerator has been operating for approximately a year. Here, we focus on the recent results achieved with the latter. A description of the facility is given in [1]. The final design report has more detailed information [2].

After achieving the threshold KPP’s during initial commissioning, the focus has been to optimize performance, troubleshoot many issues, and establish routine operation, while also providing stable x-ray beams to the experimental areas for instrument commissioning. Currently, most of the SC beam program focuses on the soft x-ray undulators. The NC-based systems are in use almost exclusively to the user program and are delivering beams with excellent performance.

The current status of machine performance is summarized in Table 1. A significant effort has been to continue diagnostic development, which allowed a more efficient tuning of the accelerator and FEL systems. This included the installation of an S-band transverse cavity (STCAV) for longitudinal phase space characterization, energy spread and slice emittance measurements of the injector. Furthermore, the X-band transverse cavities at the end of the undulators were upgraded with a new low-level RF and timing system that allows these diagnostics to be used with both the NC and SC timing systems. This was enabled by a phase locking system to both fundamental accelerator frequencies (2856 MHz for NC and 1300 MHz for SC). Other critical diagnostics such as wire scanners and bunch length monitors are nearly ready for routine operation.

The ramp up of the beam power is currently limited to 2kW due to safety system deficiencies described below.

Table 1: LCLS-II Key Performance Parameters

Parameter	Threshold	Status
SUPER CONDUCTING BASED FEL		
Beam Energy (e-)	3.5 GeV	3.8 GeV
Repetition Rate*	93 kHz	93 kHz
Bunch Charge	0.02 nC	0.1 nC
Beam Energy (γ)	0.25-3.8 keV	0.2-3.8 keV
Photon # (10^{-3} bandwidth) per bunch	$5 \times 10^8 @ 2.5 \text{ keV}$	$> 10^{11} @ 3.8 \text{ keV}$
FEL Intensity jitter	N/A	15%
Bunch charge jitter	1.5%	3%
Energy jitter	1.0e-4	0.5e-4
Bunch length jitter	N/A	4%

* 93 kHz in burst mode; routine operation is 8.25 kHz

An important aspect of machine operation is beam stability. We have demonstrated stability performance that exceeds the design specifications. The critical numbers are summarized in Table 1 and illustrated in Fig. 1.

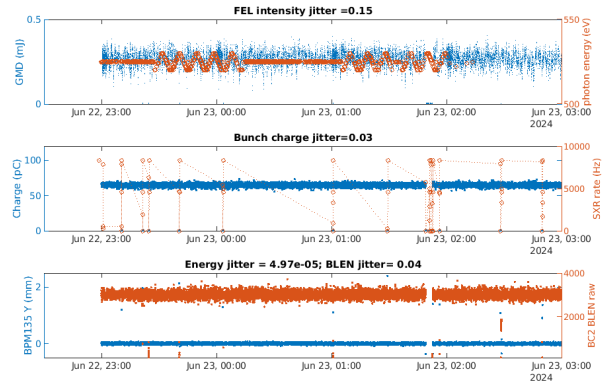


Figure 1: SC beam stability.

Beam emittances at the injector (88 MeV) are generally at the $0.5 \mu\text{m}$ level in both dimensions. At the end of the accelerator, at 3.5 GeV, best projected emittances were 1-1.5 μm Fig. 2 illustrates the emittance measurements for both parts of the accelerator. The minimization of emittance degradation will be subject to further work during the coming months.

During beam power ramp-up, we monitor the accumulated dose on the undulator segments to prevent excessive exposure that could demagnetize the permanent magnets. Over the last two weeks of $\sim 2 \text{ kW}$ beam power operation, the first undulator cell recorded a maximum integrated dose of $\sim 0.08 \text{ Gy}$, well below the 0.2 Gy/week threshold.

* Work supported by U.S. DOE contract No. DE-AC02-76F00515

[†] brachman@slac.stanford.edu

RF-BASED ENERGY SAVINGS AT THE FLASH AND EUROPEAN XFEL LINACS

J. Branlard*, V. Ayvazyan, A. Bellandi, C. Christou, M. Diomedea, T. Froehlich, S. Göller, H. Schlarb, C. Schmidt, V. Vogel (Fogel), M. Vogt, N. Walker
Deutsches Elektronen-Synchrotron DESY, Germany

Abstract

Several measures were developed and deployed at the pulsed linacs FLASH and European XFEL operated at DESY in order to reduce the energy consumption of the RF systems. A staged implementation of several techniques allowed energy savings up to 25% for both facilities, at the cost of reducing the RF overhead and increasing the complexity of the low-level radio frequency (LLRF) system. However, through tool development and automation, the energy saving linac configuration could be implemented without compromising the RF stability, maximum beam energy, accelerator availability and with minimal impact on the setup time.

INTRODUCTION

One third of the European X-ray Free Electron Laser (EuXFEL) accelerator energy consumption comes from generating the radio frequency (RF) fields necessary to accelerate the electron beam. Over the last couple of years, multiple efforts to optimize the energy consumption translated into significant energy and cost savings. A first initiative to lower the HV drive of the accelerator high-power sources (klystrons) was introduced at EuXFEL in 2022, removing the unused klystron power overhead, while preserving enough margin for field regulation. This first step already provided 10-15% savings [1]. As a second step, modifications of the high-power modulator shape combined with a more sophisticated use of the available klystron power allowed to bring the savings up to 25%, without compromising the beam quality necessary for photon science. A similar effort at the Free Electron Laser in Hamburg (FLASH) was carried out, optimizing the modulator high-voltage (HV) shape with tighter margins around the RF pulse for all accelerating stations including the RF gun. Altogether, the RF power consumption could be reduced by 200 kW, also corresponding to a 25% saving. A conceptual description of these techniques is presented in the first section of this report, including their impact on the RF and some insight on the technical solution. The second and third sections present the energy saving achieved at FLASH and EuXFEL, followed by a conclusion.

CONCEPTUAL DESCRIPTION

The approaches presented here to achieve energy saving by shaping the modulator HV can be applied separately or together to combine their benefit.

* julien.branlard@desy.de

Profiling the Modulator Shape

The most direct approach to reduce the power consumption is to lower the modulator HV, denoted as circle 1 in Fig. 1. Both FLASH and EuXFEL have different energy working points requiring different klystron power levels. Changing the HV set point affects the power level where klystron saturation occurs. One can then experimentally find the minimum HV settings that will guarantee the maximum klystron power required to cover typical operation scenarios, with the caveat that not all modulator voltages result in a stable klystron working point. Optimizing the modulator HV will effectively reduce the RF overhead necessary for field regulation. Accurate resonance control using piezo and efficient field control using on-resonance cavity filling with the LLRF system is essential to efficiently use the available RF power [2], hence allowing for maximum HV reduction (i.e. operating just a few percent from klystron saturation).

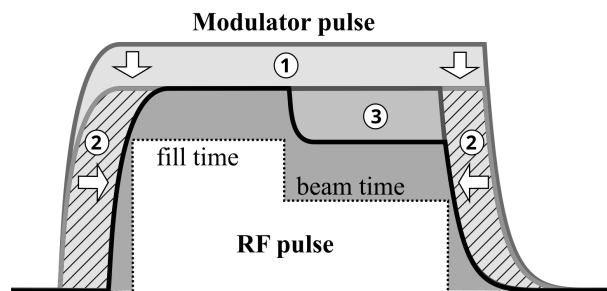


Figure 1: Different stages of modulator HV pulse shaping (solid line): lowering the HV (1), shortening the modulator pulse (2), introducing a step in the second half of the pulse (3). The dotted line illustrates the RF pulse scheduled during the modulator pulse.

The next step in profiling the modulator pulse focuses on its time duration. In the original high power settings, the width of the modulator HV pulse is chosen so that a stable plateau is reached and kept for the entire duration of the RF pulse, including some margins before and after. Some power savings can hence be achieved by reducing, more or less aggressively the duration of the HV pulse, eating up the margin before and after the pulse. For reference, the duration of the fill time and beam time (or flat top) are listed in Table 1 for both facilities. This point is illustrated Fig. 1 circle 2. The reduction in pulse duration is combined with a change of trigger delays so that the savings are distributed before and after the RF pulse. Due to the non-symmetrical shape of the modulator pulse (i.e. soft knee at the end of the fill time against an abrupt drop at the end of the pulse), the

DEVELOPMENT FOR BEAM INJECTOR USING LASER-DRIVEN ION ACCELERATION

H. Sakaki[†], S. Kojima, T. -H. Dinh, M. Hata, T. Miyatake, M. Nishikino, T. Shirai, K. Kondo
QST, Kyoto, Japan

K. Ohtomo, H. Tsutsui, Sumitomo Heavy Industry, Tokyo, Japan

H. Kuroki, N. Inoue, Hitachi Zosen, Osaka, Japan

H. Matsumoto, Kyushu Univ., Fukuoka, Japan

S. Oishi, A. Okano, K. Ishii, Nara-Women's Univ., Nara, Japan

Abstract

A quarter of a century has passed since the discovery of the mechanism of laser-driven ion acceleration [1, 2]. This mechanism makes a compact ion accelerator than the present accelerators, and many applications, especially an ion therapy, are proposed on the ion user's studies. To develop ion applications, it is necessary to increase the beam delivery efficiency using in the beam line adapted to the characteristics of the energetic ions transported. However, 25 years after the discovery of laser-driven ion acceleration with ultrashort pulsed high-current ions, there are currently no benchmark codes to simulate its transport system for application. We are beginning to construct a prototype of laser-driven ion injector for benchmarking and to investigate the beam parameters in a simulation. In this report, we describe our ongoing project "Quantum Scalpel" for heavy ion therapy using laser-driven ion acceleration and the commissioning of a prototype for this application.

QUANTUM SCALPEL PROJECT

HIMAC in Japan, a facility dedicated to heavy particle therapy, has been in operation since 1996. HIMAC had a huge site area of 120 x 65 m to accelerate various heavy-ions other than carbon beams, which are usually used for heavy particle therapy.

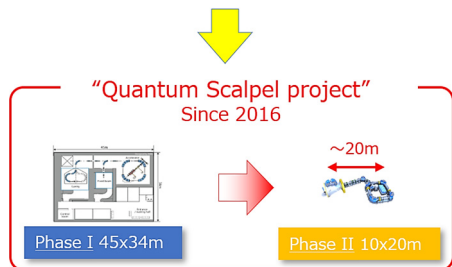
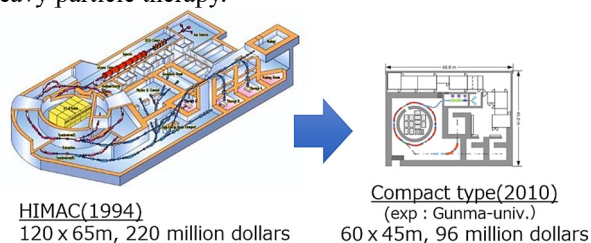


Figure 1: Accelerator for advanced heavy-ion therapy in Japan.

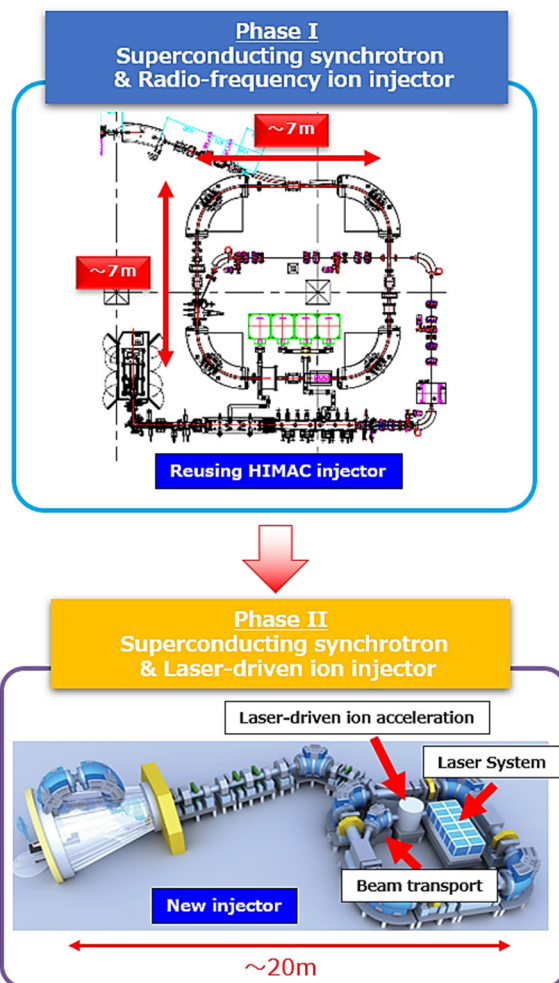


Figure 2: General view of Quantum scalpel project.

A dedicated 60 x 45 m carbon therapy facility was developed around 2010. However, it was also too large to be installed in an urban area in Japan, so a downsizing project, Quantum Scalpel [3], with novel ion acceleration technologies was started in 2016. The project was named "Quantum Scalpel" to describe the quantum-effect ion beam those cuts through the affected area like a surgical scalpel. The project is divided into two phases. In Phase I, an accelerator unit will be built in a newly developed 7 x 7m superconducting synchrotron using the current high-frequency ion injector: reusing HIMAC injector.

[†] email address: sakaki.hironao@qst.go.jp

DEVELOPMENT OF ADDITIVELY MANUFACTURED 750 MHz RFQ*

T. Torims[†], A. Ratkus, G. Pikurs, Riga Technical University, Riga, Latvia
 M. Vretenar, W. Wuensch, V. Bjelland, C. Garion, H. Kos, A. Cherif, CERN, Geneva, Switzerland
 M. Vedani, T. Romano, Politecnico di Milano, Italy
 S. Gruber, Fraunhofer IWS, Dresden, Germany
 M. Pozzi, Rösler Italiana S.R.L, Concorezzo, Italy
 N. Delerue, IJCLab, Orsay, France
 P. Wagenblast, TRUMPF Laser und Systemtechnik GmbH, Ditzingen, Germany

Abstract

Additive manufacturing (AM) technologies, especially powder bed fusion, are rapidly taking their place in the technological arsenal of the accelerator community. A wide range of critical accelerator components are being manufactured additively today. However, there is still much scepticism as to whether additive manufacturing can address the stringent requirements set to complete accelerator components. Therefore, as an advanced proof-of-principle, a full-size, pure-copper Radio Frequency Quadrupole (RFQ) prototype was developed and additively manufactured in the frame of the I.FAST EU project. Gradually improved RFQ prototypes and related pure copper samples manufactured by laser powder bed fusion were submitted to a series of standard tests at CERN to demonstrate that this novel technology and suitable post-processing can deliver the required geometrical precision, surface roughness, voltage holding, vacuum tightness, and other relevant parameters. The results obtained are very promising and could be of great benefit to the linac community at large. The paper is outlining the technological developments and RFQ design improvement process along with the obtained results and future endeavours.

DEVELOPMENT OF RFQ BY AM

AM solutions are becoming an integral part of the accelerator community technological portfolio. A dedicated survey revealed that several challenging parts of accelerator components already are already produced by AM, mainly through powder bed fusion technology [1]. Nonetheless, there is still scepticism on the possibility for AM parts to attain some challenging requirements of accelerator components, i.e. surface roughness, geometrical precision, vacuum-tightness, etc [2].

The RFQ is considered as one of the most complex and arduous part and for this reason was considered as an excellent test bed for AM technologies because of its very stringent mechanical requirements [3]. The recent development of high-frequency RFQ structures at 750 MHz [4-6] provides an excellent opportunity for AM since their reduced dimensions are compatible with modern AM machines. A summary of specific requirements for a 750 MHz RFQ is presented in Table 1.

* This project has received funding from the European Union's Horizon 2020 Research and Innovation programme under grant agreement No 101004730.

[†] toms.torims@rtu.lv

Initially, an *iteration 1* prototype RFQ section was additively manufactured by Fraunhofer IWS, corresponding to one-quarter of a 750 MHz 4-vane RFQ – see Fig. 1 [7]. To achieve the required surface roughness parameters, three samples were post-processed by three different surface treatment technologies.

Table 1: Standard RFQ Requirements

Requirement	Value
Geometrical accuracy	20 μm on vane tip 100 μm elsewhere
Surface roughness	$R_a < 0.4 \mu\text{m}$ for all inner surfaces
Porosity, degassing	Vacuum 10^{-7} mbar
Peak electric field on surface	~ 40 MV/m
Electrical conductivity	90% IACS

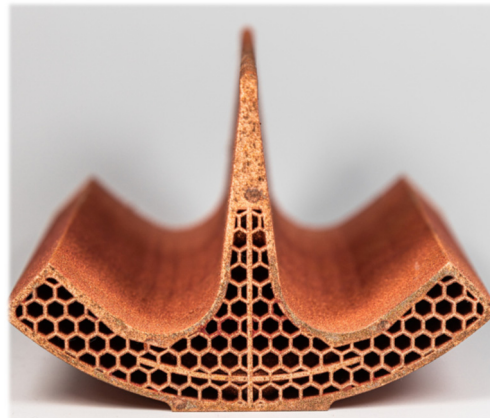


Figure 1: *iteration 1* - 95 mm $\frac{1}{4}$ RFQ.

Subsequently, a complete 4-vane RFQ prototype *iteration 2* was designed by RTU and manufactured by TRUMPF. The design was optimised for AM production and involved improved features – see Fig. 2 [8]. Based on results obtained with *iteration 1*, the printed part was treated with a two-step mass finishing process by Rösler, aiming to address hard-to-reach areas, such as the vane tip.

Benefiting from the valuable experience gained by the I.FAST WP10 partners [9] and excellent collaboration, an *iteration 3* of the RFQ was manufactured with a length of 390 mm, considered as an optimum to realise segmented RFQ's – see Fig. 3. Its design was optimised by RTU and realised by TRUMPF [10].

FIRST RESULTS FROM TWO Nb₃Sn CAVITIES ASSEMBLED IN A CEBAF QUARTER CRYOMODULE

G. Ereemeev, S. Cheban, S. Posen, B. Tennis, Fermi National Accelerator Laboratory, Batavia, IL, USA
 G. Ciovati, M. Drury, J. Fischer, K. Macha, M. McCaughan, U. Pudasaini, A. Reilly, R. Rimmer,
 M. Weeks, Thomas Jefferson National Accelerator Facility, Newport News, VA, USA

ABSTRACT

Two 1.5 GHz CEBAF C75-shape 5-cell accelerator cavities were coated with Nb₃Sn film using the vapor diffusion technique at Fermilab and Jefferson Lab coating facilities. Both cavities were measured at 4 K and 2 K in the vertical cavity test facility (VCTF) in each lab, then assembled into a CEBAF quarter cryomodule at Jefferson Lab. The cryomodule was tested at 4 K and 2 K in the CryoModule Test Facility (CMTF) at Jefferson Lab. RF test results for both cavities in the cryomodule are similar to those in the qualification test in VTS, with one cavity reaching $E_{acc} = 7.9$ MV/m and the other - 13.3 MV/m at 4 K.

INTRODUCTION

Nb₃Sn is a promising superconductor for accelerator cavities, which has been shown to sustain magnetic fields close to 100 mT, corresponding to accelerating gradients of about 20 MV/m [1–5]. There are several cryomodule development projects underway that aim to exploit this superconducting RF technology for accelerator applications [6–12]. The present contribution discusses the progress and challenges in installing and qualifying two C75 cavities [13] coated with Nb₃Sn into a spare CEBAF quarter cryomodule. The goal for this cryomodule is to be installed in the Upgraded Injector Test Facility (UITF) at Jefferson Lab and to have its operation tested with the beam as well as to provide the electron beam to UITF experiments [14].

CAVITY QUALIFICATION

Two niobium 5-cell cavities, built by RI Research Instruments, GmbH, according to Jefferson Lab C75 specifications [13], were coated with Nb₃Sn coating. 5C75-RI-NbSn01 cavity was made from fine grain material, and 5C75-RI-004 cavity cells were made from large grain material. The cavities received the standard processing and were tested to $E_{acc} \approx 29$ MV/m for 5C75-RI-NbSn01 limited by the high field Q-slope, and to $E_{acc} \approx 19$ MV/m for 5C75-RI-004 limited by multipacting-induced quench.

5C75-RI-004 was coated with Nb₃Sn at Jefferson Lab [15]. The cavity was found to be uniformly coated with a matte appearance typical for the developed multi-cell cavity coating protocol [16].

A slow cooldown protocol was implemented during the vertical test to cool the cavity uniformly. The temperature gradient across the cavity was maintained at about 100 mK while cooling down through the superconducting transition temperature. RF test results at 4 K are shown in Fig. 1. The

cavity quality factor was about $2 \cdot 10^{10}$ at the low fields and was above $1 \cdot 10^{10}$ at $E_{acc} \approx 10$ MV/m at 4 K. The quality factor was measured up to $E_{acc} \approx 13.3$ MV/m before a multipacting barrier was encountered and the test was stopped. The low-field quality factor was above $3 \cdot 10^{10}$ at 2 K. The quality factor exhibited a field dependence similar to that in 4 K test, but with a high quality factor.

The 5C75-RI-NbSn01 cavity received 35 μ m of electropolishing in the Argonne National Laboratory facility to reset the Nb₃Sn-coated surface for the new coating. The complete cavity was then anodized at 30 V in a 0.1 M diluted sulfuric acid solution as a part of the coating protocol followed at Fermilab. The anodized cavity was coated following the coating protocols developed for multi-cell Nb₃Sn coating at Fermilab [17]. This was the first time a C75-shape five-cell cavity was processed and coated at these facilities.

The cavity was visually inspected and found to be uniformly coated and glossy, similar to several other cavities coated at Fermilab. The coated surface appeared shinier than the one at Jefferson Lab, likely due to the thinner coating.

RF test was done at 4 K and 2 K after a slow cooldown. The cavity quality factor was above $1 \cdot 10^{10}$ at low fields and was close to $1 \cdot 10^{10}$ at $E_{acc} \approx 10$ MV/m at 4 K. The maximum gradient was limited to $E_{acc} \approx 14$ MV/m by multipacting-induced quench. The quality factor was about $6 \cdot 10^9$ at the maximum field. The low-field quality factor was above $4 \cdot 10^{10}$ at 2 K. The quality factor exhibited a field dependence similar to that in the 4 K test, but with a high quality factor.

Since both cavities met the gradient targeted for the quarter cryomodule to be installed in the UITF, they were progressed to the pair assembly. After the pair assembly, a warm leak was detected in the ceramic window attached to the fundamental power coupler of the 5C75-RI-004 cavity. Since the pair needed to be re-assembled, each cavity was re-tested individually in VCTF at Jefferson Lab.

Following the disassembly from the pair, each cavity followed the typical processing steps for RF testing. It was discovered that the 5C75-RI-004 cavity performance was degraded compared to the test before the pair assembly. The low field quality factor dropped to about $1 \cdot 10^{10}$ at low fields at 4 K, and a sharp Q-drop was observed starting at $E_{acc} \approx 3$ MV/m. The cavity was limited to $E_{acc} \approx 8$ MV/m, as shown in Fig. 1. 5C75-RI-NbSn01, on the other hand, did not show any noticeable degradation. The cavity reached $E_{acc} \approx 20$ MV/m at 2 K after multipacting processing.

After the cavities were re-tested, they were assembled again into a pair. The assembly was evacuated, leak checked,

PROGRESS TOWARDS HALO MODELING AT THE SNS BEAM TEST FACILITY *

K. Ruisard[†], A. Aleksandrov, A. Hoover, T. E. Thompson, A. Zhukov
Oak Ridge National Laboratory, Oak Ridge, TN, USA

Abstract

The SNS beam test facility is a model of the SNS front end (source through medium-energy transport). On-going work at the BTF focuses on accurate modeling of the beam distribution to enable the prediction of halo losses (<100 parts per million). This presentation will discuss the latest progress towards this goal, including recent results after a reconfiguration of the test beamline. Good agreement within the 90% beam core is shown for a 30 mA beam at 2.5 MeV.

INTRODUCTION

The aim of research at the SNS Beam Test Facility (BTF) is to demonstrate accurate modeling of bunch evolution including space charge and early halo growth. The project uses advanced beam phase space measurements developed at the BTF, including a full-and-direct 6D phase space measurement and a high-dynamic-range 2D phase space measurement capable of more than 6 orders of magnitude in dynamic range. The scope of the project is to characterize an initial bunch (1.4 meters downstream of the RFQ) at 2.5 MeV, reconstruct the distribution for simulation, and compare to measured output at the end of the 2.5 MeV beamline (12 meters downstream of RFQ).

We show the performance of the model at 30 mA RFQ output. This is below typical beam currents in the SNS linac. Ongoing efforts to build a benchmark case at 50 mA include use of a large-aperture ion source capable of higher LEBT current. This benchmark is limited to “optimal” transport near the matched solution for the FODO line.

SIMULATION MODEL PARAMETERS

The current best benchmark case uses the PyORBIT code [1]. This case uses 200,000 macroparticles and a maximum space charge step of 1 cm to model a 30 mA beam from the “input” position (1.4 meters downstream of the RFQ) to the “output” near the beamline end. The model also includes

* This work relies on expertise and support from SNS Operations and the Research Accelerator Division at ORNL. The US government retains and the publisher, by accepting the article for publication, acknowledges that the US government retains a nonexclusive, paid-up, irrevocable, worldwide license to publish or reproduce the published form of this manuscript, or allow others to do so, for US government purposes. DOE will provide public access to these results of federally sponsored research in accordance with the DOE Public Access Plan (<https://www.energy.gov/doe-public-access-plan>). This material is based upon work supported by the U.S. Department of Energy, Office of Science, Office of High Energy Physics. This work has been authored by UT-Battelle, LLC under Contract No. DE-AC05-00OR22725 with the U.S. Department of Energy. This research used resources at the Spallation Neutron Source, a DOE Office of Science User Facility operated by the Oak Ridge National Laboratory.

[†] ruisardkj@ornl.gov

a “multi-bunch” field solver, which takes into account the fact that, due to debunching, the 402.5 MHz bunches start to overlap in the FODO section of the beamline.

The section of lattice under study contains 10 electromagnetic quadrupoles and 19 permanent magnet quadrupoles in a FODO arrangement (108 degrees phase advance per cell). The quadrupole focusing function is drawn in Fig. 1. The field model consists of soft-edged, pure quadrupole fields parameterized by magnet geometry.

BENCHMARK CASE AT 30 mA

Reconstruction of the input distribution is done from 3 2D phase space projections, under the assumption $f_{6D} = f(x, x') \cdot f(y, y') \cdot f(\phi, dE)$. Transverse phase space measurements $f(x, x')$ and $f(y, y')$ used a 2-slit system and Faraday cup. The dynamic range of this measurement is limited to 10^2 . The longitudinal phase space $f(\phi, dE)$ is done with a dipole, vertical slit and bunch shape monitor, as well as two vertical slits upstream of the dipole for energy resolution. At the time of the transverse measurements, the RFQ transmitted 30 mA and for longitudinal, 32 mA.

The output distributions $f_{out}(x, x')$ and $f_{out}(y, y')$ are measured using the slits and Faraday cup at the end of the beamline. No longitudinal measurement is possible at this location. The output distributions are characterized at 30 mA from the RFQ.

Figure 2 shows the latest result from model/measurement comparison at the end of the beamline (approximately 9.5 meters downstream of the input). The density contours are at the 79%, 32%, 10% and 1% levels. The measurement of input phase space had a relatively low dynamic range of 10^2 , although the emittance diagnostic is capable of dynamic range in excess of 10^6 .

The bunch evolution between diagnostic areas is shown in Fig. 1. This plot includes data points from measured beam profiles from 1D slit-scans measurements. The rms calculation includes a threshold at 1% of the peak density. The rms value is sensitive to the tail distribution, therefore the discrepancy in rms sizes is consistent with the contour plots in Fig. 2.

TRANSPORT MATRIX ELEMENTS

Measurement of lattice matrix elements allows an independent benchmark of subsections of the BTF lattice. This measurement requires scanning the coordinates of a (x, x', y, y') collimated beamlet and measuring the response with a sensitive luminescent screen.

Table 1 compares the measured matrix elements to simulated values for the same optics case investigated above.

RESEARCH AND DEVELOPMENT OF COHERENT TERAHERTZ SOURCES AT LEBRA LINAC, NIHON UNIVERSITY*

T. Sakai[†], Y. Hayakawa, K. Hayakawa, T. Tanaka, Y. Takahashi, K. Nogami
LEBRA, Nihon University, Funabashi, Japan
N. Sei, AIST, Tsukuba, Japan
Y. Sumitomo, CST, Nihon University, Funabashi, Japan

Abstract

The Laboratory for Electron Beam Research and Application (LEBRA) at Nihon University has developed free electron laser (FEL), parametric X-ray radiation (PXR), and terahertz (THz) wave sources in collaboration with KEK and the National Institute of Advanced Industrial Science and Technology (AIST) using a 100 MeV electron linac. Each of these light sources are used for both internal and external collaborations. We are developing THz coherent edge radiation (CER), coherent transition radiation (CTR), and plane-wave coherent Cherenkov radiation (CCR) sources in the THz band for the FEL and PXR beamlines, respectively. In particular, we are developing THz wave sources using an artificial quartz hollow conical tube for the CCR source and a thin aluminum plate with a spiral target surface for THz-CTR optical vortex source. So far, we have performed parameter measurements, including beam profile and spectrum measurements, for the THz-CCR and the THz-CTR vortex beams. In this paper, we describe the development and characteristics of each THz wave source.

INTRODUCTION

At the Laboratory for Electron Beam Research and Application (LEBRA), Nihon University, we are engaged in collaborative research with KEK and National Institute of Advanced Industrial Science and Technology (AIST). Through this collaboration, we are working to improve a 100 MeV electron linear accelerator and to develop free electron laser (FEL), parametric X-ray radiation (PXR), and terahertz (THz) sources. These light sources are utilized in collaborative research both within and outside the university [1-8]. The development of THz sources are being carried out in both the FEL and PXR beamlines. In the FEL beamline, we are developing a coherent edge radiation (CER) source in the THz range. In the PXR beamline, we are advancing the development of CER, coherent transition radiation (CTR), planar-wave coherent Cherenkov radiation (CCR), and a CTR vortex light source. For the development of the THz CTR vortex light source, we are using a target with a spirally shaped metal-dielectric surface as the source. We are advancing with fundamental measurements, including beam profile and spectral analyses. In this paper, we present the development of these various THz sources.

* This work was supported by JSPS KAKENHI Grant Numbers JP19H04406, 21K12539, 23K28360, and JKA through its promotion funds from KEIRIN RACE.

[†] sakai.takeshi@nihon-u.ac.jp

LEBRA LINAC AND THZ SOURCES

At LEBRA, Nihon University, we are advancing the enhancement of a 100 MeV electron linear accelerator, as illustrated in Fig. 1. Utilizing the electron beam accelerated by this linear accelerator, we are making progress in the development of THz radiation sources within the FEL and PXR beamlines. Table 1 shows the specifications of the LEBRA linac. In the FEL line, we are developing CER in the THz band, which is emitted at the entrance of the bending magnet, just before the beam dump, from the electron beam passing through the undulator within the FEL optical resonator. The CER generated in the FEL line is intended for applications such as bunch length evaluation and FEL control. A transport optical system employing a perforated mirror and an ITO mirror has been constructed to superpose and transport both the FEL and THz beams. We have successfully achieved the simultaneous measurement of FEL and THz-CER using this transport line [9-11].

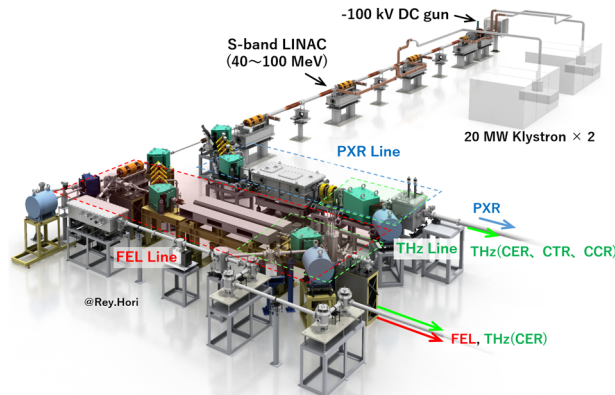


Figure 1: LEBRA 100 MeV Linac, FEL and PXR beamlines.

Table 1: Specifications of LEBRA Linac and Light Sources

Beam Energy	40 - 100	MeV
RF frequency	2856	MHz
Macropulse duration	5 - 20	μ s
Repetition rate	2 - 10	Hz
FEL wave length	1.3 - 7.5 (*0.4 - 1.2)	μ m
PXR energy	5 - 47	keV
THz wavelength	0.1 - 4.0	THz

(*Generated by a nonlinear optical crystal.)

THE SARAF-LINAC PROJECT JULY 2024 STATUS

N. Pichoff[†], A. Chance, J. Dumas, G. Ferrand, F. Gougnaud,
T. Plaisant, F. Senée, D. Simon, D. Uriot
CEA/IRFU, Gif-sur-Yvette, France
J. Luner, A. Kreisel, A. Perry, E. Reinfeld, I. Shmueli, L. Weissman
Soreq NRC (SNRC), Yavne, Israel

Abstract

SNRC and CEA collaborate to the upgrade of the SARAF accelerator to 5 mA CW 40 MeV deuteron and proton beams (Phase 2). CEA is in charge of the design, construction and commissioning of the linac downstream the existing RFQ (SARAF-LINAC Project).

The MEBT is now installed at SNRC and has been commissioned with both proton (cw) and deuteron (pulsed) beams. Transverse and longitudinal emittances have been measured and beam transport has been compared with TraceWin simulations.

Cryomodules have been assembled and tested at Saclay. CM1 has been delivered to SNRC and is being integrated at SNRC.

This paper presents the results of the qualification of the cryomodules at Saclay and the commissioning at Soreq.

subsystems (MEBT and Cryomodules) and have been qualified at Soreq (MEBT) and Saclay (Cryomodules).

This paper presents the last results of these qualifications tests.

MEBT COMMISSIONING

The MEBT has been delivered in August 2020, but its commissioning has been complicated by the COVID19 travel restrictions and the co-activity in the facility. After an update (to EPICS) of the ECR Ion source, LEBT and RFQ control system, the proton and deuteron beams have been transported to a D-plate downstream the MEBT [2]. The transmission reaches close to 100% of the RFQ accelerated particles. The results of the beam characterization are in accordance with the simulations with TraceWIN [3].

Longitudinal Emittances Measurements

The longitudinal beam profile and emittances were measured with a FFC through the gradient variation method. The measured profiles were compared with the one obtained with TraceWin simulations from RFQ input with Gaussian beam, including diagnostic transfer function simulation (Fig. 1). The profiles fit remarkably well.

INTRODUCTION

The last status has been presented in IPAC23 [1]. After design (2015-2016), prototype (2017-2018), series manufacturing (2018-2022), individual qualification (2020-2023), critical components are now integrated into linac

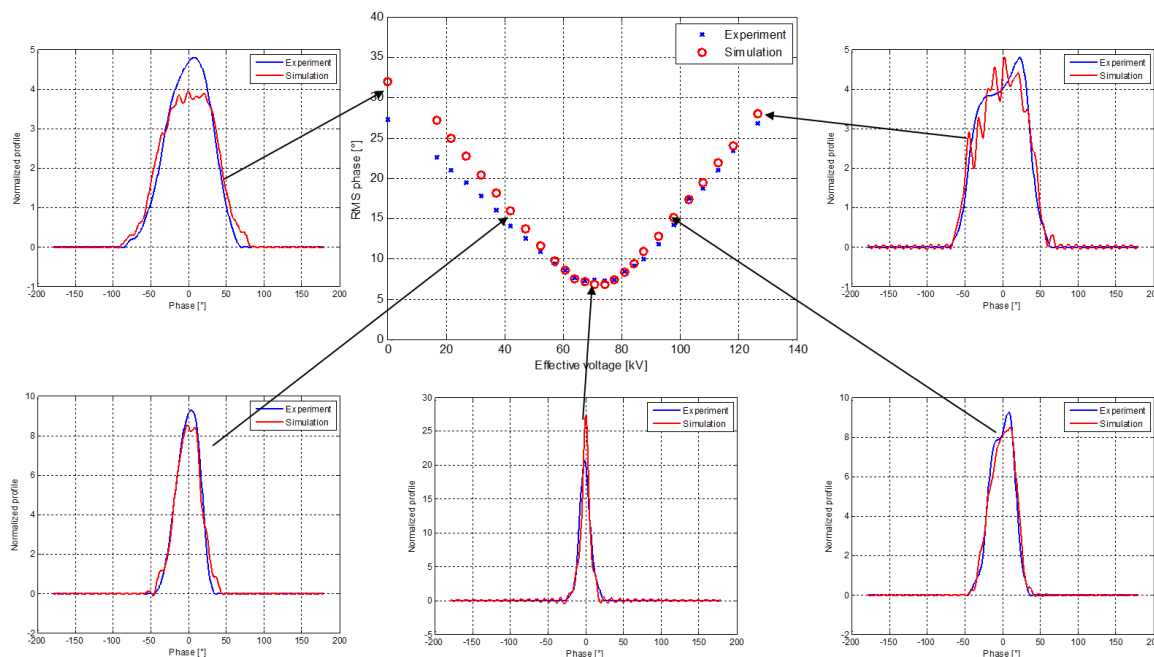


Figure 1: comparison between calculated and measured longitudinal beam profiles at FFC position.

THz-DRIVEN ACCELERATION OF SUB-RELATIVISTIC ELECTRONS IN TAPERED RECTANGULAR DIELECTRIC-LINED WAVEGUIDES

L. J. R. Nix^{*1,4}, R. B. Appleby^{2,4}, J. T. Bradbury^{2,4}, G. Burt^{1,4}, D. M. Graham^{2,4},
M. T. Hibberd^{2,4}, S. P. Jamison^{3,4}, R. Letizia^{1,4}, C. T. Shaw^{2,3,4}

¹School of Engineering, Lancaster University, Bailrigg, Lancaster, United Kingdom

²Department of Physics and Astronomy & Photon Science Institute,
The University of Manchester, Manchester, United Kingdom

³Department of Physics, Lancaster University, Bailrigg, Lancaster, United Kingdom

⁴The Cockcroft Institute, Sci-Tech Daresbury, Daresbury, United Kingdom

Abstract

We have designed a tapered dielectric-lined waveguide for the acceleration of sub-relativistic electron bunches with THz-frequency electromagnetic pulses. We consider an example design based on a commercial 100 keV electron gun and a THz generation scheme driven by a mJ-level regenerative amplifier laser system. With a 12 μ J THz pulse we simulated acceleration of a 100 keV electron bunch to 162 keV with very low energy spread. A second example design shows energy doubling from 100 keV to 205 keV using a 22.5 μ J pulse. The former of these two designs has been assembled for experimental testing. We also discuss methods to improve the efficiency of the design process using 1D particle tracking to provide better estimates of the initial geometry before optimization.

THz-DRIVEN ACCELERATION

THz-driven acceleration has received significant research interest in recent years as a novel technique for compact accelerators with fs-level bunch control [1–3]. In this work, we study THz-driven acceleration in rectangular dielectric-lined waveguides (DLWs). Such a structure consists of a rectangular metal waveguide with a layer of a dielectric material fitted to the top and bottom surface. This type of structure allows for accelerating modes with phase velocities below c [4, 5], and it is therefore possible for a subluminal electron to travel in synchronism with the THz pulse in the DLW.

The THz-driven acceleration method discussed in this work uses the interaction between a μ J-level THz pulse and an initially sub-relativistic electron beam. At sub-relativistic energies, electron velocity changes significantly under acceleration. Therefore, to keep particles at the correct phase, the phase velocity v_p of the pulse must start well below c and must increase along the interaction length. The phase velocity of a rectangular dielectric-lined waveguide (DLW) depends on the dielectric constant ϵ_r , the thickness of the dielectric layer t_d , the total waveguide width w , and the width of the dielectric layer w_d . Of these parameters, the latter two are practical for a tapering scheme and a taper geometry may be optimized by performing parameter sweeps across



Figure 1: Photograph of the dielectric-lined waveguide structure and integrated coupler as assembled at STFC Rutherford Appleton Laboratory.

the widths at several markers along the length. For manufacturing reasons, we restricted our dielectric taper to a single linearly tapered region between two non-tapered regions, while the metal taper was allowed to be more complex. This methodology and the simulation results for our example designs are presented in detail in [6].

TAPERED DLW STRUCTURE

Our accelerating structure has been manufactured by STFC Rutherford Appleton Laboratory and will be experimentally tested in the near future.

The structure, shown in Fig. 1, will be mounted on a multi-axis alignment stage. To limit dielectric charging during alignment, multiple channels are machined into the structure, visible as the middle and right apertures in Fig. 1. If the electron bunch passes through the coarse alignment channel (right aperture), the whole structure can be shifted and its alignment adjusted until the electron bunch passes through the fine alignment channel (middle aperture). This will ensure minimal charging when doing final alignment adjustments for the interaction channel. Simulations on THz coupling have shown that the power reaching the accelerating mode is negligibly affected by misalignment on the achievable scale [7], but performance is expected to be very sensitive to electron beam alignment.

* l.nix@lancaster.ac.uk

PROGRESS AND CHALLENGES IN TRAVELING-WAVE (TW) SRF CAVITY*

F. Furuta†, V. Yakovlev, T. Khabiboulline, K. McGee, S. Kazakov
Fermi National Accelerator Laboratory, Batavia, IL, USA
R. Kostin, P. Avrakhov, Euclid Techlabs, Bolingbrook, IL, USA

Abstract

Traveling-wave technology can push the accelerator field gradient of niobium SRF cavity to 70MV/m or higher beyond the fundamental limit of 50~60MV/m in Standing-Wave regime. The early stages of TW SRF cavity developments had been funded by several SBIR grants to Euclid Techlabs and completed in collaboration with Fermilab through a 1-cell prototype and a *proof-of-principle* 3-cell TW cavity development and testing. The TW resonance excitation in a SRF cavity at 2K liquid helium was demonstrated as the 1st time using the TW 3-cell at Fermilab. To advance TW technologies necessary more for future accelerator-scale TW cavity, Fermilab proposed a half-meter scale TW RF design. Here we report the recent progress in the 3-cell and the challenges towards a half-meter scale TW cavity.

INTRODUCTION

Presently all SRF cavities operate in a standing wave (SW) resonance field in which particles experience an accelerating force alternating from zero to peak. Niobium SRF cavities have a theoretical peak magnetic field which limits the accelerating field to 50 - 60 MV/m using standard available designs. A travelling wave (TW) regime evades this limit by generating a resonance field propagates along the cavity length. Particles in such traveling resonance field can experience a *constant* acceleration force, thus an energy gain per unit length can be higher than that of SW regime. This phenomenon is defined by the cavity's transit time factor T ($T = E_{acc}/E_{ave}$, E_{acc} - accelerating gradient including variation in time, E_{ave} - accelerating gradient without time dependence). A TW structure proposed in the early study showed a T of 0.9 [1], which is >20% higher than T of most common 1.3GHz SW 9-cell design ($T \sim 0.7$). This approach explores the path to 70 MV/m and higher for the same peak surface magnetic field condition of standard Niobium materials and processing technology. A higher cavity quality factor with higher R/Q of TW design can also be expected [2], which will lower the heat load and cryogenic power. Increased cavity energy gain per unit length and higher cavity quality factor can dramatically reduce the scale and running cost of SRF accelerators. An example, the proposed TW-based linear collider HELEN can achieve a 250 GeV center-of-mass energy in only 7.5 km, in stark contrast to the 30-km scale of the SW ILC structure [3].

*Fermilab is managed by Fermi Research Alliance, LLC (FRA), acting under Contract No. DE-AC02-07CH11359 with the U.S. Department of Energy, Office of Science, Office of High Energy Physics.

† ffuruta@fnal.gov

3-CELL TRAVELING WAVE CAVITY

Early Achievements

The early stages of TW SRF cavity developments have been funded by several SBIR grants to Euclid Techlabs (DOE SBIR Grant # DE-SC0006300) and completed in collaboration with Fermilab through a 1-cell prototype and a 3-cell *proof-of-principle* TW cavity fabrication and testing. It demonstrated the feasibility of the fabrication and processing of multi-cell TW structure [4] and achieved the TW resonance excitation in the 3-cell TW cavity at room temperature [5, 6].

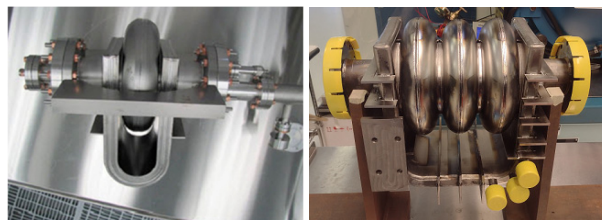


Figure 1: 1-cell prototype (left) [4] and 3-cell *proof-of-principle* TW cavity (right).

TW Resonance Control in the 3-cell Cavity

To excite TW resonance in the 3-cell cavity, the following technical concepts were investigated and demonstrated during the early R&Ds; 1) the stiffened cavity design, 2) RF control using two input power couplers, and 3) a special tuner device [5, 6].

The loaded quality factor Q_{load} at 2 K in VTS will be around 10^8 , making the cavity bandwidth very narrow and sensitive to microphonics. The stiffening ribs were welded on the waveguide (WG) to reinforce the resonator (Fig. 1 right). Based on the simulations, the stiffened cavity design and fine tuning of RF input signals would be enough to withstand microphonics detuning.

The WG of the 3-cell cavity has two RF input couplers and three RF monitoring couplers (Fig. 2). During the study at room temperature, a “forward” and a “backward” traveling waves inside the cavity and WG loop were mathematically extracted from the monitoring coupler signals. The “backward” traveling wave was suppressed by RF power redistribution and phase control between the two input signals. With these controls and signal processing, the desired “forward” traveling wave was successfully established in the 3-cell cavity at room temperature. Figure 3 shows RF feed and measurement scheme at room temperature for the 3-Cell TW cavity by Euclid [5].

DUST CONTAMINATION IN THE TRIUMF E-LINAC

A. Mahon^{*1}, T. Junginger¹, J. Keir, P. Kolb, D. Lang, T. Planche¹ TRIUMF, Vancouver, Canada
¹also at University of Victoria, Victoria, Canada

Abstract

The presence of dust particulates inside the vacuum space of particle accelerators has been linked to a variety of issues: At the Large Hadron Collider (LHC), beam loss events have been linked to the interaction of charged dust with the proton beams. In superconducting rf cavities, dust contamination leads to field emission, limiting the accelerating gradient and causing damage to external beamline components. Facilities such as the TRIUMF electron linear accelerator see progressive onsets in field emission that cannot simply be explained by vacuum events. The environment of a particle accelerator provides an ideal opportunity for dust to gain charge, which is one of the main drivers of dust grain dynamics in vacuum. However, fundamental parameters such as the dust composition and charge to mass ratio of these grains are unique to each accelerator environment and remain largely unknown. We will present an analysis of dust samples taken from TRIUMF linear accelerators, detailing their size, composition and potential sources.

INTRODUCTION

TRIUMF is undertaking a significant expansion of its rare isotope program via the addition of the Advanced Rare Isotope Laboratory (ARIEL). The ARIEL facility will add two new target stations to increase isotope production; one will be driven by a 520 MeV proton beam from the existing cyclotron, the other by a 30 MeV electron beam from a recently commissioned superconducting electron linear accelerator, the e-Linac (Fig. 1). The electron beam will be used to generate high purity isotope products via photofission, a technique which yields more isotopes in the neutron rich region of the nuclear landscape [1].

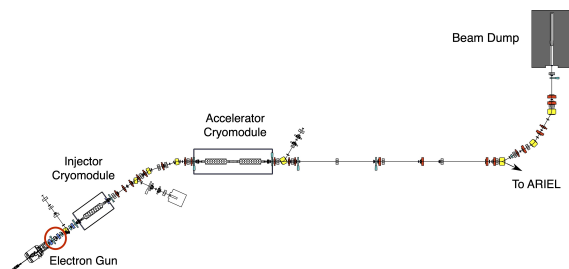


Figure 1: Schematic of ARIEL e-Linac.

High Gradient Requirements

As the overall isotope production yield at ARIEL is expected to depend strongly on the electron beam energy [2], maintaining the output at – or above – 30 MeV is essential for the ARIEL science program. Three 1.3 GHz 9-cell elliptical

* amahon@triumf.ca

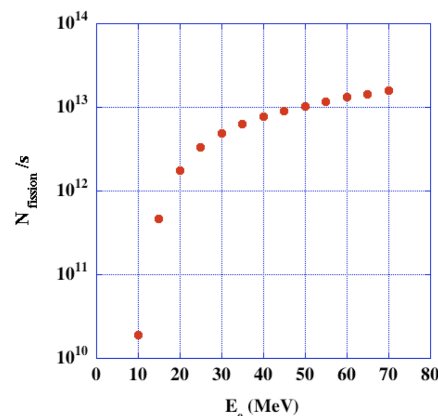


Figure 2: Isotope photofission yield as a function of 100kW electron beam energy [2].

superconducting rf (SRF) cavities, made of bulk niobium, are used to accelerate the electron beam. To reach the design specification of 30 MeV, each cavity must deliver an energy gain of 10 MeV or higher. Figure 2 demonstrates the steep dropoff in isotope production when the electron beam energy, and by association the SRF accelerating gradient, dips below this operational imperative.

Present Limitations

One practical limitation in SRF cavities is field emission [3], wherein rogue electrons are emitted from regions of high surface electric field inside the cavities. Field emission electrons cause a range of detrimental effects in accelerators. They draw energy from the rf field, lowering the quality factor (Q) of the resonator [4]. This increases the heat being dissipated in the cavity surface, requiring more liquid helium consumption to maintain cryogenic temperatures at the same gradient, ultimately forcing facilities with finite cryo power to operate at lower gradients. Field emission electrons may also reach relativistic velocities and generate intense bremsstrahlung and radiation damage to accelerator components [5–7].

The TRIUMF e-Linac actively suffers from field emission, which can be observed directly with our viewscreen diagnostics elements. Field emission electrons are accelerated by the rf fields present in the cavities, and can consequently travel outside of the confines of the cavity, which can then be picked up on our scintillator screens. An example of this is shown in Fig. 3; in this case the field emission electrons are escaping the confines of the adjacent cavity to reach the viewscreen further down the beamline. We are able to identify these particles as electrons, and not for example X-rays, as we are able to steer them with the optical elements of the beamline, proving that they are charged particles.

A LASER PLASMA WAKEFIELD ELECTRON ACCELERATOR FOR THE ADVANCED PHOTON SOURCE AND LOW-ENERGY ACCELERATOR FACILITY*

K. P. Wootton[†], W. J. Berg, J. Calvey, S. Chemerisov, J. Dooling, M. Edelen, V. Guarino, C. Kozłowski, A. H. Lumpkin, V. Sajaev, F. Westferro
Argonne National Laboratory, Lemont, IL, USA
E. Aneke, Northwestern University, Evanston, IL, USA

Abstract

Recent developments in laser wakefield accelerators (LWFAs) lead us to consider employing this technology to accelerate electrons at the Advanced Photon Source (APS) facility. Previous experiments using LWFAs were performed at Argonne using the Terawatt Ultrafast High Field Facility. The injector complex serving the APS begins with an electron linac, producing beam energies on the order of 450 MeV. We consider that the infrastructure developed at the Linac Extension Area (LEA) could be usefully employed to develop a new LWFA injector for the APS linac. In the present work, we outline the proposed parameters of an LWFA using approximately a 100-TW-peak laser pulse focussed into a few-mm in extent pulsed gas jet. We are targeting electron beam energies in the range 300–500 MeV. Initially, we would use the LEA quads, diagnostics and electron spectrometer to demonstrate performance and characterize the LWFA beam, before moving the LWFA to inject into the Particle Accumulator Ring (PAR).

INTRODUCTION

The photon beams produced by the Advanced Photon Source Upgrade (APS-U) illuminate materials to solve the most pressing problems in science, engineering, and energy [1]. The high-power electron beams of the Low Energy Accelerator Facility (LEAF) at Argonne are used to create diagnostic radioisotopes for medicine [2]. As stewards of our facilities, we endeavour to most efficiently use electricity as we deliver needed beams.

Laser plasma wakefield accelerators (LWFAs) [3–6] are being developed to serve the needs of future electron accelerators, especially towards energy-frontier electron-positron colliders and free-electron lasers [7, 8]. We propose that an effort parallel to the high energy physics roadmap is needed to develop this technology as an injector to a storage ring lightsource [9–11], or for production of radioisotopes using electron beams. With an eye to material irradiation, previous work on LWFAs was performed at Argonne using the Terawatt Ultrafast High Field Facility (TUHFF) [12–14].

In the present work, we outline a proposal to develop a LWFA linear accelerator as for electron beam irradiation or

as an injector to the APS-U. We outline and motivate the proposal. Background and prior studies are outlined. Proposed experimental parameters are outlined using particle-in-cell simulations. To close, we discuss some of the potential opportunities enabled by such a research pursuit.

MOTIVATION

A distinguishing feature of the injector accelerator chain of the Advanced Photon Source (APS) is the Particle Accumulator Ring (PAR) [15]. Situated between the electron linac and the booster synchrotron, the PAR is used to accumulate electrons for APS electron beam operation. The large momentum aperture of the PAR ring ($\sim 0.1\%$) allows us to capture multiple injections from an LWFA before directing that beam on to the booster synchrotron. This approach is not unique: a number of studies have considered matching an LWFA to a ring [10, 11, 16–18].

Rather than attacking scientific problems associated with larger scale facilities (such as staging multiple accelerator segments together [19]), we propose to deploy a single acceleration stage. Specifically, we propose to develop a LWFA based on a supersonic transverse gas jet operated in the blowout regime, modelled along previous studies [20].

We envisage conducting this research in stages. Based on existing demonstrations of LWFAs at other laboratories, we propose to assemble and characterize a LWFA at the Linac Extension Area (LEA) [21–24] to demonstrate the feasibility of an LWFA for radioisotope production or as an injector to the APS. We would subsequently relocate the LWFA to inject into the Particle Accumulator Ring (PAR) [15], and demonstrate injection into the APS-U storage ring.

BACKGROUND

Presently at Argonne, the LEAF electron linac is used for the production of radioisotopes [2]. The linac can be configured to provide electron beams with energies up to 50 MeV and beam powers up to 25 kW.

The injector chain of accelerators at the APS begins with an S-band electron linac [15, 25]. The APS linac routinely provides electron beams of energies on the order of 450 MeV. The linac is typically operated to produce ~ 1 nC of beam charge at a linac repetition rate of up to 30 Hz (~ 13 W average beam power). The APS electron linac is illustrated in Fig. 1.

* Work supported by the U.S. Department of Energy, Office of Science, Office of Basic Energy Sciences, under Contract No. DE-AC02-06CH11357.

[†] kwootton@anl.gov

PROPOSED INVESTIGATIONS OF ELECTRON-BEAM MICROBUNCHING IN THE ADVANCED PHOTON SOURCE LINAC*

A.H. Lumpkin[†], J.C. Dooling, W.J. Berg, Y. Sun, K.P. Wootton
Argonne National Laboratory, Lemont, IL, USA

Abstract

We propose extension of the investigations on the longitudinal-space-charge-impedance mechanism for inducing microbunching of relativistic electron beams within the Advanced Photon Source (APS) S-band linac. The microbunched content is evaluated by observing the coherent enhancements of optical transition radiation (OTR) when such beam transits a vacuum-metal boundary. The facility also uniquely includes both a thermionic cathode rf gun and a photocathode rf gun as electron sources for comparisons of effects. In previous studies, we addressed mitigation of the COTR's deleterious effects in the diagnostics for the visible light 2-D beam images at 375 MeV. In this case we plan to elucidate the microbunching phenomenon.

INTRODUCTION

Relativistic electron beam micropulses may be compressed to a high degree producing kAs of peak current on the sub-picosecond time scales. In addition, the charge fluctuations may couple to the longitudinal-space-charge impedance to generate energy modulations starting from noise. These energy modulations can be converted to periodic longitudinal density modulations (microbunching) in a chicane with an R_{56} term with gain for the initial modulation wavelength [1, 2]. If a proper beam energy chirp is present the longitudinal distribution will also be compressed. These interactions lead to gain at various wavelengths which can be evaluated with coherent optical transition radiation (COTR) imaging.

In previous studies, we addressed mitigation of the COTR's deleterious effects in the diagnostics for the visible light 2-D beam images at 375 MeV [3]. By extending our wavelength coverage into the NIR, we will access the much stronger enhancements predicted (>100) [1] and elucidate their spectral content. We will use an existing optical transport line for visible to NIR COTR (0.4 to 3.0 microns) from the diagnostics cube in the tunnel to an enclosed, external optics table. The inexpensive addition of a NIR-sensitive photodiode and integrating circuit with an existing digital oscilloscope in the optical setup would provide immediate extension of the wavelength coverage of the detectors [4] and enable the testing of the current model predictions for the microbunching instability into the NIR.

* Work supported by the U.S. Department of Energy, Office of Science, Office of Basic Energy Sciences, under Contract No. DE-AC02-06CH11357.

[†] lumpkin@anl.gov

EXPERIMENTAL FACILITY

A schematic of the linac is shown in Fig. 1 with the PC rf gun, two TC rf guns, the S-band accelerating structures, the 4-dipole magnet chicane at 150 MeV, the mini-flag OTR station, the subsequent 8 accelerating structures, electron spectrometer, and Station-5. Coherent Transition Radiation (CTR) monitors in L2 and L3, based on Golay cells, detect far-infrared radiation. The THz CTR signals are maximized at maximum compression (minimum bunch length). Scanning one arm of the CTR interferometer provides an autocorrelation used to determine the bunch length.

Electron Sources

The APS linac provides electron beams to the injector complex, including the Linac Extension Area (LEA). Three electron sources can be individually selected to deliver electron beams to the linac, in different charge configurations [5]. These include: a photocathode (PC) S-band radiofrequency (rf) gun and two thermionic cathode (TC) rf guns. Parameters of beams from the different electron sources are summarized in Table 1. The higher micropulse charge of the PC gun results in stronger COTR signals.

Table 1: Parameters of Beams From the Electron Guns

Parameter	Units	PC	TC
Charge per cycle	nC	0.3	1.0
Micropulse charge	nC	0.3	0.050
Micropulse length	ps	2	0.3
Micropulses per cycle	...	1	29
Micropulse spacing	ns	...	0.35
Repetition rate	s ⁻¹	6	30

Station 5

Station-5 includes optical transport of the converter screens' light out to a shielded room with an optical table. The station has three independent pneumatic actuators to select a YAG:Ce scintillator screen plus 45° mirror, an LSO:Ce scintillator screen plus 45° mirror, or an Al mirror at 45° for OTR imaging. Currently there is one analog charge-coupled device (CCD) camera for beam profiling on the optical table and the Oriel UV-visible spectrometer with a GaAs photocathode multi-channel plate (MCP) coupled to an analog camera giving sensitivity to 880 nm. Re-commissioning of these detectors could be done with TC gun beam initially. The optical transport enables the addition of the near infrared (NIR) photodiode detector and the upgrade to a digital complementary metal-oxide semi-

SIMULATED PERFORMANCE OF A COMPACT WATER-WINDOW FEL DRIVEN BY A STRUCTURE WAKEFIELD ACCELERATOR*

R. A. Margraf-O'Neal[†], P. Piot, J. Power, J. Xu, Argonne National Laboratory, Lemont, IL, USA

Abstract

Free-electron lasers (FELs) send an accelerated electron beam through a magnetic undulator to provide a source of continuously tunable, short (10s of fs), high-peak power (GW-scale) radiation. FELs have found many applications, particularly in the infrared, extreme ultraviolet (EUV) and X-ray regimes. However, current EUV and X-ray FELs are large (100s of m) and expensive facilities, limiting the accessibility of these sources. In this work, we present FEL simulations driven by a compact accelerator combining high-gradient short pulse two-beam wakefield accelerators and short-period superconducting undulators. An FEL demo based on a GeV-scale accelerator is discussed as a driver for a water-window (2.3–4.4 nm) FEL with a ~50 m length. Such a proof-of-principle integrated facility would serve the dual purpose of supporting user-based research in the water-window regime, and providing a proving ground for these new technologies to later be applied to shorter wavelength FELs. Here, we present early design and simulation efforts with a focus on FEL-process modeling.

INTRODUCTION

In the pursuit of high-gradient accelerators for future high-energy particle physics colliders, several technologies, including structure wakefield acceleration (SWFA), plasma wakefield acceleration (PWFA), and laser wakefield acceleration (LWFA) are now nearing sufficient maturity for commissioning of intermediate-energy (~1 GeV scale) demonstrator facilities. Compact free-electron lasers (FELs), which use electron beams to produce an energy-tunable source of high intensity radiation, are a logical application of such facilities. When combined with short-period undulators [1], single GeV-scale electron beams can produce photons in the EUV and soft X-ray. FEL demonstrator facilities have already been proposed for PWFA in this regime [2, 3], and for LWFA at slightly longer wavelengths [4]. In this work, we describe the radiation stage of a "water window" FEL facility utilizing a two-beam, short pulse SWFA [5].

The wavelength range of 2.3–4.4 nm (280–540 eV) is often referred to as the "water window," so named for the transparency of oxygen (and thus water) to soft X-rays in this range. This regime is particularly useful to the study of organic molecules, containing the absorption K-edges [6] of both carbon (4.37 nm/284 eV) and nitrogen (3.09 nm/402 eV). Additionally, the oxygen K-edge (2.33 nm/532 eV) sits on the high-energy boundary of the

water window, enabling the characterization of oxygen-containing molecules with high absorption when transparency to water is not required. Common experimental uses of the water window include soft X-ray microscopy [7], where transparency to water increases the feasibility of measuring thick aqueous samples, and spectroscopy [8], particularly of organic molecules.

High harmonic generation (HHG) sources can provide low pulse intensity soft X-ray pulses with a table-top scale facility footprint [7, 9, 10]. However, electron beam-based sources, such as electron storage rings and free-electron lasers (FELs), can provide significantly higher pulse intensity, at the cost of a typically much larger and more expensive facility [8, 11]. The potential of high-gradient accelerators to reduce the size of these facilities could significantly reduce cost, making water window pulses accessible to a larger number of users.

GENERAL FACILITY PARAMETERS

The SWFA method under development at Argonne, known as short-pulse two-beam acceleration (TBA), uses a drive beam to generate short RF pulses that allow the accelerating structure to operate at a high acceleration gradient. The wakefield radiation (typically X-band) is produced as a high-charge drive bunch train travels in a decelerating structure, and is extracted and transferred to a separate high-gradient accelerating structure. Due to the beam-produced X-band pulses being much shorter ($\tau_{RF} \leq 10$ ns) than conventional klystron-produced X-band pulses, and the electrical breakdown scaling as $BDR \propto E_0^{30} \tau_{RF}^5$, the secondary structure can sustain high electric field (E_0) amplitudes. This is the key to achieving high acceleration gradients with a TBA accelerator.

The proposed facility, diagrammed in Fig. 1, utilizes a 400 MV/m 11.7 GHz X-band accelerating gun (described in [5, 12, 13]), followed by a 250 MV/m X-band linac, both driven by beam-generated X-band radiation. The X-band linac would follow the same principles of the X-band accelerating gun, and would be designed as a part of this facility's development. A subsequent 26 GHz K-band, 150 mV/m linac ("LK1") linearizes the longitudinal phase space before compression in a chicane ("BC1"). The beam then undergoes an additional stage of acceleration and compression in LK2 and BC2, followed by a final acceleration stage in LK3. LK2 and LK3 are assumed to also be 11.7 GHz, 250 MV/m linacs, but could be replaced by K-band linacs to reduce complexity at the cost of additional length. A dechirper is used to reduce the correlated energy spread before the final beam is sent into the undulator to produce soft X-rays.

* This research is based on work supported by Laboratory Directed Research and Development (LDRD) funding from Argonne National Laboratory, provided by the Director, Office of Science, of the U.S. DOE under Contract No. DE-AC02-06CH11357.

[†] rmargrafoneal@anl.gov

NB₃SN TECHNOLOGY FOR LOW-BETA LINACS*

T. Petersen†, M.P. Kelly, T. Reid, Y. Zhou, B. Guilfoyle
Argonne National Laboratory, Lemont, IL, USA

G. Ereemeev, S. Posen, B. Tennis, Fermi National Accelerator Laboratory, Batavia, IL, USA
S. Kutsaev, R. Agustsson, E. Spranza, RadiaBeam, Santa Monica, CA, USA

Abstract

Nb₃Sn is the most advanced potential successor for niobium in superconducting RF accelerator cavities. Nb₃Sn has a significantly higher critical temperature (18.3 K) compared to that of niobium (9.2 K). This has a large effect on the BCS surface resistance, and therefore, on the dynamic RF losses at 4.5 K. The higher critical temperature allows two important changes for cavity and cryomodule design. First, the lower BCS losses allow the designer to use a higher frequency, translating to physically smaller cavities and cryomodules. Second, the low dynamic losses allow the use of stand-alone cryocoolers instead of complex helium refrigerators and distribution systems. Fabrication of a prototype 218 MHz cavity, test results, and continuing challenges are discussed.

INTRODUCTION

Heavy-ion linear accelerator resonators based on niobium are necessarily designed around for relatively low frequencies to keep the BCS resistance manageable for operation. This BCS resistance is the main source of surface resistance for niobium cavities and is strongly dependent on frequency and operating temperature. Figure 1 gives a comparison of calculated BCS resistance for niobium (at two frequencies, 72 MHz and 218 MHz) and for Nb₃Sn (at 218 MHz). At the operating temperature of 4.5 K the advantage of lower frequencies for bare niobium is clear. However, Nb₃Sn, even at the higher frequency, offer the possibility of an order of magnitude lower BCS resistance. The higher frequency translates to physically smaller cavities (reducing raw material costs as well as cryomodule fabrication size and cost) and a much lower dynamic RF load allowing the utilization of cryocoolers.

With the substantially higher T_c , Nb₃Sn could allow low-beta cavity operation at frequencies up near 1 GHz with a few nΩ of surface resistance [1].

PROTOTYPE FABRICATION

A prototype quarter wave cavity was constructed with high purity (RRR>250) niobium (and reactor grade for all non-RF surfaces) to serve as a base for the thin Nb₃Sn coating. The frequency chosen was 218 MHz, a harmonic of

*This material is based upon work supported by the U.S. Department of Energy, Office of Science, Office of Nuclear Physics, under contract number DE-AC02-06CH11357, and the Office of High Energy Physics, under contract number DE-AC02-76CH03000. This research used resources of ANL's ATLAS facility, which is a DOE Office of Science User Facility †tpetersen@anl.gov

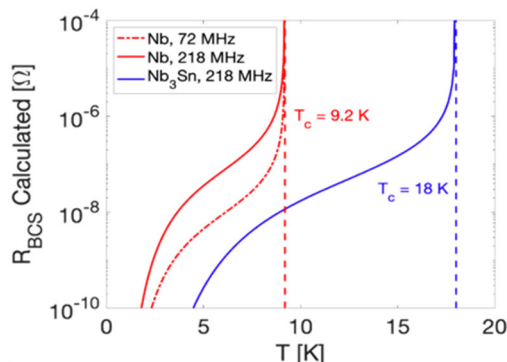


Figure 1: SRIMP calculated BCS surface resistance of Nb (at 72 MHz and 218 MHz) and Nb₃Sn (at 218 MHz) vs operating temperature.

the ATLAS clock, and substantially higher than typical quarter wave cavities. Subassemblies were hydroformed at a local shop, Stuecklen Inc. The complex center conductor tip and gussets were machined by our collaborators at RadiaBeam. All welds were performed by electron beam welding at Sciaky Inc. The finished cavity was electropolished (125 μm) before cold testing without low temperature baking (Fig. 2).

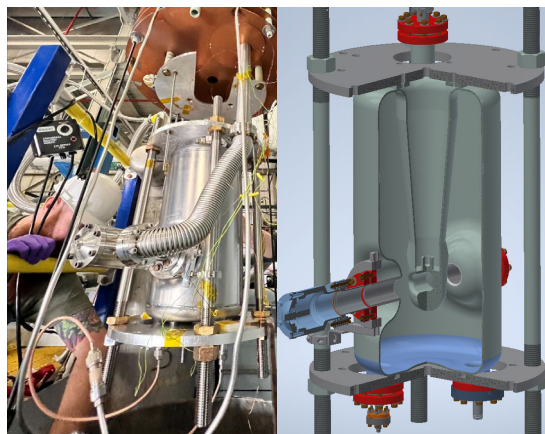


Figure 2: Cavity being inserted into 24" dewar (left) and section view of the cavity test assembly (right).

Following fabrication, the bare niobium cavity was cold tested to verify a good substrate for the thin film coating. The intent was to identify any possible defects that could cause early quench in the coated cavity testing. The cavity had a low Q of 8×10^8 , but this was expected as the cavity was not de-gassed and showed classic symptoms of Q-disease. However, the cavity met the design goal of 60 mT peak magnetic field, no defect initiated quench.

PROGRESS UPDATE ON THE RF SYSTEM REFURBISHMENT AT THE APS LINAC*

Y. Yang[†], N. DiMonte, G. Fystro, D. Meyer, A. Nassiri, T. Smith, Y. Sun, S. G. Wang
Advanced Photon Source, Argonne National Lab, Lemont, IL, USA

Abstract

A new storage ring, which utilizes a multi-bend achromat (MBA) lattice, has been built at the Advanced Photon Source. Currently, the commissioning process is ongoing in order to bring beamlines back into operation. The APS linac consists of two S-band thermionic cathode guns, one photo-cathode gun at the front end, and thirteen S-band traveling-wave RF structures, all powered by five klystrons. A significant refurbishment is underway to upgrade the RF system in the APS linac. This includes the replacement of the high power modulators and klystrons with a newly designed solid-state switching modulator RF system. In addition, the RF control and diagnostic systems are being upgraded to the new digital LLRF systems. To date, one RF station has been successfully replaced, commissioned, and has been in operation for almost two years. The RF stability, and power efficiency at this station is notably improved compared to the other stations.

INTRODUCTION

The Advanced Photon Source has been successfully upgraded after a year-long shutdown. The original storage ring has been replaced with a new ring using a multi-bend achromat (MBA) lattice. The new storage ring has been successfully commissioned. We are currently in the process of bringing each of the 71 beamlines around the ring into operation [1]. The upgraded X-ray, generated by the new storage ring will be up to 500 times brighter.

The APS linac needs to operate between 400 MeV and 500 MeV with high reliability for the new machine [2]. The linac setup is shown in Fig. 1. The electron beam is generated by one of two thermionic cathode guns (RG1 and RG2) and accelerated by three sectors of S-band traveling wave RF structures (L2, L4, and L5). Each sector consists of four linac structures powered by a klystron and a SLED power compressor. Currently, the APS linac has five operating RF stations (K1 through K5). K6 is used as a SLED test stand [3]. Each station uses a pulse-forming network (PFN) type pulse modulator to supply power to a Thales-35/45 MW klystron [4]. The original LLRF systems for the APS linac have been in operation for around 30 years, and it's challenging to find spare components and replace them when needed.

* Work supported by U.S. Department of Energy, Office of Science, Office of Basic Energy Sciences, under Contract No. DE-AC02-06CH11357.

[†] yaweiyang@anl.gov

RF STATION DEVELOPMENT

A new RF station has been developed for the APS linac. It includes a Cannon S-band klystron, a Scandinova solid-state modulator, and a Libera LLRF system.

Solid State Modulator and Klystron

The solid-state pulsed power modulator technology has been implemented globally to replace conventional klystron modulators. In contrast to a PFN-type modulator, which uses a thyratron tube as the high-power switch, a solid-state pulse modulator uses semiconductor switches such as the Insulated Gate Bipolar Transistor (IGBT). Each IGBT is powered by a DC power supply. A pulse transformer steps up the voltages from the IGBT to the high power level for the klystron. This technology offers significant improvements in power efficiency, compact footprint, pulse flatness and DC stability for RF stations used in accelerators [5].

We have selected the K400 solid-state modulator, developed by Scandinova Systems, for the new RF station. The modulator consists of two Capacitor Charging Power Supply (CCPS) units and twelve IGBT switch units. Each CCPS unit converts a three-phase AC power line to DC voltage, which charges six IGBT units to a primary voltage of around 1 kV. An external trigger gates the charged IGBT switches to discharge, generating a high-power pulse of around 350 kV through the pulse transformer. This high-power pulse is capable of powering an S-band klystron to generate RF pulses with a peak power up to 60 MW and 4.5- μ s width.

The APS linac currently utilizes Thales TH2128 klystrons, capable of generating a peak power of 35 MW. However, it is incompatible with the K400 modulator. Therefore, the Canon (Sumitomo) E3712 klystron was chosen as the new klystron to work with the new modulator.

To conduct the site acceptance test, a dedicated utility shed was developed. The first system was delivered to ANL in 2021, and a comprehensive site test was carried out in the shed. Figure 2 shows the first installed system in the utility shed. During the test, we collaborated closely with the vendor to resolve the identified issues and developed operation and maintenance procedures. Eventually, the klystron output power reached 60 MW during the test.

Digital LLRF System

A customized digital LLRF system has been developed by Instrumentation Technologies to control the APS linac RF station [6]. This system has 22 RF monitor inputs, with each input capable of providing amplitude and phase waveforms with 8 ns resolution. A customized LLRF software has been developed to extract average and peak information from

STATUS OF THE CEA CONTRIBUTION TO THE PIP-II LINEAR ACCELERATOR

N. Bazin[†], S. Berry, R. Cubizolles, G. Devanz, H. Jenhani, C. Simon, Université Paris-Saclay, CEA, Département des Accélérateurs, de la Cryogénie et du Magnétisme, Gif-sur-Yvette, France

Abstract

The Proton Improvement Plan II (PIP-II) project at Fermilab is the first U.S. accelerator project that will have significant contributions from international partners [1]. CEA joined the international collaboration in 2018, and will deliver 10 low-beta cryomodules as In-Kind Contributions to the PIP-II project, with cavities supplied by LASA-INFN (Italy) and VECC-DAE (India), and power couplers and tuning systems supplied by Fermilab. An important milestone was reached in April 2023 with the Final Design Review of the cryomodule, launching the pre-production phase. This paper presents the status of CEA activities on the construction of the LB650 pre-production cryomodule and the upgrade of the existing assembly and test infrastructures to the PIP-II requirements.

INTRODUCTION

The PIP-II project is an upgrade of the accelerator complex of Fermilab [2] to enable the world's most intense neutrino beam for the Deep-Underground Neutrino Experiment (DUNE) housed in the Long Baseline Neutrino Facility (LBNF) located in South Dakota, 1200 km from the neutrino production in Illinois.

PIP-II will deliver 1.2 MW of proton beam power from the injector, upgradeable to multi-MW capability. The central element of PIP-II is an 800 MeV linear accelerator, which comprises a room temperature front end followed by a superconducting section. The superconducting section consists of five different types of cavities and cryomodules, including Half Wave Resonators (HWR), Single Spoke and elliptical resonators operating at state-of-the-art parameters.

OVERVIEW OF THE CEA CONTRIBUTION TO THE PIP-II PROJECT

Thanks to the expertise in designing, building, testing, installing, and commissioning superconducting linear accelerators, CEA joined the PIP-II collaboration in 2018. The involvement of CEA in the PIP-II Linac construction was formally approved by the French Ministry of Research in July 2020 with the definition of the scope of work and the budget envelope.

CEA contribution focuses on the 650 MHz superconducting accelerating section, with the design, fabrication, assembly, and test of 1 pre-production and 9 production

low-beta 650 MHz cryomodules (called “LB650” hereafter) according to the PIP-II project specified requirements. This includes:

- The design of the LB650 cryomodule.
- The procurement of most of the components of the cryostat (i.e. the cryomodule without the cavities, the tuning systems, the power couplers and some standard components provided by the PIP-II collaboration).
- The assembly and cold RF tests of the 10 LB650 cryomodules.
- The design of the transport frame for the LB650 cryomodules, fabrication of 3 units, and road test of the pre-production cryomodule.
- The preparation for overseas shipment to the USA before the transfer title from CEA to the U.S Department of Energy (DOE).

DESIGN OF THE LB650 CRYOMODULE

The LB650 cryomodule houses four 5-cell $\beta=0.61$ cavities (developed by Fermilab, INFN [3], and VECC for the pre-production cryomodule and series cryomodules). The frequency tuning systems and the power couplers for the low beta and high beta cavities are identical. They are under the responsibility of Fermilab, with CEA contribution on the design studies of the power couplers. Each cavity is connected to a supporting system that stays at room temperature, called the strongback, using two support posts made of low thermal conductivity material to limit the thermal load between the room temperature strongback and the helium temperature devices.

The LB650 cryomodule is like the HB650 prototype cryomodule that was qualified at Fermilab [4, 5]. To benefit from the efforts in the HB650 cryomodule design to be applied to the LB650 one, CEA was part of the integrated design team with Fermilab, UKRI-STFC, and DAE, and was in charge of the mechanical and thermal design of the strongback of the HB650 prototype cryomodule and the design of the endcap tooling (based on the one used for the assembly of the ESS cryomodules at CEA).

Lessons learnt from the assembly and tests of the HB650 prototype cryomodule have been implemented in the design of the LB650 cryomodule. This one was independently reviewed in April 2023. The Final Design Review, which is an important milestone for the CEA activities, marks the end of the design phase and opens the construction phase of the LB650 pre-production cryomodule.

The design of the LB650 cryomodule is described in [6]. Figure 1 presents an artist view of this cryomodule.

[†] nicolas.bazin@cea.fr

COBOTISATION FOR SRF CRYOMODULES AT CEA: FOCUS ON ESS AND FUTURE PROSPECTS

S. Berry[†], A. Bouygues, J. Drant, A. Gonzalez-Moreau, C. Servouin, C. Madec, A. Madur
Université Paris-Saclay, CEA, Département des Accélérateurs,
de la Cryogénie et du Magnétisme, Gif-sur-Yvette, France

Abstract

The assembly of cavity string in the clean room is a tedious work that has noisy and painful steps such as cleaning the taped holes of a part. CEA together with the company *INGELIANCE* has developed a cobot: a collaborative robot operated by a technician one time and repeating the action without the operator. The cobot can work anytime without any operator: Therefore, it is working at night reducing the assembly duration by several hours. The cobot consists of a *FANUC* CRX-10iA a 6-axis arm on an Arvis cart. At CEA, the cobot is used to blow the flange of the cavities and the bellows inside. This allows to reduce the noisy steps that the technicians are exposed to. The process is also more reproducible since the cobot does always the same steps. The cobot is used on ESS cavity string assembly to clean flanges but also beam vacuum surface as inter-cavity bellows. Our activities, results and technical choices for next development will be presented in this article.

INTRODUCTION

Laboratories beyond CEA [1] are advancing robotization and cobotization for clean room operations. MSU in the USA has developed a robotized high-pressure rinsing system that enhances the cleaning process by adjusting to the cavity's geometry [2]. KEK in Japan is developing a system for cleaning cavities and assembling components [3]. Cavity string assembly in the clean room is a tedious work that has noisy and painful steps such as cleaning the taped holes of a part. It is recognized that humans are the biggest source of particulate contamination during assembly operations on sensitive components in cleanrooms.

A Collaborative roBOT (hereafter cobot) can work anytime with or without operators including overnight, reducing painful work and assembly duration by several hours. The use of cobot is also motivated by the fact that cavity string components are well defined, immobile and the assembly phase remains identical during the production.

The repeatability is an issue for operators, whereas it is an important advantage and objective for a cobot. The quality of cleanroom operations could be improved by limiting the inherent variability of human operators.

CEA OBJECTIVES FOR COBOTISATION

CEA's final objective is the assembly of cavity strings with a cobot. This objective contains two sub-efforts: cleaning and assembly of components (the latter being the most difficult). CEA initially cleaned parts under blowing

nitrogen. However, assembling with the vacuum surfaces exposed to the cleanroom environment has more impact on the quality (i.e. cavity specifications) and is now being addressed as a priority. The cleaning of parts with the cobot have been reported for ESS cryomodules assembly [4].

All the development presented hereafter required several steps of modeling and programming. The cobot used at CEA comes from *FANUC* and the programs are realized with Roboguide. The preparatory work consists of path programming, vision-based localization of parts, then the cobot will adapt the recorded paths. All cobot actions can be prepared in advance. The small change in our strategy since ESS experience is the introduction of the tool changer in order to be able to clean parts which requires different End-of-Arm tools (EOAT) or to insert intermediate cleaning steps during assembly. The tool changer is from *WING-MAN* company, electrical and compress air Pass-through interface depends on the need of the EOAT.

CLEANING OF COMPONENTS

The first step is the cleaning of following component:

- Environment of cavities,
- Flanges and their holes,
- Gasket groove in between flanges,
- Inter-cavity bellows (most critical parts at last).

The cleaning is performed going from the dirtier part to the cleaner such as environment of cavities, then flanges and their holes, then the cavity-to-cavity bellows (as shown in Fig. 1). Operators always install the objects to be cleaned and remove the screws and studs from the flanges to be cleaned. The cleaning is realized by blowing ionized and filtered air (6.5 bar). The cleaning efficiency is validated by particle counting performed by the cobot monitoring a particle air borne counter (28,3L per flange's hole).

The cleaning of components is implemented since May 2022 in ESS project with a CRX-10iA. Up to now, it has been used for 17 cryomodules preparation (24 cryomodules delivered). Cobot and operators can work independently in parallel or cobot works at night, it's a time-saver for ESS string assembly in the clean room: ~1/4 of assembly time. Cleaning is very efficient and meets perfectly ESS cleaning specifications.

Table 1 summarizes the statistics of the last particle counting performed by the cobot for the 17 ESS cryomodules assembled up to now. About 68 flanges of each type (coupler flanges, beam flanges with right angles valve and beam port with blind flanges) are taken into consideration.

[†] stephane.berry@cea.fr.

STATUS OF THE TEST BENCH FOR THE PIP-II LB650 CRYOMODULES AT CEA

H. Jenhani[†], C. Arcambal, N. Bazin, Q. Bertrand, P. Bredy, G. Devanz, L. Maurice, O. Piquet, P. Sahuquet, C. Simon, Université Paris-Saclay, CEA, IRFU, Gif-sur-Yvette, France

Abstract

The Proton Improvement Plan II (PIP-II) project at Fermilab is the first U.S. accelerator project that will have significant in-kind contributions (IKC) from international partners. As a part of the French IKC to this project, CEA will provide ten 650 MHz low-beta cryomodules (LB650) equipped with cavities from INFN-LASA (Italy), Fermilab (USA), and DAE-VECC (India), and power couplers and RF tuning systems from Fermilab. CEA is in charge of the design, manufacturing, assembly, and testing of these cryomodules. This paper presents the progress of the future implementation of the test stand dedicated to the cryogenic and RF power testing of the LB650 cryomodules.

INTRODUCTION

The central element of PIP-II is an 800 MeV linear accelerator that will deliver 1.2 MW of proton beam power from the main injector [1]. The CEA major contribution is the design [2], fabrication, assembly [3], and testing of ten LB650 cryomodules. An overview of the CEA contribution to the PIP-II project is given in references [4].

The construction of a new test bench dedicated to testing the LB650 cryomodules at the Saclay test facility Supratech Cryo/HF [5] represents one of the most significant activities within the CEA scope [4]. Each LB650 cryomodule will undergo comprehensive cryogenic and RF testing at CEA to evaluate its performance against a defined Acceptance Criteria List (ACL) [6]. Several important procurements have been initiated to meet the requirements of these cryomodule validation tests. An overview of the main

procurements and the related key technical requirements is also detailed in the aforementioned reference.

This paper provides an updated overview of CEA's activities related to the procurement of new cryogenic equipment and the associated distribution network, the establishment of the new RF power facility, and the upgrade of the cryomodule test cave previously used for the qualification tests of height ESS cryomodules with elliptical cavities and four SARAF cryomodules with HWR cavities.

CRYOMODULE TEST BENCH

The preparation of the LB650 cryomodule test bench is well advanced. The exact position of the cryomodule has now been finalized (see Fig. 1). This has enabled the completion of the Secondary Cryogenic Transfer Line (SCTL) and RF waveguide path definitions, as well as provided essential input for radiation calculations. These calculations are based on various cavity test configurations, particularly the maximum accelerating gradient tests and the multi-cavity nominal accelerating gradient tests, both conducted in continuous wave (CW) mode.

For a better understanding of the choices explained in this paper, it is highly recommended to see the details giving in [6] about the LB650 Cryomodule design, validation tests and main procurements technical requirements.

MAIN CRYOGENIC EQUIPMENT PROCUREMENTS

The main procurements for the cryogenic equipment are the cryogenic transfer lines, the valve box and the cold box.

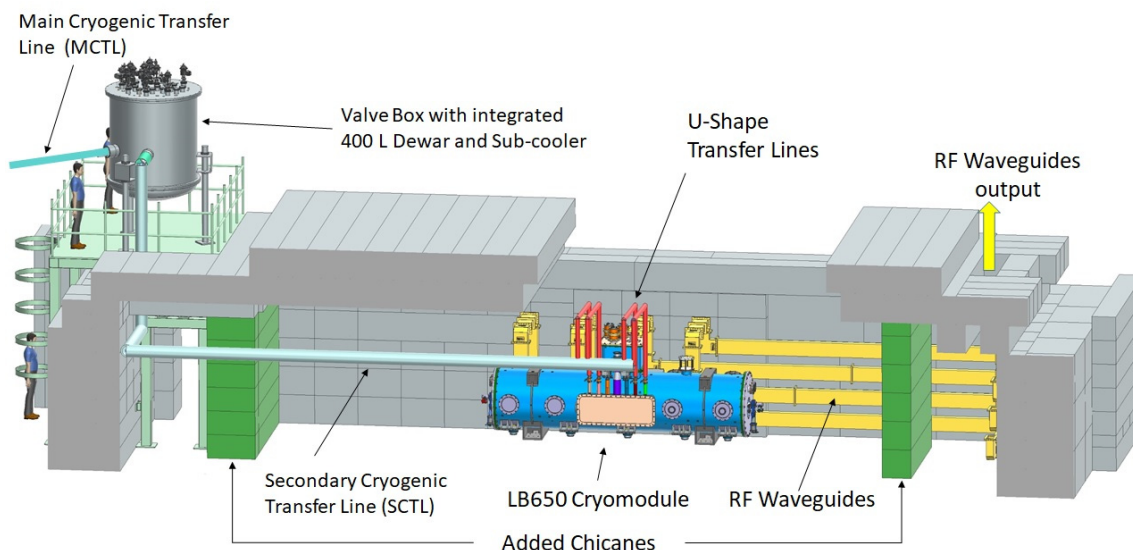


Figure 1: LB650 cryomodule test bench at CEA-Saclay.

INTRABEAM SCATTERING SIMULATION WITH A NOVEL HYBRID-KINETIC MONTE CARLO METHOD FOR LINEAR ACCELERATORS

P. Desiré ^{*,1}, A. Latina, CERN, Geneva, Switzerland
 A. Gerbershagen, University of Groningen, Groningen, Netherlands
¹ also at University of Groningen, Groningen, Netherlands

Abstract

Recent studies have identified intrabeam scattering (IBS) as one of the processes that can have a significant impact on the beam dynamics of linacs with high-density and low-energy beams, such as in free electron sources (FELs), where IBS appears to be one of the effects that most limits their performance. Most existing simulation codes have been developed for circular lattices or assume Gaussian beams and thus cannot accurately simulate the desired scenario. Motivated by this problem, this work presents the implementation of IBS in RF-Track, a tracking code developed for linear accelerators. The numerical simulation follows a novel methodology based on a hybrid-kinetic Monte Carlo approach. The method has proven to be stable using different input parameters and has shown emittance and a Sliced-Energy-Spread (SES) growth in different scenarios, demonstrating the accuracy of the tool and making it a promising solution to understand SES growth in FELs.

INTRODUCTION

Intrabeam Scattering (IBS), which consists of particle-to-particle elastic collisions by Coulomb interaction, has been extensively studied due to its critical role in the performance of circular accelerators. IBS causes emittance growth in storage rings [1] and damping rings [2, 3], leading to a deterioration of their performance. Lately, it has also been shown to limit the efficiency of linear accelerators.

The latest photoinjector technologies have allowed free-electron laser light sources (FELs) to have much more dense beams, increasing the effect of IBS, which grows for low-energy and high-density beams. In fact, recent studies have shown that IBS can be a determining factor in the performance of these machines, as it causes a growth in the Sliced-Energy Spread (SES, also known as uncorrelated energy spread), which is a key parameter for efficient light production. SwissFEL obtained a SES of 15 keV with 200 pC bunches [4], whereas European XFEL found a value of 6 keV with 250 pC bunches [5]. Finally, the PhotoInjector Test facility at DESY Zeuthen, also for 250 pC bunches, measured 2 keV [6]. The mentioned results highly differ from the SES of around 1 keV predicted from simulations, which did not consider either Micro-Bunching Instabilities or IBS effects. For a better understanding of this problem, a simulation accounting for IBS is needed.

Most of the existing simulations are based on analytical descriptions of IBS, such as Piwinski's [7] or Bjorken and Mtingwa [8] formulations which assume Gaussian beams, an unrealistic approximation for the high-intensity and low-energy beams present in many linear accelerators. Some codes model the IBS effect based on a partial differential equation that describes the system evolution [2], but in this work, each collision is reproduced individually with a Monte Carlo (MC) method, aiming to maximize the accuracy. This idea has been exploited by the tracking codes MOCAC [9] and SIRE [10–12] for circular lattices and recently has been studied in linear architectures [13]. Our work builds on this idea, introducing a novel methodology: a hybrid-kinetic MC approach.

In this paper, the implementation of IBS in RF-Track [14], a tracking code developed for linear accelerators, is presented. The IBS effect was analyzed in two different proposed cases which showed the emittance and SES growth respectively. Both scenarios used different input simulation parameters to test the stability and convergence of the method.

IMPLEMENTATION

This section describes the logic followed by the proposed IBS algorithm, which follows a novel approach different from other Monte-Carlo-based implementations. Firstly, it is named “kinetic” because it calculates the force experienced by each macro particle in the bunch at each time step (dt) and applies it in the form of a thin kick. This is the standard approach used in RF-Track to compute and apply collective effects to the beam. Secondly, it is described as “hybrid” because the deflecting force is computed colliding each particle with an *average particle* obtained from a set of 3D meshes containing charge density, velocity, and temperature of the bunch in the 3D space. In particular, three 3D meshes are needed: one for the average velocity, one for the standard deviation of the velocity, and one for the charged density. Finally, the deflection angles are computed using an MC method where the Rutherford cross-section is used to resolve the kinematics of the interaction.

After creating the described 3D meshes, the algorithm iterates over all the particles in the bunch, applying the following three steps. The 3D meshes are updated at each IBS calculation.

* pdesirev@cern.ch

VALIDATION OF HIGH EFFICIENCY KLYSTRON TECHNOLOGY

P. Alonso-Arias*, N. Catalán-Lasheras, A. Chauchet, S. González-Antón, C. Marrelli,
I. Syrathev, Z. Un-Nisa, M. Webber, CERN, Geneva, Switzerland
M. D. Jones, ASTec STFC Daresbury Laboratory and Cockcroft Institute,
Sci-Tech Daresbury, Warrington, U.K.
M. Boronat, IFIC (UV-CSIC), Valencia, Spain
T. Anno, Canon ETD, Otawara, Japan

Abstract

The delivery of high RF power—from hundreds of kW to MW—by klystrons, is linked with a high overall energy consumption. A research programme led by CERN in collaboration with the industry is being conducted to understand what limits klystron efficiency and how to develop high-efficiency klystrons. As a result of this program, two first prototypes of X-band (11.994 GHz) high-efficiency klystrons have been successfully designed and manufactured in collaboration with Canon Electron Tubes and Devices. The first results look promising, revealing a remarkable 56% efficiency, and validating the proposed HE klystron technology. A comprehensive characterisation campaign has been conducted at CERN to verify and demonstrate these results. The methodology for the HEK tubes characterisation is based in two independent measurements: a RF power measurement, and a calorimetric methodology—less subject to calibration inaccuracies. We describe the setups, principle of the calorimetry methodology, and we discuss the feasibility and precision of the results.

lowing the design provided by CERN, which maintained the electron gun and the collector, and introduced a six-cavity bunching circuit followed by a three-cell output cavity [1]. In addition, the tubes include a new ceramic window presenting lower surface electrical fields—result of a previous collaboration between CERN and Canon ETD—, which allows higher peak powers. In Fig. 1 and Table 1, we present the expected performance of the new klystrons in comparison with the original model.

Table 1: Performance Metrics of the X-band Klystron Tubes Manufactured by Canon ETD for CERN

	E37113	E37117
Beam voltage, kV	157	153
Beam current, A	96	93
Peak output power, MW	6	8
Efficiency	39	56

INTRODUCTION: AN X-BAND HIGH-EFFICIENCY KLYSTRON

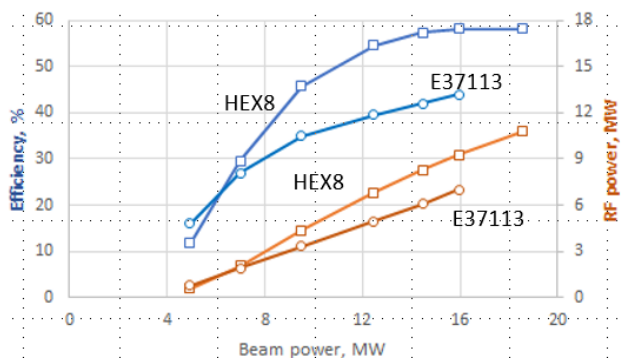


Figure 1: Expected performance of the E37117 tube (HEX8) built by CANON ETD in collaboration with CERN in comparison with the original model E37113.

The new high efficiency tube E37117 uses a retrofit approach from the original Canon E37113 model. The original model, used for years at CERN Xboxes facilities, delivered a maximum power of 6 MW for a 5 s pulse and 400 Hz repetition rate. Canon ETD delivered two new prototypes fol-

TEST STAND FOR X-BAND HEK AT CERN

The two prototypes have been installed for their testing in the Xbox3 klystron-modulator system at CERN. Xbox3 is used to evaluate and test high-gradient accelerating structures and high-power RF components in the context of the Compact Linear Collider (CLIC) project [2].

The system consists of a Scandinova 170 kV modulator system that delivers the pulsed power to the klystron cathode, waveguide network for the distribution of the RF power, pulse compressor, and auxiliary power supplies and dedicated subsystems for control, interlocking, and diagnosis. Originally, Xbox3 was designed for conditioning structures rather than testing klystrons. Consequently, the test stand has been modified for the current measurement campaign. These modifications include the addition of new channels to acquire the high-voltage pulses from the modulator, as well as signals necessary for calorimetry. These improvements enable effective measurements of the klystrons performance in a reliable and secure testing environment.

For the klystron commissioning, an assembly consisting of a X-band high power load is connected to the klystron output. At the end of the transmission line, an ion pump has been integrated to maintain vacuum levels of approx. 10^{-8} mbar.

Two directional couplers (regular, DC, and high power, HPDC) allow the measurement of the klystron's input and

* paz.alonso.arias@cern.ch

SMARTCELL X-BAND NORMAL CONDUCTING ACCELERATOR STRUCTURE PROTOTYPE FABRICATION

P. Morales Sanchez*, N. Catalan Lasheras, A. Moros, A. Perez Fontenla, E. Rodriguez Castro,
S. Gonzalez Anton, A. Gerardin, A. Magazinik
CERN, Geneva, Switzerland

Abstract

This study presents the design and fabrication of a prototype normal-conducting X-band accelerator structure, known as Smartcell. These structures, fabricated using brazing and bonding techniques, are crucial for future linear colliders. We examine the brazing and bonding geometry, material selection, and the implications of varying heat cycles and atmospheres during the brazing/bonding processes. Additionally, we analyze how copper quality and annealing procedures, conducted before, during, and after machining, influence the machinability, microstructure, and overall performance of the final component. The study evaluates different tests and five mock-ups, with results and conclusions drawn from optical examination, metrology, and scanning electron microscopy (SEM) analysis.

INTRODUCTION

Acceleration in the main linac of the Compact Linear Collider (CLIC) [1] is based on normal-conducting, X-band travelling-wave structures working with a very high accelerating gradient. Following extensive experience from the NLC projects in the US and Japan, CLIC prototypes have been manufactured using ultra-precision (UP) machined copper disks, joined together through diffusion bonding [2]. High-power tests on these structures have demonstrated their capability to operate at a gradient of 100 MeV/m with a very low breakdown rate (BDR), meeting the stringent requirements set by CLIC [3].

However, advancements in machining accuracy, improvements in surface finishing, and new assembly methods, have significantly transformed the technological landscape. Within the CLIC collaboration, it has been shown that brazed prototypes can achieve similar high-gradient performance with low BDR [4], offering a viable alternative to diffusion bonding [5].

Considering these advancements, we have redesigned the next prototype for CLIC, known as Smartcell, to be assembled by brazing, motivated by the advantages of using lower temperatures and the broader availability of suppliers, which should lead to a cheaper production.

The following sections will discuss the design considerations, material selection, and fabrication processes involved in the Smartcell prototype, with a focus on optimizing the brazing process to ensure high performance and reliability and trying to keep the cost as low as possible.

CHOICE OF BRAZING PARAMETERS

In the initial phase of this redesigning process, available UP machined cells (Fig 1) were repurposed for testing different parameters of the brazing cycle, namely Brazing

Filler Materials (BFM), brazing atmosphere, filling factor, and applied pressure (Table 1). According to the BFM specifications, the brazing cycles were conducted at temperatures between 790°C and 1010°C, with pressures from 4kPa to 40kPa (1-10 kg).



Figure 1: Existing disc model from an X-band accelerating structure 11WNSDVG1.8.

Table 1: Test Cycles Parameters

#	BFM	Atmosphere	Filling ratio	Weight
1	AuCu50	H2 dry	4.36 0.96	10
2	AuCu50	H2 dry	2.13 0.96	1
3	AuCu50	H2 dry	2.13 0.812	1
4	Palcusil5	Vacuum	4.36 0.96	1
5	Palcusil5	Vacuum	2.13 0.96	10
6	Palcusil5	Vacuum	2.13 0.812	1
7	Palcusil5	Vacuum	2.00 1.9	10
8	AuCu50	H2 dry	4.36 0.96	10
9	AuCu50	H2 dry	2.13 0.96	1
10	AuCu50	H2 dry	2.00 1.9	1
11	Pallabraz840	Vacuum	4.36 0.96	1
12	Pallabraz840	Vacuum	2.13 0.96	1
13	Pallabraz840	Vacuum	2.00 1.9	10
14	Palcusil5	Vacuum	4.36 0.96	10

All specimens were vacuum tight, up to $1 \cdot 10^{-10}$ bars. Ultrasound inspection showed good interface continuity. Subsequently, we proceeded to cutting the samples and performed optical microscope examination. Samples brazed using AuCu50 at the highest temperature presented crossing grains across the cell's interfaces, demonstrating successful diffusion bonding. In general brazing done with Ag-based BFM did not present crossing grains and in most cases, BFM flowed into the RF area. We performed an additional cycle #14, for which the heating cycle was extended by a long plateau (5 hours) right below the melting temperature of the BFM to enhance diffusion bonding. As anticipated, even at this relatively low pressure and temperature range 40kPa and 795.9°C, crossing grains were present which indicated that diffusion bonding took place

OPERATIONAL IMPROVEMENTS AND UPGRADES OF THE CLEAR USER FACILITY

P. Korysko^{1*}, I. Najmudin, C. Robertson, University of Oxford, Oxford, United Kingdom
R. Corsini, W. Farabolini, A. Aksoy, A. Malyzhenkov, A. Gilardi,
E. Granados, M. Martinez-Calderon, V. Rieker, L. Wroe, CERN, Geneva, Switzerland
¹also at CERN, Geneva, Switzerland

Abstract

The CERN Linear Accelerator for Research (CLEAR) at CERN is a user facility providing a 200 MeV electron beam for accelerator R&D and irradiation studies, including medical applications. In this paper we will outline the most recent improvements in CLEAR operation and beam control and delivery, and describe the upgrades under way, giving an update of their current status. These upgrades include a new front-end for the laser system which will enable an highly flexible time structure, better stability and higher repetition rates, and the implementation of a second beam line which will provide additional testing capability and whose optics has been designed to match user requirements. Finally, we will discuss the proposed future experimental program of the facility, particularly in view of the novel capabilities provided by the upgrades.

INTRODUCTION

The CLEAR facility offers a diverse array of electron beams with customisable parameters [1–4], as detailed in Table 1. An overview of the time structure and charge parameters achievable at CLEAR, depicted in Fig. 1, along with a schematic layout of the beamline shown in Fig. 2.

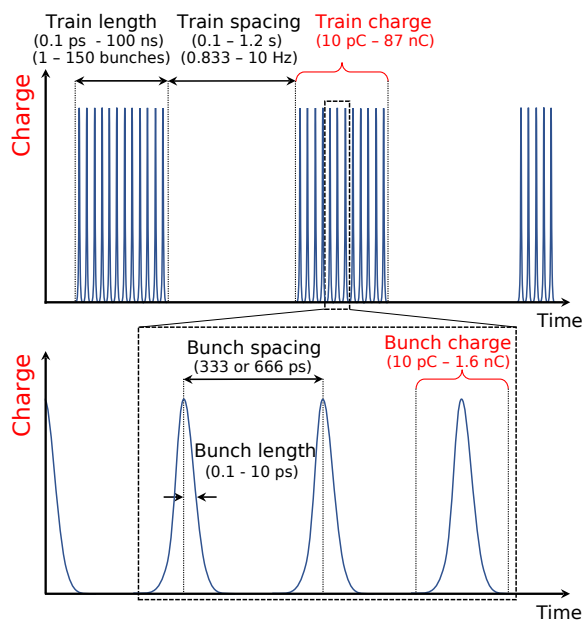


Figure 1: CLEAR beam time structure and charge parameters at the end of the beam line in 2024.

* pierre.korysko@cern.ch

Table 1: CLEAR Beam Parameters in 2024

Parameter	Value
Beam Energy	30 – 220 MeV
Beam Energy Spread	< 0.2% rms (< 1 MeV FWHM)
Bunch length RMS	0.1 – 10 ps
Bunch frequency	1.5 or 3.0 GHz
Bunch charge	0.005 – 1.6 nC
Norm. emittance	1 – 20 μm
Bunches per pulse	1 – 150
Max. pulse charge	87 nC
Repetition rate	0.8333 – 10 Hz

CLEAR operates independently from CERN’s proton machines, enabling operation during the LHC’s extended shut-downs and upgrades. Offering remarkable flexibility, the accelerator typically undergoes weekly experiment installations on Monday mornings and runs for 8 to 12 hours per day, five days a week, tailored to user demands. In 2023, CLEAR ran for 37 weeks and the beam availability was 96.7% (40 hours of fatal failure for 1209 hours of beam). In 2024, 35 experiments are planned in 39 weeks of beam. The approval of the CERN Medium Term Plan in September 2020 earmarked funding for extended CLEAR operation, subsequently endorsed by CERN management until the end of 2025.

CLEAR provides two distinct in-air test areas: VESPER (Very energetic Electron facility for Space Planetary Exploration missions in harsh Radiative environments), primarily utilised for electronics radiation hardness tests, and the In-Air Test Area offering greater flexibility for various experimental needs. Both areas have been utilised for medical applications studies such as Very High Energy Electron (VHEE) radiotherapy at Ultra High Dose Rate (UHDR), looking for the FLASH effect [5], beam instrumentation, diagnostics studies and electronics component irradiation, among others.

Notably, VESPER has played a role in testing and validating components for the ESA’s Jupiter ICy moons Explorer (JUICE) mission, successfully launched in April 2023 [6–9]. It is expected to reach Jupiter in July 2031 after four gravity assists and eight years of travel. Additionally, CLEAR features in-vacuum test areas tailored for specific experiments, including studies on novel accelerator technologies such as plasma lenses and advancements in beam instrumentation [10, 11].

MEDICAL ACTIVITIES IN CLEAR: STUDIES TOWARDS RADIOTHERAPY USING VERY HIGH ENERGY ELECTRONS (VHEE) IN THE FLASH REGIME

R. Corsini*, A. Aksoy, W. Farabolini, A. Gilardi, A. Malyzhenkov, CERN, Geneva, Switzerland
J. Bateman, M. Dosanjh¹, P. Korysko¹, C. Robertson
University of Oxford, Oxford, United Kingdom
V. Rieker¹, University of Oslo, Oslo, Norway
¹also at CERN, Geneva, Switzerland

Abstract

Given the present availability of high-gradient accelerator technology for compact and cost-effective electron linacs in the 100-200 MeV energy range, the interest for Very High Energy Electron (VHEE) radiotherapy (RT) for cancer treatment recently reached an all-time high. Particular significance is assumed by the Ultra-High Dose Rate (UHDR) regime where the so-called FLASH biological effect takes place, in which cancer cells are damaged while healthy tissue is largely spared. VHEE beams from linacs are especially well adapted for FLASH RT, given their penetration depth and the high beam current needed to treat large deep-seated tumours. In recent years, several multidisciplinary user groups carried out a number of studies on VHEE and FLASH RT issues using the CERN Linear Accelerator for Research (CLEAR) user facility, in close collaboration with the local operation team. In this paper, we give an overview of such activities and describe the main results of chemical and biological tests aimed at clarifying the damage mechanisms at the root of the FLASH effect and the relevant beam parameters needed to achieve it. We also describe the dedicated systems and methods developed and used in CLEAR for these activities, focusing on recent advances in the crucial aspects of uniform beam delivery and high dose rate real-time dosimetry.

INTRODUCTION

The CERN Linear Electron Accelerator for Research (CLEAR) is a 200 MeV electron linac followed by an experimental beam line, operated at CERN as a user facility [1]. It serves a wide and diverse scientific community covering many activities, including development of instruments and components for existing and future accelerators and tests of novel concepts as plasma and THz acceleration. In recent years, the investigation of medical applications of electron beams with energies above 100 MeV has become one of its main activities. Over the past years, the question of whether ultra-high-dose rate (UHDR) beams might offer a new modality for cancer treatment is one of the most discussed subjects in modern radiotherapy (RT). The so-called FLASH RT mode, in which the total therapeutic dose is delivered at UHDR in a fraction of a second, has been shown

in several experiments to significantly increase the differential response between healthy and tumour tissue [2–4]. Very-high-energy electron (VHEE) beams with energies above 100 MeV are promising candidates for FLASH RT due to their favorable dose distributions and accessibility of ultrahigh dose rates. Linear electron accelerators can easily provide the high intensity beams needed for UHDR, and have the additional advantage, thanks to recent advances in high-gradient technology, of being rather compact and relatively cheap. The CLEAR electron beam has a wide parameter range, offering great flexibility for experiments [5–8]. In particular, CLEAR beam energy range (30-220 MeV) and high charge per pulse (up to 75 nC) have made it so far the only facility widely available to users for complete VHEE/UHDR studies. Beam parameters are shown in Table 1. A diagram of the beamline is shown in Fig. 1.

Table 1: Updated List of CLEAR Beam Parameters

Parameter	Value
Beam Energy	30 – 220 MeV
Beam Energy Spread	< 0.2% rms (< 1 MeV FWHM)
Bunch length rms	0.1 – 10 ps
Bunch frequency	1.5 or 3.0 GHz
Bunch charge	0.005 – 3 nC
Norm. emittance	1 – 20 μm
Bunches per pulse	1 – 150
Max. pulse charge	75 nC
Repetition rate	0.8333 – 10 Hz

METHODS, DOSIMETRY AND BEAM DELIVERY TECHNIQUES

The CLEAR team has developed in the last years methods and data analysis techniques dedicated to VHEE and FLASH studies, including detailed procedures for passive dosimetry techniques, sample handling, and beam delivery. It also explored new methods for real-time dosimetry in UHDR conditions.

Radiochromic films (RCFs) change colour macroscopically due to polymerisation caused by ionising radiation. The colour change is related to the accumulated dose. After irradiation, the films are optically scanned and the resulting image is processed to determine the dose received, using an experimentally measured calibration curve. They are

* roberto.corsini@cern.ch

BEAM DYNAMICS SIMULATIONS FOR THE ERDC PROJECT: INDUSTRIAL SRF LINAC

N. Solyak[†], C. Edwards, I. V. Gonin, A. Saini, J. C. T. Thangaraj, V. P. Yakovlev
Fermilab National Laboratory, Batavia, IL, USA
R. Kostin, Euclid Techlabs LLC, Bolingbrook, IL, USA

Abstract

Compact conductively cooled SRF industrial linacs can provide unique parameters of the electron beam for industrial applications (up to 10MeV, 1MW). For ERDC project we designed normal conducting RF injector with thermal RF gridded gun integrated in the first cell. For design of the RF gun, we used MICHELLE software to simulate and optimize parameters of the beam. Output file was converted to ASTRA format and most beam dynamic simulations in multi-cell normal conducting injector and cryomodule were performed by using ASTRA software. For cross-checking we compare results of MICHELLE and ASTRA in first few cells. At the end of the injector the beam reach ~ 250 keV energy which allow to trap bunch in acceleration regime without losses in TESLA like 1.3 GHz cavity. Short solenoid at the end of injector allow to regulate transverse beam size in cryomodule to match beam to extraction system and reduce charge losses in the injector.

INTRODUCTION

The new concept of a compact linear accelerator for industrial application suggested in Ref. [1] is based on use of SRF cavities. Several proposals of the compact conduction cooled linac received funding for the R&D stage. Attractive electron beam parameters for industrial application is 10 MeV with average beam powers of 100's kW.

The Illinois Accelerator Research Center (IARC) of Fermilab has started design, construction, and validation of a compact 20 kW prototype of the linac capable of operating 10MeV, 2mA beam in a continuous wave (CW) mode (ERDC project). The linac employs a 9-cells 1.3 GHz TESLA-type Nb₃Sn coated conduction-cooled cavity. As a source of electron beam, we propose to use external injector capable to produce bunches extracted from gridded RF gun and accelerated in copper cavities up to 250-300 keV. The general design of the gun is reported in [2, 3]. The engineering design of the cathode-grid unit has been done at HeatWave Labs, Inc. and two prototypes were fabricated.

General layout of the linac, including RF injector cavity with six individually controlled cells and cryostat with SC 9-cell cavity are presented in Figure 1. On the left side, one can see resonator integrated with RF gun and providing RF voltage on the grid. Playing with RF amplitude and DC voltage on the grid and phase/amplitude of accelerating cell allows us to get required 2 mA beam current and regulate bunch length, output energy and energy spread.

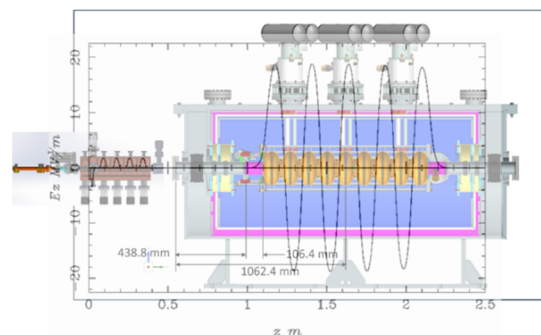


Figure 1: General layout of the 20kW accelerator with external injector and superconducting 9-cells 1.3 GHz cavity.

RF GUN OPTIMIZATION

MICHELLE Simulation

The MICHELLE code [4] is a 3D electrostatic particle-in-cell (PIC) code that has been designed to address the beam optics modelling and simulation of charged-particle transport. The MICHELLE approach uses space charge limited emission based on the Child-Langmuir law.

The beam dynamics simulation of the RF gun + injector cavity assembly was performed with MICHELLE code. An RF voltage with a DC bias is applied to the cathode-grid gap to form the electron bunches. After emission, these bunches are captured and accelerated by RF field in the gun-cell (C0) of the injector. The phase shift ϕ between the RF fields in the gun and in the first cell is one of the optimization parameters. Other parameters are DC and RF voltages between cathode and grid.

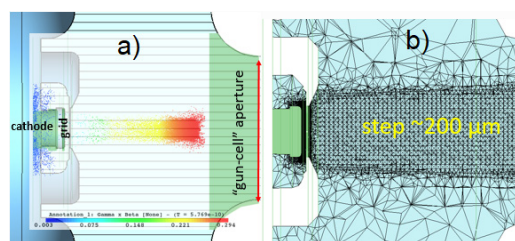


Figure 2: Example of MICHELLE simulation of RF gun. a) beam dynamics in the gun and accelerating cell. b) typical mesh-size: 25 μm -on the grid area, 200 μm in accelerating cell beam transportation area.

Figure 2 show geometry of the gun and cell and accelerated beam. For mesh size we chose fine mesh in cathode-grid area and near the axis of accelerating cell. Grid parameters were optimized for current of 2 mA and output energy of 30 keV after the first injector cell C0.

[†] solyak@fnal.gov.

CW COPPER INJECTOR FOR SRF INDUSTRIAL CRYOMODULES

R. Kostin†, C. Jing, Euclid Techlabs LLC

I. Gonin, V. Yakovlev, N. Solyak, T. Khabiboulline, C. Edwards, J. Thangaraj, FNAL, Batavia, USA

Abstract

Compact SRF industrial linacs can provide unique parameters of the beam (>1 MW CW and $>1-10$ MeV) hardly achievable by normal conducting linacs within limited space. SRF technology was prohibitively expensive until the development of conduction cooling which opened the way for compact standalone SRF systems suitable for industrial and research applications. Limited cooling capacity puts strict requirements on the beam parameters with zero losses of the beam on the SRF cavity walls. This implies strict requirements on the beam energy to be accepted by the cryomodule and most importantly the beam bunching with zero particles in between.

We designed a CW normal conducting RF injector which consists of a gridded RF gun integrated with a first cell of a copper booster cavity to satisfy these requirements. Here we present a complete design of a booster cavity including beam dynamics, RF, thermomechanical and engineering design.

INTRODUCTION

The new concept of a compact linear accelerator for industrial application suggested in [1] is based on the use of Superconducting Radio-Frequency (SRF) cavities. Several proposals of the compact conduction cooled linac has been under development [2, 3]. Attractive electron beam parameters for industrial application is 10 MeV with average beam powers of 100's kW.

The Illinois Accelerator Research Center (IARC) of Fermilab has started design, construction, and validation of a compact 20 kW prototype of the linac capable of operating 10MeV, 2mA beam in a continuous wave (CW) mode (ERDC project). The linac employs a 9-cells 1.3 GHz TESLA-type Nb₃Sn coated conduction-cooled cavity. As a source of electron beam, we propose to use external injector capable to produce bunches extracted from gridded RF gun and accelerated in normal conducting CW injector up to 250-300 keV. The general design of the gridded RF gun is reported in [4, 5]. The engineering design of the cathode-grid unit has been done at HeatWave Labs, Inc. and two prototypes were fabricated. This paper focuses on the injector preliminary design covering the whole spectrum of engineering problems towards its fabrication.

1.3 GHz INJECTOR DESIGN

The schematic representation of the normal conducting CW injector is presented in Fig. 1. The injector consists of several accelerating single-cells boosting the beam energy out of the gridded gun up to 250-300 keV which is enough to successfully capture the beam by the SRF Tesla-cavity

in the cryomodule which has all cells with $\beta=1$. The gridded RF gun is integrated into the first cell of the injector cavity. Bunch length, output energy and energy spread can be changed adjusting RF amplitude and DC bias of the grid and phase/amplitude of the first injector cell.

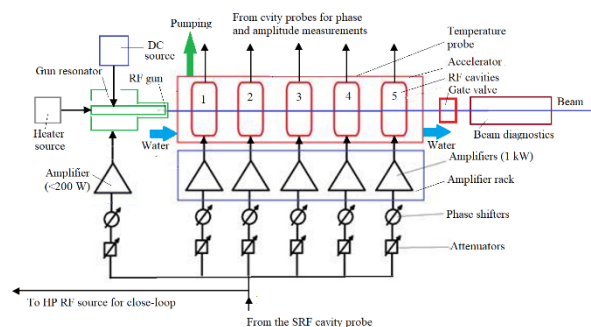


Figure 1: General layout of the normal conducting injector.

All of the cells of the injector are fed through their own separate solid-state amplifiers (SSA's) providing a lot of flexibility in cell's design and beam manipulations. Single cells can have higher shunt impedance as inter-cell coupling is not required and any phase advance can be realized which gives improvement in transit time factor. RF focusing can also be employed. The injector will be locked to the SRF cavity frequency. SRF Nb₃Sn cavity is brittle, and the mechanical tuning is not foreseen for the cavity, thus the injector needs to have the ability of frequency adjustment of several 100's kHz. RF tuning plungers are desired in each cell for this purpose. A preliminary mechanical design of the injector is presented in Fig. 2.

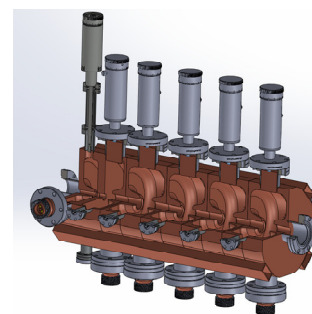


Figure 2: Injector preliminary mechanical design.

The injector has total of six cells with different length to provide the highest energy gain, not to match beam β as it is not required due to each cell individual control. Each cell has a pick-up probe, a loop-style fundamental power coupler (FPC), an RF plunger/tuner and vacuum port. Four cooling channels at the cell's OD are reserved for cavity cooling. The next sections will focus on RF parameters, cooling, multipacting and beam dynamics.

† r.kostin@euclidtechlabs.com

TRANSFER OF EP AND DOPING TECHNOLOGY FOR PIP-II HB650 CAVITIES FROM FERMILAB TO INDUSTRY*

V. Chouhan†, D. Bice, S. Chandrasekaran, G. Ereemeev, A. Netepenko, D. Passarelli, H. Park, J. Ozelis, G. Wu, Fermi National Accelerator Laboratory, Batavia, USA
 A. Shabalina, Science and Technology Facilities Council, UK Research and Innovation, UK
 P. Barbero^{1,2}, A. Gresele¹, A. Tsymbaliuk¹,
¹Zanon Research and Innovation Srl, Italy,
²Simic Spa, Italy

Abstract

Fermilab has optimized the surface processing conditions for PIP-II high beta 650 MHz cavities. This encompasses conditions for bulk electropolishing, heat treatment, nitrogen doping, post-doping final electropolishing, and post-processing surface rinsing. The technology has been effectively transitioned to industry. This paper highlights the efforts made to fine-tune the process and to smoothly share them with the partner labs and an associated vendor.

INTRODUCTION

The Proton Improvement Plan II (PIP-II) is an upgrade to the Fermilab accelerator complex, designed to deliver an 800 MeV proton beam to create the world's most intense neutrino beam for the Deep Underground Neutrino Experiment (DUNE). The PIP-II linear accelerator (LINAC) will be developed with support from international partners and industry, focusing on the integration of various types of niobium (Nb) superconducting RF (SRF) cavities into the LINAC. The international partner laboratories responsible for delivering the high-beta (0.92) 650 MHz (HB650) cavities are Raja Ramanna Centre for Advanced Technology (India) and Science and Technology Facilities Council, UK Research and Innovation (UKRI, UK), with additional support from industry. For UKRI, Zanon Research and Innovation Srl (Italy) is tasked with fabricating these cavities and conducting the necessary surface processing.

Previous projects like LCLS-II and LCLS-II HE, led by the United States with industrial collaboration, have set a successful precedent. The achievements of these projects were made possible through effective technology sharing with industry partners [1, 2]. Surface processing of the Nb cavities is a critical step in ensuring the cavities meet the performance specifications required for the cryomodules. The knowledge gained from these projects is invaluable for future endeavors and is currently being applied to the ongoing PIP-II project.

This paper reports on the surface processing technology and the lessons learned, which have been shared with partner labs and the vendor working on the HB650 cavities.

LESSONS LEARNED ON EP OF HB650

Fermilab and other SRF facilities have extensive experience in electropolishing (EP) 1.3 GHz cavities and other surface processing techniques [1, 3]. The HB650 cavity is significantly larger, with nearly twice the surface area of a 1.3 GHz cavity, making the same standard EP conditions unsuitable for achieving a smooth surface, as shown in our latest EP study conducted with LB650 and HB650 cavities [3, 4]. Based on the studies performed, key findings and lessons learned were identified as summarized below.

The standard 18 V was found to be insufficient for the EP of HB650 cavities, resulting in a rough equator surface and premature quench of the cavities [3]. This conclusion is supported by I-V curves measured for 650 MHz cavities under various conditions. The I-V curve with two major regions, linear and plateau regions, provides insight into the chemistry of the cavity surface. A smooth surface is achieved when EP is conducted at a voltage within the plateau region.

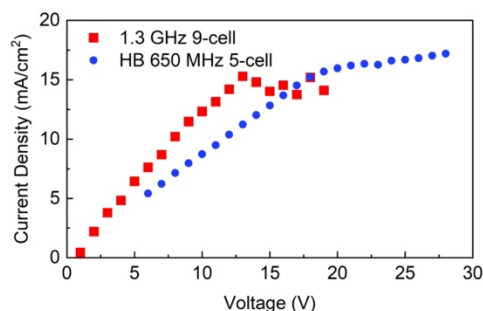


Figure 1: I-V curves measured for 1.3 GHz and HB 650 MHz cavities. The I-V curve for HB650 was obtained with new cathode structure.

Unoptimized cathode structure and surface area fail to yield the current plateau even up to 25 V [3]. A new cathode was designed to enhance the surface area and acid flow conductance, and to reduce cathode polarization. The plateau onset (V_{onset}) was obtained at relatively lower voltage as compared to the initial cathodes. A lower EP voltage is also important to mitigate sulfur generation. However, HB650 cavities still requires an EP voltage higher than the standard voltage. The I-V curves for a 1.3 GHz 9-cell cavity and an HB650 cavity are compared in Fig. 1. V_{onset}

* This work was supported by the United States Department of Energy, Offices of High Energy Physics and Basic Energy Sciences under contract No. DE-AC02-07CH11359 with Fermi Research Alliance.

† vchouhan@fnal.gov

STUDY OF MECHANICAL GRINDING EFFECTS ON NIOBIUM SURFACE*

V. Chouhan†, T. Ring, D. Smith, G. Wu, Fermi National Accelerator Laboratory, Batavia, IL, USA

Abstract

Mechanical grinding is commonly employed to eliminate surface defects such as scratches and pits from niobium cavity surfaces or sheets before cavity fabrication. Subsequently, chemically buffered polishing or electropolishing is often utilized to completely remove residues of the polishing media and any defects induced by mechanical grinding, ensuring a pristine surface. In this study, we conducted a systematic investigation to assess the influence of mechanical grinding using silicon carbide and aluminum oxide polishing media on niobium surfaces. Additionally, the study examines the effects of post-mechanical grinding chemical treatments on surface quality.

INTRODUCTION

Niobium (Nb) superconducting RF (SRF) cavities for modern superconducting accelerator machines are fabricated by following various steps, including Nb sheet fabrication from Nb ingot deep drawing, electron beam welding, buffered chemical polishing (BCP), electropolishing (EP), and other surface processing methods [1, 2]. Mechanical grinding is also required at different stages to polish the surface defects when they appear. Surface grinding is often applied during the preparation of the Nb sheet, before deep drawing the sheets to form half cells, and even to a fabricated cavity when a defect appears on the interior surface.

The thickness of the cavity wall must be maintained at a desired value, and the surface should be defect-free as required for the good performance of the cavities. Therefore, a precise grinding process is essential [3], typically using silicon carbide (SiC) or aluminum oxide (Al_2O_3) media. However, understanding the optimal grinding media, grit size, and post-grinding removal through BCP or EP for Nb remains limited.

This study aims to provide insights into the grinding process and the necessary EP removal to achieve a defect-free surface, free from embedded contaminants.

EXPERIMENTAL

Nb samples (1×1 cm) were prepared from the same Nb sheet. The samples were electropolished for 100 μm removal to eliminate any initial surface defects. These electropolished samples were mechanically ground using SiC and Al_2O_3 media with varying grit sizes. A target sample was pressed against a rotating disk with sandpaper attached for grinding. For each media type, 5 samples were ground initially with grit size 80 and finished with finer grits

* This work was supported by the United States Department of Energy, Offices of High Energy Physics and Basic Energy Sciences under contract No. DE-AC02-07CH11359 with Fermi Research Alliance.

† vchouhan@fnal.gov

ranging from 120 to 320. The grinding steps and average removal are detailed in Table 1.

After grinding, all samples underwent three EP sequences, removing a total of 20, 40, and 80 μm . EP was performed in a temperature-controlled electrolyte bath using a standard mixture of sulfuric (96wt%) and hydrofluoric (70wt%) acids in a 10:1 volumetric ratio. EP was conducted at 18 V, with Nb as the anode and an aluminum electrode as the cathode.

The sample surfaces were analyzed using scanning electron microscopy (SEM) and energy-dispersive X-ray spectroscopy (EDS) to identify any embedded particles. Laser confocal scanning microscopy (LCSM) was used to study surface morphologies to assess the effects of grit size and removal on the surface quality.

RESULTS AND DISCUSSION

After grinding, all the surfaces were observed using SEM and analyzed with EDS. Figure 1 shows typical SEM images of the niobium surfaces ground with grit sizes 80 and 320 of SiC and Al_2O_3 . The coarse grit of 80 clearly caused more surface damage, as observed for both SiC and Al_2O_3 media. It was evident that grinding with SiC, especially with grit size 80, resulted in greater surface damage compared to Al_2O_3 . Additionally, the SEM images revealed bright spots, which are presumed to be embedded abrasive particles. The number of bright spots increased with finer grit sizes for both types of media. However, the surfaces ground with SiC consistently exhibited more bright spots compared to those ground with Al_2O_3 .

To analyze these bright spots, EDS was performed on all the samples. Figure 2 presents the EDS spectra of the surfaces of SC-G320 and AO-G320, which were ground with a fine grit size of 320 and contained the highest number of bright spots. The EDS spectra for SC-G320 and AO-G320 show peaks corresponding to Si and Al, indicating the presence of embedded SiC and Al_2O_3 abrasives in the niobium surface. The strong Si peak confirmed that the surfaces ground with SiC contained a higher number of embedded particles compared to those ground with Al_2O_3 .

After the EP steps, the samples were again examined using SEM and EDS to detect any remaining embedded particles. Thorough SEM scanning and EDS analysis revealed that no embedded SiC particles remained after the first EP step, which removed 20 μm of material. However, some Al_2O_3 abrasives were still embedded in the surfaces of samples AO-G80 and AO-G320. Figure 3 shows an SEM image of AO-G320 after the first EP step, along with its corresponding EDS spectrum. The image and spectrum indicate the presence of an embedded Al_2O_3 particle. However, after subsequent EP steps, no abrasives were detected on any of the samples.

EXCELLENT PERFORMANCE OF 650 MHz SINGLE-CELL NIOBIUM CAVITY AFTER ELECTROPOLISHING*

V. Chouhan†, D. Bice, A. Cravatta, T. Khabiboulline, O. Melnychuk, A. Netepenko, G. Wu
Fermi National Accelerator Laboratory, Batavia, IL, USA
B. Guilfoyle, T. Reid, Argonne National Laboratory, Lemont, IL, USA

Abstract

Electropolishing process and cathodes have undergone modification and optimization for both low- and high-beta 650 MHz five-cell niobium cavities for PIP-II. Cavities treated with these modified electropolishing conditions exhibited smooth surfaces and good performance in baseline tests. Nonetheless, due to administrative constraints on project cavities, maximum gradient performance testing was not conducted. This paper presents a study conducted on a single-cell 650 MHz cavity utilizing the optimized electropolishing conditions, highlighting the maximum performance attained for this specific cavity. The cavity tested at 2 K in a vertical cryostat reached a superior accelerating field gradient of 53.3 MV/m at Q_0 of 1.6×10^{10} , which is the highest gradient attained for this type of large-sized cavities.

INTRODUCTION

Modern superconducting accelerator machines utilize niobium superconducting RF cavities, which operate in a superconducting state at 2 K. Various types of superconducting cavities are essential for building an efficient accelerating machine. Medium (~ 650 MHz) and high frequency (~ 1.3 GHz) elliptical cavities are used to accelerate high-energy particles. For an efficient accelerator, it is crucial to have cavities with both high gradient and high Q_0 . SRF R&D focuses on enhancing these aspects, with surface processing playing a critical role in achieving optimal performance. Key processes include electropolishing, heat treatment, nitrogen doping (N-doping), mid-temperature baking, 120°C baking, and high-pressure water rinsing. Electropolishing is an electrochemical technique designed to remove interior material from the cavity, ensuring a defect-free and smooth surface.

1.3 GHz cavities have demonstrated excellent SRF performance with a high accelerating gradient of around 50 MV/m [1]. The corresponding surface peak magnetic field B_{pk} reaches ~ 210 mT. 650 MHz niobium cavities should also be capable of reaching similarly high gradients and corresponding B_{pk} . However, the performance of 650 MHz cavities and cavities with similar frequencies reported so far have not met such a high performance.

Recently, we have demonstrated significant improvements in the surface quality and SRF performance of low- and high-beta five-cell 650 MHz cavities developed for the Proton Improvement Plan (PIP-II) linac [2, 3]. Notably,

one of the HB650 cavities was tested beyond the administrative limit, achieving 29 MV/m without quenching [3]. The maximum performance potential of these cavities, following processing with the modified EP technique and upgraded cathode design, has yet to be fully assessed. This study focuses on applying the optimized EP conditions to a 650 MHz single-cell cavity with a β value of 0.9 and evaluating its maximum quench field. This paper presents the surface processing methods applied and the resulting SRF performance of the 650 MHz single-cell cavity.

EP SETUP AND CONDITIONS

The horizontal electropolishing (EP) setup and the cathode used in this study are illustrated in Fig. 1. The single-cell cavity (B9AS-AES-003) was processed using EP parameters detailed in Table 1. The cathode design used for the 5-cell cavities was scaled down and replicated for the cavity B9AS-AES-003. These EP parameters and cathode structure were consistent with those optimized for the 5-cell high- β 650 PIP-II cavities [3].

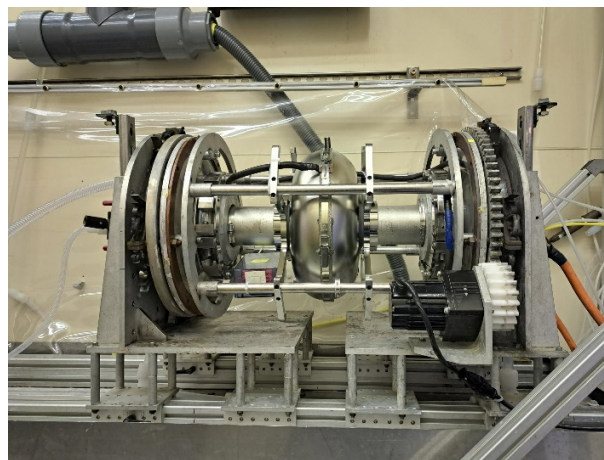


Figure 1: EP tool with the cavity B9AS-AES-003 (top). Patented cathode structure used for EP the cavity (bottom).

* This work was supported by the United States Department of Energy, Offices of High Energy Physics and Basic Energy Sciences under contract No. DE-AC02-07CH11359 with Fermi Research Alliance.

† vchouhan@fnal.gov

OPTIMIZATION OF STATIC HEAT LOADS OF THE PIP-II CRYOMODULES BASED ON PROTOTYPE HB650 CRYOMODULE TEST RESULTS*

V. Roger †, J. Bernardini, B. J. Hansen, J. P. Holzbauer, J. Makara, A. Martinez, J. Ozelis, D. Passarelli, M. J. White, D. Porwisiak, S. Yoon, J. Subedi, Fermilab, Batavia, USA

Abstract

During the first cool-down of the prototype HB650 cryomodule (pHB650 CM), high static heat loads have been measured compared to the estimation. Several analysis and calculations have been performed to explain this difference which led to cool-down this cryomodule two additional times. Before each cool-down, repairs and upgrades have been done, and instrumentations were added to identify the issues and quantify their impact on the heat loads. Based on these findings, the production cryomodule design and assembly process have been updated to align the future heat loads measurements with the estimations.

INTRODUCTION

From March 2023 to July 2024, the pHB650 CM underwent three cooling cycles. Extensive cryogenic testing conducted during the initial cooldown, detailed in Table 1, prompted a thorough analysis to identify discrepancies between calculated and measured static isothermal heat loads [1]. The analysis revealed several issues:

- Radiation from the room temperature parts of the couplers inside the coldmass.
- Thermal Acoustic Oscillations (TAO) in the cool-down valve.
- Rollin film going up in the pressure transducer lines making a short with the thermal shield.

In addition, heat loads estimations were checked and refined using a Simulink/Simscape model of the pHB650 CM [2] supplemented by measurements obtained from the 1st cool-down.

Table 1: Estimated and Measured Static Heat Loads

	Estimated heat loads	1 st Cool-down
High Temperature Thermal Shield (HTTS)	160 W	260 W
Low Temperature Thermal Source (LTTS)	17.6 W	29.7 W
2K (Cavities at 4K)	9.8 W	33.8 W
2K (Cavities at 2K)	10.1 W	~ 50 W

STATIC HEAT LOADS MEASURED DURING THE 1ST AND 2ND COOL-DOWN

Prior to the 2nd cool-down of the cryomodule, several modifications were implemented, Multi-Layer Insulation (MLI) was added around the room temperature parts of the

* This manuscript has been authored by Fermi Research Alliance, LLC under Contract No. DE-AC02-07CH11359 with the U.S. Department of Energy, Office of Science, Office of High Energy Physics.

† vroger@fnal.gov

couplers, the material of the cool-down valve stem has been changed from Stainless steel to G10, and heaters have been added at the base of the pressure transducer lines. Following overseas transportation, which aimed to validate the design of the cryomodule and its transport frame [3], a 3rd cool-down was conducted. During this phase, additional MLI was applied around the couplers, a check valve was installed on the relief line, and heaters along with temperature sensors were added to the valve intercepts. Additionally, a light warm-up procedure was performed to facilitate the replacement of the G10 stem with a stainless-steel stem equipped with wipers, similar to the method used for the LCLS-II cryomodules [4]. Heat loads results for the 2nd and 3rd cool-down are summarized in Table 2.

Table 2: Measured Static Isothermal Heat Loads During Cool-Downs

	2 nd Cool-down	3 rd Cool-down	
HTTS	240 W	240 W	
LTTS	23.3 W	19.5 W	
2K (Cavities at 4K)	27.2 W	23.0 W	
2K (Cavities at 2K)	38.2 W	29.6 W (Before putting wipers)	27.5 W (After putting wipers)

An analysis of the heat loads for both the Low Temperature Test Stand (LTTS) and the 2K stage with cavities at 4K, indicates that radiation from the room temperature parts of the couplers impacts both LTTS and 2K heat loads similarly. To address the discrepancies observed between the estimated and measured heat loads, the contributions of the main components of the cryomodule [5] have been studied in detail in the subsequent chapters.

CRYOGENIC VALVES

During the 1st cool-down of the cryomodule, TAO were observed in the cool-down valve. Although replacing the stainless-steel stem with a G10 stem during the 2nd cool-down reduced the heat load associated with TAO by approximately 5.2 W, it did not completely eliminate the issue. TAO were fully mitigated in the final phase of the 3rd cool-down after installing wipers on the stainless-steel stem, which reduced the heat load by an additional 2.1 W.

The installation of temperature sensors on the valve intercepts during the 3rd cool-down (as shown in Fig. 1) enabled the calculation of heat transfer through the thermal straps with cavities at 2K and 8K for which TAO are not possible. The comparison of this data confirmed that the TAO issue in the cool-down valve was effectively

THE 648 MHz KLYSTRON POWER SOURCE SYSTEM OF CSNS-II LINAC SUPERCONDUCTING ELLIPSOID CAVITY

Zhencheng Mu¹, Maliang Wan¹, Hui Zhang², Xie Zhixin¹, Hexin Wang¹, Bo Wang¹, Linyan Rong¹

¹Institute of High Energy Physics, Beijing, China

²Spallation Neutron Source Science Center, Dongguan, China

Abstract

The CSNS-II superconducting Linac accelerator includes 20 sets of 324 MHz superconducting spoke cavities and 24 sets of 648 MHz superconducting ellipsoidal cavities. The beam energy at the end of the superconducting Linac accelerator reaches 300 MeV. The 324 MHz solid-state power source supplies RF power to superconducting spoke cavity, while the 648 MHz klystron power source supplies RF power to superconducting ellipsoid cavity. The RF pulse width of the 648 MHz klystron is 1.2 ms, the repetition rate is 50 Hz, and the peak power is 1.2 MW. The 1.5 ms long pulse solid-state modulator provides high voltage pulse for the klystron, and each modulator is equipped with four klystrons.

INTRODUCTION

At the end of March 2024, the phase II of China Spallation Neutron Source (CSNS-II) project began, 20 sets of 324 MHz spoke cavities are connected behind the DTL accelerators, the spoke cavities increase the energy of the H⁻ ions from 80 MeV to 173 MeV. Then, 24 sets of 648 MHz medium β ellipsoidal cavities further increase the energy of the H⁻ ions to 300 MeV.

THE RF POWER SOURCE SYSTEMS

The RF power source systems provide RF power required for 50 mA of peak beam current over a pulse length of 700 μ s at a repetition rate of 50 Hz. The beam cutting rate is 40%. The fill and fall time of the ellipsoidal cavities will be on the order of 300 μ s, the RF pulse length of the RF power source is set 1.2ms, the duty factor of the RF power is 6%. The RF peak power demands of the CSNS Linac superconducting cavities are shown in Fig. 1. According to the RF peak power demand, the 324 MHz spoke cavities are powered by solid state amplifiers, and the 648 MHz klystron power sources are adopted to supply RF power for superconducting ellipsoidal cavities.

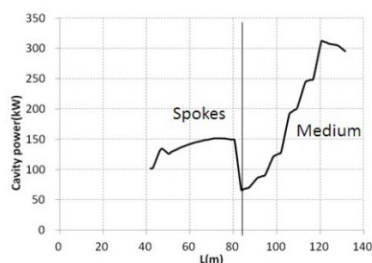


Figure 1: RF power demands of spoke cavities and ellipsoidal cavities.

THE 648 MHz KLYSTRON POWER SOURCE OF ELLIPSOID CAVITY

Each 648 MHz klystron power source of ellipsoidal cavities consists of a modulator, a 648 MHz klystron, a circulator and dummy load, WR1500 waveguides to deliver the RF power to cavities. One modulator provides the high voltage pulse to four klystrons.

Klystron

The klystrons operates at a frequency of 648 MHz and the saturation peak power is 1.2 MW. With the 6% duty cycle for CSNS-II Linac RF system, this means that the average power level at saturation is about 72kW, the specifications of the 648 MHz klystron are shown in Table 1 [1].

Table 1: The Specifications of 648 MHz Klystron

Parameter	Value	Unit
Center Frequency	648	MHz
Bandwidth	± 0.5	MHz
RF Peak Power	≥ 1.2	MW
RF Pulse Width	1.2	ms
Repetition rate	50	Hz
Gain	≥ 45	dB
Efficiency	50	%
Cathode Voltage	-105	kV

The 648 MHz klystron is designed with mod-anode configuration, and the modulator outputs high voltage pulse to the klystron cathode, the high voltage pulse applied to the mod-anode can be adjusted through resistive divider. The electron gun part of the klystron includes two section ceramics, this part is placed in an oil tank to protect the ceramics from high voltage breakdown. After receiving the prototype of the 648 MHz klystron, we aged the klystron with a hi-potter, and the withstand voltage between the mod-anode and the cathode was aged to 90 kV, the withstand voltage between the mod-anode and the ground was aged to 70 kV. The prototype passed the site acceptance test in October 2023, the test results have met all the specification requirements. The 648 MHz klystron operates in horizontal orientation, it has a separate magnet, and the photograph of the klystron installed at CSNS site is shown in Fig. 2.

INVERSE INFERENCE OF INITIAL BEAM PROFILE AND KEY PARAMETERS BASED ON AUTOMATIC DIFFERENTIATION METHOD*

Z. Sun[†], T. Xin, X. Li, C. Meng, O. Xiao, Z. Liu

Institute of High Energy Physics, Chinese Academy of Sciences, Beijing, China

also at University of Chinese Academy of Sciences, Beijing, China

Z. Song, Tsinghua University, Beijing, China

Abstract

For experiments requiring the longitudinal shaping of the beam at the exit of an electron linear accelerators, it is crucial to infer the initial beam profile at the entrance of the linear accelerator and key parameters. After passing through the dispersion section of beam bunch compressor, and the high-frequency system, the electron beam will undergo modulation on the longitudinal density. Based on the longitudinal dynamic process, this paper proposes to use automatic differentiation to provide the design of beam initial conditions and key parameters corresponding to a specific longitudinal profile of the beam at the exit of the linear accelerator. Finally, we implemented this method on a section of linear accelerator consisting of two L-band accelerating cavities, one S-band accelerating cavity, and a bunch compressor.

INTRODUCTION

The advancement of accelerator technologies, including free-electron lasers, terahertz radiation sources, and plasma accelerators, underscores the critical need for precise control over the temporal characteristics of electron beams [1]. These applications benefit from customized current profiles, which are vital for achieving optimal performance. For example, in plasma acceleration, specialized electron beam profiles play a key role in achieving high transformer ratios. This often involves using an asymmetric driver beam with a triangular shape, characterized by a gradual increase in density at the front and a sharp decrease at the rear to minimize the decelerating field experienced by the driver beam. Furthermore, utilizing a trapezoidal distribution for the beam to be accelerated results in a flatter longitudinal wakefield at the accelerated beam's location, facilitating the production of a beam with low energy spread for efficient acceleration [2]. Additionally, the elimination of current fluctuations is crucial for enhancing the operation of free-electron lasers, underscoring the significance of advanced beam shaping techniques in accelerator physics for designing optimal current profiles for various FEL applications. To address these requirements, shaping the temporal profiles of electron beams is indispensable, emphasizing the importance of advanced beam shaping techniques in accelerator physics.

Several reliable methods have been developed to shape the beam profiles. One common method involves directing an electron beam with a particular energy spread through an energy dispersion section, such as a bunch compressor with multiple bending magnets, and possibly additional

sextupoles and octupoles [3]. These components offer a more flexible combination of dispersion terms. By selecting the appropriate combination of parameters in the compressor and an initial beam with a particular energy chirp, it is possible to achieve the desired beam profiles. Furthermore, understanding the impact of the RF system on the energy chirp, and anticipating the longitudinal distribution of the beam in advance, will be a crucial step. This is also the main issue that this paper work aims to address.

With the application of automatic differentiation in the reconstruction of beam phase space, more and more attention is being focused on using automatic differentiation to solve problems with high complexity, high dimensionality, and difficulties in convergence. R. Roussel and A. Edelen's team proposed using automatic differentiation techniques to rapidly reconstruct the 6-dimensional information of the initial beam based on neural network structures, utilizing the 6-dimensional information of the beam images observed at the diagnostic screen [4]. This laid the foundation for the application of automatic differentiation techniques in solving inverse problems.

Based on this method, we analyzed the longitudinal dynamics of the beam and provide the relationship between the longitudinal particle coordinates of the beam at the exit and the initial RF system parameters, chicane parameters, and initial particle longitudinal coordinates. By using automatic differentiation methods, the initial beam profile and the parameter design of the linear accelerator can be rapidly determined.

LONGITUDINAL DYNAMICS

For generality, we discuss the longitudinal dynamics process of an electron beam passing through an RF system consisting of two L-band traveling wave tubes and one S-band traveling wave tube, as well as a chicane design similar to that described in Ref. [3] (comprising 4 dipoles and 2 quadrupoles, 2 sextupoles, and one octupole, providing a more flexible combination of dispersion terms) as shown in Fig 1. Assuming the initial electron beam is monoenergetic with an initial energy of 200 MeV, the electron energy (charge e) at the chicane after passing through the three RF systems is

$$E_f \approx E_0 + eV_1 k_L \cos(\varphi_1 + k_L z_0) + eV_2 k_L \cos(\varphi_2 + k_L z_0) + eV_3 k_S \cos(\varphi_3 + k_S z_0) \quad (1)$$

where $k_{L,S} = (2\pi/\lambda_{L,S})$ is the RF wavenumber, z_0 is the longitudinal position of the electron with respect to the reference particle (bunch center), and the bunch head is at

[†]sunzheng@ihep.ac.cn

COMPLETION OF PHASE B+ BEAM COMMISSIONING OF LINEAR IFMIF PROTOTYPE ACCELERATOR (LIPAc)*

T. Akagi^{†, 1}, A. De Franco¹, T. Ebisawa, K. Hasegawa, K. Hirose, J. Hyun¹, N. Kaneko¹, A. Kasugai, K. Kondo, K. Kumagai¹, S. Kwon¹, K. Masuda¹, A. Mizuno⁴, M. Sugimoto¹
QST, Rokkasho, Japan

F. Benedetti², Y. Carin¹, J. Chambrillon¹, F. Cisondi, H. Dzitko, D. Gex¹, D. Jimenez-Rey³, I. Moya¹, F. Scantamburlo¹, F4E, Garching, Germany
¹also at IFMIF/EVEDA Project Team, Rokkasho, Japan
²also at CEA Paris-Saclay, France
³also at CIEMAT, Madrid, Spain
⁴also at JASRI, Sayo, Japan

Abstract

The Linear IFMIF Prototype Accelerator (LIPAc) is being commissioned under the international collaboration between the EU and Japan. LIPAc aims to accelerate a deuteron beam of 125 mA to 9 MeV and operate in CW mode, and consists of an injector, an RFQ, a Superconducting RF Linac (SRF Linac), a beam transport line, and a beam dump. Until recently, the LIPAc beamline was in its final configuration except for the SRF Linac, which was for a high-duty beam operation called Phase B+ commissioning. The main objective of this commissioning was to validate high duty cycle deuteron beam operation and characterization of the beam. Phase B+ was completed at the end of June 2024, with a beam current of about 119 mA and duty cycle of up to 8.75% have been achieved. After the completion of the Phase B+, the SRF will be delivered to the accelerator room and installed in the beamline. The results of Phase B+ are presented in this paper.

INTRODUCTION

As one of the Broader Approach (BA) projects, an international cooperation between Europe and Japan in the field of fusion energy, the International Fusion Materials Irradiation Facility (IFMIF) Engineering Validation and Engineering Design Activity (IFMIF/EVEDA) is underway [1]. This is to research and develop an accelerator-driven intense neutron source using the D-Li stripping nuclear reaction to study the effects of 14 MeV high-energy neutrons produced in the D-T fusion reaction on potential candidate materials constituent of a fusion reactor.

The prototype accelerator of IFMIF, called Linear IFMIF Prototype Accelerator (LIPAc), is being commissioned in Rokkasho-mura, Japan as part of the IFMIF/EVEDA project. The IFMIF accelerator concept is designed to operate in continuous wave (CW) mode with two deuteron beams with a total of 250 mA (2×125 mA) at 40 MeV. LIPAc is designed to demonstrate the low-energy part of the accelerator, which is the most challenging part from a beam dynamic standpoint, and its goal is to accelerate a 125-mA deuteron beam to 9 MeV and operate in CW mode. LIPAc

consists of an injector, an RFQ driven by 175 MHz eight 200 kW RF power system, an SRF Linac, a beam transport system and a Beam Dump (BD). Each system was designed and manufactured at European research institutes and shipped to QST Rokkasho Institute for Fusion Energy in Rokkasho for installation and commissioning. The commissioning of LIPAc is performed in several phases: Injector Stand-Alone Validation (Phase A), RFQ Validation (Phase B) and SRF-Linac Validation (Phase C/D) as shown in Fig. 1. Phase B was completed in July 2019 with the successful acceleration of a 125-mA deuteron short pulse beam (1 ms, 1 Hz) at 5 MeV thanks to the RFQ [2]. The installation of the MEBT Extension Line (MEL) in place of the SRF Linac, the High Energy Beam Transport (HEBT) line and the beam dump enabled to begin the Phase B+ in 2021 toward high-duty beam operation and it was completed at the end of June 2024. The SRF Linac installation preparations are currently underway for Phase C. The following sections report on the test results obtained from the Phase B+.

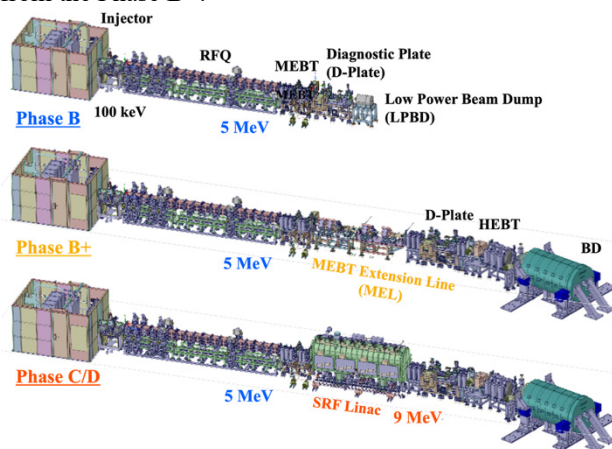


Figure 1: The three configurations of the LIPAc stepwise commissioning phase.

PHASE B+

The main purpose of Phase B+ is to demonstrate the operation of the 5 MeV deuteron beam with long pulses and to characterize the beams injected into the SRF-Linac (which will be installed after the completion of Phase B+).

* IFMIF/EVEDA Integrated Project Team with QST, IFMIF/EVEDA PT, F4E, CEA, CIEMAT, INFN
[†] akagi.tomoya@qst.go.jp

PLAN FOR TERAHERTZ-WAVE SOURCE OF SUPERIMPOSED COHERENT TRANSITION RADIATION USING RING-TYPE RESONATOR AT LEBRA

N. Sei[†], H. Ogawa, Research Institute for Measurement and Analytical Instrumentation, National Institute of Advanced Industrial Science and Technology (AIST), Tsukuba, Ibaraki, Japan
 T. Sakai, Y. Hayakawa, Y. Takahashi, T. Tanaka, K. Hayakawa
 Laboratory for Electron Beam Research and Application, Nihon University, Funabashi, Japan
 T. Takahashi, Institute for Integrated Radiation and Nuclear Science, Kyoto University, Osaka, Japan

Abstract

We plan to generate high peak power pulses in a terahertz region by superimposing CTR pulses using a ring-type resonator. In experiments conducted at an L-band electron linear accelerator facility at the Kyoto University Institute for Integrated Radiation and Nuclear Science (KURNS-LINAC), a resonant coherent transition radiation (CTR) could be extracted with low loss from the resonator using a material with low absorption in the terahertz region as an output coupler inside the resonator. It was observed that the extracted terahertz CTR pulses were amplified owing to superimposition of their electric fields. Because the long CTR wavelength resulted in large diffraction losses of the resonator, the amplification rate of the CTR pulses was low at the KURNS-LINAC. We therefore planned to develop a device of CTR superposition with a ring-type resonator at the Laboratory for Electron Beam Research and Application (LEBRA) in Nihon University, where a short-wavelength CTR has been developed using the electron beam with the bunch length of a few sub-picoseconds is short. Our goal is to generate terahertz CTR pulses with a peak power of more than 1 MW at the LEBRA.

INTRODUCTION

We have studied intense terahertz-wave sources using a normal-conducting S-band linac at the Laboratory for Electron Beam Research and Application (LEBRA) at Nihon University [1, 2]. The developed coherent transition radiation (CTR) had a high energy of 1 mJ per macropulse [3]. However, the peak power of the CTR was approximately 100 kW and did not reach 1 MW, i.e., the level at which nonlinear optical phenomena are evident in the terahertz region. Therefore, based on our experimental results at the Kyoto University Institute for Integrated Radiation and Nuclear Science (KURNS-LINAC) [4], we planned to generate high peak-power terahertz pulses by confining CTR micropulses in a ring-type resonator and superimposing them with CTR micropulses generated late within the resonator. By inserting a plate with low absorption in the terahertz region into the resonator as an output coupler, it is possible to extract CTR pulses with high peak power while suppressing a cavity loss.

In this article, we first briefly describe pulse superposition of coherent radiations using a resonator. Then, we outline the superposition experiments of CTR micropulses

[†] sei.n@aist.go.jp

conducted at the KURNS-LINAC and describe the plan of the new superposition experiments at the LEBRA.

PULSE SUPERPOSITION USING A RESONATOR

Coherent radiation has an electric field structure which corresponds to a pulse shape of an electron bunch [5]. If a bunch train in an electron beam macropulse is accelerated at precise time intervals, the coherent radiation train generated by the electron bunches can be superimposed by confining them in a resonator whose circumference is an integer multiple of the electron bunch interval. The electric field of the superimposed coherent radiation can be amplified by using a resonator comprising an even number of mirrors. Several studies on the superimposition of coherent radiations using a resonator have already been reported [6, 7].

If a CTR in the terahertz region generated by a thin metal substrate is used as a coherent radiation source, the substrate can be also used as a mirror to construct the resonator [4]. To extract CTR pulses from the resonator, a thin parallel plate made of a material with negligible absorption in the terahertz region is used. When the parallel plate is inserted at the Brewster angle with respect to the circulating CTR pulses, the p-polarized component of the CTR pulses passes through the parallel plate without a loss. Therefore, it is possible to construct a resonator with a small cavity loss. The CTR pulses are observed using the s-polarized component extracted from the resonator. By adjusting the thickness of the parallel plate whose optical length is longer than the length of the CTR pulse, interference of reflected lights on the front and back surfaces of the parallel plate can be eliminated. If the CTR pulse length is sufficiently short, even materials with a slightly high absorption can be used as the parallel plate. When a semiconductor material is irradiated with a short-pulse laser, a plasma mirror which reflects lights in the terahertz region is generated [8]. Using Si as the parallel plate, it is possible to quickly extract the high peak-power CTR pulses accumulated in the resonator.

SUPERPOSITION EXPERIMENTS AT KURNS-LINAC

A ring-type resonator comprising two off-axis parabolic mirrors and two plane mirrors was installed on the electron beam orbit of an L-band electron linear accelerator facility

INTEGRATION OF HKL SINGLE CRYSTAL COMPUTATIONS INTO EPICS USING PYDEVICE *

Alexander Baekey^{1,2}, Kazimierz J. Gofron^{1†}

¹Oak Ridge National Laboratory, Oak Ridge, TN, USA

²University of Central Florida, Orlando, FL, USA

Abstract

In this work, we integrate and extend an HKL computation package into EPICS through a PyDevice IOC. This provides EPICS users a generalized approach to mapping real motor rotation space to HKL reflections for a wide range of diffractometers (4-circle, 6-circle, kappa geometries). Utilizing PyDevice for EPICS IOC development allows us integrate Python bindings for core calculations written in C, simultaneously taking advantage of the efficiency of C and readability of Python. The EPICS IOC provides an interface between beamline hardware and users through an intuitive Phoebus CSS GUI. Extensions are being developed to the original HKL package to handle inelastic scattering in addition to the original elastic scattering case for neutron and X-ray diffraction.

INTRODUCTION

Crystallography studies arrangement of atoms in a material, and inner atomic structure can be determined using diffraction properties of penetrating radiation such as X-ray, electron, or neutron. The single crystal studies use a diffractometer which allows precise rotation of the material under study, in order to measure diffraction pattern. The diffraction pattern identifies arrangement and symmetry of the atoms in a crystal. In this work we report development of an EPICS [1] IOC that allows integration of control of the diffractometer rotations of the crystal under studies with beamline controls and data acquisition typically present at neutron and X-ray synchrotron beamlines. The integrated controls is indispensable in order to optimize use of precious beam time assigned at the X-ray and neutron sources.

Commercial diffractometers used at beamlines typically have four or six axis of rotation (Figs. 1 and 2), but many specialized diffractometers have been tailored to specific beamline needs. For instance, inelastic neutron scattering [2] typically uses a triple-axis spectrometer to probe momentum

and energy response of sample materials. Instead of a full circle geometry, neutron specific facilities often use a triple-axis goniometer with two tilt stages on top of a rotation stage to accommodate the heavy load of magnets and cryostats.

In this work we report EPICS support for diffractometers with four and six axis of rotation in Eulerian and kappa geometries for horizontal and vertical diffractometer orientations.

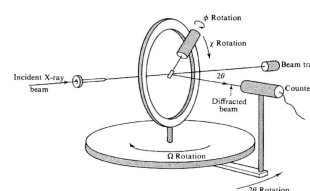


Figure 1: Four-circle diffractometer [3].

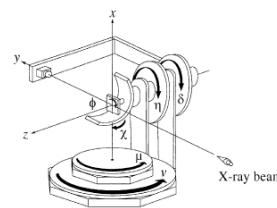


Figure 2: Six-circle diffractometer [4].

Our EPICS control of the diffractometer consists of an IOC that provides forward calculations (real space angle motor to momentum), inverse calculations (momentum to diffractometer angles), and allows for scanning in inverse space by using coordinated motion of real motors. Utilizing the HKL C library [5], This IOC is used to factorize single crystal diffraction angles computation for different kinds of diffractometer geometries. Integration is achieved with PyDevice [6], which allows for communication between Python bindings for the HKL library and EPICS Process Variables.

The UB matrix computations use Busing & Levy [3] with two reflections. The hkl package supports simplex computation with more than two reflections using the GSL library. Computations are for right handed convention for all angles, and direct space orthogonal base. The hkl library uses quaternions to describe diffractometer geometries and 3D rotations. The library also allows for addition of custom diffractometer geometries.

The Phoebus [7] .bob files shown in Figs. 3-8 show details of the EPICS control for the vertical four-circle (E4CV) diffractometer.

* 1 This manuscript has been authored by UT-Battelle, LLC, under contract DE-AC05-00OR22725 with the US Department of Energy (DOE). The US government retains and the publisher, by accepting the article for publication, acknowledges that the US government retains a nonexclusive, paid-up, irrevocable, worldwide license to publish or reproduce the published form of this manuscript, or allow others to do so, for US government purposes. DOE will provide public access to these results of federally sponsored research in accordance with the DOE Public Access Plan (<https://www.energy.gov/doe-public-access-plan>). 2 A.B. research was supported in part by an appointment to the Oak Ridge National Laboratory GEM Fellowship Internship Program, sponsored by the U.S. Department of Energy and administered by the Oak Ridge Institute for Science and Education.

† gofronkj@ornl.gov

LLM INTEGRATION INTO EPICS

E. Adams, A. Sobhani, Oak Ridge National Laboratory, TN, USA

Abstract

The last two years have seen a drastic rise in the usage of Large Language Models (commonly known as LLMs) including ChatGPT, across multiple industries and applications. This has firmly established them as broadly applicable tools, proving their flexibility and power to understand and generate human-like text. In this paper, we explore the integration of an LLM into the EPICS system. The integration will focus on using the LLM for state-of-the-art image processing and spatial analysis of the images from the beamlines. We aim to increase the accuracy and efficiency of image interpretation, enabling more precise data analysis and decision-making within EPICS through the services offered by this LLM. This integration best showcases the various potentials of LLMs in science and industry, setting the stage for future advancements in automated control systems.

INTRODUCTION

EPICS is a software system that has grown out of scientific-industrial cooperation, aiming to satisfy the emerging needs for the development of distributed control systems. Generally, EPICS has been designed to cope with the complex control requirements of large experimental setups, such as particle accelerators, telescopes, and other highly sophisticated scientific instruments. Its robust architecture and scalability have made it the natural choice for such applications. Moreover, it provides flexibility and efficiency in managing the large sets of data produced in experiments.

The core building blocks of the EPICS control system are Input/Output Controllers (IOCs). IOCs interface directly with the hardware and address tasks like data acquisition, device control, and real-time processing. They are responsible for running the devices under their control, executing commands, and gathering data from sensors and instruments. This decentralized approach offers better scalability and fault tolerance: each IOC operates independently while communicating with other IOCs and higher-level applications through a well-defined protocol.

The recent breakthrough in large language models, such as ChatGPT, has enabled numerous possibilities for enhancing control systems. Large Language Models (LLMs) have tremendously succeeded in understanding human-like text and handling complex analysis tasks, and they can easily automate many different tasks. Clearly, integrating LLMs with the EPICS system would provide real benefits in image processing. These functionalities are key to understanding the huge volumes of visual data that come from today's beamlines, where exact and efficient analysis forms the foundation of the scientific approach.

This paper discusses the integration of an LLM into the EPICS framework, specifically for image processing of beamline images at the VULCAN beamline at SNS. Build-

ing on the advanced computational capabilities enabled by LLMs, we plan to accomplish various improvements to the full ease of use of the control system.

SYSTEM DESIGN

The system is entirely written in Python, forming a robust yet flexible core for integration into EPICS. It is implemented as a PCASpy [1] IOC, which allows for seamless integration with the existing EPICS infrastructure. The input images are obtained using PyEpics [2], processed through the LLM, and the output images are then hosted with PCASpy, making them accessible to other components of the control system.

This setup includes the implementation of a Control System Studio (CSS) page to facilitate user interaction with the software's Process Variables (PVs), providing an easy way of controlling and monitoring the system (Fig. 1).

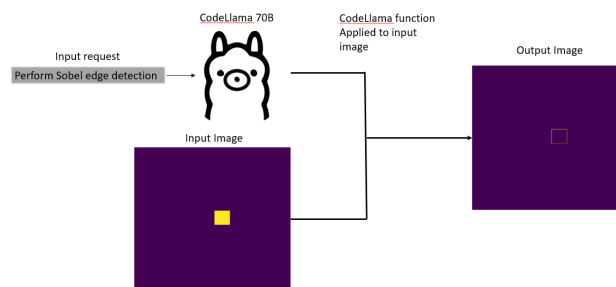


Figure 1: System Architecture Diagram showing the interaction between EPICS, CSS, and LLMs.

Upon entering the CSS page, users are presented with two major functions: image processing and spatial analysis. These options cover most of the possible analytical needs, ensuring comprehensive capabilities in data interpretation and manipulation.

The image processing function allows users to apply various transformations to input images. This includes operations such as thresholding, edge detection, image arithmetic, and Gaussian blurring. These transformations are executed by the LLM, and the processed images are then made available as PVs for other EPICS components to access.

The spatial analysis function extracts useful information directly from the input images. For example, it can determine the coordinates of centroids or other features of interest. This data is stored in PVs, enabling other parts of the EPICS system to leverage the insights provided by the LLM-powered analysis.

Additionally, the system offers an online/offline mode option. This allows users to choose how the system processes requests based on their operational context and available resources.

CALIBRATION OF THE ANALOG BEAM-SIGNAL HARDWARE FOR THE CREDITED ENGINEERED BEAM POWER LIMIT SYSTEM AT THE PROTON POWER UPGRADE PROJECT AT THE SPALLATION NEUTRON SOURCE*

C. E. Deibele†, M. Bobrek, P. Bong, K. Kasemir, K. Mahoney, C. Michaelides, Y. Tan, D. Willis
Oak Ridge National Laboratory, Oak Ridge, TN, USA
T. Allison, Osprey Digital Control Systems, Ocean City, MD, USA
C. Barbier, ITER, St. Paul-lez Durance, France

Abstract

A programmable signal processor-based credited safety control that calculates pulsed beam power based on beam kinetic energy and charge was designed as part of the Proton Power Upgrade (PPU) project at the Spallation Neutron Source (SNS). The system must reliably shut off the beam if the average power exceeds 2.145 MW averaging over 60 seconds. System calibration requires pedigree in measurements, calibration setup, and calculations. This paper discusses the calibration of the analog beam signal components up to and including the Analog Digital Convertors (ADCs) for implementation into the Safety Programmable Logic Controllers (PLCs) and Field Programmable Gate Arrays (FPGAs).

BLOCK DIAGRAM

The Beam Power Limit System (BPLS) block diagram in Fig. 1 shows redundancy in the beam current measurement with two chains, each beginning with a Fast Current Transformer (FCT) [1]. The FCTs are connected to long-haul cables that send the beam signal to an Analog Front End (AFE). Each AFE conditions the beam signal and distributes it to two different Analog to Digital Convertors (ADCs). One ADC is contained within the Digital Processing Unit (DPU), which is part of the credited Personnel Protection System (PPS), and the other is sent to the Protection System Interface (PSI) which is a Machine Protection System (MPS).

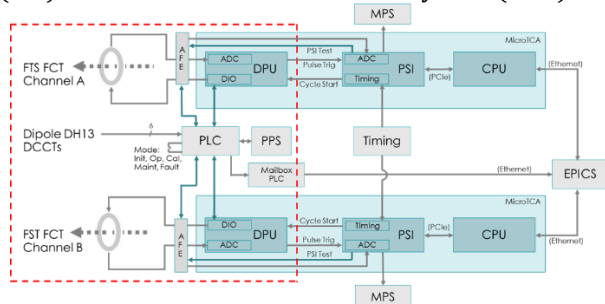


Figure 1: Block Diagram of BPLS.

* This material is based upon work supported by the U.S. Department of Energy, Office of Science and by UT-Battelle, LLC, under contract DE-AC05-00OR22725

† deibele@ornl.gov

The Safety Programmable Logic Controller (PLC) measures the beam energy through a calculation from six individual Direct Current-Current Transformers (DCCTs) [2] measurements. The DCCTs measure the dipole current used to steer the beam to the target station. The DCCTs are calibrated with the vendor.

One salient difference between the credited PPS system measurement and the non-credited MPS measurement is the use of timing. Timing is used in the MPS measurement to supply a gate to measure the beam signal, while the PPS system runs independently of timing.

The following equation [3] is used to calculate the beam charge trip limit (counts):

$$Limit = (1 + s_{11})T_{AFE}T_{cable}Z_{FCT} \frac{NP_{limit}}{k_{ADC}E \Delta t}$$

where s_{11} is the reflection looking into the ADC, T_{AFE} and T_{cable} are the transmission coefficients of the AFE and long haul cable respectively, Z_{FCT} is the transimpedance of the FCT, N is the number of seconds to average over, P_{limit} is the threshold power, k_{ADC} is the volts/count conversion of the ADC, E is the energy of the beam, and Δt is the sample rate of the ADC. This results in Limit being in units of counts, which is provided to the DPU and PSI where the beam charge algorithms and trip comparisons are implemented in Field Programmable Gate Arrays (FPGAs).

For the purpose of this paper, the FCT transimpedance, long-haul cable transmission, AFE transmission, and ADC conversion factor require calibration so that appropriate trip limits can be assigned as necessary. The quantities of the number of seconds N , the power limit P_{limit} , and sample rate Δt are fixed.

FCT CALIBRATION

The FCT transimpedance is nominally designed to be 0.25Ω at the factory. Parasitic elements in its manufacture add to deviations in the design value and therefore requires to be calibrated.

To perform this calibration [4, 5], a set of cone-shaped launches were designed to transition from a cable to the geometry consistent with the FCT. Figure 2 shows two launches that are assembled onto a long section of coax that is short circuited. The long coax is used to characterize each launch independently, so that they can be re-assembled with the FCT placed in-between.

DRIFT TUBE LINAC (DTL) STEERING MAGNETS REPLACEMENT DESIGN AT SNS*

Haitao Ren[†], Chad Helland, Sung-Woo Lee, John Moss, George Toby, Sang-Ho Kim
Oak Ridge National Laboratory, Oak Ridge, TN, USA

Abstract

The SNS Drift Tube Linac (DTL) operates at 402.5 MHz and consists of 6 RF tanks, DTL1 to DTL6, which accelerate the H- beam from 2.5 MeV to 87 MeV before entering the Coupled Cavity Linac (CCL). Each DTL tank assembly has 2 sets of horizontal and vertical electromagnetic steering magnets (24 in total) required for transverse beam steering. The steering magnets are water-cooled copper tubing coils designed to fit in the limited space inside the drift tube bodies. After 20 years of operation, some of the copper tubing steering coils have developed water leaks likely due to elevated water flow velocities. For the leaking coils, the cooling water has been removed and the steering coils have been disabled. The water leak points are inaccessible for repair so the entire drift tube will require replacement to be able to restore the electromagnet. To prepare for the possibility of drift tube replacement in the future design and fabrication of spare drift tubes is underway, including ones with steering magnets. To simplify the steering coil winding and avoid water leaking issues, a non-water-cooled steering magnet design has been developed. With the existing yoke, the new coils are designed to produce the same magnetic field with lower electrical power removing the need for water cooling. According to the CST [1] simulations, the maximum temperature of the coils is below 50°C with no water cooling. A prototype development is in progress and will be used for thermal testing and magnetic field verification. Details of the steering magnet design and calculation results are presented in this paper.

INTRODUCTION

The Spallation Neutron Source (SNS) Drift Tube Linac (DTL) tanks employ four distinct types of drift tubes to accelerate and control the H- beam [2]. Among these, the Permanent Magnet Quadrupole (PMQ) drift tubes utilize 16 permanent magnets to provide transverse beam focusing with a gradient of 3.70 kG/cm. Additionally, some drift tubes are empty, constructed of solid copper, while others incorporate Electromagnetic Dipoles (EMDs) for beam steering or Beam Position Monitoring (BPM). Each DTL tank assembly has 2 sets of the “x” and “y” EMD steering magnets. Two Drift tubes downstream of the EMD Drift tubes house a BPM, which will provide beam location feedback [3].

The current EMD magnets feature a carbon steel yoke and water-cooled copper coils encapsulated in epoxy,

* ORNL is managed by UT-Battelle, LLC, under contract DE-AC05-00OR22725 for the U.S. Department of Energy. This research was supported by the DOE Office of Science, Basic Energy Science, Scientific User Facilities.

[†] renh@ornl.gov

designed to fit within the drift tube bodies. This existing design involves complex and costly winding of copper tubing and necessitates additional water-cooling circuits. Unfortunately, this design has experienced issues with water leaks after 20 years of operations, with two incidents reported in the past a few years: one in DTL2 in 2020 and another in DTL3 in 2023. Although these leaks did not affect the cavity pressure because they are outside the vacuum, we need to remove the water cooling and disable these steering coils, and restore the beam operation by adjusting other beamline steering magnets. To address these issues, a new design featuring solid copper wire magnet without water cooling has been proposed.

EXISTING EMD COILS

As the first step of the new coils design, we developed a CST model of the existing EMD vertical steering magnet (see Fig. 1) to calculate the field distribution as a reference. Table 1 shows EMD magnet requirements of DTL3 as an example in this paper.

Table 1: Required Field Strength of EMD in DTL3

Steel Length	Gap	Current	Steering Field
2.88 cm	2.83 cm	110 A	560 Gs-cm

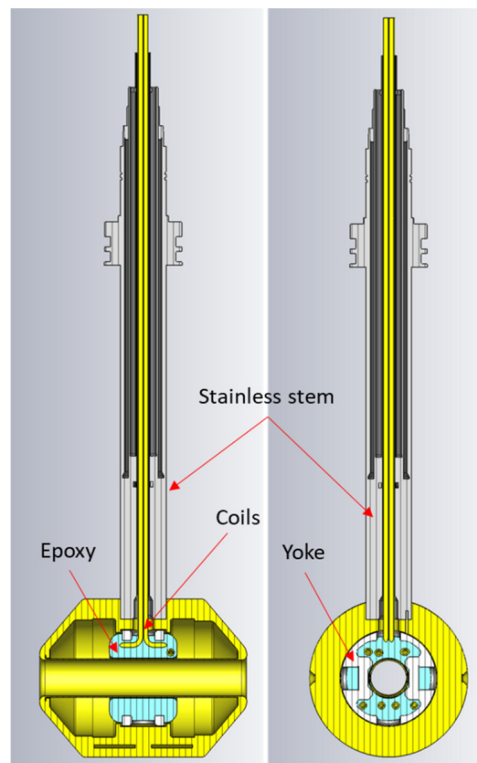


Figure 1: CST model of the DTL3 EMD magnet.

USING TimePix3 DETECTOR FOR NEUTRON AND X-RAY STUDIES*

Kazimierz J. Gofron[†]

Spallation Neutron Source and High Flux Isotope Reactor,
Oak Ridge National Laboratory, Oak Ridge, TN, USA

Abstract

The 65k pixel TimePix3 chip with ToA of 1.5625 [ns] nominal time resolution allows for timing and imaging studies using X-ray, neutron, and electron spectroscopies. The EPICS ADTimePix3 areaDetector driver enables detector control and integration into a neutron beamline acquisition system. This presentation will discuss the recent development of the detector's integration into neutron and X-ray beamlines and selected results.

INTRODUCTION

Here we discuss the integration of the TimePix3 detectors purchased from Amsterdam Scientific Instruments (ASI) [1] into the EPICS [2] control system. The TimePix3 detector was integrated into EPICS [2] using the areaDetector [3] framework by developing the ADTimePix3 [4] driver. Using ADTimePix3, data collection with neutron spectroscopy was reported by Funama *et al.* [5].

DETECTOR

The thermal neutron detection process uses detection of neutron fission energy in reaction with ${}^6\text{Li}$ or ${}^{10}\text{B}$ embedded in a Microchannel Plate (MCP) [4, 5]. The two stacked MCP typically have bias voltage levels of -2500 [V], -1300 [V], and -300 [V] for the front, middle, and back MCP double stack. The detector is kept at 0 [V]. The detection efficiency is dependent on neutron energy. The quad detector has a gap between four chips, for which influence on detection is not yet currently clear. The preview image of neutron clusters is shown in Fig. 1 using the CSS Phoebus client [6].

TimePix3 requires calibration files typically provided by the vendor (ASI). The equalization files consist of .bpc (Binary Pixel Configuration) and .dacs (DACs settings) files. Both equalization files are loaded during the IOC boot process. The calibration files can also be loaded from the dedicated .bob screen in the "Load Files" menu. The detector calibration is typically performed with vendor software, such as SoPhy or Accos. The quad detector calibration shown in Fig. 2 was done with SoPhy version 1.6.5.

* This manuscript has been authored by UT-Battelle, LLC, under contract DE-AC05-00OR22725 with the US Department of Energy (DOE). The US government retains and the publisher, by accepting the article for publication, acknowledges that the US government retains a nonexclusive, paid-up, irrevocable, worldwide license to publish or reproduce the published form of this manuscript, or allow others to do so, for US government purposes. DOE will provide public access to these results of federally sponsored research in accordance with the DOE Public Access Plan (<https://www.energy.gov/doe-public-access-plan>).

[†] gofronkj@ornl.gov

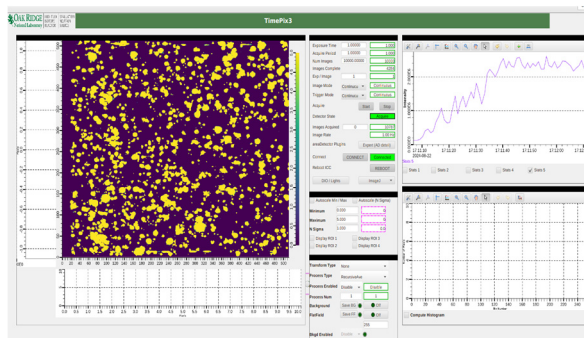


Figure 1: The ADTimePix3 Phoebus [6] control window with an image of neutron clusters.

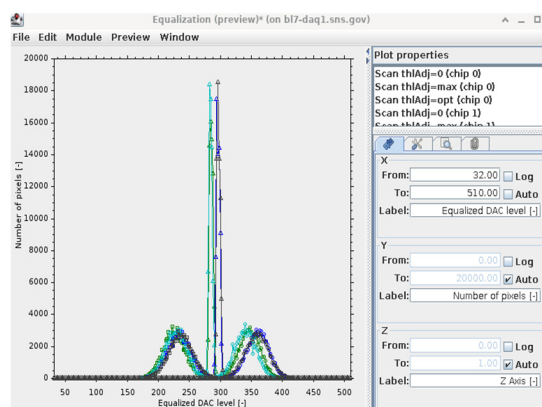


Figure 2: A four-chip TimePix3 detector equalization of DAC level using SoPhy.

The ASI vendor provides two programs for data acquisition: SoPhy (older) and Accos (newer). Either one of these programs can generate equalization files (Figs. 2 and 3).

ADTimePix3 allows integration of the detector into the EPICS beamline control environment. The ASI also provides SERVAL server and detector Emulator programs. The SERVAL connects to a physical TimePix3 detector over 10Gb ethernet, or to a detector Emulator program. The Emulator was very useful during the initial ADTimePix3 driver development.



Figure 3: Loading .bpc and .dacs detector calibration from CSS screen of ADTimePix3 driver.

COMPLETION OF THE PROTON POWER UPGRADE PROJECT AT THE SPALLATION NEUTRON SOURCE*

M. Champion[†], M. Connell, N. Evans, J. Galambos, M. Howell, G. Johns, S. Kim, J. Moss,
G. Stephens, K. White, Oak Ridge National Laboratory, Oak Ridge, USA

Abstract

The Proton Power Upgrade (PPU) project at the Spallation Neutron Source (SNS) at Oak Ridge National Laboratory (ORNL) has completed the installation and testing of all project scope required to meet threshold key performance parameters (KPPs), supported beam commissioning in June 2024, and transitioned to operations in July 2024. Increasing the beam energy from 1.0 to 1.3 GeV required the installation of seven additional cryomodules in the SNS Linac along with supporting RF systems. The accumulator ring injection and extraction regions were upgraded, a 2 MW mercury target was developed, and ancillary target systems were upgraded to support high-flow gas injection, mercury off-gas treatment, and ortho-para fraction control in the cryogenic moderator hydrogen loop. Three of four threshold KPPs have been demonstrated, and the project is planning for its final review in early 2025. Beam power on the first target station (FTS) will be ramped up to 2 MW over the next two years. Completion of the PPU project supports increased scientific capability at the FTS and will support operation of the second target station (STS) upon its completion. Lessons learned will be documented and a project closeout report will be written prior to the final closeout of the project.

INTRODUCTION

The PPU project has been underway for more than six years since establishing the conceptual design and cost range (Critical Decision-1, CD-1) as depicted in Fig. 1. The upgrade increases the accelerator beam power capability from 1.4 to 2.8 MW, provides a 2-MW-capable mercury target for the first target station, and constructs a tunnel extension for future connection to the second target station. The detailed technical scope has been described previously [1], and the project status will be presented in an invited talk at this conference [2]. The long installation outage began in August 2023 and concluded in April 2024. All remaining PPU technical components required for threshold

* ORNL is managed by UT-Battelle, LLC, under contract DE-AC05-00OR22725 for the U.S. Department of Energy. This research was supported by the DOE Office of Science, Basic Energy Science, Scientific User Facilities.

Notice: This manuscript has been authored by UT-Battelle, LLC, under contract DE-AC05-00OR22725 with the US Department of Energy (DOE). The US government retains and the publisher, by accepting the article for publication, acknowledges that the US government retains a nonexclusive, paid-up, irrevocable, worldwide license to publish or reproduce the published form of this manuscript, or allow others to do so, for US government purposes. DOE will provide public access to these results of federally sponsored research in accordance with the DOE Public Access Plan (<http://energy.gov/downloads/doe-public-access-plan>).

[†] championms@ornl.gov

KPP demonstration were installed and tested during this outage. An external accelerator readiness review was conducted in May 2024, and authorization for beam commissioning and routine operations was granted in early June. Beam commissioning commenced June 7th and was completed in less than one month. Neutron production for the user program resumed July 11th as planned at 1.3 GeV and 1.7 MW. Three project threshold KPPs related to beam parameters have been achieved. Demonstration of the fourth KPP, for target lifetime, is progressing and expected to be achieved in October 2024.

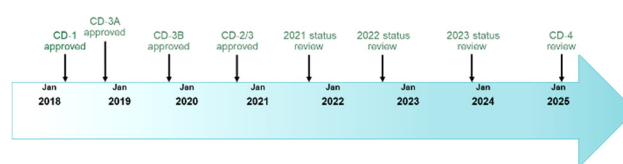


Figure 1: The PPU project execution spans seven years from CD-1 approval to CD-4 project completion review.

BEAM COMMISSIONING

PPU beam commissioning commenced June 7th, 2024, and proceeded quickly as shown in the timeline (Fig. 2). First up was commissioning of the Linac with seven new PPU cryomodules. Tune-up of the SNS Linac is a well understood process, and 1.33 GeV low-duty-factor beam was delivered to the Linac injection dump within a few hours. Accumulator ring commissioning began June 8th at 1.05 GeV for comparison with accelerator performance during the final run prior to the long outage. After successfully delivering low-duty-factor 1.05 GeV beam to the ring extraction dump, the energy was increased to 1.3 GeV, and full-energy beam was delivered to the extraction dump on June 11th.

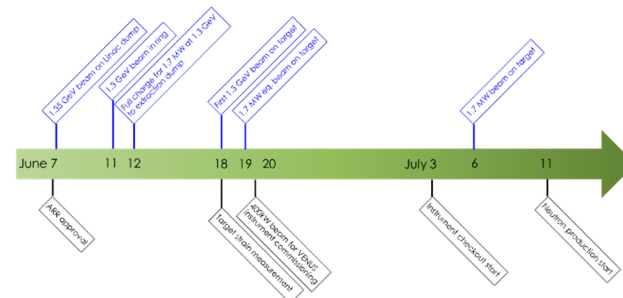


Figure 2: PPU beam commissioning was accomplished in approximately one month from start to neutron production.

1.7-MW-equivalent charge (22uC) at 1.3 GeV was circulated in the ring and sent to the extraction dump on June 12th at low duty factor. Tuning for low beam loss throughout the accelerator proceeded for several days, and

RF AND MECHANICAL DESIGN OF A 915 MHz SRF CAVITY FOR CONDUCTION-COOLED CRYOMODULES *

G. Ciovati^{†1}, A. Castilla-Loeza, G. Cheng, K. Harding, J. Henry, J. Vennekate
Jefferson Lab, Newport News, VA, USA

J. Lewis, Mechanical & Aerospace Engineering Department, Old Dominion University,
Norfolk, VA, USA

J. Rathke, TechSource, Los Alamos, NM, USA

T. Schultheiss, TJS Technologies, Commack, NY, USA

¹also at Center for Accelerator Science, Physics Department, Old Dominion University,
Norfolk, VA, USA

Abstract

Conduction-cooled SRF niobium cavities are being developed for use in compact, continuous-wave electron linear accelerators for a variety of industrial applications. A 915 MHz two-cell cavity has been designed to achieve an energy gain of 3.5 MeV. The design of the cell shape aims at minimizing the peak surface magnetic field. Field flatness is achieved by adjusting the length of the outer end half-cells. The higher-order mode analysis shows that absorbers are not required for a moderate beam current of 5 mA. One of the beam tubes has two side-ports for insertion of coaxial fundamental power couplers. The mechanical design and analysis were done to maintain a stress near or less than 15.5 MPa for all anticipated loading conditions. This is half the measured yield strength and is to provide relief from creep when the cavity is evacuated and stored with outside atmospheric pressure.

INTRODUCTION

Superconducting radio-frequency (SRF) cavities are commonly used in modern particle accelerators to increase the energy of a charged-particle beam. R&D projects in the last few years have demonstrated the possibility to operate SRF cavities cooled by commercial cryocoolers at an accelerating gradient of up to ~ 12 MV/m [1, 2].

These results may allow envisioning compact, high-power, continuous-wave electron accelerators with energy of up to 10 MeV for industrial irradiation applications, such as wastewater treatment, medical device sterilization and phytosanitary treatment [3, 4]. The beam power of these possible novel accelerators has to be greater than hundreds of kilowatt, ideally up to 1 MW, to reduce the unit cost of treatment. Given the high beam power requirements, the RF source of the accelerator has to have a high efficiency to reduce the operating cost of the accelerator. Commercially available 915 MHz industrial magnetrons have an electrical efficiency of $\sim 90\%$ with an output power of ~ 100 kW. An ongoing R&D project at Jefferson Lab and General Atomics is tar-

geting to demonstration of efficient power combining from multiple magnetrons and developing the control system to drive an SRF cavity [5].

In this contribution we present the RF design and the mechanical analysis of a 915 MHz two-cell cavity as part of a larger R&D project aiming at developing a conduction-cooled cryomodule, which includes cryocoolers, a coaxial fundamental power coupler (FPC) and warm-to-cold beam-line transitions. The number of cells was determined by the available cryocoolers and space within a vacuum vessel developed for a preceding project. Details about the FPC design, done by RadiaBeam, can be found in Ref. [6].

RF DESIGN

The cavity was designed aiming to provide an energy gain of at least 3.5 MeV to a relativistic electron beam. SUPERFISH [7] was used for the electromagnetic design of the cell shape. The shape design aimed at reducing the ratio of the peak surface magnetic field, B_p , to the accelerating gradient, E_{acc} , while maintaining a wall angle, α , that facilitates surface chemical and cleaning processes. The iris radius, R_{iris} was chosen to be close to the largest possible value that could fit within the beamline flange used in 1.3 GHz TESLA-type cavities, allowing the use of testing hardware already available. The cell shape design includes a short straight segment, L_{eq} , that is used as a parameter to tune the frequency of the end half-cell. This allows using a single die for pressing both center and end half-cells. Furthermore, the presence of a straight section at the equator facilitates electron-beam welding of a Nb ring for conduction cooling. The equator radius, R_{eq} , was used as a parameter to tune frequency of the center half-cell. Table 1 lists the geometric parameters of the center half-cell. The equator weld-prep is included in the cell-shape design and an arc with 2 mm radius is used to connect the straight section at the equator to the equator ellipse's arc. The end half-cell is identical to the center half-cell other than $L_{eq} = 3.1$ mm.

The list of electromagnetic parameters of the 2-cell cavity is given in Table 2. The highest B_p measured on a conduction-cooled Nb₃Sn-coated cavity was 50 mT, which would correspond to $E_{acc} = 13.6$ MV/m and an energy gain of 4.3 MeV for this cavity shape.

* Work supported by U.S. DOE Office of Accelerator R&D and Production through Jefferson Science Associates, LLC under U.S. DOE Contract No. DE-AC05-06OR23177

[†] gciovati@jlab.org

EXTENSION OF REFERENCE TRACKING METHOD TO REDUCE RF AMPLITUDE DRIFT IN PARTICLE ACCELERATORS

Jinyul Hu†, Chang-Ki Min, Hoon Heo, Yong Jung Park, PAL, POSTECH, South Korea

Abstract

RF long-term stability (drift) is as important as RF short-term stability for the stable operation of particle accelerators including PAL-XFEL. Increasing the performance of LLRF itself becomes an important factor in maintaining the long and short-term stability of the RF field. The reference tracking method applied to LLRF is effectively used as a method of reducing the drift of the RF phase. However, this drift improvement method was not applied to the RF amplitude. This time, the method of reference tracking was newly expanded to improve the RF amplitude drift. As a result of applying this new function to PAL-XFEL LLRF, it is showing some effect in improving the RF amplitude drift. We would like to share the progress so far.

INTRODUCTION

In the operation of an accelerator, not only short-term stability but also long-term stability is important. In particular, in the case of sensitive accelerators such as XFELs (X-ray Free Electron Lasers), the influence of short-term and long-term stability is critical. An illustrative Fig. 1 shows a typical XFEL intensity. The left side of the dotted line is a case where long-term stability is well maintained, and the right side is a case where long-term stability is poor and normal user service cannot be provided. Through this, it can be seen that long-term stability must also be well maintained. In order to do so, it is very important to improve the long-term stability of the LLRF (Low Level RF controller) itself. We will present the improvement of the long-term stability of the LLRF by applying reference tracking to the amplitude as well.

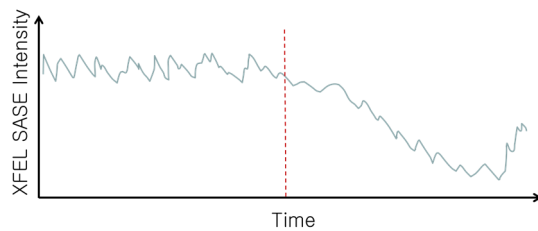


Figure 1: An illustrative sketch of typical XFEL intensity graph.

REFERENCE TRACKING METHOD

The reference tracking method is occasionally used to improve the long-term stability of LLRF systems. There is also the method of reference injection applied to European XFEL [1]. Although the method is considered more accurate, it is needed to add hardware configurations, while reference tracking has the advantage of simple implementation with little additional hardware. Reference tracking is mainly used to improve the stability of the phase.

† hjy@postech.ac.kr

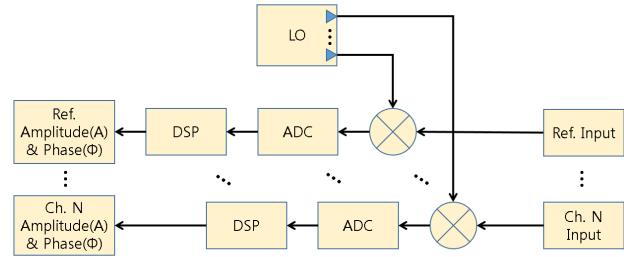


Figure 2: A typical structure of a LLRF receiver.

Figure 2 is a diagram of a typical LLRF receiver. The input RF signals are downconverted to IF signals, then the analogue signals are converted to digital signals, and the phases and amplitudes of the RF are calculated. The reference tracking method of the phase is a method of compensating for the phase drift of other channels by using the phase variation of the reference, and can be implemented as shown in Eq. 1.

$$Ch. N \Phi (Ref. track) = Ch. N \Phi - \Delta (Ref. \Phi) \quad (1)$$

where $Ch. N \Phi (Ref. track)$ is the compensated phase of nth channel, $Ch. N \Phi$ is a phase before compensation, and $\Delta (Ref. \Phi)$ is the change in the reference phase.

Similarly, the reference tracking of the amplitude can be written as in Eq. 2. This method has been applied to the LLRF of PAL-XFEL.

$$Ch. N A (Ref. track) = Ch. N A - \Delta (Ref. A) \quad (2)$$

APPLICATION TO PAL-XFEL

The implemented amplitude reference tracking was applied to PAL-XFEL during the winter maintenance in 2023. The layout of PAL-XFEL is shown in Fig. 3. PAL-XFEL is based on a copper linac which accelerates electron bunches to 10 GeV at a repetition rate of 60 Hz. It generates ultra-strong and short X-ray pulses in each of hard X-ray and soft X-ray beamline for experiments. The linear accelerator (linac) of PAL-XFEL consists of a total of 51 RF stations, which are divided into five sections, named INJ, L1, L2, L3, and L4. The amplitude reference tracking (ART) has been applied to all 51 LLRFs and has been used to date. Some RF stations are selected and the data comparing before and after the application of the amplitude reference tracking are shown in Figs. 4-8.

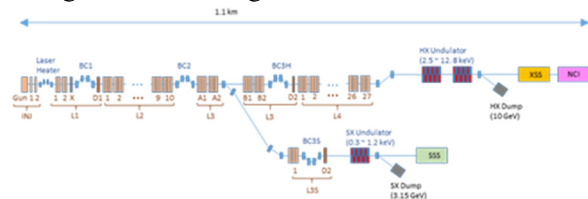


Figure 3: PAL-XFEL layout.

HIGH-RESPONSE PLC-BASED MACHINE PROTECTION SYSTEM DEVELOPMENT AND PERFORMANCE FOR SRILAC

A. Uchiyama[†], M. Komiyama, M. Fujimaki, T. Nishi, K. Kumagai
RIKEN Nishina Center, Wako, Japan

H. Yamauchi, K. Kaneko, SHI Accelerator Service, Ltd., Tokyo, Japan

Abstract

The RIKEN linear accelerator (RILAC), which is among the injectors for cyclotrons at the radioactive isotope beam factory (RIBF), was upgraded by installing a superconducting RILAC (SRILAC) to search for superheavy elements with element numbers 119 and above. Prior to conducting the SRILAC upgrade, the machine protection system in RILAC was constructed using simple relay circuits. However, most of the accelerators at RIBF other than RILAC have been equipped with machine protection systems using Mitsubishi MELSEC-Q programmable logic controllers (PLCs) since 2006. They follow a mechanism that was triggered an anomalous signal to drive the beam chopper to stop the beam, and are called beam interlock systems (BIS). Machine protection was required in the SRILAC project to prevent vacuum deterioration of the superconducting cavity owing to changes in the beam envelope. Thus, we developed an FA-M3 PLC-based system to realize a BIS with high response performance at a lower cost than conventional systems. This system was characterized by implementing both relatively slow response and I/O requiring high response performance. For example, in the case triggered by an anomalous signal from the electromagnet power supply, the simulation of the beam envelope indicated that the response performance was relatively slow, with a few milliseconds being sufficient.

INTRODUCTION

One of the injectors in the RIKEN radioactive isotope beam factory (RIBF) is the RIKEN linear accelerator (RILAC) [1]. RILAC serves as an injector for the RIBF and provides beams for standalone experimental courses. Experiments are underway to search for superheavy elements with atomic numbers greater than 119, facilitated by an upgraded project. The primary upgrades to the RILAC include two significant improvements. The first is the installation of a new 28 GHz superconducting electron cyclotron resonance ion source (ECRIS) upstream, which enhances the beam intensity [2]. The second upgrade involves the implementation of a superconducting linear accelerator (SRILAC) downstream of the existing RILAC cavities to boost the beam energy [3]. Because of the increased beam intensity and energy from the upgrade, minor errors in the accelerator components could easily cause significant problems for the experimental equipment and the RIBF beamline downstream of SRILAC.

In addition, issues with superconducting cavities, such as quenching owing to vacuum deterioration caused by beam loss, must be avoided. Therefore, the machine

[†] a-uchi@riken.jp

protection system (MPS), a mechanism for protecting hardware from the beam, must be more advanced. In response to these requirements, an MPS was developed to operate SRILAC.

PREVIOUS SYSTEM

Before the SRILAC project, the RILAC interlock system was implemented using hardware composed of mechanical relays. Consequently, the response performance of the previous system was not high, typically on the order of tens of milliseconds. In contrast, at RIBF facilities other than the RILAC, an interlock system based on the MELSEC Q-series programmable logic controller (PLC) is employed as the MPS [4]. This system prevents hardware failures caused by deviations in the beam trajectory from its normal orbit by driving a beam chopper located just downstream of the ECRIS in response to abnormal signals from components, such as power supplies, RF systems, and vacuum systems. In addition to the beam chopper, the system outputs signals to insert the Faraday cups depending on the type of input signal. This system is referred to as the beam interlock system (BIS), and its response time is of the order of 10 ms.

SYSTEM REQUIREMENT

The following system requirements have been established to develop the MPS for the SRILAC project. The system is designed to minimize the complexity of both hardware and software. In addition, human and machine protection systems are clearly separated, with the core logic of the system following the RIBF BIS. The selected hardware prioritizes long-term maintainability. Furthermore, all stages of system development and operation are handled by the team to facilitate system upgrades and rapid troubleshooting. The development of the upper-level system is based on the experimental physics and industrial control system (EPICS) channel access (CA) protocol, which is the standard control protocol at RIBF. For example, with abnormal RF signals, the system achieves a performance that exceeds the typical response of the capabilities of conventional PLC-based system such as RIBF BIS and drives the beam chopper.

SRILAC BIS SPECIFICATIONS

Controller

When selecting hardware for the SRILAC BIS, the goal was to develop and operate the system entirely within a team, thereby ensuring long-term maintainability. Consequently, the decision was made to construct the system

PERFORMANCE OF THE SUPER-CONDUCTING RIKEN HEAVY-ION LINAC AT THE RIKEN RADIOACTIVE ISOTOPE BEAM FACTORY

N. Sakamoto*, O. Kamigaito, K. Ozeki, K. Suda, K. Yamada, T. Nagatomo, T. Nishi, Y. Higurashi, A. Uchiyama, RIKEN Nishina Center, Saitama, Japan

Abstract

The RIKEN superconducting heavy-ion linear accelerator (SRILAC) has been steadily supplying beams for super-heavy element synthesis experiments since its commission in January 2020 by addressing relevant issues. The decrease in the available acceleration voltage due to the increase in X-rays i.e. field emission (FE) from superconducting (SC) cavities has been a major issue. However, this issue has been mitigated via high-RF power processing (HPP). This presentation reports on the current performance of SRILAC and its prospects.

INTRODUCTION

The mission of the RIKEN Radioactive Isotope Beam Factory (RIBF [1]) in Japan is to improve our understanding of the element synthesis mechanism via experiments using intense heavy-ion beams.

In 2016, the RIKEN Nishina Center (RNC) started a comprehensive super-heavy element (SHE) research program. The main objective was to expand the periodic table of elements by synthesizing new super-heavy elements. After the discovery of oganesson (Og, $Z = 118$), the aim of the SHE project was to discover elements beyond $Z = 118$. To synthesize the $Z = 119$ element, the RNC adopted a combination of ^{51}V as the beam and ^{248}Cm as the target [2]. For this experiment, a beam energy of $^{51}\text{V} = 6$ MeV/u with an intensity of 2.5 μA is required. Thus, the primary focus of this project was to upgrade the accelerator by introducing a SC linear accelerator to increase the final beam energy from 5.5 to 6.5 MeV/u and a SC electron-cyclotron-resonance ion source (SC-ECRIS) to multiply its beam intensity by a factor of five (see Fig. 1).

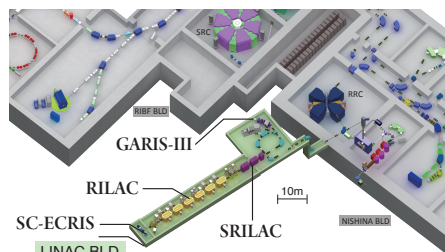


Figure 1: Birds-eye view of the RILAC.

In 2020, beam commissioning for SRILAC was successfully conducted [3], with user beam service subsequently starting [4]. Ar and V beams are provided for the experiment with an energy ranging between 4.2 and 6.3 MeV/u. Owing

* nsakamot@ribf.riken.jp

to the newly constructed SC-ECRIS [5] and the improvement in the RILAC transmission efficiency [6], the maximum beam intensity of 5.2 μA (duty 100%) exceeded the project's primary target intensity. In this report, an overview and operation status of SRILAC and its relevant issues are presented. Additionally, FE and vacuum leakage from input couplers are described.

SRILAC OVERVIEW

The SRILAC layout is illustrated in Fig. 2. SRILAC comprises three cryomodules (CM1, CM2, and CM3) and a medium-energy beam-transport line (V00, V10, V20, and V30) that connects the CMs, RILAC DTLs, and a high-energy beam-transport line. As shown in Fig. 2, CM1 and CM2 contain four SC-QWRs, whereas CM3 contains only two SC-QWRs. Each SC-QWRs are labeled SC01–SC10 from upstream to downstream. The SC-QWR specifications are listed in Table 1. The operating temperature was 4.5 K. The SC-QWRs were fabricated from highly purified Nb sheets with an RRR of 250. The inner surfaces were treated using a standard processing method as follows: (i) bulk etching via buffered chemical polishing (BCP); (ii) annealing (750 °C, 3 h) in a vacuum furnace; (iii) light etching via BCP; (iv) high-pressure rinsing (HPR) with ultrapure water; and (v) baking (120 °C, 48 h). All SC-QWRs achieved the target $Q_0 \times 10^9$ with $E_{\text{acc}} = 6.8$ MV/m in the acceptance tests [7]. The operating frequency of the SC-QWRs was 73 MHz. The amplitude and phase of the accelerating field could be set independently for each SC-QWR. The independent RF system for each SC-QWR enables the seamless tuning of the energy of the accelerated beams. The gap length was optimized for $\beta = 0.078$.

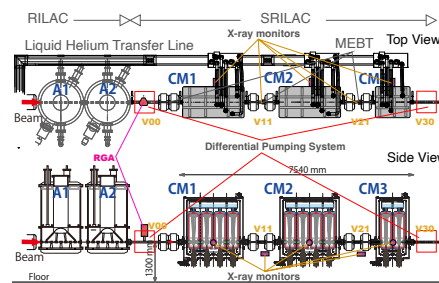


Figure 2: SRILAC layout.

One of the most crucial issues in beam-transport-line design is preventing SC cavity contamination by dust transported from the room-temperature (RT) section through gas flow owing to the vacuum pressure gradient. While the vacuum pressure level of the SC part decreases to as low as

STUDIES ON HIGH REPETITION RATE OPERATION OF SACLA WITH X-BAND NORMAL CONDUCTING ACCELERATOR

T. Inagaki[†], K. Yasutome, H. Maesaka, T. Hara, H. Tanaka, RIKEN SPring-8 Center, Sayo, Japan
E. Iwai, T. Ohshima, C. Kondo, T. Tomai, JASRI, Sayo, Japan

Abstract

The next upgrade plan for the XFEL facility SACLA is to increase the repetition rate of the accelerator, which is currently 60 Hz, by one order of magnitude to 1 kHz maintaining the performance of the current SASE and electricity usage. To improve the power efficiency, we choose X-band as the radio frequency (RF) of the main accelerator instead of current C-band. A basic design and optimization of the accelerator are undergoing. As a testbed, we plan to introduce an X-band transverse deflector cavity to measure the temporal distribution of the electron beam downstream of the undulator. The development of equipment such as pulse compressors, dummy loads, low-level RF control, which are common to the systems for high repetition, has begun.

INTRODUCTION

The RIKEN SPring-8 Center and JASRI operate SPring-8, the 3rd generation synchrotron radiation facility, and SACLA, an X-ray free electron laser facility, providing synchrotron radiation for many scientific experiments. The upgrade project “SPring-8-II” is underway to replace the entire storage ring and obtain X-ray radiation with 100 times higher brilliance by 2029 [1]. SACLA has already been in operation for 13 years since 2011 [2]. We consider an upgrade in the 2030s, along with the replacement of aging equipment [3]. In this upgrade program SACLA-II, the increase in light intensity, the expansion of the wavelength range, and the increase in pulse repetition rate are being considered, which are strongly requested by users. To increase the light intensity, improvements to the electron gun and bunch compression section are being considered. To expand the wavelength range and increase the pulse repetition rate, part of the C-band (5.7 GHz) main accelerator is being replaced by an X-band (11.4 GHz) accelerator.

For higher pulse repetition rates, superconducting RF cavities are also being used in XFEL [4-6]. However, the use of superconducting cavities requires a large amount of liquid helium and huge cryo-plants to cool them, as well as investments almost equivalent to building a new facility, such as extending the accelerator length and strengthening radiation shielding. On the other hand, in many experiments using XFEL, MHz pulse repetition rates are not necessary, and repetition rates of 1 kHz are often sufficient.

We therefore aim to increase the power efficiency of the normal conducting accelerator by one order of magnitude and increase the pulse repetition rate to 600 Hz - 1 kHz, more than ten times the current 60 Hz, without increasing power usage. This will enable high-repetition XFEL with the current building, power, and cooling facilities. The acceleration energy can be increased by increasing the width

of the RF pulses, which will enable the wavelength range to be extended to the higher energy side.

The SACLA-II project is studying each item with the aim of building a prototype in 2029. It also plans to introduce an X-band deflector cavity downstream of the BL3 undulator around 2027, combined with operational tests of X-band RF. These are currently being designed and prototype tested [7].

SYSTEM DESIGN

Accelerator Configuration

The layout of SACLA is shown in Fig. 1. In the compact 400 m long accelerator section, a 1 ns, 1 A low-emittance electron beam generated by a CeB₆ thermal cathode electron gun [8] is compressed to 10 fs and 10 kA in a buncher cavity [9] and three bunch compressors (BCs), and accelerated up to 8 GeV in a high gradient C-band accelerator [10]. The electron beam, generated and accelerated at a 60 Hz repetition rate, is distributed by high-precision kicker magnets [11] to two XFEL beamlines, BL2 and BL3, and the injection into the SPring-8 storage ring [12]. In BL1, the accelerator that was originally used as the SCSS prototype accelerator [13] has been relocated and its energy increased to 800 MeV and used for user experiments as an EUV-FEL facility [14].

In the upgrade program SACLA-II, part of the downstream C-band accelerator will be replaced by an X-band accelerator. As described in the next chapter, the X-band accelerator can provide an average acceleration gradient of 42 MV/m even at a 600 Hz repetition rate, thus providing a margin of acceleration energy. On the other hand, the remaining C-band accelerators and the S-band accelerators are planned to remove the pulse compressor and operate at short pulse RF to increase the repetition rate. As this change lowers the acceleration gradient to about half of the current level, we plan to compensate for the energy with the high-gradient X-band accelerator and obtain more than 8 GeV energy at the exit of the accelerator. If the repetition rate of the X-band accelerator is reduced to 200 Hz and the RF pulse width is increased, the acceleration gradient can be increased to 48 MV/m. The energy of the electron beam could be increased to 10 GeV to produce shorter wavelength XFELs.

As SACLA is currently also used as an injector of SPring-8, it is difficult to make a large-scale replacement work with a long shutdown period. Therefore, the X-band accelerator will consist of a unit with a total length of 4 m, same as the current C-band accelerator, and will be replaced by several units every shutdown period. In this way, the replacement can be carried out while the operation of SPring-8 and SACLA continues.

[†] inagaki@spring8.or.jp

ISIS INJECTOR LINAC EMITTANCE MEASUREMENT AND PHASE-SPACE TOMOGRAPHY

A. P. Letchford[†], S. Ahmadiannamin, R. Williamson, B. Kyle

ISIS Neutron and Moun Source, Rutherford Appleton Laboratory, Harwell, Didcot, UK

Abstract

Accurate beam emittance measurement is vital for optimizing high-intensity proton accelerators. Traditional methods often only approximate the phase space ellipse linearly, limiting their effectiveness. Comprehensive analysis of phase space distribution, including nonlinearities, is essential for better characterization. This study focuses on the ISIS neutron spallation source, which is being upgraded to increase beam intensity to 300 microamps while minimizing losses. We present tomographic reconstruction and quadrupole scan results for emittance measurement at the end of the ISIS injector, showing strong alignment between measurements and simulations.

INTRODUCTION

The ISIS neutron spallation source, a pulsed high-power proton accelerator, generates high-intensity neutron radiation for various applications [1]. It includes a 70 MeV injector linac and an 800 MeV rapid cycling synchrotron (RCS) [2]. A key goal for ISIS, like other high-intensity hadron accelerators, is to minimize beam loss and radiation activation while increasing beam power and stability. Achieving this requires advanced diagnostics, precise beam measurement techniques, and an accurate beam dynamics model to optimize performance.

The High Energy Drift Section (HEDS), positioned after the injector linac, hosts diagnostics and magnets essential for beam characterization before RCS injection [3]. Accurate emittance and Twiss parameter characterization at the injector linac's end is crucial, with the HEDS setup offering robust capabilities for these measurements through both traditional and innovative methods.

Widely used measurement techniques include three-screen and quadrupole scans, with tomographic phase space reconstruction becoming increasingly valuable for analysing nonlinearities in beam phase space [4]. Algorithms like Filtered Back Projection (FBP), Algebraic Reconstruction Technique (ART), and Maximum Entropy (MENT) facilitate phase space reconstruction from one-dimensional beam profiles [5]. The MENT algorithm stands out for its efficiency with fewer beam profile measurements, addressing challenges related to beam loss and magnet strength. In Computational Tomography (CT), one-dimensional beam profiles are converted into two-dimensional phase space distributions [6].

This paper details the experimental setup at ISIS, including the quadrupole scan, three-screen monitor, and

MENT-based CT method, and presents preliminary emittance measurements and phase space reconstruction results at the injector's output within the first diagnostics setup of the HEDS section.

EXPERIMENTAL SETUP

The ISIS linac, operating at 202.5 MHz, includes a Penning ion source delivering a 45-mA output, followed by a Low Energy Beam Transport (LEBT) section with 75% transmission efficiency, achieved through three solenoids for matching to the RFQ. The RFQ raises the beam energy to 0.665 MeV with over 97% transmission. The beam then enters a drift section, lacking matching before being transferred directly to the Drift Tube Linac (DTL), where four tanks accelerate it to 70.5 MeV. Due to the absence of an MEBT (under development for machine upgrade), significant beam loss occurs in the first DTL tank, resulting in 75% and 100% transmission in the first and last three DTL tanks, respectively. However, the beam's low energy prevents activation in this section. Approximately 22.5 mA of the beam is transmitted through the DTL tanks and injected into the RCS synchrotron. Fig. 1. shows the schematic of the injector and HEDS section.

Our primary measurement section is in the initial part of the HEDS injector, utilizing quadrupole magnets and wire scanners (Fig. 2.). A beam dump is positioned between the IPM3 and IPM4 wire scanners to minimize beam loss during measurements, with the first three profile monitors in use during machine physics experiments. Quadrupoles QF1, QF2, QD3, and QF4 (highlighted in green) operated at currents of 2.1, 6.25, 112.5, and 6.35 Amperes, respectively. Wire scanners 1, 3, and 4 were used for the three-screen method, while wire scanner 3 (IPM3) was employed for quadrupole scans and tomographic phase space reconstruction. The parameters for the beamline and its configuration are provided in Table 1.

RESULTS

The ISIS injector was modelled using Parmila and Trace-3D beam dynamics codes, with simulation results shown in Fig. 3 and Fig. 4. Horizontal and vertical beam profiles, measured with the IPM3 wire scanner under various quadrupole settings and rotation angles, are presented in Fig. 5. Applying maximum entropy techniques, commonly used in image processing, the transverse phase space distributions at the injector linac's output were calculated and shown in Fig. 6. We used three screen monitors and quadrupole scan procedures to benchmark these calculations against topographically reconstructed phase spaces. Beam phase space ellipse

[†] alan.letchford@stfc.ac.uk

THE UK XFEL CONCEPTUAL DESIGN AND OPTIONS ANALYSIS PROJECT

D. J. Dunning^{*1,2}, P. Aden¹, D. Angal-Kalinin^{1,2}, J. A. Clarke^{1,2}, J. L. Collier³, B. D. Fell¹, J. S. Green³, J. P. Marangos⁴, S. L. Mathisen^{1,2}, B. L. Milityn^{1,2}, M. D. Roper^{1,2}, E. W. Snedden^{1,2}, N. R. Thompson^{1,2}, D. A. Walsh^{1,2}, P. H. Williams^{1,2}, M. D. Wilson³

¹STFC Daresbury Laboratory, Warrington, UK

²The Cockcroft Institute, Warrington, UK

³STFC Rutherford Appleton Laboratory, Didcot, UK

⁴Imperial College London, Blackett Laboratory, London, UK

Abstract

The UK is conducting a multi-stage project to analyse the case for major investment into XFELs, through either developing its own facility or by investing at existing machines. The project's 2020 Science Case identified a clear need for 'next-generation' XFEL capabilities including near-transform limited x-ray pulses across a wide range of photon energies and pulse durations, evenly spaced high-repetition rate pulses, and a high-efficiency facility with a step-change in the simultaneous operation of multiple end stations. The project is developing a conceptual design to meet these requirements, significantly aided by collaboration with international XFELs. It is also guided by an extensive ongoing user engagement programme of Town Hall meetings and other activities (see <https://xfel.ac.uk>). Both the science requirements and the emerging conceptual design are expected to be of general interest to the community.

INTRODUCTION

In 2019, the UK initiated a project to develop the science case for a UK XFEL, which was published in 2020 [1, 2]. Subsequent exercises demonstrated the support of the UK community and UK Research and Innovation provided funding for the next phase of the project: a 3-year conceptual design and options analysis (CDOA), which started in October 2022. This phase includes developing a conceptual design for a unique new UK facility, alongside examining investment opportunities at existing facilities e.g., [3–12], both with the aim of realising 'next-generation' XFEL capabilities (the features of which are discussed below). By the end of the CDOA phase (October 2025), we will have:

- explored a conceptual design for a unique new machine aiming to fulfil all the required capabilities;
- examined other investment options and collaborations in existing XFELs;
- updated the Science Case to feed into the process and inform future decisions;
- held multiple Town Hall Meetings around the UK engaging with the user community;
- investigated the socioeconomic impact of a next-generation XFEL.

Year 1 focused on surveying the science requirements, preliminary engagement with overseas XFEL facilities, planning the Town Hall meetings and initial conceptual design scoping. Year 2 is focusing on producing a self-consistent design, identifying gaps in key physics and technology areas, working with overseas XFEL facilities, and the continuation of Town Hall meetings. In Year 3, existing R&D activities will continue and roadmaps to address gaps in key areas will be defined. The CDOA report will be written, detailing the preferred options; this will include associated costs, socio-economic analysis, and an update to the Science Case. This paper provides a summary of progress to date.

NEXT-GENERATION XFEL CAPABILITIES

Next-generation capabilities were defined by distilling the key messages within the Science Case, focusing on transformational future opportunities that can't yet be delivered at existing facilities. These have been refined through a wide-ranging consultation process between the science team, the facility design team and with external experts. The Science Case and ongoing engagement clearly set an emphasis on both enhancing XFEL capabilities and on widening access to such capabilities, defined as follows:

- A high-efficiency facility, with a step-change in the simultaneous operation of multiple end stations.
- Near-transform-limited operation across the entire X-ray range (~0.1 - 20 keV and ~100 as - 100 fs). Non-transform-limited pulses from ~20-50 keV.
- Evenly-spaced, high repetition rate pulses to match samples and detectors (~100 kHz - 1 MHz per FEL).
- Synchronisation/timing with external lasers to <1 fs.
- Widely separated multiple-colour X-rays to at least one end station.
- Full array of synchronised sources: XUV-THz, e-beams, high power and high energy lasers at high rep. rate.
- Data and computing systems matched to the demands of high repetition rate acquisition.
- Minimal carbon footprint with minimal energy consumption for both operation and build.

NEXT-GENERATION XFEL CONCEPT

To develop a next-generation XFEL concept, we have chosen to initially assume a new-build facility at an international

* david.dunning@stfc.ac.uk

CBXFEL DESIGN, PRODUCTION, AND INSTALLATION STATUS*

M. White[†], J. Anton, L. Assoufid, A. Bernhard, D. Bianculli, M. Golebiowski, X. Huang, W. Jansma, A. Karales, K. Kauchha, S. Kearney, K.-J. Kim, K. Lang, R. Lindberg, P. Liu, R. Margraf-O'Neal, M. Martens, S. Mashrafi, A. Miceli, Jeong-Wan Park, P. Pradhan, M. Rivers, X. Shi, D. Shu, Y. Shvyd'ko, J. Sullivan, J. Tijerina, D.A. Walko

Argonne National Laboratory, Lemont, IL, USA

N. Balakrishnan, M. Balcazar, C. Curtis, F.-J. Decker, G. Gassner, A. Halavanau, Z. Huang, B. Jocson,

E. Kraft, G. Lanza, A. Lutman, J. Mock, M.A. Montironi, X. Permanyer, S. Saraf,

T. Sato, J. Tang, D. Zhu, SLAC National Accelerator Laboratory, Menlo Park, CA, USA

T. Osaka, K. Tamasaku, RIKEN SPring-8 Center, Saitama, Japan

W. Lewis, S.J. Stein, OspreyDCS, Ocean City, MD, USA

M. Camarena, C. Jing, B. Wyderski, Euclid Beamlabs LLC, Bolingbrook, IL, USA

Abstract

Use of a cavity-based X-ray free electron laser (CBXFEL) is potentially a way to dramatically improve the stability and coherence of existing XFELs. A proof-of-principle project is underway as a collaboration between Argonne National Laboratory (ANL), The Institute of Physical and Chemical Research in Japan (RIKEN), and SLAC National Accelerator Laboratory. The CBXFEL is expected to operate using 9.831 keV photons from LCLS, using synthetic diamonds as cavity Bragg mirrors. The LCLS copper linac will deliver two electron bunches 624 RF buckets apart, resulting in a total X-ray cavity length of 65500.87 mm. The X-ray cavity design, and installation and production status will be presented.

EXPERIMENTAL LAYOUT

As shown in Fig. 1, the first seven LCLS hard X-ray undulators are within the optical cavity delineated by the four diamond Bragg-reflecting crystal mirrors C1, C2, C3, and C4. A chicane diverts the incoming electron beam around the crystal mirror C4 in Fig. 1. The electron beam passes through the seven undulators creating x-rays, and continues on to be diverted around the C1 crystal mirror by a second chicane. The design allows for precision alignment of the diamond mirrors using sophisticated nano-positioning systems, such that the produced x-rays can continue to be reflected around the cavity. Stations A & B contain the four diamond crystal mirrors and their nano-positioning systems. Stations C, D, E, F, and G also shown in Fig. 1, host additional X-ray diagnostics.

Diamond Crystal Mirrors

The diamond crystals, grown by Sumitomo under contract to RIKEN, were qualified after extensive testing [1]. Processes were developed to machine and anneal the diamonds for optimal shape and performance. The left side of Fig. 2 shows the results of the process, where strain relief cuts have been machined into the crystal to prevent strain

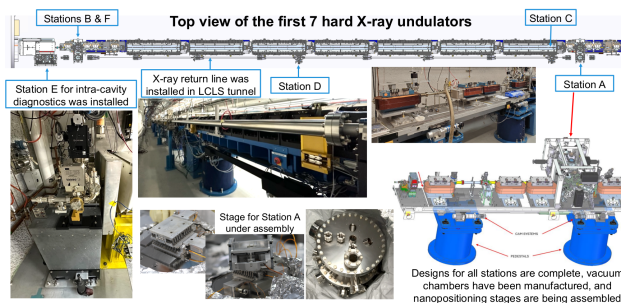


Figure 1: Overview of the CBXFEL cavity, including stations A and B that house the diamond crystal mirrors and beryllium x-ray lenses, chicanes that divert the electron beam around the crystals, X-ray diagnostics stations C, D, E, and F, and the X-ray return line.

from the mounting clamps on the right to affect the working area boxed in red. After high-temperature annealing, X-ray Rocking Curve Imaging (RCI) shows a nearly ideal Darwin width that is nearly constant over a 2 mm² working area.

In addition to the usual treatment that is applied to the nearly 100% reflective crystals C2, C3, and C4, thin, “drum-head” membranes were laser-ablated into C1 to allow for outcoupling of ~5% of the X-rays [2]. We show RCI results in Fig. 2 both before (middle top) and after (middle bottom) laser ablation. The bottom shows that while the Darwin width increases somewhat because of the crystal thickness reduction, the center of mass of the reflection is unchanged. This indicates a nearly strain-free membrane whose thickness of ~17 microns results in a measured Rocking curve that agrees very well with ideal simulations as shown on the right of Fig. 2.

Simulations

Extensive simulations were performed to understand the ideal CBXFEL performance, the required mechanical tolerances, and the effects of cavity misalignments. Figure 3 shows the expected 2-bunch gain and source properties obtained from GENESIS simulations. The top row plots the power along the undulator (left), along with the X-ray spectrum generated by the first bunch (middle) and the second

* Work supported by U.S. Department of Energy, Office of Science under contracts DE-AC02-06CH11357 and DE-AC02-76FO0515.

[†] mwhite@anl.gov

BEAM POSITION MONITORS (BPMS), USING THEIR CHARGE INFORMATION AT SLAC*

F.-J. Decker†, W. Colocho, S. Hoobler, B.T. Jacobson, T. Kabana, SLAC, Stanford, CA, U.S.A.

Abstract

BPMS have been used for decades since their easy-to-use absolute transverse position capability. Left signal minus right signal divided by the sum times the radius gives the beam position. The charge is “just” a relative measurement and has to be calibrated (or ironed) against a toroid signal. Even when the incoming charge variation is high (like 3% rms for the superconducting LCLS2), the relative variations are only 0.1%. This opens up quite some uses. Besides even small charge losses at beam restrictions like collimators or septum magnets it has been found that this signal is very useful in quantifying the charge loss during a wire scan since losses of around 2% are observed. By taking the difference of a few BPMS before and after the wire scanners signal-to-noise levels of up to 5000 are observed, making this method compatible to the typical scintillator plus photomultiplier setup. This is especially helpful where the first beam loss is hundreds of meters downstream since most of the scattered electron make it down the relatively wide bore of the superconducting cavities. An SVD method to analyze the data independent by human judgement is discussed.

INTRODUCTION

First, we will investigate the BPM signals and their sensitivity. Then we look for beam loss patterns along the accelerator, followed by using the loss generated by a wire scanner. Finally, we use the SVD method, which generates distinctive eigenvectors in time and location.

BPM SIGNALS

The four BPM raw signals are processed to get the best transverse beam position information [1, 2]. The charge or TMIT (TransMITted number of electrons) value is the sum of all four channels. RF BPMS have only one charge related signal making them a factor of two worse. The Cryo-modules have button BPMS with a big bore which are even worse, see Fig. 1. Beam losses at collimators in the SC beamline are quite common. The beam is often steered close to a jaw since many (>7) of the deferred BPMS are still missing. This initiated the 30-times zoomed-in display around $100 \pm 2\%$ instead of the usual 0 to 120%.

A few individual BPMS showed much higher RMS jitter. Some reasons were found where the signal raw waveform was hitting the ± 32000 -count digitizer limit. Other BPMS had four signals with very different waveform counts. The cause for bad performances for some RF BPMS in the undulators are not yet identified.

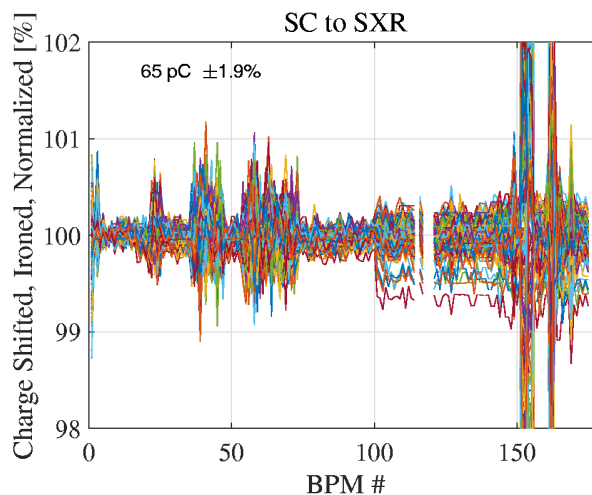


Figure 1: Charge Ratio along the SC (Super Conducting) linac to the SXR (Soft X-Ray) dump. After normalizing to the “incoming” charge (average of #5 to #20), the charges are the same within an RMS of 0.05% for the best BPMS. The cryo BPMS are 5 times worse indicating the four linac regions L0, L1, L2 and L3 at #3, around #25, #40 and #60. Beam losses of at least 0.5% at a halo collimator (BPM #100) are indicated by a step up in the RMS value.

BEAM LOSSES

Beam losses down to 0.1% can be localized with a display like Fig. 1. Mostly they were at collimators and septum magnets needing steering the beam away from a jaw or some beam beta mismatch or emittance tuning. A few times, we had losses at unexpected (and not water-cooled) locations like in the BSYS (Beam Switch Yard to the Soft x-ray line) where a sparse BPM region with bends caused the beam to have less than 1 mm wiggle room. Another place to watch is just three BPMS away from the final dump where the XTCAV (X-band Transverse deflecting CAVity) is located.

When looking at numbers even a small loss of 0.1% is too much at higher beam rates for the SC linac. At 10 kHz, this loss is equivalent of a 100% beam loss at 10 Hz. The BPM TMIT loss method has also helped to locate which LBLM (Long Beam Loss Monitor) have a rate dependant behaviour and therefore photon beam versus not rate dependant dark current losses.

For the Copper Linac we identified a loss location where the holed-out mirror for the BC2 (Bunch Compressor) peak current detector was slowly creeping into the beam path creating small losses. It was found earlier [3] that being close to an obstruction increases the emittance to the point that no FEL intensity at hard x-rays is generated, even before losses are obvious.

*Work supported by U.S. Department of Energy, Contract DE-AC02-76SF00515.

† Decker@SLAC.Stanford.edu

AUTONOMOUS BEAM ALIGNMENT THROUGH QUADRUPOLE TRIPLETS USING BAYESIAN ALGORITHM EXECUTION

R. Roussel*, D. Kennedy, A. Edelen

SLAC National Accelerator Laboratory, Menlo Park, CA, USA

A. Ody, E. Wisniewski, Argonne National Laboratory, Lemont, IL, USA

Abstract

A common challenge in online accelerator operations is aligning beams through a series of quadrupole magnets, especially when in situ beam position monitors are not present. Accelerator operators generally use a trial-and-error approach to solve this problem by sequentially measuring the centroid deflection of the beam as a function of quadrupole strengths. This is a challenging process that necessitates dedicated effort by operational experts, requiring significant beam time and personnel resources to configure basic accelerator operations. In this work, we use Bayesian Algorithm Execution (BAX) with virtual objectives to autonomously control steering magnets at the Argonne Wakefield Accelerator to center the beam through a quadrupole triplet. This technique uses virtual objectives to reduce the number of measurements needed to converge to an optimal solution, resulting in a turn-key algorithm for finding the optimal steering configuration for a set of accelerator magnets from scratch.

INTRODUCTION

Effectively steering particle beams through magnetic elements is a necessary part of routine accelerator operations. Beams that travel off-axis through magnetic elements, such as quadrupoles or solenoids, are deflected when varying the field strength of these elements due to “feed-down” effects of multipole magnets which result in dipole fields. This complicates automated optimization of magnetic fields as varying the field of each magnet might cause the beam to be further misaligned with elements downstream, such as diagnostic screens or small apertures. Additionally, beams that travel off-axis in magnetic elements may be subjected to non-ideal magnetic field geometries due to fringe field effects, which can degrade beam quality. As a result, steering beams through the center of magnetic elements is a critical part of accelerator operations.

Several methods have been developed to effectively determine and minimize the misalignment of beams travelling through magnetic accelerator elements such as quadrupole magnets, often referred to as beam-based alignment (BBA). In some cases, these methods use a model of the beamline including the locations of quadrupole magnets and steering magnets (e.g. [1]). On the other hand, other model-free approaches have been developed to determine misalignments without the need for knowledge of the accelerator structure (e.g. [2]). However, these methods are relatively inefficient,

as multiple measurements are necessary to determine the magnitude of deflection when varying magnet strengths as a function of steering parameters.

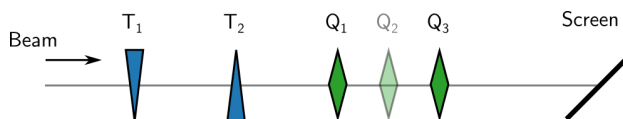


Figure 1: Simple example beamline of alignment through a quadrupole focusing triplet. Two steering / trim magnets (T1, T2) are used to steer the beam through the center of two quadrupole magnets (Q1, Q2) while measuring the beam centroid location at a downstream diagnostic (in this case a screen).

In this work, we introduce a technique that can be used to correct for beam misalignments in magnetic elements in an efficient, model-free way. This technique utilizes recent developments in Bayesian Algorithm Execution (BAX) [3], which is a generalization of conventional Bayesian optimization algorithms [4] to optimize so-called “virtual objectives”. We demonstrate that this technique efficiently steers the beam through the centers of 2 quadrupoles in a triplet configuration with little to no prior information about the accelerator beamline, all while respecting operational constraints and accounting for measurement noise. As a result, this technique can be incorporated into future systems for autonomous accelerator control.

BAYESIAN ALGORITHM EXECUTION

In some optimization tasks, such as beam alignment as shown in Fig. 1, each acquisition requires a secondary scan in a separate domain to calculate the objective function. Instead of directly measuring objectives of interest, BAX builds a Gaussian process (GP) model [5] of observables that can then be used to compute the objective as a function of tunable parameters. To do this the parameter space is divided into so-called “tuning parameters” which effect the virtual objective and “measurement parameters” which are used to compute the virtual objective to predict the dependency on tuning parameters. The BAX acquisition function uses these predictions to evaluate which future measurements will provide the most information about the steering current that leads to a minimization of the centroid deflection. An example application of BAX is minimizing transverse beam emittances [6]. In this case, the virtual objective involves fitting polynomials to the beam size squared as a function of quadrupole strength using predictions from a GP model. At FACET-II, BAX was able to match the best emittance

* rroussel@slac.stanford.edu

ADVANCEMENTS IN BACKWARDS DIFFERENTIABLE BEAM DYNAMICS SIMULATIONS FOR ACCELERATOR DESIGN, MODEL CALIBRATION, AND MACHINE LEARNING

R. Roussel¹, G. Charleux², A. Edelen¹, A. Eichler³, J. P. Gonzalez-Aguilera⁴,

A. Huebl², J. Kaiser³, R. Lehe², A. Santamaria Garcia⁵, C. Xu⁵

¹ SLAC National Accelerator Laboratory, Menlo Park, CA, USA

² Lawrence Berkeley National Laboratory, Berkeley, CA, USA

³ Deutsches Elektronen-Synchrotron DESY, Hamburg, Germany

⁴ University of Chicago, Chicago, IL, USA

⁵ Karlsruhe Institute of Technology, Karlsruhe, Germany

Abstract

Many accelerator physics problems such as beamline design, beam dynamics model calibration or interpreting experimental measurements rely on solving an optimization problem that use a simulation of beam dynamics. However, it is difficult to solve high dimensional optimization problems using current beam dynamics simulations because calculating gradients of simulated objectives with respect to input parameters is computationally expensive in high dimensions. To address this problem, backwards differentiable beam dynamics simulations have been developed that enable computationally inexpensive calculations of objective gradients that are largely independent of the number of input parameters. In this work, we highlight current and future applications of differentiable beam dynamics simulations in accelerator physics, such as improving accelerator design, model calibration, and machine learning. We also describe current collaborative efforts between SLAC, DESY, KIT, and LBNL to implement fast, backwards differentiable beam dynamics simulations in Python. These tools will enable unprecedented improvements in optimization efficiency and speed when using beam dynamics simulations, leading to enhanced control and detailed understanding of physical accelerator systems.

INTRODUCTION

Solving challenging optimization problems is critical to accelerator design, interpreting experimental measurements, and calibrating physics models to realistic beam dynamics. However, current beam physics simulations can present a bottleneck in the optimization process. Most current beam dynamics simulations used in accelerator physics are “gradient-free” simulations, where only the input and output of the model is available. This limits the applicability of powerful gradient-based optimization algorithms, such as first- or second-order gradient descent, which often outperform optimization algorithms that do not use gradient information [1]. The only available methods for estimating gradients of gradient-free simulations is finite difference methods, which require higher computational costs proportional to the number of optimization parameters. As a result, optimization problems that include beam dynamics simulations

are often restricted to optimizing a handful of parameters at once.

An alternative simulation paradigm to gradient-free simulations is so-called “differentiable simulations”, illustrated in Fig. 1. In addition to making conventional predictions, differentiable simulations also provide the gradient of simulations with respect to input parameters. Differentiable simulations are enabled through the use of a computational technique known as “automatic differentiation” [2]. Computational programs, such as beam dynamics simulations, can be broken down into a set of atomic operations (addition, multiplication, exponentiation etc.) for which the derivative is analytically known. Differentiable simulations track the derivative of each calculation step alongside normal computation and use the chain rule to calculate total derivatives of simulation outputs with respect to simulation inputs.

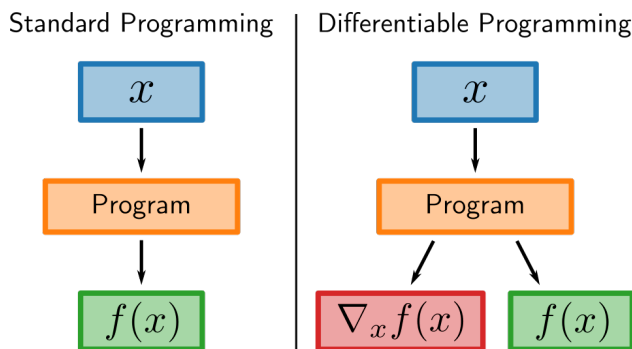


Figure 1: Block diagram showing the difference between standard programming used to model physical phenomena, which produces outputs $f(x)$ as a function of model inputs x , and differentiable programming, which produces gradients of model outputs $\nabla_x f(x)$ in addition to model outputs.

Several existing beam dynamics software packages [3–5] use a technique known as “forward differentiation” [2] to calculate arbitrary order Taylor maps of accelerator elements, and more recently, to optimize accelerator design parameters for beam dynamics under the influence of space charge [6]. However, the efficacy of this method is restricted to computing derivatives with respect to a small number of input parameters, making it impractical for optimizing problems that contain a large number of free parameters. On the other

A COMPACT, ULTRAFAST HIGH-VOLTAGE PULSER FOR TRANVERSE ELECTROMAGNETIC KICKERS*

T. Le†, A. Krasnykh, SLAC National Accelerator Laboratory, Menlo Park, CA, USA

Abstract

A compact, high-voltage (HV) pulser in the nanosecond regime for transverse electromagnetic (TEM) kickers is presented. TEM kickers are electromagnetic deflectors used in particle accelerators to redirect bunches of particles out of their original trajectory into a new path, such as alternate beam paths, detectors, or other instrumentation devices. The circuit proposed in this design consists of two main portions: a gate driver and a HV switch. The gate driver consists of an isolated and high-speed gate driver, powered by an isolated DC/DC converter with dual output voltages. The HV switch portion was simulated in Ansys HFSS and is composed of a SiC MOSFET, LC resonance components, and specialized diodes. When switched, the MOSFET is used to pump a high voltage into the LC circuit and diode stack, and the ultrafast diode turnoff delivers the final HV pulse to the resistor load. Careful layout techniques were implemented for the MOSFET driver to reduce pulse to pulse instability.

BACKGROUND

All particle accelerators require some form of electromagnetic deflector mechanism to redirect, or kick, particle bunches from their original trajectory into a new path, typically for alternate beam paths, detectors, or other instrumentation devices [1, 2]. These kickers must quickly reach the desired field, maintain that field for a certain time, and then quickly return to zero field. Thus, the drivers need to pump the required current into the kicker impedance, and therefore must operate with nanosecond rise and fall times, adjustable pulse top durations, fast repetition rates, and low jitter. This paper will focus on the design of the driver portion of the TEM kicker consisting of a HV Silicon Carbide (SiC) MOSFET, isolated high-speed gate driver, and an isolated DC/DC converter.

SIC MOSFET CHARACTERISTICS

Compared to their Silicon (Si) counterparts, SiC MOSFETs have different intrinsic material characteristics, summarized in Table 1 [3]. The greater bandgap energy and critical electric field breakdown means higher voltage operation and lower leakage current. Their faster saturation velocity means faster switching and lower power loss, and their better thermal conductivity means better thermals, leading to a smaller die for the same temperature rise. One downside to SiC is their lower electron mobility, which means a higher channel resistance that requires a higher gate drive voltage. These differences make SiC MOSFETs the preferred choice over Si in drivers for kicker designs.

Table 1: Comparison of Intrinsic Material Properties of SiC and Si MOSFETs

Property	Definition	SiC	Si
E_G [eV]	Bandgap Energy	3.2	1.12
E_C [MV/cm]	Critical Electric Field	2.2	0.25
V_s [$\times 10^6$ cm/s]	Saturation Velocity	20	10
μ_e [$\text{cm}^2/\text{V}\times\text{s}$]	Electron Mobility	950	1350
λ [W/cm \times K]	Thermal Conductivity	3-4	1.5

GATE DRIVER FOR HV SiC MOSFETS

For this TEM kicker design, a high voltage is required to be supplied to the LC circuit and diode stack that supplies the final HV pulse to the resistor load. Due to the large voltage at the drain of the SiC MOSFET and fast switching, an isolated gate driver is needed to isolate the low-voltage circuitry from the high voltage and to enhance the common-mode transient immunity (CMTI) from high dv/dt . Two common methods for implementing isolation in gate drivers are galvanic and optical isolation.

Galvanic isolation uses a transformer to transmit the gate drive signal across an air gap. The signal that is applied on the primary winding creates a magnetic field in the core, which induces a corresponding voltage on the secondary winding. The main benefits of using galvanic isolation are low propagation delay and not needing any additional bias circuitry. However, the main drawbacks are its relatively larger size and potential for overshoot or ringing on the secondary due to parasitics and large leakage inductance.

Optical isolation uses an LED and phototransistor to transmit the gate drive signal across a barrier. The drive signal is applied to the LED, and the phototransistor converts the received light signal into a corresponding current. This signal is then usually buffered by a CMOS circuit to provide the final gate drive output. Compared to galvanic isolation, the drawbacks are its larger propagation delay and need for bias circuitry. However, the primary benefits of a smaller footprint, minimal parasitics, and lack of overshoot or ringing on the output is critical for TEM kickers.

PROPOSED GATE DRIVER DESIGN

A simplified schematic diagram of the proposed design of a HV SiC MOSFET gate driver for TEM kicker is shown in Fig. 1. For the HV SiC MOSFET, Microchip's MSC080SMA330B4 was selected due to its high voltage breakdown of 3.3 kV and lower total gate charge across the gate-to-source voltage range when compared to other alternatives with that high of a breakdown voltage.

* Work supported by U.S. DoE contract DE-AC02-76SF00515.

† thiele@slac.stanford.edu

LCLS-II LONGITUDINAL BEAM DIAGNOSTICS BASED ON A SHORT S-BAND DEFLECTOR *

V. A. Dolgashev[†], E. Williams, E. M. Kraft, K. M. Ratcliffe, M. Kosovsky, A. Brachmann
SLAC, Menlo Park, CA, USA

Abstract

We designed, built and commissioned a beam diagnostic system based on a short S-band deflector and a commercial klystron transmitter. A two feet long transverse-horizontally deflecting S-band rf structure is installed the LCLS-II post-laser-heater diagnostic beamline at 100 MeV electron beam energy to measure the absolute electron bunch length and to allow time-resolved beam quality measurements such as vertical slice emittance and slice energy spread. The deflector is designed to produce 0.48 MeV peak kick at 300 kW of input power. The klystron transmitter, which uses a commercial solid-state modulator, is installed in the klystron gallery at the grade level. The low-level RF system is based on Advanced Telecommunications Computing Architecture and developed in-house. We will report on the overall performance of the project, which was successfully completed, on May 31, 2024.

INTRODUCTION

The parameters of the X-ray beam generated by a linac-based Free Electron Laser (FEL) depend to a large extent on the quality of the electron beam entering the undulators. The quality of the electron beam is determined by the performance of the electron injector and the means of maintaining this quality through the linac. To tune and improve the performance of the injector, we use a set of diagnostic tools. One such tool is the longitudinal beam diagnostics, which uses a radiofrequency deflector to create a transverse momentum chirp on the electron beam. The beam is then displayed on a profile monitor screen located after the bending magnet, which serves as an energy spectrometer. Therefore, this method allows direct measurement and tuning of the longitudinal phase space of the beam.

SLAC has a long history of developing and using rf deflectors [1, 2]. For example, the SLAC FEL LCLS [3] uses S-band deflectors for pre-undulator and X-band deflectors for post-undulator beam diagnostics [4, 5]. This paper describes the concept and basic approaches to LCLS-II [6] longitudinal beam diagnostics based on a 2856 MHz rf deflector. A photograph of the deflector during its field profile measurement after tuning is shown in Figure 1.

STACAV2 SYSTEM

A 2 ft long transverse-horizontally deflecting S-band rf structure (STCAV2) is installed in the post-laser-heater diagnostic beamline at 100 MeV to measure the absolute electron

* Work supported by supported by the U.S. Department of Energy contract DE-AC02-76SF00515.

[†] dolgash@slac.stanford.edu



Figure 1: STCAV2 - traveling wave backward wave rf deflector during its after-tuning microwave characterization. The measured data shows that the rf deflector is well tuned.

bunch length and to allow time-resolved beam quality measurements such as vertical slice emittance and slice energy spread. The main parameters of the STCAV2 system are listed in Table 1. The commercial klystron transmitter is installed in klystron gallery at grade level between penetrations 1-8 and 1-9, and the cavity is installed on a table with 43.623 m from the rf gun cathode to the cavity its center. Overview of the STCAV2 system is shown in Fig. 2.

Table 1: Main STCAV2 System Parameters [7]

Parameter	Value	Unit
Beam energy	100	MeV
Nominal rms bunch length (100 pC)	1.0	mm
Nominal rms vertical norm. emittance	0.45	μm
RMS slice energy spread	1-10	keV
Cavity length	60	cm
RF frequency	2856	MHz
RF phase stability (rms) at all $f > 1$ Hz	< 0.2	deg-S
Fast rf phase-flip capability (< 8 ms)	180	deg-S
Fast rf phase-flip accuracy	< 1	deg-S
RF phase setting range	360	deg-S
Max rf power required	500	kW
Max deflecting voltage (on crest)	0.5	MV
Max electron beam power (120 Hz)	4	W

RF System

RF deflector The STCAV2 rf deflector type is a traveling-wave backward-wave waveguide. It is based on the original SLAC's LOLA-II structure [1, 2]. It was recently built with improved couplers and a smaller than the original beam pipe. The redesign of the coupler was done by Zengai Li of SLAC in 2018. The main parameters of the deflector

EFFECTIVE THERMAL LOAD MITIGATION IN CERL INJECTOR COUPLER THROUGH WARM SECTION MODIFICATION

Pragya Nama*, The Graduate University for Advanced Studies (SOKENDAI), Hayama, Japan

Ashish Kumar¹, Dai Arakawa, Kensei Umemori¹, Eiji Kako, Hiroshi Sakai¹, Takako Miura¹

High Energy Accelerator Research Organization (KEK), Tsukuba, Japan

¹also at The Graduate University for Advanced Studies (SOKENDAI), Hayama, Japan

Abstract

The prototype of cERL (compact ERL) injector coupler experienced excessive thermal load during high power transmission in continuous wave (CW) mode operation. Hence, some modifications has been introduced in the warm sections of the coupler which includes a scheme for active water cooling for the inner and outer conductors. The material of the warm inner conductor was also replaced from copper coated stainless steel to pure oxygen-free copper. The high power test results with modified warm section shows effective thermal load mitigation. For the unmodified coupler, the warm inner conductor's temperature reached 183°C at 27 kW power level, while for the modified coupler with active water cooling, this temperature was mere 25°C. Due to the conduction cooling effect from the modified warm inner and outer conductor, the temperature rise of the entire coupler was suppressed. Furthermore, high power test was conducted using the forced convection cooling by a fan which additionally suppressed the temperature rise of the entire coupler components. The results demonstrate the effectiveness of the implemented modifications and suggests that the 100 kW class high power transmission in CW mode could be possible.

INTRODUCTION

In superconducting radio-frequency (SRF) accelerators, input couplers transfer power from the source to the SRF cavities. The SRF cavities have the ability to accelerate high-power beams in continuous wave (CW) mode. However, during power transmission, the coupler's components experience excessive thermal loads, leading to potential damage. Essentially, the configuration of accelerator to generate high current beams is constrained by the power transfer capability of the input coupler rather than the SRF cavities.

This problem was notably encountered by the cERL injector coupler's test stand during 100 kW power transmission in CW mode for one minute, about 15 years ago [1]. The cERL injector coupler, designed for power transmission in L-band SRF cavities, achieved power transfer up to 30 - 40 kW in CW mode at the test stand (Fig. 1(a)) [2]. However, while transferring 100 kW power for a minute, the coupler's warm inner conductor was burned due to excessive thermal load. The temperature measurement of the warm inner conductor shows that maximum temperature reached about 180°C during RF transmission of 20 kW in CW mode [3]. The ANSYS

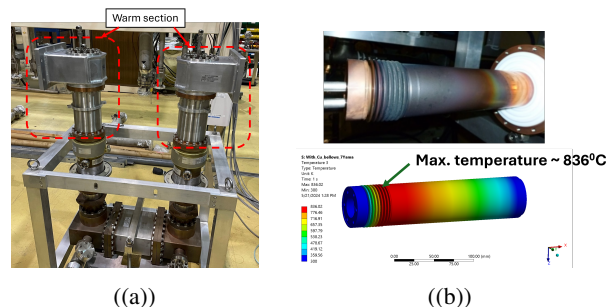


Figure 1: (a) cERL injector coupler test stand and (b) burned warm inner conductor by 100 kW RF transmission and temperature profile by ANSYS thermal simulation.

thermal simulation of the warm inner conductor also suggests that the expected maximum temperature near bellows will be around 836°C for 100 kW power transmission. The temperature profile by ANSYS simulation and the burned inner conductor are shown in the Fig. 1(b). To address this issue, some modifications were introduced in the coupler's warm section. The high-power test with modified components were performed with and without fan. The following sections highlight the implemented modifications and the results of high power test.

MODIFICATIONS IN CERL INJECTOR COUPLER

The warm inner and outer conductor of the cERL injector coupler were fabricated from stainless steel with 20 μm copper coating. This design exhibited poor thermal conductivity, leading to overheating and subsequent burning of the warm inner conductor. Additionally, substantial temperature rise was observed in the outer conductor and other components.

To address these thermal issues, modifications were implemented in the warm section of the cERL injector coupler. The revised components are as follows:

- **Warm inner conductor:** The inner conductor was re-fabricated using oxygen-free copper, which significantly improves thermal conductivity. Figure 2(a) illustrates the modified inner conductor, which includes integrated water cooling channels. These channels allow chilled water from the chiller to circulate through the space adjacent to the bellows.
- **Warm outer conductor:** The outer conductor was re-fabricated with added jacket on its outer surface. This jacket is designed to be filled with chilled water, as depicted in Fig. 2(b).

* pragya@post.kek.jp

THE PIP-II DEDICATED RADIO FREQUENCY PROTECTION INTERLOCK SYSTEM FULL SCALE PROTOTYPE DESIGN AND INTEGRATION*

W. Cichalewski[†], P. Amroziak, G. Jablonski, W. Jalmuzna, R. Kielbik, K. Klys, R. Kotas, P. Marciniak, B. Pekoslawski, W. Tylman, Technical University of Łódź, Department of Microelectronics and Computer Science (DMCS), Łódź, Poland
J. Holzbauer, N. Patel, P. Varghese, Fermi National Accelerator Laboratory, Batavia IL, USA

Abstract

The Radio Frequency Protection Interlock (RFPI) system watches over fifty signals near the superconducting cavities cryomodule. Its major role is to recognize faulty situations instantly and drop permits for the Low-Level Radio Frequency control system (LLRF) and solid-state amplifier (SSA) operation. The full-scale prototype RFPI is a recent version of the PIP-II dedicated system capable of fulfilling the requirements of this newly constructed Linac project. Its hardware structure is compact but still modular. It provides enough capability to protect four superconducting resonators and their close environment at the same time. This work summarizes the production phase and the integration process of this designed RFPI system. The work introduces also the hardware and software structures of this system. Moreover, we also summarize the on-the-bench testing experiences from the individual hardware module verification and integrated RFPI studies.

INTRODUCTION

The newly designed and under construction linac named Proton Improvement Plan II (PIP-II) is located in Fermilab [1]. This significant upgrade to the existing accelerator infrastructure will allow for new scientific studies within such projects as, for instance, Deep Underground Neutrino Experiment (DUNE) [2].

This design and construction triggered the need for the development of existing and new accelerator systems. An example of such a system is the RFPI. Its main role is to protect the RF system in case of faulty cavities and cryomodule behavior or state. This goal can be achieved by instantaneous operation permits dropping while monitored signals begin to deviate from predefined safety limits. The PIP-II version of the RFPI system must provide enough channels to protect four cavities from a single cryomodule independently.

The first phase of the system design has resulted in the proof of concept prototype preparation [3]. That device provided valid information on the correctness and performance of each input/output signal. The second prototype covers a full list of input and output signals. Its structure changed in-

ternally on the hardware and software level. Still, protection functionality for 4 cavities remained unchanged.

This design consists of one central HW unit (carrier module) that hosts the system-on-chip module responsible for main protection logic realization and the other SOM responsible for the overall RFPI management. Additionally, it carries 7 FMC (FPGA Mezzanine Card) slots to be used for modules dedicated to different input/output signals. Such modularity provides possibility of different system configuration depending on the individual implementation requirements.

MAIN LOGIC UNIT AND MANAGEMENT SUBSYSTEM CARRIER MODULE (KC)

Main logic unit is a FPGA based hardware module that collects all the input signals (in digital representation) and compare their levels against safety limits. It is also responsible for managing output (permit) signals. Moreover, via the FMC connectors it allows individual inputs management and configuration (see Fig. 1).

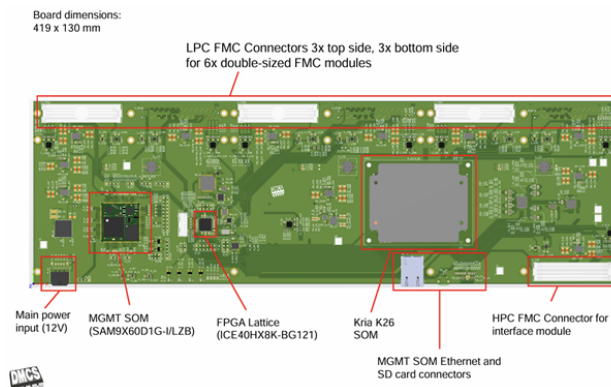


Figure 1: FMC/KRIA carrier module.

The management processor is responsible for: individual system modules power management, voltages and currents monitoring, resetting KRIA SOM, providing UART interface to the main (KRIA carrier) logic, and providing the JTAG access to KRIA chip.

FMC MODULES

The list of input and output signals required for the full-scale design RFPI system includes more than 60 elements (based on the current specification). To cover all

* Work supported, in part, by the U.S. Department of Energy, Office of Science, Office of High Energy Physics, under U.S. DOE Contract No. DE-AC02-07CH11359.

[†] wchical@dmcs.pl

PARTICLE MEASUREMENT ON ALL-METAL GATE VALVE FOR CEBAF BEAMLINE VIA LASER-BASED PARTICLE COUNTER*

M. Ge[†], A.-M. Valente-Feliciano, S. Balachandran, R. Ruber, T. Powers, R. Geng
Thomas Jefferson National Accelerator Facility, Newport News, USA

Abstract

The Viton gate valves installed in the CEBAF beamline degrade significantly after long-term operation in a radiation environment, generating numerous particles that cause heavy contamination and increased risk of field emission. All-metal gate valves have been proposed as a replacement for installation in the CEBAF beamline. In this paper, we present thorough comparison tests between the Viton gate valves and the all-metal gate valves, including evaluations of particle levels, aging tests of the gate valves, and analysis of the particle material.

INTRODUCTION

During CEBAF operation, various beamline components, such as Viton gate valves, may generate microscopic particulates. Those that migrate onto SRF cavity surfaces can become field emitters, causing field emission (FE) and leading to performance degradation of the SRF cavities [1-3]. Frozen gases can also activate non-field-emitting particulates [4, 5].

The Viton gate valves (VAT 01.0 Mini UHV Gate Valve [6]) have been widely used in the CEBAF beamline. Each CEBAF cryomodule has two Viton gate valves, one at each extremity, resulting in approximately 190 Viton gate valves installed in the CEBAF accelerator. Although the root cause of the field emitters has not been definitively identified, one of the primary suspicions is that the Viton seals become hardened and shattered into microparticles after long periods of accelerator operation under a high-level radiation environment.

Viton gate valve failures have occurred many times in the CEBAF beamline. In some cases, a small piece of the Viton seal was missing. There were two instances of complete Viton gate valve failure. In both cases, the Viton seals had hardened after over 12 years of use in cryomodules with excessive field emission. When the Viton seals shattered, adjacent cavities became inoperable due to gas discharges. Following the failure, the operational gradient of cryomodule 1L25 dropped from 79 MeV to 59 MeV, accompanied by a significant increase in radiation. Similarly, cryomodule 1L26, which operated at 82 MeV before the failure, dropped to 38-45 MeV afterward. Upon disassembly of the Viton gate valve, it was observed that the Viton seal had shattered into numerous dark particles, as shown in Fig. 1 (a).

To eliminate the potential risk of field emission from the Viton gate valve, the VAT 47.2 XHV RF All-Metal Gate

Valve [6], as shown in Fig. 1 (b), is proposed to replace all the Viton gate valves on the CEBAF cryomodules. Unlike the Viton seals, the materials of this all-metal valve should not shatter after long periods of operation under high-level radiation. The critical metric for qualifying the all-metal valve is that the particle level generated during valve operation (i.e., opening and closing) should be equal to or less than that of a brand-new Viton gate valve. In this work, we present the setup and results of particle-level measurements comparing the all-metal valve and the Viton gate valve using a laser-based vacuum particle counter system.

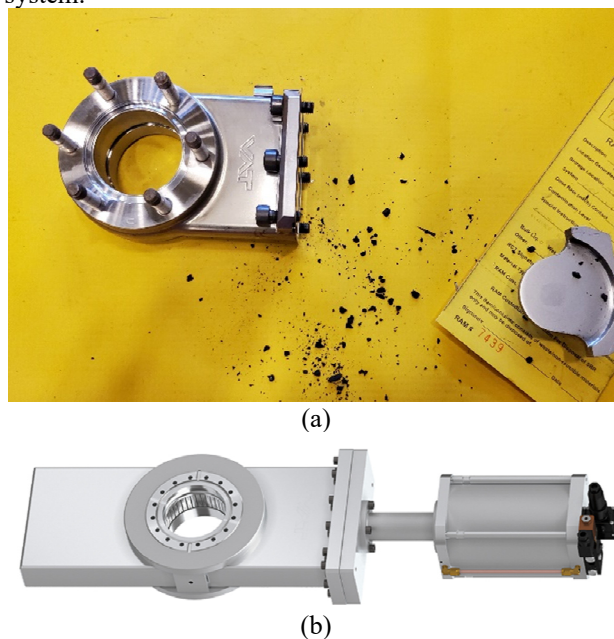


Figure 1: (a) Numerous dark particles from the Viton gate valve after disassembly from CEBAF cryomodule 1L26; (b) Photograph of the VAT 47.2 XHV RF All-Metal Gate Valve.

LASER-BASED PARTICLE COUNTER SYSTEM

The particle counter system was first developed at Jefferson Lab around 2018-2020 [7]. This system utilizes a laser-based vacuum particle sensor [8], capable of measuring particle sizes up to 3.6 μm and counting particles in a 2.75-inch OD vacuum pipeline in real-time. In 2022-2023, the system was upgraded with new features, such as slow pumping. The diagram and photograph of the particle counter system are shown in Fig. 2 (a) and (b), respectively. During a measurement, a gate valve is mounted above the particle sensor. Slow pumping is performed before data collection to prevent particle movement and agitation.

* Work supported by DOE contract DE-AC05-06OR23177

[†] mingqi@jlab.org.

RECENT PROGRESS ON HF-FREE SURFACE TREATMENT BY BIPOLAR PULSED ELECTROPOLISHING FOR SRF Nb CAVITIES*

M. Ge[†], H. Tian, J. Musson, M. Lester, N. Brock, A.-M. Valente-Feliciano, E. Stallworth
Thomas Jefferson National Accelerator Facility, Newport News, VA, USA

Abstract

The bipolar pulsed electropolishing (BPEP) process, due to its HF-free nature, offers a safer, more environmentally friendly, and cost-effective alternative to conventional electropolishing, which uses concentrated HF and H₂SO₄ as the electrolyte. Jefferson Lab has developed a BPEP system that utilizes only diluted H₂SO₄ for the final surface processing of niobium superconducting radio frequency (SRF) cavities. This includes single cells, 7-cell CEBAF C100 cavities, and 9-cell TESLA-style cavities.

In this report, we present recent progress for BPEP-treated single-cell cavities at Jefferson Lab. Notably, one single-cell cavity, following a 120°C bake, achieved an accelerating gradient (E_{acc}) of 37 MV/m with a quality factor (Q_0) exceeding 1×10^{10} at 2 K. This result demonstrates the potential for the BPEP process.

INTRODUCTION

The bipolar pulsed electropolishing (BPEP) technique for niobium superconducting radio frequency (SRF) cavities was patented by Faraday Technology, Inc., through collaborative SBIR work with Jefferson Lab [1-3]. Previous studies by Cornell University, in collaboration with Faraday, reported that a 1.3 GHz TESLA-shaped 9-cell Nb SRF cavity treated with BPEP achieved an accelerating gradient of 35 MV/m [4]. Additionally, developments at Jefferson Lab have demonstrated the successful commissioning of its own BPEP setup for 1.3 GHz single-cell and multi-cell Nb cavities [3, 5].

BPEP uses an HF-free electrolyte and employs a novel approach to treat Nb SRF cavities. An anodic pulse anodizes the Nb surface to form Nb oxides, while intervening cathodic pulses mechanically erode the oxide layer through the action of hydrogen gas bubbles formed at the niobium surface via electrolysis.

Systematic studies on Nb samples have demonstrated that the removal rate and uniformity can be finely controlled using this method [3, 5]. The studies indicate that the removal rate of BPEP is proportional to the pulse repetition frequency (PRF). When the PRF is set at approximately 60 Hz, the BPEP removal rate is comparable to that of conventional EP, i.e., $\sim 0.25 \mu\text{m}/\text{min}$ [5]. Conventional EP can lead to the formation of sulfur particles, in the form of sulfate and/or sulfite, on the niobium surface when using aged electrolyte with a 1:10 volume ratio of HF (49%) and H₂SO₄ (98%) [6]. These sulfur particles can act as field emitters, thereby limiting the RF performance of SRF cavities. In contrast, BPEP typically employs a lower concentration of H₂SO₄ (37% or less) and uses mixed metal oxides

as the counter electrode, which exhibit a low overpotential for the hydrogen evolution reaction, approximately 20-50 mV at a current density of 10 mA/cm² in acidic media [7]. Consequently, BPEP significantly reduces the likelihood of sulfur particle formation on Nb surfaces [8]. Furthermore, the HF-free nature of BPEP offers substantial environmental benefits and is more cost-effective than other surface processing methods.

BPEP SYSTEM AT JLAB

A BPEP system has been implemented at Jefferson Lab and applied to various SRF cavities, including single-cell cavities, 1.5 GHz 7-cell CEBAF C100 cavities, and 1.3 GHz 9-cell TESLA-shaped cavities. This system utilizes a recently upgraded pulser system [9] that enables an adjustable PRF and operating voltage. It offers potential improvements in surface removal for different types of SRF cavities. Figure 1(a) illustrates the schematic diagram of the Jefferson Lab patented high power pulse generator and controller system [9]. The pulser depicted in the figure can generate the designed pulse structures, including anodic and cathodic pulse durations, off-time, and the potentials of both anodic and cathodic pulses. Diluted sulfuric acid is used as the electrolyte.

During the process, the oxide layer grows when the niobium cavity is at a positive potential, and the removal of niobium oxides occurs when the cavity alternates from a positive to a negative potential, thereby removing the niobium pentoxide formed. Figure 1(b) shows the setup for a 1.5 GHz 7-cell CEBAF C100 Nb SRF cavity inside a closed chemical cabinet, which is equipped with ultrasonic thickness gauges and thermocouples for in-situ monitoring of material removal and temperatures.

In order to evaluate the improved BPEP system, a series of comparative tests were performed between BPEP and conventional horizontal EP (HEP) using two 1.3 GHz TESLA-shaped single-cell Nb cavities, RDT-13 and RDT-5. Initially, both cavities underwent surface resetting through HEP, followed by further surface removal using BPEP. Vertical tests were subsequently carried out after each removal to assess RF performance. Comparable or superior RF performance achieved after BPEP, relative to HEP, would validate the successful development of the BPEP system at JLab. This study highlights BPEP's potential as a viable and effective surface processing technique for SRF cavities.

* Work supported by DOE contract DE-AC05-06OR23177

[†] mingqi@jlab.org.

NUMERICAL STUDY OF 5 MeV SRF ELECTRON LINAC FOR WASTEWATER PURIFICATION*

A. B. Kavar[†], S. Kashiwagi, T. Muto, H. Abiko, F. Hinode, K. Kudo, I. Nagasawa, K. Nanbu, K. Shibata, K. Takahashi, H. Yamada, H. Hama

Research Centre for Accelerator and Radioisotope Science, Tohoku University, Sendai, Japan

Abstract

Superconducting Radio Frequency (SRF) technology is a proven solution for generating high-power electron beams (EB), suitable for tasks like purifying wastewater from challenging impurities such as PFAS. This study elaborates on effectiveness of EB treatment and outlines design considerations for a 1.3 GHz SRF linac operating at 5 MeV with an average beam current of 10 mA. Numerical analyses for the accelerator system, ensuring that the beam reaches 5 MeV with the desired characteristics, lead to a compact beamline structure. This structure includes a 100 kV thermionic gridded electron gun, a 1.3 GHz 3-cell low beta buncher cavity, and three 2-cell 1.3 GHz accelerator cavities, along with necessary focusing solenoids, all fitting within 3 meter. Given the need for high beam current, achieving a high bunch repetition rate is important. We therefore will employ the RF gating to the grid of the electron gun. The results of the numerical studies will be presented at this conference.

INTRODUCTION

Increased population and their rising demands for improved living standards have spurred significant industrial advancements. This progress has led to the generation of numerous new impurities, among which per- and polyfluoroalkyl substances (PFAS) stand out due to their carbon-fluorine (C-F) bonds. These bonds impart exceptional chemical and thermal stability resulting in their widespread use in various applications. However, their persistence in the environment—evident from their detection in soil, water, and human blood globally—has highlighted the urgent need for effective methods to decompose and remove these chemicals from the environment.

To address the challenge of PFAS remediation in water, several technologies are employed. One promising approach is Electron Beam (EB) technology [1], which has shown efficacy in neutralizing such stubborn pollutants. However, effective PFAS treatment requires high dosages of EB, necessitating the development of high-power accelerators. Our research is centred on utilizing superconducting radio-frequency (SRF) technology to create a compact, high-current electron linear accelerator. In collaboration with KEK and the National Institute for Material Science (NIMS) in Japan, we are developing Nb₃Sn SRF cavities and designing an electron gun and buncher cavities at Research centre for accelerator and radioisotope science

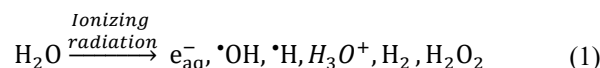
* Work supported by pioneering research support project by Tohoku University, Japan

[†] kavar.anjali.bhagwan.r4@dc.tohoku.ac.jp

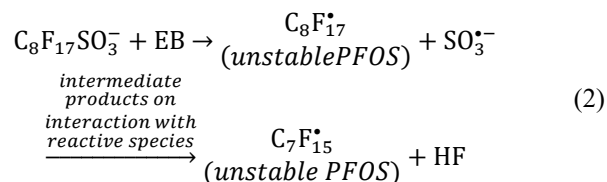
(RARiS), Tohoku University. We aim to develop a reliable and compact electron linac system that produces short electron bunches with minimal complexity and cost, utilizing a DC high voltage thermionic cathode for high current density and ease of maintenance.

EB WORKING

EB treatment [2, 3] is unique in that it produces highly oxidizing and reducing species simultaneously as shown in the Eq. (1) with the capability of generating these species higher than any other hydrolysis method.



Interactions of these species with impurities in water lead to the degradation of the contaminants. PFASs [4, 5] also after EB irradiation decomposes on interaction with these species as given in the Eq. (2).



The reaction chain continues to further cleave the C-F bonds reducing PFAS into less toxic and simple compounds. The destruction of PFAS by cleavage of these C-F bonds require doses of more than 100 kGy [1]. EB accelerator having the ability to provide 100s of kGy make EB treatment a practical and sustainable alternative for PFAS and wastewater treatment.

DESIGN & PARAMETERS

To design the accelerator for environmental applications, we need to set parameters such as beam energy and beam current. Specifically, the beam energy must be below 10 MeV to avoid inducing radioactivity in water. Additionally, lower energy levels allow for a smaller and more cost-effective accelerator. However, the penetration depth of electrons in water decreases with lower energy [6] as shown in the Fig. 1, complicating the construction of an effective irradiation system. Therefore, we chose a beam energy of 5 MeV, striking a balance between being neither too high nor too low. For beam current, there is no upper limit, but the achievable beam current is constrained by the available power coupler. As an initial target, we aim for a

DEVELOPMENT OF HIGH-POWER 4K Nb₃Sn SUPERCONDUCTING RF ELECTRON LINAC FOR MEDICAL RADIOISOTOPE PRODUCTION

S. Kashiwagi[†], A. B. Kavar, K. Shibata, H. Abiko, F. Hinode, H. Hama, K. Kudo, T. Muto, K. Nanbu, I. Nagasawa, K. Takahashi, H. Yamada,
Research Center for Accelerator and Radioisotope Science, Tohoku University, Sendai, Japan
K. Umemori, H. Sakai, H. Ito, T. Yamada, S. Shanab, KEK, Tsukuba, Japan
A. Kikuchi, S. Ooi, M. Tachiki, S. Arisawa, NIMS, Tsukuba, Japan

Abstract

Various radioisotopes (RIs) are used in the field of nuclear medicine for diagnosis, such as PET and SPECT. In recent years, RIs are applied to therapy of cancer and the actinium-225 has been confirmed to be effective in the therapy of advanced cancer. One of the promising RI production methods for medical application is the use of high-intensity beam in accelerators. In the case of an electron accelerator, a photonuclear reaction is used in the RI production process. We have started research and development of a 4K niobium-tin (Nb₃Sn) superconducting RF (SRF) electron accelerator system for RI production, which can be operated with a compact conduction cooling system and does not require a large-scale cooling system. As a first step, we plan to develop a single-cell Nb₃Sn superconducting cavity and a cryomodule, and to demonstrate its performance by beam acceleration experiments. In this presentation, we report the basic design of the SRF electron linear accelerator (linac) and R&D of Nb₃Sn SRF cavity.

INTRODUCTION

Radioisotopes (RIs) are widely used in nuclear medicine for nuclear diagnosis. In recent years, the use of RIs for medical use has taken a new development from diagnostics to therapy, as evidenced by the confirmation of the efficacy of RI-based internal therapy (Radionuclide Therapy, RNT) in therapy for cancer. In particular, the radionuclide therapy using actinium-225 (²²⁵Ac), an α -emitter RI, is attracting worldwide attention as a therapy for advanced cancer [1]. At present, ²²⁵Ac can only be produced with less than 100 GBq per year by a radioactive decay from thorium-229 (²²⁹Th) at research institutes in Germany, the U.S., and Russia. Three times doses of nuclear pharmaceuticals for one patient requires 20 MBq of ²²⁵Ac, therefore, it is difficult to deploy a full-scale radionuclide therapy worldwide at the current production rate. Medical RIs can also be produced using nuclear reactors and particle accelerators. Advantage of accelerator-based RI production can produce the required amount of RI when it is necessary. The ²²⁵Ac can be produced by the reaction of ²²⁶Ra(p, 2n)²²⁵Ac using proton beam. The amount of production cannot be increased by using the high intensity beam or a thick target, since the proton beam has a short range in a target material. On the other hand, in the case of ²²⁵Ac production by photonuclear reaction (γ, n) using electron beams, the amount of RI production can be increased by using a high

current electron beam and a thick target (Fig. 1). The advantage of this method using electron beam is that there are fewer impurities (unnecessary isotopes).

To achieve mass production of medical RIs using an electron accelerator, we have started research and development of a 4K niobium-tin (Nb₃Sn) SRF electron linac capable of high-current beam acceleration. From the development of SRF cavities in the United States, it is known that, in the case of a Nb₃Sn SRF cavity, the performance (Q_0) is almost equivalent to that of a bulk niobium SRF cavity cooled to 2 K by cooling the cavity to 4 K which can be achieved by conduction cooling [2]. Since a Nb₃Sn SRF cavity does not require a large-scale cooling plant, it is possible to construct a superconducting accelerator even in small facilities such as universities. As a first step, we plan to fabricate the S-band single-cell Nb₃Sn SRF cavity and build cryomodule with a conduction cooling for the SRF cavity. Experiments will be performed to demonstrate a beam acceleration using the Nb₃Sn cavity.

In this paper, we describe the basic design of the 35 MeV SRF linac for RI production and the demonstration of beam acceleration using the Nb₃Sn cavity.

RADIOISOTOPE PRODUCTION BASED ON ELECTRON ACCELERATOR

Bremsstrahlung γ -ray photons are generated by electron beam injecting a heavy metal such as platinum (Pt) or tantalum (Ta). Photonuclear reactions occur when atomic nuclei are excited via the capture of incident photons and relax by emitting one or several elementary particles or nuclei fragments. For photon energies below 30 MeV near the Giant Dipole Resonance (GDR), that are generally used for photonuclear production of RI production [3].

In the production of ²²⁵Ac using an electron beam, radium-226 (²²⁶Ra) is irradiated with γ -rays to produce radium-225 (²²⁵Ra) by photonuclear reaction, and then ²²⁵Ac is produced by its β -decay. The photonuclear reaction cross section of ²²⁶Ra is shown in Fig. 2 [4]. For efficient RI production, a large number of γ -ray photons around

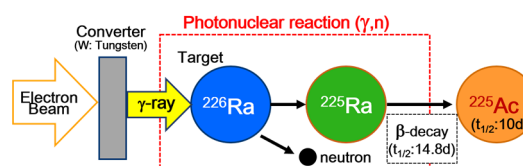


Figure 1: Actinium-225 (²²⁵Ac) production via photonuclear reaction.

[†] kashiwagi@raris.tohoku.ac.jp

DEVELOPMENT OF PLASMA PROCESSING OF 1.3 GHz SUPERCONDUCTING RADIOFREQUENCY CAVITIES AT TRIUMF

D. Hedji^{1,2,†}, R. E. Laxdal^{1,2}, P. Kolb¹, Z. Yao¹, V. Zvyagintsev¹, T. Junginger²

¹TRIUMF, Vancouver, B.C., Canada

²Department of Physics and Astronomy, University of Victoria, Victoria, B.C., Canada

Abstract

Superconducting Radio Frequency (SRF) technology is a key component in many particle accelerators operating in a continuous wave, or high duty cycle, mode. The on-line performance of SRF cavities can be negatively impacted by the gradual reduction in the accelerating gradient that can be attained within a reasonable field emission level. Conventional cleaning procedures are both time- and resource-exhaustive as they are done *ex-situ*. Plasma processing is an emerging *in-situ* method of cleaning which chemically removes hydrocarbon-based field emitters through plasma. An R&D program is underway at TRIUMF with the goal to develop fundamental power coupler (FPC) driven plasma processing of the installed 1.3 GHz nine-cell cavities in the ARIEL 30 MeV SRF eLINAC. Processing recipes have been systematically studied in single-cell and multi-cell cavities off-line. The progress on these developments will be reported.

INTRODUCTION

TRIUMF's Advanced Rare Isotope Laboratory (ARIEL) program includes a 3 mA, 30 MeV SRF electron linear accelerator (eLINAC) operating in continuous wave (cw) as a driver to produce radioactive ions through photo-fission [1,2]. The eLINAC consists of three 1.3 GHz nine-cell ARIEL cavities housed in two cryomodules; one within an "injector" module, and the remaining two residing in an "accelerator" cryomodule. Each cavity is specified to operate at a minimum accelerating gradient of 10 MV/m to achieve a threshold Rare Isotope Beam (RIB) production energy of 30 MeV.

The yield of the photo fission process is highly dependent on the electron energy, as seen in Fig. 1. Reductions in the cavity gradient significantly decrease RIB yield and must be avoided. Particulate contamination therefore poses a serious concern for operational efficiency. Field emitters reduce cavity performance through local heating effects and radiation emission, degrading the quality factor of the affected cavity.

Various techniques have been developed to mitigate field emission, but each suffer from some intrinsic limitation. Either large resource and time allocation is needed as they are done *ex-situ*, or they are insufficient at removing hydrocarbon contamination. Plasma processing is an *in-situ* cleaning technique that has been demonstrated to be effective for a number of linac facilities [4,5,6]. Plasma processing utilizes a mixture of an inert gas (i.e. helium or argon) and a reactive gas, oxygen, in the form of a glow discharge to chemically clean the inner cavity surface.

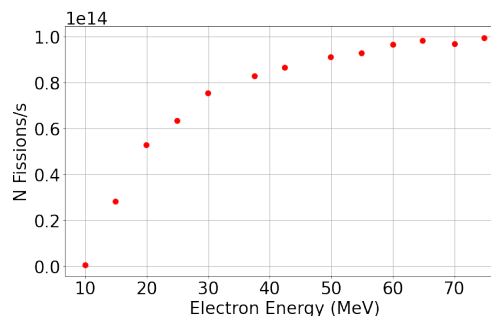


Figure 1: Photo-fission production rates as a function of electron energy for the ARIEL target stations [3].

TRIUMF is pursuing plasma processing for application at the eLINAC to derisk the potential of field emission reducing the available gradient past a point in which RIB yield is compromised. However, ignition through Higher Order Mode (HOM) couplers used in other applications of plasma processing cannot be directly applied on our current configuration. Specifically, the ARIEL cavities are a unique variant of the TESLA design, with modified end groups equipped with two FPCs each. HOM dampers are also utilized at the upstream and downstream beam pipe locations to absorb HOMs [7]. For this reason, we are exploring plasma ignition using FPCs in the TM_{010} passband. In this paper, we will report on our developments in single-cell and multi-cell structures.

METHODS

The apparatus is shown in Fig. 2. A gas supply system continuously injects the process gasses into the cavity, while a pumping system is used to remove byproducts from the plasma reaction. In addition, an RF system is used to excite the cavity fields to strike a plasma at a mode-dependent location. Figure 3 shows an example of a plasma generated within a 1.3 GHz single-cell cavity using this setup.

Gas Supply System

As part of our early studies we have chosen helium as the inert support gas. The gas supply system manages the gas flow within the cavity environment. Gas injection is done using a series of shutoff and leak valves to regulate the percentage of helium gas to oxygen gas, keeping oxygen levels within the range of 5–10%. Total gas pressure within the cavity is measured using a CDG-500 capacitance diaphragm gauge such that total pressure can be regulated to be within the range of 80 mTorr to 200 mTorr.

THE STATUS OF ARIEL e-LINAC RF SYSTEM*

Y. Ma †, K. Fong, P. Kolb, R.E. Laxdal, R. Leewe, K. Piletskiy, V. Zvyagintsev
TRIUMF, Vancouver, BC, Canada

Abstract

Now the stage of the 30 MeV portion of ARIEL (The Advanced Rare Isotope Laboratory) e-Linac (1.3 GHz, SRF) is under commissioning which includes an injector cryomodule (ICM) with a single nine-cell cavity and the 1st accelerator cryomodule (ACM1) with two cavities configuration. This paper is focused on the recent advances towards high power operation which includes ICM MRO and e-gun tuner upgrade, PID loop test, continuous operation test.

INTRODUCTION

ARIEL e-Linac is a continuous-wave (CW) superconducting electron linear accelerator. The ‘Demonstrator’ phase of ARIEL was installed for initial technical and beam tests with successful beam acceleration to 22 MeV [1]. The ACM1 cryomodule, initially installed with one cavity, was then updated to 2 cavities [2] but still driven by a single klystron in vector sum as shows in Fig. 1. 30 MeV beam has been achieved after ACM1 which energy gain is about 20.6 MeV [3, 4].

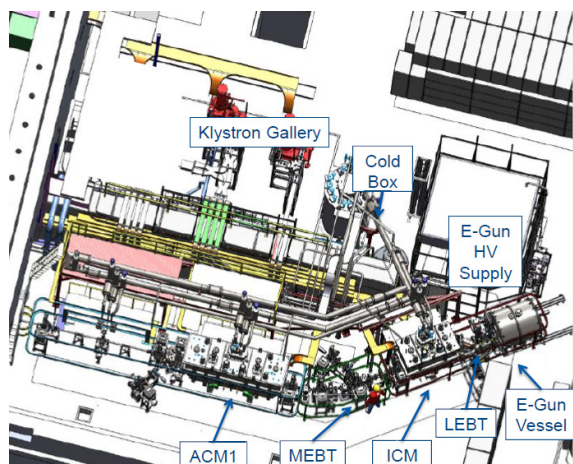


Figure 1: The present configuration of the e-Linac.

During the 2020-2021 shutdown, we made MRO for the ICM to recover performance. In 2021, 10 kW beam operation had been achieved with a 500 μ A beam, using an Iterative Learning Controller (ILC) for beam loading compensation [5], and in 2023 upgraded the e-gun RF tuner. At the beginning of 2024, we successfully maintained three days of continuous operation. Recently, to improve beam current stability due to temperature fluctuations, we implemented a PID loop for current regulation using the ACCT signal as feedback.

* TRIUMF receives funding via a contribution agreement with the National Research Council of Canada.

† mayanyun@triumf.ca

TEST PROGRESS

ICM MRO

The ICM cavity experienced a significant degradation in Q_0 due to pollution from venting and pumping. In 2016, the RF space of the ICM was vented too fast. Additionally, a 10 Torr pressure step occurred during pumping, increased the problem, particularly when the pressure dropped from 716 Torr to 708 Torr while the cavity was on the lower side.

Figure 2 illustrates the impact of these events. After the event, the cavity couldn’t operate at 10 MV/m due to strong field emission. After pulse conditioning, it became possible to run at 10 MV/m, though this was accompanied by strong x-ray emissions and a reduced Q_0 factor, around 4×10^9 . To prevent such operational errors, a slow pumping and venting system has been developed and implemented for each cryomodule. The ICM cavity was later refurbished in a clean room and pumped with slow venting/pumping system on beamline. The test results show successfully restoring its performance to a Q_0 factor of 1×10^{10} at a 10 MV/m gradient.

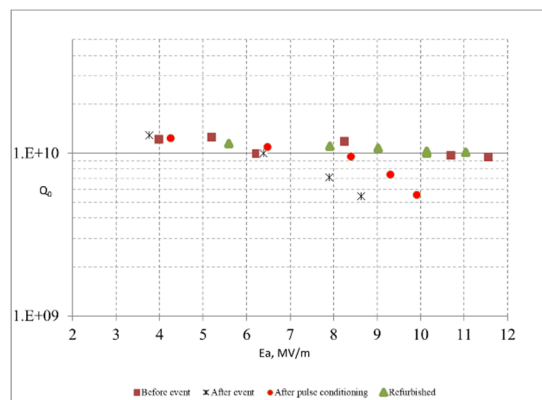


Figure 2: ICM Q_0 .

Iterative Learning Controller

The e-Linac must operate at much lower power levels during commissioning and beam development. To achieve this, the e-Linac is pulsed with varying repetition rates and pulse lengths, which results in significant transient beam loading in the SRF cavities. Especially when the beam power ramp-up, which is accomplished by increasing the duty factor.

To improve beam loading compensation, Iterative Learning Control (ILC) is employed in parallel with the constant-gain feedforward controller [5] in each cryomodule LLRF. With the optimized ILC controller parameters, it can effectively compensate beam loading with varying repetition rates and pulse widths, as shown in Fig. 3. The average beam power successfully reached 10 kW with a current of 500 μ A and an energy of 30.2 MeV.

PHYSICAL DESIGN OF THE INJECTOR FOR XIPAF-UPGRADING*

C.B. Yue^{1,2,3}, P.F. Ma^{1,2,3,4}, Q.Z. Xing^{†1,2,3}, B.C. Wang⁴, C.T. Du^{1,2,3}, S.X. Zheng^{1,2,3},
X.L. Guan^{1,2,3}, M.T. Zhao⁴, W.L. Liu⁴, M.W. Wang⁴, W. Lv⁴, Z.M. Wang⁴, X.W. Wang^{1,2,3}

¹Key Laboratory of Particle and Radiation Imaging, Tsinghua University, Ministry of Education, Beijing, China

²Laboratory for Advanced Radiation Sources and Application, Tsinghua University, Beijing, China

³Department of Engineering Physics, Tsinghua University, Beijing, China

⁴State Key Laboratory of Intense Pulsed Radiation Simulation and Effect, Xi'an, China

Abstract

This paper describes the physical design of one linac injector for the proton/heavy ion synchrotron, which is under construction for Xi'an 200 MeV Proton Application Facility (XiPAF) heavy ion upgrading project. A heavy ion linac injector will be constructed close to the existing proton linac injector. The heavy ion injector consists of one electron cyclotron resonance (ECR) source, one low energy beam transport (LEBT) section, one radio frequency quadrupole (RFQ) accelerator, one interdigital H-type drift tube linac (IH-DTL), and one linac to ring beam transport (LRBT) section. Heavy ion beams will be accelerated to 2 MeV/u. The unnormalized 99%-particles emittances at the injection point of proton and heavy ion are optimized to be lower than 10 and 16 π mm·mrad, respectively. Besides, low dispersion at the injection point is obtained to minimize the beam offset caused by the dispersion mismatch in the synchrotron. Three scrapers are installed in the LRBT to meet the requirement of emittance and dispersion.

INTRODUCTION

Xi'an 200 MeV proton application facility (XiPAF) is the first facility in China specifically designed to simulate space radiation environments. It was officially launched in 2014 and completed overall beam emission in 2020 [1–3]. XiPAF can currently provide a stable proton beam of 20~200 MeV, and the on-target particle flux can reach an adjustable range of $10^5 \sim 10^8$ p/cm²/s [3]. XiPAF is currently composed of a negative hydrogen ion linac, a medium energy beam transport line (MEBT), a proton synchrotron [4], a high energy beam transport line (HEBT), and an experimental target station.

In recent years, the demand of heavy ion single event effect (SEE) experiments is rapidly increasing. The XiPAF-upgrading project has been proposed in order to improve the heavy ion SEE experimental facilities. Based on the proton synchrotron at present, a new heavy ion injector will be constructed to provide heavy ions with a charge-mass ratio in the range of 1/3 ~ 1/6.5, at the energy of 2 MeV/u.

The heavy ion injector consists of an electron cyclotron resonance (ECR) heavy ion source, an low energy beam transport (LEBT), an radio frequency quadrupole (RFQ), an interdigital H-type drift tube linac (IH-DTL), and a linac to ring beam transport (LRBT) section. The RFQ and IH-DTL can accelerate heavy ions to 400 keV/u and 2 MeV/u respectively, which can meet the injection energy requirement of the synchrotron. For the proton injector, existing RFQ and Alvarez-DTL will be reused, and modifications will be mainly made on ECRIS and LRBT.

The overall conceptual design has been completed [5], and this article mainly introduces the physical design of the entire linear injector.

REQUIREMENT OF THE INJECTOR

Because there are various kinds of heavy ions, Bi³²⁺ ions with the smallest charge-mass ratio are selected for heavy ion injector optimization design. The type of proton source has changed from the H⁻ to H⁺ due to the change of injection method from stripping injection to multiturn injection. The requirement parameters of the injector are shown in Table 1. The sketch diagram of the whole injector is shown in Fig. 1.

Table 1: Design Parameters of the Linac Injector

Parameter	Proton	Heavy ion
Injected ion	H ⁺	C ⁴⁺ ~ Bi ³²⁺
Charge-mass ratio	1	1/3 ~ 1/6.5
Injection energy	7 MeV	2 MeV/u
Peak current exit of the ECRIS	20 mA (H ⁺ , H ₂ ⁺)	50 e μ A (Bi ³²⁺)
Injected current	2~4 mA	≥ 17 e μ A (Bi ³²⁺)
Unnorm. emit. 99%-particles	$\leq 10\pi$ mm·mrad	$\leq 16\pi$ mm·mrad
Momentum spread 99%-particles	$\leq 0.3\%$	$\leq 0.3\%$
RF Frequency	325 MHz	108 MHz
Repetition rate	0.1 ~ 0.5 Hz	0.1 ~ 0.5 Hz
Beam pulse width	60 ~ 100 μ s	60 ~ 100 μ s

* Work supported by the National Natural Science Foundation of China (Grant No. U1730120 and 11975138) and the fund of the State Key Laboratory of Intense Pulsed Radiation Simulation and Effect (Grant No. SKLIPR2001).

† xqz@tsinghua.edu.cn

IMPACT OF COHERENT SYNCHROTRON RADIATION EFFECT ON GENERALIZED LONGITUDINAL STRONG FOCUSING INSERTION UNIT*

Jihong Bian, Zizheng Li, Wenhui Huang[†], Chuanxiang Tang

Department of Engineering Physics, Tsinghua University, Beijing, China
Xiujie Deng, Institute for Advanced Study, Tsinghua University, Beijing, China

Abstract

The generalized longitudinal strong focusing (GLSF) scheme is a potential approach for a steady-state microbunching (SSMB) storage ring, leveraging the ultra-low vertical emittance in the storage ring. It achieves active vertical-longitudinal coupling through an insertion unit, further compressing bunch length from the hundreds of nanometers scale in the main ring to the nanometers scale, thus emitting coherent radiation. Due to the extremely short bunch length, coherent synchrotron radiation (CSR) effect may significantly impact beam dynamics. We developed a particle tracking program based on one-dimensional CSR model to preliminarily evaluate the influence of CSR effect in the GLSF scheme under current design parameters. Our work contributes to the future optimization of the GLSF scheme.

INTRODUCTION

Steady-state microbunching (SSMB) storage ring [1-4] is a promising solution for high average power and high peak power extreme ultraviolet (EUV) light source. In principle, SSMB storage rings can stably form electron bunches with nanometer-scale lengths per revolution, capable of generating coherent EUV radiation. The generalized longitudinal strong focusing (GLSF) [5] is a possible SSMB scheme. In the GLSF scheme, the main ring is a low-alpha ring, where hundreds of nanometer-scale bunch lengths are achieved using laser modulators with modulation wavelengths much shorter than traditional RF cavities in conventional storage rings. The core of the GLSF scheme is an insertion unit. Through active vertical-longitudinal coupling, this section projects the inherently ultra-low vertical emittance of the storage ring into the longitudinal direction, further compressing the bunches from the main ring to nanometer-scale for radiation generation. To achieve steady-state operation, the latter part of the insertion unit decouples the bunches after radiation emission and returns them to the main ring.

In a typical layout of the GLSF insertion unit, there are four vertically dispersive lattice sections, labeled as part 1-4, along with two laser modulators, MOD1 and MOD2, as illustrated in Fig. 1. Bunch compression is achieved through the combined action of part1, MOD1, and part2.

To maintain the steady-state operation, the beam must return to an uncouple and unmodulated state after passing through the whole insertion unit. Therefore, part3 is introduced to form an isochronous and achromatic lattice, together with part2, allowing MOD2 to directly eliminate the modulation caused by MOD1 through an opposite modulation. Finally, part4 clears out any remaining vertical-longitudinal coupling effects. Note that the drastic variations of bunch length occur in part2 and part3.

Coherent synchrotron radiation (CSR) effects become particularly pronounced when short bunches pass through bending magnets, potentially adversely affecting beam quality by increasing beam energy spread and causing transverse emittance dilution. In the GLSF insertion unit, where the bunch length is extremely short and varies significantly, CSR effects may prevent the beam from compressing to the expected length at radiation spot. Additionally, it may also interfere with the cancellation of modulation, thereby disrupting the maintenance of the steady-state operation. To assess the impact of CSR, we have developed a particle tracking program that incorporates CSR effects based on linear beam dynamics. We have evaluated and analyzed the influence of CSR in the GLSF insertion unit using the current design parameters. And we found that the influence is acceptable for a single pass case.

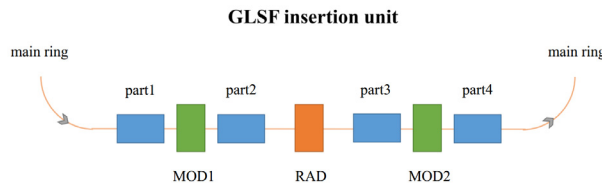


Figure 1: GLSF insertion unit layout.

SIMULATION METHOD

The theory of CSR has been extensively studied. Currently, the most commonly used model in particle tracking programs is the one-dimensional CSR wakefield model, which treats the beam as a thread charge distribution. Murphy et al. [6] have provided a detailed description of the one-dimensional steady-state CSR model. The CSR wake can be expressed as:

$$w(\mu) = \frac{\gamma^4}{3\pi\epsilon_0\rho^2} \phi(\mu), \quad (1)$$

* Work supported by the National Natural Science Foundation of China (NSFC Grant No. 12035010)

[†] huangwh@mail.tsinghua.edu.cn

COMPACT FIELD EMISSION ELECTRON GUN DRIVEN BY THz WAVE*

W. Yu, K. Peng, S. Fan, Y. Fu, L. Wang, C. Song, W. Huang[†]
 Department of Engineering Physics, Tsinghua University, Beijing, China

Abstract

Accelerator-based light sources require high brightness electron beams to improve performance in exploring structure of matter. Higher acceleration gradient is the key to generate high brightness electron beams and is more feasible with higher frequency and shorter pulse length electromagnetic wave according to previous empirical formulas. A tapered rectangle waveguide structure driven by terahertz (THz) wave is designed as a compact electron gun. A nanotip is fabricated by focused ion beam (FIB) in the centre to enhance the field and to emit electrons. The average emission charge per pulse is measured by a Picoammeter, and the peak value reaches 10 fC. The max electron energy beyond 4 keV is measured from the signal of channel electron multiplier behind a -4 kV metal grids, revealing that maximum acceleration gradient is beyond 100 MeV/m. These results indicate promising performance of compact THz electron gun in high brightness electron injection. Further research will be done in the future.

INTRODUCTION

Compact terahertz (THz) electron accelerators and injectors have emerged as an active research focus with the development of strong-field THz technologies, providing the

potential for high-gradient acceleration as suggested by previous empirical formulas [1, 2]. This capability is beneficial to generating high-brightness electron bunches, thereby enhancing the performance of accelerator-based light sources for the investigation of matter's structure. THz-driven acceleration of electron beams has been achieved with an effective acceleration gradient of 85 MeV/m and an energy gain of up to 204 keV [3]. The electron beam emitted by THz photocathode electron gun, with a charge of approximately 10 fC, achieves a maximum electron energy of 14 keV [4]. This corresponds to an acceleration gradient of approximately 280 MeV/m, which is much higher than that of an X-band photogun, yet the maximum electron energy is significantly lower. Further research is required to enhance the performance of THz accelerators and electron guns.

In this paper, we report on the setup of experimental platform for THz electron guns research in Tsinghua University. Beam experiments were carried out using the designed compact THz field emission gun. Emission charges up to 10 fC were obtained with the maximum energy detected exceeding 4 keV. This corresponds to an acceleration gradient over 100 MeV/m, which was limited by our available THz pulse energy. Despite the limitation, it shows promising high-gradient acceleration capabilities.

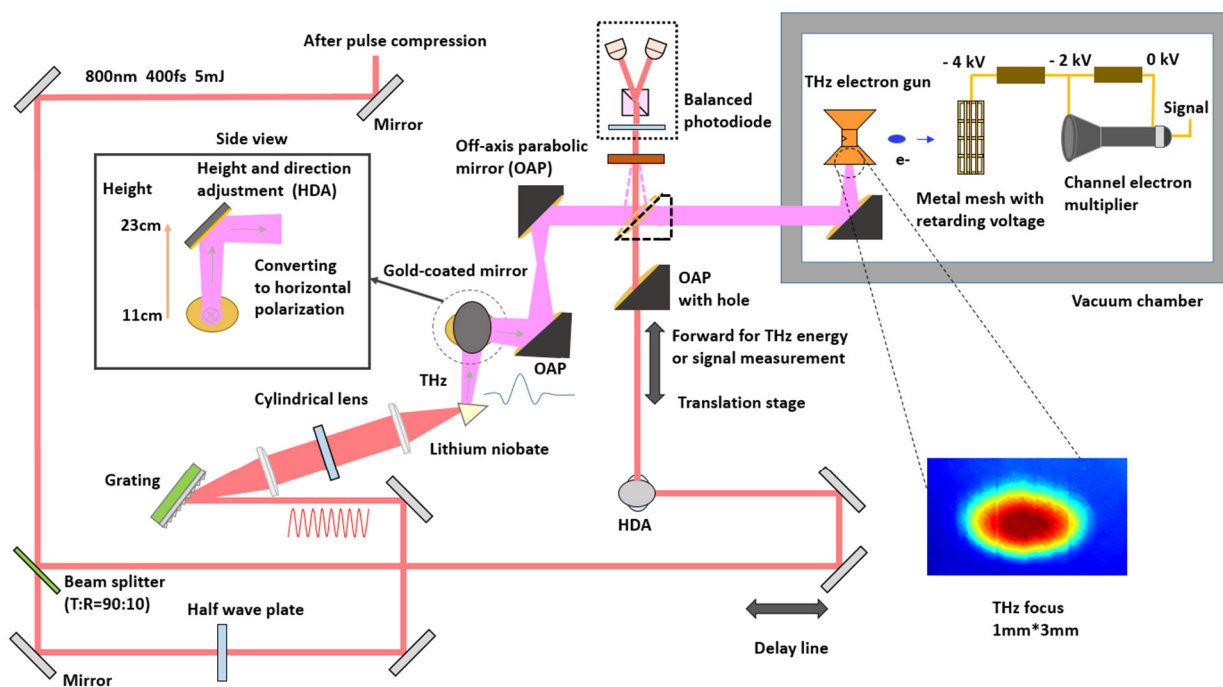


Figure 1: The schematic layout of the experiment.

* This work is supported by National Natural Science Foundation of China (NSFC Grant No. 12035010).

[†] huangwh@mail.tsinghua.edu.cn

DESIGN AND SIMULATION OF VIRTUAL PEPPER-POT METHOD FOR LOW ENERGY PROTON BEAM

E. Cosgun*, M. S. Hur, Ulsan National Institute of Science and Technology, Ulsan, South Korea
 S. Moon, D. Kim, Korea Multipurpose Accelerator Complex, Gyeongju, South Korea
 M. Chung, Pohang University of Science and Technology, Pohang, South Korea

Abstract

The Virtual Pepper-Pot (VPP) is a 4D transverse phase space measurement technique based on pepper-pot-like patterns that are generated by crossing each measured horizontal slit-based beamlet with all measured vertical slit-based beamlets. The VPP beam phase space distribution reconstruction and simulation are performed using the Beam Delivery Simulation (BDSIM) code, which is a Geant4 toolkit. The configuration includes a VPP 3D model slit, a scintillator screen, and a user-defined 1 MeV energy and 10 mA current proton beam distribution, characteristic of the KOMAC RFQ beam test stand. Besides VPP, pepper-pot mask simulation is carried out, and the intensity and emittance differences are observed. The input beam distribution is generated from a TraceWin output file for comparison of results. The comparison between the VPP analysis results and the TraceWin input shows satisfactory results, ensuring accurate estimation of the emittance.

INTRODUCTION

The measurement and analysis of transverse phase space in particle beams are vital for optimizing accelerator performance and improving beam quality. Traditional techniques, such as slit-based and pepper-pot methods, have been widely used for these measurements. Besides these, the Virtual Pepper-Pot (VPP) technique has been developed to achieve high resolution and to provide fast scanning, offering a novel approach to 4D transverse phase space measurements.

The VPP technique generates pepper-pot-like patterns by crossing horizontal slit-based beamlets with vertical slit-based beamlets, providing a comprehensive view of the beam's phase space distribution [1]. This method is implemented using the Beam Delivery Simulation (BDSIM) code [2], a sophisticated simulation tool based on the Geant4 [3] toolkit. BDSIM allows to simulate both the transport of particles in an accelerator and their interaction with the accelerator material.

A key application of the VPP technique is its use in the Korea Multi-purpose Accelerator Complex (KOMAC) Radio Frequency Quadrupole (RFQ) beam test stand. Here, a user-defined proton beam distribution with 1 MeV energy and 10 mA current is employed. The simulation configuration includes a 3D model slit and a scintillator screen, considering the main beam parameters of test stand.

To validate the VPP method, simulations are compared with traditional pepper-pot mask techniques. These compar-

isons focus on intensity and emittance differences, providing insights into the advantages of VPP over conventional methods. Additionally, the input beam distribution is generated from a TraceWin output file, allowing for a direct comparison between VPP analysis results and TraceWin inputs. The satisfactory agreement between these results highlights the accuracy and reliability of the VPP technique in estimating emittance.

This paper aims to present a comprehensive overview of the VPP technique, its construction, and its validation through comparative analysis.

KOMAC BEAM TEST STAND LAYOUT

Radio-Frequency Quadrupole Beam Test Stand (BTS) is a proton accelerator structure at Korea Multipurpose Accelerator Complex (KOMAC) that accelerates beams to 1 MeV/n. In addition to the microwave ion source, an LEBT, and an RFQ, the BTS consists of two beamlines, each with triple quadrupole magnets and a wire scanner. A detailed ion source extraction simulation study [4] shows that beams are transmitted to LEBT with 25 keV energy and 10~15 mA current.

There are two beamlines at the KOMAC BTS, one of which has a straight beamline (BL1) and another consisting of a bending magnet at 30°. Since the phase space measurement will be carried out BL1 in this study we will focus on this beamline. The BL1 features four small quadrupoles immediately after the RFQ and has a triplet quadrupole structure to optimize beam transportation to the target chambers by adjusting the quadrupole gradients. The TraceWin code [5] shows that the beam distribution from RFQ exit is fully transmitted to diagnostic chamber. Figure 1 gives the RMS beam trajectories along the beamline, and the horizontal and vertical phase space distributions at the measurement point are given in Fig. 2.

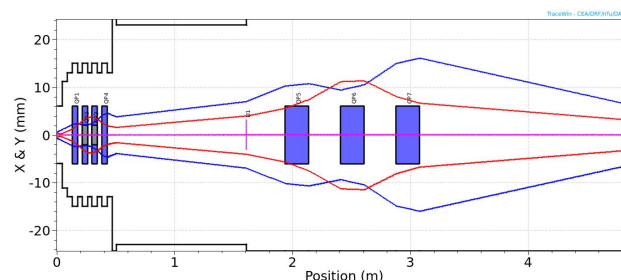


Figure 1: KOMAC BTS straight beam line envelope simulation. Blue line indicates x axis while red shows y axis.

* emrecosgun@unist.ac.kr

CHROMATIC INDEX TO FIND A WORKING POINT FOR A 4TH GENERATION SYNCHROTRON LIGHT SOURCE

E. Sánchez^{*,1}, A. Flores-Tlalpa², J. Hernández-Cobos¹, M. Moreno³, A. Antillón¹

¹Instituto de Ciencias Físicas, Universidad Nacional Autónoma de México, Morelos, México

²Departamento de Bioingeniería y Ciencias, Tecnológico de Monterrey, Puebla, México

³Instituto de Física, Universidad Nacional Autónoma de México, Cd. de México, México

Abstract

Optimizing the electron dynamics generated by MBA cells involves adjusting a large number of parameters while meeting complex constraints. These optimizations are typically performed using methods that involve calculating standard nonlinear functions, such as dynamic aperture. These methods are often computationally expensive. Recently, a quasi-invariant surface technique for optimizing nonlinear electron dynamics in storage rings has been reported. Building on this approach, a framework for optimizing the linear parameters of a lattice without the need for particle tracking, or similar nonlinear calculations, is proposed. This framework enables the definition of the distorted chromatic index $\zeta_{D,\delta}$, a valuable function for analyzing and tuning a cell to identify a suitable working point for a machine. As an example, these techniques are applied to identify a working point for a ring model based on a 7BA cell, which comprises 20 cells and has a circumference of approximately 490 meters. After conducting nonlinear optimization, this approach achieves stable horizontal amplitudes exceeding 5 mm for momentum deviations between -3% and 3% .

INTRODUCTION

Fourth-generation synchrotron light sources heavily rely on MBA cells. However, controlling the complex electron dynamics generated by these magnetic structures presents significant challenges. For instance, adjusting numerous parameters and meeting stringent constraints require sophisticated and computationally intensive tools. To address these challenges, various techniques are employed, including global analyses of storage ring lattices [1], global optimizations of storage ring lattices [2], frequency map analysis [3], and the calculation of dynamic and momentum apertures using particle tracking [4, 5]. Additionally, methods such as minimization of resonance driving terms [6–8] and hybrid or unconventional approaches [9–14] are also used. However, to the best of our knowledge, there are few studies focused on optimizing the linear designs of a cell [1, 2], and no established protocols specifically address this type of optimization without relying on typical nonlinear functions, such as dynamic aperture.

Recently, polynomial quasi-invariants of motion [15–18] have been employed to optimize the nonlinear design of a fourth-generation synchrotron light source storage ring [19]. This approach eliminates the need for particle tracking cal-

culations, thereby reducing the reliance on costly computational resources. Here, we propose a framework that extend this approach to optimize the linear parameters of a lattice without requiring particle tracking or other similar nonlinear calculations. This framework utilizes the distorted chromatic index $\zeta_{D,\delta}$, a valuable tool for analyzing and tuning a cell to identify a suitable working point for a machine. As an example, this technique is used to identify a working point for a ring model based on a 7BA cell, which consists of 20 cells and has a circumference of approximately 490 meters. Following nonlinear optimization, this approach enhances the horizontal dynamics of the ring.

THE METHOD

The work in Ref. [6] demonstrates that a storage ring can be modeled using a two-dimensional nonlinear Hamiltonian that incorporates chromatic effects

$$H(x, p_x, y, p_y, s) = \frac{1}{2}(p_x^2 + p_y^2) (1 - \delta + \delta^2 + \dots) - b_1(s) x \delta + \frac{b_1^2(s)}{2} x^2 + \frac{b_2(s)}{2} (x^2 - y^2) + \frac{b_3(s)}{3} (x^3 - 3xy^2) + \frac{b_4(s)}{4} (x^4 - 6x^2y^2 + y^4) + \dots, \quad (1)$$

where the functions $b_1(s)$, $b_2(s)$, $b_3(s)$, and $b_4(s)$, are related to the magnetic field derivatives, and $\delta = \frac{\Delta p}{p_0}$ is the percentage deviation from the momentum p_0 . A quasi-invariant polynomial surface [18, 19] can be associated with this system. Up to order δ^2 , it can be written as follows

$$S(x, p_x, y, p_y, \delta) = \sigma_1 + \sigma_{nl} + \sigma_{\delta 1} \delta + \sigma_{\delta 2} \delta^2, \quad (2)$$

with σ_1 , σ_{nl} , $\sigma_{\delta 1}$ and $\sigma_{\delta 2}$ its non-chromatic linear, non-chromatic nonlinear, first-order chromatic and second-order chromatic contributions, respectively.

After substituting Eq. (2) into the invariance condition

$$\frac{d}{ds} S = \{S, H\} + \frac{\partial}{\partial s} S = 0, \quad (3)$$

* esanchez@icf.unam.mx

MICROSCOPIC UNDERSTANDING OF THE EFFECTS OF IMPURITIES IN LOW RRR SRF CAVITIES*

K. Howard[†], Y.-K. Kim, University of Chicago, Chicago, IL, USA

D. Bafia, Z. Sung, W. Dzedzic-Misiewicz, Fermi National Accelerator Laboratory, Batavia, IL, USA

Abstract

The SRF community has shown that introducing certain impurities into high-purity niobium can improve quality factors and accelerating gradients. We question why some impurities improve RF performance while others hinder it. The purpose of this study is to characterize the impurities of niobium coupons with a low residual resistance ratio (RRR) and correlate these impurities with the RF performance of low RRR cavities so that the mechanism of impurity-based improvements can be better understood and improved upon. The combination of RF testing, temperature mapping, frequency vs temperature analysis, and materials studies reveals a microscopic picture of why low RRR cavities experience low BCS resistance behavior more prominently than their high RRR counterparts. We evaluate how differences in the mean free path, grain structure, and impurity profile affect RF performance. The results of this study have the potential to unlock a new understanding on SRF materials and enable the next generation of high Q/high gradient surface treatments.

INTRODUCTION

As we approach the theoretical limit of niobium for superconducting radio-frequency (SRF) cavities, the last decade has brought immense improvements in quality factor (Q_0) and accelerating gradients though intentionally added impurities into the niobium surface [1, 2]. Many SRF studies follow a “clean bulk dirty surface” technique to optimize the BCS resistance (R_{BCS}) by adding impurities to the surface layer of high purity niobium such as nitrogen through N-doping and oxygen through a low temperature bake [3–10].

The success of intentionally added impurities to the niobium surface has drawn deeper questions about how these impurities affect cavity behavior, and has prompted an investigation of cavities with a low residual resistance ratio (RRR). Low purity niobium has been studied previously for the purpose of cost reduction and possible high Q_0 [11]. In this study, we look at the intrinsic impurities as a resource to optimize the R_{BCS} and understand the mechanism of impurity-based improvements. From the free electron model and the Wiedemann-Franz law, RRR and mean free path (mfp) have a direct relationship $l(nm) \approx 2.13 \cdot RRR$ [12]. As a result, we might expect to experience low R_{BCS} behavior at low

RRR, as seen in Fig. 1. We ask if the intrinsic impurities can improve performance, as we observe in extrinsic impurities.

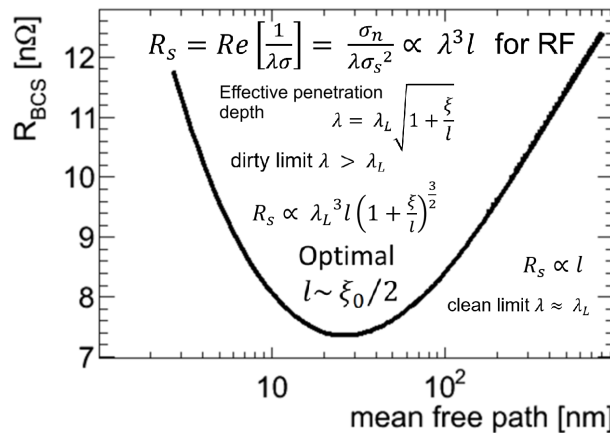


Figure 1: A moderately dirty surface optimizes the BCS resistance versus mean free path, adapted from [13].

RESULTS

Cavity Performance

In this study, we investigate a single-cell TESLA-shaped 1.3 GHz low RRR cavity in electropolished (EP) condition, where the surface and bulk are uniform [14]. We measure the Q_0 at a given gradient by maintaining the cavity at its resonant frequency, inputting power via antenna, and then measuring the reflected and transmitted power [12]. We compare the performance of the low RRR cavity to a high RRR counterpart to understand how the intrinsic impurities affect RF behavior. In Fig. 2, we observe the lower Q_0 of the low RRR cavity at all gradients, which is expected from the increased dissipation and decreased thermal conductivity from intrinsic impurities.

The surface resistance is the geometry factor divided by Q_0 . R_{BCS} is the difference between the surface resistance at 2 K and low temperature (< 1.5 K). This component represents the breakdown of cooper pairs with increasing temperature [3, 15]. In Fig. 3, we highlight the low R_{BCS} of the low RRR cavity. The low mfp of the low RRR material does enable low R_{BCS} since it is much closer to the optimal value, recalling Fig. 1.

Material Characterization

We conduct a sample study using low RRR coupons cut from the same sheet as the cavity to correlate the RF behavior with the material properties. In EP condition, we measure the ratio of the resistivity at room temperature to its residual

* This manuscript has been authored by Fermi Research Alliance, LLC under Contract No. DE-AC02-07CH11359 with the U.S. Department of Energy, Office of Science, Office of High Energy Physics. This work was supported by the University of Chicago.

[†] khoward99@uchicago.edu

FABRICATION STATUS OF PRODUCTION SSR1 JACKETED CAVITIES FOR PIP-II AT FERMILAB*

T. Aiuzzi[†], M. Parise, L. Grassellino, D. Passarelli, FNAL, Batavia, IL, USA

Abstract

This paper provides an overview of the current fabrication status of superconducting SSR1 spoke cavities intended for integration into the PIP-II SRF linac at Fermilab. It explores the ongoing development and fabrication processes of the jacketed SSR1 cavity, highlighting key modifications made in the mechanical design to enhance structural integrity.

INTRODUCTION

The Proton Improvement Plan II (PIP-II) project aims to upgrade the accelerator complex at Fermilab to produce the world's most intense high-energy neutrino beam for the Deep Underground Neutrino Experiment at the Long-Baseline Neutrino Facility (LBNF). This upgrade includes the development of a linear particle accelerator with five types of Superconducting Radio Frequency (SRF) cavities: Half-Wave Resonator (HWR), Single-Spoke Resonator 1 (SSR1), Single-Spoke Resonator 2 (SSR2), and low-beta and high-beta 650 MHz elliptical cavities (LB650 and HB650) [1].

Operating at 325 MHz, the SSR1 cryomodules will use continuous wave RF power to accelerate H- beams from 10 MeV to 32 MeV (Table 1) [2]. The mechanical design of the SSR1 cavities has been presented in an earlier work [3]. After finalizing the design by adding four reinforcement ribs to the endwalls, the production of nine SSR1 cavities has started. This paper presents the final design revision and the current status of cavity fabrication and processing.

Table 1: Parameters of the SSR1 Cavity

Parameter	Value
Nominal Frequency	325 MHz
Target Frequency Allowable Error	± 50 kHz
MAWP @ RT	2.05 bar
MAWP @ 2 K	4.1 bar

FINAL DESIGN REVISION

The structure of the bare cavity consists of four main components Electron Beam (EB) welded together: the two endwalls, the shell, and the spoke [4]. The endwalls are the most challenging components to form, and they are manufactured using the metal spinning technique. This technique provides a more reliable forming process by minimizing the risk of tearing, but it does result in a significant reduction in thickness. A maximum thickness reduction of 30%

* This manuscript has been authored by Fermi Research Alliance, LLC under Contract No. DE-AC02-07CH11359 with the U.S. Department of Energy, Office of Science, Office of High Energy Physics.

[†] taiazz@fnal.gov

was observed in the endwalls, necessitating the addition of reinforcing ribs.

Reinforcing Ribs

Four niobium ribs are welded to each endwall and connected to a reinforcing ring (Fig. 1).

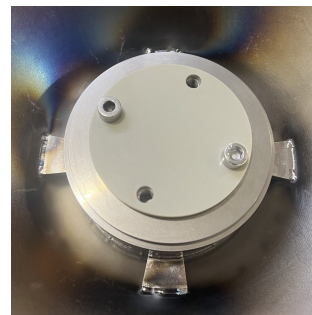


Figure 1: Welded reinforcing ribs.

The design accounts for both structural integrity and the feasibility of the welding process. The cavity is engineered to withstand an external Maximum Allowable Working Pressure (MAWP) of 0.205 MPa. At an operational temperature of 2 K, this MAWP increases to 0.410 MPa. Additionally, an internal pressure load up to 0.205 MPa, which could result from helium leakage into the main volume during the warm-up process, was also considered. The cavity has a tuning range of 0.26 mm.

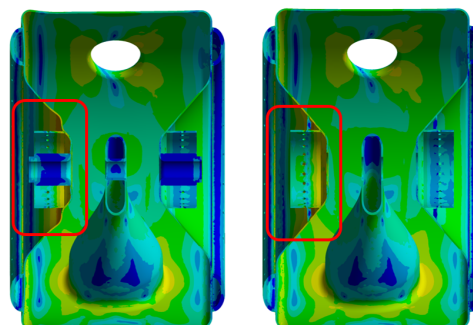


Figure 2: Mechanical analysis of a SSR1 bare cavity without ribs (left) vs with ribs (right).

The Fermilab ES&H manual mandates that the cavity be rated for a MAWP in accordance with the relevant sections of the ASME Boiler and Pressure Vessel Code [5]. In compliance with Chapter VIII, Division 2 (Design by Analysis), several finite element analyses have been performed using ANSYS [6] to determine the MAWP of the cavity, considering the reduced thickness of the endwalls and the addition of the reinforcing ribs. These analyses ensure that the cavity

LONGITUDINAL BEAM DYNAMICS OPTIMIZATION FOR INFRARED TERAHERTZ FEL LINAC

Y. M. Yang, S. C. Zhang, Z. G. He, G. Y. Feng[†]
University of Science and Technology of China, Hefei, China

Abstract

The high-repetition-rate infrared terahertz free-electron laser (IR-THz FEL) facility is progressing in the preliminary research stage, which can achieve the demand for a tunable high-power light source in the long wavelength spectrum and form a complementary structure of advantages with the Hefei Advanced Light Facility (HALF). In this paper, we present the design of a bunch compressor, enabling compress the bunch length to reach the peak current of 118 A. We also introduce an approach to optimize the RF parameters for the accelerating modules, which makes it feasible to generate a high-quality beam bunch that can reach the requirements for future FEL applications.

INTRODUCTION

The paper introduces the design and optimization of a high-repetition-rate IR-THz FEL facility [1–4], which leverages optical resonator-based FEL technology to achieve a higher mean power output by increasing pulse frequency. Electron beam of the facility will be generated from a photocathode RF gun injector and further accelerated with a superconducting linear accelerator. The C-type bending magnet chicane is used to increase the peak current by compressing the bunch length. During the beam dynamics simulations, space charge effects, coherent synchrotron radiation (CSR) effects and longitudinal cavity wake field effects have been taken into account with the codes of ASTRA [5] and CSRTrack [6].

LAYOUT

The schematic layout of the IR-THz FEL facility is shown in Fig. 1. The injector consists of a photocathode RF gun, an L-band accelerating section and a third-harmonic accelerating section. The electron bunches are generated by using a normal conducting 1.3 GHz RF gun.

reaching 5 MeV [7-8]. After the gun, the electron bunches are accelerated in a superconducting 9-cell TESLA cavity [9] with resonant frequency of 1.3 GHz: ACC1. Downstream of the ACC1 section, a third-harmonic RF system [10,11], operating at 3.9 GHz and referred to as ACC39, will be used to linearize the longitudinal phase space distribution with RF curvature distortion and to minimize the bunch tails in the subsequent chicane. The electron beam energy is 20 MeV at the exit of ACC39 section. There is a bunch compressor chicane (BC) with a C-type structure downstream of the ACC39 section. The beam energy is increased to 58 MeV after passing through the main linac, which is equipped with two L-band superconducting 9-cell TESLA cavities, named ACC2.

The IR-THz FEL will operate in the oscillator mode, which generates FEL radiation with wavelengths ranging from 5 μm to 1000 μm . After the ACC1 section, electron bunches are deflected to the undulator (U1) by a beam distribution system, and THz radiation with wavelength range of 200–1000 μm can be generated in the U1. Following the ACC2 section, the electron bunches are distributed into two distinct undulators, which generate mid-infrared (5–40 μm) and far-infrared (40–200 μm) radiation respectively.

BUNCH COMPRESSION

The linac-based free-electron laser require very short bunches of high-brightness electron beams with high peak currents. The bunches cannot be directly generated in rf-gun, as space charge forces would result in the deterioration of the beam quality in a short distance. Therefore, electron bunches must start with a low intensity and a few tens of Amperes peak current, and subsequently be accelerated to energy where the space charge effects are sufficiently weakened. In this case, the peak current can be increased by compressing the bunch length.

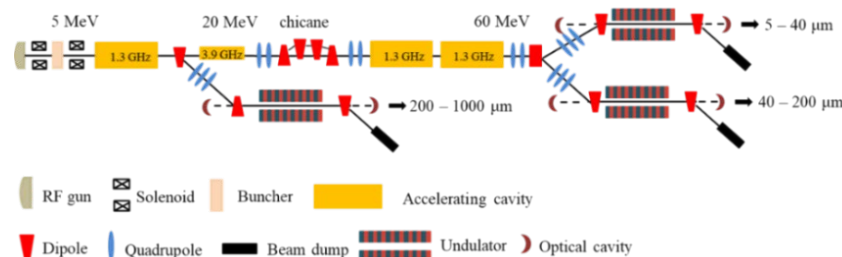


Figure 1: The schematic layout of the IR-THz FEL facility.

* Work supported by Supported by the Hundred-person Program of Chinese Academy of Sciences

[†] fenggy@ustc.edu.cn

PIP-II LINAC CRYOGENIC DISTRIBUTION SYSTEM DESIGN CHALLENGES

T. Banaszekiewicz*, M. Chorowski, P. Duda, M. Stanclik

Wroclaw University of Science and Technology, Wroclaw, Poland

R. Dhuley, A. Martinez, W. Soyars, Fermi National Accelerator Laboratory, Batavia, USA

Abstract

The PIP-II linac Cryogenic Distribution System (CDS) is characterized by extremely small heat inflows and robust mechanical design. It consists of a Distribution Valve Box (DVB), Intermediate Transfer Line, Tunnel Transfer Line, comprising 25 Bayonet Cans, and ends with a Turnaround Can. Multiple helium streams, each characterized by distinct helium parameters, flow through each of these elements. The CDS geometry allows maintaining an acceptable pressure drop for each helium stream, considering the planned flows and helium parameters in different operation modes. This is particularly crucial for the return line of helium vapors, which return from cryomodules to the cold compressors and thus have very restrictive pressure drop requirements. On both sides of the DVB there are fixed supports for process pipes. One of the DVB design challenges was to route the process pipes in such a way that their shape provided sufficient compensation for thermal shrinkage. This ensures that the forces resulting from thermal shrinkage acting on the cryogenic valves remain at a level acceptable to the manufacturer. The required thermal budget of the CDS was achieved by thermo-mechanical optimization of its components, like process pipes fixed supports in Bayonet Cans.

PIP-II CDS OVERVIEW

The Cryogenic Distribution System is tasked with providing cooling power from the cryogenic plant to the linear accelerator (linac) cryomodules. The simplified layout of the CDS is shown in Fig. 1.

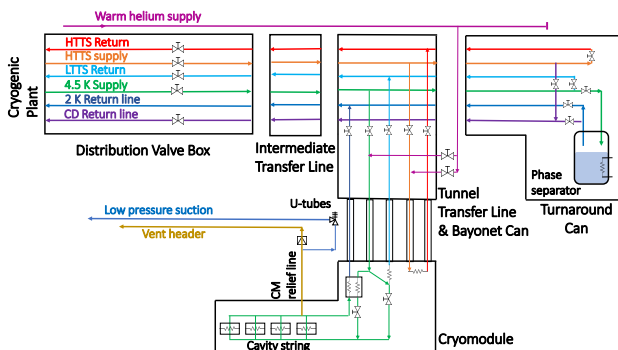


Figure 1: PIP-II CDS layout.

The linac consists of five distinct types of cryomodules, each of which is connected to the CDS via its own dismantable, bayonet connection for each process line. The CDS

spans approximately 285 meters, running from the Distribution Valve Box at the cryogenic plant interface, through twenty-five Bayonet Cans which are the points where the main helium stream branches into streams that supply the cryomodules, to the Turnaround Can at the linac's end.

The CDS process circuits with size of the main and the branch line and nominal operating conditions (temperatures and pressures) are:

- 4.5 K Supply - DN50/DN15 at 4.5 K and 2.9 bara
- 2 K Return - DN250/DN65 at 3.8 K and 3.1 mbara
- Low Temperature Thermal Shield Return (LTTS)- DN50/DN15 at 9 K and 2.9 bara
- High Temperature Thermal Shield Supply (HTTS-S) - DN50/DN20 at 40 K and 18 bara
- High Temperature Thermal Shield Return (HTTS-R) - DN50/DN20 at 80 K and 18 bara
- Cooldown Return (CD) - DN80/DN20 at 80 K

PRESSURE DROP

The first discussed challenge was designing the helium transfer line and the helium branched lines in such a way as to meet the constraints of allowable pressure drop budgets. Special attention was given to the helium vapor return line from the cryomodules (2 K Return line). This is a vacuum line used to return the evaporated helium stream from the cryomodules to the cold compressors located in the cryoplant building. During the design of the process lines, all operational modes had to be considered, from the cool-down of the installation through the nominal operating mode to emergency modes. Examples of the helium stream requirements in the nominal operating state and the corresponding pressure drop budget requirements are shown in Table 1.

Table 1: CDS Process Circuit Pressure Drop Budget

CDS circuit	Press. drop budget	Mass flow
HTTS	280 mbar	≥ 65 g/s
4.5 K Supply	30 mbar	≥ 172 g/s
LTTS Return	30 mbar	≥ 25 g/s
2 K Return	4.3 mbar	≥ 147 g/s

The calculations considered all influences on the pressure drop due to the geometry of the individual process circuits, including straight sections, elbows, tees, constrictions, valves, etc. Additionally, geometric constraints related to the actual placement of the individual system elements were taken into account in the calculations. For example,

* tomasz.banaszekiewicz@pwr.edu.pl

HIGH POWER TESTS OF AN ADDITIVE MANUFACTURING IH-TYPE CAVITY*

H. Hähnel^{1,2†}, A. Ateş¹, B. Dedić¹, J. Kaiser^{1,2}, C. Wagner¹, U. Ratzinger^{1,2}

¹Institute of Applied Physics, Goethe University, Frankfurt a. M., Germany

²Helmholtz Forschungsakademie Hessen für FAIR (HFHF), Frankfurt a. M., Germany

Abstract

Additive manufacturing (AM) has become a powerful tool for rapid prototyping and manufacturing of complex geometries. A 433 MHz IH-DTL cavity has been constructed to act as a proof of concept for direct additive manufacturing of linac components. In this case, the internal drift tube structure has been produced from 1.4404 stainless steel, as well as pure copper using AM. We present the most recent results from high power tests with the AM IH-type structure.

INTRODUCTION

A prototype IH-type cavity was constructed as the basis for a proof of concept of additive manufacturing for the production of linac structures (see Fig. 1). The cavity is designed to operate at 433.632 MHz and to provide a total acceleration voltage of 1 MV to a 1.4 MeV proton beam. The inner length of the cavity on the beam axis is 146 mm, resulting in an effective acceleration gradient of 6.8 MV/m at full design power [1–3]. AM of stainless steel stems or drifttubes with CNC postprocessing and copper plating has been implemented in some projects already [4, 5]. A recent focus of AM research for linac production has been production of pure copper parts [6–10]. In this paper we present first high power RF tests up to 25 kW, 5 MV/m with a 3D printed copper linac structure.

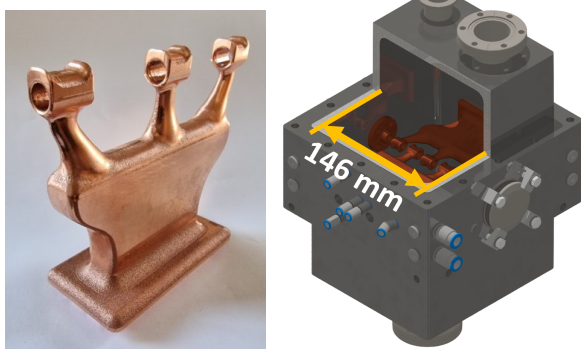


Figure 1: Printed copper parts after CNC post-processing (left) and cross-section of the cavity geometry (right).

EXPERIMENTAL SETUP

For the prototype, a stainless steel cavity was manufactured to house AM produced girder-drifttube structures to

* Work supported by BMBF 05P21RFRB2

† haehnel@iap.uni-frankfurt.de



Figure 2: Top view of the assembled prototype cavity with AM copper girders mounted. (AM copper components got a surface finish by CNC controlled milling.)

be tested. The inside of the test cavity was copper plated and is sealed by an aluminum wire backed by a pre-vacuum and o-ring (see Fig. 2). At the mount-point of the 3D printed drifttube structure, a similar vacuum seal with a pre-vacuum backed aluminum wire is performed interfacing directly on the printed part. Using this concept, reliable vacuum pressures around 1×10^{-7} mbar were achieved using stainless steel, as well as copper AM parts [2]. Due to its modular design and precision mounting points for the drifttube structures, multiple 3D printed structures could be tested in this cavity.

Printed Parts

To date, three different revisions of the drifttube structure were designed and printed from stainless steel and finally pure copper. The current revision features cooling channels running through the girder and up to just below the drifttubes. AM copper parts after manufacturing have a surface roughness in the order of $R_z = 15\text{--}30\ \mu\text{m}$. Therefore, for first tests with these structures, the contour of the parts was CNC machined to remove $200\ \mu\text{m}$ from all surfaces, providing a near mirror finish on the flat sides (see Fig. 1). Additionally, the sealing surfaces for the vacuum und water seals on the bottom of the printed part also have to be machined. In future investigations, the focus will be on achieving the same performance by utilizing surface polishing techniques to reduce the complexity of part manufacturing.

RF Coupler

Due to the small dimensions of the cavity and the largest flange size being CF40, a compact RF coupler had to be developed for high power RF tests. A first revision without any active cooling [2] was used for first low power condi-

SRF COAXIAL RESONATORS FOR HADRON ACCELERATION

P. Kolb*, R. E. Laxdal, TRIUMF, Vancouver, B.C., Canada

Abstract

SRF technology using niobium accelerating cavities enables high performance and efficient acceleration for modern accelerator projects. While electron LINACs accelerate particles with common structures designed for relativistic acceleration, hadron LINACs require acceleration over a broad velocity range. SRF technology is now being adopted at hadron energies in some cases starting from the RFQ exit but with top end energies such that a velocity range of a factor of ten has to be considered in the LINACs configuration and cavity design. Different structures in the TEM mode (coaxial) class (QWR, HWR, SSR, DSR) are employed with customized rf frequency, design beta and cavity structure. The coaxial cavities are now operating at very high performance rivaling the achievements in the 1.3 GHz elliptical cavities. This paper gives an overview of the state of the art of usage of coaxial cavities and highlights research on the performance of these cavities.

INTRODUCTION

Superconducting radio-frequency (SRF) cavities allow particle acceleration at high gradients in continuous wave (cw) operation due to the low surface resistance R_s and resulting high quality factors Q_0 . Over the past years, performance of SRF cavities have increased significantly. Both Q_0 and accelerating gradients E_{acc} have been increased due to improved surface preparation and novel heat treatments of the niobium material. Conventional treatments like the 120 °C/48hr vacuum bake result in a relatively constant Q_0 as a function of accelerating field, while new treatments like N2-doping [1] and O2 diffusion [2] result in Q_0 's that rise with increasing E_{acc} .

These new treatments were discovered using elliptical 1.3 GHz cavities operating at 2 K, which are the typical choice of cavity for e^- accelerators, such as EU-XFEL [3], LCLS-II [4], and SHINE [5]. While the gradient E_{acc} defines the accelerating performance, SRF cavity performance is bounded by the peak magnetic and electric rf fields at the cavity surface B_p and E_p . Nine-cell 1.3 GHz elliptical cavities used in pulsed, high gradient applications routinely reach accelerating gradients E_{acc} of 30 MV/m, which corresponds to peak surface magnetic fields B_p of 120 mT and electric surface fields of 60 MV/m. Performance of continuous wave (CW) electron linacs (LCLS-II) are specified at gradients near 20 MV/m corresponding to B_p values of 80 mT and $E_p = 40$ MV/m. As will be summarized in the next section, a new generation of large hadron LINACs are now being realized or developed with SRF sections starting at energies of a few MeV/u (ie $\beta \sim 0.06$) and extending to near relativistic energies. As elliptical cavities are only

practical for velocities of $\beta > 0.6$, the community relies on different variations of TEM mode coaxial resonators (quarter wave resonators (QWR) for $\beta < 0.15$ and half wave resonators (HWR) and single or double spoke resonators (SSR, DSR) for higher velocities) to span the 'low β ' velocity range. As the longitudinal emittance scales as $1/(\beta\gamma)$, cavities in the lower velocity range require lower frequencies to provide sufficient longitudinal acceptance favouring QWRs near 100 MHz with HWRs adopted for $f \sim 200$ MHz and SSRs around $f \sim 300$ MHz. The RF surface resistance R_s is inversely proportional to the quality factor Q_0 and for superconducting cavities follows

$$R_s = R_{BCS}(T) + R_{res} , \quad (1)$$

with R_{res} as a temperature independent residual resistance and R_{BCS} as temperature dependent resistance, which can be approximated [6] as

$$R_{BCS} = \frac{A}{T} \omega^2 e^{-\frac{\Delta}{k_b T}} , \quad (2)$$

with A as a material properties constant, T as temperature, ω as rf frequency and Δ as superconducting gap. The quadratic increase in R_{BCS} with ω means that lower frequency cavities like QWRs and HWRs can be operated near atmospheric pressure liquid helium ($T \sim 4.2$ K) while higher frequency cavities usually adopt operation below the λ point at $T = 2$ K.

Since the gap structure of a coaxial cavity is proportional to $\beta\lambda$ and the transverse dimensions are proportional to λ , the low β coaxial cavities have necessarily more compressed geometries than elliptical cavities with larger ratios of B_p/E_{acc} and E_p/E_{acc} . This results in lower accelerating gradients compared to $\beta = 1$ elliptical cavities but performances of coaxial resonators are now rivaling those reached in elliptical resonators in terms of achieved B_p and E_p .

Much of the SRF performance research has focused on the elliptical 1.3 GHz $\beta = 1$ cavity as the same cavity is used 100's to 1000's of times in many different projects worldwide. Developments include both efforts to increase Q_0 and E_{acc} to lower operating costs and decrease capital costs. On the other hand, for hadron accelerators, cavity designs are typically project specific with a few unique cavity types to cover the required velocity range. This makes dedicated performance research and development challenging to transfer between labs. Nonetheless there is a strong need for improved performance of TEM mode cavities as more hadron accelerators using SRF cavities come online. Not only high Q_0 and high E_{acc} are important topics for these accelerators, but also maintaining performance and reliability.

This paper will discuss the current landscape of SRF based hadron accelerators and showcase individual R&D, as well as covering dedicated, purpose-built research cavities from TRIUMF and JLab.

* kolb@triumf.ca

OPERATIONAL EXPERIENCE AND RELIABILITY OF THE NEW CERN LINAC4

E. Sargsyan*, A. M. Lombardi, G. Bellodi, J.-B. Lallement, P. K. Skowronski, R. Wegner
CERN, Geneva, Switzerland

Abstract

Since its completion in 2017, Linac4, the new 160 MeV proton injector for the CERN accelerator complex, has undergone some tests to assess and improve reliability, until being connected to the Proton Synchrotron Booster (PSB) during the 2018–2020 Long Shutdown 2 (LS2). The performance requirements for the LHC high-luminosity upgrade have been successfully met, and during its first three complete years of operation the linac has shown high reliability figures. Recent improvements of the H^- ion source enable the increase of the beam current from the nominal 35 mA to 50 mA, opening the possibility for increasing the intensity of the Booster beams, for the benefit of the experimental programmes. This paper presents the operational experience and reliability of Linac4 in its first three years of operation.

INTRODUCTION

Linac4 [1] is a normal conducting linac consisting of a 45 keV caesiated RF H^- ion source, Low Energy Beam Transport (LEBT), 3 MeV Radio Frequency Quadrupole (RFQ), Medium Energy Beam Transport (MEBT) with a chopper and 3 bunching cavities, 3 Drift Tube Linac (DTL) tanks up to 50 MeV, 7 Cell-Coupled DTL (CCDTL) modules up to 102 MeV, 12 Pi-Mode Structure (PIMS) cavities up to 160 MeV, and 1 de-buncher cavity, all resonating at 352.2 MHz. The chopper modulates the beam pulse time structure to reduce beam losses during the beam capture process in the Proton Synchrotron Booster (PSB) and when switching between its 4 rings. The peak beam current from the source is 35 mA, resulting in 27 mA out of the RFQ and 25 mA at the PSB injection with shot-to-shot modulated pulse length of 0–600 μ s at 0.83 Hz repetition rate. Linac4 became the injector of the CERN proton accelerator complex in 2020, replacing the 50 MeV Linac2 after 40 years of service. Providing 160 MeV H^- ions, it has been the first step of the LHC Injectors Upgrade (LIU) project [2], implementing a charge exchange injection process and doubling the PSB injected intensity, resulting in a luminosity increase in the LHC injector chain. The commissioning staged in beam energy steps started in 2013, reaching its final beam energy in 2016. Several reliability and performance improvement runs took place [3], until it was finally connected to the PSB. Since then, Linac4 performance and reliability were continuously analysed and improved.

OPERATIONAL EXPERIENCE

In Dec. 2020, the beam was sent to the PSB for the first time. The charge exchange injection was commissioned

according to the plan [4]. The PSB beam brightness goal was quickly reached and even surpassed [5]. The experience from the first year of Linac4 operation is described in [6, 7]. The achieved beam performance is within the specifications [6]. The normalized rms emittance measured at the PSB injection is 0.26π .mm.mrad in both transverse planes (the requirement is 0.4π .mm.mrad for a 40 mA beam current). The measured optics mismatch factor (Eq. 7.98 in [8]) was 0.08. The pulse flatness in terms of bunch position and energy are one of the key parameters. The beam loading effect in the cavities is compensated by feedback and adaptive feedforward (AFF) systems operating concurrently. When the pulse length or chopping factor are changed, the feedforward correction is automatically reset, while feedback is kept active. By observing deviations in the measured cavity amplitudes and phases from the requested values, AFF develops corrective waveforms that are applied on the subsequent pulse of the same type. This permits to achieve smaller than 10 keV energy deviations at the PSB injection.

The pulse position stability in the horizontal plane is well within the specified 1 mm. In the worst case, it is measured to be 0.4 mm and the deviation is visible only for the very first couple of microseconds. On the other hand, in the vertical plane it is slightly above 1 mm, and the slope is visible all along the pulse. The most likely reason is the 3 MeV chopper voltage.

The pulse-to-pulse beam stability in terms of intensity, position, and energy deviations is within the defined margins of 2%, 1.5 mm and 100 keV, respectively. A feedback system keeps the measured beam intensity in the LEBT constant by regulating the amplitude of the 2 MHz RF power of the source [9]. This system is also capable of automatically adjusting the intensity in the MEBT; however, it is not enabled for operational beams because no drift in the RFQ transmission was ever observed.

A dedicated web service (Beam Performance Tracking) was developed at CERN that provides plots showing evolution of the key accelerator parameters [10]. For Linac4, it shows plots of beam intensity, transmission, position, and phase for the past week for each beam user. The RF amplitudes and phases are plotted for the past 60 days. Results of various statistical analyses are also made available. This helps to monitor the machine status and to detect problems with the machine stability.

Startup, Commissioning, and Operation

Linac4 yearly operation typically starts in March after the beam re-commissioning, when the beam is sent to the PSB, and ends in November, when a year-end technical stop starts to allow for maintenance of the accelerator complex. During the first week after the end of the run, experts

* edgar.sargsyan@cern.ch